

Improved Human Soft Tissue Thigh Surrogates for Superior Assessment of Sports Personal Protective Equipment

A doctoral thesis submitted in partial fulfilment of the requirements for the award of Doctor of
Philosophy of Loughborough University

by

Thomas Payne

Wolfson School of Mechanical and Manufacturing Engineering

Loughborough University

United Kingdom

March 2015

© Thomas Mark Payne

There should be no boundary to human endeavour

Prof. Stephen Hawking

Abstract

Human surrogates are representations of living humans, commonly adopted to better understand human response to impacts. Though surrogates have been widely used in automotive, defence and medical industries with varying levels of biofidelity, their primary application in the sporting goods industry has been through primitive rigid anvils used in assessing personal protective equipment (PPE) effectiveness. In sports, absence from competition is an important severity measure and soft tissue injuries such as contusions and lacerations are serious concerns. Consequently, impact surrogates for the sporting goods industry need a more subtle description of the relevant soft tissues to assess impact severity and mitigation accurately to indicate the likelihood of injury.

The fundamental aim for this research study was to establish a method to enable the development of superior, complementary, increasingly complex synthetic and computational impact surrogates for improved assessment of sports personal protective equipment. With a particular focus on the thigh segment, research was conducted to evaluate incremental increases in surrogate complexity. Throughout this study, empirical assessment of synthetic surrogates and computational evaluation using finite element (FE) models were employed to further knowledge on design features influencing soft tissue surrogates in a cost and time efficient manner.

To develop a more representative human impact surrogate, the tissue structures considered, geometries and materials were identified as key components influencing the mechanical response of surrogates. As a design tool, FE models were used to evaluate the changes in impact response elicited with different soft tissue layer configurations. The study showed the importance of skin, adipose, muscle and bone tissue structures and indicated up to 15.4% difference in maximum soft tissue displacement caused by failure to represent the skin layer. FE models were further used in this capacity in a shape evaluation study from which it was determined that a full-scale anatomically contoured thigh was necessary to show the full diversity of impact response phenomena exhibited. This was particularly pertinent in PPE evaluations where simple surrogate shapes significantly underestimated the magnitudes of displacements exhibited (up to 155% difference) when rigid shell PPE was simulated under impact conditions.

Synthetic PDMS silicone simulants were then fabricated for each of the organic soft tissues to match their dynamic responses. The developed simulants exhibited a superior representation of the tissues when compared to previous single material soft tissue simulant, Silastic 3483, which showed 324%, 11,140% and -15.8% greater differences than the PDMS when compared to previously reported target organic tissue datasets for relaxed muscle, skin and adipose tissues respectively. The impact response of these PDMS surrogates were compared in FE models with previously used single material simulants in representative knee and cricket ball sports impact events. The models were each validated through experimental tests and the PDMS simulants were shown to exhibit significantly closer responses to organic tissue predictions across all impact conditions and evaluation metrics considered.

An anatomically contoured synthetic thigh surrogate was fabricated using the PDMS soft tissue simulants through a novel multi-stage moulding process. The surrogate was experimentally tested under representative sports impact conditions and showed a good comparison with FE model predictions with a maximum difference in impactor displacements and peak accelerations of +6.86% and +12.5% respectively at velocities between 2 - 4 m.s⁻¹.

The value of increased biofidelity in the anatomical synthetic and virtual surrogate thighs has been proven through the incremental adoption of important surrogate elements (tissue structures, material and geometries). The predictive capabilities of each surrogate have been demonstrated through their parallel developments and staged comparisons with idealised organic tissue responses. This increase in biofidelity is introduced at modestly higher cost compared to Silastic 3483, but, given the benefits of a more representative human impact response for PPE evaluations, this is shown to be worthwhile.

Acknowledgments

First and foremost, I would like to acknowledge the support of my supervisor for the past seven years, Dr. Séan Mitchell. I am grateful for his patience, pragmatic attitude and unwavering belief in my abilities. I certainly would not have achieved what I have without his help.

I would also like to recognise my co-supervisor Dr. Richard Bibb who has provided a constant source of support and offered valuable contributions throughout my project. In addition, I would like thank Prof. Mark Waters and his colleagues at Technovent who have been a great help and source of knowledge on all silicone related matters.

The academics and technicians at the Sports Technology Institute have all supported me throughout my studies. A special acknowledgement should be reserved for the lab technicians, Stephen Carr and Max Farrand, who have been essential to the manufacture and testing of the surrogate structures. Further thanks must also go my colleagues at the Sports Technology Institute. Their good humour, helpfulness and support have made my three years an enjoyable experience.

Finally, I would like to acknowledge the support of my friends and family without whom none of this would have been possible. They have always provided a relief from PhD related stresses, a solution to issues and, above all, believed in me.

Publications arising from this research

Payne, T., Mitchell, S. and Bibb, R. 2013. Design of human surrogates for the study of biomechanical injury: a review. *Critical Reviews™ in Biomedical Engineering*; 41 (1), pp. 51-89. DOI: 10.1615/CritRevBiomedEng.2013006847.

Halkon, B.J., Mitchell, S.R., Payne, T. and Carbo, J. 2014. Biomechanical measurements of human impacts in basketball. *Procedia Engineering*; 72, pp. 214-219. DOI: 10.1016/j.proeng.2014.06.038.

Payne, T., Mitchell, S.R., Bibb, R. and Waters, M. 2014. Initial Validation of a Relaxed Human Soft Tissue Simulant for Sports Impact Surrogates. *Procedia Engineering*; 72, pp. 533-538. DOI: 10.1016/j.proeng.2014.06.092.

Payne, T., Mitchell, S., Bibb, R. and Waters, M. 2015. Development of novel synthetic muscle tissues for sports impact surrogates. *Journal of the Mechanical Behavior of Biomedical Materials*; 41, pp. 357-374. DOI: 10.1016/j.jmbbm.2014.08.011.

Payne, T., Mitchell, S., Halkon, B.; Bibb, R. and Waters, M. 2015. Development of novel synthetic muscle tissues for sports impact surrogates. *Journal of the Mechanical Behavior of Biomedical Materials*; 41, pp. 357-374. DOI: 10.1016/j.jmbbm.2014.08.011.

Payne, T., Mitchell, S., Halkon, B., Bibb, R. and Waters, M. 2015. Development of an anatomical synthetic human thigh impact surrogate for sports personal protective equipment testing. *IMechE, Part P: Journal of Sports Engineering and Technology*. [in press]

Table of Contents

1. Introduction.....	1
1.1. Chapter Overview	1
1.2. Background.....	1
1.3. Research Aim.....	3
1.4. Research Questions	4
1.5. Research Approach	5
1.6. Chapter-by-Chapter Summary	6
2. Literature Review.....	8
2.1. Chapter Overview	8
2.2. Sports Injury Context.....	8
2.2.1. Injury Statistics	8
2.2.2. Injury Modes	10
2.2.3. Sports Personal Protective Equipment.....	13
2.3. Anatomy of the Thigh Region	16
2.3.1. Tissue Structures.....	16
2.3.2. Organic Tissue Properties	20
2.4. Human Surrogates.....	27
2.4.1. Organic Surrogates.....	27
2.4.2. Artificial Surrogates.....	33
2.5. Surrogate Development Approach.....	44
3. Methods to Enable the Formulation of Improved Sports Impact Assessments.....	46
3.1. Chapter Overview	46
3.2. Introduction.....	46
3.2.1. Components of Sports Impact Assessments.....	46
3.2.2. Review of Sports Impact Assessments	46
3.2.3. Review of Previous Conceptual Frameworks.....	47
3.2.4. Aims and Objectives.....	49
3.3. Formulation of Improved Conceptual Framework	49
3.3.1. Core Model	50
3.3.2. Influencing Factors.....	51
3.4. Model Evaluation through Application.....	53
3.4.1. Injury Scenario Definitions	53
3.4.2. Experimental Protocol Development for Controlled Scenario Reproduction	56
3.5. Specification for Improved Sports Impact Assessments	56
3.5.1. Target Surrogate.....	56
3.5.2. Striker Surrogate.....	57
3.5.3. Levels of Constraint.....	57
3.5.4. Impact Parameters.....	57
3.5.5. Methods of Assessment/Evaluation Criteria	57

3.6. Target Surrogate Research Approach	58
3.6.1. Anatomical Simplifications	58
3.6.2. Materials.....	58
3.6.3. Evaluation Metrics.....	58
3.6.4. Surrogate Development Work Flow.....	59
4. Determining the Effects of Anatomical Simplifications in a Soft Tissue Surrogate using FEA Methods	60
4.1. Chapter Overview	60
4.2. Introduction.....	60
4.2.1. Aims and Objectives.....	62
4.3. Computational Modelling Parameters	62
4.3.1. Selection of Solver Methods.....	63
4.3.2. Geometries	64
4.3.3. Material Models.....	66
4.3.4. Model Definition	71
4.4. Investigation of the Importance of Surrogate Tissue Layers	81
4.4.1. Introduction	81
4.4.2. Methodology	81
4.4.3. Results.....	83
4.4.4. Sensitivity Analysis.....	87
4.5. Discussion.....	91
4.5.1. Organic Tissue Data.....	91
4.5.2. FE Modelling Techniques	91
4.5.3. Biofidelity of Surrogate Response.....	93
4.5.4. Importance of Tissue Layers	94
5. Surrogate Soft Tissue Simulant Formulation	95
5.1. Chapter Overview	95
5.2. Introduction.....	95
5.2.1. Previous Surrogate Soft Tissue Simulants.....	95
5.2.2. Simulant Development Approach.....	95
5.2.3. PDMS Silicones	96
5.2.4. Silicone Behaviour.....	97
5.2.5. Aims and Objectives.....	98
5.3. Methodology.....	98
5.3.1. Fabrication Procedures	98
5.3.2. Test Conditions	99
5.3.3. Mechanical Testing Procedures.....	99
5.4. Silicone Formulations	103
5.4.1. Base Formulations	103
5.4.2. Effects of Changes in Cross-Linker Concentrations	104
5.4.3. Effects of Changes in Polymer Concentration	105

5.4.4. <i>Bespoke Silicone Formulations</i>	106
5.5. Mechanical Properties of Bespoke Silicones	107
5.5.1. <i>Low Strain Rate Tests</i>	107
5.5.2. <i>Intermediate Strain Rate Tests</i>	110
5.5.3. <i>Stress Relaxation Tests</i>	112
5.5.4. <i>Durability Tests</i>	113
5.5.5. <i>Consistency of Response</i>	114
5.6. Material Models	115
5.6.1. <i>Hyperelastic</i>	115
5.6.2. <i>Viscoelasticity</i>	117
5.7. FE Specimen Tests.....	118
5.8. Discussion.....	119
5.8.1. <i>Mechanical Characterisation Procedures</i>	119
5.8.2. <i>PDMS Silicone Behaviour</i>	119
5.8.3. <i>Quality of PDMS Silicone Formulations</i>	120
5.8.4. <i>Constitutive Modelling</i>	123
5.9. Conclusions.....	124
6. Experimental Impact Testing of Soft Tissue Surrogates and FE Model Validation.....	125
6.1. Chapter Overview	125
6.2. Introduction.....	125
6.2.1. <i>Validation Approaches</i>	125
6.2.2. <i>Aims and Objectives</i>	127
6.3. Surrogate Instrumentation.....	127
6.3.1. <i>Load Cells</i>	127
6.3.2. <i>Pressure Measurement Systems</i>	127
6.3.3. <i>Strain Gauges</i>	128
6.3.4. <i>Accelerometers</i>	129
6.3.5. <i>Motion Tracking</i>	129
6.4. Instrumentation Evaluation	130
6.4.1. <i>Selection of Instrumentation</i>	130
6.4.2. <i>Mould Development</i>	130
6.4.3. <i>Experimental Tests</i>	131
6.5. Closed Loop Surrogate Validation.....	135
6.5.1. <i>Introduction</i>	135
6.5.2. <i>Materials</i>	135
6.5.3. <i>Experimental Test Configuration</i>	137
6.6. Results.....	138
6.6.1. <i>Surrogate Validation Results: Knee Impact</i>	138
6.6.3. <i>Discussion</i>	143
6.7. Open Loop Predictive FE Simulation of Surrogate Behaviour	145
6.7.1. <i>Introduction</i>	145

6.7.2. Methodology.....	145
6.7.3. Results.....	145
6.7.4. Discussion.....	150
6.8. Conclusions.....	151
7. Investigation of the Importance of Anatomical Geometric Complexities and their Effect on PPE Interactions	152
7.1. Chapter Overview	152
7.2. Introduction.....	152
7.2.1. Previous Surrogate Geometries.....	152
7.2.2. Aims and Objectives	154
7.3. Study 1 – Evaluation of Surrogate Shape	154
7.3.1. Introduction.....	154
7.3.2. Methodology.....	154
7.3.3. FE Modelling.....	157
7.3.4. Results	158
7.3.5. Discussion.....	165
7.4. Study 2 – Evaluation of Surrogate Response in an Anatomically More Representative Surrogate	167
7.4.1. Introduction.....	167
7.4.2. Methodology.....	167
7.4.3. Results	170
7.4.4. Discussion.....	173
7.5. Study 3 - PDMS Divergence Study	175
7.5.1. Introduction.....	175
7.5.2. Results	175
7.5.3. Discussion.....	176
7.6. Study 4 - Sensitivity Analysis: Tensile Soft Tissue Loads	177
7.6.1. Introduction.....	177
7.6.2. Results	177
7.7. Study 5 - PPE Interactions.....	178
7.7.1. Introduction.....	178
7.7.2. Methodology.....	178
7.7.3. Results	180
7.7.4. Discussion.....	183
7.8. Conclusions.....	184
8. Fabrication of an Anatomical Synthetic Thigh Surrogate	185
8.1. Chapter Overview	185
8.2. Introduction.....	185
8.2.1. Aims and Objectives.....	185
8.3. Methodology.....	185
8.3.1. Surrogate Skeletal Component.....	185
8.3.2. Mould Tooling Development.....	186

8.3.3. <i>Surrogate Fabrication</i>	192
8.3.4. <i>Costing</i>	196
8.4. <i>Discussion</i>	197
8.4.1. <i>Quality of Synthetic Surrogate Thigh</i>	197
8.4.2. <i>Further Surrogate Improvements</i>	198
8.4.3. <i>Geometric Dataset and Anatomical Simplifications</i>	200
8.4.4. <i>Cost of Manufacture</i>	201
9. Experimental Impact Testing of the Synthetic Surrogate Thigh and Validation of a Parallel FEA Model	202
9.1. <i>Chapter Overview</i>	202
9.2. <i>Introduction</i>	202
9.2.1. <i>FEA Approaches</i>	202
9.2.2. <i>Impact Testing Configurations</i>	202
9.2.3. <i>Aims and Objectives</i>	203
9.3. <i>Test Methodology</i>	203
9.3.1. <i>Experimental Test Configuration</i>	203
9.3.2. <i>Instrumentation and Methods of Evaluation</i>	204
9.3.3. <i>Impact Parameters</i>	205
9.3.4. <i>FE Modelling</i>	206
9.4. <i>Results</i>	208
9.4.1. <i>Synthetic Surrogate Responses</i>	208
9.4.2. <i>FE Model Comparison</i>	210
9.5. <i>Discussion</i>	217
9.5.1. <i>Correlation between Experimental Data and FE Model Responses</i>	217
9.5.2. <i>Test Rig Configuration</i>	220
9.6. <i>Conclusions</i>	221
10. Discussion, Conclusions and Recommendations for Future Work	222
10.1. <i>Chapter Overview</i>	222
10.2. <i>Discussion</i>	222
10.3. <i>Limitations of Study and Recommendations for Future Work</i>	227
10.3.1. <i>Diversity and Range of Tissue Structures</i>	227
10.3.2. <i>Organic Soft Tissue Characterisation</i>	227
10.3.3. <i>Synthetic Soft Tissue Materials</i>	228
10.3.4. <i>Constitutive Modelling</i>	228
10.3.5. <i>Geometric Representation of External and Internal Tissue Structures</i>	229
10.3.6. <i>Measurement and Injury Evaluation</i>	229
10.3.7. <i>Human Impact Testing</i>	230
10.3.8. <i>Safety Standards</i>	230
10.4. <i>Conclusions</i>	231
Reference List	233

List of Figures

Chapter 1

Figure 1.1 - Iterative Enhancement Development Cycle.	3
Figure 1.2 – A sample of thigh PPE worn in: (a) basketball; (b) cricket; (c) American football; (d) martial arts.	6

Chapter 2

Figure 2.1 - Femur fracture injury risk curve (adapted from Tencer <i>et al.</i> (2002)).	11
Figure 2.2 - Commercial thigh PPE: (a) Nike Pro Combat Hyperstrong American Football Compression Hard Plate (www.nike.com); (b) Kookaburra Blade Cricket Thigh Guard (www.kookaburra.biz).	13
Figure 2.3 - Schematic showing a typical sports safety standard protocol used to assess projectile impacts (BS:13546:2002 - Field Hockey Goalkeeper Protective Clothing; BS 6183-3:2000 - Cricket Leg Protectors).	14
Figure 2.4 - Axial plane section through the human male thigh (Gray, 1918).	16
Figure 2.5 - Femur bone anatomy and position in thigh in: (a) anterior femur; (b) posterior femur; (c) anterior frontal cross-section and (d) posterior frontal cross-section views (Gray, 1918).	17
Figure 2.6 - Musculature in the thigh region with some key muscles labelled in: (a) anterior; (b) posterior and (c) deep medial locations (Gray, 1918).	17
Figure 2.7 - (a) Hip joint; (b) knee joint (posterior view); (c) knee joint (sagittal plane) (Gray, 1918).	19
Figure 2.8 - Engineering stress - strain graphs for a range of organic skin tissue samples at different strain rates (T - transverse; L - longitudinal).	22
Figure 2.9 - Compressive engineering stress - strain graphs for a range of organic adipose tissue samples at different strain rates in (a) linear and (b) log-linear plots.	23
Figure 2.10 - Compressive engineering stress - strain plot showing data from previous organic muscle tissue characterisation studies.	24
Figure 2.11 - Cross-section through human femur showing cortical and trabecular bone regions (Gray, 1918).	26
Figure 2.12 - Compressive engineering stress - strain plots showing response of: (a) cortical bone (McElhaney, 1966) and (b) trabecular bone (Schoenfeld <i>et al.</i> , 1974).	26
Figure 2.13 - Surrogate thigh components developed by Hrysonmallis (2009) showing Silastic 3483 soft tissue surface, wooden surrogate backing, and steel skeletal component (<i>Image reproduced with permission of the rights holder, Elsevier</i>).	36
Figure 2.14 - Durable surrogate lower leg developed by Tatar <i>et al.</i> (2014) with boot mounted pendulum end-effector (<i>Image reproduced with permission of the rights holder, JSSM</i>).	37
Figure 2.15 – (a) Components of the FSL; (b) Fully assembled FSL (Bergeron <i>et al.</i> , 2006).	39
Figure 2.16 – Images showing FE model mesh definitions in Untaroiu <i>et al.</i> (2013) highlighting additional consideration afforded to joint structures and skeletal components (<i>Image reproduced with permission of the rights holder, Springer</i>).	43

Chapter 3

Figure 3.1 - Multifactorial model (Meeuwisse, 1994).	47
Figure 3.2- Load-injury model (Wismans, 2000).	48
Figure 3.3 - DCS core framework.	50
Figure 3.4 - From left: basketball knee impact to the anterior thigh; cricket ball impact to the lateral thigh.	53
Figure 3.5 - Surrogate development approach.	59

Chapter 4

Figure 4.1 – Log-linear stress - strain plot showing the quasi-static compressive response of Silastic 3483 when compared to skin (Shergold <i>et al.</i> , 2006), relaxed muscle (Song, 2007; McElhaney 1966), and adipose tissue (Comley & Fleck, 2012).	61
Figure 4.2. (a) Axial plane section through the human thigh showing the diversity of tissue structures (Gray, 1918); (b) Anatomical simplification of the thigh.	62
Figure 4.3 – Image showing separation lines from bone centroid (<i>Reproduced courtesy of EPFL, Visible Human Visualization Software, http://visiblehuman.epfl.ch and Gold Standard Multimedia (GSM) www.gsm.org</i>).	64
Figure 4.4 – Cylinder surrogate geometry and sagittal plane section.	66
Figure 4.5 – Log-linear intermediate strain rate properties of: skin (Shergold <i>et al.</i> , 2006), adipose (Comley & Fleck, 2012) and relaxed muscle (McElhaney, 1966; Song <i>et al.</i> , 2007).	67
Figure 4.6 – Single element cube in original and deformed state after tensile test.	70
Figure 4.7 - Tensile engineering stress - strain plots showing tensile response of the quasi-static skin tissue compressive material model (Shergold <i>et al.</i> , 2006) compared with previous characterisation studies in literature (L - longitudinal; T - transverse).	70

Figure 4.8 - (a) C3D8 linear brick element; (b) C3D20 quadratic brick element; (c) C3D10 second order tetrahedral element; (d) S4 conventional shell element; (e) SC8 continuum shell element (ABAQUS, 2014).....	71
Figure 4.9 – (a) Mesh distortion in continuum shell skin; (b) continuous stress profile in continuum solid element skin.	73
Figure 4.10 - Four continuum solid elements through skin layer.....	74
Figure 4.11 - Adipose layer element penetration when no distortion control was applied.	74
Figure 4.12 - von Mises Stress on the adipose layer surface in models with and without distortion control.....	74
Figure 4.13 - Artificial energy/internal energy vs. time graphs for: (a) cricket ball and (b) knee impacts.	75
Figure 4.14 - Exponential pressure-overclosure relationship.....	76
Figure 4.15 – (a) Hard contact element distortion and areas of high stress concentrations; (b) softened contact continuous stress profiles.	76
Figure 4.16 – (a) Skin layer displacement and (b) von Mises surface stress in models with and without tied layers.....	77
Figure 4.17 - Bone tissue mesh convergence graphs showing: (a) $\sigma_{22,max}$ on bone surface vs. element size; (b) computational time vs. element size.	78
Figure 4.18 - Skin tissue mesh convergence graphs showing: (a) x_{max} on surrogate surface vs. element size; (b) t_x vs. element size; (c) $\sigma_{v,max}$ on skin surface vs. element size; (d) computational time vs. element size.....	79
Figure 4.19 - Adipose tissue mesh convergence graphs showing: (a) x_{max} on surrogate surface vs. element size; (b) t_x vs. element size; (c) $\sigma_{v,max}$ on adipose surface vs. element size; (d) computational time vs. element size.	79
Figure 4.20 - Muscle tissue mesh convergence graphs showing: (a) x_{max} on surrogate surface vs. element size; (b) t_x vs. element size; (c) $\sigma_{v,max}$ on muscle surface vs. element size; (d) computational time vs. element size.	80
Figure 4.21 - FE model configuration for impact simulations.	81
Figure 4.22 – x_{skin} - time plots for: (a) cricket ball and (b) knee impactor loading conditions.....	83
Figure 4.23 – P_{base} - time plots for: (a) cricket ball; and (b) knee impactor loading conditions.....	84
Figure 4.24 - Layer thicknesses for (a) skin; (b) adipose; (c) muscle (left: cricket ball; right: knee impactor).	85
Figure 4.25 – von Mises stresses on the: (a) skin; (b) adipose and (c) muscle layer surfaces (left: cricket ball; right: knee impactor).	86
Figure 4.26 – x_{skin} - time plots showing responses for variations in skin thickness in: (a) cricket ball and (b) knee impact simulations.	87
Figure 4.27 – P_{base} - time plots showing variations in response in surrogates with different skin thickness for: (a) cricket ball and (b) knee impact simulations.....	88
Figure 4.28 – x_{skin} - time plots showing variations in response in surrogates with different adipose thicknesses for: (a) cricket ball and (b) knee impact simulations.	89
Figure 4.29 – P_{base} - time plots showing variations in response in surrogates with different adipose thicknesses for: (a) cricket ball and (b) knee impact simulations.	90
Figure 4.30 - Image showing relative magnitudes of maximum principal strain in the FE surrogate in knee impact simulation.....	93
Figure 4.31 - Hertzian contact model for a rigid impactor indenting elastic half-space (Popov. 2010).	93
 Chapter 5	
Figure 5.1 – Chain length of PDMS polymer chains.	96
Figure 5.2 - Chemical structure of additive cure PDMS silicone reaction.	97
Figure 5.3 - ASTM D395 compressive test specimen.	98
Figure 5.4 - Instron 5569 test configuration with compressive platens.....	99
Figure 5.5 - Programmed triangular loading profile for quasi-static uniaxial compressive tests.....	100
Figure 5.6 - Instron 9250HV drop tower intermediate strain rate materials testing configuration.	100
Figure 5.7 - Instron ElectroPuls E3000 mechanical test machine.	101
Figure 5.8 - Processing of intermediate strain rate drop tower data: (a) raw data; (b) load-time and displacement-time curves with coincident time scales; (c) unfiltered stress - strain output; (d) smoothed stress - strain plot.....	103
Figure 5.9 – Quasi-static compressive engineering stress - strain plot of silicones with different cross-linker concentrations in: (a) linear and (b) log-linear graphs.	104
Figure 5.10 – Brittle failure of 1:1 PDMS silicone specimen.	104
Figure 5.11 – Log - linear engineering stress - strain plot showing differences in response based on changes in polymer concentrations....	105
Figure 5.12 – Log - linear engineering stress - strain plot showing target organic tissue properties for bespoke PDMS simulants.	106
Figure 5.13 - Quasi-static stress - strain curves showing closeness of fit of PDMS silicones with organic tissue datasets in: (a) relaxed muscle (McElhaney, 1966; Song <i>et al.</i> , 2007); (b) contracted muscle (Zheng <i>et al.</i> , 1999); (c) skin (Shergold <i>et al.</i> , 2006); (d) adipose (Comley & Fleck, 2012).....	107
Figure 5.14 - Log-linear plot of quasi-static compressive responses of PDMS simulants compared to Silastic 3483.....	108
Figure 5.15 – Graphs showing closeness of fit of silicone simulants with contracted muscle target organic tissue dataset (Zheng <i>et al.</i> , 1999) for: (a) PDMS simulant and (b) Silastic 3483.....	108

Figure 5.16 - Intermediate strain rate stress - strain curves for PDMS simulants: (a) relaxed muscle; (b) contracted muscle; (c) skin; (d) adipose.	110
Figure 5.17 – Log - linear intermediate strain rate engineering stress - strain plots showing comparisons between PDMS simulants and organic tissues in: (a) relaxed muscle; (b) contracted muscle; (c) skin; (d) adipose.	111
Figure 5.18 – Normalised stress - time plot showing stress relaxation of PDMS simulants compared with organic tissue data in: (a) relaxed muscle (Van Loocke <i>et al.</i> , 2009); (b) contracted muscle (Van Loocke <i>et al.</i> , 2009); (c) skin (Wu <i>et al.</i> , 2003); (d) adipose (Gefen & Haberman, 2007).....	112
Figure 5.19 - Engineering stress - strain plots showing quasi-static simulant responses before and after repeated loading cycles for: (a) PDMS skin; (b) PDMS relaxed muscle and (c) PDMS adipose simulants.....	113
Figure 5.20 – Engineering stress - strain plots of six identical PDMS silicone test specimens.....	114
Figure 5.21 - Hyperelastic model fits for: (a) relaxed muscle; (b) contracted muscle; (c) skin; (d) adipose.	116
Figure 5.22 - Compressive specimen test comparisons in PDMS simulants: (a) adipose - quasi-static; (b) adipose - strain rate; (c) relaxed muscle - quasi-static; (d) relaxed muscle - strain rate; (e) skin – quasi-static; (f) skin – strain rate.	118
Figure 5.23 – Intermediate strain rate PDMS relaxed muscle simulant engineering stress - strain response compared with human muscle characterisation studies by Chawla <i>et al.</i> (2009) and Balaraman <i>et al.</i> (2012).....	121

Chapter 6

Figure 6.1 - Common FE model usage procedures: (a) Investigative closed loop; (b) Predictive open loop.	126
Figure 6.2 - Puck surrogate mould with instrumentation cable access point.....	131
Figure 6.3 - Graph showing a comparison between Instron and Dytran load cell peak forces with a linear fit.....	132
Figure 6.4 - Pressure map visualisation of: (a) surface sensor; (b) embedded sensor and (c) base sensor.	132
Figure 6.5 - Differences in nett force between the Instron 9250HV load cell and the Tekscan sensor (20cm, 6.8kg drop).	133
Figure 6.6 - Differences in Instron 9250 drop tower load cell output with and without a Tekscan F-Scan sensor on the surface of the gelatin puck.....	133
Figure 6.7 - Embedded Tekscan sensor creating delamination within the surrogate.....	134
Figure 6.8 - Compressive engineering stress - strain graphs of Silastic simulants and ballistic gelatin at representative intermediate strain rates.....	135
Figure 6.9 - Cylindrical puck geometry and sagittal plane section.	137
Figure 6.10 - Schematic showing experimental drop test configuration.	137
Figure 6.11 - HSV stills of puck surrogates at maximum displacement in: (a) 10% gelatin; (b) PDMS; (c) Silastic 3481.	138
Figure 6.12 - Experimental differences in mean surrogate response in different simulants for knee impacts.	138
Figure 6.13 - Displacement vs. time and force vs. time graphs showing a comparison between experimental data and FE model predictions for knee impacts in: (a) Silastic 3481; (b) Silastic 3483; (c) Silastic 3487; (d) 10% Gelatin; (e) 20% Gelatin and (f) PDMS surrogates.....	139
Figure 6.14 – Corrected displacement vs. time and force vs. time graphs showing a comparison between experimental data and optimised FE model predictions for: (a) 10% gelatin and (b) 20% gelatin.	140
Figure 6.15 - HSV stills of cricket ball puck surrogates at maximum displacement: (a) 10% gelatin; (b) PDMS; (c) Silastic 3481.....	141
Figure 6.16 - Experimental differences in mean surrogate response in different simulants for cricket ball impacts.....	141
Figure 6.17 - Displacement vs. time and force vs. time graphs showing a comparison between experimental data and FE model predictions for cricket ball impacts in: (a) Silastic 3481; (b) Silastic 3483; (c) Silastic 3487; (d) 10% Gelatin; (e) 20% Gelatin and (f) PDMS surrogates.	142
Figure 6.18 – x_{skin} - time plots of simulant surrogates in: (a) cricket ball and (b) knee impactor simulations.....	145
Figure 6.19 - Sagittal plane sections showing impactor penetrations of surrogate under cricket ball: (a) organic tissues, (b) PDMS, (c) 10% gelatin; and knee impactor loading conditions: (d) organic tissues, (e) PDMS, (f) 10% gelatin.	146
Figure 6.20 - P_{base} - time graphs for: (a) cricket ball and (b) knee impactor simulations.....	147
Figure 6.21 – (a) $\sigma_{v,skin}$ - time graphs and (b) $\sigma_{v,muscle}$ - time graphs (left: cricket ball; right: knee impacts).....	148
Figure 6.22 - Tissue layer thicknesses in the cylinder surrogate showing responses under the cricket ball (left graph) and knee impactor (right graph) loading conditions for: (a) skin; (b) adipose; (c) muscle tissues.	149

Chapter 7

Figure 7.1 - (a) BS 6183:3:2000 Cricket Leg Guards - Shin Region; (b) BS:EN 13277 Martial Arts Limb Segment Protection – Shin, Instep and Forearm Protectors; (c) BS 13546:2002 – Field Hockey Goalkeeper Clothing – Abdominal, Chest, Breast Thigh, Hip Protection.....	152
Figure 7.2 – 75 mm puck surrogate configuration dimensioned in sagittal plane section.....	155
Figure 7.3 – Shaped anvil surrogate configurations and dimensions shown in sagittal plane section for: (a) 50 mm; (b) 75 mm and (c) 100 mm surrogates.	156
Figure 7.4 – 75 mm cylinder surrogate geometry and dimensions shown in sagittal plane section.	157

Figure 7.5 - x_{skin} - time comparisons between different surrogate geometries for: (a) 50 mm surrogate-cricket ball; (b) 50 mm surrogate-knee impact; (c) 75 mm surrogate-cricket ball; (d) 75 mm surrogate-knee impact; (e) 100 mm surrogate-cricket ball; (f) 100 mm surrogate-knee impact.....	159
Figure 7.6 - x_{skin} - time graphs showing differences in response in the following impacts: (a) puck-cricket ball; (b) puck-knee; (c) shaped anvil-cricket ball; (d) shaped anvil-knee; (e) cylinder-cricket ball; (f) cylinder-knee.	160
Figure 7.7 - P_{base} - time comparisons between different surrogate geometries for: (a) 50 mm surrogate-cricket ball; (b) 50 mm surrogate-knee impact; (a) 75 mm surrogate-cricket ball; (b) 75 mm surrogate-knee impact; (a) 100 mm surrogate-cricket ball; (b) 100 mm surrogate-knee impact.	161
Figure 7.8 - P_{base} - time graphs for: (a) puck-cricket ball; (b) puck-knee; (c) shaped anvil-cricket ball; (d) shaped anvil-knee; (e) cylinder-cricket ball; (f) cylinder-knee.	162
Figure 7.9 - $\sigma_{v,skin}$ - time plots in the following impacts: (a) puck-cricket ball; (b) puck-knee; (c) shaped anvil-cricket ball; (d) shaped anvil-knee; (e) cylinder-cricket ball; (f) cylinder-knee.	163
Figure 7.10 - $\sigma_{v,muscle}$ - time plots in the following impacts: (a) puck-cricket ball; (b) puck-knee; (c) shaped anvil-cricket ball; (d) shaped anvil-knee; (e) cylinder-cricket ball; (f) cylinder-knee.	164
Figure 7.11 - Anatomically contoured cylinder surrogate and constituent tissue components.	168
Figure 7.12 - Anatomical contoured cylinder mesh images showing density of tissue layers and mesh biasing.....	169
Figure 7.13 - Impact types to the anatomical contoured surrogate in: (a) anterior; (b) posterior and (c) lateral directions.	170
Figure 7.14 - Images of anatomical contoured cylinder at maximum displacement for: (a) anterior; (b) posterior; (c) lateral impacts (left: cricket ball; right: knee).	170
Figure 7.15 - x_{skin} - time graphs for the anatomically contoured surrogate in (a) cricket ball and (b) knee impact simulations.	171
Figure 7.16 - $\sigma_{v,bone}$ - time graphs on the bone surface of the anatomical contoured surrogates in (a) cricket ball and (b) knee impact simulations.	171
Figure 7.17 - x_{skin} - time graphs showing the differences in response between a 75 mm surrogate and the anatomically contoured surrogate in: (a) cricket ball and (b) knee impact simulations.	174
Figure 7.18 - Tensile soft tissue loads applied to ends of surrogate.....	177
Figure 7.19 - x_{skin} - time and $\sigma_{v,bone}$ - time plots showing differences in response when different tensile loads were applied.	177
Figure 7.20 - Commercial thigh PPE: (a) Nike Pro Combat Hyperstrong American Football Compression Hard Plate; (b) Kookaburra Blade Cricket Thigh Guard.....	178
Figure 7.21 - CAD images of: (a) hard shell and (b) foam leg guard geometries.	178
Figure 7.22 - (a) Undeformed PPE with pressure on underside; (b) deformed PPE configuration.....	179
Figure 7.23 - PPE-surrogate configurations for foam and shell PPE across each surrogate.	180
Figure 7.24 - x_{skin} - time plots for each surrogate geometry with PPE affixed: (a) cricket ball-foam; (b) cricket ball-shell; (c) knee-foam; (d) knee-shell.	181
Figure 7.25 - von Mises stress distributions on surfaces of surrogates showing areas of high stress concentration immediately after impact when shell PPE was simulated.	182
Figure 7.26 - von Mises stress distributions on the surface of anatomically contoured surrogates when: (a) foam and (b) shell were simulated.	182
Figure 7.27 - $\sigma_{v,bone}$ - time plots for anatomical contoured surrogates with foam and shell PPE in: (a) cricket ball and (b) knee impact simulations.	183

Chapter 8

Figure 8.1 - Sawbones® 4 th generation large left composite femur (www.sawbones.com).....	186
Figure 8.2 - Composite femur coated in developer spray and retroreflective markers.	186
Figure 8.3 - Process stage diagram for thigh surrogate development.....	188
Figure 8.4 - Images of small scale surrogate development stages showing: (a) Stage 1 cured solid PDMS skin simulant and liquid sacrificial gelatin core;(b) Stage 1 cured PDMS skin on outside of mould with positioning stud; (c) Stage 4 final moulding of adipose; (d) Complete surrogate (inverted) showing positioning stud.....	190
Figure 8.5 - Skin mould assembly with highlighted design features.....	191
Figure 8.6 - Mould assembly components: (a) CAD image of distal femur attachment; (b) attachments between femur and intermediate base plates (c) cavity base plate femur seal.	192
Figure 8.7 - Images showing the stage 1 and 2 development stages for the surrogate skin layer: (a) gelatin being cooled in skin inner mould; (b) cured gelatin removed from mould; (c) gelatin positioned in skin outer mould assembly; (d) PDMS skin simulant poured into gap between the gelatin and mould cavity through funnels; (e) gelatin removed from the mould and PDMS skin layer cleaned from contaminate.	193
Figure 8.8 - Stage 3 moulding process: (a) PDMS muscle simulant moulded around femur; (b) cured PDMS simulant removed from the mould.	194

Figure 8.9 – Stage 4 Adipose layer moulding process: (a) muscle positioned in skin mould; (b) funnel used to pour adipose into cavity; (c) full leg assembly in environmental chamber.	194
Figure 8.10 - Full synthetic thigh model in: (a) anterior; (b) lateral; (c) posterior; (d) medial views.....	195
Figure 8.11 – FEA images of surrogate after 0.05s when subject to gravitational accelerations.....	199
Figure 8.12 - Reduction of wrinkling effect when skin subject to manual axial tension.....	199
Figure 8.13 - Small scale cylindrical surrogate with 1.5mm skin layer.	200

Chapter 9

Figure 9.1 – Pendulum test rig configuration with mounted striker and surrogate bodies.	203
Figure 9.2 – Accelerometer screw mounted into rear of the striking object.....	204
Figure 9.3 – High speed video camera and lighting arrangement for impact testing.	204
Figure 9.4 – Images showing the speckle pattern on surrogate surface for GOM ARAMIS DIC tracking and the camera and lighting orientation.	205
Figure 9.5 - GOM ARAMIS camera orientations for impact trials.....	205
Figure 9.6 - Comparison in quasi-static mechanical response between specimens from the reference and surrogate material batches for: (a) skin; (b) relaxed muscle; and (c) adipose simulants.	206
Figure 9.7 - Image showing the distribution of sampling points relative to the impact location at x_{max}	207
Figure 9.8 – Perpendicular high speed video stills of $2\text{ m}\cdot\text{s}^{-1}$ impacts at maximum displacement to: (a) anterior and (b) lateral thigh regions.	208
Figure 9.9 – Mean acceleration - time graphs for the impactor in: (a) anterior and (b) lateral impacts.....	209
Figure 9.10 – Mean displacement - time graphs for the impactor in: (a) anterior and (b) lateral impacts.....	209
Figure 9.11 - Examples of surface strain maps generated in GOM ARAMIS, attained from anterior impacts using: (a) frontal and (b) side camera arrangements.....	209
Figure 9.12 – (a) Torn skin on anterior surrogate surface due to off-centre impact; (b) Delamination of skin and adipose tissues in lateral regions.....	210
Figure 9.13 - x_{skin} - time and x_{bone} - time graphs showing the differences in impact kinematics between experimental data and FE model predictions in lateral impacts: (a) $1\text{ m}\cdot\text{s}^{-1}$; (b) $2\text{ m}\cdot\text{s}^{-1}$; (c) $3\text{ m}\cdot\text{s}^{-1}$; (d) $4\text{ m}\cdot\text{s}^{-1}$	211
Figure 9.14 – x_{skin} - time and x_{bone} - time graphs showing the differences in impact kinematics between experimental data and FE model predictions in anterior impacts: (a) $1\text{ m}\cdot\text{s}^{-1}$; (b) $2\text{ m}\cdot\text{s}^{-1}$; (c) $3\text{ m}\cdot\text{s}^{-1}$; (d) $4\text{ m}\cdot\text{s}^{-1}$	212
Figure 9.15 – a_{max} - time graphs showing the differences in impactor decelerations between experimental data and FE model predictions in lateral impacts: (a) $1\text{ m}\cdot\text{s}^{-1}$; (b) $2\text{ m}\cdot\text{s}^{-1}$; (c) $3\text{ m}\cdot\text{s}^{-1}$; (d) $4\text{ m}\cdot\text{s}^{-1}$	213
Figure 9.16 – $a_{impactor}$ - time graphs showing the differences in impactor accelerations between experimental data and FE model predictions in anterior impacts: (a) $1\text{ m}\cdot\text{s}^{-1}$; (b) $2\text{ m}\cdot\text{s}^{-1}$; (c) $3\text{ m}\cdot\text{s}^{-1}$; (d) $4\text{ m}\cdot\text{s}^{-1}$	214
Figure 9.17 – Surface strain images of lateral impacts at x_{max} showing differences in response between GOM ARAMIS data and FE model predictions in (a) $1\text{ m}\cdot\text{s}^{-1}$; (b) $2\text{ m}\cdot\text{s}^{-1}$; (c) $3\text{ m}\cdot\text{s}^{-1}$	215
Figure 9.18 - Graphs showing the divergence in response between experimental data and FE model predictions at sampling point: (a) A; (b) B; and (c) C (left: anterior; right: lateral).....	216
Figure 9.19 – Axial cross-section of the thigh showing the potential error introduced through impactor misalignment.....	218
Figure 9.20 - a_{max} vs. velocity plot for anterior and lateral impacts.....	219
Figure 9.21 - Cross-sectional sagittal plane images showing potential alignment issues introduced in experimental trials,.....	219
Figure 9.22 – Schematic showing the constraints in the thigh region.	220

List of Tables

Chapter 1

Table 1.1 – Overview of severity of potential injuries and PPE compositions in each body region.	2
---	---

Chapter 2

Table 2.1 - Injury incidence to thigh region (% of reported injuries).....	9
Table 2.2 - Femur maximum bending moments reported in literature.....	12
Table 2.3 - Tibia maximum bending moment and energy to failure thresholds (adapted from Schreiber <i>et al.</i> (1998)).	12
Table 2.4 - Percentage differences in momentum and impact energy between safety standards and 'in play' estimates (adapted from Payne <i>et al.</i> , 2013).	15
Table 2.5 - Tensile and compressive mechanical properties of a 4 th generation composite Sawbones [®] compared with organic bone (adapted from Heiner (2008)).	37

Chapter 3

Table 3.1 - DCS influencing factors.	52
Table 3.2 - Cricket ball impact injury scenario model.....	54
Table 3.3 - Basketball knee impact injury scenario model.	55

Chapter 4

Table 4.1 – Measurements from the VHP human thigh (mm).	65
Table 4.2 – Densities of organic tissues (kg.m ⁻³).	67
Table 4.3 - First order Ogden model coefficients for skin and adipose tissues (Comley & Fleck, 2012).	68
Table 4.4 – First order Ogden model coefficients for relaxed muscle (McElhaney, 1966; Song <i>et al.</i> , 2007) and cortical bone (McElhaney, 1966).	69
Table 4.5 - Prony series coefficients for organic tissues (adapted from Wu <i>et al.</i> (2003); Gefen & Haberman (2007); Van Looke <i>et al.</i> (2009)).	69
Table 4.6 – FE impactor approximations.....	71
Table 4.7 - Parameters for sensitivity analysis of tissue thicknesses.	82
Table 4.8 - x_{max} and t_x for cricket ball and knee impactor simulations.	83
Table 4.9 – $P_{base,max}$ for cricket ball and knee impactor simulations.	84
Table 4.10 – $\sigma_{v,max}$ (MPa) and t_o (ms) on the tissue layer surfaces for cricket ball and knee impactor simulations.	87
Table 4.11 - x_{max} and t_x for cricket ball and knee impact simulations in skin thickness sensitivity analysis (% differences from standard dimensions in brackets).	87
Table 4.12 – $P_{base,max}$ and t_p for cricket ball and knee impact simulations in skin thickness sensitivity analysis (% differences from standard measures in brackets).	88
Table 4.13 - x_{max} and t_x for cricket ball and knee impactor simulations in adipose thickness sensitivity analysis (% differences from standard dimensions in brackets).	89
Table 4.14 – $P_{base,max}$ and t_p for cricket ball and knee impact simulations in skin thickness sensitivity analysis (% differences from standard measures in brackets).	90
Table 4.15 - FE model definitions.	92

Chapter 5

Table 5.1 - Part A and B component base constituent concentrations (% by mass).....	103
Table 5.2 – Failure strains for each cross-linker specimen.	104
Table 5.3 – Constituent Part A polymer ratios.....	105
Table 5.4 - Failure strains of PDMS silicone specimens.	106
Table 5.5 - Part A and B silicone constituent concentrations (% by mass).	106
Table 5.6 - Calculated Poisson's ratio values of PDMS simulants.	109
Table 5.7 - Percentage reduction in stress from first to last cycle in PDMS silicone simulants.	109
Table 5.8 - Compressive stresses at different strains for six identical test specimens.....	114
Table 5.9 - Hyperelastic model coefficients for PDMS simulants with RMS error from experimental data.....	117
Table 5.10 - Prony series coefficients for PDMS simulants.	117

Chapter 6

Table 6.1 - Differences in peak force between Dytran and Instron 9250HV load cells.	131
Table 6.2 - Hyperelastic and viscoelastic material coefficients for PDMS skin, adipose and relaxed muscle tissues.	136
Table 6.3 – Comparison of x_{\max} , t_x , RF and t_{rf} between experimental data and FE model predictions in the knee impact.	140
Table 6.4 - Comparison of x_{\max} , t_x , RF and t_{rf} between experimental data and FE model predictions in the cricket ball impact.	143
Table 6.5 - x_{\max} and t_x values for cricket ball and knee impacts (% difference from organic tissue predictions in brackets).	146
Table 6.6 - $P_{\text{base,max}}$ and t_p values from cricket ball and knee impact simulations (% difference from organic tissue predictions in brackets).	147

Chapter 7

Table 7.1 – Sagittal plane sections of simple surrogate at maximum deformation.	158
Table 7.2 - x_{\max} (mm) and t_x (ms) for surrogates in cricket ball and knee impacts.	160
Table 7.3 – $P_{\text{base,max}}$ (MPa) and t_p (ms) for surrogates in cricket ball and knee impacts.	162
Table 7.4 – $\sigma_{v,\max}$ (MPa) and t_σ (ms) for surrogates in cricket ball and knee impacts.	163
Table 7.5 – $\sigma_{v,\max}$ (MPa) and t_σ (ms) for surrogates in cricket ball and knee impacts.	164
Table 7.6 - Computational expenditure for each surrogate type.	165
Table 7.7 – Mesh descriptions for anatomically contoured surrogate.	169
Table 7.8 - x_{\max} (mm) and t_x (ms) for the anatomical contoured surrogate in cricket ball and knee impact simulations.	171
Table 7.9 – $\sigma_{v,\max}$ and t_σ on bone surface of the anatomical contoured surrogate in cricket ball and knee impacts.	172
Table 7.10 – $\sigma_{v,\max}$ (MPa) and t_σ (ms) on skin, adipose and muscle surfaces of the anatomical contoured surrogate in cricket ball and knee impact simulations.	172
Table 7.11 - x_{\max} and t_x responses recorded for PDMS simulant surrogate impacts (percentage differences from organic tissue predictions in brackets).	175
Table 7.12 – $\sigma_{v,\max}$ and t_σ responses on the bone surface recorded for PDMS simulant surrogate impacts (percentage differences from organic tissue predictions in brackets).	175
Table 7.13 – $\sigma_{v,\max}$ (MPa) and t_σ (ms) layer stress responses recorded for PDMS simulant surrogate impacts.	175
Table 7.14 – Single-term Ogden model coefficients for EVA foam (adapted from (Mills <i>et al.</i> , 2003)) and elastic material properties for CFRP (adapted from Davies <i>et al.</i> (2008)).	179
Table 7.15 - x_{\max} (mm) and t_x (ms) values for PPE impact simulations (percentage differences from anatomically contoured surrogate predictions in brackets).	181

Chapter 8

Table 8.1 - PDMS simulant constituent quantities (kg) for full surrogate thigh.	192
Table 8.2 - Cost breakdown for single thigh surrogate manufacture.	196
Table 8.3 - Estimation of cost per surrogate based on larger production volumes for: PDMS, Silastic 3483 and 10% ballistics gelatin.	197
Table 8.4 - Comparison of mid-thigh adipose thickness measurements between basketball players (mean \pm 1SD) and VHP.	200

Chapter 9

Table 9.1 - Material properties for 4th generation composite femur (adapted from Heiner <i>et al.</i> (2008) and Thielen <i>et al.</i> (2014)).	206
Table 9.2 - Mean synthetic surrogate outputs in anterior and lateral impacts (\pm 1 SD).	208
Table 9.3 - Comparison of accelerometer outputs between experimental data and FE model predictions for lateral impacts.	213
Table 9.4 - Comparison of accelerometer outputs between experimental data and FE model predictions for anterior impacts.	214
Table 9.5 - Maximum principal strain magnitudes experienced at each sampling point in FE and experimental trials.	216
Table 9.6 - Differences in a_{\max} magnitude introduced through angular impactor deviation.	218
Table 9.7 - Estimations of divergences in a_{\max} at different velocities.	219

Nomenclature

<i>50th Percentile</i>	50% of the measured values in a given population are smaller than the 50 th percentile measurement and 50% are larger; the 'mean' value.
<i>Abduction</i>	Movement of limb away from median plane in body.
<i>Adduction</i>	Movement of limb towards median plane in body.
<i>Acceleration</i>	Rate of change of velocity with respect to time in metres per second squared (m.s ⁻²).
<i>Aetiology</i>	Attribution of the cause of a disease or condition.
<i>Anisotropic</i>	Exhibition of directional dependent material responses.
<i>Anterior</i>	Located on or near the front of an organ or on the ventral surface of the body in humans.
<i>Anthropometry</i>	Study of physical measurements of the human body to determine differences in individuals and groups.
<i>Autolysis</i>	Breakdown of all or part of a cell or tissue by self-produced enzymes.
<i>Biofidelity</i>	The degree of transferability of the test surrogate's response characteristics to that of the human body in identical test conditions.
<i>Bipeds</i>	Any animal with only two feet.
<i>Bovine</i>	Of, relating to, or like a cow.
<i>Coagulation</i>	Process by which blood becomes more viscous into a coherent mass.
<i>Condyle</i>	A rounded prominence at the end of a bone, most often for articulation with another bone.
<i>Distal</i>	Anatomically located far from a point of reference, such as an origin or a point of attachment.
<i>Edema</i>	An abnormal infiltration and excess accumulation of serous fluid in connective tissue or in a cavity.
<i>Epicondyle</i>	A rounded projection at the end of a bone, located on or above a condyle and usually serving as a place of attachment for ligaments and tendons.
<i>Epidemiology</i>	Study of the incidence, causes and effects of a disease or condition in a population.
<i>Frangible</i>	Brittle, fragile and easily broken.
<i>Frontal Plane</i>	Also known as the coronal plane, a plane parallel to the long axis of the body and perpendicular to the sagittal plane that separates the body into front and back portions.
<i>Haematoma</i>	Mass of usually clotted blood that forms in a tissue, organ, or body space as a result of a broken blood vessel.
<i>Heterogeneous</i>	Not uniform in structure or composition.
<i>Homogeneous</i>	Uniform in structure or composition.
<i>Hydrophilic</i>	Having a tendency to mix with, dissolve in, or be wetted by water.
<i>Hyperelastic</i>	A type of constitutive model for which the stress-strain relationship varies as a function of the strain energy density.
<i>Hypofunction</i>	Diminishes, abnormally low or inadequate functioning.
<i>Inferior</i>	Situated below and closer to the feet than another.
<i>in vivo</i>	In the living body of a plant or animal.
<i>in vitro</i>	Outside the living body and in an artificial environment.

<i>Isotropic</i>	Exhibition of the same material response when measured along axes in all directions.
<i>Kinetics</i>	The study of the motion of bodies and containment systems with reference to mass or force.
<i>Lateral</i>	Relating to, or situated at or on the side, or directing away from, the midline.
<i>Malleolus</i>	A rounded bony prominence, such as those on either side of the ankle joint.
<i>Medial</i>	Relating to, situated in, or extending toward the middle.
<i>Morphology</i>	The form and structure of an organism or any of its parts.
<i>Orthogonal</i>	Lying or intersecting at right angles.
<i>Osseous</i>	Of, relating to, or composed of bone.
<i>Pathophysiology</i>	The disordered physiological changes that accompany a particular disease or condition.
<i>Porcine</i>	Of, relating to, or like a pig.
<i>Posterior</i>	Located behind a part or toward the rear of a structure.
<i>Post-Mortem Human Subject/Cadaver</i>	A human corpse as a surrogate in impact biomechanics research.
<i>Proximal</i>	Nearer to a point of reference such as an origin, a point of attachment, or the midline of the body.
<i>Quadrupeds</i>	An animal having four feet.
<i>Rigor Mortis</i>	Temporary rigidity of muscles occurring after death.
<i>Sagittal Plane</i>	A longitudinal plane that divides the body of a bilaterally symmetrical animal into right and left sections.
<i>Shock</i>	Rate of change, or onset of acceleration with respect to time in metres per second cubed ($\text{m}\cdot\text{s}^{-3}$).
<i>Superior</i>	Situated toward the head and further away from the feet than another.
<i>Transection</i>	Division by cutting transversely.
<i>Transverse Plane</i>	Also known as the axial plane, a plane passing horizontally through the body, at right angles to the sagittal and frontal planes, and dividing the body into upper and lower portions.
<i>Viscoelasticity</i>	The property of a substance exhibiting both elastic and viscous behaviour.
<i>Viscoplasticity</i>	The property of a substance exhibiting both non-recoverable plastic and viscous behaviour.

Abbreviations

3D	Three-dimensional
ABS	Acrylonitrile butadiene styrene
AP	Anti-Personnel
A-P	Anteroposterior
ASCII	American Standard Code for Information Interchange
ASTM	American Society for Testing and Materials
BMI	Body Mass Index
BSI	British Standards Institute
CAD	Computer Aided Design
CFRP	Carbon-Fibre-Reinforced Composite
CPU	Central Processing Unit
CT	Computer Tomography
Da	Daltons
DCS	Determinative Contextual Sequential
DEAP	Dielectric Electro Active Polymer
DIC	Digital Image Correlation
DOF	Degrees of Freedom
ERI	Effective Remote Inertia
EVA	Ethylene-vinyl Acetate
FBI	Federal Bureau of Investigation
FDM	Fuse Deposition Modelling
F-E	Flexion-Extension
FE	Finite Element
FEA	Finite Element Analysis
FEM	Finite Element Method
fps	Frames per second
FSL	Frangible Surrogate Leg
H301	MethylHydrosiloxane-Dimethylsiloxane Copolymer
HSV	High Speed Video
HURP	Human Use Review Panel
I-E	Internal-External
IPHRG	International Hip Protection Research Group
ISO	International Organization for Standards
LED	Light Emitting Diode
L-M	Lateromedial
LVDT	Linear Variable Differential Transformer
MADYMO®	Mathematical Dynamic Model
MRI	Magnetic Resonance Imaging

NATO	National Atlantic Treaty Organisation	
NBA	National Basketball Association	
NFL	National Football League	
NHTSA	National Highway Traffic Safety Administration	
PDE	Partial Differential Equation	
PDMS	Polydimethylsiloxane	
PE	Polyethylene	
PMHS	Post-Mortem Human Subjects	
PPE	Personal Protective Equipment	
PU	Polyurethane	
PVA	Polyvinyl Acetate	
QLV	Quasi-Linear Viscoelastic	
RMS	Root Mean Square	
SD	Standard Deviation	
SHPB	Split Hopkinson Pressure Bar	
SLS	Selective Laser Sintering	
SPAMM	Spatial Modulation of Magnetism	
THUMS®:	The Total Human Model for Safety	
TRL	Transport Research Laboratories	
VHP	Visible Human Project	
$\sigma_{v,max}$	Maximum von Mises stress at any given time interval.	(Pa)
$P_{base,max}$	Deep tissue pressure given by the maximum Cauchy stress tensor normal to the impact direction at any given time interval.	(Pa)
RF	Reaction force	(N)
t_x	Time to peak displacement	(s)
t_{rf}	Time to peak force	(s)
t_p	Time to peak pressure	(s)
t_σ	Time to peak stress	(s)
t_{impact}	Duration of impact	(s)
T_{skin}	Thickness of skin tissue layer	(m)
x_{max}	Peak displacement	(m)
a_{max}	Peak acceleration	(m.s ⁻²)

Chapter 1 – Introduction

1.1. Chapter Overview

In this chapter, the background of the research has first been presented, outlining the fundamental function of human surrogates, their applications within relevant industries and potential benefits. In addition, the rationale addressing the choice of thigh segment surrogates has been detailed. An overall research aim has been determined as well as a series of complementary research questions with brief descriptions of how they have been investigated. A chapter-by-chapter summary has also been presented, outlining the content addressed in each chapter.

1.2. Background

In the field of injury biomechanics, a fundamental goal is concerned with replicating “real life” injurious scenarios in a laboratory environment through an understanding of the mechanisms of injury, characterisation of human response to loading conditions and development of protective methods to prevent injury occurrence or limit severity (Viano *et al.*, 1989).

Human surrogates attempt to provide an artificial representation of a living human and thus offer a means of achieving these goals. For any surrogate the ultimate aim is ‘biofidelity’, which is the term used to describe the exactness with which a given surrogate approximates the behaviour of a human when subjected to comparable loading conditions (Crandall *et al.*, 2011).

There are several industries that use surrogates to improve their understanding of the human response to different injurious scenarios. Human surrogates arguably have the most widespread usage within the automotive industry where they are typically used in dynamic impact testing, evaluation of restraint systems, and investigations of pedestrian impacts. Within the military, human surrogates are commonly used to assess the effectiveness of personal protective equipment (PPE) under extreme loading conditions from impacts such as penetrating bullets or anti-personnel (AP) landmines (NATO, 2007; Owens *et al.*, 2007; Ramasamy *et al.*, 2009). Surrogates are also used in the medical industry, where the most prevalent usage is in training models and simulation of orthopaedic surgical procedures such as joint replacements or osteotomies (Scheepers *et al.*, 1997; Sato *et al.*, 2000; Schmitt *et al.*, 2001; Blemker *et al.*, 2007).

Human surrogates are similarly used within the sports PPE domain. The primary goal of surrogates in this field is to evaluate the impact protective capabilities of the PPE to prescribed loading conditions, commonly defined by safety standards. In many sports, PPE is a requirement outlined by governing bodies to ensure the safety of the participant and prevent avoidable impact injuries. Injuries to athletes performing at a professional level place a significant financial burden on many stakeholders (e.g. sponsors, teams), whilst injuries to recreational players incur cost in terms of the number of productive societal days lost through injury. In a recent survey of the UK population (Barclays, 2005), 13.4 million people in the UK were found to have had a sporting injury and, on average, each person participating in sport sustained 1.65 injuries every year resulting in 5 days absent from work (~ 300 million societal days lost). A study by Schmikli *et al.* (2009) conducted in the Netherlands estimated the indirect cost of work absence from physical activity-related injury to be \$525 million annually.

Sports PPE typically performs one or more of the following functions: impact energy attenuation; acceleration management; load distribution and force limitation (McIntosh, 2011). In an ideal scenario, all PPE should enable optimal performance whilst preventing impact injury. However, athlete performance is critical and the introduction of weight, range of motion restriction, increased temperature and chaffing through use of PPE, can adversely affect performance (Webster & Roberts, 2009). Due to these potentially conflicting aspirations, a trade-off is required to engineer products with due consideration to both safety and performance of the user. The challenge presented has been highlighted through a qualitative questionnaire conducted by Torell (2011), which indicated that professional association football players would, for example, when asked about their opinions on shin guards, rather be fast than well protected.

Current safety standards used to assess PPE typically use rigid anvils of unrepresentative geometries, constrained to a massive base. These practices potentially overlook many important human response phenomena that affect the manner in which load is transferred and hence the perceived effectiveness of PPE. Improved, more realistic, human surrogates for this field can better inform an evaluation of the effectiveness of PPE and enable superior engineering of novel PPE materials, constructions and manufacturing techniques. Improved surrogates can also potentially lead to a better understanding of the causal factors and mechanical phenomena relating to injury and even inform the likelihood of injury occurrence.

Different areas of the human body require different amounts of protection typically dependent on the constitutive tissue structures, presence and locality of vital organs, and likelihood of injury occurrence in the region. Table 1.1 presents a subjective ranked evaluation of the severity of injuries in each body region and broadly details the key tissue structures and types of PPE commonly worn in the segments.

Table 1.1 – Overview of severity of potential injuries and PPE compositions in each body region.

Body Region	Major Tissue Structures	Severity	Primary Sports PPE Worn
<i>Head & Neck</i>	Skull, Brain, Cervical Vertebra, Skin, Nervous Tissues.	●●●●	Helmets or faceguards: typically rigid shell with foam padding.
<i>Thorax</i>	Heart, Lungs, Liver, Kidneys, Stomach, Intestines, Skin, Muscle, Adipose, Ribs, Sternum, Thoracic & Lumbar Spine.	●●●	Chest protector: typically panelled high density foam construction.
<i>Pelvic Region</i>	Reproductive Organs, Pelvic Girdle, Femur Bone, Skin, Muscle, Adipose.	●●	Genital protectors: typically rigid shell.
<i>Upper Leg</i>	Femur Bone, Muscle, Adipose, Skin.	●●	Thigh pads or padded shorts: typically high density foam constructions.
<i>Lower Leg</i>	Tibia Bone, Fibula Bone, Foot and Ankle Bones, Ligaments, Muscle, Skin.	●●	Shin guards: typically rigid shell exterior with low density foam padding.
<i>Upper Arm</i>	Humerus Bone, Muscle, Adipose, Skin.	●	No protection commonly worn. Optional elements generally available.
<i>Lower Arm</i>	Radius Bone, Ulna Bone, Hand and Wrist Bones, Muscle, Skin.	●	Wrist guards and gloves: typically panelled high density foam constructions.

The most substantial body of research in the sports domain has been focussed on high severity, life threatening injuries to the head, neck and thorax regions. There is a significant overlap in this regard with the regions of the body primarily focussed on by other industry sectors (e.g. military, security services, automotive). However, given the underlying dependence of athlete performance in sport on mobility, less severe but still debilitating injuries are a pertinent concern. Injuries to these fleshy regions of the body are being mitigated by a range of PPE, where achieving an optimal balance between protection and mobility requires a more subtle approach than a rigid surrogate provides. There are obvious commercial benefits for the sports industry from having better surrogates for PPE research in these areas and significant potential for these to benefit other industries concerned with enhancing the mobility of personnel wearing PPE.

The presence of a wide range of tissue structures, structural interactions and joint degrees of freedom in a body region significantly influence the necessary levels of anatomical complexity of surrogates. This, in turn, introduces increased expense. Consequently, to make cost-effective and time-efficient progress, a useful approach is to initially focus on a single body segment.

1.3. Research Aim

The overall aim for this research study has been defined as follows:

To establish a method to enable the development of superior, complementary, increasingly complex synthetic and computational impact surrogates for improved assessment of sports personal protective equipment.

The development of parallel, complementary synthetic and computational surrogates is a desirable approach to better understand the effects of human anatomical simplifications and the worth of different levels of surrogate complexity. The incremental validation of these two types of surrogate, through iterative stages of complexity (Fig 1.1) can provide a reliable, efficient and cost effective route to appropriate sports impact assessments to understand injuries and evaluate PPE. This systematic staged process ensures that surrogates which are overly complex are not attempted prematurely as there can often be too many unknowns in such systems (e.g. structural interactions, DOF) to methodically validate.

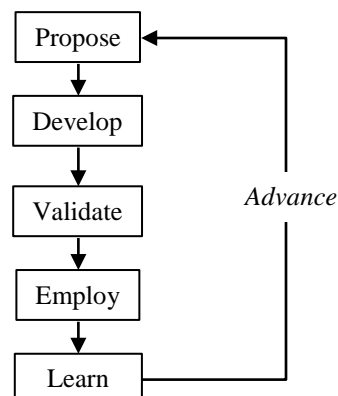


Figure 1.1 - Iterative Enhancement Development Cycle.

1.4. Research Questions

A series of key research questions have been formulated to enable investigation of the research aim and provide a structure to objectively assess the success of the research study.

Q1. Can Finite Element models be formulated to better inform the development of improved human surrogates?

Finite element (FE) models are simulation tools used to predict the behaviour of real systems. Their potential worth and merit in this research study is twofold and relates to both their ability as a design tool to examine relative differences between different surrogate design features and as a predictive tool to better understand human surrogate impact response. The practical capabilities of FE models in both of these scenarios have been examined in this research study.

Q2. Can durable, biofidelic human soft tissue simulants be fabricated using materials that exhibit a consistent impact response?

Soft tissue simulants are commonly selected through best fit ‘off the shelf’ elastomers or gelatins. These simulants are usually either developed to represent overall composite response of all soft tissues in a given body segment or are developed for different purposes to their intended use as human tissue simulants and consequently are unlikely to accurately represent the mechanical properties of their organic soft tissue equivalents. The formulation of bespoke blends of durable soft tissue simulants to match specific mechanical properties of target soft tissues can potentially improve the manner in which human surrogates respond to impact.

Q3. Is a significant difference in surrogate response elicited in more anatomically complex geometries?

Surrogate shapes vary greatly between safety standards, industry applications and academic studies. There is, however, a paucity of research explicitly investigating the changes in surrogate response caused by different surrogate geometries. Using FE models, an investigation into the effects of different surrogate geometries can inform important geometric features of future surrogates and can potentially save time and expense of engineering unnecessarily complex surrogates.

Q4. To what extent do different human soft tissue structures influence impact response?

Conventional synthetic impact surrogates have typically only considered a single soft tissue simulant to represent all of the tissue structures within the target body segment. Although this is a gross simplification of the complexities of actual human structures, it is not clear whether this approach adequately represents human impact response or whether a greater consideration of the individual human tissues is required. Using FE models, an investigation into the effects of different tissue structures on impact response can be conducted and can provide information to better inform the development of future surrogates.

Q5. Given thorough consideration of kinetic and kinematic impact parameters of specific injury scenarios, can bespoke reconstructions provide the basis for more realistic PPE evaluations?

Typical PPE evaluations, exemplified by safety standards, commonly approximate sports loading conditions using unrepresentative target and striker geometries, masses, velocities and levels of constraint. Through systematic consideration of the factors influencing an injury event, it is possible to better define the parameters for real play impact reconstructions. Synthetic and computational methods can be used to determine the relative merits of such an approach when compared with existing practices.

Q6. Can human impact surrogates be developed at an affordable cost when compared to previous surrogates?

For improved surrogates to be adopted by standards testing bodies and sporting goods manufacturers it is important that they can be fabricated at an affordable cost. Current impact surrogates range in cost based on their functionality and levels of instrumentation. A full costing and comparison with other surrogate designs can aid in the determination of affordability and added value.

Q7. Can the developed surrogates provide a better understanding of injury causation and PPE effectiveness?

The principal application for sports impact surrogates has traditionally been in the assessment of the impact protective capabilities of PPE. Secondary applications of surrogates have been in the measurement of injury inducing phenomena and prediction of the likelihood of sustaining injury. The parallel development of mutually validating computational and synthetic surrogates can provide a superior resource for both PPE assessments and evaluations of injury phenomena.

1.5. Research Approach

The human body is very complex and consists of many interacting tissue structures. To make achievable, time efficient progress in the field of human surrogates it is necessary to prioritise the development of a single body segment instead of attempting to engineer overly complex multi-segmented surrogates without sufficient prior knowledge. This approach allows for a greater consideration of contributory surrogate elements and progression through validated levels of complexity rather than attempting a complicated multi-body system with insufficient knowledge to effectively develop it, having to rely on unverified simplifying assumptions.

The thigh region represents a segment of the human body in which the tissue structures are clearly defined; there is a singular skeletal component (femur) positioned relatively centrally in the soft tissue. There are no secondary interfacing skeletal structures which may complicate surrogate modelling approaches. Injuries to the thigh region are common and debilitating in many sports such as rugby, cricket, martial arts, American football and basketball. In these sports, non-contact injuries such as sprains and strains occur most frequently (Leary & White, 2000; Bathgate *et al.*, 2002), however, impact injuries to the thigh are also common with contusions, lacerations and even in severe cases fractures occurring as a result of contact. Consequently, PPE is commonly worn by players in this region to mitigate the risk of injuries. The types of

PPE used are specific to the given sports application and differ in coverage and levels of protection (Fig. 1.2).



Figure 1.2 – A sample of thigh PPE worn in: (a) basketball; (b) cricket; (c) American football; (d) martial arts.

Due to the wide applicability of PPE in this region across many sports and the potentially debilitating nature of injury sustained, the thigh segment has been prioritised as the region of interest in this investigation.

1.6. Chapter-by-Chapter Summary

This research study has been conducted to develop improved human surrogates for enhanced assessment of sports PPE. Current sports impact surrogates fail to adequately represent real sports impact injury events and, in particular, poorly address the target and striker surrogates, the impact parameters and levels of constraint. Research has been conducted to: better describe injury events and identify key influencing factors through a conceptual impact injury model; establish the effects of anatomical simplifications on surrogate responses through FE models; and develop improved human soft tissue simulants. The culmination of research in these areas has informed and enabled the development and validation of superior synthetic and computational human thigh surrogates for assessment of sports PPE.

The body of research has been conducted as a series of discrete studies linking to inform the development of the improved surrogates. A chapter-by-chapter summary has been provided outlining, in brief, the subjects detailed in each section.

Chapter 2 – Literature Review

A literature review has been conducted, firstly examining the anatomy of the human thigh and constitutive tissue properties as well as pertinent sports injuries and PPE used. The field of human surrogates has also been reviewed outlining their historical uses, advantages, disadvantages and industry applications.

Chapter 3 – Methods to Enable the Formulation of Improved Sports Impact Assessments

The fundamental components of sports impact assessments have been reviewed and a conceptual model has been created to describe the causal sequence of events involved in two impact injury scenarios to the thigh. This informed a specification for improved sports impact assessments and a surrogate research approach.

Chapter 4 – Determining the Effects of Anatomical Simplifications in a Soft Tissue Surrogate using FEA Methods

The effects of different soft tissue layers have been determined through use of FE models. The universal modelling techniques used in each surrogate impact study have been outlined in this chapter with consideration to: material models, surrogate geometries, meshing techniques and contact definitions.

Chapter 5 – Surrogate Soft Tissue Simulant Formulation

Soft tissue simulants were developed to match the specific mechanical properties of organic skin, adipose, relaxed and contracted muscle tissues. The materials have been characterised through a range of mechanical test procedures at different strain rates and described using constitutive models.

Chapter 6 – Experimental Impact Testing of Soft Tissue Surrogates and FE Model Validation

The predictive capabilities of the FE models were established through experimental impact tests of simple surrogates. The validated material models were then used to demonstrate the relative benefits of the developed soft tissue simulant formulations when compared to previously used simulants and organic tissue surrogate predictions.

Chapter 7 – Investigation of the Importance of Anatomical Geometric Complexities and their Effect on PPE Interactions

The effects of different shape complexities on surrogate impact response have been established using FE models. The geometries considered ranged from simple cylindrical pucks to full anatomically contoured thigh geometries to establish the benefit at each complexity level. The further worth of the geometries has been investigated through modelling of their interactions with different types of PPE.

Chapter 8 – Fabrication of an Anatomical Synthetic Thigh Surrogate

A full-scale multi-material synthetic human surrogate thigh was fabricated using the best practice soft tissue simulants, materials and geometries established. The manufacturing techniques used in the construction have been reported in detail at each process stage. The cost-benefit of fabricated surrogate was also evaluated based on the production costs compared to single material simulants.

Chapter 9 – Experimental Impact Testing of the Synthetic Surrogate Thigh and Validation of a Parallel FE Model

Experimental testing of the synthetic thigh surrogate was conducted under simulated sports impact conditions using a range of evaluation techniques to determine kinetic and kinematic impact responses. The experimental data were then compared to FE model predictions to determine the correlation and predictive capabilities of the models.

Chapter 10 – Discussion, Conclusions and Future Work

The research aim and questions detailed in §1 have been addressed with reference to the findings of entire research study. The limitations of the research and potential areas for future work have also been reflected upon.

Chapter 2 – Literature Review

2.1. Chapter Overview

Chapter 2 provides an extensive review of existing literature examining the current state of the art in the field of human surrogates. Common injury modes pertinent to the thigh region were first reviewed, evaluating incidence and severity measures. The PPE industry was next examined with reference to the safety standards used to assess them. The anatomy of the thigh region was also considered with a subset of key organic tissue structures investigated to provide a complete overview of their morphology, function and mechanical response behaviour. Finally, different types of organic and artificial surrogates have been evaluated with accompanying description of their historical use, current practices, merits and drawbacks. The direction of research has then been outlined with consideration to the parallel development of synthetic and computational surrogate approaches.

2.2. Sports Injury Context

2.2.1. Injury Statistics

Human surrogates have been used to assess PPE and better understand injury risk in a wide range of industrial contexts. The injuries sustained can vary significantly between approaches dependent on their operational environment and levels of threats. In automotive and military environments, very serious or life threatening injuries are the primary concern (e.g. penetrating bullets or vehicular impacts). This is reflected by the risks identified in the Abbreviated Injury Scale (AIS) (Champion, 2012) and Mine Trauma Score (MTS) (Harris, 2001) injury scales developed to rank the severity of injuries in automotive and military industries respectively.

In the sporting goods industry, however, the threats are typically far less severe and the seriousness of an injury is often determined by the time a player is absent from competition (Velani *et al.*, 2012). Despite this, the prevalence of these injuries makes them a pertinent concern. Nicholl *et al.* (1995) estimated that, in the UK, each year, there are 29 million incidents resulting in new or recurrent sports-related injuries, whilst in the Netherlands, every sixth hospital-treated injury is sustained during physical activity (Schmikli *et al.*, 2009). Though many of these injuries are chronic and related to overuse exercise, Nicholl *et al.* (1995) stated that 21.6% of injuries reported were sustained as a result of mechanical trauma.

Impact injuries to the thigh region are common and debilitating in many sports and typically occur as a result of blunt force trauma from contact with: other players, equipment or the playing environment. Thigh injuries can range in severity from relatively mild contusions which can affect the ability of players to perform at an optimal level to severe contusions, lacerations or fractures which can prevent players from training or competing for prolonged periods. A study by Diaz *et al.* (2003) reported that a blunt force trauma to the thigh during basketball gameplay resulted in haematoma and edema which took 3.5 months to fully recover. Severe or repeated impacts can also have further complications through disorders such as myositis ossificans traumatica or partial ruptures. Myositis ossifications are a proliferation of bone and cartilage within skeletal muscle sustained at the site of a previous major trauma or repeated injury and can result in surgery (Jarvinen *et al.*, 2005; Hrysomallis, 2009). This injury is suggested to be

associated with prior sports-related muscle injuries and is most common in sports where PPE is not usually worn (e.g. rugby, Australian rules football) (Mitchell, 2000; Beiner & Jokl, 2002). Partial ruptures are tears in the muscle tissue and are also a serious complication from thigh impacts. They most frequently occur in the quadriceps at the patella tendon as a result of impact against a contracted muscle, such as when a player's knee hits an opposing player's thigh (Chomiak *et al.*, 2000).

These injuries represent a prevalent and serious concern in a number of sports including but not limited to: rugby, cricket, field hockey, ice hockey, American football, basketball and martial arts. The incidence of common impact injuries to the thigh region have been shown in Table 2.1.

Table 2.1 - Injury incidence to thigh region (% of reported injuries).

Sport	Study	Gender and Level of Competition	Detail	% of Total Gameplay Injuries		
				Fractures	Lacerations	Contusions
<i>Cricket</i>	Orchard <i>et al.</i> (2002)	Male, state/national level	Thigh, batting injuries	3.1%	21.9% (combined)	
	Walker <i>et al.</i> (2010)	Male and female, all abilities	Lower limb, all positions	30%	12%	4%
<i>Field Hockey</i>	Dick <i>et al.</i> (2007a)	Female, collegiate level	Thigh, all positions	-	-	29.4%
	Murtaugh (2001)	Female, high school, university and national levels	Lower limb, all positions	6.3%	0.8%	2.9%
<i>Martial Arts</i>	McPherson & Pickett (2010)	Male and female, Canadian martial arts, all levels, hospital reports	Lower limb injuries, all martial arts	19.0%	1.7%	-
<i>Rugby</i>	Brooks <i>et al.</i> (2005)	Male, English professional rugby	Thigh, all positions	-	-	50.6%
	Garraway & Macleod (1995)	Male, Scottish club rugby	Lower limb, all positions	6.3%	13.6% (combined)	
<i>Association Football</i>	Agel <i>et al.</i> (2007)	Male, collegiate level	Upper leg, all positions	-	-	44.0%
	Hägglund <i>et al.</i> (2009)	Male and female, Swedish professional level	Thigh, all positions	-	-	22.6%
	Junge <i>et al.</i> (2004)	Male, professional, World Cup 2002	Thigh, all positions	-	-	33.3%
<i>Lacrosse</i>	Dick <i>et al.</i> (2007b)	Male, collegiate level	Upper leg, all positions	-	-	51.5%
<i>American Football</i>	Dick <i>et al.</i> (2007c)	Male, collegiate level	Upper leg, all positions	-	-	50.6%
<i>Basketball</i>	Dick <i>et al.</i> (2007d)	Male, collegiate level	Upper leg, all positions	-	-	67.3%

2.2.2. Injury Modes

To effectively mitigate the risk of injuries it is important to understand the human body's response to specific events including causal injury mechanisms and thresholds (Merkle, 2013).

a) Contusions

In sports, contusion injuries are often considered as the highest risk impact injury due to their frequency of occurrence (Crisco *et al.*, 1994; Khattak *et al.*, 2010; Smith *et al.*, 2008; Conforti, 2013). They are generally considered to be caused by a blunt non-penetrating trauma, leading to compression and shearing forces, which results in damage to the muscular layer directly adjacent to the bone (Walton & Rothwell, 1983). On a local scale, contusions result in damage to blood vessels which lead to leaking of blood into extracellular spaces (Cavanaugh *et al.*, 1986). When a muscle is contracted it is suggested that the contusion will impact more superficial tissues, while in a relaxed state, structural damage and consequently haematoma will generally occur at a depth nearer the bone (Conforti, 2013).

Due to ethical constraints, however, little is known about *in vivo* organic tissue response to impact and the pathophysiological sequelae succeeding it. Previous studies have typically utilised mechanical drop test procedures on the hind limbs of anaesthetised rodents and have investigated the effect of regenerative aids to reduce the long term severity of resulting injuries. Few studies have investigated the mechanical causation for contusions (Crisco *et al.* 1994; Crisco *et al.*, 1996; Sherman *et al.* 2005; McBrier *et al.*, 2009; Desmoulin & Anderson, 2011), with only a single study investigating the onset in humans (Desmoulin & Anderson, 2011).

Existing studies lack comparable control over their inputs in terms of masses and drop heights used and are therefore difficult to compare or correlate meaningfully. In terms of physical measures to quantify the onset of contusions, whilst strain is generally considered to be the injury mechanism, there is little consensus on which indirect mechanical phenomenon value (e.g. force, pressure) to consider (Beiner & Jokl, 2001). Ankrah & Mills (2004) suggested a value of 1 MPa could be considered as a metric to represent the onset of contusions, however a recent study by Desmoulin & Anderson (2011) showed a human participant experienced far greater pressures (up to 4.52 MPa) without a visible bruise. One of the main issues with such approaches is that there are no common measures for evaluating the effects of the impacts. The severity of the contusion is suggested to be dependent on the site of impact, activation status of muscles involved, age of patient and presence of fatigue (Conforti, 2013). Desmoulin & Anderson (2011) qualitatively assessed the size and colour of bruises, though these can vary greatly depending on the athlete's levels of muscle contraction and characteristics of vascularisation and coagulation (Conforti, 2013). Other approaches have used MRI to identify specific tissue damage (McBrier *et al.*, 2009) though the distinctions between severities of contusions are similarly not well defined.

b) Lacerations

In sports, lacerations are a rare but serious injury and occur as a result of direct trauma (Huard *et al.*, 2002; Kragh Jr. *et al.*, 2005). They can result in athletes incapacitation for long periods of time and in severe cases leads to permanent damage and hypofunction (Menetrey *et al.*, 1999). Lacerations are sustained when tissue is subject to crushing forces or sharp objects leading to a local destruction of tissue (including membrane myofibrils and innervations) or even a volumetric loss of muscle tissue (Menetrey *et al.*, 1999; Turner *et al.*, 2012).

Animal impact surrogates have typically been used to assess the mechanical loading required to elicit lacerations *in vivo* and evaluate the response of specific treatment interventions. Similar to contusion injury studies, the hind limbs of anaesthetised rodents have been most commonly used with a typical study involving a transection of the muscle belly (Souza & Gottfried, 2013). Studies have also been conducted in forensic fields to investigate the mechanical impact forces required to cause lacerations. For example, Sharkey *et al.* (2011) used porcine head cadavers as impact models to determine injury thresholds under different loading stimuli. A laceration was observed from stamping of trainer shoe at force of 5,259 N and a fall of 4,300 N. However, potentially more pertinent to gameplay sports impacts, a hammer and broom stick impact elicited the greatest incidence of laceration. These objects are geometrically similar to sports equipment such as football boot studs or hockey sticks and would imply small diameter impactor and localised pressures are a causal factor.

c) Fractures

Skeletal tissues are inhomogeneous structures, which vary in mechanical response dependent on the loading direction. Therefore, for a complete understanding of behaviour, different injury mechanisms (e.g. torsion, bending) must be considered. The primary aetiology of femoral fractures is through either falls on greater trochanter or proximal femur, axial compression from automotive vehicle impacts, or bending in pedestrian-vehicle impacts (Tencer *et al.*, 2002; Cristofolini *et al.*, 2007). These injuries almost always require medical care and may involve an intra-articular component resulting in permanent disability (Mackenzie *et al.*, 1993a, 1993b). Most studies have characterised the mechanical properties of the bone using *in vitro* PMHS specimens tested in three-point bending or axial compression scenarios.

Tencer *et al.* (2002) reported that from low-speed frontal automotive collisions the only injuries sustained were femur fractures; all fractures sustained from simulations of axial conditions were transverse with comminution. The axial load thresholds of the femur have been defined by the National Highway Traffic Safety Administration (NHTSA) in Figure 2.1 and approximate compressive fracture load threshold for femurs between 7,500 - 15,000 N with an accepted threshold load of 8,900 N suggested as being sufficient to elicit fracture (Donnelly & Roberts, 1987). However, Tencer *et al.* (2002) reported that 14 out of the 19 specimens tested experienced fracture below the reported threshold.

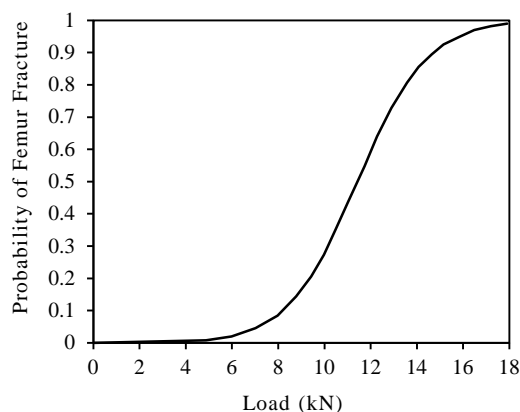


Figure 2.1 - Femur fracture injury risk curve (adapted from Tencer *et al.* (2002)).

The maximum bending moments for the femur have also been reported extensively (Table 2.2). Tests have typically been conducted under three point bending conditions, loaded in the anteroposterior (A-P) or lateromedial (L-M) directions at the mid-diaphysis (Schreiber *et al.*,

1998). This type of loading is likely to be more pertinent to sports impacts sustained to the thigh where the segment is remotely constrained at both the hip (upper body mass) and lower leg (planted foot-turf interaction).

Table 2.2 - Femur maximum bending moments reported in literature.

Source	Description	Femur maximum bending moment (N.m)
Weber (1859)	Quasi-static 3-pt bending	233 Males; 182 Females
Messerer (1880)	Quasi-static 3-pt L-M bending	310 Males; 180 Females
Mather (1968)	Quasi-static 3-pt A-P bending	318 Males; 202 Females
Yamada (1970)	Quasi-static 3-pt A-P bending	211
Stromsoe <i>et al.</i> (1995)	Quasi-static 3-pt L-M bending	185 Males; 125 Females
Kerrigan <i>et al.</i> (2003)	Dynamic 3-pt L-M bending	412

The three-point bending tests reported (Table 2.2) show a significant discrepancy between quasi-static and dynamic loading conditions. This is suggested as being due to increases in stiffness and strength of bone at higher strain rates as well as the viscoelastic contribution of the structures (§2.3.2.d). This is further demonstrated by Schreiber *et al.* (1998) who reported a 69% higher breaking strength of the tibia in dynamic loading than specimens subjected to quasi-static loading with fractures showing a higher degree of comminution (Table 2.3).

Table 2.3 - Tibia maximum bending moment and energy to failure thresholds (adapted from Schreiber *et al.* (1998)).

	Mean maximum bending moment (N.m)	Mean energy to failure (J)	Relation
<i>Quasi static three-point bending</i>	241	59.2	Moment = $0.938 \times \text{Area} + 1.93$, $R^2 = 0.847$
<i>Dynamic three-point bending</i>	408	68.6	Moment = $1.12 \times \text{Area} + 60.7$, $R^2 = 0.634$

Given the variances in bone strength associated with factors such as impact site, age and gender (§2.3.2.d), bone failure cannot accurately be represented using absolute values. An impact force to bone strength ratio has been increasingly used as an improved measure of fracture likelihood (Keaveny & Bouxsein, 2008). It is, however, very difficult to predict the exact impact forces that are sustained in an impact or accurately measure the strength or mechanical response of the surrounding tissue structures. Furthermore, muscles are expected to contribute significantly to the compressive force on the femur in impacts. The exact levels of bracing and muscle tension cannot be empirically determined, though it is suggested the knee flexors can produce approximately 3000 N of force for males and 1800 N for females and are likely to contribute to the *in vivo* differences in dynamic loading (Tencer *et al.*, 2002).

2.2.3. Sports Personal Protective Equipment

(a) Overview

PPE is commonly worn by participants in sport to both mitigate the risk of injury occurrence and lessen the subsequent severity of injuries sustained. Given its widespread usage, the sports PPE industry is highly lucrative and is estimated to be worth in excess of \$1.8 billion in the USA (BCC Research, 2013). Sporting goods manufacturers therefore tender substantial sums of money on the research and development of their product ranges.

The function and form of PPE differs significantly dependent on the sports application, body region and common injury mechanisms. In many sports, however, the thigh region is not an area traditionally protected by PPE. Nevertheless the worth of thigh PPE in contact sports has been identified by Mitchell (2000) who conducted a study investigating the efficacy of thigh protectors in Australian rules football. Two under-18 teams were divided into a protected group (wearing thigh PPE) and an unprotected group. Over the course of a season the protected group sustained no blunt trauma injuries to this region, whilst the unprotected group suffered nine injuries, two of which resulted in repeat injury (thigh strains).

In recent years, thigh PPE has attracted increased attention from sporting goods manufacturers, is being more frequently worn by players and has been adopted as mandatory safety equipment within the regulations of an increasing number of sports (e.g. NFL, 2013). There are two common protection types adopted by sporting goods manufacturers for impacts to large fleshy regions of the body such as the thigh. The traditional approach involves use of foam padding (e.g. Arensdorf & Tobergte, 2012). This padding can be of varying density or stiffness and has been constructed in layered or segmented designs dependent on the intended applications. The second approach has been to use a thin rigid shell construction (e.g. Henry, 2014) with curvature representative of the outer tissue morphology of the target body segment (Fig. 2.2). A further approach adopted involves a hybrid of the foam and shell constructions.



Figure 2.2 - Commercial thigh PPE: (a) Nike Pro Combat Hyperstrong American Football Compression Hard Plate (www.nike.com); (b) Kookaburra Blade Cricket Thigh Guard (www.kookaburra.biz).

There is a paucity of research studies investigating the specific differences in impact attenuation capabilities between PPE constructions. Most research in the sporting goods industry has been focussed on the lower limb for association football shin guard protection (Francisco *et al.*, 2000; Ankrah & Mills, 2003; Tatar *et al.*, 2014). However, the fundamental PPE construction in this region differs from the thigh due to the locality of a skeletal component (tibia). Hrysmallis (2009) conducted the only study investigating the impact protection afforded by thigh guards (§2.4.2a)

but there was insufficient detail reported to distinguish between PPE types. The target surrogate arguably wasn't detailed enough and evaluation metrics used also only provided a partial assessment of PPE performance and was not able to identify significant differences between PPE.

The difference in construction and mechanism by which human soft tissues are involved in the impact response potentially gives rise to significant differences in performance between PPE designs and application contexts. Gross simplifications when evaluating performance are, therefore, likely to cause misrepresentation of these differences.

(b) Review of Safety Standards

Sports PPE is governed by safety standards which prescribe the form and minimal acceptable levels of impact protection that the garment must embody, providing a baseline for comparison between designs. There is a general procedure for impact testing of PPE in British Standards Institute (BSI) safety standards.

The general standards dictate the nature of the striker and surrogate bodies as well as the loading conditions (Fig. 2.3). In many instances both the striking element and target component (anvil) used in standards can be considered as human surrogates and as such should aim to represent the mass, shape and stiffness of the relevant human tissue. The target surrogates are typically single body, high mass, rigid anvil surrogates fixed to a massive base with outer geometries based on simple geometric shapes with approximate outer surface curvature relevant to the specific human body segment (e.g. half cylinder, truncated cone). The striker surrogates are generally linear-guided rigid drop masses with hemispherical geometries.

The intensities of the impacts are prescribed by target impact energies attained through adjustment of drop heights. Force measurements are recorded using load cells beneath the target surrogate to determine the transmitted force through the PPE and thus assess its effectiveness.

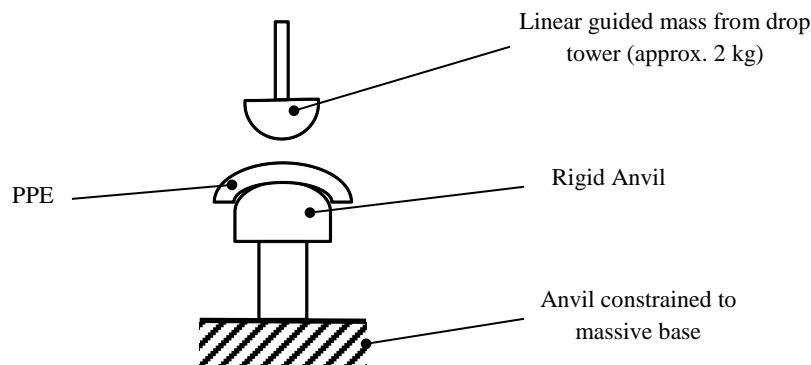


Figure 2.3 - Schematic showing a typical sports safety standard protocol used to assess projectile impacts (BS:13546:2002 - Field Hockey Goalkeeper Protective Clothing; BS 6183-3:2000 - Cricket Leg Protectors).

Minor variations in anvil and striker geometry and mass are apparent between standards, however they are typically heavier, stiffer, and in general provide poor representations of impacts in actual sporting environments. As a result, many PPE test standards embody inaccurate approximations of in use performance scenarios and may give misleading measures of PPE suitability.

With a particular focus on the target surrogates, the anvils provide a poor representation of the structures within the human body and may cause issues in the way in which the surrogate responds to impact. There are also fixed constraints on the surrogate, which prevents it from

recoiling in a manner similar to that observed in the body. Specific issues that can be potentially introduced through such tests are differences in:

- The magnitude and rate of deformation of the body segment.
- The magnitude of stress and strain in the body segment.
- The extent of damage that may be caused to the body segment.
- The proportion of strain energy absorbed by the PPE and body segment.
- The interaction of the PPE with the body segment and subsequent distribution of pressure.
- The magnitudes of stress and strain experienced by the PPE.

There are also issues with the impact conditions used. Ankrah & Mills (2003) suggested that current BSI protocols have been developed to prevent test rigs from breaking as opposed to matching impact conditions experienced in sporting environments. This can lead to inaccurate measures of PPE suitability. Payne *et al.* (2013) indicated the potential discrepancies in momentum and impact energy between safety standards and reported kinematics from sports impacts. Using the BS 6183-3:2000 (2000) safety standard for cricket leg guards, BS:EN 13061:2009 (2009) for football shin guards and BS:EN 13546:2000 (2000) for field hockey goalkeeper PPE, the potential inaccuracies in impact conditions have been outlined (Table 2.4).

Table 2.4 - Percentage differences in momentum and impact energy between safety standards and 'in play' estimates (adapted from Payne *et al.*, 2013).

	% Difference from 'in play' estimate	
	Momentum	Impact Energy
<i>BS:EN 13061:2009 (Blunt Impact)</i>	-53.0	+2.10
<i>BS:EN 13061:2009 (Stud Impact)</i>	-97.3	-99.7
<i>BS 6183-3:2000</i>	+157	-58.0
<i>BS:EN 13546:2000</i>	+146	-60.9

There are no sports safety standards which solely focus on thigh PPE. However, their assessment is included in the following standards:

- **BS 6183-3:2000** - Protective equipment for cricketers: Part 3: leg protectors for batsmen, wicketkeepers and fielders, and thigh, arm and chest protectors for batsmen.
- **BS EN 13546:2002** - Protective clothing - Hand, arm, chest, abdomen, leg, foot and genital protectors for field hockey goalkeepers and shin protectors for field players - Requirements and test methods.
- **DD CEN/TS 15256:2005** - Protective clothing - Hand, arm, leg, genital and neck protectors for use in ice hockey - Protectors for players other than goalkeepers - Requirements and test methods.
- **DD 7971-9:2005** - Protective clothing and equipment for use in violent situations and in training - Part 9: Training suits and equipment - Requirements and test methods.

Each of these safety standards embody the same inadequacies as those discussed in the general example (Fig. 2.3). The shortcomings associated with safety standards all influence the quality of PPE assessment and consequently the manner in which PPE is developed. Improved, more biofidelic surrogates have the potential to significantly improve the assessment of PPE and can inform future designs to both protect the athlete and enhance performance.

2.3. Anatomy of the Thigh Region

2.3.1. Tissue Structures

A detailed overview of the specific structural components in the human thigh region has been documented. An axial cross-section through a central region of the thigh is shown in Figure 2.4 illustrating the range and diversity of structural components present in the segment.

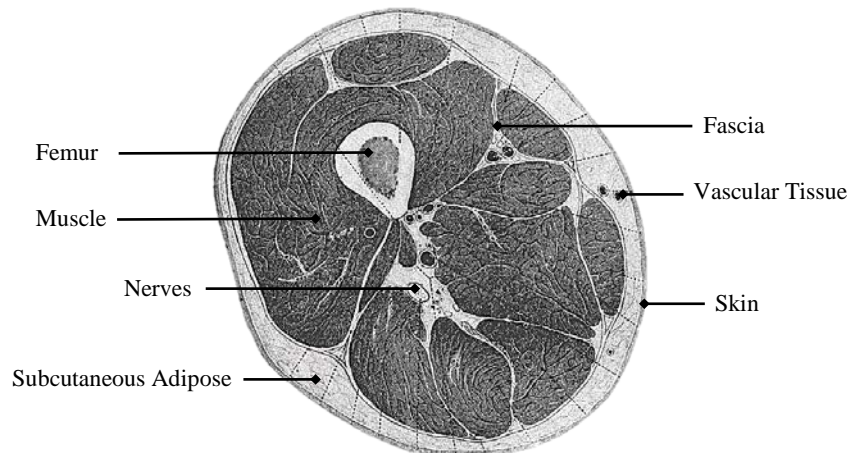


Figure 2.4 - Axial plane section through the human male thigh (Gray, 1918).

a) Skeletal Components

Bone, in particular long bones, are the integral support structure throughout the human body and are essential in providing leverage for locomotion. The single skeletal component in the thigh is the femur bone; this is the largest and heaviest bone in the human body and transmits body weight from pelvis to tibia. The femoral head is connected to the femoral shaft by a narrow neck, which lies at an angle of 125° with the shaft. The femur descends in the frontal plane from lateral to medial at an angle of 7° from vertical. The distal portion of femur diverges into a medial and lateral condyle, which are separated by an intercondylar fossa and is joined anteriorly where they articulate with the patella. Anterior and posterior views of the femur are shown in Figure 2.5a and Figure 2.5b with anterior and posterior frontal cross-sectional views of the thigh (Fig. 2.5c, Fig. 2.5d) showing the location of the femur relative to the outer surface of the thigh. Due to its presence as a structural support for soft tissues, the femur is a key constitutive structure in the thigh region. Its high relative stiffness and proximity to outer surface tissues in places is likely to have a significant influence on the mechanical response of the thigh on impact.

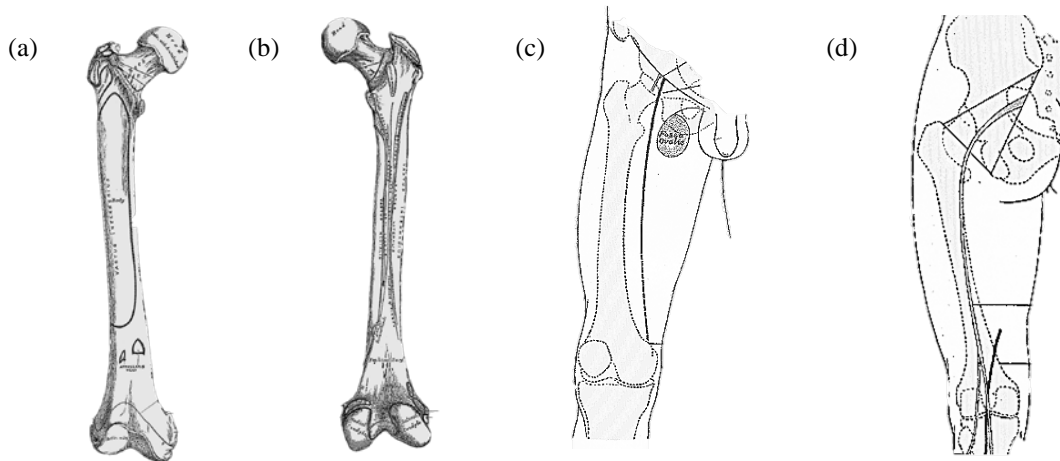


Figure 2.5 - Femur bone anatomy and position in thigh in: (a) anterior femur; (b) posterior femur; (c) anterior frontal cross-section and (d) posterior frontal cross-section views (Gray, 1918).

b) Muscles

Skeletal muscle constitutes the bulk of soft tissue in the human limb segments, accounting for 40 - 50% of body mass (Wang *et al.*, 1997; Salem *et al.*, 2006). The microstructure of skeletal muscle tissues are characterised by a hierarchy of densely packed muscle fibres arranged in fascicles surrounded by connective tissues.

The muscles in the thigh are divided into three compartments: anterior, medial and posterior (Fig. 2.6). Each compartment is surrounded by a very strong resilient membrane called fascia that supports muscles when exercising (Fig. 2.4). The anterior compartment (quadriceps femoris) contains hip flexors and knee extensors, the medial compartment contains a group of adductors and the posterior compartment (hamstrings) contains knee flexors and hip extensors. The thigh also has an outer layer of fascia which forms a deep stocking like membrane covering all the muscles. It is particularly thick in the thigh and gluteal region and is termed the fascia lata. The muscles are attached to the bone through tendons, which are tight bands of soft connective tissue that are responsible for transferring force from the muscle to the bone to facilitate joint movement. Due to its constitutive mass and volume in the thigh region, muscle tissue is certain to have a significant influence on the mechanical response of the body segment to impact.

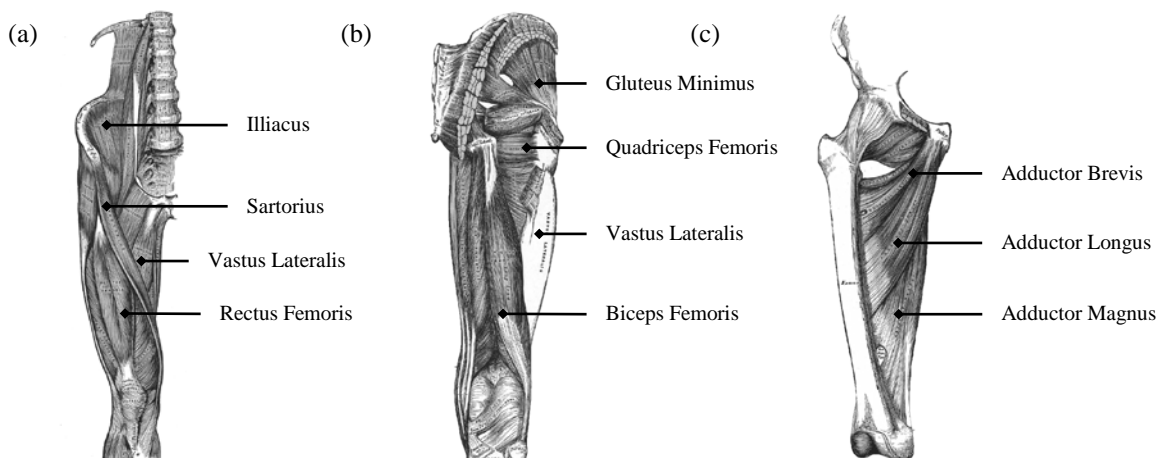


Figure 2.6 - Musculature in the thigh region with some key muscles labelled in: (a) anterior; (b) posterior and (c) deep medial locations (Gray, 1918).

c) Subcutaneous Adipose

Subcutaneous adipose tissue, also known as the hypodermis, is a connective fatty tissue located between the dermis and the aponeuroses and fascia of muscles, and is bonded strongly to the dermis. It plays an important role as a mechanical load absorbing and distributing member that absorbs shock and protects against local stresses (Robbins *et al.*, 1989; Miller-Young *et al.*, 2002; Geerligs *et al.*, 2008; Sims *et al.*, 2010; Comley & Fleck, 2012; Alkhouli *et al.*, 2013). Adipose consists of 90 - 99% triglyceride, with the remaining tissue containing 5 - 30% water and 2 - 3% proteins (Albright & Stern, 1998). The tissue is a loose association of lipid filled cells called white adipocytes (80 μm diameter approximately) held in two extracellular networks of collagen fibres penetrated by fibroblasts, neural and vascular cells, and multipotent progenitor cells (Geerligs *et al.*, 2008; Young & Christman, 2012; Sommer *et al.*, 2013). The smaller network is a reinforcement basement membrane, comprised of collagen fibres, which acts as the walls of a closed-cell foam with the adipocyte forming the cavity. The larger network is called the interlobular septa comprised of type I collagen fibres and is roughly 1 mm in size acting as an open-celled foam (Comley & Fleck, 2010). Due to its significant volume within the thigh and function as a mechanical load absorbing tissue, it is suggested that subcutaneous adipose will influence the impact response of the body region.

d) Skin

Skin is the outermost tissue in the human body and represents a protective barrier from mechanical trauma and stiff interface surrounding other tissues (Edwards & Marks, 1995; Pailler-Mattei *et al.*, 2008). With the exception of muscle and skeletal tissues it represents the largest organ, constituting approximately 5.5% of body mass (Goldsmith, 1990). It consists of two major structures, the dermis and epidermis, though the structural response is largely determined by the dermal layer, which is primarily populated by collagen fibres (75% of dry weight). The fibres at rest are twisted and knotted in a very complex network with interspersed elastin fibres and lymphatic elements (Pailler-Mattei *et al.*, 2008; Wu *et al.*, 2003); this makes the fibres very stiff in tension but able to carry little load in compression. The continuous presence of a layer of skin in all regions of the thigh as well as its increased relative stiffness to surrounding soft tissues suggest that it will significantly influence the impact response of the body region.

e) Other Structures

There are a number of other tissue structures in the thigh, most significantly a series of vascular components and nerves that intersect through the region (Fig. 2.4). The nerves pass information to and from the muscles with information in the form of chemical impulses. Axons pass electrical information down limbs to perform specific functions while other nerves pass from sensation organelles to connect with the brain. Large bundles of nerves are present in the thigh and pass distally down the limb originating from the spinal foramina of the lumbar and sacral spine branching off to innervate different muscle groups. The three major nerves providing information to the thigh are the: femoral nerve (anterior compartment), obturator nerve (medial compartment) and sciatic nerve (posterior compartment).

The vascular components are responsible for blood flow with arteries transporting oxygen rich blood away from the heart and to the tissues and veins transport de-oxygenated blood back to the heart through a series of vessels. There is also a smaller network of blood transportation known as the lymphatic system which is responsible for collecting excess blood that has leaked into

interstitial tissues. The femoral artery, deep profunda artery, obturator artery, iliac artery and superior and inferior gluteal arteries are the major blood supplies to the thigh region. Venous drainage in the human leg occurs at two distinct levels: superficial and deep. Superficial veins are located in subcutaneous connective tissue and take blood into the deep venous system (femoral vein) through the long and short saphenous veins.

These structures constitute a small volume of the tissues in the thigh. They are clearly integral to the physical function of the region but when not assessing the physiological or neuromuscular responses of the region, it is believed that they have a much lower significance.

f) Joints

There are two joints with which the thigh segment (femur) articulates: the knee (tibiofemoral) joint and the hip (acetabulofemoral) joint (Fig. 2.7). The hip joint is a synovial articulation between the head of the femur and the acetabulum of the pelvis, which is formed superiorly by the ilium, anteriorly by the pubis and posteroinferiorly by the ischium. There are three ligaments which reinforce the joint and stabilise the movements: iliofemoral ligament, ischiofemoral ligament and the pubofemoral ligament; the joint is therefore stable from dislocations. The joint permits three rotational DOF along the sagittal, frontal and transverse planes. In the sagittal plane a normal hip joint is capable of 120° movement with the knee in flexion and 90° with the knee in extension, the joint also permits approximately 45° abduction, 30° adduction, 40° internal rotation and 45° external rotation (Banks & Hodge, 2004; Robertson *et al.*, 2003; Grood *et al.*, 1988).

The knee joint is a synovial hinge joint that has six DOF and involves the articulation of the femoral condyles located on the distal femur with the proximal tibia condyles. The knee joint permits the following movements: F-E rotation (0 - 140°); I-E rotation (at 90° flexion, 45° Ext., 30° Int.); A-P translation; ML rotation; ML translation; and longitudinal translation (Banks & Hodge, 2004; Robertson *et al.*, 2003; Grood *et al.*, 1988). The knee joint is held intact by ligaments connecting the tibia and femur as well as the surrounding muscle and tendon. There are two collateral ligaments (one on each side of the joint) which provide lateral stability to the hinge-like motion. There are also two cruciate ligaments located in the intercondylar region of the knee and connect the tibia and femur bones: the anterior cruciate ligament prevents anterior displacement, whilst the posterior cruciate ligament restricts posterior displacement.

The hip joint clearly has a significant direct effect on the kinematics of the thigh segment, whilst the knee joint influences the remote inertia from the lower leg. Each of these joints is likely to influence, to some extent, the mechanical response of the body region.

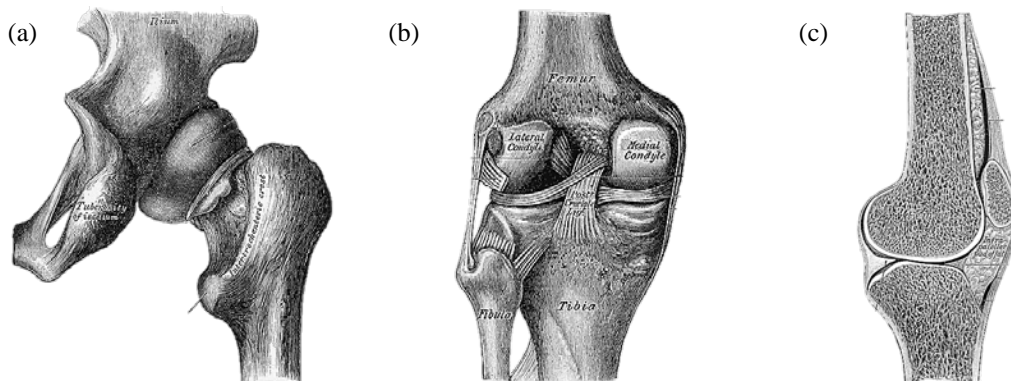


Figure 2.7 - (a) Hip joint; (b) knee joint (posterior view); (c) knee joint (sagittal plane) (Gray, 1918).

2.3.2. Organic Tissue Properties

The mechanical properties of organic tissues have been extensively studied in literature through measurements on human and animal specimens (§2.4.1). Within the human thigh segment: skin, subcutaneous adipose, muscle and bone tissues constitute the most significant volumes of material (Fig. 2.4) and are believed to govern the mechanical response behaviour. The morphology, structure and mechanical behaviour of these tissues have been investigated.

It is very challenging to practically obtain *in vivo* human tissue data from mechanical tests and as such most studies are conducted *in vitro*. There is also a paucity of good quality research of human tissue properties due to difficulties in obtaining post-mortem human subjects (PMHS) and the degradation in properties associated with the time the body is kept post-mortem prior to testing and storage conditions. Consequently, very few studies presented are of human tissues (Chawla *et al.*, 2009; Balaraman *et al.*, 2012). Much more of the organic tissue characterisation research published has been obtained from testing on more accessible animal specimens, such as bovine or porcine sources. It is suggested that these tissues exhibit comparable morphology, physiological and structural properties to humans (Douglas, 1972; Schmook *et al.*, 2001; Snedeker *et al.*, 2005a; Avon & Wood, 2005; Shergold *et al.*, 2006; Paus *et al.*, 2007). Although, Balaraman *et al.* (2012) reported that human muscle tissues studied exhibited stiffer behaviour than both bovine and porcine equivalents.

All organic tissues exhibit inhomogeneous, non-linear, viscoelastic behaviour and inherently vary as a function of the following test specific factors, which influence their reported mechanical behaviour.

- **Specimen site:** The location on the body from which the specimen is taken for testing can significantly affect the mechanical properties. For example, Keaveny *et al.* (2001) reported that the strength of bone can vary by an order of magnitude across sites, whilst Balaraman *et al.* (2012) observed significantly greater stiffness in tests conducted on *in vitro* human gastrocnemius muscles compared to neighbouring soleus muscles when tested at comparable strain rates. Similar location dependent differences have been reported in skin specimens (Haut, 1989; Sugihara *et al.*, 1991; Ní Annaidh *et al.* 2012).
- **Test temperature:** The temperature at which the specimens have been preconditioned to, and tested at, can affect the reported mechanical responses. For example, a decreased test temperature has been shown to increase the measured modulus of bone (Smith & Walmsley, 1959).
- **Hydration levels of specimens:** The pre-induced levels of artificial hydration can affect the viscoelastic properties of tissues. For example, Adharapurapu *et al.* (2006) tested bovine femoral cortical bone in compression in dry and rehydrated states at a range of strain rates and observed increases in modulus from 5.3 - 20 GPa to 5 - 30 GPa. It was also noted that when soaked in a saline bath, the transition from ductile to brittle behaviour was delayed (Hansen *et al.*, 2008).
- **Specimen geometry:** Inaccuracies may be introduced due to the specimen shape. For example, it was reported that it was almost impossible to cut perfect shapes of fresh muscle tissue due to its high mobility (Böl *et al.*, 2012; Van Loocke *et al.*, 2006). Differences in shape were also reported to significantly affect the properties of bone tissues (Ferreira *et al.*, 2006).

- **Time before testing:** The time left post-mortem prior to testing can significantly affect mechanical response with dehydration and decomposition occurring. For example, Van Sligtenhorst *et al.* (2006) showed that there was a significant difference in the mechanical properties of muscle specimens 1.5 and 3.5 hours post-mortem when compared to specimens tested 5, 6, 7, 9 and 27 hours post-mortem; this was largely supported by Van Loocke *et al.* (2006) who suggested that dehydration of tissues may lead to an increased stiffness.

a) Skin

Organic skin exhibits properties that are greatly inhomogeneous, non-elastic, time-dependent and in a state of biaxial tension *in vivo*. Its properties are based on the concentration and the orientation of the collagen fibres (Edwards & Marks, 1995; Wu *et al.*, 2003; Flynn & McCormack, 2008; Lim *et al.*, 2011; Ní Annaidh *et al.*, 2012). The fibres at rest are twisted and knotted in a very complex network with interspersed elastin fibres and lymphatic elements (Pailler-Mattei *et al.*, 2008; Wu *et al.*, 2003); this makes the fibres very stiff in tension but able to carry little load in compression.

The mechanical behaviour observed is influenced by many factors relating to both the specimen and loading conditions. Skin exhibits significant anisotropy underpinned by the presence of Langer lines which describe natural lines of pre-tension in the skin and have a significant effect on the mechanical response (Edwards & Marks, 2005; Ní Annaidh *et al.*, 2012). Liu & Yeung (2008) observed a greater stress relaxation in specimens cut perpendicular to the fibre direction and a greater viscoelasticity at higher strains. Similarly Ankersen *et al.* (1999) and Lim *et al.* (2011) observed a clear distinction in material stiffness in tensile tests between the two orthogonal directions.

The loading conditions employed such as the mechanical loading type and loading rate can also influence the response. The morphology of the tissue results in a loading type dependent behaviour whereby skin exhibits a greater stiffness in compression than in tension (Lanir & Fung, 1974; Dunn *et al.*, 1985), though this response can differ between *in vivo* and *in vitro* studies. The mechanical properties of skin have also been shown to be highly dependent on loading rate (Finlay, 1978; Potts *et al.*, 1984; Jamison *et al.*, 1968). At high loading rates, a more viscous response has been observed (Jee & Komvopoulos, 2014), perhaps due to an increased fluid (blood, water, lymph) loss from the compressed dermis (Edwards & Marks, 1995). The age of the mammalian surrogate is also a pertinent consideration. The collagen content of skin decreases with age and young skin is typically less protective against large strain trauma than older skin which has a proportionally greater elastic region. Older skin also has a lower water content, which has a significant effect on its viscous response (Potts *et al.*, 1984).

The typical stress - strain response of skin can be divided into three regions, described by Brown (1973). In the initial region, the skin is compliant and large deformation occurs at low applied loads with the fibres largely unaligned, the constitutive response at this phase is largely governed by the bending stiffness of collagen fibres and viscous shear between the fibres and extrafibrillar matrix (Cohen *et al.*, 1976). The second phase, the stiffness gradually increases as fibres align themselves in the direction of the load and in the third phase skin behaves almost linearly with the stiffness increasing rapidly as the collagen fibres are mostly aligned and the response becomes dependent on the tensile mechanical response of the collagen fibres which are three orders of

magnitude stiffer than the elastin fibres (Ní Annaidh *et al.*, 2012); this region has been suggested to occur at approximately 0.4 strain (Comley & Fleck, 2012).

Skin is commonly tested in tension (Wu *et al.*, 2003). Most studies have characterised the properties under quasi-static loading conditions (e.g. Ankersen *et al.*, 1999; Ní Annaidh *et al.*, 2012), though quasi-static responses may not be simply extrapolated to high strain rates without experimental validation. Lim *et al.* (2011) and Gallagher *et al.* (2012) conducted dynamic tensile testing on porcine and human skin tissues respectively using a modified Split Hopkinson Pressure Bar (SHPB). A significant strain rate dependency was observed in both sets of tests, though there was a significant difference in the magnitude of stiffness reported, which has varied widely between previous studies. Few studies have been reported on *in vitro* skin tissues in compression. Wu *et al.* (2003) conducted *in vitro* compressive tests on porcine tissues from the upper neck and back, and Shergold *et al.* (2006) tested porcine rump skin in uniaxial compression. Data from a subset of representative studies are shown in Figure 2.8.

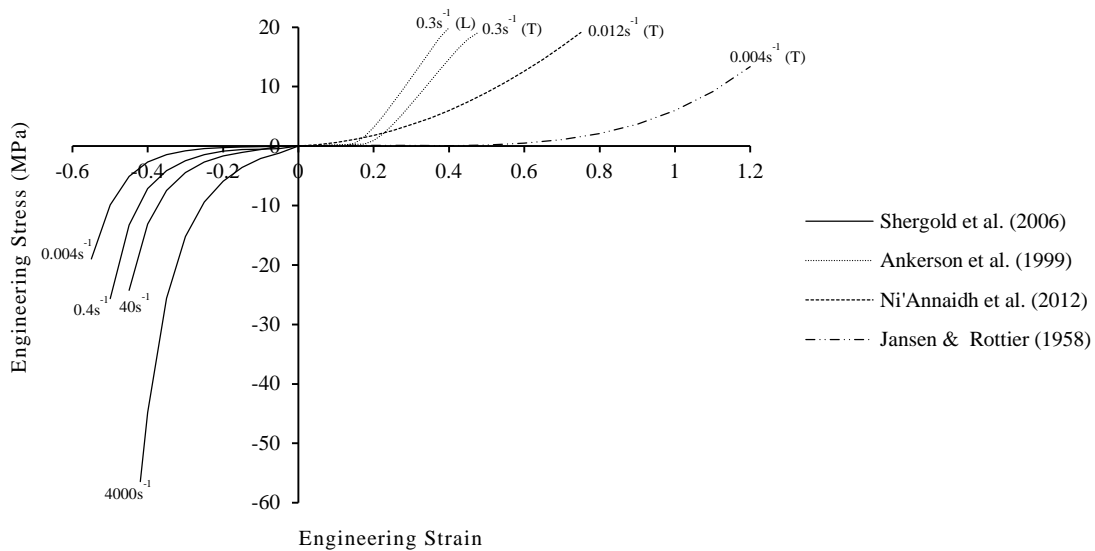


Figure 2.8 - Engineering stress - strain graphs for a range of organic skin tissue samples at different strain rates (T - transverse; L - longitudinal).

Given available sources, the compressive datasets by Shergold *et al.* (2006) potentially present the best quality data conducted in a deformation mode of interest tested at sports relevant strain rate ranges believed to be between 50 - 500 s^{-1} , based on an expected maximal velocity projectile impact from a cricket ball of 34.6 $m.s^{-1}$ (Penrose *et al.*, 1976).

b) Subcutaneous Adipose

Adipose, as with most biological tissues, exhibits heterogeneous, rate-dependent, viscoelastic behaviour and experiences large non-linear deformations (Holzapfel, 2004; Sapozhnikov & Ignatova, 2013). It is suggested that adipose is approximately isotropic in structure and due to the large liquid content is almost incompressible (Samani *et al.*, 2003; Comley & Fleck, 2010), though a recent study by Sommer *et al.* (2013) observed some anisotropy in specimens.

In comparison to the relative wealth of research on the mechanical properties of skin, there is a paucity of studies characterising the response of adipose. Much of current research only presents linear material parameters (e.g. Young's modulus) at quasi-static strain rates, whilst it is widely

acknowledged that the tissue exhibits a non-linear response and significant rate dependence (Comley & Fleck, 2012; Samani & Plewes, 2004; Alkhouli *et al.*, 2013; Sommer *et al.*, 2013).

Adipose is commonly characterised using samples from the human heel pad region (Miller-Young, *et al.*, 2002; Erdemir *et al.*, 2006; Natali *et al.*, 2013), though fat pads on the hands and feet differ from subcutaneous tissues elsewhere in the body as they contain higher ratios of unsaturated versus saturated fatty acids (Geerligs *et al.*, 2008). They also have morphological differences due to their anatomical function and high levels of stress experienced in normal loading conditions (Gefen & Haberman, 2007). Adipose properties have also been characterised using samples from human breast tissues (e.g. Azar *et al.*, 2002; Krouskop *et al.*, 1998; Van Houten *et al.*, 2003; Sarvazyan *et al.*, 1994; Samani *et al.*, 2007) or porcine subcutaneous specimens (e.g. Geerligs *et al.*, 2008; Comley & Fleck, 2010; Comley & Fleck, 2012).

Under compression adipose tissue has low stiffness initially (< 0.3 strain) but then, under increased loads, the collagen fibres of fat and skin come under tension, restricting the movement of the adipose and increasing the stiffness (Miller-Young *et al.*, 2002; Fontanella *et al.*, 2012). This observation is supported by Alkhouli *et al.* (2013) who reported a mean elastic modulus of 1.6 ± 0.8 kPa up to 0.3 strain and a mean elastic modulus of 11.7 ± 6.4 kPa from 0.3 strain to failure. This theory was extended by Sapozhnikov & Ignatova (2013) who suggested that between 0.4 - 0.5 strain, adipose exhibits non-linear behaviour followed by a transition at 0.5 - 0.7 strain where stresses decrease attributed to the collapse of cell walls, with an expulsion of fluid. This is then followed by a hardening with a rapid increase in compressive stress governed by a high bulk modulus of the remaining cell shells.

Under quasi-static strain rates, studies have shown the elastic modulus of adipose to be approximately between 1 - 4.5 kPa (Azar *et al.*, 2002; Samani & Plewes, 2004; Samani *et al.*, 2007; Sims *et al.*, 2010; Comley & Fleck, 2012) with little strain rate sensitivities between $2 \times 10^{-3} - 10 \text{ s}^{-1}$ (Comley & Fleck, 2012). Beyond 10 s^{-1} , significant sensitivity has been observed (Miller-Young *et al.*, 2002; Gefen & Haberman, 2007; Comley & Fleck, 2012). Comley & Fleck (2012) reported an increase in Young's by three orders of magnitude from 2 kPa at 10 s^{-1} to 4 MPa at 3000 s^{-1} , a similar modulus to the dermis. Comparable responses were observed by Egelbretsson (2011) when conducting high strain rate compressive tests. Representative stress - strain data from a subset of characterisation studies are shown in Figure 2.9.

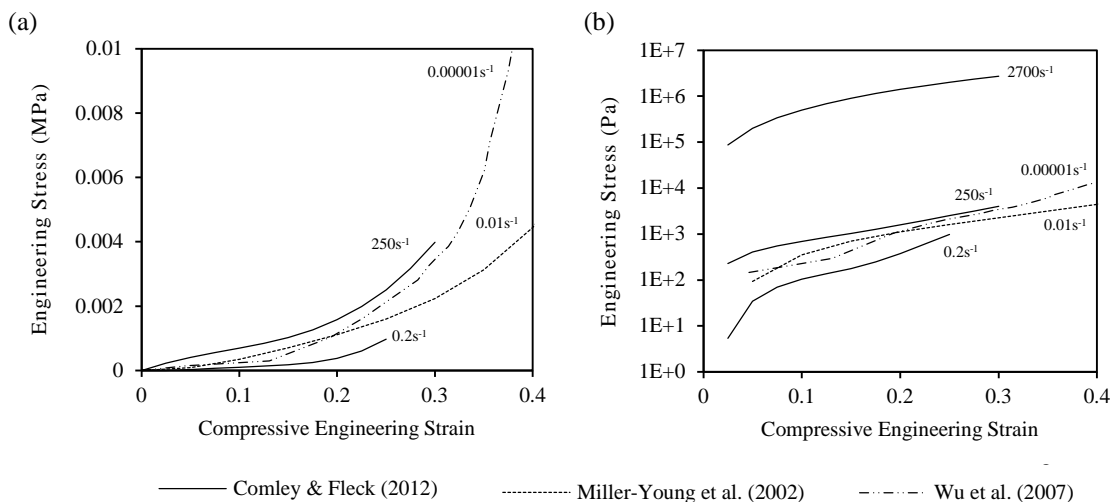


Figure 2.9 - Compressive engineering stress - strain graphs for a range of organic adipose tissue samples at different strain rates in (a) linear and (b) log-linear plots.

Subcutaneous adipose clearly exhibits a wide variation in mechanical responses dependent on the strain rate in which it is deformed. Therefore, the study by Comley & Fleck (2012) presents the most applicable data as responses are reported over a wide range of strain rates, including those relevant to sports impacts.

c) Muscle

Muscle tissue is heterogeneous and exhibits anisotropy, viscoelasticity, and strain rate dependencies. The anisotropy present in muscle is well documented and it is widely acknowledged that tissues behave stiffer when tested perpendicular to the direction of the muscle fibres (Van Looke *et al.*, 2006; Böl *et al.*, 2012; Song *et al.*, 2007). The mechanical properties of muscle have also been reported to vary significantly dependant on the age of the animal tested. Song *et al.* (2007) noted differences in mechanical response compared with the study conducted by Van Looke *et al.* (2006) and partly attributed differences to the age of the specimens (3 and 5 month old animals respectively). In accordance with studies on the skin and adipose tissues, it is expected that these differences will be amplified in older animals.

Many characterisation studies have been conducted investigating the mechanical properties of muscle tissues. Most tests are conducted in uniaxial compression and have been performed under quasi-static loading conditions (Yamada, 1970; Fung 1993), which are unrepresentative of the dynamic loading experienced from sports impacts. McElhaney (1966) conducted a seminal study characterising *in vitro* bovine tissues around the femur in uniaxial compression using both a Tinius-Olsen electromatic test machine and an air operated test machine for tests at low and high strain rate tests respectively. In recent years, authors have typically investigated the high strain rate response of soft tissues using a polymeric SHPB, capable of testing in the order of 10^3 s^{-1} (Van Sligtenhorst *et al.*, 2006; Song *et al.*, 2007; Chawla *et al.*, 2009; Balaraman *et al.*, 2012). There is, however, a paucity of information conducted under intermediate strain rate conditions in a similar range to those expected in sports impact scenarios. Data from a subset of compressive muscle characterisation studies are shown in Figure 2.10.

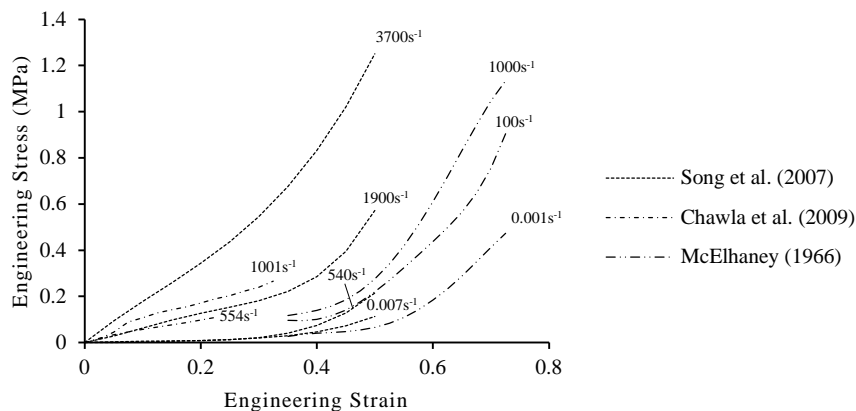


Figure 2.10 - Compressive engineering stress - strain plot showing data from previous organic muscle tissue characterisation studies.

The muscle property data, however, lacks tonicity that would be present in live humans; a very different mechanical response may occur when an athlete's limb segment is contracting, braced or tensed reflexively in anticipation of an impact (Muggenthaler *et al.*, 2008). Although, it is widely suggested that muscles exhibit a greater stiffness when contracted (Hoffer & Andreassen, 1981), there is no consensus quantifying the effect that muscle tonicity introduces.

Many different studies have investigated the effect of contraction using a variety of techniques such as ultrasound and motion capture (Blackburn *et al.*, 2009), magnetic resonance elastography (Bensamoun *et al.*, 2006), vibro-ultrasound (Wang *et al.*, 2012) and manual ultrasound indentation (Zheng *et al.*, 1999); the effects measured varied. Crisco *et al.*, (1996) also observed a 44% reduction in the delay between peak force and peak displacement between contracted and relaxed muscles when testing Wistar rats *in vivo*; this is an indication of reduced viscoelasticity in contracted muscles. Muggenthaler *et al.* (2008) also noted an increase in tissue stiffness of up to 49% when the muscle was contracted in human impact tests. Given a variable and inconsistent characterisation of this effect, a direct measurement by Zheng *et al.* (1999) potentially provides the best approximation of the increased stiffness of a contracted skeletal muscle. The study used a manual ultrasound indentation system on the human forearm and lower limb soft tissues and recorded a mean increase in effective Young's modulus of $4.2 \times$ when gripping a pen.

There are many studies which have reported the mechanical properties of muscle; however, there exists a wide variation in the reported mechanical properties. Characterisation studies by Song *et al.* (2007) and McElhaney (1966) present data in relevant strain rate ranges and potentially have the greatest application in sports impact research

d) Bone

The mechanical responses of bone tissues are important in surrogate research both in terms of impact response behaviour and failure thresholds. Skeletal components comprise osseous tissue consisting of hydroxyapatite (mineral), collagen, water and trace amounts of other protein (Erickson *et al.*, 2002). Of these constituents, hydroxyapatite is the stiffest and most brittle component with an elastic modulus of approximately 110 GPa (Currey, 1985), whilst collagen is a tough, pliant fibrous component with a modulus of approximately 350 MPa (Currey, 1985). The individual concentrations of each of these components significantly influence the mechanical properties of the tissues.

Bones are typically categorised into two types of structure: compact cortical bone, which is usually present in the shell of structures and in the diaphysis (central section) of long bones, and trabecular bone which is a relatively spongy 3D lattice continuous within the inner surface of the cortical shell and at the epiphysis (ends) of the femur (Carter & Hayes, 1977) (Fig. 2.11). The two structures are intrinsically similar and are generally distinguished by their porosity (percentage of volume occupied by non-mineralised tissues) (Keaveny *et al.*, 2001). Cortical bone typically has a porosity of between 5 - 30% whilst trabecular bone has a porosity of between 30 - 90% (Guedes *et al.*, 2006). The similar microstructural properties means that distinctions between porous cortical bone and dense trabecular bone can sometimes be arbitrary (McElhaney *et al.*, 1970; Martin, 1972). The structural properties of trabecular bone differ between tissues based on the arrangement of trabeculae that divide the inner volume of bone into intercommunicating pores of different dimensions. This produces a structure of variable porosity and apparent density. The pores are commonly in the order of 1 mm and are filled with red and yellow marrow, blood vessels, nerve tissues and interstitial fluid (Keaveny *et al.*, 2001).

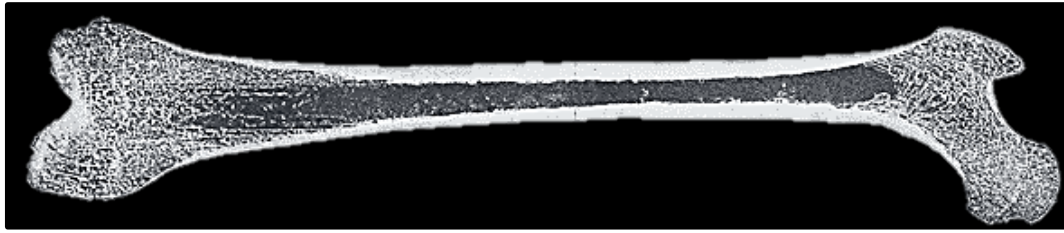


Figure 2.11 - Cross-section through human femur showing cortical and trabecular bone regions (Gray, 1918).

Both cortical and trabecular bone structures exhibit anisotropic (Ferreira *et al.*, 2006), non-linear rate dependence (McElhaney, 1966), viscoelasticity (Lakes *et al.*, 1979) and viscoplasticity (Johnson *et al.*, 2010) that is dependent largely on the spatial architecture and composition of bones, primarily governed by the porosity and apparent density (Currey, 1988; Martin, 1993; Keaveny *et al.*, 2001; Ferreira *et al.*, 2006). Typical values for apparent density vary between $1.7 - 2.0 \text{ kg.m}^{-3}$ for cortical bone (Guedes *et al.*, 2006) and between $0.18 - 0.95 \text{ kg.m}^{-3}$ (Lotz *et al.*, 1990) for trabecular bone.

Most studies have been conducted looking at the physiological strain rate ranges for walking and running, which were determined to be in the range $0.005 - 0.08 \text{ s}^{-1}$ (Rubin & Lanyon, 1982). The quasi-static properties of bone are therefore most commonly reported. Elastic modulus values of cortical and trabecular bone have ranged between 14 - 30 GPa (McElhaney, 1966; Currey & Butler, 1975; Lucksanasombool *et al.*, 2003; Reilly *et al.*, 1974) and 6 - 14 GPa (Ashman & Rho, 1988; Rho *et al.*, 1993; Hogan *et al.*, 2000) respectively. Values for the ultimate strength have typically varied between 100 - 350 MPa (Reilly *et al.*, 1974; McElhaney, 1966; Ferreira *et al.*, 2006) for cortical bone and 4 - 23 MPa (Carter & Hayes, 1976; Hogan *et al.*, 2000).

However, the stiffness and failure characteristics of bone have been shown to be rate dependent (Carter & Hayes, 1977; Currey, 1989; Kulin *et al.*, 2011). The rate dependency of bone tissues is well demonstrated in a study by Crowninshield & Pope (1974) who tested bovine femoral cortical bone between $0.001 - 250 \text{ s}^{-1}$ and observed that the elastic modulus increased from 10 - 12.5 GPa. McElhaney (1966) similarly observed strain rate dependencies with an increase of elastic modulus in bovine femoral bone specimens of 18.6 - 42 GPa between $0.001 - 1500 \text{ s}^{-1}$. Typical stress - strain responses from a representative subset of bone tissue studies are presented in Figure 2.12.

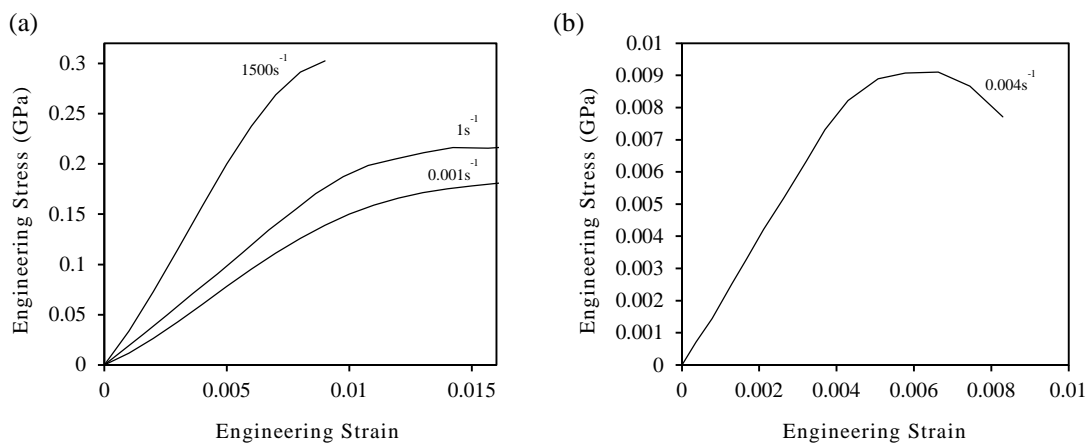


Figure 2.12 - Compressive engineering stress - strain plots showing response of: (a) cortical bone (McElhaney, 1966) and (b) trabecular bone (Schoenfeld *et al.*, 1974).

Given the increased relative stiffness of skeletal tissues compared to surrounding soft tissues, the exactness to which the mechanical properties are matched is of lower importance. The increased stiffness also results in lower strain rates being elicited in the tissue structure from impact. The study presented by McElhaney (1966) provides useful data through strains and strain rates relevant to sports impacts.

Mechanical characterisation studies for organic tissues, particularly soft tissues, have, to date, provided highly varied responses in most cases related to differences in species types, loading type and loading conditions employed. Consequently, previous studies have often only provided a partial description of actual tissue behaviour, typically in strain rate ranges relevant to automotive or military industry applications where the impact duration is often much faster or much slower than those experienced in typical sports impacts (<10 ms or >100 ms) (van der Horst *et al.*, 2005). The presence of more representative datasets conducted in deformation modes of interest on human tissue would be greatly beneficial in assimilation of organic tissue behaviour for sports impacts both in computational modelling and the fabrication of simulants for synthetic surrogate research.

2.4. Human Surrogates

2.4.1. Organic Surrogates

Organic surrogates refer to any biological tissue, living or post-mortem that aims to emulate the response of humans. They are widely used to determine the impact response and mechanical properties of tissue structures. Organic surrogates can be broadly categorised into three primary types: human volunteers, PMHS and animal surrogates.

a) Human Volunteers

Human volunteers as representative samples of a target demographic group present a key testing resource in impact biomechanics research. Studies utilising surrogates of this type have been conducted for many years to determine *in vivo* human injury response. One of the first volunteer studies was published in 1954 by John Stapp, where military personnel were tested through rapid decelerations from a rocket sled to simulate an aircraft crash.

The primary advantage of using volunteers is that they allow researchers to consider the *in vivo* response of a living human without having to make assumptions about, or approximations of, the internal structure, tissue composition and physiology. Studies generally involve either retrospectively determining injury epidemiology from vehicle crash occupants or through laboratory-based experiments; however both of these approaches have severe practical limitations (Kent & Bass, 2007).

Laboratory test experiments must be performed at non-injurious levels of exposure, below the pain threshold in compliance with the Nuremberg Code of 1947 and the Helsinki Declaration of 1964 (revised in World Medical Association (2008)), which provides ethical guidelines for human experimentation. In addition, proposed testing protocols must be reviewed by an international review board to determine whether they meet all legal and ethical standards (King *et al.*, 1995; Crandall *et al.*, 2011). This severely limits the nature of testing that can take place and makes the testing more time-consuming and expensive to perform.

Further practical limitations include the lack of direct measurements that can be taken because most instrumentation must be non-invasive to comply with ethical guidelines. Consequently, internal loads must generally be inferred from measured external parameters rather than directly acquired (Crandall *et al.*, 2011). There is also decreased control and repeatability in testing humans because human tissues exhibit significant inhomogeneity and as such there is considerable variability within and between trials. This leads to a difficulty in determining accurate relations between external loading parameters and specific injury mechanisms or phenomena. In addition, there are issues predicting, by extrapolation, an accurate description or model of human response from one loading regime (e.g. low intensity loading) into another (e.g. high intensity injurious loading). Nevertheless, laboratory testing has been instrumental in understanding the physiological human impact response; in particular considerations such as muscle tonicity and activation levels that cannot be accurately defined on other organic surrogates.

Epidemiological studies of crash occupants inadvertently subject to impacts are also useful and provide data unobtainable in a laboratory environment such as intrinsic conditions (age, gender, anthropometrics) and multi-directional dynamic loading (James, 1991; Evans, 2001; Evans & Gerrish, 2001). The studies are, however, inherently inaccurate because in retrospective studies it is impossible to control the setting or collect sufficiently detailed information about the crash loading environment (Kent & Bass, 2007). The lack of knowledge of the loading environment generally limits the utility of these studies as it is extremely difficult to define relationships with injury mechanisms.

In the sports impact domain, human volunteers have been most extensively used to determine both the kinematics of human movements in impact scenarios and the human impact response in real play laboratory replications. Studies have typically either considered human-on-human impacts (e.g. Pain *et al.*, 2008; Halkon *et al.*, 2012) or artificial impactor-on-human impacts (e.g. Hrysmallis, 2009; Tsui & Pain, 2008). Human-on-human impacts often lack ecological validity as the prescribed laboratory scenarios are innately different from real play environments and the impact intensities are different from games. In artificial impactor-on-human impacts, the impactor lacks biofidelity and the subjects are often anticipating injuries and as such the replications do not accurately represent the gameplay injury scenario. To overcome some of these practical challenges and in pursuit of this research (§3.4.2), a three-phase protocol has been developed to quantify basketball impacts (Halkon *et al.*, 2014). Human volunteers impacted an instrumented synthetic surrogate to provide an understanding of the impact intensities, the author then developed a simplified artificial impactor capable of replacing the human impacts to strike the volunteers in a controlled laboratory environment.

A representative sample of human volunteers that could be tested to injurious levels and invasively measured would present the ultimate testing medium for sports PPE. However, the severe constraints and extensive legislation that must be adhered to practically limit the nature of testing that can be performed and hence the usefulness of the surrogate type in this field.

b) Post-Mortem Human Subjects

PMHS, also known as cadavers, were first introduced in the field of injury biomechanics in the 19th century (Weber, 1859; Messerer, 1880) and have since been widely used to characterise human impact responses (Crandall *et al.*, 2011).

PMHS can be tested through a variety of different methods. However, in general, whole body tests have been conducted through an impact sled test, whilst local tests on body segments have been conducted using a linear impactor, pendulum or falling weight (King *et al.*, 1995). Body regions are instrumented to provide both a direct (tissue damage) and indirect measure (instrumentation feedback) of injury prediction. Accelerometers are generally attached directly to the bone, and the surface usually contacted is frequently backed by load cells to measure the impact force. Pressure transducers are sometimes used in re-pressurised blood vessels and positional markers are sometimes used to track body segments with high speed video (HSV) (King *et al.*, 1995). However the predominant means of injury evaluation is through autopsy based procedures to assess visible damage to tissues, which requires trained medical staff to determine the extent of injuries (Bergeron *et al.*, 2006; Cronin *et al.*, 2003).

PMHS have not commonly been used in the sports impact domain, however their limited usage is most widespread in assessing head impacts in sports where protective headgear is worn (e.g. cycling, American football, ice hockey or baseball) (Heald & Pass, 1994). Hrysonallis (2009) reported an application of PMHS in the sports impact domain when developing a surrogate thigh segment. The author conducted drop tests on lower limb specimens to determine the impact response from which a synthetic thigh surrogate was validated. PMHS are, however, most extensively used in automotive and military industries, determining injury response criteria and validating artificial surrogates. For example, tests have been performed on PMHS lower leg specimens to provide validation data for both synthetic and numerical models (Geurts *et al.*, 2006; Bir *et al.*, 2008). Kajzer *et al.* (1997, 1999) performed a series of tests on PMHS to study the response of the knee in lateral dynamic shear and lateral dynamic bending, which has since been used as a key piece of human response literature from which to validate artificial surrogates. PMHS have also been used to evaluate the effectiveness of PPE. Bergeron *et al.* (2006) utilised a series of lower leg PMHS to both validate an artificial surrogate and investigate the protective capabilities of landmine protective boots.

A key strength of PMHS is that they are exact geometrical and anatomical representations of the human tissue structures being tested (Snyder, 1973; Verriest, 1984); there is currently no artificial substitute that can model the complexities of the human anatomy as accurately (King *et al.*, 1995; Cronin *et al.*, 2003; Bergeron *et al.*, 2004). This makes them extremely useful in determining the extent of tissue damage under injurious impacts.

Despite this, a key disadvantage associated with the use of PMHS concerns their lack of physiological response. The surrogates do not possess any cardiovascular activity and hence tissues remain unpressurised. There is also no neurological activity which causes an absence of active flexure or reflexive response, which greatly affects their impact behaviour and thus diminishes biofidelity (Mertz & Patrick, 1967; Krstic *et al.*, 2002; Bergeron *et al.*, 2006; Crandall *et al.*, 2011). Although PMHS contain all human tissue complexities, the structures are flaccid and do not represent the tonicity of living human tissues.

PMHS are biological structures and hence there is a limited time period before decomposition processes such as autolysis and rigor mortis occur, which dramatically changes their mechanical properties (Sakezles, 2009); Van Ee *et al.* (2000) noted that failure stresses significantly decreased following decomposition. After these processes have occurred, PMHS are essentially atonal and unable to simulate resting muscle tone and contraction of living humans (Crandall *et al.*, 2011). This is an essential aspect of testing in many industries, for example, it has been determined that more than 50% of occupants in frontal crashes engage in bracing behaviour (Ore, 1992; Petit *et al.*, 1997). The manner in which these post-mortem changes affect responses is not fully understood and consequently data from human volunteers are often used to better understand the differences in *in vitro* and *in vivo* human responses (Shaw *et al.*, 2002).

Several different techniques have been used to preserve cadavers and extend their useful condition. Embalmed PHMS were traditionally used as a means of preserving specimens; however, the process has been largely abandoned due to the artificially inaccurate tissue properties generated such as excessive tissue rigidity, limited joint ranges of motion, and modified ultimate strength of embalmed tissue (Sakezles, 2009; Crandall & Pilkey, 1994). Similarly freezing PMHS specimens has been shown to increase their useful life; however, additional facilities are required for the process, which makes it more complex and expensive. In addition, undesirable damage is caused to the tissue structure during the freezing and thawing process, which has been shown to decrease the failure strengths of the tissue (Menz, 1971; Lee & Pelker, 1985; Clavert, 2001). Researchers have also attempted to restore some physiological function of the body through processes such as pressurising the cardiovascular systems or electrically stimulating muscles; however, these must be performed in the limited time scale before post-mortem changes occur (Kent *et al.*, 2004). This commonly introduces further issues regarding the availability of PMHS specimens, as test studies often require numerous specimens, which can be considered to be practically unobtainable without preserving the PMHS in some manner. Generally, for studies in the field of injury biomechanics, comparable PMHS are required; however, variations in age, gender, and anthropometry make this an increasingly difficult, if not impossible task.

Due to ethical and social acceptance issues there are often difficulties associated with obtaining PMHS specimens (King *et al.*, 1995; Krstic *et al.*, 2002; Guillotin *et al.*, 2004; Roach, 2003), and the age of available specimens is generally biased towards the elderly population. In injury biomechanics research, the 'Association of Anatomy Chairmen' ethical guidelines stipulate that the age range of the subjects must be between 19 - 70 years (King *et al.*, 1995). This frequently leads to a wide variation in the anthropometric and mechanical properties of the specimens. For example, cortical bone strength and has been shown to decrease significantly with age, which makes specimens significantly more susceptible to fracture (Helelä, 1969; Chaloner *et al.*, 2002). Furthermore younger PMHS are generally required for females because of the potential changes in bone mineral density and strength of the skeleton after the menopause (King *et al.*, 1995; Cronin *et al.*, 2003). Consequently, it is unlikely that the age and medical history of the PMHS used in experimental studies would be representative of an athletic population, and an elite athletic population in particular (Woo *et al.*, 1991; Crandall *et al.*, 2011; King *et al.*, 1995; Krstic *et al.*, 2002). Limitations in the availability of representative PMHS dictate that specimens are often impacted multiple times; however, the PMHS become damaged through testing and injury tolerances and response corridors consequently vary between trials (Sakezles, 2009; Crandall *et al.*, 2011).

PMHS are treated as a level 2 biohazard and therefore require specialised facilities, protocol and personnel when handling human tissue, which add both cost and complexity to the experiments (Bergeron *et al.*, 2006; Cronin *et al.*, 2003; Sakezles, 2009; Guillotin *et al.*, 2004; Roach, 2003). Furthermore there is a high cost in bio-contamination safeguards required for the handling and disposal of human biological material (Krstic *et al.*, 2002). For example, Shaw *et al.* (2002) required approval from their organisation's 'Human Use Review Panel' and screening of blood for disease prior to acceptance into the research program. In general, host nations legislation will constrain organisations or individuals acceptable use and treatment of PMHS. For example, in the UK, the Human Tissue Act 2004 (c. 30) would apply and a licence would be required adding further delay and cost to any such research.

Nevertheless, PMHS continue to make an important contribution to understanding of the human response to impacts. The greatest utility of PMHS in sports injury assessments is related to testing of injurious impacts where a single damaging impact will be conducted. They are useful in limited passive applications where the lack of tonicity is either preferable or acceptable; however they would only be beneficial in sports applications in these contexts if restrictions for use permit and these restrictions don't make testing impractical. When considering a single impact test, they currently present the only ethically acceptable and feasible way to get structural definition at this level of detail.

c) Animal Surrogates

Animals have been extensively used in injury biomechanics research for many decades and have seen continued usage to the present day. They are primarily used to provide *in vivo* responses to impacts. Given the ethical issues associated with performing injurious impacts on humans, anaesthetised animals present the only source for obtaining behavioural information, permitting the ability to follow the pathophysiological response following an injury (Crandall *et al.*, 2011; King *et al.*, 1995). This is particularly pertinent when studying injuries which take time to develop (e.g. mild traumatic brain injury).

Few animals have bone structures that are comparable in size and geometry to that of humans (Krstic *et al.*, 2002). Rats, primates, rabbits and pigs are most commonly used for specific body parts; however, they all have obvious anatomical and physiological differences with human subjects that lead to inaccuracies in data interpretation. For example, considering the limbs used for locomotion, most animals used in injury biomechanics research are quadrupeds that walk on their toes whilst humans are upright bipeds, which inevitably affect their physical structure (e.g. the calcaneus bone does not have to withstand axial loading) (Chaloner *et al.*, 2002). This affects factors such as stride lengths, joint angles and torques from which erroneous assumptions can be made (Alexander, 2004). The great apes represent the most anatomically and physiologically similar species to humans due to their similar skeletal components and arrangement of internal organs (Cavalieri & Singer, 1993). However, due to the highly developed cognitive and behavioural characteristics present in great apes, ethical concerns have led to restrictions and bans in a large number of European countries (Crandall *et al.*, 2011). The data from these studies are often scaled so that they can be applied to humans due to differences in anatomy and level of tolerance between animals and humans; however this conveys its own associated inaccuracies (King *et al.*, 2005).

Animal cadaver surrogates have also been used in certain applications where it would be grossly unethical to use living animals (e.g. blast surrogates for AP landmines). Animals with comparable

human morphology (e.g. primates) are difficult to use due to ethical constraints, therefore animal cadavers from domesticated animals commercially farmed and killed for food represent a less complex and expensive alternative. However, as with PMHS, the issues with animal cadaver surrogates are primarily concerned with the absence of physiological response present in live animals (Krstic *et al.*, 2002). Testing using animal cadavers can, however, be employed to determine relationships between the behaviour of PMHS and living humans, as comparisons can be made between the differences present between living and dead animals (Lowenhielm *et al.*, 1977; Verriest, 1984).

There are strict ethical guidelines and legislation governing testing of animals in most developed countries. For example, in the US testing is governed by the Laboratory Animal Welfare Act of 1966 (P.L. 89 - 544), whilst in the UK, testing is governed by The Animal Welfare Act 2006 (c 45). In addition, institutions performing experiments must create an 'Institutional Animal Care and Use' committee to ensure conformance to the act (King *et al.*, 1995; Sakezles, 2009; Crandall *et al.*, 2011). Adherence to the legislation and guidelines results in a significant financial burden which makes testing unfeasible for many organisations. Further issues arise from the general public who take particular exception to animal testing; animal rights groups heavily scrutinise experimental testing and have succeeded in encouraging many institutions to have formal policies to eliminate animal testing (King *et al.*, 1995; Crandall *et al.*, 2011).

The greatest utility of animal surrogates in sports injury evaluation is through the ability to follow the physiological progression of injuries. Animal surrogates have been widely studied to examine the *in vivo* impact response of organic tissues particularly with regards to the onset of injuries. For example, Crisco *et al.* (1994, 1996) used anaesthetised Wistar rats to attempt to determine contusion thresholds. Cadaver animal surrogates are also commonly used to determine the mechanical properties of organic tissues (§2.3.2).

Using anaesthetised animals it is possible to determine injurious thresholds of tissues under less severe ethical and logistical constraints than other organic surrogates. It can be assumed, to a limited degree of accuracy that humans are biologically similar to other mammals and as such behave in a similar manner on impact. Even so, there are few clinical invasive instrumentation opportunities and as such methods of determining response are difficult to employ. Furthermore, sporting goods brands will try to avoid all associations with animal testing given the impact of ethical sensitivities to their brand image and revenues.

2.4.2. Artificial Surrogates

Artificial surrogates are inorganic simplified representations of living humans, which use data obtained from measurements on organic surrogates to inform their development. Artificial surrogates can be broadly categorised into two major groups: synthetic and computational surrogates.

a) Synthetic Surrogates

Synthetic surrogates were originally used to aid in injury prevention in military aircrafts; however they are currently more commonly used in assessing safety measures in automotive impacts (Caldwell *et al.*, 2012). They present a feasible alternative to organic surrogates which inherently have many ethical and logistical limitations and offer a means of experimentally studying human impact response without physically harming a participant (or animal) (Ramasamy *et al.*, 2011). As synthetic surrogates are simplifications of a real organic system, key challenges exist with regards to appropriate tissue structures, simulants materials, geometries and methods of evaluation.

Due to their simplicity, synthetic surrogates typically use engineering materials that respond to stresses consistently and repeatedly instead of like biological living organisms, which exhibit complex deformation behaviours and respond non-uniformly to impacts (Bedewi, 2001). However, this means that they can provide a controlled, repeatable structure from which to test PPE as the geometric and material parameters of synthetic tissue can be fixed within pre-established limits. This eliminates issues associated with inter-subject differences in tissue stiffness, strength and density present between organic surrogates (Krstic *et al.*, 2002; Bergeron *et al.*, 2006). Two common benefits traded for this lower biofidelity are sensitivity and repeatability. Repeatability refers to the ability of the surrogate to reproduce comparable results for each test with the same loading conditions, which is important to ensure that the surrogate provides a standardised response and means of comparison between trials. Sensitivity refers to the ability of the surrogate to produce different results if the specific injury producing stimulus is changed (Bergeron *et al.*, 2006).

Manufacturers of synthetic surrogates have typically considered 50th percentile US male anthropometry as a standardised dataset for the development of their models (Backaitis & Mertz, 1993; Beach *et al.*, 1998; Krstic, 2005). This sizing is intended to represent an average across a population and therefore inherently does not match any specific individual within it. Payne *et al.* (2013) indicated that using this dataset, body size can be overestimated by up to 17.1% in some demographic groups. If PPE is manufactured using this dataset as a guideline, significant inaccuracies could be introduced in the fit of the garment and the manner in which it interacts with the skin. Similar issues exist with the mass and inertia of the body segments. If a 50th percentile US male dataset is adopted in surrogates, an underestimation of up to 65.7% could be introduced from a 95th percentile US male anthropometry. Despite this, using standardised body dimensions provides an accurate means of comparison with PMHS data and other synthetic surrogates (Bergeron & Chichester, 2003). However, the anthropometric profiles of humans have changed over the past few decades and traditional assumptions about sizing made are potentially not as representative of the current user population as they once were. A useful solution to this issue may be to develop a surrogate technology where it is cost-effective to manufacture surrogates that better represent the target demographic.

To develop a more complete description of human structures, it is necessary to consider internal tissue geometries. In recent years, imaging techniques such as magnetic resonance imaging (MRI) and computer tomography (CT) have been used extensively in the medical industry due to the improved accuracy of the scans (Esat & Osada, 2010). MRI machines generally have the greatest overall utility in human surrogate research as they are suitable for simultaneous examination of hard and soft tissues (Assassi *et al.*, 2009). The use of MRI's has led to the emergence of more individualised, accurate and detailed musculoskeletal models (Blemker *et al.*, 2007).

The Visible Human Project (VHP) (Ackerman, 1998) is a human geometry database that includes high quality MRI data with axial, sagittal and frontal plane anatomical cross sectional images (Silvestri & Ray, 2009). This has provided the basis for previous human surrogates such as the Human Torso Model (Merkle, 2013). However, the generated model is only valid in the one measured position and will cause errors when extrapolated to other positions (Horsman *et al.*, 2007). It should also be noted that the position was prone and post-mortem. As previously stated, the major issue with a generic dataset is that it is inherently not individualised and therefore will not accurately represent any individual member of the target population (Scheepers *et al.*, 1998). However, imaging approaches result in surrogate geometries that are completely individualised and therefore lack comparability with other surrogates that use standardised 50th percentile measures. This limits the utility of many validation measures in literature as they cannot be directly compared. Uses of these techniques are also currently limited due to the expense and availability of equipment.

Another essential consideration in the development of synthetic surrogates is the feedback mechanisms and manner that they are provided. Embedding instrumentation can introduce artificial stress concentrations adversely affecting the impact response of the surrogate. The responses of synthetic surrogates are often validated against organic surrogates (most commonly PMHS) to determine their biofidelity (King *et al.*, 1995). Force - time curves and deflection - time curves are commonly attained from PMHS and recorded and averaged across different specimens. At each instant the mean \pm 1 standard deviation (SD) is widely considered as the human response corridor (Kajzer *et al.*, 1997; Cronin *et al.*, 2003). Organic tissue data for validation, however, is scarce and often not appropriate, therefore bespoke studies are often required to provide specific validation data; this can be both expensive and time consuming.

Current synthetic impact surrogates are typically categorised as either “durable” or “frangible” based on their levels of intended durability and biofidelity.

(i) Durable Surrogates

Durable surrogates are multi-use testing devices that give consistent, repeatable mechanical responses and can measure physical parameters, such as force and acceleration that can ultimately be linked to injury predictions (Bir *et al.*, 2008). They aim to exhibit internal biofidelity in the form of comparable deformations, accelerations and articulations, as well as external biofidelity in similar interactions with the surrounding environment (Crandall *et al.*, 2011).

Durable surrogates often differ by industry application and typically either use stiff, durable materials, relying on instrumentation to assess rigid segment response with respect to organ damage (e.g. automotive crash test dummies) or use a combination of a stiff skeletal component and a single durable simulant to represent the composite response of all soft tissues.

The two most fundamental characteristics of the durable surrogates are mass and size, with which basic human impact response can be determined. Durable surrogates also aim to embody the articulations, inertial properties and mechanical response of living human structures (NATO, 2007; Cronin *et al.*, 2003; Schneider, 1983). In these surrogates the requirements for repeatability exceed those for biofidelity and hence durable surrogates are constructed from very robust, resilient materials that can be impacted many times under extreme loading conditions without affecting their response characteristics (Crandall *et al.*, 2011; Merkle, 2013).

Artificially high mechanical tissue simulant strengths are often desirable to ensure premature failure does not occur (Cronin *et al.*, 2003; NATO, 2007). This is demonstrated by Owen *et al.* (2001) who reported that for non-injurious testing on the Hybrid III crash test dummy, the peak axial force experienced at the tibia was approximately 1.2 - 1.6× higher than measured on a PMHS. This is suggested as being due to differences in the modulus of elasticity of bone and steel as bone stiffness increases with strain rate (§2.3.2.d). Therefore the responses of the PMHS are dependent on the velocity of the impact, which is not the case for the Hybrid III's metal shaft skeletal components (Bir *et al.*, 2008). Donnelly & Roberts (1987) also conducted a study on the Hybrid III femur and showed a higher force than a PMHS femur under the same velocities (288% difference for a 9.1 m.s⁻¹ impact). The anvils used in safety standards for sports PPE also typically reflect these robustness requirements and embody many related inaccuracies where rigid steel anvils are often prescribed (e.g. BS:EN 13546:2002; BS:EN 13061:2009).

Durable surrogates do not visually exhibit any physical signs of injury in response to the same loads that would cause evident injury in humans and consequently the information obtained from instrumentation must be correlated with injury data from organic surrogate studies in order to determine a risk of injury; this is usually expressed as a probability curve rather than a definitive threshold as the likelihood of injury is dependent on many predisposing factors (e.g. previous injuries) (Kimpura *et al.*, 2010; Crandall *et al.*, 2011). Previous researchers have prioritised measures such as accelerations, forces, moments and displacements and as such surrogates generally include instrumentation in the form of load cells, strain gauges, accelerometers and displacement transducers. HSV is also often employed separately to determine displacements (Krstic *et al.*, 2002; Cronin *et al.*, 2003). Safety standards for sports PPE typically evaluate performance in terms of the force transmitted through the garment to the load cell beneath the surrogate. When the force exceeds prescribed values the PPE is failed. This is a very limited assessment of the effectiveness of a garment of PPE and potentially restricts some effective designs from being adopted.

To provide full characterisation of the interactions occurring in a whole body surrogate during the impact event, Been *et al.* (2007) suggested that head-to-toe transducers with more than 135 channels of instrumentation would be required. Therefore limb segments are generally isolated for testing to reduce expense and time spent through redundant data capture as well as unnecessary recalibrations of sensors. The commercial cost of a standard Hybrid III surrogate is approximately \$35,000 (AA, 2013) and this cost is more than tripled when the dummy is fully instrumented.

There has only been one durable impact surrogate of the human thigh developed for investigating impact response in sports. Hrysmallis (2009) fabricated a synthetic surrogate thigh using data attained from drop tests on human volunteers and PMHS. The surrogate soft tissue structures were represented using silicone elastomer, Silastic 3483, moulded in a two-thirds cylindrical section of representative mid-thigh girth (550 mm) measured from human volunteers. The

posterior third of the soft tissue surrogate was a wooden section to enable easier mould release. The skeletal component was represented using two 0.025 m × 0.025 m sections of stainless steel with a length of 0.67 m (Fig. 2.13). The surrogate was tested in a drop tower configuration with a drop mass, instrumented with an accelerometer, used to determine impactor deceleration and peak local force on impact.



Figure 2.13 - Surrogate thigh components developed by Hrysomallis (2009) showing Silastic 3483 soft tissue surface, wooden surrogate backing, and steel skeletal component (*Image reproduced with permission of the rights holder, Elsevier*).

The study provided a good human simplification through quantitative selection of materials compared to organic surrogates and reasoned simplifications of geometries. However, the surrogate only used a single simulant to represent all of the soft tissue structures in the body segment (Fig. 2.4). Although not explicitly stated within the study, the length of the soft tissue structure is much smaller than in humans. This could cause issues in impact response and edge effects both in the loading phase and through initial shock wave propagation. As stated within the study, the accelerometer used only provides a measure of local kinetics above the surrogate and does not necessarily represent the deep tissue or skeletal response behaviour.

Other durable sports impact surrogates have been developed for the lower leg. Francisco (2000) developed a durable surrogate of the lower leg for testing of association football shin guards. The surrogate consisted of a rubber-covered foam surrounding a Sawbones[®] composite tibia bone. The surrogate was again tested in a linear guided drop test configuration; the falling drop mass embedded a load cell and accelerometer. There was also a strain gauge mounted on the posterior tibia specimen. Ankrah & Mills (2003) similarly developed a lower leg impact surrogate and used a Sawbones[®] tibia component and Senflex 435 foam soft tissue component with a SkinFx rubber skin. The surrogate was simply supported, horizontally, at distal and proximal ends and tested in a linear guided drop test configuration. Tekscan Flexiforce sensors (§6.3.2.b) were mounted on the surrogate surface in seven locations and used alongside HSV to determine impact response.

A more recent study by Tatar et al. (2014) investigating shin guards in association football also used a composite Sawbones[®] tibia component and used EVA foam to represent the soft tissues. The surrogate was impacted in a pendulum impact configuration with a load cell backed prosthetic foot and boot end-effector (Fig. 2.14).



Figure 2.14 - Durable surrogate lower leg developed by Tatar *et al.* (2014) with boot mounted pendulum end-effector (Image reproduced with permission of the rights holder, JSSM).

Each of these surrogates, however, embodies significant simplifications to the diversity of organic tissue structures present in the body region and their mechanical properties. In all of the studies, a best fit ‘off the shelf’ soft tissue simulant was adopted without detailed consideration to the actual constitutive materials and their impact behaviour. Elastomers are generally considered to be good tissue equivalents due to their durability, consistency of response and comparable material densities to organic tissues, whilst foams have been criticised for their unrepresentative densities, resiliency and impact response characteristics (Lawrence & Hardy, 1998; Hrysomallis, 2009). The instrumentation used in each of the tests and methods of evaluating impact response each only provide a partial description of the actual surrogate impact response and, in some cases, introduce artificial stress concentrations.

The composite skeletal components used in each of these research studies, however, provide a geometrically accurate and mechanically representative bone structure. Sawbones® develop commercially available composite bones, which are widely used in both orthopaedic research and reconstructions of surgical procedures (Gardner *et al.*, 2010). The composite femur is based on a 90.8 kg, 183 cm tall adult male and is intended to match the mechanical properties of healthy adult bones up to 80 years old. The bones are constructed from short glass-fibre reinforced epoxy pressure injection moulded around a rigid PU core (with a hollow intramedullary canal) to represent cortical and trabecular bones respectively.

The 4th generation composite is the most recent iteration and has been shown to exhibit comparable mechanical responses under quasi-static loading conditions with similar compressive and tensile modulus, ultimate tensile strength, fracture toughness and fatigue crack propagation to literature on fresh frozen cadavers (Chong *et al.*, 2007; Gardner *et al.*, 2010). The composites also showed similar brittle failure modes to organic bone (Tencer & Johnson., 1994; Johner *et al.*, 2000; Gardner *et al.*, 2010). Comparisons between the mechanical properties of the composite and organic bone are presented in Table 2.5.

Table 2.5 - Tensile and compressive mechanical properties of a 4th generation composite Sawbones® compared with organic bone (adapted from Heiner (2008)).

	4 th Gen. Composite	Organic Bone
<i>Tensile Elastic Modulus (GPa)</i>	16.0	17.0
<i>Tensile Strength (MPa)</i>	107	130
<i>Compressive Elastic Modulus (GPa)</i>	16.6	17.0
<i>Compressive Strength (MPa)</i>	154	170

The composite bones have also been shown to exhibit little inter-specimen variations with reported values of 5% (Heiner, 2008), 4.5% (Heiner & Brown, 2001), 10% (Gardner *et al.*, 2010). A study by Zdero *et al.* (2010), however, showed significant discrepancies in loading rate dependence compared to organic bone. This could significantly affect the biofidelity of the surrogate component under high rate loading conditions.

(ii) Frangible Surrogates

Frangible surrogates are test structures that are designed to offer greater biofidelity and sustain permanent damage in a manner similar to a human body (Bir *et al.*, 2008). This makes the surrogates single use and consequently more expensive per test than durable alternatives (Krstic *et al.*, 2002; Cronin *et al.*, 2003).

Frangible surrogates are the design solution when tissue failure biofidelity is the main design goal. The surrogates are more concerned with specific failure modes for single-use injury evaluation; therefore more closely matched human material properties are necessary to provide an indication for accurate post-mortem evaluation.

Frangible soft tissue components have commonly used water-based gels. Ballistic gelatin is often used as the preferred soft tissue simulant for military applications and has served as an international standard for ballistic wound research (Fackler, 1988; Sellier & Kneubuehl, 1994). It is often fabricated in either 10% (FBI protocol, Fackler, 1988) 20% (NATO protocol) gelatin concentrations (by mass). Hydrogels have also been used in the development of soft tissue simulants. They were first synthesised by Wichterle & Lim (1960) and have since been used extensively within tissue engineering, pharmaceutical and biomedical fields (Hoare & Kohane, 2008). Hydrogels consist of a three-dimensional (3D) network of structures obtained from a class of synthetic and/or natural hydrophilic polymers which absorb and retain significant amounts of water between macromolecules (Rosiak & Yoshii, 1999). The key characteristic of these gels are their water retention capabilities. In their swollen state, hydrogels have a mass fraction significantly greater than the polymer which gives them properties similar to humans. Polymer engineers can design and synthesise polymer networks with molecular scale control over structures to tailor specific mechanical properties as well as chemical and biological responses to stimuli (Ahmed, 2013). SyndaverTM specialise in the commercial development of hydrogels to represent the mechanical properties of human soft tissues; the simulants are validated directly against accompanying *in vitro* human or animal tissue tests.

Human tissue engineering is a highly active research area and could potentially yield future developments in human surrogate materials, though at present this technology is not sufficiently established for use in mechanical impact evaluations.

Although, these materials are formulated to exhibit superior biofidelity, there is still, however, a requirement for high levels of consistency between individual surrogates so that comparisons can be legitimately made. One of the key issues associated with frangible surrogate materials (e.g. gelatins), however, is that the properties often change over time and often requires refrigeration to prolong useful storage life (Cronin *et al.*, 2003; Bergeron *et al.*, 2006).

Frangible surrogates are designed to replicate the actual damage mechanisms experienced by living humans under similar loading conditions. As a result frangible surrogates are predominantly evaluated through autopsy-based procedures to determine mechanical damage and as such require an expert medical prognosis in the same manner as PMHS. However, a lack of

detailed internal structures representative of soft tissues and organs in surrogates is often an issue and consequently measurements of force or acceleration must be utilised to infer loading phenomena rather than observe stresses within a given structure of interest (Crandall *et al.*, 2011). Therefore a variety of instrumentation such as load cells, pressure transducers and strain gauges are commonly incorporated and complimented by HSV. Cronin *et al.* (2011) assessed trauma of a lower leg landmine surrogate through use a qualified surgeon alongside a combination of load cells, strain gauges, pressure gauges, manganin gauges and high speed x-ray. This approach, however, can introduce artificial stress risers and lead to premature fractures (NATO, 2007). The requirement for a medical expert to determine particular injury modes also makes frangible surrogate evaluation expensive.

No published literature has been identified for frangible lower limb surrogates developed for assessment of PPE or study of injury in the sporting goods industry. Frangible surrogates are primarily used within the military industry when considering life-threatening or very serious debilitating injuries such as penetrating bullet impacts or AP land mine blasts. The most representative frangible surrogates have been designed for axial landmine impacts such as the Red Deer Lower Leg (Skelton *et al.*, 2000), Simplified Lower Leg (Bourget *et al.*, 2008) and Complex Lower Leg (Biokinetics, 2003). The Frangible Surrogate Leg (FSL) (Krstic, 2005), in particular represents one of the most complex and sophisticated frangible surrogates developed.

The surrogate consisted of four skeletal components: a femur, tibia, patella, and fibula, with the bones in the foot being modelled separately in two sub-assemblies (Bergeron *et al.*, 2006). The bones were moulded from a mineralized plastic with an x-ray agent to provide a good CT contrast (Bergeron *et al.*, 2001). Cartilage material was simulated in considered positions on the surrogate and was modelled using a high temperature, high flexibility polyamide glue (Bergeron *et al.*, 2001; Bergeron *et al.*, 2006). Similarly tendons were simulated at anatomical positions to strengthen certain areas, such as the ankle and the knee capsule (Fig. 2.15).

To model the muscle tissue the existing structure was placed in a two-part fibreglass mould while a ballistic gelatin (20% aq. at 10°C) was poured in and left to cure (Bergeron *et al.*, 2006). The FSL also contained embedded instrumentation in the form of strain gauges to measure wave propagation speeds as well as local bending and compression, and triple rosettes placed on the femur and tibia.

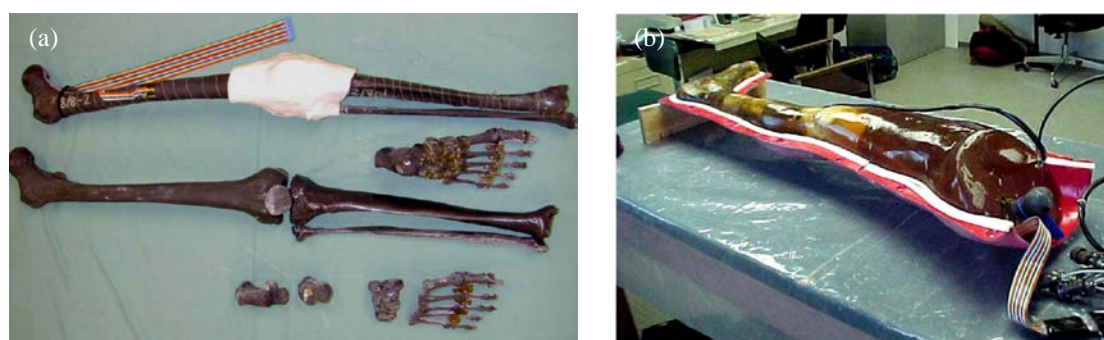


Figure 2.15 – (a) Components of the FSL; (b) Fully assembled FSL (Bergeron *et al.*, 2006).

The FSL represents a structurally detailed and anatomically accurate frangible surrogate with extensive instrumentation. However, the FSL embodies many of the shortcomings associated with frangible surrogates, in that it is only suitable for a single use, instrumentation causes artificial stress concentrations and the soft tissues require specialised storage facilities. A more recent

iteration of the FSL (eFSL) has, however, used a synthetic, non-biological tissue simulant called 'Ausgel', which does not require specialised storage conditions.

b) Computational Models

The utility of computational models in injury biomechanics research has markedly increased in the past few decades. Since their inception (McHenry, 1963) computational models have become important in facilitating determination of human response in impact scenarios (Crandall *et al.*, 2011). Computational models in injury biomechanics research typically refer to virtual human surrogates that aim to predict and explain the structural response of the anatomy when combined with a mathematical description of environmental and impact conditions (Merkle, 2013). It is widely considered that further development in the field towards more accurate, validated models can reduce the requirement for expensive experimental set ups.

One of the key advantages of computational modelling in injury biomechanics research is that different injury mechanisms can be studied without causing harm to the participant. The virtual nature of the surrogates means that there is no physical material cost associated with each model and this can support the exploration of a wide range of variable permutations without physical manufacturing costs or significant delays. Computational models can replace time-consuming and expensive experimental measures and provide a method of predicting internal measurable phenomena such as muscle forces (Ambrósio *et al.*, 1997). However the immense complexity of the human body continues to make accurate computational modelling a significant challenge and the development time associated with even a single body segment is non-trivial (Lee *et al.*, 2009). In most cases, however, a limited set of observable external phenomena are used to validate the accuracy of an increasingly complex set of internal phenomena, therefore a level of caution is warranted.

The ultimate goal of computational modelling in injury biomechanics research is a unified model, scalable from consistent geometries with the ability to accurately predict injuries from omnidirectional impacts. The rapid advancement in computer technologies shown in the past two decades serves as a good indicator of future growth in the area. Development in computer hardware and software increases the potential capabilities of future computational models (Yang *et al.*, 2006; Vezin & Verriest, 2005).

There are different types of computational models which are generally categorised relative to their complexity into: lumped mass, multi-body and discrete element models (Yang *et al.*, 2006).

(i) Lumped Mass Models

Lumped mass models consist of concentrated masses connected with mass-less single dimensional springs and Newtonian dashpots (Lee *et al.*, 2009; Crandall *et al.*, 2011). They aim to represent the basic dynamic response of a human during an impact and are often used to simulate the simplified mechanical responses of body segments remote from the impact event (e.g. upper and lower cervical spine ligaments in neck impact simulations (Panzer *et al.*, 2011)). However, lumped mass models are restricted by their simplicity and thus have limited application where environmental loading conditions become too complex (Crandall *et al.*, 2011). The Brinkley Dynamic Response criteria is an example of a simple lumped parameter single DOF model used within the aerospace industry to predict whole body response to accelerations based on the acceleration of the seat (Caldwell *et al.*, 2012).

(ii) Multi-Body Models

A multi-body system consists of a number of interconnected bodies, which can be flexible, rigid or a combination of both. These bodies are connected together by means of kinematic joints described mathematically by constraint equations (Muggenthaler *et al.*, 2008; Al Nazer, 2008). Multi-body models are used in a wide range of industrial applications (e.g. robots, bridges, satellites) as well as bio-dynamical systems (such as human body, animals and insects) (Al Nazer, 2008). Multi-body human body models are typically more complicated than industrial multi-body systems, because human body models require a large variety of joint properties and articulations, body forms and complex actuators in the forms of muscles and neighbouring soft tissue (Kraus *et al.*, 2005). The Mathematical Dynamic Model (MADYMO®) is an example of a multi-body model used within the automotive industry. It consists of a series of ellipsoid segments representative of human structures and is used to estimate impact response (Caldwell *et al.*, 2012).

In general, multi-body models provide an efficient balance of accuracy relative to computational costs. They are particularly useful in scenarios where optimisation and parameter sensitivity are involved, which would be too computationally expensive to model with discrete element models and not presented in sufficient detail using lumped mass models. However, multi-body models are limited by their lack of failure descriptions at tissue level, simple approximations of contact forces, and inability to accurately model body deformation.

(iii) Discrete Element Models

Discrete element models are the most sophisticated and accurate computational models (Yucesoy *et al.*, 2002; Tang & Hui, 2009). The finite element method (FEM) is a powerful tool for finding approximate numerical solutions through transforming partial differential equations (PDEs) into a set of algebraic equations (Oomens *et al.*, 2003).

In the FEM, the body is divided into a series of finite volumes, surfaces or lines interconnected at points called nodes, which together form the model mesh. Most FE models are typically displacement based. The displacements and positions of the elements are determined by interpolation functions, which are often selected based on their geometry, accuracy and computational budget. Stresses are determined through deformations and constitutive properties of the materials modelled. The material models are assigned to each of the elements corresponding to the associated tissues to define the mechanical properties (Yang *et al.*, 2006; Lee *et al.*, 2009). Given a dynamic problem to be solved, equilibrium equations are derived in terms of quantities of interest (e.g. stress or strain) and are expressed as PDEs, which are then approximated by the FEM (Lee *et al.*, 2009).

FE models have several advantages over simpler model types. They are capable of modelling anisotropic, inhomogeneous, non-linear tissues that are present in the human body. They are also capable of modelling delineated stress distributions across tissues that allow for injury predictions based on local values of stress and strain and thus are capable of determining deformations, forces, pressures, and alignments (Muggenthaler *et al.*, 2008; Al Nazer *et al.*, 2008; Crandall *et al.*, 2011). They present the most complex and accurate means of determining human response without introducing artificial stress concentrations and can provide a more continuous description of tissue behaviour (e.g. stress profiles) than synthetic surrogates. The ability of models to accurately predict local stresses and strains based on controlled external loading conditions is useful in the development of more refined injury threshold criteria. Computational models can be tested at sub-

injurious levels, which can lead to a greater understanding of human response under failure loads (Yang *et al.*, 2006).

However, one of the major potential limitations of FE models is that they are heavily dependent on the quality of the human model and simplifications made with regards to geometries and material properties; this affects the accuracy of the results (Perillo-Marccone *et al.*, 2003). Hence, experimental verification is often considered a necessity.

The computational cost of FE models is another pertinent consideration. Higher order interpolation functions and fine mesh densities often used in human models require greater computation per element, which can be time consuming and costly (Muggenthaler *et al.*, 2008; Lee *et al.*, 2009; Esat & Osada, 2010). This has meant that FE is typically restricted to small body segments or single tissues (Al Nazer, 2008). Furthermore, due to expensive computation, FE models usually need to be applied in a static or short term dynamic solution because they are considered computationally impractical to be used in long dynamic analysis where a number of bones and muscles as well as interactions need to be taken into consideration (Al Nazer, 2008).

For a model to provide accurate information it must be validated against experimental data, however, there is currently insufficient data available from organic surrogates to fully validate the models and thus their response patterns may be inaccurate and unrepresentative of human behaviour (Yang *et al.*, 2006; Horsman *et al.*, 2007; Lee *et al.*, 2009; Ramasamy *et al.*, 2011). Furthermore much of the data used to validate existing models were not acquired for the purposes of validation and therefore likely have inherent differences in the experimental protocol (Yang *et al.*, 2006). Therefore, complex simulations must rely on assumptions and simplifications to deal with the nondeterministic nature of the equations driving the dynamics (Krosshaug *et al.*, 2005).

Crandall *et al.* (2011) has expressed these problems succinctly when he states “At best FE models approximate human response based on a set of simplifying assumptions. At worst they provide an accurate representation of inaccurate data if proper procedures for verification and validation are not followed”.

Many different commercial FE solvers have been used in surrogate impact analyses, primarily in the automotive industry. Common solvers are LS-DYNA®, RADIOSS® and PAM-CRASH®. The Total Human Model for Safety (THUMS®) developed by Toyota is an example of a whole body FE model widely used in the automotive industry. The model contains a full human biofidelic skeleton with muscle, ligaments and internal organs (Caldwell *et al.*, 2012).

When considering simulations of the thigh region, there has been no published research investigating sports impacts. The most sophisticated studies have considered automotive impacts. For example, Li *et al.* (2013) investigated pedestrian impact response to vehicle collisions using a FE model of the leg. In their model, the soft tissues were treated as a homogenous block, with a greater consideration afforded to the skeletal structures and ligaments in the knee joint. All soft tissues were modelled with quasi-linear viscoelastic material models whilst skeletal tissues were modelled using elasto-viscoplastic models. The FE model was validated against PMHS data under quasi-static and dynamic strain rates using constant velocity impactors with the bending moment and fracture force of the skeletal tissues in the upper and lower leg acting as evaluation criteria.

Similarly, Untaroiu *et al.* (2013) developed a lower limb FE model for simulating automotive impacts (Fig. 2.16). The model was designed to simulate AIS 2+ injuries (moderate to fatal) and

consequently, again, focussed on the skeletal tissue structures and joints. The trabecular and cortical bone tissues were both assigned elasto-plastic material models, with varying stiffness in three separate regions on the femur: head, neck and shaft. The “fleshy” tissues were assigned a simple rubber/foam model based on data from representative dynamic tests. The FE model was compared to PMHS data under quasi-static and dynamic impact conditions using femoral deflections and bending moments as validation criteria.

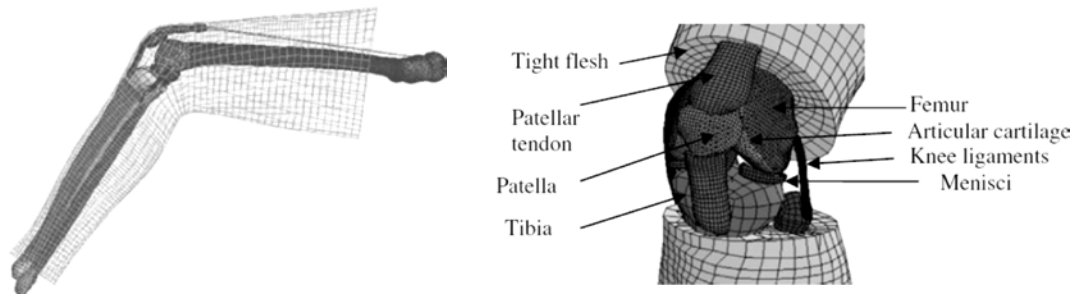


Figure 2.16 – Images showing FE model mesh definitions in Untaroiu *et al.* (2013) highlighting additional consideration afforded to joint structures and skeletal components (Image reproduced with permission of the rights holder, Springer).

The high driven masses used in each of the FE impact simulations are innately different from the conditions typically experienced in sports impacts. In each of the research studies reviewed, failure of the skeletal tissues has been assessed as the primary damage mechanisms. However, in sports impacts where lower mass, higher velocity impacts are common (e.g. projectiles), soft tissue injuries such as contusions or lacerations are more prevalent (§2.2.1). A related issue exists that, despite an abundance of data on PMHS responses under automotive impact conditions, there is a paucity of data at sports relevant strain rates from which to validate sports surrogates.

In the sports industry, the vast majority of FE models have been formulated to simulate head impacts. For example, Patton *et al.* (2013) developed a FE model to investigate brain tissue deformations to the unprotected head sustained during sports impacts. The model considered a wide diversity of soft tissues with the: scalp, skull, brain, meninges, cerebrospinal fluid, eleven pairs of the parasagittal bridging veins and neck muscles all considered. Each of these tissues were modelled using hyper-viscoelastic constitutive models. The model was extensively optimised against experimental PMHS data and, using kinematic data from real play impacts in which concussions were and were-not sustained, simulations were conducted to evaluate the differences in acceleration and strain in the constitutive tissues. However, validations of the FE model were made based on data attained from other research studies concerned with automotive relevant impacts. This can cause issues as it is practically very difficult to match experimental conditions precisely, particularly when the exact loading environment is unknown. Furthermore, due to the complex range of the soft tissues modelled, the optimisations made have potentially only corrected global response kinematics as opposed to ensuring the biofidelity of each tissue from representative impacts.

Without more extensive verification, the main use of computational models at this time in sports impacts surrogates is perhaps not so much to provide absolute values but to explore and so better understand the potential interaction of complex structures and multiple tissue phenomena. In studies which utilise complex geometries of strikers, targets and PPE, they are important in providing a good approximation of general human behaviour.

2.5. Surrogate Development Approach

Human surrogates are required in the sporting goods industry, primarily for conducting impact evaluations of PPE. Considering the key requirements of a surrogate for this application, it is important that it embodies the same size and shape as the target human, whilst responding consistently to repeated impacts. Each type of surrogate has its individual merits and specific applications where it is particularly useful in sports impact scenarios.

Organic surrogates are inherently poor candidates for an impact surrogate as they are biological and hence not durable enough to withstand repeat injurious loads without degradation in tissue properties. The consistency and repeatability of responses are a key requirement in sports impact testing; this cannot be achieved using organic surrogates. The ethical and logistical constraints associated with testing organic surrogates also complicate matters and limits their utility as a primary impact surrogate. Organic surrogates are, however, useful in informing the development and validation of artificial substitutes.

Artificial surrogates present a preferable solution for experimental impact testing as studies can be performed without harming the participants. Although they inherently lack many of the tissue complexities and biofidelity present in organic alternatives, artificial surrogates typically provide a consistent, repeatable means of determining human response.

Both synthetic and computational surrogates possess merits which make them attractive as sports impact surrogates. Computational models are useful in that they are capable of modelling complex scenarios where there are many variables and environmental conditions. There is also no physical material cost and as such models are flexible and permit manipulation of variables without having to fully re-generate the formulations. They are particularly useful in sports applications where specific design optimisations can be evaluated before physical models are manufactured. They are also useful in enhancing understanding into performance phenomena and unobservable equipment and surrogate interactions at levels of detail beyond what can be physically measured. Despite this, computational expenditure of modelling impacts is very high and thus remains a pertinent concern. Computational surrogates are also undermined by the quality of the input data, particularly material models, which often negates any theoretical advantage.

Synthetic surrogates provide a physical body that can be used to attach PPE, which is desirable in the sporting goods industry where experimental testing of PPE is considered a necessity. During the new product evaluation phase it is arguably unethical to rely on computational analysis alone before human-use trials are conducted. Superior synthetic surrogates that enable manufacturers to evaluate physical prototype PPE performance, without the risk of human injury, are needed to test the effectiveness of 'what has been made' rather than relying on 'what was intended or predicted'. The PPE industry, including the sporting goods sector, recognises that physical human surrogates are essential in this second phase. For the testing of PPE and exploration of injury below catastrophic or permanent levels, durable surrogates are the most likely to provide a cost-effective platform for future research and development. Existing durable surrogates are typically developed for automotive and military industries and are generally too stiff to model many pertinent mechanical impact phenomena related to sports injuries. Greater sophistication of the soft tissue materials, structures and morphologies are required to model subtler, more sensitive injury types pertinent to sports impacts. Scenarios where repeat impact testing is necessary (e.g. cyclic fatigue testing of a garment of PPE) also dictate that a durable surrogate would be required to provide a

consistent and reliable response to impact without degradation in the surrogate's properties through its useful life.

Given the merits and limitations of each surrogate type, superior research in this field is, therefore, likely to be based on complementary, mutually validating synthetic and computational human surrogates which provide a greater confidence in each of the individual approaches (Payne *et al.*, 2013). A similar parallel approach has been outlined and successfully exploited by Merkle (2013) when considering head impacts through the 'Human Surrogate Head Model' and the 'Human Head Finite Element Model'. This has also been adopted in sports equipment research by Ankrah & Mills (2003) and Ankrah & Mills (2004) to evaluate the effectiveness of association football shin guards and ankle protection.

The idealised solution for a sports impact surrogate is a validated set of computational and synthetic models which provide kinetic and kinematic feedback of the injury event that can be directly linked to specific injury mechanisms. The progression towards more biofidelic models should be staged and consider advancement through predetermined levels of complexity, which are constantly validated.

However, it is not just the biofidelity of the target surrogate that influences the quality of sports impact assessments. It is important to ensure that the environment in which sports impacts of interest are sustained are replicated as precisely as possible. This requires consideration of the impact test configuration, loading conditions and methods of evaluation, which have not been adequately considered in safety standards and previous sports impact assessments

Chapter 3 – Methods to Enable the Formulation of Improved Sports Impact Assessments

3.1. Chapter Overview

Chapter 3 provides an overview of the key components of sports impact assessments and presents an improved conceptual model to enable a systematic description of the factors relating to a specific impact injury event. The model has been applied to define two distinct injury scenarios to the thigh region: cricket ball and basketball knee impact. This information was then used to establish a set of specifications for improved sports impact assessments and the systematic formulation of key surrogate development approaches.

3.2. Introduction

3.2.1. Components of Sports Impact Assessments

There are many variables within each sports impact assessment, a series of integral components have been listed:

- *Target Surrogate*: The physical body, representative of the target human structure, to which PPE is attached.
- *Striker Surrogate*: The physical body, representative of the impacting structure in the sports scenario, with which the target structure is impacted.
- *Levels of Constraint*: The physical restraint mechanisms preventing the target and striker surrogates from freely recoiling on impact.
- *Impact Parameters*: The kinetic and kinematic parameters attributed to the target and striker surrogates at the instant of the impact event.
- *Methods of Assessment/Evaluation Criteria*: The measurements recorded in the impact assessment that are used to identify the mechanical phenomena occurring and the protective capabilities of the PPE.

3.2.2. Review of Sports Impact Assessments

a) Previous Assessments

Issues associated with existing sports impact assessments have been highlighted in the review of safety standards in §2.2.2.b and relate to unrepresentative simplifications to each of the listed components. For example, the impact parameters adopted significantly differ from ‘in play’ estimates of kinetic energy and momentum (Table 2.4). Similarly, the impact assessments conducted in academic literature (§2.4.2.a), although improved in some aspects, embodied many simplifications of the components that detract from the quality of their representation of the real sports impact scenario. §2.5 addresses the need for improved sports impact assessments in the evaluation of PPE.

b) Potential for Improved Assessments

To improve the quality of PPE evaluations, it is important to make sports impact assessments more representative of ‘in-play’ sports impact scenarios. Improved impact-specific assessments could potentially enable the production of superior PPE, with balanced consideration to the safety and performance of the user. This could include the engineering of PPE to address particular injury types or threat levels (e.g. high velocity cricket ball impacts). It could also result in the introduction of new materials and construction methods for PPE that would not have been acceptable in previous test standards.

In order to develop improved PPE assessments, it is important to first have a methodical, systematic approach to understanding the specific sports impact problem. This can be achieved using a framework to describe the sequence of events comprising an injury, addressing each of the assessment components (§3.2.1). Through knowledge of the factors involved in the specific injury event, informed judgements can be made on appropriate simplifications relating to each sports impact assessment component to enable cost-effective testing.

3.2.3. Review of Previous Conceptual Frameworks

There have been several attempts to design a conceptual framework, describing the relationship between factors determining an injury event. These models are typically deterministic and can be categorised by three distinct approaches:

- A risk accumulation and intensification model (i.e. injury occurs because of the accumulation of risk factors making the injury outcome increasingly probable).
- A mechanical phenomena sequence (i.e. injury occurs due to a sequence of interrelated mechanical loading events).
- An event sequence entity matrix (i.e. the Haddon matrix).

The first risk accumulation and intensification model was named the ‘multifactorial model’ (Meeuwisse, 1994). It is based on the principle that multiple causal factors contribute towards a single injury outcome (Fig. 3.1). It is considered that the likelihood of injury is dependent on internal risk factors (e.g. biomechanics, conditioning of the athlete), exposure to external risk factors (e.g. equipment, weather) and an inciting event (e.g. contact).

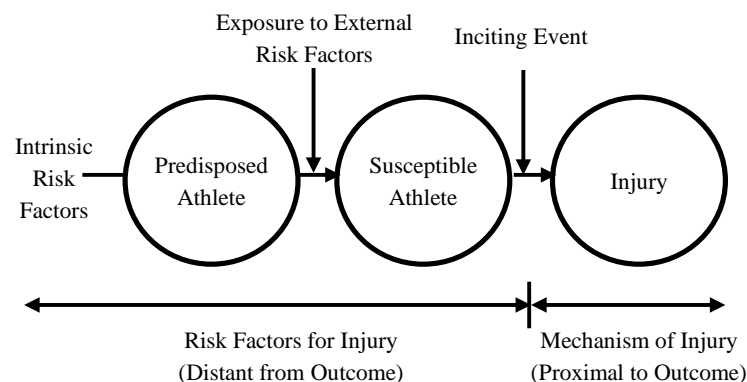


Figure 3.1 - Multifactorial model (Meeuwisse, 1994).

This model has since been adapted, notably by Bahr & Krosshaug (2005) who identified specific risk factors influencing an ACL injury. This model substantiated the multifactorial model framework and applied it to aid in the identification of the aetiology of a specific sports injury scenario. Another significant adaptation to the model was introduced by Meeuwisse (2007) who proposed a dynamic causal injury model that considered a reflective change in risk, related to previous impacts altering the predisposition to athletes to injuries. A similar approach was also undertaken by Gissane *et al.* (2001).

The mechanical phenomena sequence was first presented by Wismans (2000) and named the 'biomechanical dependency chain' (Fig. 3.2). It highlights the causal series of events from initial contact to injury occurrence. The general model suggests that when a body is subjected to external loading it deforms and in doing so triggers a biomechanical response from the body, which varies within and between people. If the body deforms beyond a recoverable limit, the injury tolerance level will be exceeded, leading to a specific injury, which is the function of the injury mechanism, resulting in damage to anatomical structures and impairment. This model has since been adapted by McIntosh (2005), who presented a similar core structure with a specific focus towards the effects of training interventions and psychological developments on mitigating injury risk. The model expanded the general approach using elements from the multifactorial model to identify many external factors that influence injury risk and provided an indication of potential areas for interventions.

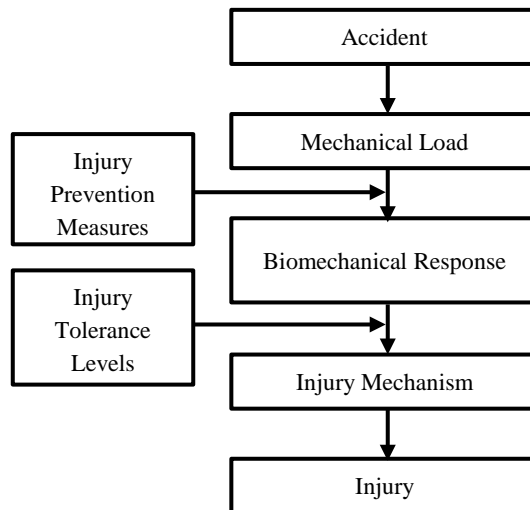


Figure 3.2- Load-injury model (Wismans, 2000).

The Haddon matrix (Haddon, 1980) is a cross-tabulation of important elements relating to injury, presented in a nine-cell matrix. It provides the opportunity to offer a preventative strategy in each cell corresponding to the relevant headings. This simple chart was initially designed to analyse injury prevention methods in the automotive industry. The structure of the matrix ensures systematic consideration is given to a range of known pertinent factors and can reveal areas in which knowledge is lacking. The matrix has also been presented in a sports context, notably by Bahr & Mæhlum (2004) who suggested the use of the model to conceptualise risk factors with a given injury problem using the headings: human, equipment and environment. This has since been applied by authors to describe injuries in American football (Crandall & Kent, 2011) and association football (Verhagen & van Mechelen, 2010).

Each of these models presents a different method for describing the injury event but none of them ensure all factors are given full consideration. The risk accumulation and intensification model does not describe in sufficient detail the deterministic series of events preceding injury and fails to address the nature of the body's response to impact. The mechanical phenomena sequence lacks specificity and does not provide sufficient differentiation between sequential entity types. The point of application for intervention methods (i.e. injury prevention measures) is also too narrow and does not consider opportunities to mitigate risk at other stages (Fig. 3.2). In addition, both of these model types are conceptual and somewhat academic; they suggest a method of describing injuries but do not provide a direct useful application. Whilst the Haddon matrix is a useful tool, it does not provide sufficient regulation to distinguish between key elements leading to injury and the absence of a list of influencing factors makes it possible to overlook certain elements of importance.

3.2.4. Aims and Objectives

The research presented in this chapter is an enabling stage to provide structure for subsequent experimental studies. As a result, the following aims and objectives for this chapter have been established:

1. To develop a sports impact model that can be applied to comprehensively describe the causal factors pertaining to any specific impact injury including systematic collation of a near complete list of influencing factors to describe an injury.
2. To apply the developed model to investigate specific impact events.
3. To apply the model to inform a specification for improved sports impact assessments and a considered surrogate research approach.

3.3. Formulation of Improved Conceptual Framework

To establish the specific requirements for human surrogate testing of sports PPE and so develop superior and cost-effective surrogate designs, it would be useful to formulate a more comprehensive conceptual framework to systematically collate factors affecting the specific injury scenarios. Thus, there is a requirement within the sports impact injury research domain to develop a comprehensive systematic description of the injury event.

A deterministic contextual sequential (DCS) model has been developed to provide a framework from which sports injury scenarios can be systematically studied. The causal factors relating to injuries have been extensively categorised to present a comprehensive tool to describe specific sports scenarios, develop experimental protocols to better understand scenarios and apply to surrogate development practices.

3.3.1. Core Model

The DCS model uses a simple flow diagram at its core with a dependency chain reflecting the deterministic relationships between the factors arising from elements relating to context, physiology and impact mechanics. This DCS framework maps the path from the participant performing the sports activity to the injury occurrence. Figure 3.3 shows just such a dependency chain from general context to specific injury occurrence using diagrammatic elements from traditional flow chart construction.

A contextual example of the framework has been provided in reverse from injury occurrence to context. It is believed that injury occurs when human tissue experiences an overload condition. This condition is dependent on several factors, which can be arranged in a dependency chain. For example, the overload occurrence in a particular structure will depend on the tissue type (e.g. muscle) and pre-conditioning physiological factors (e.g. fatigue); overloading will concern a particular tissue response (e.g. strain) to a load transfer mechanism (e.g. tensile stress) imposed by a load condition (e.g. impact) and associated resistance (e.g. inertia); the loading condition will depend on the type of incident (e.g. human on human impact) resulting from a particular sport (e.g. Rugby).

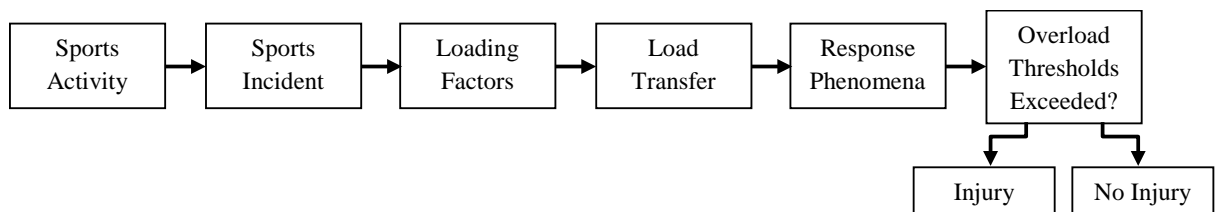


Figure 3.3 - DCS core framework.

The elements start at a general contextual level and become more focussed as the particular scenario becomes more defined, eventually resolving to a specific injury event. Seven major elements of the dependency chain are identified:

- (i) **Sporting Activity:** the sport being performed when the injury is attained. This element describes factors relating to the regulations of the sport, playing environment, style of play and playing conditions.
- (ii) **Sporting Incident:** the exact parameters between the target and striking object(s) immediately prior to contact. This element describes factors relating to the types of objects involved, constraints and impact locations.
- (iii) **Loading Factors:** the specific kinematic, kinetic and spatial parameters influencing the target and striker objects at the point of impact.
- (iv) **Load Transfer Factors:** the conditions at the target object at the point that it experiences impact from the striker. This element considers factors relating to the physical size, material properties and joint properties of the target.
- (v) **Response Phenomena:** the manner in which the loading phenomena are being experienced by the target body.
- (vi) **Overload Thresholds Exceeded:** at this stage it must be established whether the stresses and strains placed upon the body have exceeded the natural tolerance of the tissues.
- (vii) **Injury:** if the thresholds have been exceeded an injury will occur as a function of the type of loading and tissues that have been overloaded.

3.3.2. Influencing Factors

The framework provided by Figure 3.3 enables systematic identification, classification and ordering of all factors that may influence any sports injury event. An attempt has been made to exhaustively list without redundancy the factors relating to each of the elements in the deterministic framework (Table 3.1), i.e. the conditions dictating the outcome. Each set of factors presents a basis to characterise the individual components of the injury event, each set being intrinsically linked to the previous series. For example, if the ‘sports incident’ involves a football stud impact, the ‘loading factors’ will consider factors such as the geometry and stiffness of the stud. The framework attempts to provide a clear succession of exhaustible factors that aim to completely describe the phenomena occurring in the injury event.

Table 3.1 - DCS influencing factors.

1. Sports Activity	1.1. Game rules (contact/no contact).
	1.2. Equipment (goals, projectiles, apparel, implements, surfaces).
	1.3. Player exposure.
	1.4. Gender propensity (mixed/single sex).
	1.5. Team/individual.
	1.6. Popularity (no. of participants, frequency of play).
	1.7. Attitude/behaviour.
	1.8. Tactics.
	1.9. Temperature and humidity.
2. Sports Incident	2.1. Contact type: human (with or without PPE) versus: <ul style="list-style-type: none"> - Human (with or without PPE). - Projectile. - Surface. - Obstacles (goals, nets, posts, boards etc.). - Implements (bats, sticks etc.).
	2.2. Deliberate (active) or accidental (passive) contact.
	2.3. Two or more (striker & target(s)).
	2.4. Constraints (striker & target): free, driven, planted.
	2.5. Impact location – segment detail.
3. Loading Factors	3.1. Relative incoming velocity (target & striker).
	3.2. Relative surface alignment (target & striker).
	3.3. Specific surface geometry (target & striker).
	3.4. Surface properties (target & striker); external friction, lubrication.
	3.5. Effective inertia of striker (mass, moment of inertia, distribution).
	3.6. Striker stiffness (inertial resistance).
	3.7. DOF/constraints (pivot friction, moments, secondary inertia).
4. Load Transfer Factors	4.1. Effective inertia of target (mass, moment of inertia, mass distribution).
	4.2. Anthropometrics.
	4.3. Material characteristics: <ul style="list-style-type: none"> - Type (bone, muscle etc.). - State (tensed/relaxed/flexed/extended). - Mechanical properties (immediate surface and affected structures).
	4.4. Spatial geometry (physical location of material).
	4.5. Target DOF (at each of the joints; rotational and translational degrees).
	4.6. Internal friction & lubrication.
	4.7. Ground reaction forces.
5. Response Phenomena	5.1. Impact duration.
	5.2. Tissue displacement.
	5.3. Segment velocity (target & striker).
	5.4. Joint displacement.
	5.5. Acceleration.
	5.6. Shock.
	5.7. Vibration.
	5.8. Physiological factors (e.g. muscle tension, tendon reflex, localised pressure change).
	5.9. Temperature change.
6. Overload Thresholds Exceeded?	6.1. Compressive stresses & strains.
	6.2. Tensile stresses & strains.
	6.3. Shear stresses & strains.
	6.4. Cyclic fatigue.
	6.5. Subject specific property variation (e.g. age, physical condition, pre-existing damage or deformity).
	6.6. Multi-axial stress (resulting in yield or failure of tissue).
7. Injury	7.1. Muscle contusions.
	7.2. Bone fractures.
	7.3. Joint dislocations.
	7.4. Lacerations (compression, tearing of body tissue by blunt impact).
	7.5. Blistering (friction, rubbing).
	7.6. Incisions (cutting by sharp implement).
	7.7. Puncture (penetrating with sharp implement).
	7.8. Avulsions (forceful tearing of body tissue).
	7.9. Sprains/strains.
	7.10. Nerve entrapment.
	7.11. Organ failure.
	7.12. Concussion/Brain injuries.

3.4. Model Evaluation through Application

Given the dependency chain and factors defined, the general scope of the potential deterministic injury scenarios has been established in the subsequent sections. It can be used to:

- Generate a comprehensive description of particular sports specific injury scenarios, highlighting which aspects are known and where gaps in the knowledge exist.
- Develop a detailed set of experimental protocol, considering all aspects that need to be approximated, controlled and measured in an experiment.

3.4.1. Injury Scenario Definitions

The model framework has been used to generate a comprehensive description of the causal factors relating to two specific sports injury scenarios in the thigh region: a projectile-on-human cricket ball impact and a human-on-human basketball knee impact (Fig. 3.4). The two injury scenarios are good examples of the range of impacts that can be sustained in sports from a low velocity-high mass human impact, to a high velocity-low mass projectile impact.



Figure 3.4 - From left: basketball knee impact to the anterior thigh; cricket ball impact to the lateral thigh.

In cricket, injuries to the thigh region of a batsman from cricket ball impacts are a frequent and pertinent consideration with contusions a common occurrence (§2.2.1). Impacts from a cricket ball can result in severe contusions that can prevent an athlete performing for a prolonged period. In the thigh region, PPE is worn by most batsmen and as such injuries to this region must be addressed.

Human-on-human knee-on-thigh impacts in basketball are also common and potentially severe (Hrysomallis, 2009). A longitudinal study conducted by Dick *et al.* (2007d) investigated the injury incidence amongst collegiate basketball players and noted that the overall rate of injury was 9.9 per 1000 athlete exposures for games. Of those injuries 76.6% can be directly attributed to contact experienced in gameplay, 52.3% of which as a result of contact with other players. Similar knee-on-thigh trauma has been reported to be prevalent in Australian rules football where it ranks as the 2nd most common injury sustained (Mitchell, 2000). An indication of the severity of these injuries is provided by Diaz *et al.* (2003) who used imaging techniques to investigate quadriceps contusions in athletes. A case report considered a blunt trauma to the anterior thigh from a knee impact in basketball. The range of motion at the knee decreased by nearly 85% and a subsequent MRI scan showed that it took 3.5 months for the athlete to fully recover. Knee-on-thigh trauma has also been reported to be linked to partial ruptures of muscle tissue (Chomiak *et al.*, 2000). The scenario definitions for a cricket ball-on-thigh impact and a knee-on-thigh basketball impact have been presented in Table 3.2 and Table 3.3 respectively.

Table 3.2 - Cricket ball impact injury scenario model.

	Cricket ball - impact to batsman's lateral thigh from a legal delivery from a fast paced bowler
1. Sports Activity	<p>1.1. Non-contact sport, however accidental contact sustained in ball impacts to batsmen and fielders.</p> <p>1.2. Cricket ball used as playing object, the ball is bowled from 22 yards (20.12 m) to stationary batsman, who strikes the ball with a wooden bat into the field where it must be stopped and retrieved by the opposition. Batting players typically wear: a helmet, wrist guards, gloves, thigh guards, genital protectors, leg guards, and protective footwear.</p> <p>1.3. Player exposure: dependant on format, 20 over games (2 hour continuous exposure); 50 over games (4 hours continuous exposure) 4 - 5 day games (broken down into sessions, max. 3 hours continuous exposure).</p> <p>1.4. Single-sex sport played by males and females separately.</p> <p>1.5. Team sport (11 players per team).</p> <p>1.6. Played by 215,500 people in England at least once a week (Sport England, 2011).</p> <p>1.7. Not typically considered an aggressive sport.</p> <p>1.8. Fast paced bowlers can adopt styles where they bowl directly at batsmen to force them into mistakes.</p> <p>1.9. Played predominantly in summer months in England (April–September).</p>
2. Sports Incident	<p>2.1. Projectile-human impact, PPE worn on target.</p> <p>2.2. Accidental contact.</p> <p>2.3. Single striker.</p> <p>2.4. Remote constraints on target (i.e. upper body mass, ground reaction force); no constraints on striker.</p> <p>2.5. Impact with cricket ball (striker) on lateral thigh of batsman (target).</p>
3. Loading Factors	<p>3.1. Striker velocity: up to 34.5 m.s^{-1} (77.1 mph) (90 mph release velocity, with a reported loss of 14.3% before batsman (Penrose <i>et al.</i>, 1976)); target velocity: stationary.</p> <p>3.2. Assumed normal impact.</p> <p>3.3. Spherical ball ($72 \pm 2 \text{ mm}$ diameter) with approx. 2 mm elevated seam.</p> <p>3.4. Synthetic cricket trousers worn over thigh guard; ball coated with lacquer, both striker and target surfaces generally free from contaminate. (<i>Unknown: Surface Properties</i>).</p> <p>3.5. Ball mass: 0.155 - 0.163 kg, ball moment of inertia, approx. $3.3 \times 10^{-4} \text{ kg.m}^2$.</p> <p>3.6. Ball typically constructed from a bound cork core with a leather exterior; 69 MPa bulk modulus; 41 MPa instantaneous shear modulus (Kant <i>et al.</i>, 2013).</p> <p>3.7. Ball freely constrained.</p>
4. Load Transfer Factors	<p>4.1. Target segment mass: $8.4 \pm 0.9 \text{ kg}$ (Petersen <i>et al.</i>, 2010) [scaling factor of 0.1 used to determine thigh segment mass (Winter, 1990)]; moment of inertia: 0.169 kg.m^2.</p> <p>4.2. Segment length: $0.44 \pm 0.04 \text{ m}$ (Petersen <i>et al.</i>, 2010) [scaling factor of 0.245 used to determine thigh segment length (Winter, 1990)].</p> <p>4.3. Material Properties</p> <p>4.3.1. Relaxed muscle, not expecting impact.</p> <p>4.3.2. Human thigh segment stiffness values (§2.3.2) with PPE approx. 15mm thick foam [e.g. EVA, $E = 0.2 \text{ MPa}$; $\rho = 150 - 250 \text{ kg.m}^{-3}$ (Mills <i>et al.</i>, 2003)].</p> <p>4.4. Physical location of target on impact in free space.</p> <p>4.5. 3 DOF at hip joint (abduction-adduction, F-E rotation, L-M rotation).</p> <p>4.6. <i>Unknown: internal friction and lubrication.</i></p>
5. Response Phenomena	<p>5.1. Impact duration.</p> <p>5.2. Displacement of skin, adipose and muscle tissues.</p> <p>5.3. Global velocity of thigh segment.</p> <p>5.5. Peak acceleration of the segment on impact.</p> <p>5.6. Transient shock force through segment on impact.</p> <p>5.8. Physiological tendon reflex on impact.</p>
6. Overload Thresholds Exceeded?	<p>6.1. Compressive and tensile stresses and strains at: skin, subcutaneous tissue, vascular tissue, nerves and muscular tissue and bone.</p> <p>6.3. Shear stresses on skin, adipose and underlying muscle tissue.</p> <p>6.5. Increased age reduces mechanical tissue strength and increases predisposition. Repeat injury sites more susceptible.</p>
7. Injury	<p>7.1. Muscle contusions.</p> <p>7.4. Lacerations.</p>

Table 3.3 - Basketball knee impact injury scenario model.

	Knee impact - basketball knee impact to the thigh from offensive player when driving to the basket
1. Sports Activity	<p>1.1. Non-contact sport, frequent accidental contact sustained between opposition players in gameplay.</p> <p>1.2. 0.62 kg inflated ball used as only playing object, indoor courts, 28.65 m × 15.24 m with 0.46 m diameter hoops suspended 3.05 m from the ground at either end.</p> <p>1.3. Typical professional game play consists of 4 × 12 min quarters.</p> <p>1.4. Single-sex sport played by males and females separately.</p> <p>1.5. Team sport, five players on court at any one time.</p> <p>1.6. Most popular US team sport, professional basketball played between October and June, 3-4 games per week.</p> <p>1.7. High intensity, fast-paced, physical sport.</p> <p>1.8. Players can intentionally position themselves to receive contact in order to draw contact fouls from the opposition.</p>
2. Sports Incident	<p>2.1. Human-human impact, PPE worn on the upper leg region of the target body.</p> <p>2.2. Accidental contact.</p> <p>2.3. Single striker.</p> <p>2.4. Target commonly grounded, striker driven into target.</p> <p>2.5. Impact from the offensive player’s knee to the anterior or lateral thigh of the target player.</p>
3. Loading Factors	<p>3.1. <i>Unknown: striker velocity</i>; target velocity: stationary.</p> <p>3.2. Frontal impact, striker and target assumed normal on impact.</p> <p>3.3. Striker geometry: patella bone, 50 mm diameter, 37.5 mm radius of curvature (Osterhoff <i>et al.</i>, 2007); target geometry: human thigh segment.</p> <p>3.4. Striker surface: bare human skin; target surface: synthetic shorts worn over thigh PPE; <i>Unknown: surface properties.</i></p> <p>3.5. <i>Unknown: Effective mass and inertial properties in knee impact.</i></p> <p>3.6. Patella stiffness governed by cortical bone (§2.3.2.d).</p> <p>3.7. Six DOF at knee through: F-E rotation, internal-external (I-E) rotation and A-P translation.</p>
4. Load Transfer Factors	<p>4.1. Target segment mass: 10 kg (NBA, 2007) [scaling factor of 0.1 used to determine thigh segment mass (Winter, 1990)]; moment of inertia: 0.25 kg.m².</p> <p>4.2. Segment length: 0.49 m (NBA, 2014) [scaling factor of 0.245 used to determine thigh segment length (Winter, 1990)].</p> <p>4.3. Material properties</p> <p style="padding-left: 20px;">4.3.1. Relaxed muscle, not expecting impact.</p> <p style="padding-left: 20px;">4.3.2. Human thigh mechanical response (§2.3.2) with PPE typically an array of foam cylinders, ~ 10 mm thick foam [e.g. Ethylene-vinyl acetate (EVA), $E = 0.2$ MPa; $\rho = 150 - 250$ kg.m⁻³ (Mills <i>et al.</i>, 2003)].</p> <p>4.4. Impact typically in free space though possibility of other players influencing.</p> <p>4.5. 3 DOF at hip joint (abduction-adduction, flexion-extension (F-E) rotation, L-M rotation).</p> <p>4.6. <i>Unknown: internal friction and lubrication.</i></p>
5. Response Phenomena	<p>5.1. Impact duration.</p> <p>5.2. Tissue displacement of skin, adipose and muscle tissues.</p> <p>5.3. Resultant velocity of thigh segment.</p> <p>5.4. Displacements of tendons and ligaments and hip and knee joints.</p> <p>5.8. Physiological tendon reflex on impact.</p>
6. Overload Thresholds Exceeded?	<p>6.1. Compressive and tensile stresses and strains at: skin, subcutaneous tissue, vascular tissue, nerves, muscular tissue and femur bone.</p> <p>6.2. Tensile stresses on ligaments and tendons at the knee and hip joints.</p> <p>6.3. Shear stresses and strains at: skin, subcutaneous tissue and muscle tissues.</p> <p>6.5. Increased age reduces mechanical tissue strength and increases predisposition. Repeat injury sites more susceptible.</p>
7. Injury	<p>7.1. Muscle contusions.</p> <p>7.3. Joint subluxations, dislocations.</p> <p>7.4. Lacerations.</p> <p>7.9. Strains/sprains remote from impact.</p>

3.4.2. Experimental Protocol Development for Controlled Scenario Reproduction

To further investigate particular elements relating to a specific injury it may be necessary to recreate the injury event experimentally. This can be achieved through: laboratory reconstructions, human gameplay scenarios or virtual simulations. The DCS model can be used as a checklist for factors to approximate, control and measure; assessing each individual element sequentially to define a complete list of full protocol specification.

- Approximations are factors that can or must be simplified to make testing feasible. It is important to identify fully which factors are being approximated, the reasons for their approximation and the likely outcomes of the decisions made.
- Control factors are those often relevant to the experiment but cause unnecessary complications or confusing variations if included.
- Factors to measure are the dependent variables of the experiment.

A cross-tabulation of the influencing factors model (Table 3.1) has been employed with the headings: approximations, controls and measures to provide a framework from which each element can be categorically assessed.

The scenario definition for the basketball knee-on-thigh impact (Table 3.3) highlighted that there were some unknown factors influencing the likelihood of injury, in particular loading factors which must be better understood. Due to inter-individual variability associated with human impacts, it was difficult to approximate both the anticipated effective mass and velocities involved in the basketball knee impact. Further experimental characterisation was required to more closely define specific impact kinematics resulting from this type of gameplay scenario.

Halkon *et al.* (2014) performed a game play reconstruction of the basketball knee-on-thigh impact scenario to determine appropriate effective masses and velocities involved for mechanical approximations. Following testing of elite basketball players in a laboratory environment, it was determined that a 2.8 kg rigid mass provided the most comparable pressure profiles to the player tests. It was also recorded that players impacted at velocities up to 5 m.s⁻¹.

3.5. Specification for Improved Sports Impact Assessments

The DCS model has been used to provide detailed descriptions of the cricket ball and knee impact scenarios to the thigh region (Table 3.2, Table 3.3). Given this information, a specification for an improved sports impact assessment can be generated addressing each of the individual components.

3.5.1. Target Surrogate

The target surrogate in these impact scenarios is the thigh component and as such should provide a representation of the tissue structures and morphologies present in the body segment. Given the complexity of the human body, it is necessary to abstract appropriate simplifications to make simulations and synthetic surrogate manufacture, cost effective and worthwhile. Consequently, the purpose of target surrogate research in this investigation is to establish the cost-benefit of adopting increased levels of human complexity.

The only previous study investigating sports impacts to the thigh region using human surrogates was by Hrysomallis (2009) (§2.4.1.a). Therefore, the fundamental requirement for improved target thigh surrogates are that they exhibit superior biofidelity to the Hrysomallis model without significantly increased cost.

3.5.2. Striker Surrogate

The striker surrogate differs between impact scenarios. However, both impacts are from objects that can, in a simplified view, be considered to be rigid due to the relative differences in stiffness between the impactor (patella and cricket ball) and target human soft tissues. The cricket ball and knee impactor were simplified to 72 mm diameter hemispherical geometries with total masses of 0.16 kg and 3 kg respectively.

3.5.3. Levels of Constraint

The target thigh surrogate should permit representative DOF at both the knee and hip joints to ensure biofidelic body kinematics are exhibited. The target surrogate constraints should be representative of the intended game play scenarios and simulate the braced (foot planted) behaviour of the target in both the cricket ball and knee impact scenarios. For increased gameplay fidelity, the striker surrogate should remain unconstrained and free to recoil in any direction following impact.

3.5.4. Impact Parameters

The two impact types were selected due to their different strain rate loading conditions, which can elicit varied material behaviour in non-linear strain rate dependent materials. This can provide a more comprehensive understanding of surrogate behaviour. The cricket ball and knee impact approximations were given 10 m.s^{-1} and 3 m.s^{-1} velocities respectively. These velocities are a conservative estimation of those that may be experienced in gameplay scenarios but are believed to be of sufficient intensity enough to provide a realistic description of surrogate performance. Conservative velocities also aid in the development of synthetic laboratory reconstructions as increased velocities may be challenging to attain. In addition, at reduced velocities, a greater stability can be achieved in finite element algorithms, which aids in the accuracy and computational cost of solutions.

3.5.5. Methods of Assessment/Evaluation Criteria

In both scenario definitions, blunt trauma contusions and lacerations were identified as the main injury outcomes likely to be sustained. The causal factors for both injuries have been explored in §2.2.2. Current literature suggests that localised pressures are the indirect mechanical phenomena causing injury with mechanical strain in the tissues representing the direct injury mechanism. Therefore, a measure of the mechanical pressure and tissue strain are important to assess the potential of injury to the target surrogate and consequently represent key metrics to evaluate the levels of protection afforded by PPE.

3.6. Target Surrogate Research Approach

The DCS model informed a series of requirements for improved sports impact assessments. The target surrogate component represents a key element of the assessments that requires particular consideration. The parallel development of synthetic and computational sports impact surrogates has been adopted as the chosen development approach. Incremental progressions from current safety standards of PPE assessment are necessary to improve knowledge of both human impact response and PPE effectiveness and make steps to more complex, biofidelic surrogates. The continual development of mutually validated surrogates can act as complimentary diagnostic tools to enable greater understanding of each individual approach and informed decision-making when developing more complex surrogates. For each stage of surrogate complexity, three key elements have been identified as being integral to the success of an impact surrogate: the anatomical simplifications, materials and evaluation metrics.

3.6.1. Anatomical Simplifications

The selection of appropriate anatomical simplifications pertains to both the diversity of tissue structures modelled and the anatomical complexity of the geometries used. Using FE models as a design tool, the relative differences in surrogate response to changes in each of these variables can be explored. This can inform the levels of complexity at which appreciable differences in response are attained and can prevent engineering of unnecessarily complex surrogates.

3.6.2. Materials

The simulant materials used in surrogates are fundamental to their mechanical response. There are many tissue structures that contribute to the *in vivo* mechanical response of the human thigh (§2.3.2); however, existing sports impact surrogates typically only consider single soft tissue simulants to represent all tissues in the segment. It is unknown as to whether this is an acceptable approximation or if significant mechanical phenomena are overlooked through this approach.

To effectively mimic organic tissue mechanical behaviour using synthetic simulant materials, a thorough consideration of the mechanical properties associated with each tissue is necessary (§2.3.2). A further related aspect of this research pertains to the application of constitutive material models for the simulant materials to describe their mechanical behaviour and FE simulations to predict their impact response.

3.6.3. Evaluation Metrics

To effectively assess surrogate response to impact, a consistent set of evaluation metrics relevant to blunt trauma sports injuries are necessary. In a synthetic surrogate, embedded instrumentation has been used previously to provide a measure of the response phenomena experienced at a specific point in the surrogate. The instrumentation generally offers a partial performance assessment and can introduce artificial stress concentrations affecting the biofidelity of the surrogate. Computational models present a method of studying complex mechanical interactions without introducing artificial foreign bodies and can provide a more continuous description of tissue behaviour (e.g. stress profiles).

The development of FE models, validated against experimental data, can provide sufficient confidence in the accuracy of solutions and better inform the mechanical phenomena experienced within the surrogate from a given impact stimulus.

3.6.4. Surrogate Development Work Flow

Given the key surrogate design elements identified, a surrogate development approach has been formulated showing the workflow and interactions linking each element to the improved anatomical surrogates (Fig. 3.5).

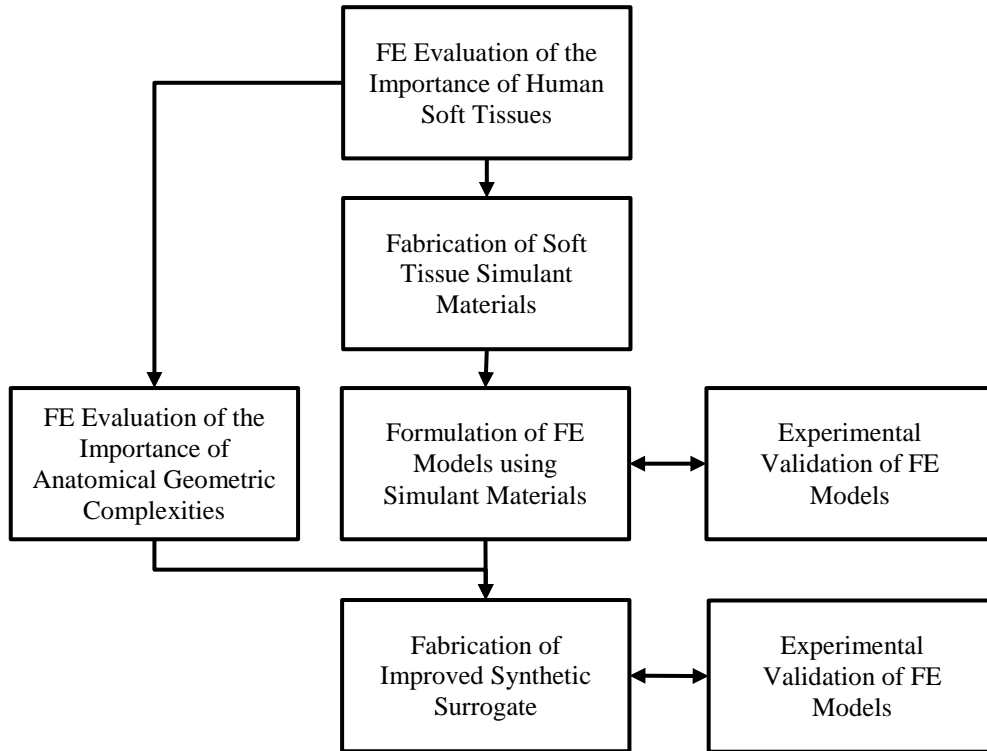


Figure 3.5 - Surrogate development approach.

Chapter 4 - Determining the Effects of Anatomical Simplifications in a Soft Tissue Surrogate using FEA Methods

4.1. Chapter Overview

Chapter 4 presents an investigation, using FE modelling techniques, into the importance of a multi-material surrogate. The model formulations adopted to simulate any sports impacts on human surrogates have been outlined in a simplified cylindrical geometry including: mesh descriptions, material models and contact definitions. The organic tissue properties obtained from previous *in vitro* mechanical tests in the literature were used to approximate predicted human impact behaviour. The importance of skin and adipose tissue layers on surrogate impact response were then demonstrated through simulations of cricket ball and knee impacts.

4.2. Introduction

The anatomical structures present in the human thigh region have been described in §2.3.1. In human surrogates, it is often considered desirable to attempt a full musculoskeletal representation of the target body region embodying all tissue structures as this is assumed to achieve a greater biofidelity. However, the additional complexity is introduced at a cost. In synthetic surrogates, this can be in the form of manufacturing difficulty, manufacturing time, facilities and expense; whilst in virtual models, this can be in the form of model development time, analysis run time, software capabilities and operator expertise. Furthermore, Robinson *et al.* (2008) also stated that simple models are more flexible, require less data to formulate and the results are easier to interpret. Consequently, many researchers turn to volume data to approximate the net effects of groups of tissue structures (Teran *et al.*, 2005).

Given a particular research question, assuming high levels of complexity are needed to adequately resolve the issue can result in unnecessarily high cost-benefit ratios. Incremental development of increasingly complex solutions, evaluating the benefit at each iteration, allows for solutions with a lower cost-benefit ratio and ensures subsequent iterations are based on a growing knowledge base rather than increasingly large, difficult to prove assumptions.

In the human thigh segment there are many interacting tissue structures, which in some form influence the mechanical response to impact. All of the structures are biological and exhibit a degree of inhomogeneous, non-linear, rate-dependent behaviour. Bone is established as a necessary component integral to provide structural support and stiffness in all human surrogates. Shen *et al.* (2010) noted a significantly increased stiffness in the chest wall due to the presence and proximity of the skeletal tissues. The stiffness of these skeletal structures is well represented by the rigid target anvils used in safety standards.

Surrogates modelling an additional level of tissue complexity have considered both muscle and bone components. Many previous research studies have considered a single off-the-shelf soft tissue simulant material as an acceptable simplification of the overall soft tissue response in durable impact surrogates. Muscle tissue constitutes the bulk of soft tissue in human limbs and accounts for 40 - 50% of human body mass (Wang *et al.*, 1997; Salem *et al.*, 2006). Hrysomallis (2009) developed a two material surrogate with Silastic 3483 (Dow Corning Corporation, Michigan, USA) to match the composite behaviour of all soft tissues in the thigh segment.

A further level of complexity modelled in some sophisticated durable surrogates is the skin tissue. Skin is the outermost layer of tissue on the human body and represents a protective barrier from mechanical trauma and stiff interface surrounding other tissues (Edwards & Marks, 1995; Pailler-Mattei *et al.*, 2008). With the exception of muscle and skeletal tissues, skin represents the largest organ, constituting approximately 5.5% of body mass (Goldsmith, 1990). Ankrah & Mills (2003) used a skin tissue simulant alongside muscle and bone in a lower leg impact surrogate (§2.4.2a). Beyond this, subcutaneous adipose is believed to play an important role in the mechanical impact response of the body segment as a mechanical load absorbing and distributing member that absorbs shock and protects against local stresses (Robbins *et al.*, 1989; Miller-Young *et al.*, 2002; Geerlings *et al.*, 2008; Sims *et al.*, 2010; Comley & Fleck, 2012; Alkhouli *et al.*, 2013).

Although the synthetic human surrogate proposed does not intend to replicate either the vascular or nervous function within the thigh, it is acknowledged that the tissues may affect the mechanical impact response of the surrogate. The simplification of the current surrogate does not consider these components as it is believed that they are not the most significant structures governing the mechanical response and represent an area for future research once more sophisticated surrogates able to show visible injury mechanisms are required.

As an initial simplification it is believed to be acceptable to assume that the mechanical response of large fleshy areas surrounding a bone (e.g. thigh, upper arm, lower leg) are primarily governed by skin, subcutaneous adipose, muscle and bone tissues. When considering the levels of over-simplification potentially introduced through use of a single material simulant, Figure 4.1 shows a quasi-static compressive stress - strain comparison between Silastic 3483 and organic soft tissues (Fig. 4.1).

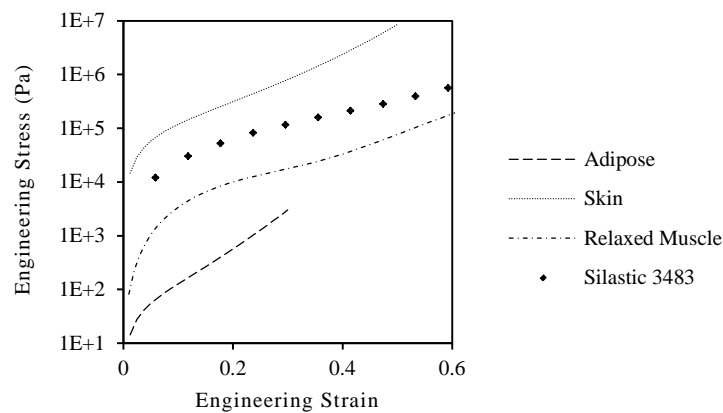


Figure 4.1 – Log-linear stress - strain plot showing the quasi-static compressive response of Silastic 3483 when compared to skin (Shergold *et al.*, 2006), relaxed muscle (Song, 2007; McElhaney 1966), and adipose tissue (Comley & Fleck, 2012).

It is unknown currently, without further analyses, whether such a simplification translates to a difference in overall surrogate response. Though limited data from previous literature suggests that it may, Shen *et al.* (2010) observed that under high strain rate ballistic impacts deformation waves passing through different soft tissue layers varied significantly. It is proposed that there are other mechanical response phenomena and inter-tissue interactions that are ignored through use of a single material surrogate (e.g. relative movement between structures, pressure distribution and deformation of tissues distant from the impact site). The nature of these interactions will generate impact phenomena unrepresentative of those experienced by the human body in sport.

In the human thigh, the muscle compartments have been considered as single homogenous structure. The interactions within and between compartments have been neglected in this approach and represent an area for future research once incremental improvements have been made. Similarly, the fascias supporting the muscles, and the tendons attaching the muscles to the bone have also been ignored in this initial early stage of complexity. Consequently, the individual muscles, fascia and tendon components in the thigh have all been considered as a homogenous muscle component. The internal geometries presented by the nerves and vascular tissues have also been disregarded and considered as homogenous with their surrounding tissue boundaries (Fig. 4.2).

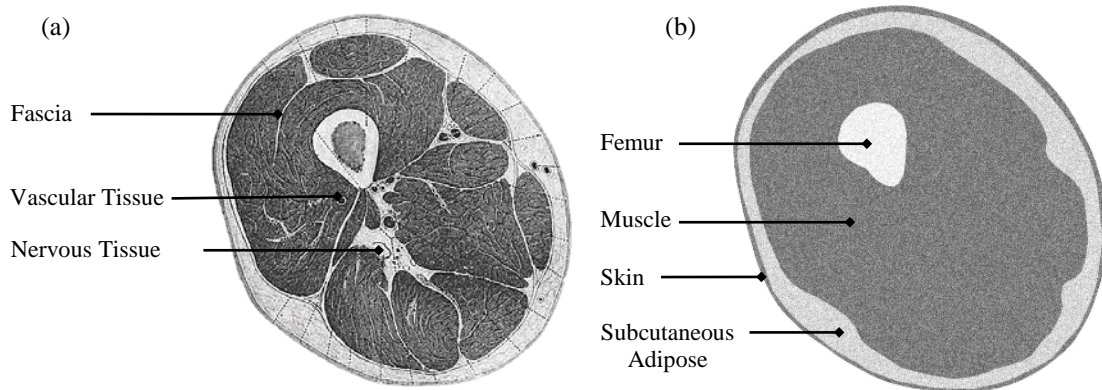


Figure 4.2. (a) Axial plane section through the human thigh showing the diversity of tissue structures (Gray, 1918); (b) Anatomical simplification of the thigh.

4.2.1. Aims and Objectives

- 1) To establish appropriate FE modelling parameters to simulate sports impacts in human surrogates.
 - Selection of appropriate geometric simplifications.
 - Determination of suitable material models.
 - Determination of representative contact conditions.
- 2) To investigate the importance of different human soft tissue layers on the mechanical impact response of a surrogate thigh.

4.3. Computational Modelling Parameters

FE modelling techniques to simulate sports impacts on human surrogates have been established in this chapter. The techniques defined have been applied to specifically investigate the importance of a multi-material soft tissue surrogate. However, their general application transcends the bounds of this particular study and they have been consistently used elsewhere throughout the research.

There are six key components to a FE model: discretised geometries, element section properties, material data, loads and boundary conditions, selection of analysis type and output requests (ABAQUS, 2014). Each of these factors has been examined in §4.3 with supporting literature establishing the basis for the methods.

4.3.1. Selection of Solver Methods

Abaqus FE solver, version 6.13 (Dassault Systèmes Simulia Corp., Providence, RI, USA) was selected as the most suitable, available FE software due to its powerful processing capabilities and reported applications in automotive impact analyses (e.g. Gholami *et al.*, 2003; Ionescu & Wernicke, 2006). It consists of two packages with different solving algorithms:

Abaqus/Standard and Abaqus/Explicit. The selection of the most appropriate algorithm is important for both accuracy and computational cost. Both packages use the same fundamental solving method. The analysis is broken down into a series of incremental load or displacement steps (increments); at the end of each increment, the structure geometry and material response changes and the stiffness matrix is adjusted before the next increment.

In Abaqus/Standard a series of static equilibrium equations must be satisfied at each increment step before the subsequent step is solved. Given a non-linear problem to be solved, Abaqus/Standard uses a series of linear approximations (Newton-Raphson equations) to incrementally determine a solution. Complex mechanical responses that occur due to impact such as large element deformation, highly non-linear material behaviour or contacts between surfaces require a large number of small iterative steps (Harewood & McHugh, 2007). The solver must iterate to satisfy all conditions, which means that contact conditions, force equilibrium and moment equilibrium are satisfied at every node. This results in very small displacement corrections compared to incremental displacements. 3D impact models have a significant number of possible contact points and changing contact conditions which can lead to a large number of iterations per increment and reduced increment size. In Abaqus/Standard, the contacts may also cause local instabilities such as wrinkling increasing the difficulty of achieving contact equilibrium, which can cause convergence issues (Rebelo *et al.*, 1992; Prior, 1994; Sun *et al.*, 2000; Choi *et al.*, 2002).

Abaqus/Explicit was developed to solve dynamic problems involving deformable bodies using wave propagation theory. The solver does not need to resolve equilibrium equations at each increment; the update to the stiffness matrix is performed at the end of each increment based on geometric and material changes. The solution is determined without iterating by explicitly advancing the kinematic state (displacements, velocities and accelerations) from the previous increment (central difference formulas). Accelerations and velocities at particular point in time are assumed constant during time increments and used to solve for the next point in time (Harewood & McHugh, 2007). The solver performs analyses using a large number of small, computationally inexpensive time increments. If the increments are sufficiently small the results will be accurate; however, if they are too small, increments can be time consuming. This makes Abaqus/Standard the preferable choice when the analysis can be performed in relatively few time increments such as solving smooth linear problems (Harewood & McHugh, 2007). The Standard solver can analyse static and quasi-static events easily as it is unconditionally stable with respect to the size of the time increment (Prior, 1994; Sun *et al.*, 2000).

Explicit solutions are only conditionally stable. The stability limit for an Explicit analysis is dependent on the stable time increment, which is the minimum time that a dilatational wave takes to move across any element in the mesh (Sun *et al.*, 2000) and is given by Equation (4.1) (ABAQUS, 2014).

$$\Delta t = \min\left(\frac{L^e}{c_d}\right) \quad (4.1)$$

Where: L^e is a characteristic element length and c_d is the dilatational wave speed of the material.

Explicit analyses are advantageous when analysing large 3D contact problems (Prior, 1994). The size of the time increment is only dependent on element dimensions and material properties not the complexity of analysis (Harewood & McHugh, 2007). The solution time is therefore generally not affected by complex contact conditions (e.g. local wrinkling instabilities does not increase run time) and therefore is better suited than Abaqus/Standard for analysing complex non-linear problems (Prior, 1994). Sun *et al.* (2000) noted that the CPU cost for an Abaqus/Explicit analysis was 1/10th of the cost of Abaqus/Standard when considering an impact problem involving an elastic cylindrical disk against a rigid wall.

In summary, Abaqus/Explicit provides a superior method for solving transient dynamic impact events with wave propagation analysis and complex contact conditions pertinent to sports impact scenarios. The non-linear, rate dependent nature of both organic tissues and elastomer materials also lends itself to the Explicit solver.

4.3.2. Geometries

The VHP (U.S National Library of Medicine) was used as a reference dataset to establish the required anthropometric parameters for the surrogate thigh (§2.4.2.a). The VHP in an online database of axial CT transverse plane scans at 1 mm intervals from a white, 38 year old, 90.2 kg, 180 cm male of US origin taken shortly after death (Spitzer *et al.* 1996).

To generate the required 3D volumetric geometries, data points from the cross-sectional images were first extracted in image processing software to provide tissue boundaries representative of the three major soft tissue structures (Fig 4.2). Images were used at regular intervals on the femur, in locations where other skeletal structures (i.e. the pelvis and patella) were not present in the soft tissue. The data points were then used to determine the proximity of each tissue boundary to the bone centroid (Fig. 4.3).

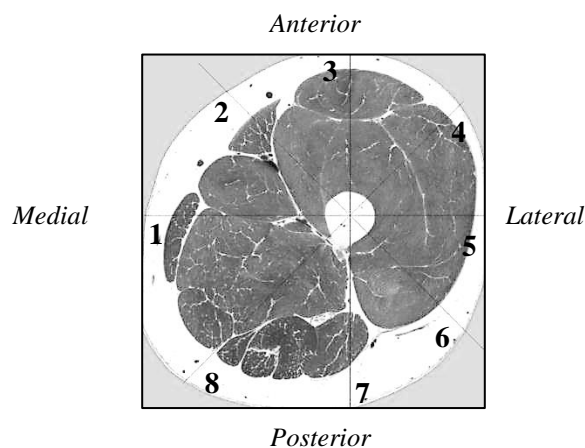


Figure 4.3 – Image showing separation lines from bone centroid (Reproduced courtesy of EPFL, Visible Human Visualization Software, <http://visiblehuman.epfl.ch> and Gold Standard Multimedia (GSM) www.gsm.org).

The proximities of each tissue boundary to the bone centroid have been presented in Table 4.1.

Table 4.1 – Measurements from the VHP human thigh (mm).

	Distance to Bone Outer Boundary			Distance to Adipose Outer Boundary			Distance to Skin Outer Boundary		
	Max.	Min.	Mean	Max.	Min.	Mean	Max.	Min.	Mean
<i>Slice 1 (84 mm superior to distal femur)</i>	20.3	12.5	16.2	69.1	50.5	41.8	80.3	46.0	59.7
<i>Slice 2 (156 mm superior to distal femur)</i>	17.3	11.4	13.8	81.3	49.4	62.2	91.4	56.1	69.3
<i>Slice 3 (222 mm superior to distal femur)</i>	14.4	11.4	12.6	93.0	56.8	70.8	104.9	64.4	79.1
<i>Slice 4 (294 mm superior to distal femur)</i>	15.0	11.8	12.7	96.3	62.3	76.1	116.9	67.1	88.5
<i>Slice 5 (360 mm superior to distal femur)</i>	14.4	8.74	12.6	90.6	44.9	72.4	99.9	67.0	88.9
Mean	16.3	11.2	13.6	86.1	52.8	64.7	98.7	60.1	77.1

The geometries used in impact surrogates have been acknowledged to influence their impact response (§3.6.1). A range of geometries have been examined within this research study (puck, shaped anvil, cylinder and anatomically contoured thigh). Initially, to assess the importance of a multi-material surrogate, a cylindrical geometry was selected (Fig. 4.4). Cylindrical geometries have been used previously in human impact surrogates (e.g. Hrysonallis, 2009) and are believed to provide an approximate representation of segment morphologies. The modelling parameters and contact definitions presented in this chapter, unless otherwise stated, are consistent with those used in all other FE impact investigations.

The cylinder was given a length of 276 mm as it represents the largest fleshy area visible on the VHP scans where there were no other conflicting skeletal tissues (e.g. pelvis or patella bones). This was also of sufficient length to reduce potential issues introduced by edge effects from the 72 mm diameter impactor. The mean distance from the bone centroid to the outer tissue was 77.1 mm and the mean adipose tissue thickness was 12.4 mm. These dimensions were simplified to 75 mm and 12 mm for the skin outer radius and adipose tissue thickness respectively. The skin was given a uniform thickness of 3 mm inferred from the VHP images and previous thicknesses used in impact surrogates (Manning, 2007). This is consistent with measurements from previous studies which have reported the thickness of the skin layer in the thigh to be between 0.9 - 3.3 mm (Akkus *et al.*, 2012; Jain, 2013; Derraik *et al.*, 2014); though this may represent a slightly increased thickness for some demographic group (e.g. subjects with body mass index (BMI) less than 25) (Akkus *et al.*, 2012). The cylinder surrogate was constrained in all translational axes at the ends of the bone using a boundary condition.

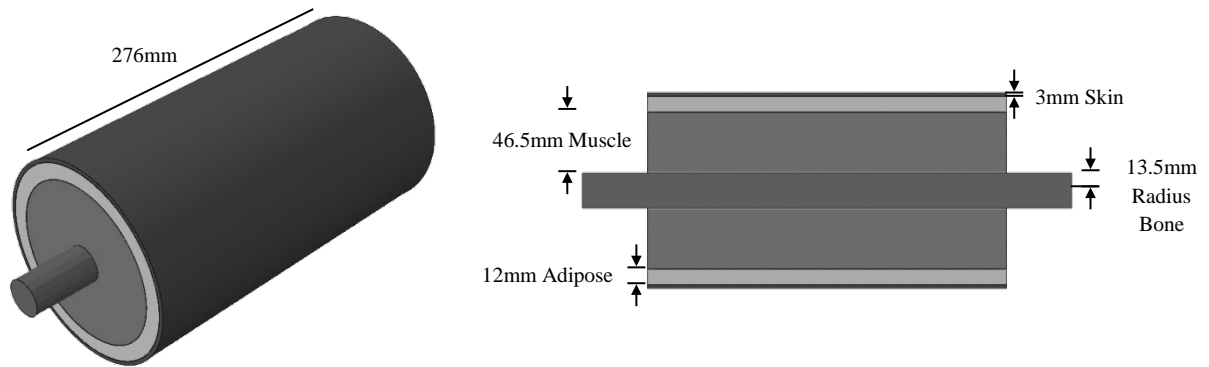


Figure 4.4 – Cylinder surrogate geometry and sagittal plane section.

4.3.3. Material Models

a) Mechanical Properties of Organic Tissues

As an initial point of comparison, the organic tissue properties of skin, adipose, muscle and bone adapted from previous research studies have been used to show an idealised surrogate response and the potential benefits of multi-material approaches.

Given the large degree of variation in organic tissue properties between characterisation studies based on the specimen type and nature of mechanical loading, it is clear that there is no consensus on the definitive structural response (§2.3.2). Therefore, it is to be noted that in this study a single absolute representative dataset has been selected for each tissue structure. The mechanical properties of all organic tissues were attained from uniaxial compression tests in the cross-fibre direction as this is most pertinent to blunt force trauma in the thigh region.

In organic structures, both skin and muscle tissues exhibit significant anisotropy, whilst adipose tissues have been reported as practically isotropic when subject to most loading conditions. The compressibility of skin (Ní Annaidh *et al.*, 2012; Wu *et al.*, 2003) and muscle tissues (Van Looke *et al.*, 2009; Böl *et al.*, 2012) are low and thus have Poisson's ratios of approximately 0.5 whilst adipose tissue is considered to be significantly more compressible and has a Poisson's ratio approximately 0.38 (Van Houten *et al.*, 2003), undergoing non-recoverable deformations (Patel *et al.*, 2005; Sims *et al.*, 2010). For simplicity and as an intermediate step in anticipation of the use of superior anisotropic material definitions in the future (when adequately researched), the tissues have been considered as incompressible and isotropic, with the response in all directions governed by the data from characterisation studies measured perpendicular to the fibres. Approximating the behaviour of these anisotropic organic materials with tailored isotropic ones should yield useful results when the anticipated loading of the subsequent soft tissue simulant corresponds with the characterisation conditions for the organic tissue (e.g. normal blunt trauma impacts to fleshy regions).

Compressive engineering stress - strain data from Shergold *et al.* (2006) and Comley & Fleck (2012) were selected to represent skin and adipose tissues respectively (Fig. 2.8, Fig. 2.9). Compressive datasets from Song *et al.* (2007) and McElhaney (1966) conducted in cross-fibre direction were selected to represent relaxed muscle (Fig. 2.10). Their responses recorded in the overlapping strain ranges at both quasi-static and intermediate strain rate ($100 - 540 \text{ s}^{-1}$) ranges are nearly coincident and were consequently combined to provide a wider strain range. With no definitive data to inform the effects of muscle contraction, the mechanical response of contracted muscle was estimated through scaling of relaxed muscle engineering stresses by a uniform scaling

factor of $4.2 \times$ (Zheng *et al.*, 1999). In the first instance, however, relaxed muscle tissue properties were selected for the cylinder surrogate as a priority since impact injuries are believed to be both more prevalent and serious when the participant is not anticipating the impact (Conforti, 2013). Muggenthaler *et al.* (2008) also suggested that the human monosynaptic stretch reflexes occur between 30 - 60 ms such that, in the majority of sports impacts, the most severe compressive stage is likely to have occurred before the body actively responds.

Due to the dynamic nature of sports impacts, it is necessary to consider the mechanical properties of organic tissues under representative strain rates. A simple theoretical calculation of the strain rates of interest has been performed assuming a soft tissue thickness of 62 mm and no slowing of the impactor. Considering the knee (3 m.s^{-1}) cricket ball (35 m.s^{-1}) impacts, strain rates of between 48.5 s^{-1} and 564 s^{-1} were calculated. Data from compressive experiments at intermediate strain rates have been provided and shown in Figure 4.5. Due to a paucity of information on the mechanical behaviour of organic tissues at increased strain rates, unmatched strain rate material properties are an issue and as such the mechanical responses must be inferred from the banded strain rate responses given.

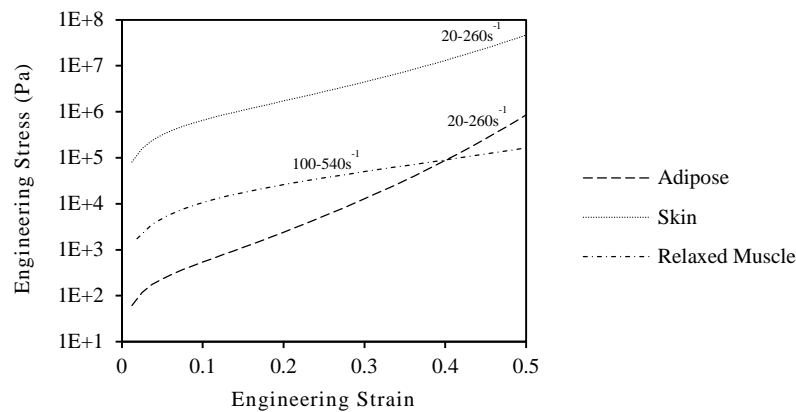


Figure 4.5 – Log-linear intermediate strain rate properties of: skin (Shergold *et al.*, 2006), adipose (Comley & Fleck, 2012) and relaxed muscle (McElhaney, 1966; Song *et al.*, 2007).

The mechanical properties of bone were also adapted from a quasi-static compressive experiment conducted by McElhaney (1966) on cortical bone. Cortical bone is significantly stiffer than trabecular bone (Rho *et al.*, 1993) and it is believed that this constitutes a more significant part of the overall tissue response and it was therefore used as an initial simplification (§2.3.2.d). The densities of each tissue structure have been detailed in Table 4.2.

Table 4.2 – Densities of organic tissues (kg.m^{-3}).

Skin	1100 (Sarvazyan <i>et al.</i> , 1998)
Adipose	920 (Fidanza <i>et al.</i> , 1954; Farvid, 2005)
Relaxed Muscle	1110 (Mendez & Keys, 1960; Ward & Lieber, 2005)
Cortical Bone	1880 (Yeni <i>et al.</i> , 1998)

b) Constitutive Material Models

The primary goal of any material model is to describe the multi-dimensional material behaviour based on material constants derived from simpler tests (Krstic, 2002). FE modelling is a powerful tool to analyse non-linear, rate dependent, viscoelastic materials that cannot easily be calculated theoretically (Kaliske *et al.*, 2001). The selection of a good material model and determination of appropriate parameters have a great influence on accuracy and reliability of results (Ghoreishy, 2012). Organic tissues, similar to elastomers, exhibit, amongst other behaviour, both an elastic and viscous resistance to deformation as the materials retain the recoverable strain energy partially but dissipate energy if the deformation is maintained. Consequently combinations of hyperelastic and viscoelastic models are needed to represent the non-linear and time dependant behaviours of the materials.

(i) Hyperelastic

Constitutive hyperelastic models follow either phenomenological or micromechanical approaches. Micromechanical models are based on the assumption that changes of free energy are entropic in nature. These models have been considered to be unsuitable for describing the constitutive behaviour of elastomers as the principal source of free energy is due to internal energy as opposed to entropy (Shergold *et al.*, 2006). Phenomenological models are based on the strain energy density of the material, the mechanical behaviour of elastomers and organic tissues are largely determined by their elastic energy and as such provide good material fits.

Considering phenomenological models, the mechanical behaviour of hyperelastic materials can be described in terms of a strain energy function based on the strain invariants I_1, I_2, I_3 (Equation (4.2)).

$$W = f(I_1, I_2, I_3) \quad (4.2)$$

Compressive data has been solely used as the basis to describe the mechanical response of organic tissues; therefore, it is widely suggested that lower order models ($N \leq 3$) provide a more accurate description of the material behaviour. Shergold *et al.* (2006) and Comley & Fleck (2012) proposed single term first-order Ogden models to describe the mechanical response of skin and adipose tissues (Table 4.3). The Ogden model (Ogden, 1972) is a commonly used hyperelastic model to describe the material behaviour of soft solids that are both isotropic and incompressible (up to 700% strain). The model proposes that the strain energy function (W) is based on the principal stretches ($\lambda_1, \lambda_2, \lambda_3$), with μ describing the shear behaviour and α describing the strain hardening. A first order Ogden model is represented in Equation (4.3).

$$W = \frac{2\mu}{\alpha^2} (\bar{\lambda}_1^{\alpha} + \bar{\lambda}_2^{\alpha} + \bar{\lambda}_3^{\alpha} - 3) \quad (4.3)$$

Table 4.3 - First order Ogden model coefficients for skin and adipose tissues (Comley & Fleck, 2012).

	μ		
	$0 - 10 \text{ s}^{-1}$	$20 - 260 \text{ s}^{-1}$	$1000 - 5700 \text{ s}^{-1}$
Skin ($\alpha = 12$)	4.00×10^5	2.20×10^6	7.50×10^6
Adipose ($\alpha = 23$)	4.00×10^2	1.70×10^3	1.10×10^6

A first-order Ogden model was also generated for relaxed muscle and cortical bone tissues using the least squares method with the automated coefficient generator in Abaqus/Explicit using raw compressive stress - strain data attained from Figure 4.5 (Table 4.4).

Table 4.4 – First order Ogden model coefficients for relaxed muscle (McElhaney, 1966; Song *et al.*, 2007) and cortical bone (McElhaney, 1966).

	μ	α
<i>Relaxed Muscle (100 - 540 s⁻¹)</i>	3.63×10^4	4.5
<i>Cortical Bone (0.4 s⁻¹)</i>	4.58×10^9	25

(ii) Viscoelastic

A generalised Maxwell model, known as the Prony series (Tschoegl, 1989), has been used to model the viscoelastic properties of the organic tissues. The Prony series expansion (Equation (4.4)) describes a series of Maxwell models in parallel with a single spring element and considers the relaxation of the materials through a series of time intervals. A time dependant Prony series was employed, which is based on changes in the shear and bulk modulus over time and consists of two stress terms: deviatoric and volumetric related to the shear and bulk moduli respectively.

$$G(t) = E_{\infty} + \sum_{i=1}^n E_i e^{-t/\tau_i} \quad (4.4)$$

The force-time data from stress relaxation tests in previous research studies were manipulated to determine the compressive stresses, $\sigma(t)$ at each time interval. The stresses were normalised from the point of maximal stress and used to determine the shear modulus parameter $g(t)$. The materials are assumed to be incompressible and as such the bulk modulus parameter, $k(t)$ is considered to equal zero. The viscoelastic properties of organic soft tissues have been presented in the form of a Prony Series (Table 4.5) for skin (Wu *et al.*, 2003); adipose (Gefen & Haberman, 2007) and relaxed muscle (Van Looke *et al.*, 2009).

Table 4.5 - Prony series coefficients for organic tissues (adapted from Wu *et al.* (2003); Gefen & Haberman (2007); Van Looke *et al.* (2009)).

	i	$g(i)$	$k(i)$	$\tau(i)$
<i>Skin</i>	1	5.01×10^1	3.80×10^{-1}	5.73×10^{-1}
	2	4.44×10^{-1}	5.59×10^{-1}	9.47
<i>Adipose</i>	1	1.59×10^{-2}	0.00	7.83×10^{-5}
	2	-7.97×10^{-2}	0.00	1.17×10^{-3}
	3	5.89×10^{-1}	0.00	1.61
	4	1.25×10^{-1}	0.00	7.29×10^1
<i>Relaxed Muscle</i>	1	3.39×10^1	0.00	2.37
	2	2.56×10^{-1}	0.00	7.02×10^1

c) Skin Anisotropy Check

In the human body, skin tissue is in a constant state of biaxial tension and hence acts as a diaphragm type structure. Therefore, it is tempting to neglect the compressive response. However, there are no reproducible studies reporting the mechanical properties of skin under tension at sports relevant strain rates. Shergold *et al.* (2006) conducted a good quality and well-recognised study evaluating the *in vitro* responses of porcine skin in unconfined compressive tests. Given quasi-incompressibility of the tissue, this compressive data also provides an averaged tensile in-plane response. As organic skin is a highly anisotropic tissue, simple FE simulations were performed to determine whether using solely compressive data as the basis for the material model provides an acceptable approximation of actual tensile response. Quasi-static material data from Shergold *et al.* (2006) were used in the model, as there is a greater body of comparable test data at this strain rate. A single element hexagonal cube of 1 mm dimensions was pinned at one corner node and displaced 0.5 mm at the opposite side at a rate of 0.004 s^{-1} (Fig. 4.6).

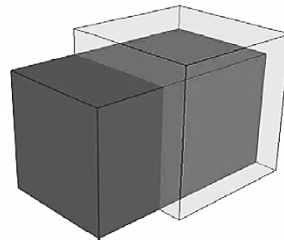


Figure 4.6 – Single element cube in original and deformed state after tensile test.

Figure 4.7 shows the predicted equivalent tensile test behaviour of the Shergold *et al.* (2006) model against previously reported quasi-static tensile data from human (Jansen & Rottier, 1958; Ní Annaidh *et al.*, 2012) and porcine (Ankersen *et al.*, 1999) tests. Experimental responses have been reported as engineering stress and strain to enable a greater ease of comparison with published data. The tensile response of the compressive model exhibits a response within the large reported experimental range and closest to the most recent study conducted on human skin (Ní Annaidh *et al.*, 2012).

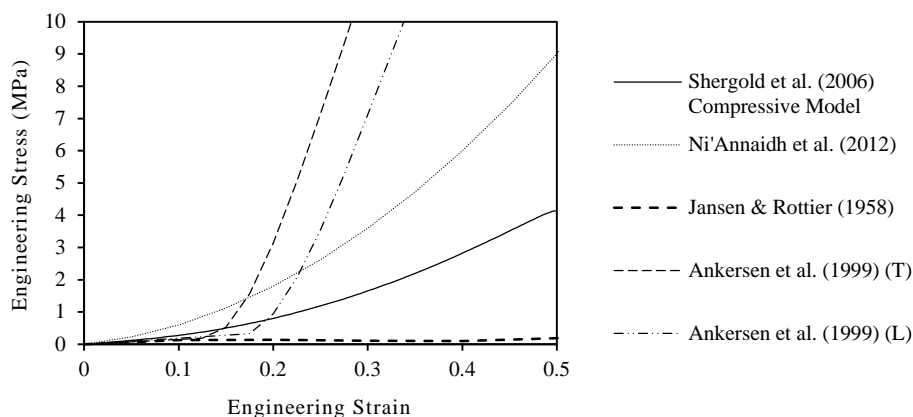


Figure 4.7 - Tensile engineering stress - strain plots showing tensile response of the quasi-static skin tissue compressive material model (Shergold *et al.*, 2006) compared with previous characterisation studies in literature (L - longitudinal; T - transverse).

4.3.4. Model Definition

The formulation of a FE model consists of many integral concurrent components. The meshing techniques, simulation parameters and model definitions used in the development of the surrogate FE model have been detailed in this section.

a) Impact Types

Using the impactor definitions developed previously (§3.5.4), cricket ball and knee impact approximations were modelled (Table 4.6). A simulation time of 40 ms and 20 ms were used for the knee impactor and cricket ball impacts respectively.

Table 4.6 – FE impactor approximations.

	Shape	Diameter (mm)	Mass (kg)	Velocity (m.s ⁻¹)
<i>Cricket Ball</i>	Hemisphere	72	0.16	10
<i>Knee</i>			3.0	3

The impactor was treated as a rigid body due to the large difference in stiffness between the impactor and surrogate soft tissue components and the anticipated small magnitude of displacements in the impactor. The rigid body structure increased the computational efficiency, as no calculations are required at impactor body elements; only the mass densities of the impactor are needed to govern the inertial behaviour.

b) Meshing

(i) Element Types

Abaqus/Explicit elements all use lumped mass formulations and calculate the stiffness and mass of an element at sampling points called integration points (Fig. 4.8). A numerical algorithm is then used to integrate these variables to inform element response. Elements are grouped into families of similar types that perform comparable functions; continuum solid elements and shell elements are two commonly used types with applicability in this research domain (ABAQUS, 2014). The selections of appropriate element types to represent organic soft tissues are a key consideration affecting the model outputs.

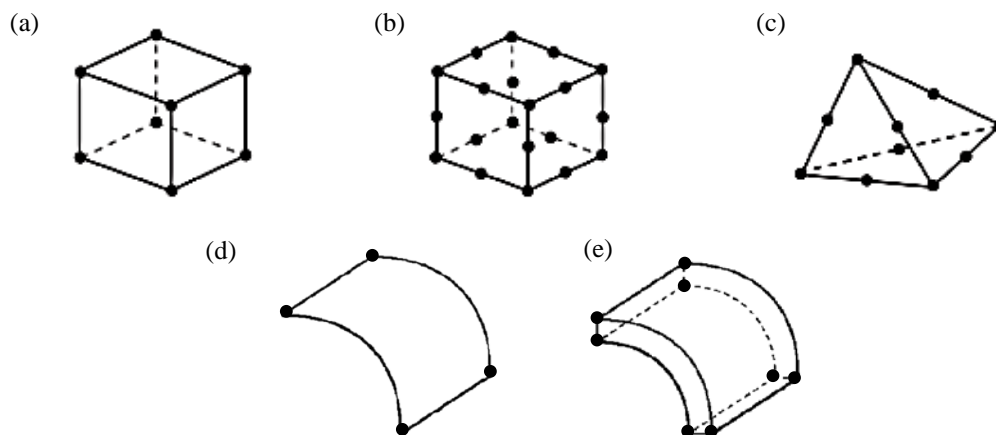


Figure 4.8 - (a) C3D8 linear brick element; (b) C3D20 quadratic brick element; (c) C3D10 second order tetrahedral element; (d) S4 conventional shell element; (e) SC8 continuum shell element (ABAQUS, 2014).

Hexahedral elements are the most widely used continuum solid element and generally provide the best accuracy solution for minimum cost and therefore, in simple geometries, isoparametric hexahedral elements (e.g. C3D8) are commonly relied on (Cifuentes & Kalbag, 1992). Tetrahedral meshes are more versatile and capable of representing complex geometries. They are commonly used where the 3D geometry cannot be decomposed into hexahedral elements; however they can generate an increased computational expense.

Shell elements approximate the behaviour of 3D continuum solids with a two-dimensional surface theory and typically model bending and in-plane deformations computationally efficiently. Two different types of shells are typically used: conventional shells and continuum shells. Conventional shells discretise geometry by a reference surface and have rotational and displacement DOF, and a thickness defined by section properties. Continuum shells discretise an entire 3D geometry of a solid and only have displacement DOF with the element thickness defined by nodal geometries. Continuum shells allow for changes in the thickness of the geometry which are not accounted for by conventional shells and can also provide more accurate impact results as they can represent two sided contacts (Diehl & Carroll, 2000). However, continuum shells are more susceptible to hourglassing and can take significantly more time to solve than comparable conventional shell models (ABAQUS, 2014).

Given the multi-layered approach suggested, the significant tissue bodies (bone, muscle, adipose) are best represented by solid elements as they can model structures without any simplification to geometric, constitutive or loading assumptions. A hexagonal element type has been selected in this instance due to the simplified cylindrical geometries and ease of discretisation without compromising geometric accuracy. Consequently, first-order interpolation C3D8R continuum solid hexagonal brick elements were used due to their low computational cost and high rate of convergence.

The skin layer, however, has a single dimension (thickness), which is significantly smaller than the other two dimensions and could potentially be represented by a shell layer at a lower computational cost than using solid elements. The skin layer was discretised into both solid (C3D8R) and continuum shell (SC8) elements and subject to a cricket ball impact conditions. Significant mesh distortion was observed in the continuum shell layer where the elements behaved overly stiff with areas of isolated high stress concentrations under the high-rate loading conditions (Fig. 4.9).

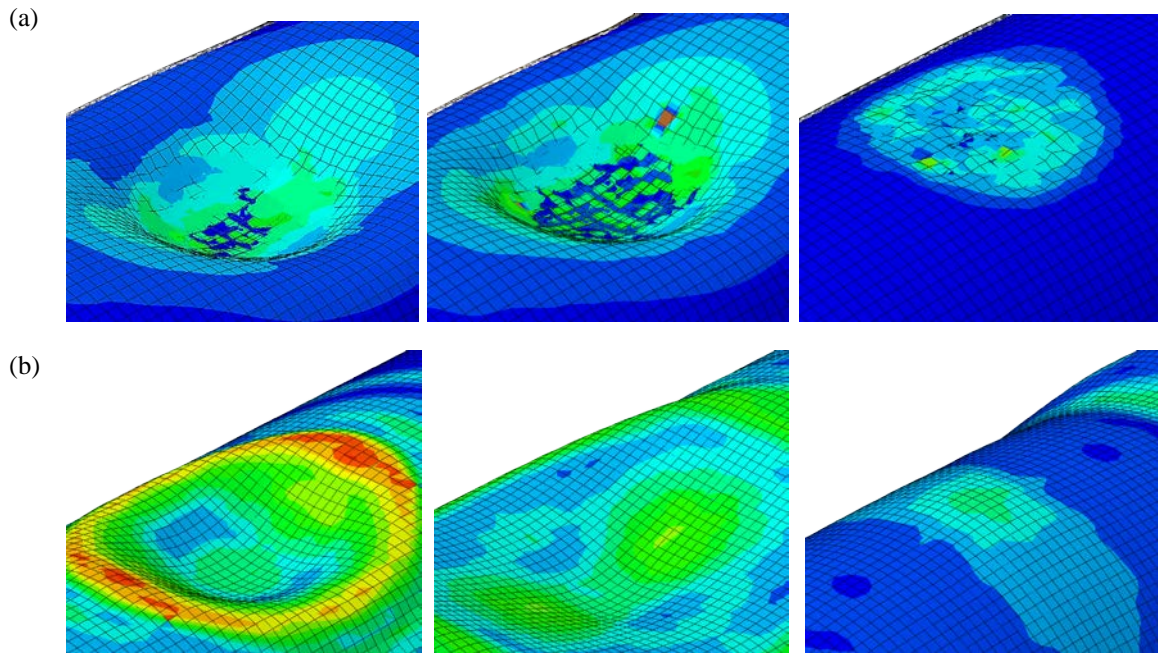


Figure 4.9 – (a) Mesh distortion in continuum shell skin; (b) continuous stress profile in continuum solid element skin.

(ii) Element Attributes

Given the incompressible or near incompressible nature of organic materials, a reduced integration approach was employed to avoid volumetric and shear locking phenomena. Volumetric locking phenomena may be experienced where the requirement for no volumetric change over-constrains the kinematically admissible displacement field and results in artificial mesh stiffness (Joldes *et al.*, 2009). A shear locking phenomena is experienced in elements subject to bending, whereby nonphysical shear strains are detected at the integration points because the element experiences shearing rather than bending due to the element formulation, resulting in overly stiff behaviour (Sun, 2006).

In reduced integration, a reduced number of integration points are used (typically one in first-order elements). Reduced integration is significantly more computationally efficient than full integration and alleviates convergence issues for nearly incompressible materials (Podnos *et al.*, 2012); but may result in hourglassing (Sun, 2006). Hourglassing is a form of mesh instability where an element may deform to a trapezoid shape without changing the position of, or applying strain to, the single integration point leading to inaccuracies in response. With a single element through the thickness, the element experiences deformation but no strain. This has been effectively prevented with at least four elements discretised through the thickness of the section as each element captures, compressive or tensile, axial strains and the overall axial strains are measured correctly (Fig. 4.10). Furthermore, enhanced hourglass control formulations adopted and provide a more robust element, less susceptible to hourglassing.



Figure 4.10 - Four continuum solid elements through skin layer.

Distortion control is a feature of Abaqus/Explicit designed to prevent elements inverting or distorting excessively from large strain gradients or high amounts of compression (Li *et al.*, 2009). It was applied to the very soft adipose tissue layer, as there is a high rate deformation in this layer that can cause excessive deformation and premature material failure. A distortion control of 0.1 was applied to this layer, which restricts the deformation of the elements at 0.9 nominal strain using a penalty function approach. Figure 4.11 shows the deformations of the adipose layer without distortion control present. The solver failed at approximately 1/20th of the step time and significant element distortion and mesh penetration.

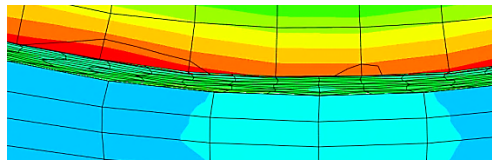


Figure 4.11 - Adipose layer element penetration when no distortion control was applied.

The von Mises stress on the surface of the adipose tissue layer also shows unexpected behaviour: the stresses rapidly increased with the mesh distorting (Fig. 4.12).

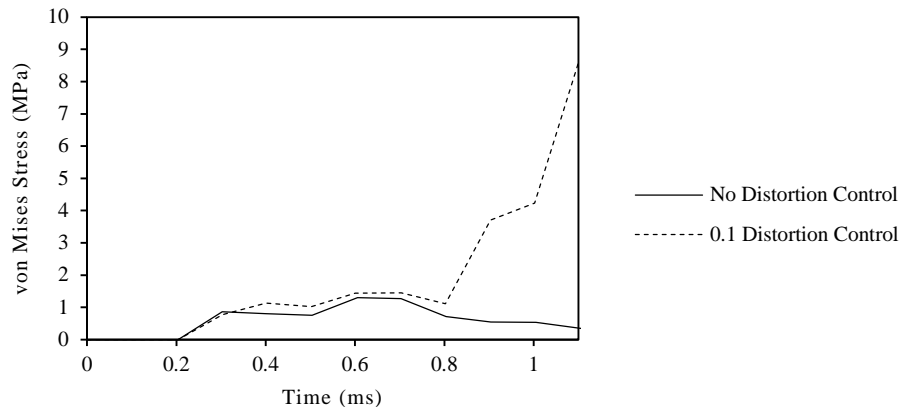


Figure 4.12 - von Mises Stress on the adipose layer surface in models with and without distortion control.

It is noted that care must be taken when interpreting results with this artificial deformation constraint that can inhibit legitimate deformation modes; however in this instance, it is necessary for numerical stability and convergence. As a general rule the kinetic energy of the deforming material should not exceed a small fraction (5 - 10%) of the internal strain energy (Wang *et al.*, 2006). In addition, the energy histories should be smooth so an acceptable solution can be obtained. The relative internal and artificial energies from each simulation type are shown in

Figure 4.13. The higher strain rate cricket ball impact exhibits a significantly higher proportion of artificial energy, however this is necessary to maintain stability.

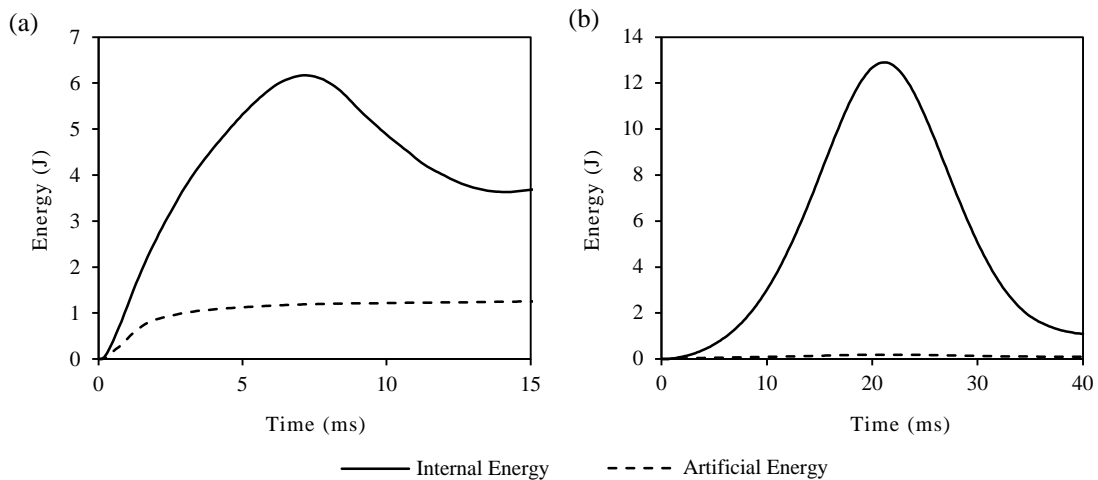


Figure 4.13 - Artificial energy/internal energy vs. time graphs for: (a) cricket ball and (b) knee impacts.

c) Contact

(i) Impactor-on-Surface

A surface-to-surface contact pair was enforced with a kinematic contact algorithm and finite sliding. Kinematic contact achieves precise compliance with the loading conditions and strictly enforces contact constraints permitting no penetrations. Abaqus/Explicit advances the kinematic state of the model adjusting the displacements and velocities of the nodes at the end of each increment into the predicted configuration without regard to the contact conditions (Prior, 1994). The solver calculates which slave nodes will penetrate the master surfaces, the depth of node penetrations, mass associated with it and the time increment to determine the resistive force to oppose the penetration. This is preferential to penalty contact in which contact constraints are enforced less stringently and can result in element penetration and distortion for these types of analyses. Furthermore, in kinematic contact, the time increment size is independent of number of contact points and complexity of contact, whilst in penalty contact the time decreases as the contact stiffness increases (ABAQUS, 2014).

Pure master-slave surface assignments were employed for the impactor and surrogate bodies due to the significant relative differences in stiffness. Refined slave mesh densities were also employed to prevent mesh penetrations associated with coarse mesh discretisation.

By default, a hard pressure-overclosure relationship is set for kinematic contact algorithms where no pressure is applied until nodes are in contact at which point unlimited contact pressure is enforced; there is also no damping in this interaction. A softened kinematic pressure-overclosure relationship has been used to more gradually enforce the contact pressure, reducing the element distortion on the skin layer surface from the impactor. An exponential pressure-overclosure relationship was employed (Fig. 4.14) whereby the contact pressure (p) between the two surfaces increases exponentially as the clearance (h) between the surfaces, measured in the normal direction, diminishes from a user-defined threshold for penetrations in the range $-c$ to $6c$ (Rohan *et al.*, 2013). The surfaces come into contact when the gap is slightly positive with special treatment at ' $h = c$ ' to avoid numerical issues with low stiffness.

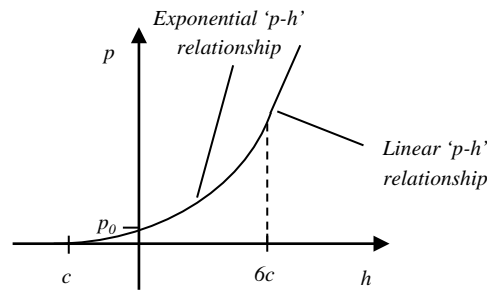


Figure 4.14 - Exponential pressure-overclosure relationship.

The exponential pressure-overclosure relationship was defined through an iterative process based, initially, on the hard contact pressures experienced at the skin layer. A pressure at zero overclosure (p_0) of 100 kPa and a clearance at zero pressure (c) of 1×10^{-4} m were used. A tangential frictional coefficient of 0.75 was enforced with finite sliding parameters to allow some sliding friction; this parameter has been used previously to define human impact surrogate behaviour (Ankrah & Mills, 2003). A critical damping fraction of 0.1 was also employed in the normal and tangential directions. The coefficient applies a constant damping to the simulation based on the contact stiffness enforced.

Figure 4.15 shows the differences in contact between simulations conducted with a hard normal contact and a softened contact. The hard contact shows element distortion and areas of high stress concentration whilst the softened simulation exhibits a more continuous stress profile.

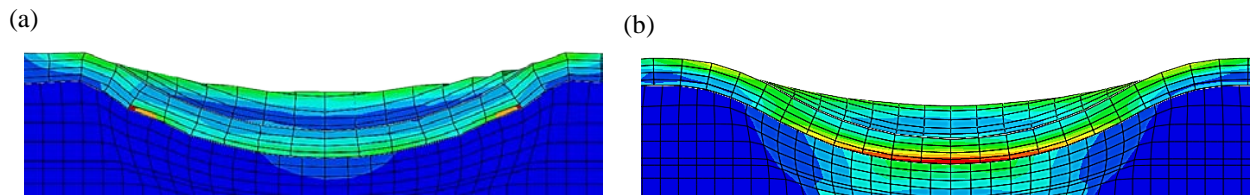


Figure 4.15 – (a) Hard contact element distortion and areas of high stress concentrations; (b) softened contact continuous stress profiles.

(ii) Inter-Layer

The soft tissue layers were tied together using the Lagrange multiplier method for reduced computational cost of the contact interaction. These ties represent the adhesion between tissue layers in the human body where sliding and separation are expected to be insignificant. The constraint completely connects all nodes on the master and slave surfaces constraining all translational and rotational DOF of the slave nodes such that all stresses transmitted are unchanged in quantity and direction (Ihde *et al.*, 2008). Rohan *et al.* (2013) studied compression levels on varicose veins in the leg and considered the bone-muscle and skin-fat layers to be tied; they have been considered in such a manner in this study.

The contact between the adipose and muscle tissue layers was investigated to determine whether the nature of contact changed the loading behaviour. A hard contact with a rough tangential frictional coefficient was compared with a tied contact in the cricket ball loading conditions. At maximum displacement, the hard contact surrogate model exhibited an overall displacement 0.52% greater than the tied surface model (Fig. 4.16a) with a 6.4% difference in peak von Mises stress between tied and hard contact models at the muscle layer (Fig. 4.16b). Due to the closeness of hard and tied contact responses and the unknown levels of actual tissue adhesion, all layers were tied with penalty contacts as a simplification of human behaviour.

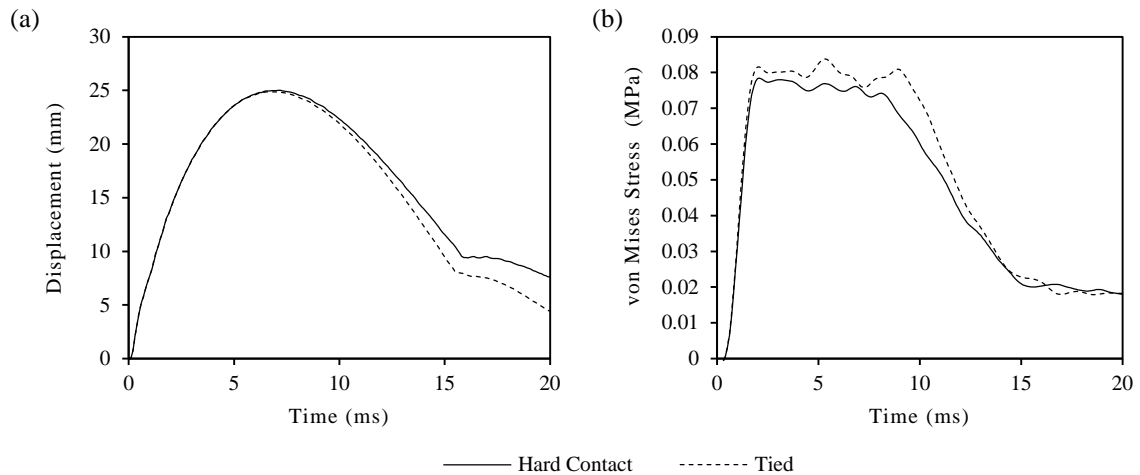


Figure 4.16 – (a) Skin layer displacement and (b) von Mises surface stress in models with and without tied layers.

d) Mass Scaling

The computational expenditure in Abaqus/Explicit can be reduced through either decreasing the time scale (artificially increasing loading rates) or through introducing mass scaling (Harewood & McHugh, 2007). Given the rate dependency present in both organic tissue and elastomers it is important to conduct simulations in the materials natural time scale, therefore mass scaling is a preferable approach.

Mass scaling artificially increases the density of the material, increasing the stable time increment and reducing the number of increments required to solve a job (Wang *et al.*, 2006). The stable time increment (Equation (4.1)) is affected by the dilatational wave speed, which, in a linearly elastic material, is given by Equation (4.5).

$$c_d = \sqrt{\frac{E}{\rho}} \quad (4.5)$$

Where: c_d is the dilatational wave speed of the material; E is the elastic modulus; ρ is the material density.

Through introduction of mass scaling with a factor of f^2 , the wave speed increases by a factor of f and the stable time increment increases by a factor of f . In some contacts involving high deformation rates, mass scaling had the additional benefit of stabilising contacts where the ratio of deformation rate to wave speed exceeds 1.0, which means that the impactor is deforming an element faster than a stress wave can propagate. However, mass scaling also results in increased inertial effects where the kinetic energy artificially increases, which can lead to unrealistic dynamic effects and erroneous solutions (Prior, 1994; Harewood & McHugh, 2007).

Semi-automatic mass scaling was applied in these simulations with a minimum time increment of 1×10^{-6} s.

With no mass scaling applied, a cricket ball impact simulation took 21 hours 46 min to complete on a single core compared to a computational time of 3 hours 34 min when mass scaling was applied with less than a 0.1% difference in maximum displacement or surface stress. When a greater mass scaling (minimum time increment: 1×10^{-5} s) was applied, the surface stresses were overestimated by over 400%.

e) Mesh Refinement Study

A mesh refinement study was conducted for each tissue layer to determine the density at which key evaluation metrics converge. This is a necessary component of any FE analysis as an overly fine mesh has a high associated computational cost whilst a coarse mesh can yield inaccurate results. Due to the simplicity of geometries, a uniform mesh was considered. All meshes were checked to ensure the maximum angle was no greater than 120° , minimum angle was no less than 20° and the element was not less than 50% of the target nominal size.

Hyperworks® 12.0 (Altair Engineering Inc., Troy, MI) pre-processor Hypermesh® was used to discretise the geometries as automatic mesh generators within generic FE packages have difficulty producing good quality graded elements (Parthasarathy *et al.*, 1994). Due to the dynamic nature of impacts, mesh densities were refined dependent on their master and slave assignments. The stiffer tissue layers were assigned master surfaces with slave surfaces having finer densities to prevent coarse mesh discretisation, element distortion and penetration of surfaces.

Brekelmans *et al.* (1972) noted that convergence tests could be conducted by comparing model displacements, strain energy or stresses and strains. The maximum top surface displacements (x_{\max}), time to maximum displacement (t_x), the maximum Cauchy stress, normal to the direction of impact ($\sigma_{22,\max}$), the maximum von Mises stresses ($\sigma_{v,\max}$) and computational time (based time for one CPU to run the simulation) were the evaluation metrics. Stolk *et al.* (2001) noted that a completely converged stress/strain distribution may not be obtained, since stress strain singularities locally cause stresses and strains to diverge with increasing mesh refinement. Therefore, the mesh densities selected were based on the accuracy relative to computational costs. The study was conducted sequentially with the bone tissue considered first with a 3 mm element size muscle layer as the impact surface. The skin layer was next introduced, followed by adipose and then muscle was considered in the full tissue assembly. Figures 4.17 - 4.20 show a comparison between evaluation metrics for different element sizes in convergence studies for each tissue layer.

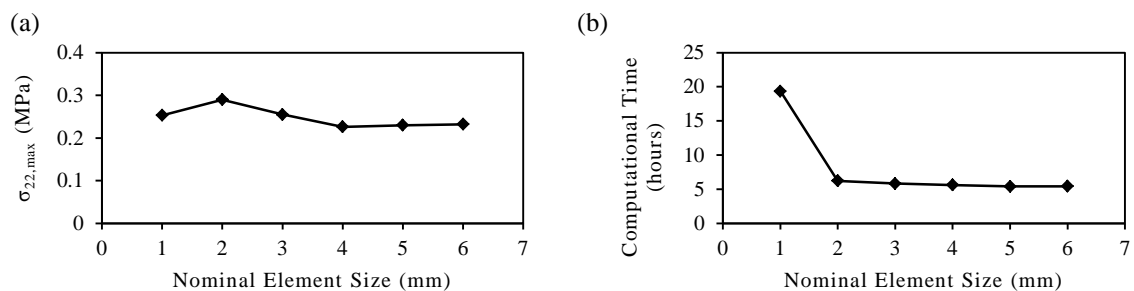


Figure 4.17 - Bone tissue mesh convergence graphs showing: (a) $\sigma_{22,\max}$ on bone surface vs. element size; (b) computational time vs. element size.

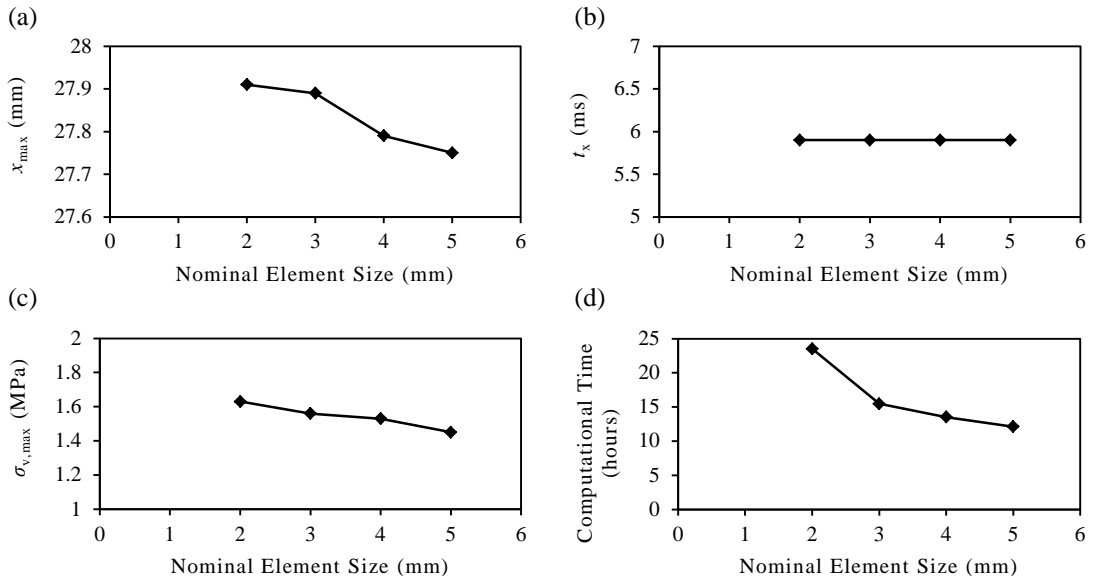


Figure 4.18 - Skin tissue mesh convergence graphs showing: (a) x_{\max} on surrogate surface vs. element size; (b) t_x vs. element size; (c) $\sigma_{v,\max}$ on skin surface vs. element size; (d) computational time vs. element size.

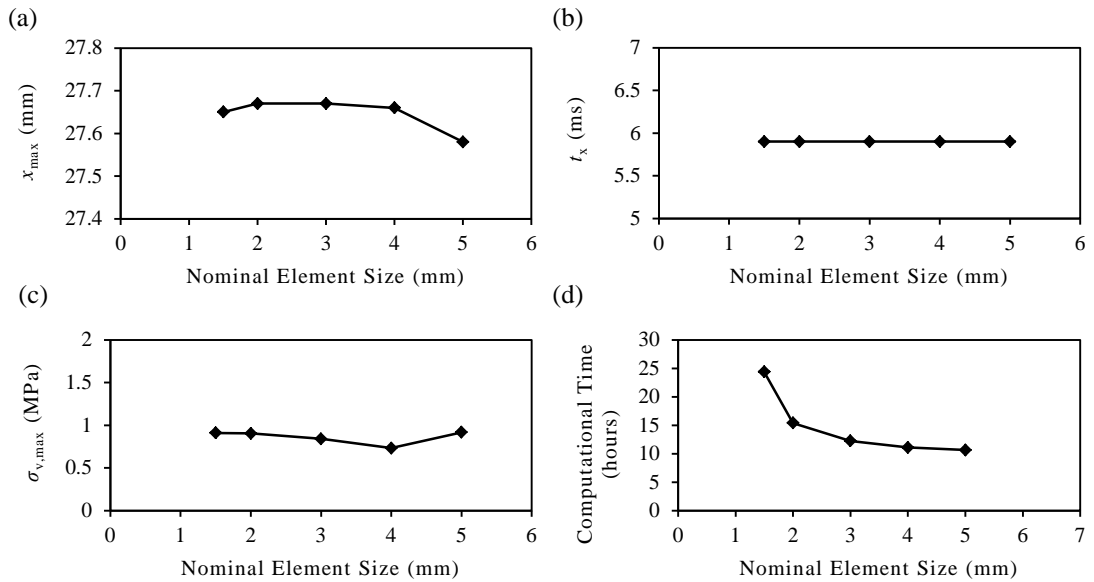


Figure 4.19 - Adipose tissue mesh convergence graphs showing: (a) x_{\max} on surrogate surface vs. element size; (b) t_x vs. element size; (c) $\sigma_{v,\max}$ on adipose surface vs. element size; (d) computational time vs. element size.

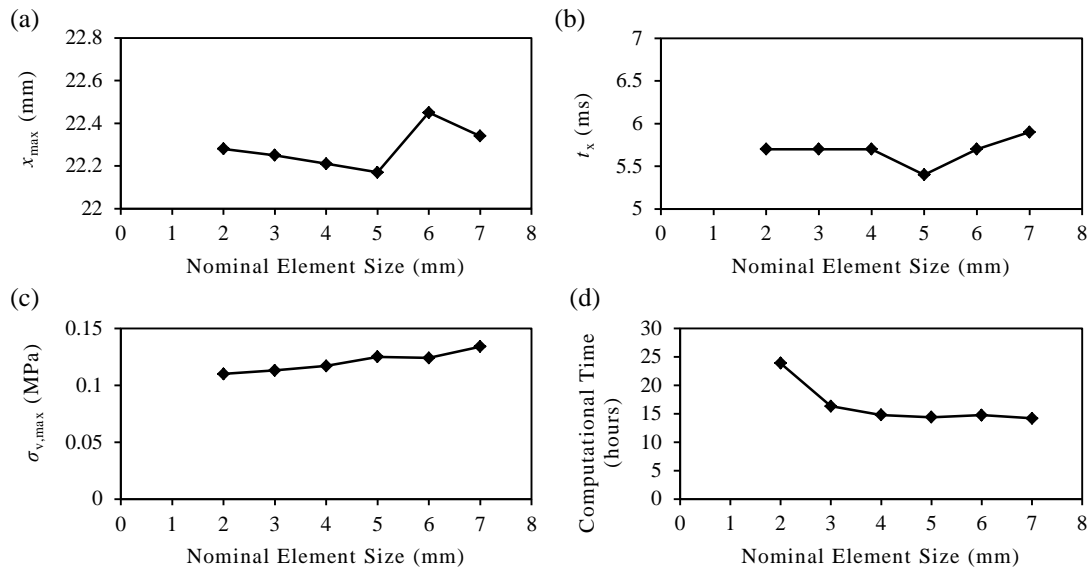


Figure 4.20 - Muscle tissue mesh convergence graphs showing: (a) x_{max} on surrogate surface vs. element size; (b) t_x vs. element size; (c) $\sigma_{v,max}$ on muscle surface vs. element size; (d) computational time vs. element size.

The mesh refinement study showed convergence in most evaluation metrics considered, particularly, x_{max} at the skin and adipose layers and $\sigma_{v,max}$ on the outer surface of the muscle and adipose layers. Other metrics considered were fairly insensitive to changes in element size, particularly, t_x across all tissues, $\sigma_{22,max}$ on the bone surface, x_{max} on the muscle surface and $\sigma_{v,max}$ on the skin surface. Therefore, the accuracy of the mesh was considered relative to the computational costs of the solutions.

In the bone layer, the 3 mm element size exhibited a $\sigma_{22,max}$ on the bone surface just 0.79% difference to the 1 mm element size at a significantly reduced computational cost (311% lower than 1 mm). The skin layer showed the best accuracy relative to computational time at 3 mm with only a 0.07% difference in x_{max} compared to 2 mm but with a 194% lower computational time. The 2 mm adipose layer exhibited just a 0.07% and -0.55% difference in $\sigma_{v,max}$ and x_{max} from the finest increment (1.5 mm) respectively; whilst, simulations with a 3mm element size exhibited a -7.48% difference in $\sigma_{v,max}$ layer stress. The muscle layer exhibited the best accuracy relative to computational time at 4 mm as there was only a 2.72% reduction in $\sigma_{v,max}$ from 2 mm element size with a 161.7% reduction in computational time.

A fine impactor mesh was employed to avoid faceted surface deformations where the surface is poorly discretised and unrepresentative of the target geometry. A 9834 element C3D4 tetrahedral mesh was used to represent the hemispherical impactor. Figure 4.21 shows the FE model configuration for the impact simulations.

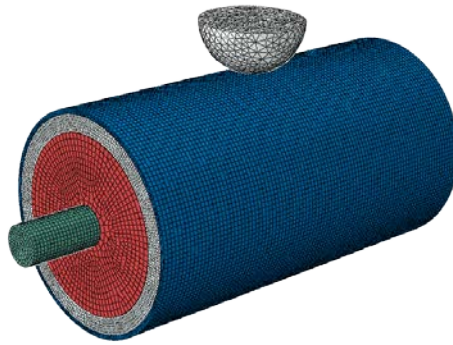


Figure 4.21 - FE model configuration for impact simulations.

4.4. Investigation of the Importance of Surrogate Tissue Layers

4.4.1. Introduction

To assess the influence of different soft tissue layers on the mechanical impact response of a thigh surrogate, a series of simulations were performed. Of the tissues in the thigh region, it is widely accepted that the bone and muscle tissue components are essential to the mechanical response of the limb segment. Muscle constitutes the most significant proportion of human soft tissue in the region (§2.3.1.b), whilst bone is significantly stiffer than any other tissue in the segment. Skin and adipose tissue have also been suggested to contribute to the mechanical response, this study aims to investigate their significance.

4.4.2. Methodology

a) Test Plan

Three surrogate configurations have been established to investigate the effects of skin and adipose layers on the body's impact response; they included the following tissues arrangements:

- 1) Muscle and bone (MB)
- 2) Muscle, skin and bone (MSB)
- 3) Muscle, skin, adipose and bone (MSAB)

In each of the surrogate tissue arrangements, the layers shown in Figure 4.21 are preserved but the material models used in skin or adipose layers can be the muscle tissue to allow comparison of potential errors introduced. Each surrogate was subject to two impact simulations (cricket ball and knee) central and perpendicular to the longitudinal axis.

b) Evaluation Criteria

To objectively assess the significance of the soft tissue layers a series of evaluation metrics were necessary. Although the exact causation of soft tissue injuries remains unknown, the metrics were based on the pertinent mechanical response phenomena believed to be exhibited in blunt trauma cricket ball and knee impacts to the thigh (§3.5.5) and an external relevance to PPE evaluations. These evaluation metrics have been used consistently throughout this research study to provide a direct comparison to assess the effects of different surrogate variations. The metrics considered have been listed:

- *Impactor penetration:* The magnitude of impactor penetration (x_{skin}) is a pertinent metric for contusion injury evaluation as it relates to the mechanical strain elicited in the surrogate tissues. The amount of deformation influences the manner in which the body segment interacts with PPE and also provides a measure of the composite stiffness of the surrogate tissue structures. x_{skin} - time graphs have been generated to show the displacement - time history of the impact with the maximum top surface surrogate displacement (x_{max}) and time to maximum deformation (t_x) values recorded.
- *Deep tissue pressure:* The pressure experienced in deep soft tissues (P_{base}) provides a measure of the mechanical load transfer through the surrogate and the susceptibility to deep tissue injury (e.g. contusions). Given the tied contact between the muscle and bone surfaces, the stress on the bone top surface is equivalent to the muscle bottom surface. The Cauchy stress tensor, σ_{22} , normal to the direction of impact was selected as the specific evaluation metric. The mechanical contact pressure applied to humans is suggested as being an indirect mechanical phenomena relating to contusion and laceration injuries. The internal normal stress experienced in the muscle tissue, given the incompressibility of the materials being considered, should be equivalent to this contact pressure. P_{base} - time graphs were generated for each impact with the maximal Cauchy stress, normal to the direction of impact ($P_{base,max}$) and time to peak pressure (t_p) values also recorded.
- *Layer effects:* The magnitudes of displacement and stresses experienced at each tissue layer surface have been recorded. The stresses provide an indication of the load transfer phenomena occurring in the surrogate and the time course over which they were achieved. In human impacts, multi-directional stress fields are generated, the von Mises stress on the surface of each tissue layer was considered as it provides a representation of the multi-directional stress conditions experienced and relates to the failure of the tissue structures. The displacements of the tissues have been expressed in terms of changes to the thickness of the tissue layers (T_{skin} , $T_{adipose}$, T_{muscle}). In a sports injury context, these layer effects also provide information on the susceptibility to superficial or deep tissue damage and an indication of the differences in responses attained from different body types (e.g. athletic lean vs. sedentary fatty body types).

c) Sensitivity Analysis

A sensitivity analysis has also been performed to both further indicate the importance of the tissue layers and investigate their sensitivity to changes in thickness. The skin and adipose tissue layers were altered independently with all other tissue thicknesses and overall surrogate diameter kept consistent. The surrogate tissue thicknesses in the variant configurations are shown in Table 4.7.

Table 4.7 - Parameters for sensitivity analysis of tissue thicknesses.

	Tissue Thickness (mm)			
	<i>Skin</i>	<i>Adipose</i>	<i>Muscle</i>	<i>Bone</i>
A	2	12	46.5	13.5
B	4	12	46.5	13.5
C	3	6	46.5	13.5
D	3	18	46.5	13.5

4.4.3. Results

a) Top Surface Displacements

The top surface displacements (x_{skin}) of the surrogate at each time interval have been presented for both the cricket ball and knee impact conditions (Fig. 4.22).

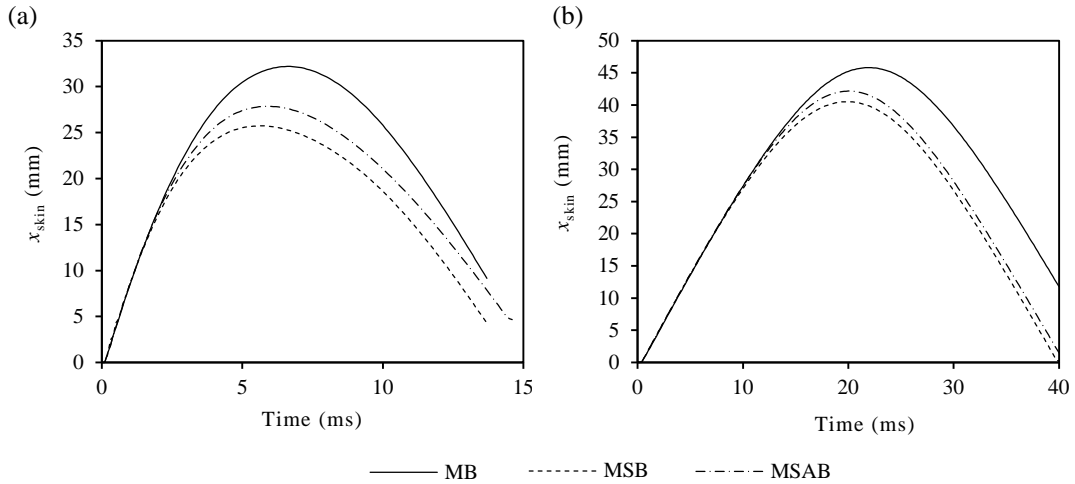


Figure 4.22 – x_{skin} - time plots for: (a) cricket ball and (b) knee impactor loading conditions

The x_{max} and t_x for the cricket ball and knee impacts on each surrogate have been reported in Table 4.8. Increased displacements were predicted in both impact conditions in the MB surrogate with minimum differences of +15.4% and +10.0% in x_{max} and t_x respectively. The MSB surrogate exhibited lowest x_{max} and t_x values whilst the MSAB showed an increase in both x_{max} than t_x compared to the MSB surrogate across both loading conditions.

Table 4.8 - x_{max} and t_x for cricket ball and knee impactor simulations.

	Cricket Ball		Knee	
	x_{max} (mm)	t_x (ms)	x_{max} (mm)	t_x (ms)
MB	32.2	6.70	45.8	22.0
MSB	25.7	5.60	40.5	19.8
MSAB	27.9	5.90	42.2	20.0

b) Deep Tissue Pressure

The deep tissue pressure (P_{base}) experienced in each surrogate has been plotted in Figure 4.23.

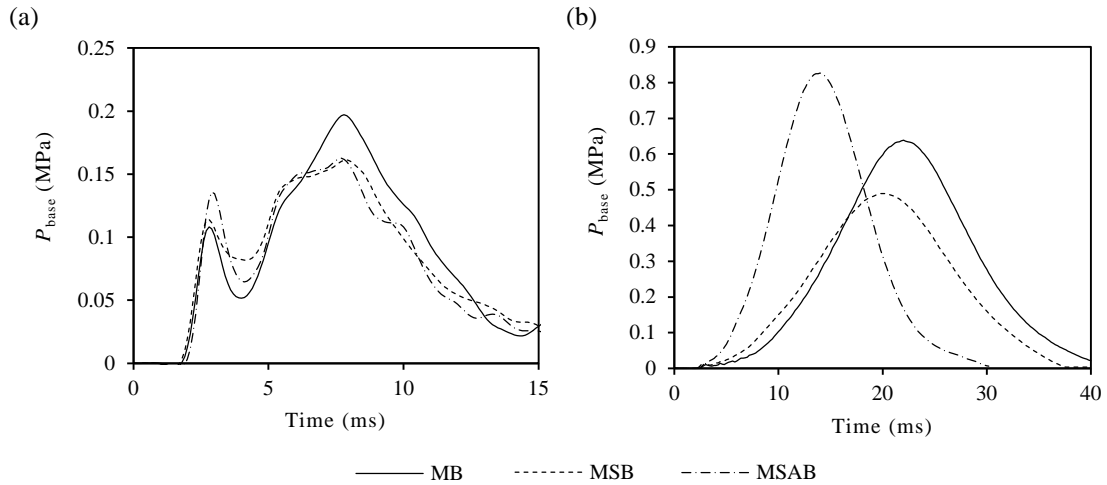


Figure 4.23 – P_{base} - time plots for: (a) cricket ball; and (b) knee impactor loading conditions.

The magnitudes of $P_{\text{base,max}}$ and time to peak pressure (t_p) recorded in the cricket ball and knee impactor surrogate simulations have been detailed in Table 4.9. The results show an increased $P_{\text{base,max}}$ in the MB surrogate when subject to the cricket ball impact (min. 20.1% difference). Similar magnitudes of pressure were observed between the MSB and MSAB surrogates, though the MSAB surrogate exhibited a -3.80% difference in t_p . In the knee impact simulations, the MB and MSAB exhibited similar $P_{\text{base,max}}$ (3.04% difference) though the MSB surrogate showed significantly lower pressures (-23.2% difference). Both MSB and MSAB surrogates experienced lower t_p to the MB surrogate (min. -8.18% difference).

Table 4.9 – $P_{\text{base,max}}$ for cricket ball and knee impactor simulations.

	Cricket Ball		Knee	
	$P_{\text{base,max}}$ (MPa)	t_p (ms)	$P_{\text{base,max}}$ (MPa)	t_p (ms)
MB	0.203	7.90	0.638	22.0
MSB	0.166	7.90	0.490	20.0
MSAB	0.169	7.60	0.658	20.2

c) Layer Effects – Tissue Thicknesses

The thicknesses of the surrogate tissue layers have been evaluated throughout the cricket ball and knee simulations (Fig. 4.24). In both impact conditions the MSAB and MSB surrogates showed significantly lower skin layer displacements than the MB surrogate. The MSAB surrogate also exhibited more rapid initial deformations than all other surrogates in both impact conditions.

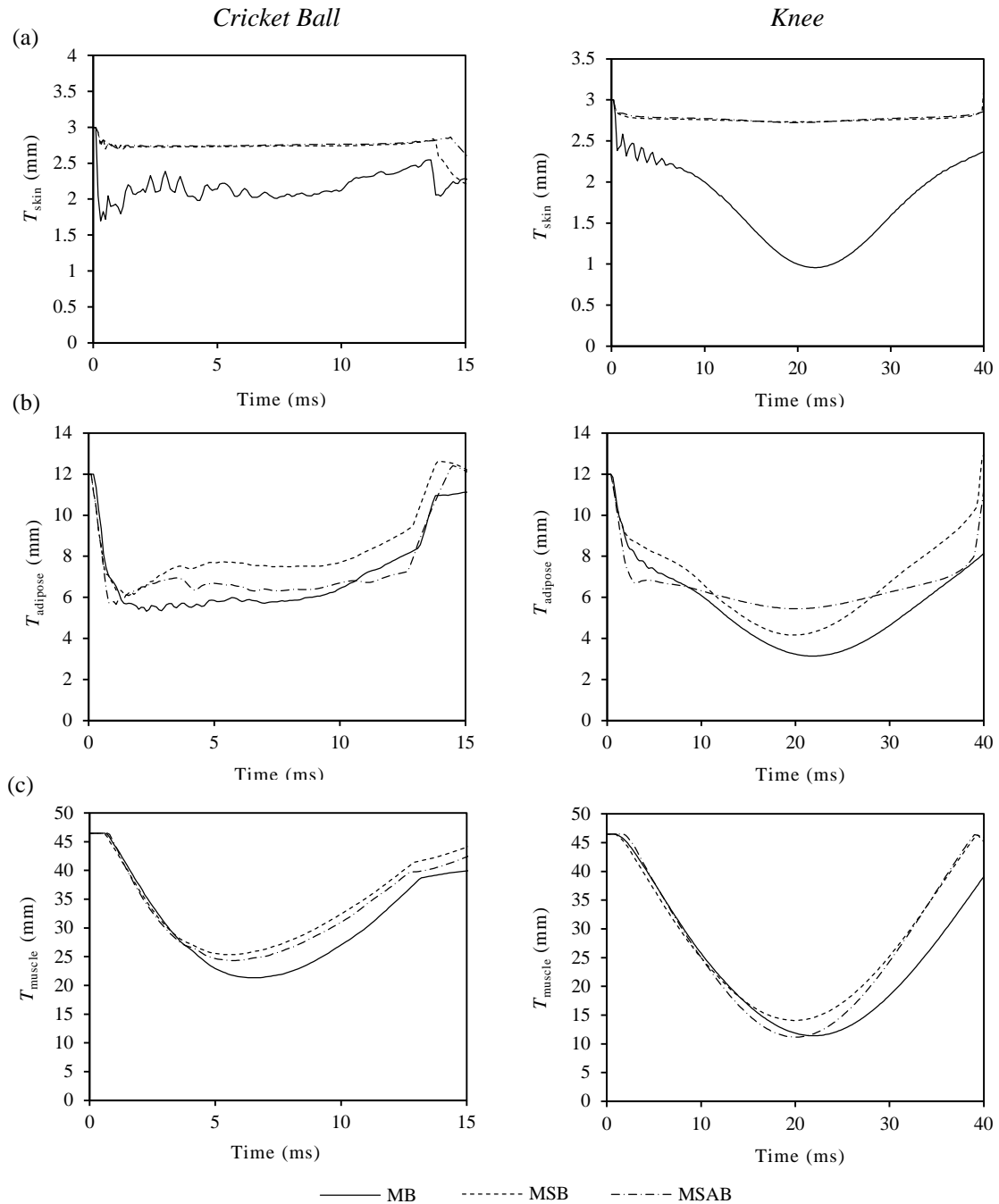


Figure 4.24 - Layer thicknesses for (a) skin; (b) adipose; (c) muscle (left: cricket ball; right: knee impactor).

d) Layer Effects – Tissue Stresses

The peak von Mises stresses at the tissue layers have been recorded for both the cricket ball and knee impactor simulations (Fig. 4.25). The $\sigma_{v,max}$ and t_σ values for each simulation at skin, adipose and muscle layers are detailed in Table 4.10.

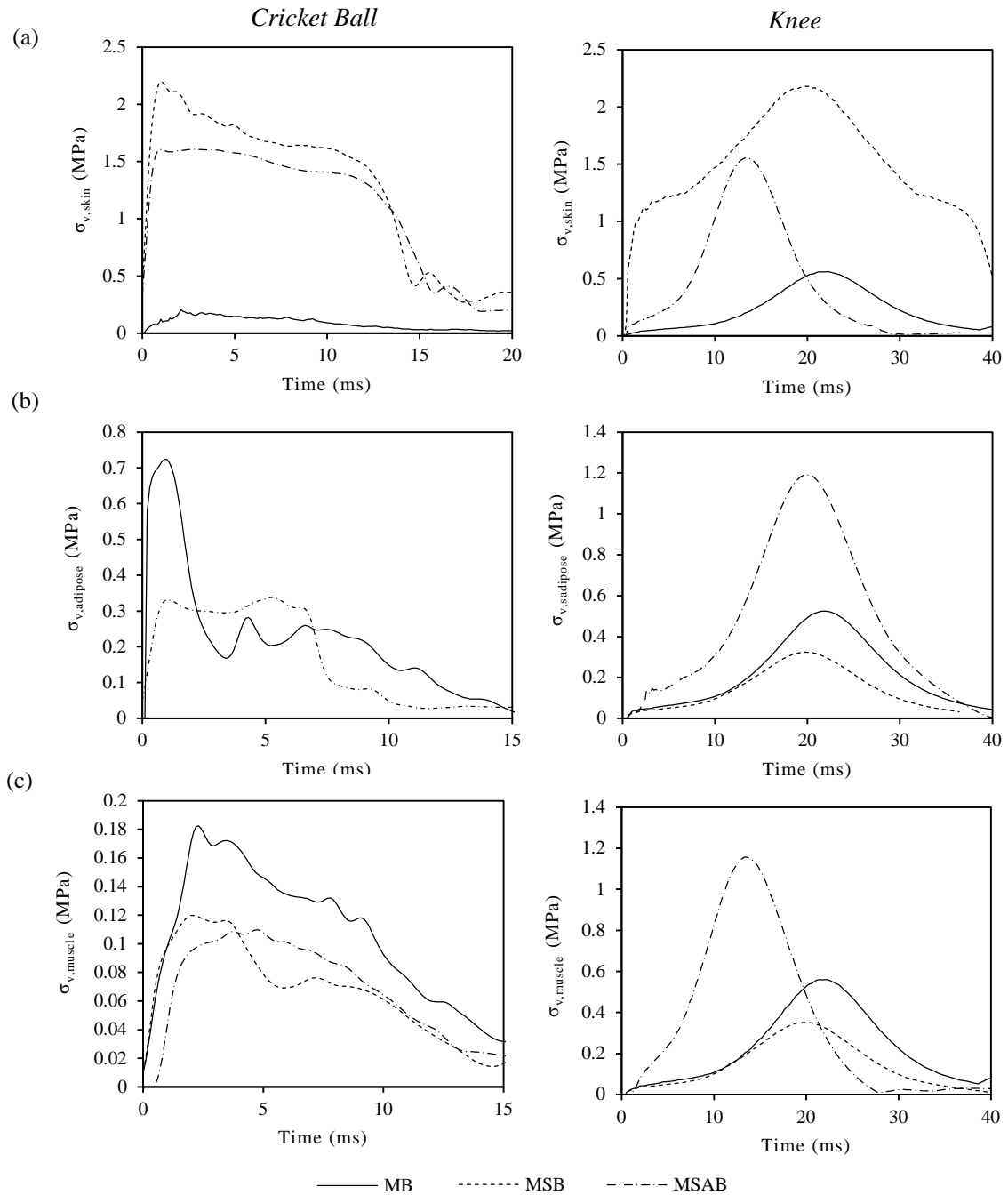


Figure 4.25 – von Mises stresses on the: (a) skin; (b) adipose and (c) muscle layer surfaces (left: cricket ball; right: knee impactor).

The MSB and MSAB surrogates both exhibit significantly greater $\sigma_{v,max}$ at the skin layer (min. 433% greater than MB surrogate). The MSAB surrogate also showed much greater $\sigma_{v,max}$ on the muscle layer outer surface under both impact conditions. At the muscle layer, the MB surrogate exhibited relatively high $\sigma_{v,max}$ under both impact conditions, whilst the MSB surrogate showed

relatively low $\sigma_{v,max}$. The MSAB surrogate exhibited higher relative stresses in the knee impact compared to the cricket ball impact condition.

Table 4.10 – $\sigma_{v,max}$ (MPa) and t_σ (ms) on the tissue layer surfaces for cricket ball and knee impactor simulations.

	<i>Skin</i>				<i>Adipose</i>				<i>Muscle</i>			
	Cricket Ball		Knee		Cricket Ball		Knee		Cricket Ball		Knee	
	$\sigma_{v,max}$	t_σ	$\sigma_{v,max}$	t_σ	$\sigma_{v,max}$	t_σ	$\sigma_{v,max}$	t_σ	$\sigma_{v,max}$	t_σ	$\sigma_{v,max}$	t_σ
MB	0.207	2.10	0.372	21.6	0.170	1.50	0.524	21.8	0.162	3.70	0.554	21.8
MSB	2.34	1.10	2.17	19.8	0.125	1.90	0.324	19.8	0.122	2.40	0.356	19.8
MSAB	1.63	1.00	1.77	19.2	0.724	0.90	1.19	19.8	0.109	4.70	0.561	20.2

4.4.4. Sensitivity Analysis

a) Variations in Skin Thickness

(i) Top Surface Displacements

x_{skin} - time plots for the cricket ball and knee impactor simulations have been shown in Figure 4.26 with the magnitudes of x_{max} and t_x values for each surrogate detailed in Table 4.11.

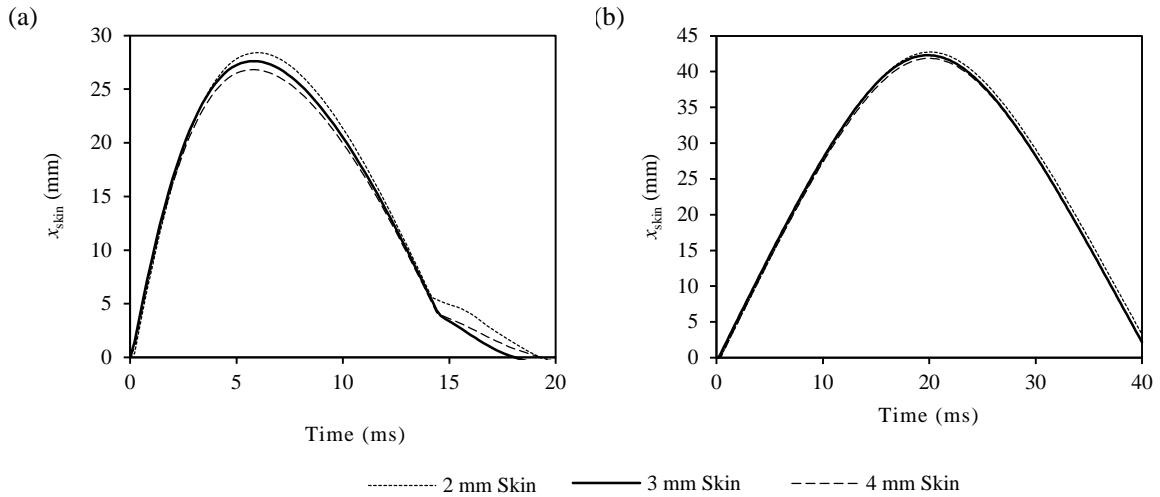


Figure 4.26 – x_{skin} - time plots showing responses for variations in skin thickness in: (a) cricket ball and (b) knee impact simulations.

Reduction in the skin thickness to 2 mm resulted in increased x_{max} and t_x under both loading conditions most evident in the cricket ball impacts with +2.09% and +3.44% differences respectively. The increased skin thickness to 4 mm resulted in reductions in x_{max} , once again more apparent in the cricket ball impact with a -2.90% difference from the 3 mm skin thickness surrogate.

Table 4.11 - x_{max} and t_x for cricket ball and knee impact simulations in skin thickness sensitivity analysis (% differences from standard dimensions in brackets).

	Cricket Ball		Knee	
	x_{max} (mm)	t_x (ms)	x_{max} (mm)	t_x (ms)
3 mm Skin (Normal)	27.6	5.80	42.3	19.8
2 mm Skin	28.4 (+2.90%)	6.00 (+3.44%)	42.7 (+0.95%)	20.0 (+1.01%)
4 mm Skin	26.8 (-2.90%)	5.80 (0%)	41.9 (-0.95%)	20.2 (+2.02%)

(ii) Deep Tissue Pressures

P_{base} - time plots for each simulation have been shown in Figure 4.27 with the magnitudes of $P_{\text{base,max}}$ and t_p detailed in Table 4.12.

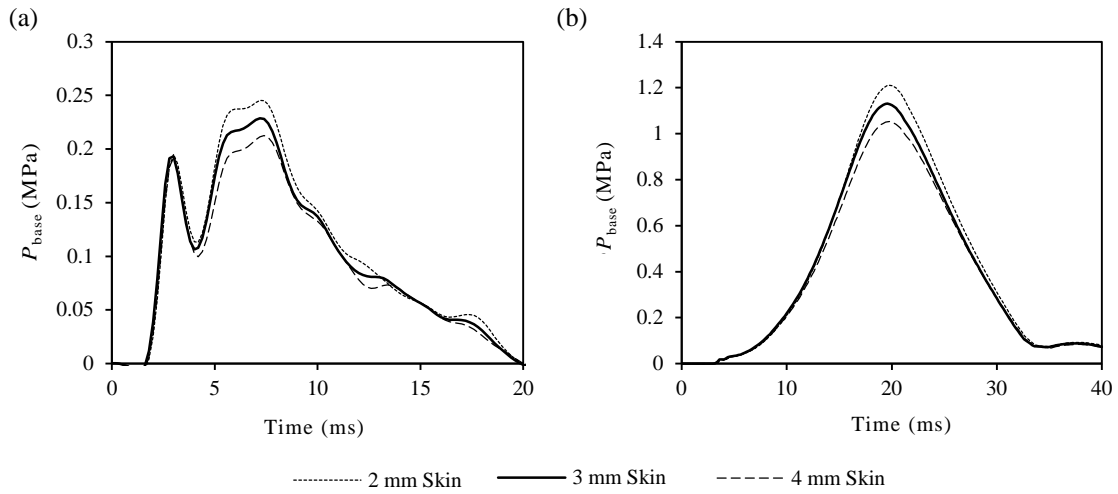


Figure 4.27 - P_{base} - time plots showing variations in response in surrogates with different skin thickness for: (a) cricket ball and (b) knee impact simulations.

The most significant differences were observed in the $P_{\text{base,max}}$ with increased magnitudes shown in the 2 mm skin thicknesses (min. +7.08% difference). The 4 mm skin thickness exhibited reduced $P_{\text{base,max}}$ magnitudes in both impacts (min. -7.02%).

Table 4.12 – $P_{\text{base,max}}$ and t_p for cricket ball and knee impact simulations in skin thickness sensitivity analysis (% differences from standard measures in brackets).

	Cricket Ball		Knee	
	$P_{\text{base,max}}$ (MPa)	t_p (ms)	$P_{\text{base,max}}$ (MPa)	t_p (ms)
3 mm Skin (Normal)	0.228	7.20	1.13	19.6
2 mm Skin	0.245 (+7.46%)	7.30 (+1.39%)	1.21 (+7.08%)	19.8 (+1.02%)
4 mm Skin	0.212 (-7.02%)	7.20 (0%)	1.05 (-7.08%)	19.8 (+1.02%)

b) Variations in Adipose Thickness

(i) Top Surface Displacement

x_{skin} - time plots for the cricket ball and knee impactor simulations have been shown in Figure 4.28 with x_{max} and t_x values for each surrogate detailed in Table 4.13.

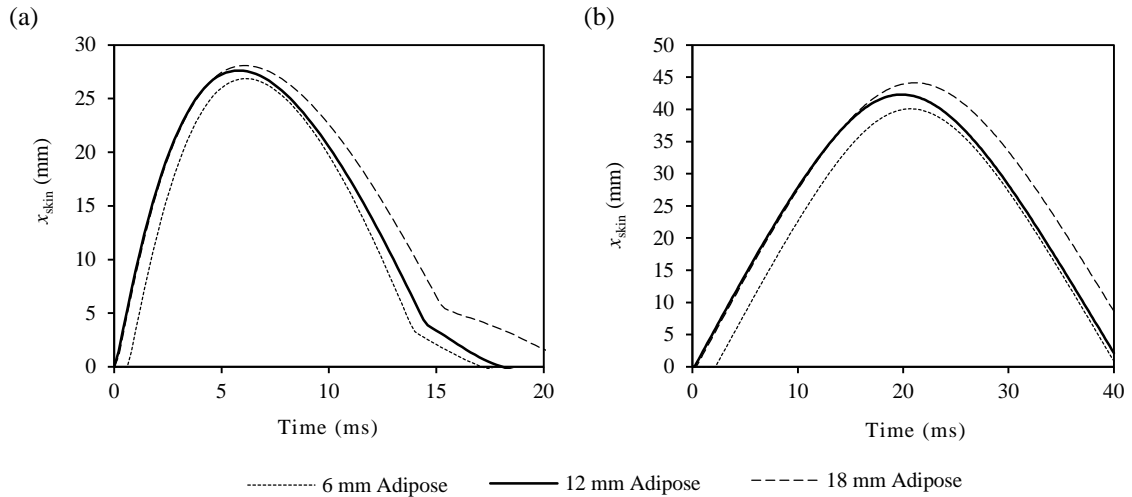


Figure 4.28 – x_{skin} - time plots showing variations in response in surrogates with different adipose thicknesses for: (a) cricket ball and (b) knee impact simulations.

The most significant differences in x_{max} were reported in the 6 mm adipose layer surrogate, particularly in the knee impact where there was a -5.20% difference compared to the 12 mm adipose surrogate. The 6 mm adipose layer surrogate, however, also unexpectedly exhibited a lower t_x than the 12 mm adipose surrogate. The 18 mm adipose layer surrogate elicited increased x_{max} response in both impacts but most significantly in the knee impact (+4.26% difference).

Table 4.13 - x_{max} and t_x for cricket ball and knee impactor simulations in adipose thickness sensitivity analysis (% differences from standard dimensions in brackets).

	Cricket Ball		Knee	
	$x_{\text{max}}(mm)$	$t_x(ms)$	$x_{\text{max}}(mm)$	$t_x(ms)$
12 mm Adipose (Normal)	27.6	5.80	42.3	19.8
6 mm Adipose	26.9 (-2.54%)	6.2 (-6.90%)	40.1 (-5.20%)	20.8 (+5.05%)
18 mm Adipose	28.1 (+1.81%)	6.00 (+3.45%)	44.1 (+4.26%)	21.0(+6.06%)

(ii) Deep Tissue Pressures

P_{base} - time plots for each simulation have been shown in Figure 4.29 with magnitudes of $P_{\text{base,max}}$ and t_p detailed in Table 4.14.

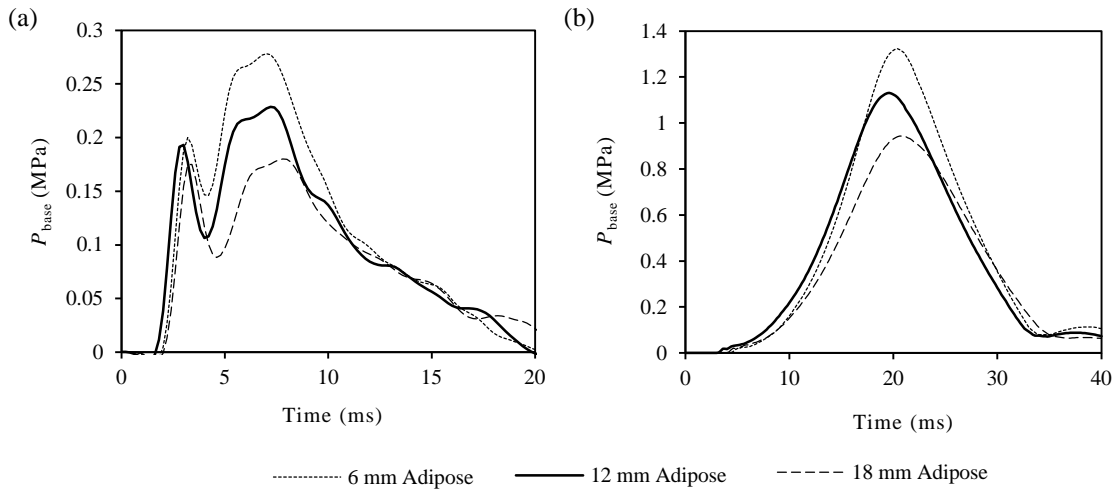


Figure 4.29 - P_{base} - time plots showing variations in response in surrogates with different adipose thicknesses for: (a) cricket ball and (b) knee impact simulations.

The results indicate an increased $P_{\text{base,max}}$ in both 6 mm adipose layer impact simulations (min. +16.8% difference). A similar magnitude of $P_{\text{base,max}}$ reduction was recorded in the 18 mm adipose surrogates with -21.1% and -16.5% differences in cricket ball and knee impact simulations respectively.

Table 4.14 – $P_{\text{base,max}}$ and t_p for cricket ball and knee impact simulations in skin thickness sensitivity analysis (% differences from standard measures in brackets).

	Cricket Ball		Knee	
	$P_{\text{base,max}}$ (MPa)	t_p (ms)	$P_{\text{base,max}}$ (MPa)	t_p (ms)
12 mm Adipose (Normal)	0.228	7.20	1.13	19.6
6 mm Adipose	0.278 (+21.9%)	7.00 (-2.78%)	1.32 (+16.8%)	20.4 (+4.08%)
18 mm Adipose	0.180 (-21.1%)	7.80 (+8.33%)	0.943 (-16.5%)	20.8 (+6.12%)

4.5. Discussion

4.5.1. Organic Tissue Data

Organic tissues are greatly inhomogeneous and exhibit anisotropy, viscoelasticity, and strain rate dependencies (§2.3.2). These complex material behaviours are not currently well understood, particularly *in vivo*. Furthermore, the available reported mechanical properties of organic tissues have varied greatly between characterisation studies based on factors related to the species tested, specimen type and loading conditions (§2.3.2). Therefore, it is impossible to define an ultimate dataset to describe the mechanical response of organic tissues; and, even if it were possible, this would only be representative of a specific individual and not universal.

Consequently, a useful approach adopted was to adapt data from previous good quality characterisation studies reporting representative data in a strain rate range of interest. The mechanical properties of each tissue were attained from uniaxial compression tests in the cross-fibre direction, as this is most pertinent to blunt force trauma impacts in the thigh region. Relaxed muscle data were adapted from studies by McElhaney (1966) and Song *et al.* (2007) conducted in the cross-fibre direction and was utilised as an initial simplification of the anisotropic behaviour exhibited by muscle tissues (Van Loocke *et al.*, 2006; Song *et al.*, 2007; Böl *et al.*, 2012). Studies by Shergold *et al.* (2006) and Comley & Fleck (2012) were used to provide an indication of the organic skin and adipose tissue behaviour under compressive loading conditions. Each of the tissues was also considered to be incompressible and isotropic in the FE models as an initial simplification of their actual behaviour. Given available data, the simplifications made are believed to be appropriate as an initial progression when considering blunt force cricket ball and human knee trauma evaluations.

Should further data become available, the organic tissue datasets used within this study could potentially be improved. A fundamental issue with all the organic tissue data is that it has been gathered post-mortem *in vitro* and lacks tonicity, which is always present to some degree in humans due to latent neurological activity. Much current research has also either been conducted at quasi static strain rates or much higher loading rates relevant to automotive or ballistic impacts; there is currently a paucity of data at intermediate strain rates pertinent to sports impacts. This can cause issues in extrapolating outputs to apply to these data ranges.

A greater confidence in the mechanical behaviour could be obtained through internal testing of organic tissues at strains and strain ranges pertinent to sports impacts. This is particularly relevant in muscle as the datasets adapted were obtained from two previous studies through a range of unmatched strain rates and loading conditions. Nevertheless, without improved data available at sports relevant strain rate ranges for each of these tissues, the datasets selected provide a relevant representation of organic soft tissue response to blunt trauma impacts normal to a fleshy region of the body.

4.5.2. FE Modelling Techniques

FE models have been adopted in this study to provide a simplification of actual human impact behaviour from which sensible predictions of human impact response can be estimated. A series of simplifying assumptions were adopted in order to generate each component of the FE model and primarily related to material descriptions and contact conditions formulated within the software. Therefore, key modelling challenges associated with the FE models were: ensuring a

good mechanical representation of real impact response behaviour; the computational expenditure of the model; and its stability when subject to dynamic impacts. The methods used to overcome these challenges have been summarised in Table 4.15.

Table 4.15 - FE model definitions.

		Definition
Material Model	<i>Hyperelastic</i>	First-Order Ogden Model
	<i>Viscoelastic</i>	QLV Prony Series
Mesh	<i>Element Type</i>	C3D8R Hexahedral Elements. Distortion Control: Adipose (0.1)
	<i>Element Attribute</i>	Reduced Integration Enhanced Hourglass Control
	<i>Nominal Element Size</i>	Skin: 3 mm; Adipose: 2 mm; Muscle: 4 mm; Bone: 3 mm
Contact	<i>Impactor-Surface</i>	Exponential Softened Contact $p_0 = 100$ kPa; $c = 1 \times 10^{-4}$ m
	<i>Inter-Layer</i>	Penalty tie contact
Boundary Condition	<i>Pinned</i>	Translational constraints on bone ends.
Mass Scaling	<i>Semi-Automatic</i>	To a minimum time increment: 1×10^{-6} s

Combinations of hyperelastic and viscoelastic material models were used to represent the viscous and non-linear elastic behaviour exhibited by the organic tissues. This approach was proposed by Fung (1993) to model soft tissues and has since been widely adopted in organic tissue studies (Taylor *et al.*, 2009; Basdogan, 2012; Rashid *et al.*, 2012). First-order Ogden models were used to represent the hyperelastic material behaviour whilst Prony series were used to describe the viscoelastic material behaviour. These models usefully provided a simplified representation of the non-linear material stress response to deformation based on previous good quality research studies.

The material models could, however, potentially be improved through consideration of the anisotropic properties of the materials, should they become more conclusively defined and readily available. This would provide a more representative description of the anticipated multi-directional behaviour. The hyperelastic models used also only represent the properties of the material at a single strain rate, whilst in an actual impact scenario, tissues will experience an initial peak in strain rate (shock) followed by a decreasing strain rate to maximum deformation. There is currently no function within the ABAQUS solver to employ such a material model and consequently represents an area for future study. A further potential issue with the material models adopted are that hyperelastic and viscoelastic properties have been obtained from different studies and amalgamated, which may result in some misrepresentation of actual material behaviour. Given representative, detailed organic tissue data from the same source this could have practically been overcome.

The contact conditions used in the FE models were derived from best practice usage guidelines stipulated by ABAQUS (2014). The critical interaction in any surrogate impact simulation is between the impacting object and the surrogate surface. Given the significant differences in relative stiffness between the two bodies, a sophisticated exponential softened contact was introduced, gradually increasing pressure to reduce instabilities and mesh distortion related issues. The level of adhesion between tissue layers is unknown and although believed to be a strongly bonded, it is not clear to what extent the tie constraint represents actual behaviour. Should further

data become available quantitatively describing this relationship, these inter-layer interactions could potentially be improved. Overall, given available information, the contact conditions established provided a good estimation of mechanical deformations without introducing significant artificial energies.

4.5.3. Biofidelity of Surrogate Response

Given the previously established predictive capabilities of FE models in human impact surrogate studies (§2.4.2.b), the combination of representative materials, geometries and contact parameters should yield a human-like impact response in blunt force normal impacts to fleshy regions of the body. However, as an initial check of the believability of the human surrogate responses, a series of checks with literature were conducted.

To ensure the contact definitions employed represent the expected mechanical response behaviour, an evaluation of the mechanical deformation modes induced in impacts was first performed. Figure 4.30 shows the relative magnitudes of maximum principal strain experienced by the surrogate at a range of time intervals. As the impactor deforms the surrogate soft tissue, there is an elliptical pattern of contact pressure with radiating strain distributions consistent with Hertzian contact theory for indentation into elastic solids (Stronge, 2004).

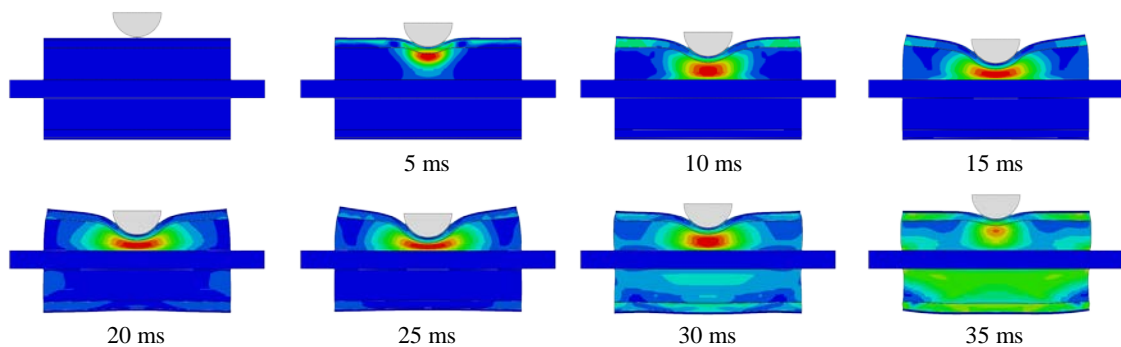


Figure 4.30 - Image showing relative magnitudes of maximum principal strain in the FE surrogate in knee impact simulation.

In Hertzian contact, a sphere of radius, R indents a half space to depth, d and hence creates a radius of contact (a) given by Equation (4.6), shown in Figure 4.31.

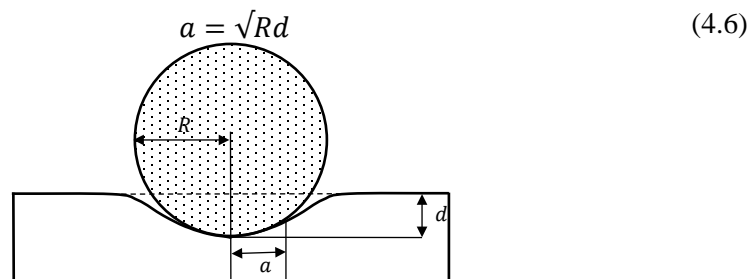


Figure 4.31 - Hertzian contact model for a rigid impactor indenting elastic half-space (Popov. 2010).

With $R = 36 \times 10^{-3}$ m, at a time interval of 2.5ms, the surrogate exhibited $d = 6.46 \times 10^{-3}$ m and $a = 1.64 \times 10^{-2}$ m.

Equation (4.6) predicts a radius of contact area for such an impact to be 1.52×10^{-2} m. The FE model predictions exhibited a difference of 7.89% from the theoretical calculation. Given the simplicity of the Hertzian contact model and the complexity of the FE contact conditions and materials employed, this is sufficiently close as to be believable.

Further checks were performed comparing the impact responses with reported human soft tissue impact studies in literature. Roberts *et al.* (2007) reported peak organ pressures between 0.1 - 2 MPa in the human torso when the region with body armour was subject to projectiles. This was consistent with the predictions from the developed FE surrogate which reported stresses between 0.1 - 1.8 MPa. Desmoulin & Anderson (2011) conducted a series of impacts to the human lower leg. Using masses between 1.9 - 2.6 kg and velocities between 1.3 - 2.5 m.s⁻¹, they reported displacements to the posterior region of the lower leg between 31 - 38 mm. These results are consistent with those attained in the FE knee impact simulations of the thigh region, in which a displacement of 42.2 mm was predicted. Given the increase magnitudes of mass and velocity as well as the increased amount of soft tissue in the region, these results are suggested to be believable.

4.5.4. Importance of Tissue Layers

The FE simulations investigating the importance of different tissue layers clearly show that muscle, skin, adipose and bone tissues are necessary components of an impact surrogate. Bone and muscle tissues have been previously established as integral structures to surrogate response (§4.2). The presence of the skin layer has been shown to significantly affect the overall composite response of the surrogates through reduced displacements and deep tissue pressures in both loading conditions. The presence of a skin layer has also been shown to significantly increase the top surrogate surface stress with 787% and 476% differences from the MB surrogate for cricket ball and knee impacts respectively.

The adipose layer has also been established as an important component due to the increased overall deformations, with the MSAB surrogate exhibiting 8.56% and 4.20% greater x_{\max} than MSB for cricket ball and knee impacts respectively. The adipose layer also introduced an increased rate and magnitude of displacements within the tissue layer.

The organic tissues used within the simulations also showed significant strain rate dependencies where the responses differed greatly between loading conditions. This is most notable in the adipose sensitivity analysis where, in both the 6 mm and 18 mm adipose layer surrogates, the knee impact simulations exhibited greater percentage differences in x_{\max} compared to the normal configuration than the cricket ball impact simulations. This could be attributed to the increased stiffness of the adipose layer at 0.3 strain (Fig. 4.5) and the more rapid rate of deformation elicited by the high rate impact.

Chapter 5 – Surrogate Soft Tissue Simulant Formulation

5.1. Chapter Overview

Chapter 5 presents the development of bespoke PDMS silicones formulated to match the specific mechanical properties of skin, adipose, relaxed and contracted muscle tissues. The silicone fabrication process has been documented thoroughly as well as the iterative development process undertaken and some preliminary formative results. The developed PDMS silicones were tested under uniaxial compression at quasi-static and intermediate strain rates and in stress relaxation conditions. The responses of the developed bespoke silicones have also been described using hyperelastic and viscoelastic constitutive models.

5.2. Introduction

5.2.1. Previous Surrogate Soft Tissue Simulants

Chapter 4 indicated the importance of a multi-material surrogate consisting of skin, adipose and muscle soft tissue layers. It is believed that superior surrogate biofidelity can be achieved by developing surrogate materials to match the mechanical behaviour of each individual human tissue type.

The simulant materials used in synthetic human surrogates are a key component significantly affecting their behaviour. It is important to match the dynamic stiffness of the human tissue structures to provide a biofidelic impact response (Saraf *et al.*, 2007). Most studies, however have typically used either static measures (e.g. Shore A hardness) or linear stiffness parameters (e.g. Young's modulus) to select the most appropriate silicones (e.g. Manning, 2007, Davison *et al.*, 2013). This, in many cases, does not adequately describe the mechanical behaviour of the non-linear silicone elastomers and can often lead to sub-optimal material selection. As previously discussed (§2.4.2.a), Hrysomallis (2009) used Silastic 3483 (Dow Corning Corporation, Michigan, USA) silicone elastomer to represent the composite response of all human soft tissues in the thigh region and the material has since been used elsewhere within the sports PPE industry. Improvement on this, therefore, represents a key requirement for improved surrogate simulants.

5.2.2. Simulant Development Approach

There is a growing body of literature concerned with quantifying the anisotropic behaviour of organic tissues (§2.3.2) but achieving consensus and a complete description of tissue behaviour *in vivo* loaded beyond quasi-static strain rates, that would enable the development of suitable anisotropic surrogate materials, is arguably some years away. In the meantime, sports and other PPE industries could benefit from improved physical surrogates based on better isotropic material combinations. Success in producing these intermediate surrogates arguably paves the way to surrogates of the future containing synthetic anisotropic tissues, particularly if these anisotropic materials are based on modified isotropic counterparts.

The mechanical properties of the target soft tissues have been thoroughly documented (§2.3.2). Given the large degree of variation between characterisation studies based on the specimen type and nature of mechanical loading (Fig. 2.8 - 2.10). This study aims to provide a close approximation of a representative target dataset, established in §4.3.3.

5.2.3. PDMS Silicones

Through manipulating the constitutive silicone components, it is possible to tailor the mechanical properties of the resultant elastomer to match specific human tissue properties. Two-part additive cure vinyl-blocked PDMS silicones (Technovent Ltd., Bridgend, UK) have been previously used in the medical industry for prostheses and soft tissue implants due to their good biocompatibility and human-like feel. Additive cure silicones provide a good solution for such a manufacturing challenge as the fabrication process is relatively simple and there is no shrinkage, which means that very accurate geometries can be achieved with no by-products from the process.

The additive cure silicones consist of four essential constituents: polymer (PDMS); filler, cross linker and catalyst which are divided into the following two-part solutions:

Part A: polymer, filler and catalyst

Part B: cross linker and polymer

In the Part A solution, three polymers with vinyl termination ($\text{CH}=\text{CH}_2$): V21 (molecular weight: 6000 Da), V31 (molecular weight: 28,000 Da) and V46 (molecular weight: 117,000 Da) have been used to provide a range of different mechanical properties (Fig. 5.1). Shorter chain length polymers have a low viscosity and are generally brittle, whilst longer chain length polymers are more viscous and have a higher tensile strength and stiffness.

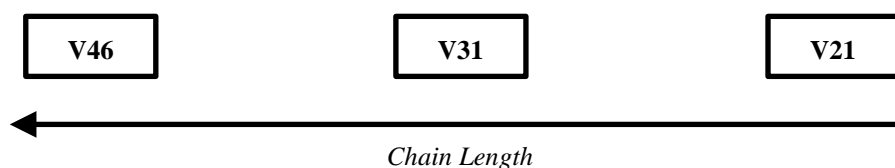


Figure 5.1 – Chain length of PDMS polymer chains.

Each of the three discussed polymers is pre-mixed with 20% (by mass) surface treated (hexamethyldisilazane) silica filler. The filler changes the properties of the polymer from hydrophilic to hydrophobic so no more moisture can be absorbed. It also acts as a material extender to provide bulk to the silicone compound. The filler reinforces the cross linked matrix as the strength of the polymers without filler is generally inadequate.

A platinum heat concentrate catalyst (platinum cyclovinylmethylsiloxane complex) is also present and is used to increase the speed of the reaction when the two parts are combined. The heat concentrate catalyst requires the application of heat to burn off masking compounds, which permits a greater work time before the silicones begin to cure.

The Part B component consisted of a MethylHydroxiloxane-Dimethylsiloxane Copolymer (H301), which was used to chemically bond the polymer chains via a hydrosilation addition reaction. The cross linker agent is a chemical which reacts with the vinyl end-blocked Si-H polymers breaking the existing hydrogen bonds which link together the silicone and creating new double $\text{CH}_2\text{-CH}_2$ bonds, which are harder and more brittle (Fig. 5.2). The concentrations of the cross linker can be altered to change the mechanical properties of the resultant silicone. A polymer is also present in this solution to act as a carrying agent for the cross-linker.

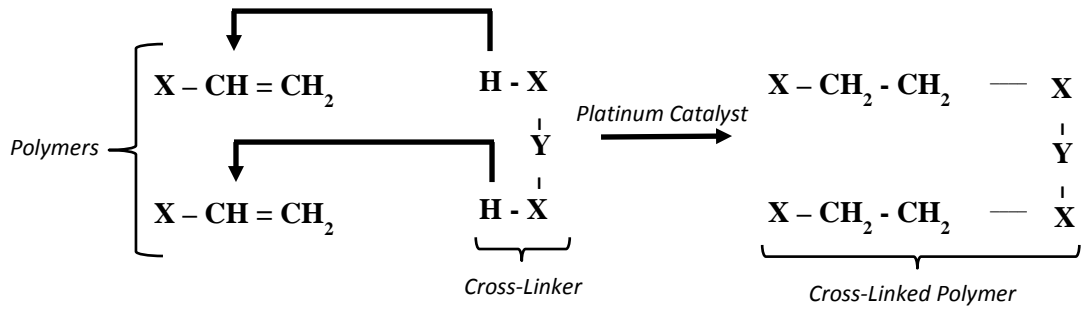


Figure 5.2 - Chemical structure of additive cure PDMS silicone reaction.

5.2.4. Silicone Behaviour

Silicone elastomers exhibit both hyperelastic and viscoelastic material behaviour, which means that they exhibit non-linear responses to deformation and strain rates dependencies. This is attributed to the timescale required for polymer chains to re-orientate during deformation. During deformation at low strain rates the polymers have significant time to reorient, whilst at high strain rates the deformation of polymer chains is restricted to bending and stretching of chemical bonds (Shergold *et al.*, 2006).

To gain a comprehensive understanding of their material behaviour, it is therefore necessary to conduct tests to characterise the simulants to show both hyperelastic and viscoelastic material responses. It is also important to characterise the material at strain rates representative of those experienced by the surrogates in sports impact scenarios. Organic tissues have been demonstrated to exhibit both large strain deformations *in vivo* and high strain rate dependencies when subject to impact stimuli (Van Loocke *et al.*, 2006; Song *et al.*, 2007). Given the nature of many sports impacts, high strain rate, high strain deformations are also likely and as such require material characterisation at comparable rates to ensure consistency of response and adequately populate associated parallel FE models. Many high strain rate characterisation procedures, however, use an oscillatory dynamic test machine (e.g. Instron ElectroPuls), which can test materials at high strain rates but compromises the degree of mechanical strain (e.g. Arbogast *et al.*, 1997; Van Loocke, 2009). These test machines also introduce ringing phenomena, inertial effects and inaccuracies from the elastic response of the machines influencing the stress - strain outputs.

Filled silicone elastomers are also widely reported to exhibit the Mullins effect (Mullins, 1969; Yan *et al.*, 2012; Rey *et al.*, 2013). The Mullins effect is the name given to the phenomenon where elastomers undergo significant softening during their first couple of load cycles and material response after that becomes repeatable (Bergström & Boyce, 1998). The presence of such an effect has been studied to understand the steady state material behaviour and was subsequently used to populate material models. This information could also potentially inform the manner in which physical synthetic surrogates are handled prior to testing and whether preconditioning may be necessary to ensure consistency of response.

5.2.5. Aims and Objectives

- 1) To establish best practice preparation methods for PDMS silicones.
- 2) To determine the changes in the mechanical properties of PDMS silicones when the constituent concentrations are changed:
 - Investigation into the effects of changes in polymer concentrations.
 - Investigation into the effects of changes in cross-linker concentrations.
- 3) To determine whether it is possible using bespoke PDMS silicones to provide an improved representation of specific target organic tissue datasets for skin, adipose, relaxed and contracted muscles when compared to existing surrogate simulants.
 - Is there scope with current *in vitro* data to develop materials that exhibit a more biofidelic response than previously used single material simulants?
 - If better *in vivo* material properties become known, is there scope to develop silicones to match the new data?
 - Is it possible to develop a silicone simulant that perfectly matches the organic tissue properties?
- 4) To create constitutive material models of the developed PDMS silicones.

5.3. Methodology

5.3.1. Fabrication Procedures

Compressive test specimens were fabricated to provide a direct comparison with compressive organic tissue studies. Also, due to the low strength and stiffness of some of the target organic tissue datasets (e.g. adipose), difficulties may arise in fabricating and testing standardised specimens for other loading modes (e.g. tensile). ASTM D395 (2008) prescribes the specimen sample size for compressive testing of vulcanised rubber compounds (Fig. 5.3).

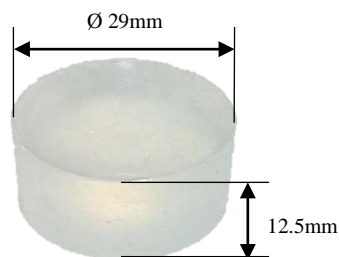


Figure 5.3 - ASTM D395 compressive test specimen.

The process by which the silicones were prepared may significantly affect the mechanical properties of the cured elastomer. Factors such as weighing inaccuracies, method of mixing, time left before curing and the temperature of cure can all alter the quality of the resulting silicones. The process employed in the silicone development is outlined below:

- (i) Weighing of constituents (± 0.1 g accuracy).
- (ii) Constituents poured and mixed manually for 2 - 3 min.
- (iii) Silicones vacuumed for 20 - 30 min until fully degassed.
- (iv) Moulds coated in several layers of release wax and Polyvinyl Acetate (PVA) release agent.

- (v) Solutions poured into specimen moulds immediately after vacuuming.
- (vi) Specimens heated at 60°C in an environmental chamber until cured (approx. 30 min).
- (vii) Cured specimens removed from moulds and cleaned from contaminate left by the release agents using a standard commercial cleaning solution.

5.3.2. Test Conditions

A series of unconfined uniaxial compressive tests were conducted using ASTM D395 cylindrical material specimens (Fig. 5.3). The accuracy of uniaxial compressive experiments is largely dependent on the planarity and parallelism of the two compressive platens and the proximity of the samples to the platens on load application. It was therefore essential that the test machines were adjusted and calibrated to ensure a good consistency between trials. Vaseline was applied to the interfacing surfaces of the test machine, to eliminate frictional forces acting on the platens, limit radial displacement and barrelling effect (Alaoui *et al.*, 2008); that can cause up to a 50% error in compressive stress (Wu *et al.*, 2004). All tests were conducted at room temperature (22°C), within the guidelines of $23 \pm 2^\circ\text{C}$ stipulated by ASTM D1349 (2009) for rubber testing. Tests were conducted at a relative humidity of between 35 - 45% though it was not directly controlled in the experiments.

5.3.3. Mechanical Testing Procedures

a) Quasi-Static Compression Tests

Quasi-static strain rate tests (0.4 s^{-1}) were conducted with an Instron 5569 screw driven universal test machine (Instron, Massachusetts, USA) (Fig. 5.4) using a range of load cells between 0.1 kN and 50 kN sensitivity dependent on the specimen tested, and a linear variable differential transformer (LVDT) to determine displacement with a sampling rate of 100 Hz. Each specimen was placed directly between flat compressive platens and aligned to ensure planarity and parallelism; the load cell and displacement transducer were zeroed prior to testing. The software was programmed to perform a triangular cyclic compressive protocol to ensure a constant strain rate was maintained in loading and unloading cycles. The specimen was compressed incrementally through six cycles in 0.1 compressive strain intervals until failure (Fig. 5.5). This incremental procedure was adopted to investigate the presence of the Mullins effect in the material following previous guidelines and usage by Dorfmann & Ogden (2004) and Diani *et al.* (2009).

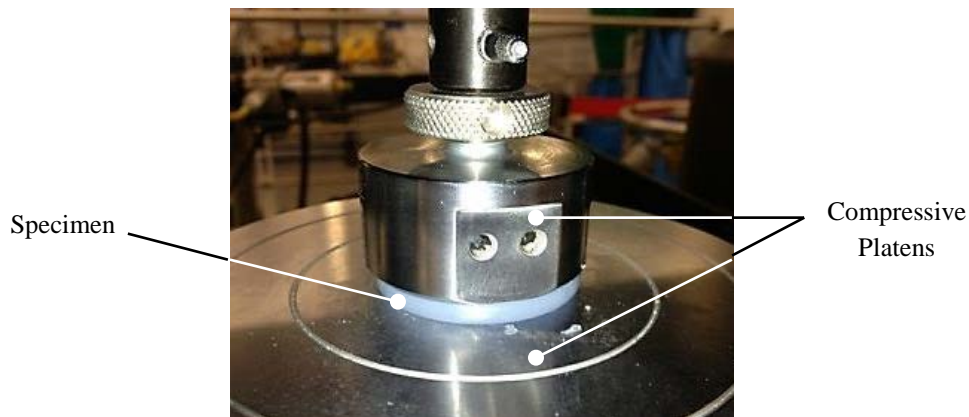


Figure 5.4 - Instron 5569 test configuration with compressive platens.

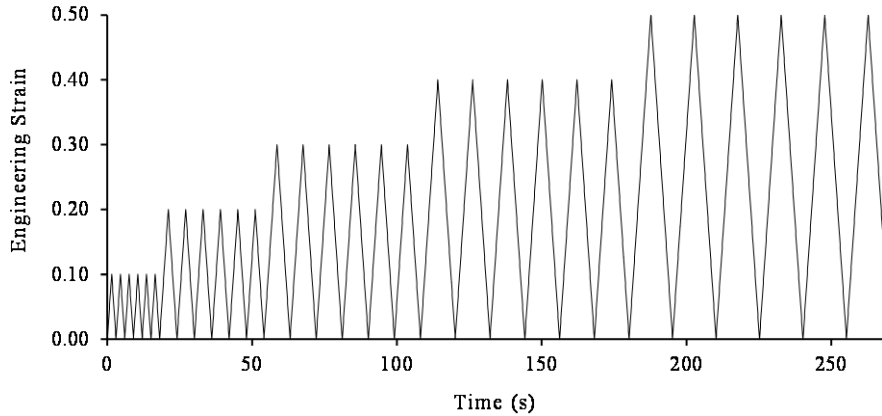


Figure 5.5 - Programmed triangular loading profile for quasi-static uniaxial compressive tests.

The Poisson's ratio was also an important parameter to measure as only compressive tests were conducted; this ratio is the sole determinant of volumetric change in the material and therefore informs the behaviour in other mechanical loading directions. The deformations were measured using a HSV camera (§6.3.5.a). The camera was set with a 256k greyscale image resolution of 1024×1024 pixels ($\approx 50\text{mm} \times 50\text{mm}$), shutter speed of $1/2000$ s, aligned perpendicular to the specimen and captured at 2000 fps.

b) Intermediate Strain Rate Compression Tests

An Instron 9250HV drop tower (Instron, Massachusetts, USA) (Fig. 5.6) was used to test the PDMS specimens at both intermediate strain rates and high strains. The test machine is equipped with three piezoelectric load cells beneath the bottom compressive platen. A HSV camera aligned perpendicular to the specimens was used to measure specimen displacement. The camera had a 256k greyscale image resolution of 1024×1024 pixels ($\approx 100\text{m} \times 100\text{mm}$), shutter speed of $1/10000$ s and was operated at a frame rate of 4000 fps to provide sufficient spatial and temporal resolution to accurately measure changes in strain. A 6.8 kg mass with a flat compressive platen end effector was dropped from a series of heights (0.01 - 0.5 m). The strain rates reported are characterised by the initial maximum value recorded.

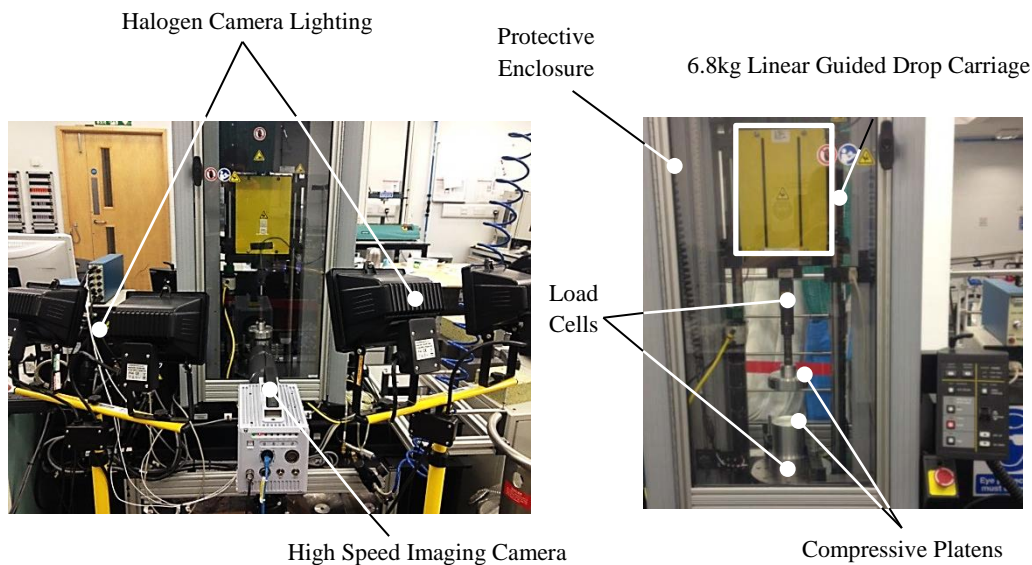


Figure 5.6 - Instron 9250HV drop tower intermediate strain rate materials testing configuration.

c) Stress Relaxation Tests

A relaxation test is the general industry standard for determining viscoelastic characteristics of a material (Mottahedi *et al.*, 2011). Uniaxial ramp-and-hold stress relaxation tests were performed on the Instron 5569 to understand the viscoelastic time-dependant properties of the material. The compressive strain levels induced in test specimens vary across standardised tests (ISO 3384-1, 2011; ASTM D6417, 2014). The strain level chosen was the highest strain attained by all materials before failure (established previously) and was selected to characterise the materials under the most representative conditions for compressive sports impacts. Each specimen was deformed to 0.5 strain at a rate of 0.4 s^{-1} and held under constant strain for a period of 300 s. The 300 s time period was used previously by Van Loocke *et al.* (2008) and was shown to be sufficient for the materials to achieve a steady relaxed state.

d) Durability Tests

One of the key requirements for a sports impact surrogate is that it exhibits consistent and repeatable responses (§2.4.2.a). Durability tests were conducted to understand if the mechanical responses of the silicones degrade following repeated loading cycles. In an ideal scenario the materials would be tested at both high strains and high strain rates through a cyclic procedure, however such a system (e.g. Instron VHS 8800 High Rate System) could not be economically obtained.

The Instron ElectroPuls E3000 test machine (Fig. 5.7) was used to test specimens through 1000 cycles to 0.5 strain, which is a pertinent operational strain value for all tissue simulants. The strain rate, however, was compromised in this study and the machine was driven at the fastest rate that it could oscillate (400 mm/min). Each specimen was tested under quasi-static loading conditions both prior to the cyclic procedure and 300 s after completion.

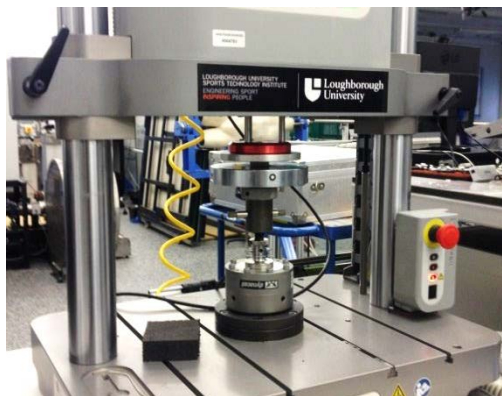


Figure 5.7 - Instron ElectroPuls E3000 mechanical test machine.

e) Analysis Procedures

Force - time and displacement - time data were obtained from the mechanical tests. The engineering strain (ϵ) at each time interval was calculated with Equation (5.1) using displacement values from the test machines and the original length measured prior to testing using a set of Vernier callipers ($\pm 1 \times 10^{-5} \text{ m}$). Engineering stress (σ) was calculated (Equation (5.2)) using data from the load cell divided by an original cross-sectional area of $6.6 \times 10^{-4} \text{ m}^2$.

$$\varepsilon = \frac{\Delta l}{l_0} \quad (5.1)$$

Where: l_0 = original length; Δl = change in length.

$$\sigma = \frac{F}{A_0} \quad (5.2)$$

Where F = applied load; A_0 = original cross-sectional area.

There is currently no consensus as to the best method to quantify the extent of the Mullins effect (Diani *et al.*, 2009). In this study, the maximal percentage stress reductions from the loading curve of the first to last cycle at maximal strain were calculated.

The Poisson's ratio (ν) was determined through post processing of the imaging output using video analysis software Image Pro Analyser (Media Cybernetics Inc.) to determine the relative ratio of transverse and axial strains (Equation (5.3)).

$$\nu = -\left(\frac{\Delta\varepsilon_{trans}}{\Delta\varepsilon_{axial}}\right) \quad (5.3)$$

Where: $\Delta\varepsilon_{trans}$ = change in transverse strain; $\Delta\varepsilon_{axial}$ = change in axial strain.

The intermediate strain rate drop tests were post-processed using the load cell data and positional output from video analysis. The loading curves from each dataset were extracted and used to calculate compressive stress - strain parameters at each time increment. The data were then smoothed using polynomial fits to remove noise within the load cell output (Fig. 5.8).

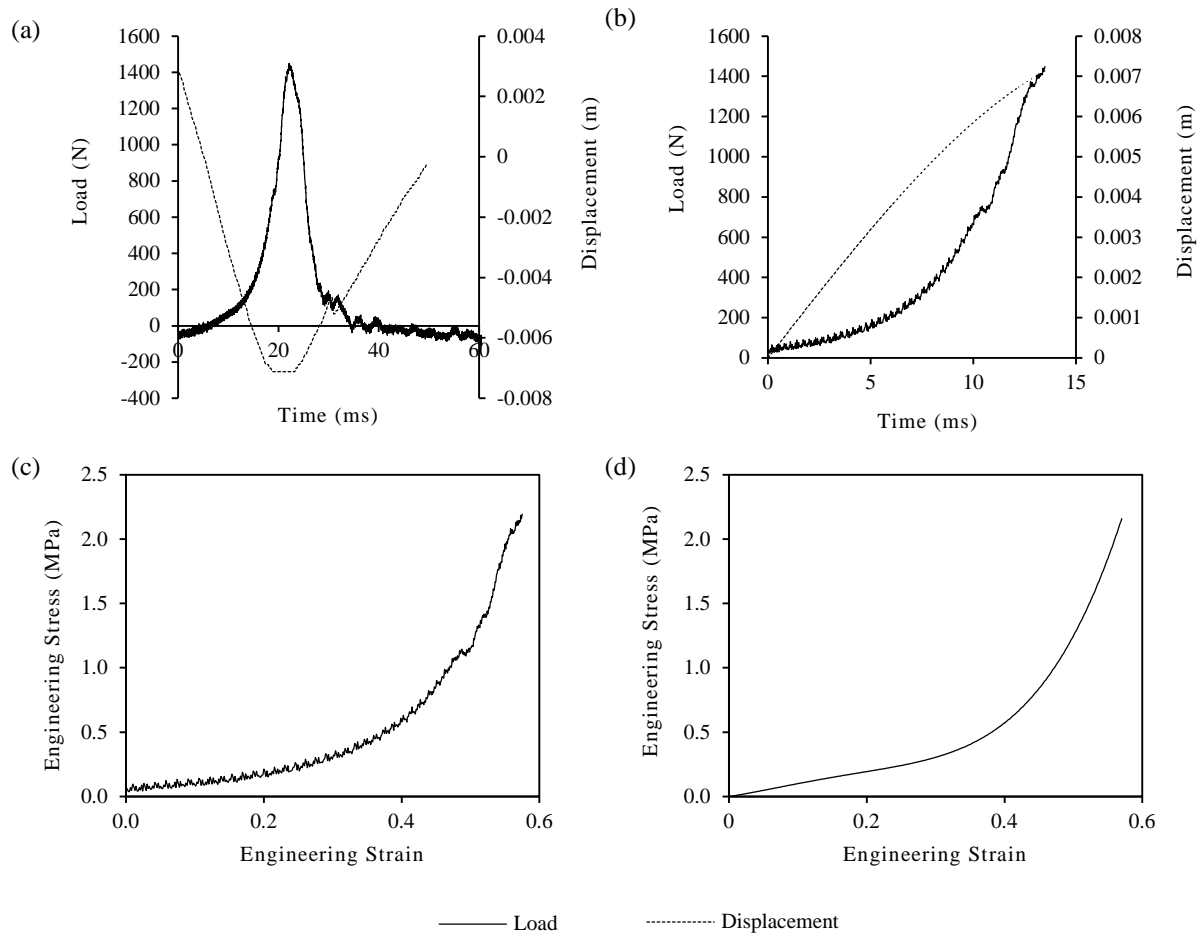


Figure 5.8 - Processing of intermediate strain rate drop tower data: (a) raw data; (b) load-time and displacement-time curves with coincident time scales; (c) unfiltered stress - strain output; (d) smoothed stress - strain plot.

5.4. Silicone Formulations

5.4.1. Base Formulations

Base concentrations of polymers in the Part A components were derived from previous work in the medical field and are detailed in Table 5.1.

Table 5.1 - Part A and B component base constituent concentrations (% by mass).

PART A		PART B	
V46 (w/filler)	63%	H301 Cross Linker	90%
V31 (w/filler)	18%	V21	10%
V21 (w/filler)	9%		
Catalyst	10%		

Initial investigations were performed to isolate the effects of changes in polymer and cross-linker concentrations on silicone response. A further iterative development study of combined changes in polymer and cross-linker concentrations provided bespoke silicone formulations to represent organic soft tissues. Comparisons with organic tissue properties were conducted using quasi-static compressive mechanical tests for ease of performance and comparison with literature due to matched strain rates.

5.4.2. Effects of Changes in Cross-Linker Concentrations

The ratio of Part A:B concentrations of the base silicones (Table 5.1) were used to alter the cross-linker concentrations within the silicones. A 10:1 Part A:B ratio is commonly given as a standard mix ratio in commercially bought silicones. Part A:B silicone ratios of 10:1, 5:1, 2:1, and 1:1 were tested in uniaxial compression. The engineering stress - strain plots for each specimen are shown in Figure 5.9.

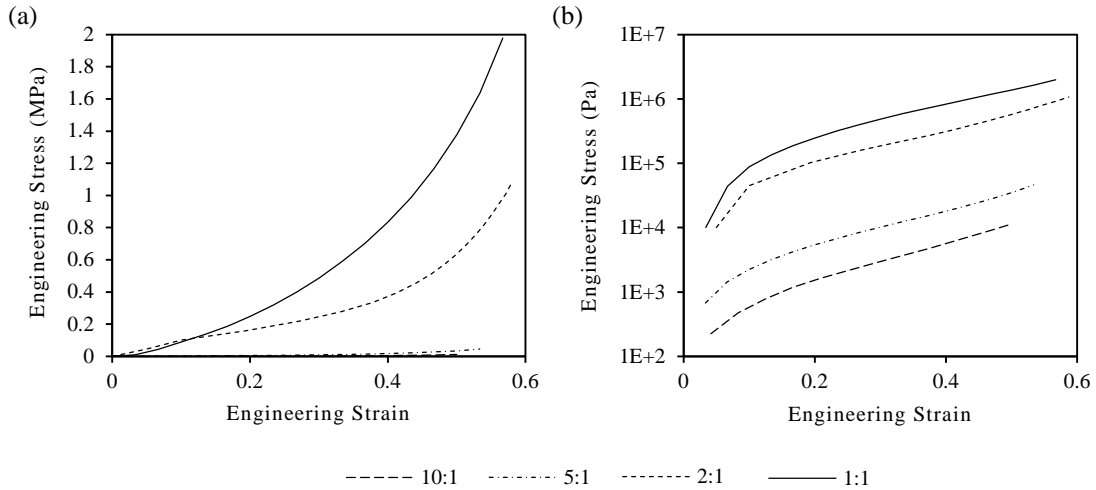


Figure 5.9 – Quasi-static compressive engineering stress - strain plot of silicones with different cross-linker concentrations in: (a) linear and (b) log-linear graphs.

The stress - strain plot shows that greater cross-linker concentrations significantly increase the stiffness of the silicones. The failure strains for each silicone specimen are shown in Table 5.2. The stiffer 1:1 specimen experienced brittle failure at 0.6 engineering strain (Fig. 5.10).

Table 5.2 – Failure strains for each cross-linker specimen.

Specimen No.	Failure Strain
10:1	N/A
5:1	N/A
2:1	0.8
1:1	0.6

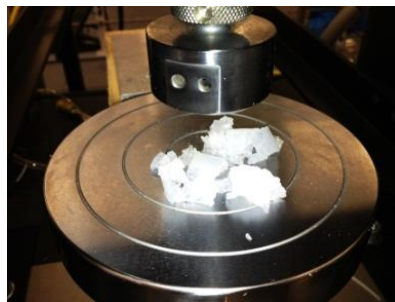


Figure 5.10 – Brittle failure of 1:1 PDMS silicone specimen.

The densities of the specimens were also recorded. A mean density of $1.01 \times 10^3 (\pm 0.05) \text{ kg.m}^{-3}$ was reported. This is comparable to the reported densities of organic soft tissues (Table 4.2).

5.4.3. Effects of Changes in Polymer Concentration

A series of tests were conducted to determine the effects of changes in polymer constituent concentrations. A systematic approach was adopted with variations from the Part A base polymer concentrations (Table 5.1). The base polymer concentrations were altered by a predetermined ratio (Table 5.3) to observe effects of changes in long chain V46 relative to constant V31:V21 ratios and the effect of changes in V31:V21 ratios at consistent lower V46 concentrations.

The samples all still maintained a 90% polymer, 10% heat cure catalyst mix in the Part A solution; however, for simplicity, the polymer ratios are varied independently (out of 100%). A 2:1 Part A:B ratio was employed somewhat arbitrarily initially as a point of comparison.

Table 5.3 – Constituent Part A polymer ratios.

Specimen No.		V46	V31	(RATIO)	V21
7			24%	1:1	24%
6	<i>Min.</i>	52%	32%	2:1	16%
5			40%	5:1	8%
4			15%	1:1	15%
3	<i>Base</i>	70%	20%	2:1	10%
2			25%	5:1	5%
1	<i>Max.</i>	85%	10%	2:1	5%

Seven specimens were fabricated initially, with ‘Specimen 1’ representing the maximum concentration of the V46 polymer and ‘Specimen 7’ with the minimum V46 and V31 polymers. Figure 5.11 shows the engineering stress - strain curves of silicones up to 0.5 strain. In general, the specimens with a greater concentration of long chain polymers exhibited the greatest stiffness. There is a strain hardening effect occurring in all of the specimens, which is particularly pronounced at strains greater than 0.1. Specimen’s 3 - 6 all exhibited similar responses to the loading stimulus, which would indicate that the amount of long chain V46 polymer has the greatest effect upon the materials stiffness. As expected, the softest silicone the contained the lowest concentrations of V46 and V31, and the greatest concentration of V21 polymer.

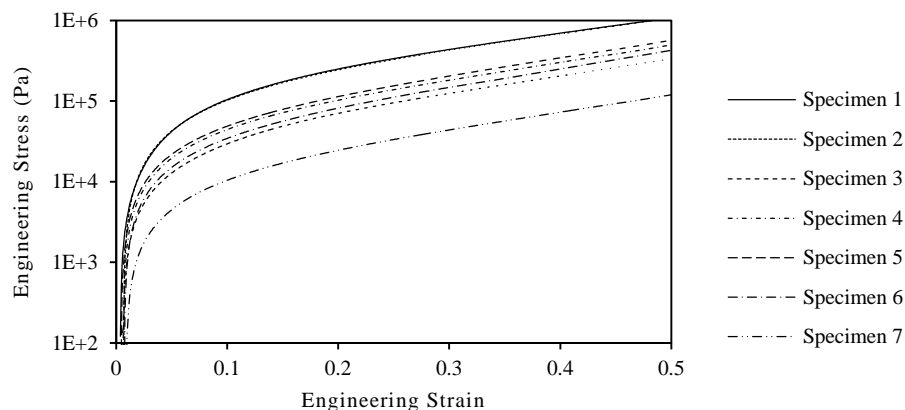


Figure 5.11 – Log - linear engineering stress - strain plot showing differences in response based on changes in polymer concentrations.

The failure strains for each of the silicones are detailed in Table 5.4. The specimens with the greatest concentrations of long chain polymer's exhibited more brittle behaviour and failed at lower strains than the predominantly shorter chain polymer silicones.

Table 5.4 - Failure strains of PDMS silicone specimens.

Specimen No.	Failure Strain
1	0.6
2	0.6
3	0.7
4	0.7
5	0.7
6	N/A
7	N/A

5.4.4. Bespoke Silicone Formulations

To provide more accurate representations of human tissues, a combination of changes in cross-linker and polymer concentrations were required. An iterative development process was undertaken varying each of the constituent parts to match the specific target organic tissue properties (§2.3.2) (Fig. 5.12). In order to be adequate, the bespoke simulants needed to at least provide a better match than previously used single material simulant, Silastic 3483 and ideally exhibit a quasi-static response within 200% of the target organic tissue dataset at any strain.

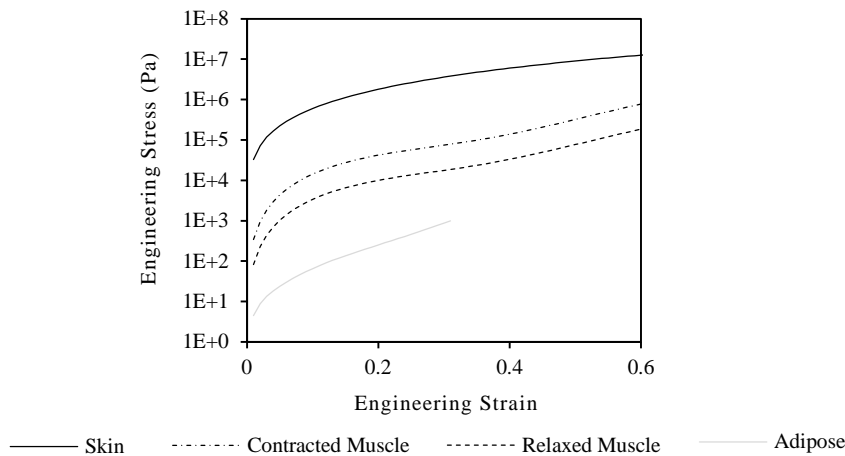


Figure 5.12 – Log - linear engineering stress - strain plot showing target organic tissue properties for bespoke PDMS simulants.

Bespoke silicone formulations were developed initially to match the quasi-static mechanical properties of the target organic tissues. The specific formulations of each tissue simulant are detailed in Table 5.5.

Table 5.5 - Part A and B silicone constituent concentrations (% by mass).

	Part A			Catalyst	Part B		Part A:B Ratio
	Polymers				H301 Cross Linker	V31 Polymer	
	V46	V31	V21				
<i>Relaxed Muscle</i>	46.8%	28.8%	14.4%				4:1
<i>Contracted Muscle</i>	46.8%	21.6%	21.6%	10%	10%	90%	3:1
<i>Skin</i>	76.5%	9.0%	4.5%				1:1
<i>Adipose</i>	46.8%	21.6%	21.6%				10:1

5.5. Mechanical Properties of Bespoke Silicones

5.5.1. Low Strain Rate Tests

a) Uniaxial Compression Tests

Engineering stress - strain graphs for quasi-static tests on the developed PDMS simulants have been presented and compared with published organic tissue data in Figure 5.13 with percentage differences plotted. The graphs illustrate that adipose, relaxed muscle and contracted muscle tissue simulants exhibit close responses to the organic tissues; however the skin tissue shows significant differences. The simulants typically initially exhibit a stiffer response up to approximately 0.4 strain at which point the organic tissues stiffen by a greater magnitude than the silicones. The PDMS adipose, relaxed muscle and contracted muscle simulants all show a maximum error of between 200 - 250% at 0.04 - 0.06 strain decreasing to 0% error in each simulant at increased strains. However, the PDMS skin simulant exhibited errors between 84 - 90% of the organic tissue properties across all strains (N.B. the significant error in quasi-static behaviour of the skin simulant is not representative of its response at higher strain rates (Fig. 5.17)).

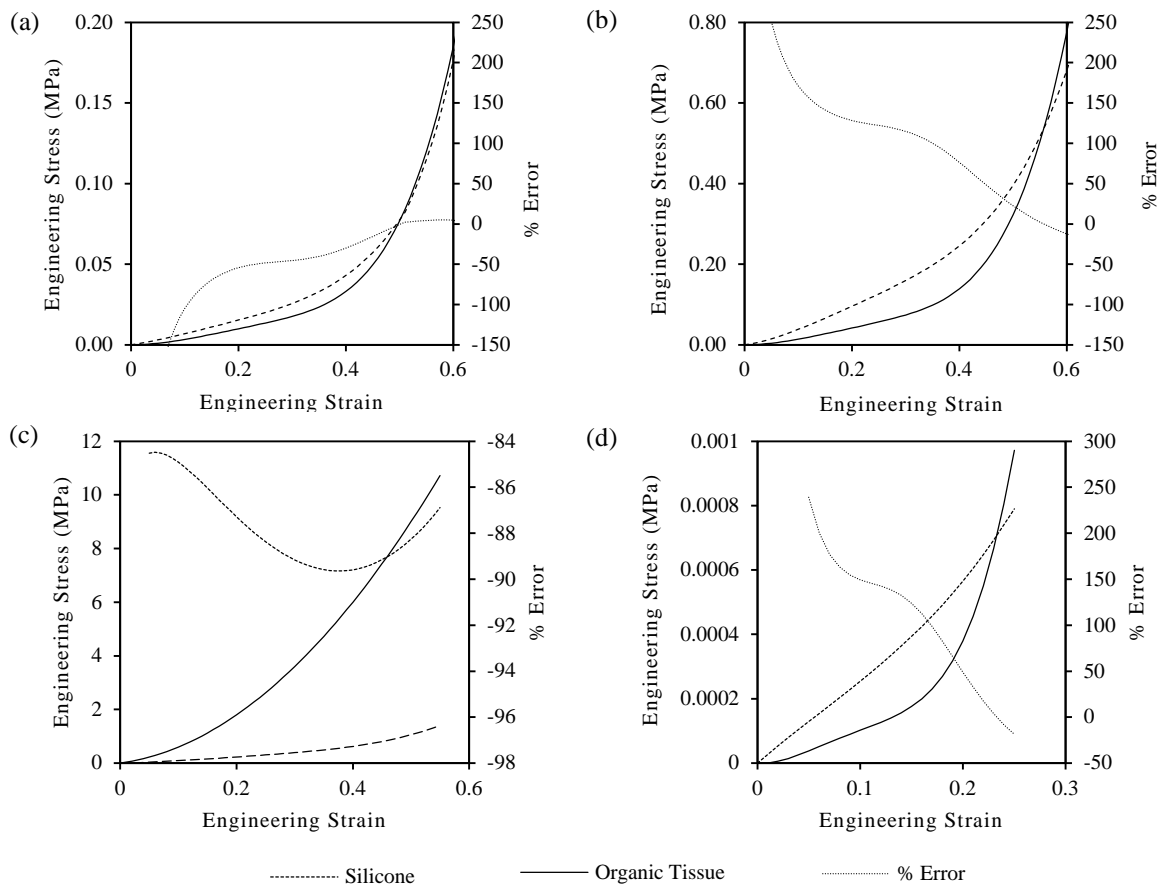


Figure 5.13 - Quasi-static stress - strain curves showing closeness of fit of PDMS silicones with organic tissue datasets in: (a) relaxed muscle (McElhaney, 1966; Song *et al.*, 2007); (b) contracted muscle (Zheng *et al.*, 1999); (c) skin (Shergold *et al.*, 2006); (d) adipose (Comley & Fleck, 2012).

The quasi-static compressive mechanical responses of each of the PDMS simulants have been compared to the quasi-static response of Silastic 3483 (Fig. 5.14).

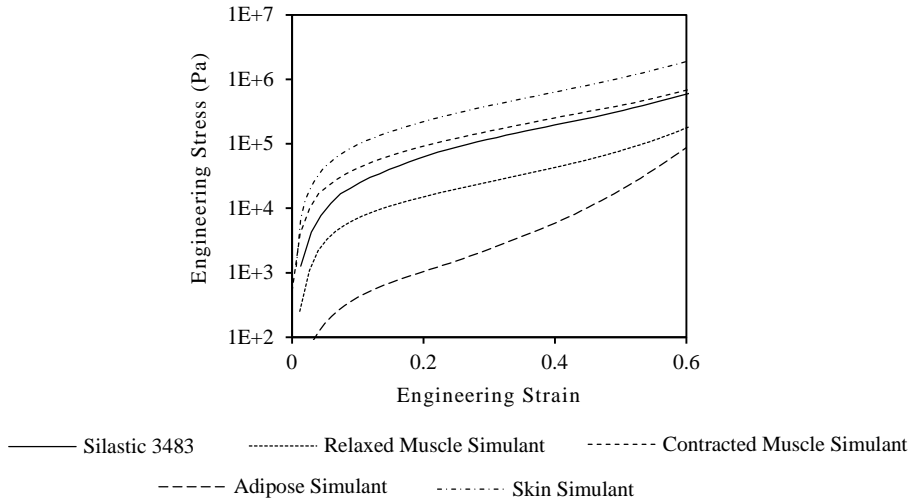


Figure 5.14 - Log-linear plot of quasi-static compressive responses of PDMS simulants compared to Silastic 3483.

Silastic 3483 exhibited significantly greater divergences from organic tissue predictions than the PDMS simulants in skin, adipose and relaxed muscle with up to 329%, 11,240% and -92.9% differences from the target organic tissue datasets at 0.3 strain respectively. Silastic 3483, however, provided the closest representation of organic contracted muscle tissue dataset. Therefore, a more detailed evaluation of the closeness of fit between Silastic 3483 and target contracted muscle tissue properties has been performed (Fig. 5.15). Both silicone simulants exhibit similar stress profiles and comparable fits when compared to the organic tissue dataset. The PDMS simulant exhibited a 250% error at 0.05 strain, whilst Silastic 3483 only showed a 201% error. At higher strains, however, the PDMS simulant showed a closer fit to the target dataset with a -12.3% error at 0.6 strain compared to a -24.7% error in the Silastic 3483.

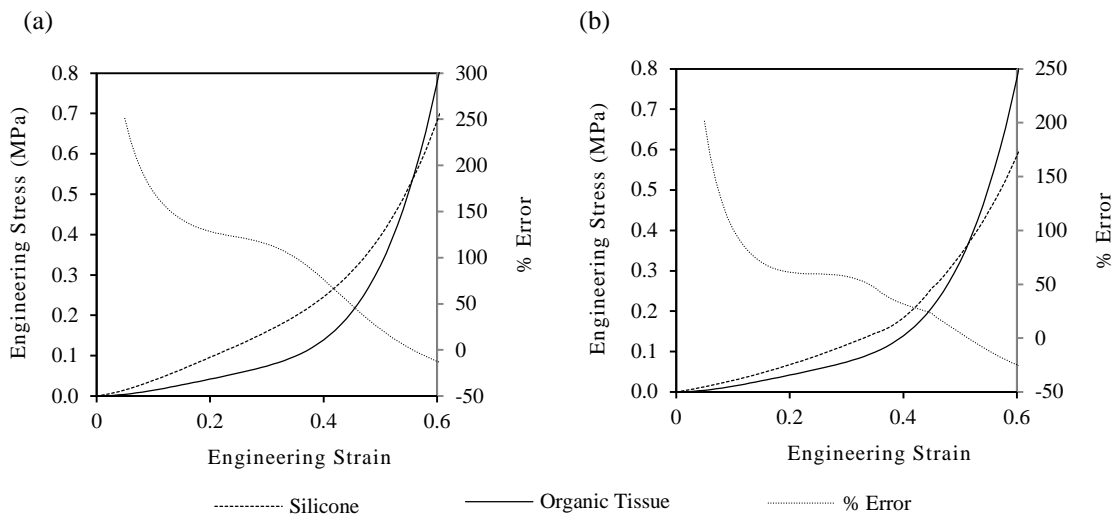


Figure 5.15 – Graphs showing closeness of fit of silicone simulants with contracted muscle target organic tissue dataset (Zheng *et al.*, 1999) for: (a) PDMS simulant and (b) Silastic 3483.

(i) Poisson's Ratio

The Poisson's ratio from each material was measured using HSV analysis. The results showed that all the silicones were practically incompressible and embodied a Poisson's ratio between 0.47 and 0.5 (Table 5.6).

Table 5.6 - Calculated Poisson's ratio values of PDMS simulants.

	Poisson's Ratio
<i>Relaxed Muscle</i>	0.493
<i>Contracted Muscle</i>	0.480
<i>Adipose</i>	0.492
<i>Skin</i>	0.476

(ii) Mullins Effect

The percentage difference in compressive stresses between the first and last loading cycle at maximal strain were recorded. The stress-softening effect was present in all simulants but most apparent in softer silicones (adipose and relaxed muscle) where a 13.5% and 12.0% stress reduction was observed respectively (Table 5.7).

Table 5.7 - Percentage reduction in stress from first to last cycle in PDMS silicone simulants.

	% Reduction in Stress
<i>Relaxed Muscle</i>	12.0
<i>Contracted Muscle</i>	0.7
<i>Adipose</i>	13.5
<i>Skin</i>	3.9

5.5.2. Intermediate Strain Rate Tests

The response of the PDMS simulants tested at a range of intermediate strain rates are shown in Figure 5.16. The graphs show the materials all exhibit stiffer material behaviour at increased strain rates.

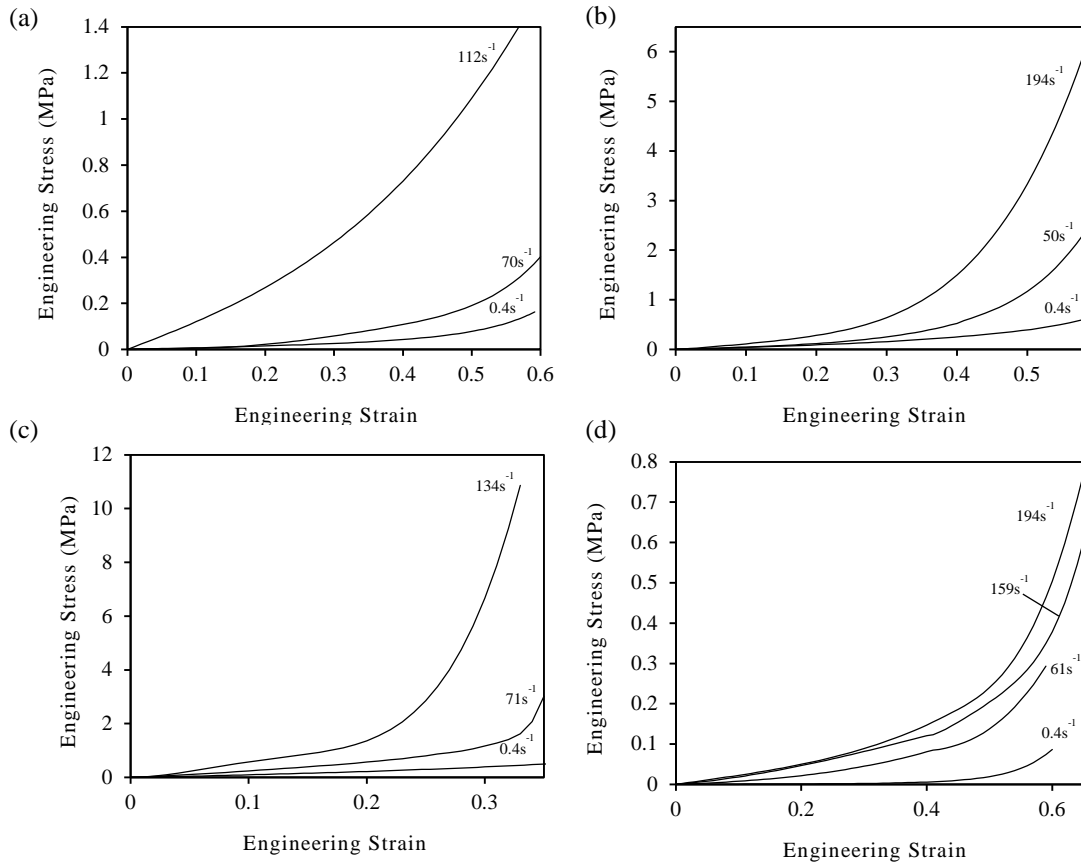


Figure 5.16 - Intermediate strain rate stress - strain curves for PDMS simulants: (a) relaxed muscle; (b) contracted muscle; (c) skin; (d) adipose.

At intermediate strain rates, the responses of the PDMS simulants were compared with the higher strain rate responses of the respective organic tissues; the banded regions indicate the PDMS responses (Fig. 5.17).

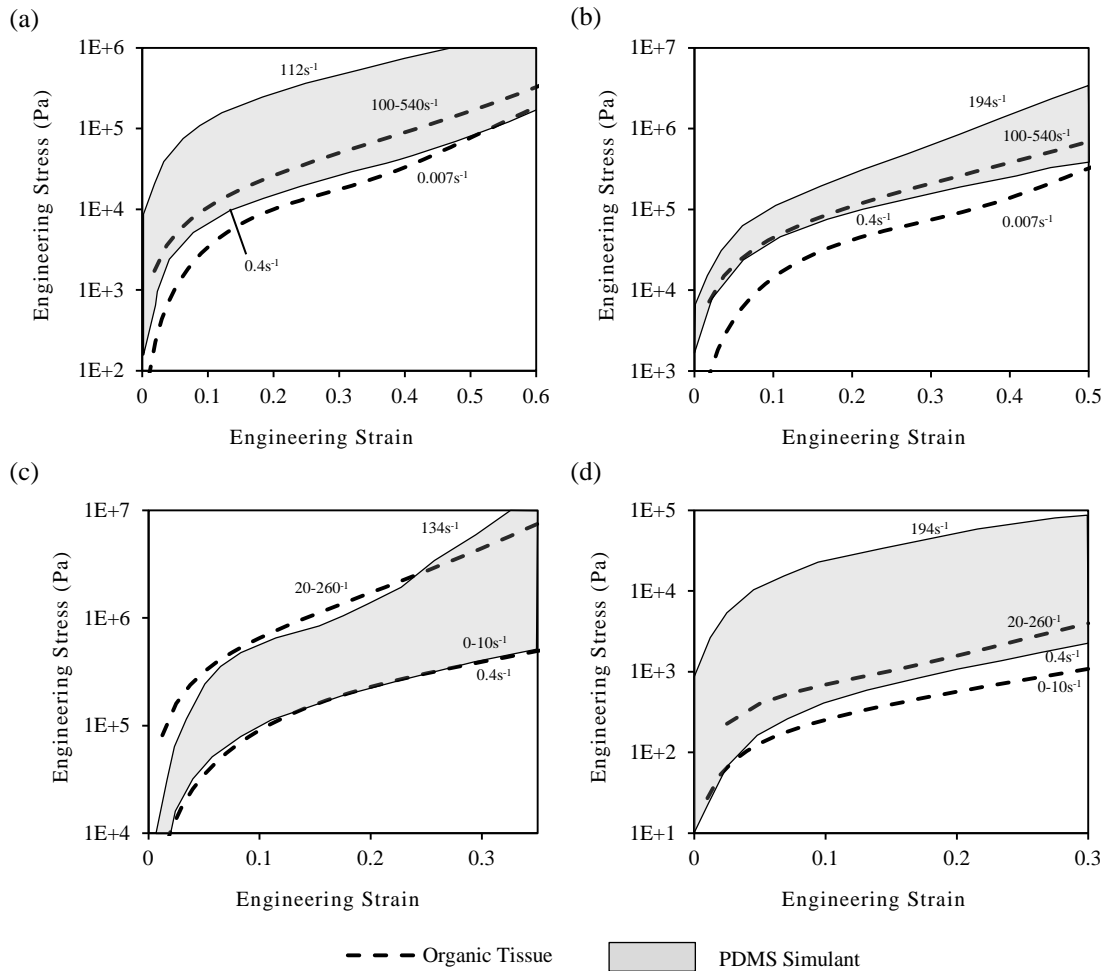


Figure 5.17 – Log - linear intermediate strain rate engineering stress - strain plots showing comparisons between PDMS simulants and organic tissues in: (a) relaxed muscle; (b) contracted muscle; (c) skin; (d) adipose.

The muscle tissue simulants, at quasi-static strain rates, demonstrated close fits with target organic tissue behaviour (Fig 5.13). There is, however, a significant divergence in the stiffness of the PDMS silicones at higher strain rates. This is most apparent in the relaxed muscle simulant between 0.1 and 0.3 strain, where the target organic tissue dataset exhibits a decreased relative stiffness. The responses of the PDMS skin tissue simulant exhibited a closer representation of organic tissue datasets at increased strain rates than under quasi-static loading conditions. The PDMS adipose simulant, however, exhibited a significantly greater stiffness than the organic equivalent, in particular at low strains and high strain rates.

5.5.3. Stress Relaxation Tests

The results from the ramp and hold stress relaxation tests are compared to tests on organic tissues (§4.3.3.b) and are displayed in Figure 5.18. In all tests, the PDMS simulants exhibited lower stress relaxations; this is most notable in the skin simulant.

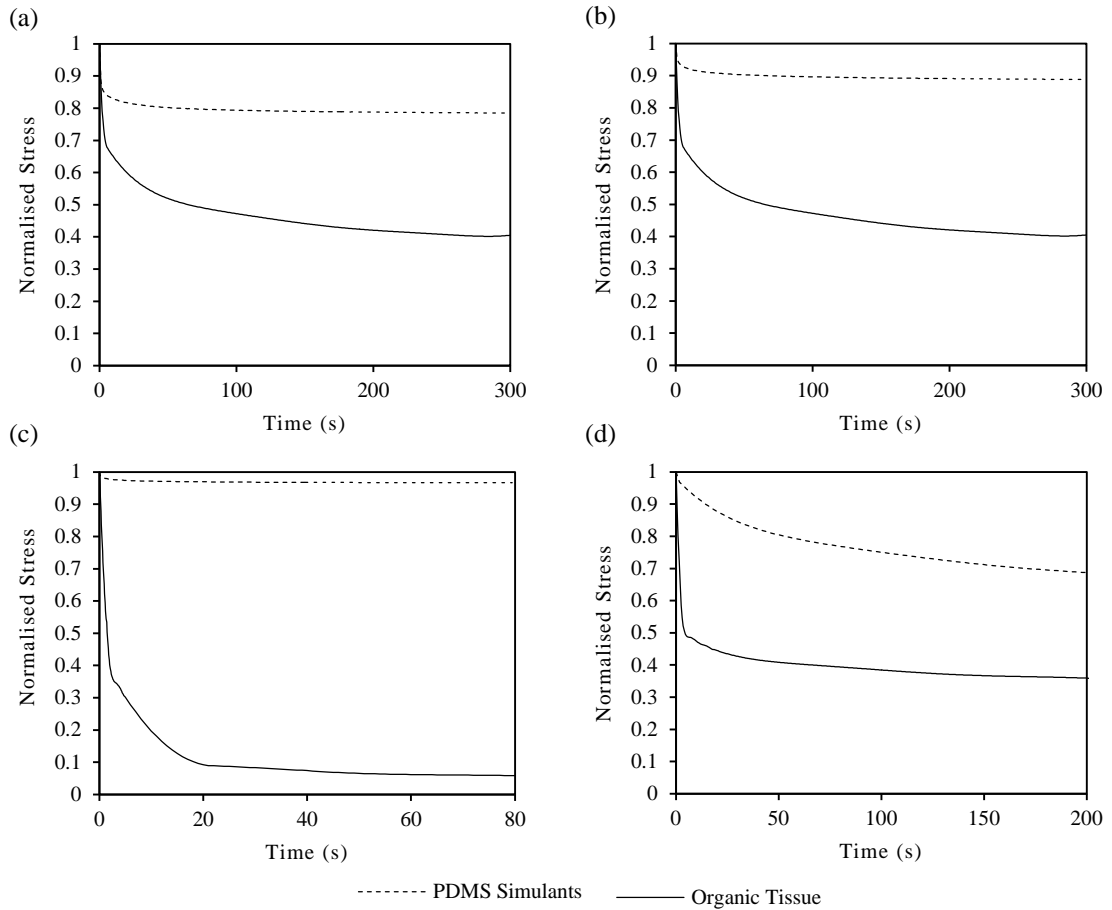


Figure 5.18 – Normalised stress - time plot showing stress relaxation of PDMS simulants compared with organic tissue data in: (a) relaxed muscle (Van Loocke *et al.*, 2009); (b) contracted muscle (Van Loocke *et al.*, 2009); (c) skin (Wu *et al.*, 2003); (d) adipose (Gefen & Haberman, 2007).

5.5.4. Durability Tests

The materials were all tested before and after the cyclic testing protocol, the results are shown in Figure 5.19. All simulants experienced no visible damage; however a softening effect is clearly present in the softer silicones, particularly adipose where there was a 25.4% reduction in stress at 0.5 strain.

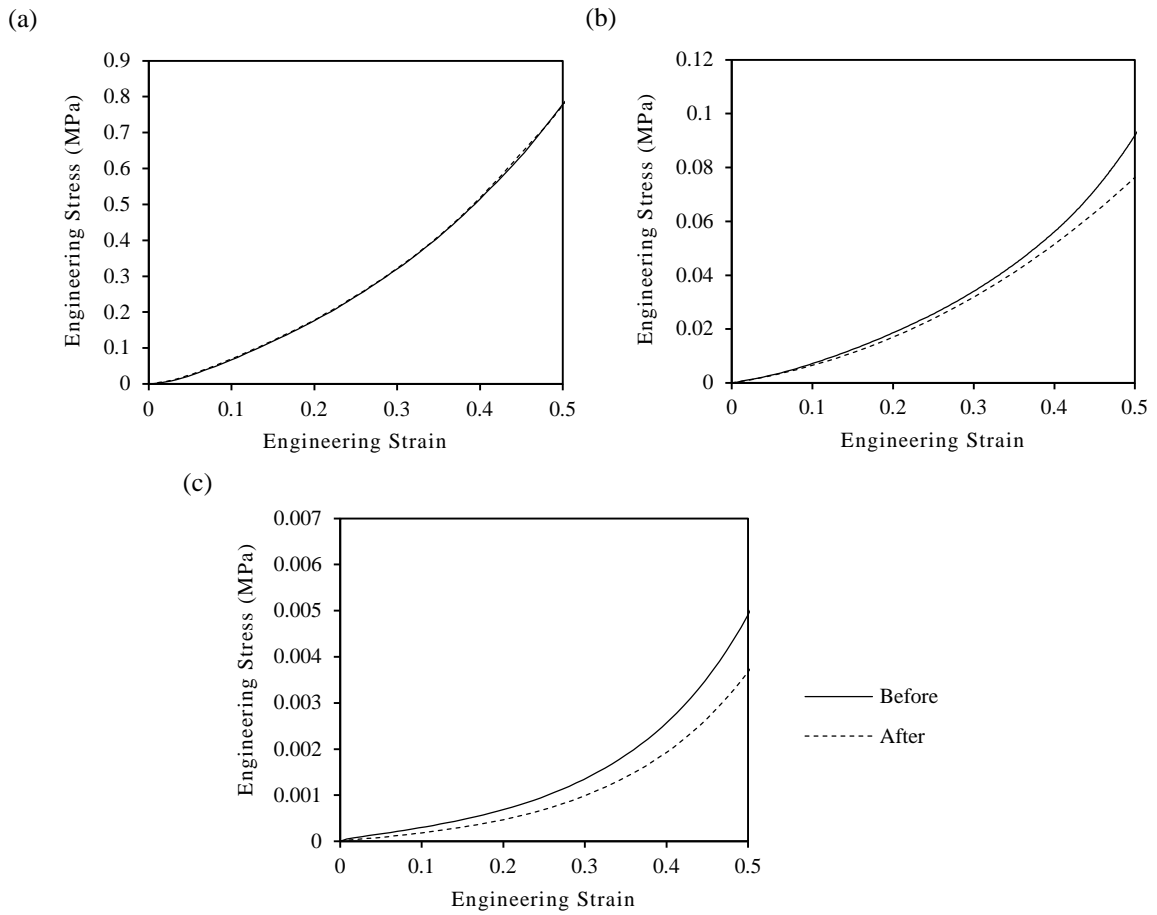


Figure 5.19 - Engineering stress - strain plots showing quasi-static simulant responses before and after repeated loading cycles for: (a) PDMS skin; (b) PDMS relaxed muscle and (c) PDMS adipose simulants.

5.5.5. Consistency of Response

The consistency of silicone responses was explored to examine the potential variability in mechanical responses from different batches under current fabrication procedures. Six identical specimens were fabricated. The differences in compressive stress are shown in Fig 5.20 with the compressive stress at different strain intervals detailed in Table 5.8.

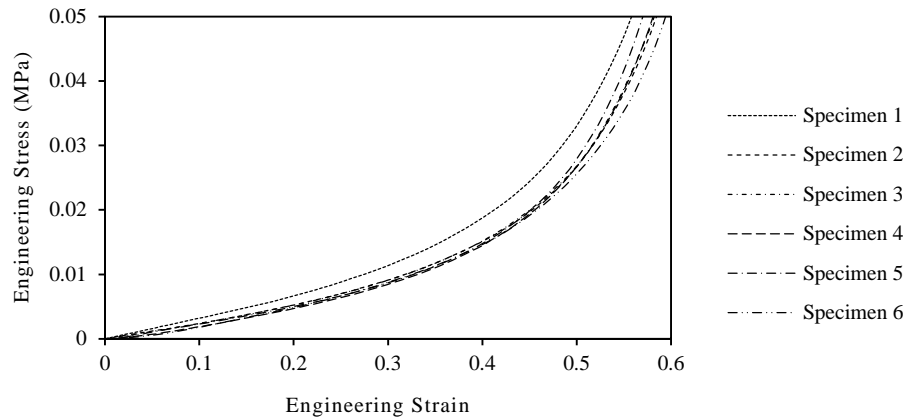


Figure 5.20 – Engineering stress - strain plots of six identical PDMS silicone test specimens.

The results show increasing magnitudes of variance at higher strains with the SD approximately an order of magnitude greater at each strain interval considered. A maximal difference in response from the experimental mean was 18.6% at 0.6 strain; however, ‘Specimen 1’ appears to be an outlier. Ignoring this data, the maximum divergences from the experimental mean were 2.07%, 2.86% and 12.3% at 0.2, 0.4 and 0.6 strain respectively.

Table 5.8 - Compressive stresses at different strains for six identical test specimens.

Specimen No.	Compressive Stress (MPa)		
	0.2 Strain	0.4 Strain	0.6 Strain
1	0.00669	0.0189	0.0719
2	0.00509	0.0155	0.0574
3	0.00515	0.0154	0.0610
4	0.00499	0.0147	0.0616
5	0.00515	0.0149	0.0680
6	0.00507	0.0150	0.0548
Mean	0.00509	0.0151	0.0606
SD	6.09×10^{-5}	2.99×10^{-4}	0.00446
Max. Difference from Mean	2.07%	2.86%	12.3%

These results suggest that during surrogate impacts, there will be a small variance between material batches through most of the operational strain levels induced in the PDMS silicones. At extreme strain deformations where significant strain hardening is present there may be a greater variance between batches. However, the duration with which the surrogate will experience these high strains will be short and therefore the differences in experimental response could be reasonably expected to be small.

5.6. Material Models

5.6.1. Hyperelastic

Constitutive material models were used to describe the mechanical behaviour of the simulants through a range of strain rates. The simulant materials all exhibit significant strain hardening effects and as such require hyperelastic models to describe their stress - strain behaviour. First-order phenomenological models were evaluated which consider changes in stiffness based on the strain energy density of the material. The Ogden (Equation (4.3)), Mooney-Rivlin and Neo Hookean have been widely used in literature to describe incompressible, hyperelastic materials (Marckmann & Verron, 2006; Ali *et al.*, 2010). The Mooney-Rivlin model (Rivlin, 1948) is a commonly used material model to describe rubber-like behaviour due to its simplicity and ability to model moderate deformations (30 - 200%) and high strain hardening (Shergold *et al.*, 2006; Meunier *et al.*, 2008). It is a first order polynomial model represented by Equation (5.3) where C_{10} is a material parameter and $C_{00} = 0$. The Neo-Hookean model (Treloar, 1943) is a first order reduced polynomial (Equation (5.4)). It is the simplest hyperelastic constitutive equation for describing rubber behaviour at low strains (up to 30%) and is often used when material data is insufficient as it only requires a single material parameter (Marckmann & Verron, 2006).

Mooney-Rivlin:

$$W = \sum_{i,j=0}^N C_{ij} (\bar{I}_1 - 3)^i (\bar{I}_2 - 3)^j \quad (5.3)$$

Neo-Hooke:

$$W = C_{10}(\bar{I}_1 - 3) + \frac{1}{D_1}(J_{el} - 1)^2 \quad (5.4)$$

Typically, FE solvers determine material parameters automatically by fitting a strain energy function to uniaxial test data based on a non-linear least squares optimisation. The commercial FEA solver, Abaqus/Explicit (Version 6.13) was used to perform this analysis; the quality of the fits are shown in Figure 5.21 with generated material coefficients presented in Table 5.9 alongside root mean square (RMS) errors showing the degree of divergence of each dataset from the experimental data.

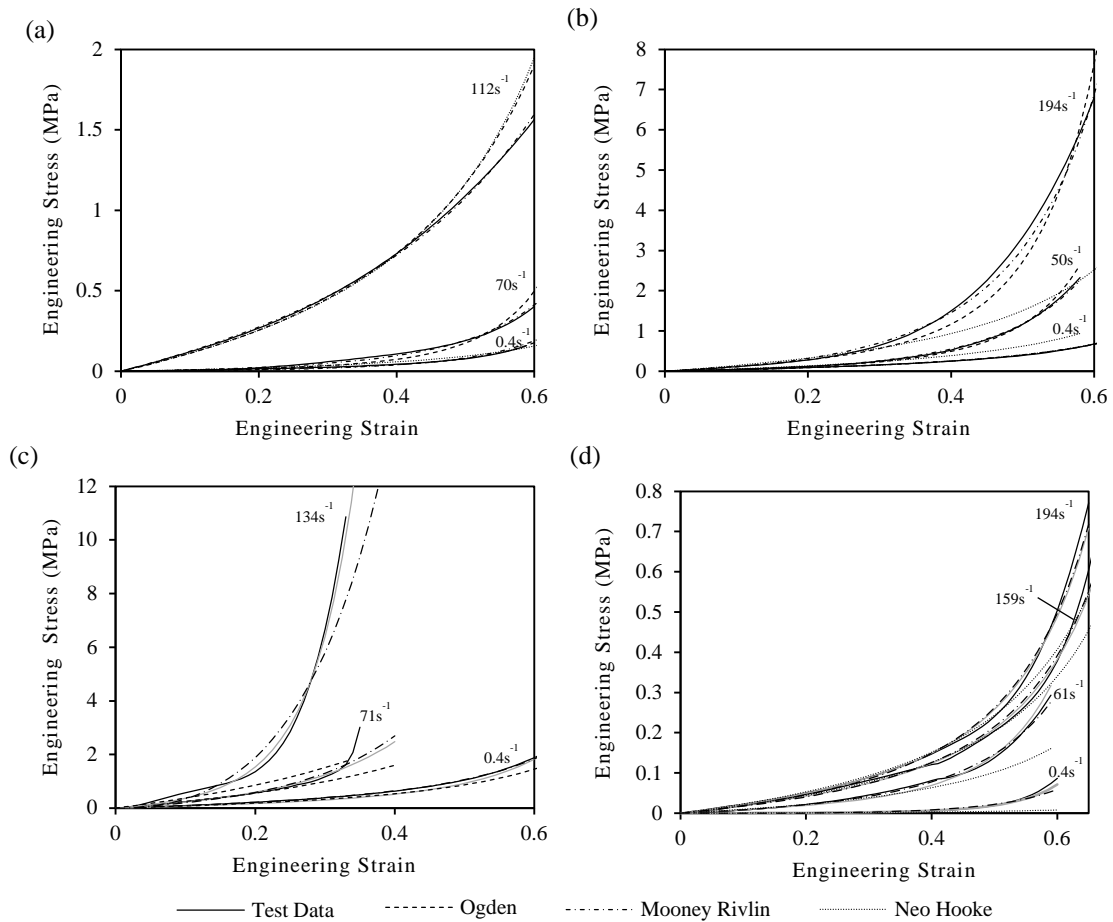


Figure 5.21 - Hyperelastic model fits for: (a) relaxed muscle; (b) contracted muscle; (c) skin; (d) adipose.

The Mooney-Rivlin model generally provided a good fit (< 0.293 MPa RMS) for relaxed muscle, contracted muscle and adipose simulants through the range of strain rates reported. The model, however typically underestimated the magnitude of strain hardening at high strains (e.g. relaxed muscle, 112 s^{-1} ; skin, 134 s^{-1}). The Ogden model also generally provided the best description of the skin simulant which exhibits a significant strain hardening effect; this is most notable at 134 s^{-1} . It also generally provided good fit (< 0.731 MPa RMS) for other simulants through the range of strain rates tested but typically under estimated the compressive stresses under low strain, low strain rate conditions and overestimated the strain hardening present at higher strains (> 0.5 strain). The Neo Hookean model provided the worst performance of the three models and was unable to capture much of the non-linearity of the silicone behaviour, particularly in the stiffer simulants (e.g. contracted muscle, 50 s^{-1} and 194 s^{-1}). The material model coefficients are detailed in Table 5.9.

Table 5.9 - Hyperelastic model coefficients for PDMS simulants with RMS error from experimental data.

		<i>Mooney-Rivlin</i>			<i>Ogden</i>			<i>Neo Hooke</i>	
		C_{01}	C_{10}	<i>RMS Error</i>	μ	α	<i>RMS Error</i>	C_{10}	<i>RMS Error</i>
<i>Relax. Musc.</i>	0.4 s ⁻¹	-4.07×10^3	8.29×10^3	0.293	1.72×10^4	5.14	0.0232	1.38×10^4	0.0843
	70 s ⁻¹	4.25×10^2	1.57×10^4	0.0368	2.51×10^4	7.36	0.00715	1.34×10^4	0.0931
	112 s ⁻¹	2.24×10^5	-3.49×10^4	0.0890	3.29×10^5	1.50	0.00942	1.67×10^5	0.0995
<i>Cont. Musc.</i>	0.4 s ⁻¹	6.00×10^4	-1.12×10^3	0.00769	1.16×10^5	1.73	0.00799	5.81×10^4	0.0119
	50 s ⁻¹	-7.76×10^4	1.23×10^5	0.0203	1.66×10^5	7.40	0.0658	8.92×10^4	0.176
	194 s ⁻¹	-1.70×10^5	3.03×10^5	0.229	4.02×10^5	7.22	0.730	2.15×10^5	1.88
<i>Skin</i>	0.4 s ⁻¹	1.27×10^5	1.21×10^4	0.00771	2.36×10^5	3.98	0.330	1.24×10^5	0.035
	71 s ⁻¹	3.17×10^5	5.62×10^5	0.107	5.92×10^5	2.61	0.125	3.68×10^5	0.258
	134 s ⁻¹	5.24×10^6	5.18×10^6	1.41	7.40×10^5	9.41	0.311	5.62×10^5	3.94
<i>Adipose</i>	0.4 s ⁻¹	4.42×10^3	3.79×10^3	0.00157	8.29×10^2	4.82	0.00209	6.83×10^2	0.0145
	61 s ⁻¹	2.55×10^3	9.19×10^3	0.00478	2.74×10^4	5.94	0.00773	1.45×10^4	0.0364
	159 s ⁻¹	2.00×10^4	5.35×10^3	0.0127	5.76×10^4	3.14	0.00806	2.90×10^4	0.0184
	194 s ⁻¹	1.76×10^4	9.90×10^3	0.0124	6.86×10^4	3.55	0.0131	3.48×10^4	0.0521

5.6.2. Viscoelasticity

The viscoelastic properties of organic soft tissues are presented in the form of quasi-linear viscoelastic (QLV) Prony Series determined from stress relaxation tests. The force - time data from the stress relaxation tests were manipulated to determine the compressive stresses at each time interval (§4.3.3.b). The uniaxial stresses were then normalised from the point of maximal stress to determine the shear modulus parameter, $g(t)$ (Equation 4.4). The model coefficients for each PDMS simulant are detailed in Table 5.10.

Table 5.10 - Prony series coefficients for PDMS simulants.

	i	$g(i)$	$\tau(i)$
<i>Relaxed Muscle</i>	1	1.28×10^{-1}	3.52×10^{-1}
	2	5.29×10^{-2}	8.07
	3	3.39×10^{-2}	7.61×10^1
<i>Contracted Muscle</i>	1	4.83×10^{-2}	3.25×10^{-1}
	2	3.66×10^{-2}	6.91
	3	2.70×10^{-2}	8.49×10^1
<i>Skin</i>	1	2.67×10^{-2}	8.51×10^{-1}
	2	8.07×10^{-3}	4.04×10^1
<i>Adipose</i>	1	1.39×10^{-1}	7.51×10^{-5}
	2	1.70×10^{-1}	3.07
	3	7.41×10^{-2}	7.90×10^1

5.7. FE Specimen Tests

The mechanical testing procedures used to characterise the PDMS simulants were reproduced in FEA to verify the accuracy of the material models. The ASTM D395 cylindrical test specimens were discretised into 20,080 C3D8R elements with a nominal element size of 8×10^{-4} m. One surface was constrained in all translational directions whilst a compressive displacement was applied from the other surface at a constant rate to match both quasi-static and intermediate strain rate loading conditions. Simulations were performed on each of the PDMS simulants. Comparisons with experimental data have been presented in Figure 5.22.

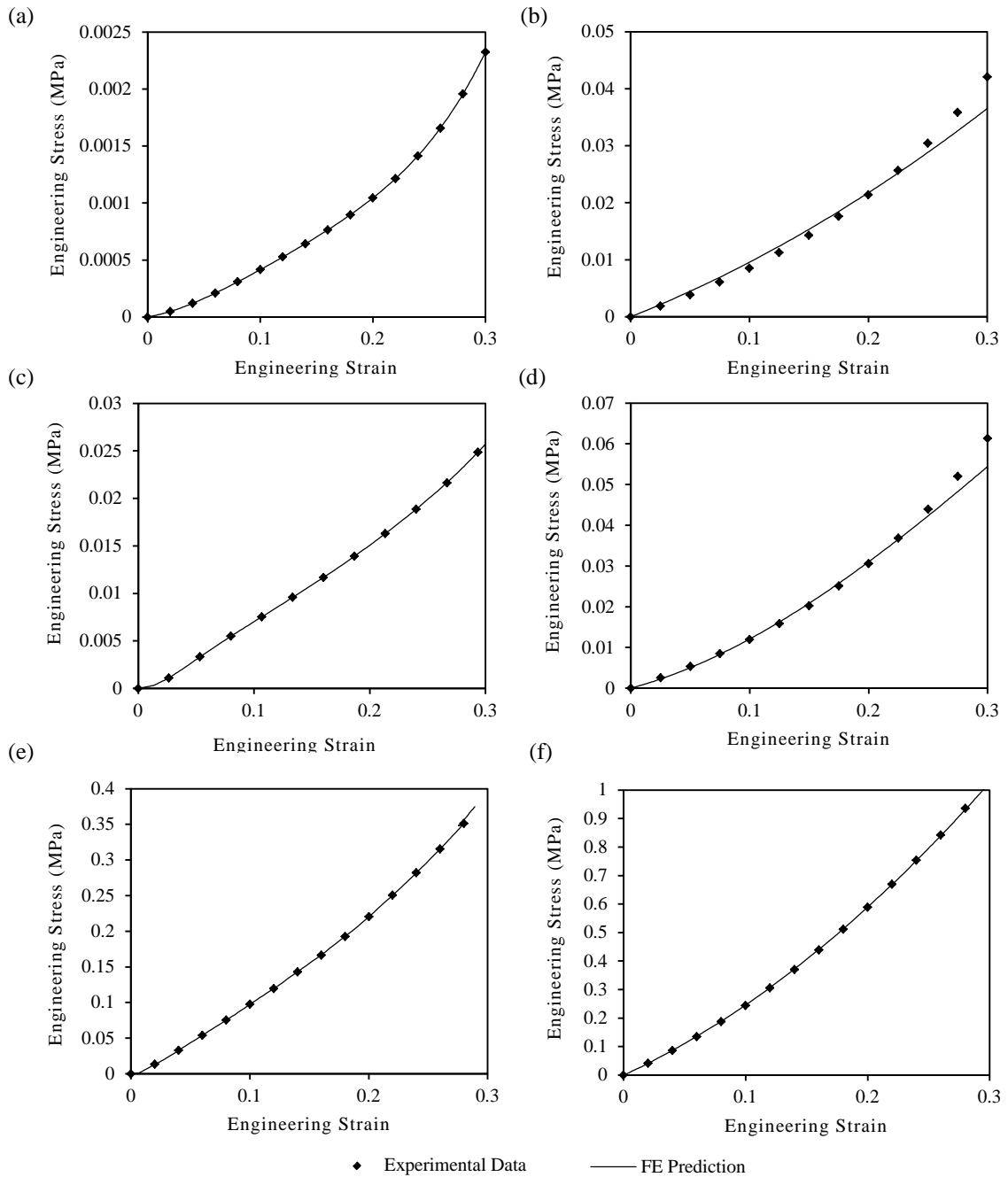


Figure 5.22 - Compressive specimen test comparisons in PDMS simulants: (a) adipose - quasi-static; (b) adipose - strain rate; (c) relaxed muscle - quasi-static; (d) relaxed muscle - strain rate; (e) skin - quasi-static; (f) skin - strain rate.

5.8. Discussion

5.8.1. Mechanical Characterisation Procedures

There are many standardised mechanical characterisation procedures defined for elastomers (e.g. ASTM D395, 2008; ISO 3384-1, 2011) However, there is a lack of agreement within and between national and international standards organisations proposing measures to test elastomers. Therefore it was important that the tests conducted corresponded with those used in the target organic tissue datasets and represented the ultimate mechanical loading modes the surrogates would be subjected to.

Unconfined compressive tests were used to characterise the mechanical behaviour of the PDMS simulants as this loading mode was used in target datasets. Compressive material behaviour is also pertinent to surrogate impact testing as a key deformation mode from normal blunt force impact trauma. In addition, as the PDMS simulants are quasi-incompressible, compressive material data incorporates simultaneous assessment of the in-plane tensile response. The mechanical behaviour values presented in this chapter are from a single characterisation study and as such are intended to represent the mechanical response of the material at the particular instant in time. Variability is inherently introduced through inconsistencies in the production environment demonstrated in §5.5.5. However the magnitude of these deviations is expected to be small during operational strain levels. Nevertheless, to ensure each material batch is representative of the absolute values presented, it is important to conduct mechanical characterisation tests and adopt the newly established properties when populating subsequent constitutive models.

In unconfined compressive tests, it was important to ensure that the surfaces of the specimens were coated in lubricant as significant shear stresses can be induced due to frictional forces resulting in an over prediction of the true compressive response. Despite these limiting measures, some frictional forces would have still been incorporated. This could potentially have been improved upon through use of biaxial tensile tests, which, in incompressible materials, can present a state of strain equivalent to pure compression (Miller, 2000). Given further research, additional mechanical loading modes could also be considered that may enhance the quality of resultant material models; this could include tensile, shear or volumetric compression modes.

5.8.2. PDMS Silicone Behaviour

Bergström & Boyce (2001) state that elastomeric materials show time-dependent behaviour exhibited by: rate dependence, where stress to reach a given strain increases with strain rate; stress relaxation, where the stress will relax with time until it reaches an equilibrium state; and hysteresis, where there are energy losses in deformation. The developed PDMS silicone simulants each exhibited near incompressibility, mechanical hysteresis, stress softening effect, stress relaxation and strain rate dependencies. The incompressibility of the PDMS simulants is also widely supported by literature concerned with elastomers (Ali *et al.*, 2010; Mottahedi *et al.*, 2011) and organic muscle tissue (Van Loocke *et al.*, 2009; Böl *et al.*, 2012), skin (Ni' Annaidh *et al.*, 2012) and adipose (Samani *et al.*, 2003; Comley & Fleck, 2010).

The effects of temperature and filler were not directly investigated in this study, though could influence the mechanical response of the silicones. The presence of filler particles in the silicone can significantly restrict the mobility of polymer chains and increase the degree of non-linearity

exhibited (Cosgrove *et al.* 1997; Cassagnau & Mélis, 2003). It is also suggested that less-filled rubber exhibits purely entropic behaviour with no mechanical dissipation, whilst filled rubber exhibits both viscous and entropic behaviour, increasing temperature sensitivity (Martinez *et al.*, 2013). The effect of temperature on the behaviour of the silicones, although controlled was not examined explicitly in this study and has potential effects on the mechanical response. Rey *et al.* (2013) noted that filled silicones exhibited an increase in stiffness at increasing temperatures which shows that the effects of entropic changes are much greater than viscous changes. A greater stress softening effect was also experienced in filled rubbers at lower temperatures below 60°C. Further manipulation of the silicone formulations may consider the concentration and type of filler present in the polymer to alter the mechanical properties of the cured silicone and create improved parallels with the target organic data.

The formulation methods used can also affect the mechanical properties of the resultant silicones (§5.3.1). Factors such as the mixing method and time, curing temperatures and times to cure all have a potential effect on the quality of the silicones. Further study could usefully investigate the specific effects of changes to each of the process variables.

5.8.3. Quality of PDMS Silicone Formulations

Given the target organic datasets established (§4.3.3.a) for a particular injury scenario (i.e. skin, adipose and muscle characterisation in an appropriate body segment, for a demographic of interest, over a relevant strain rate domain) this study explores whether superior synthetic materials can be developed to produce more biofidelic surrogates for experimental work and more biofidelic complementary constitutive models for computational analysis.

The success criteria of the developed silicone simulants were detailed previously (§5.2.5) and have been outlined again below.

- Is there scope with current *in vitro* data to develop materials that exhibit a more biofidelic response than previously used single material simulants?
- If better *in vivo* material properties become known, is there scope to develop silicones to match the new data?
- Is it possible to develop a silicone simulant that perfectly matches the organic tissue properties?

a) Are the PDMS formulations better than other surrogate materials?

(i) Quasi-static Response

Under quasi-static loading conditions, the relaxed muscle, contracted muscle and adipose tissue simulants all exhibited comparable stress - strain responses with organic tissues (Fig. 5.13). A maximal error of 250% was observed at 0.05 strain in the relaxed muscle simulant; however the error in each of the simulants decreased to 0% at a particular instant at increased strains. This was a trend across all simulants whereby the silicones exhibited a significantly stiffer response at low strains compared with the target organic tissues. This is likely to indicate an innate difference in the mechanical behaviour with organic tissues, rather than issues with the quality of the formulations. However the skin tissue simulant showed a significant divergence from the target organic tissue properties under quasi-static loading conditions with errors of up to 89% experienced between the PDMS simulant and organic tissues at 0.4 strain.

The responses of Silastic 3483 showed comparable behaviour to the target contracted muscle tissue dataset under quasi-static conditions (Fig. 5.14). When compared directly with the PDMS simulant, Silastic 3483 showed a closer response at low strains within (201% error vs. 250% in PDMS simulant), however a far greater divergence at 0.6 strain.

(ii) Intermediate Strain Rate Response

At increased strain rates, the silicones typically exhibited a greater stiffness than the organic tissues; this response was most pronounced in the adipose and relaxed muscle simulants (Fig. 5.17).

The relaxed and contracted PDMS simulants exhibited an increase in maximal stress response of $12.9 \times (0.4 - 112 \text{ s}^{-1})$ and $8.3 \times (0.4 - 194 \text{ s}^{-1})$ respectively at 0.5 strain. Previous skeletal muscle tissue characterisation studies have generated varied findings. Van Loocke *et al.* (2008) observed a $5 \times$ increase in maximal stress between 0.05 s^{-1} and 10 s^{-1} , whilst Van Loocke *et al.* (2009) observed an increase of $4.1 \times$ from $5 - 3200 \text{ s}^{-1}$ at 0.3 strain. Similarly, Chawla *et al.* (2009) observed a $1.7 \times$ increase in maximal stress between 554 s^{-1} and 1001 s^{-1} at 0.2 strain. In contrast, Van Sligtenhorst *et al.* (2006) observed an increase of maximal stress of approximately $17 \times$ between 0.01 s^{-1} and 2300 s^{-1} at 0.8 strain and Song *et al.* (2007) observed an $11 \times$ increase in maximal stress response between 0.007 and 3700 s^{-1} at 0.5 strain. The differences in magnitude appear to be largely indicative of the level of compressive strain applied and as such would suggest that the silicones are behaving in the correct response corridor at higher strain rates up to 0.5 strain.

Although the primary target dataset for relaxed muscle (McElahney, 1966; Song *et al.*, 2007) is based on porcine and bovine sources, at low strain and high strain rates the formulated PDMS relaxed muscle simulant is a close match to Chawla (2009) and Balaraman *et al.* (2012) human tissue response data (Fig. 5.23).

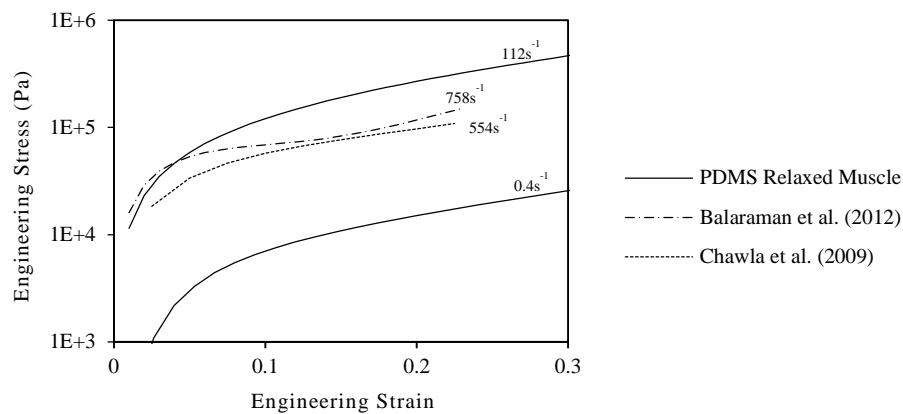


Figure 5.23 – Intermediate strain rate PDMS relaxed muscle simulant engineering stress - strain response compared with human muscle characterisation studies by Chawla *et al.* (2009) and Balaraman *et al.* (2012).

The PDMS adipose simulant, despite showing a comparable quasi-static response with the organic tissue dataset experienced a significantly greater stiffness at increased strain rates within the reported range. An increase in maximal stress response of $12.5 \times (0.4 - 194 \text{ s}^{-1})$ was recorded in the PDMS adipose simulant at 0.3 strain. Previous organic adipose characterisation studies have shown significant non-linear strain rate dependencies. Comley & Fleck (2012) reported a $4 \times$ increase in maximal stress response between 0.2 s^{-1} and 250 s^{-1} and a $680 \times$ increased stress

response between 250 s^{-1} and 2700 s^{-1} at 0.3 strain. Similarly, Egelbretsson (2011) reported an increase in maximal stress response of $2 \times$ between 0.2 s^{-1} and 250 s^{-1} , and an increase of $1344 \times$ between 250 s^{-1} and 2100 s^{-1} at 0.3 strain. The present study shows a considerably greater increase in maximal stress between quasi-static and approximately 250 s^{-1} strain rates. This is a factor that would need to be addressed in further iterations of the PDMS silicone formulations and could potentially be developed for specific sports applications based on the relevant strain rate domains.

At increased strain rates the PDMS skin simulant showed a comparable magnitude of stiffness to organic tissues in similar strain rate ranges. An increase in maximal stress response of $17 \times$ ($0.4 - 134 \text{ s}^{-1}$) was recorded in the PDMS skin simulant at 0.5 strain. Organic skin characterisation studies have typically previously reported a lower strain rate dependency than adipose. Shergold *et al.* (2006) reported a $5 \times$ increase in maximal stress between 0.004 s^{-1} and 40 s^{-1} , and a $3.4 \times$ increase between 40 s^{-1} and 4000 s^{-1} at 0.4 strain in compression, whilst Lim *et al.* (2011) reported an increase in maximal stress of $3 \times$ between 0.004 s^{-1} and 1700 s^{-1} and an increase of $1.5 \times$ between 1700 s^{-1} and 3700 s^{-1} at 0.2 strain in tension. By comparison, greater magnitudes of maximal stress increases were reported in developed PDMS skin than organic tissue. The initial differences between organic skin and the PDMS simulant under quasi-static loading conditions are compensated by a greater magnitude of strain hardening, which generates comparable behaviour. These results are in contrast to those found by Shergold *et al.* (2006) who noted that porcine skin was more strain rate sensitive than silicone rubber and exhibited a greater stiffening at increased strain rates.

(iii) Stress Relaxation Responses

The viscoelastic properties of each of the PDMS simulants have also been compared to previous organic tissue studies through stress relaxation studies. The normalised stresses for each simulant have been compared in Figure 5.18. In general, the organic tissues exhibit a significantly greater stress relaxation than the PDMS equivalents with a minimum difference in relaxed stress magnitude of 46.4% across all simulants. This could potentially be attributed to the *in vitro* nature of the organic stress relaxation experiment and the re-distribution or expulsion of fluid during a ramp and hold test.

The viscoelasticity deficit in the PDMS simulants could be theoretically improved in further iterations of the formulations through improving the viscous behaviour of the isotropic PDMS. However, it may be beneficial to consider material formulations that simultaneously introduce anisotropy and viscous behaviour.

b) Can the same approach be used to match a better organic tissue dataset?

The range of stiffness made possible by altering polymer (Fig.5.11) and cross-linker concentrations (Fig. 5.9) indicate the potential of PDMS silicones to match a wide range of target datasets. The range of viable polymer and cross linker ratios, outlined in §5.4, can be used to further refine properties, and, given the levels of agreement achieved matching four different sets of *in vitro* data in this study, it is evident there is potential for the PDMS silicone formulations to be manipulated to match new *in vivo* data to a similar level of success especially if not too dissimilar.

This is potentially most pertinent when considering contracted muscle properties. The mechanical properties of contracted muscle tissue remain unknown and almost certainly vary with the levels of muscle contraction. Some previous research has concluded that contracted muscle is less

susceptible to injuries than relaxed muscle (Crisco *et al.*, 1996; Tsui & Pain, 2008) but this is not necessarily so. Given further research to better quantify the behaviour of contracted muscle new simulants could be formulated with the methods presented.

c) Can the current PDMS simulants perfectly match organic tissue?

Given the data presented, it is not possible using PDMS silicones in their current form to exactly match organic tissue stress - strain data. As previously discussed silicones typically exhibited a greater stiffness at low strains followed by a reduced magnitude of strain hardening at higher strains. The silicone elastomers have also been shown to exhibit an increased stiffness at higher strain rates than organic tissues.

Furthermore, the simulants have only been tested and compared to target organic tissue datasets in compression. The anisotropic properties of silicones and behaviour under different loading modes (e.g. tensile, shear) have not been investigated in this study and represent an area for further study.

The anisotropy and hyperelastic material behaviour present in all organic tissue structures have been represented in some previous studies through use of fibre reinforced soft tissue simulants. There are two predominant methods which have been adopted to generate this behaviour electrospinning and textile processing techniques. Electrospinning creates fibres of approximately the same diameter as collagen or elastin fibrils and attempts to match the microscopic behaviour; however attaining accurate fibre position and orientation has been difficult (Bu *et al.*, 2012). For example, textile processing uses knitted, braided or woven fabrics to match macroscopic anisotropic properties; however the fibrous structures of commercial textiles often do not exhibit suitable deformity (Bailly *et al.*, 2014).

These fibre reinforcement techniques present a potential future area of study to enhance the biofidelity of the developed PDMS simulants. Using the PDMS simulants as the elastomer matrix, a lattice structure could be introduced to provide organic anisotropic behaviour. The reinforcement could also artificially increase the stiffness of the materials at certain strain levels; this would be most useful currently in the PDMS skin and adipose simulants, which exhibits significant divergences in strain hardening from their organic correspondents. This could help to better match organic tissue stress responses, particularly at higher strain rates.

5.8.4. Constitutive Modelling

The material models available within the Abaqus/Explicit solver provide an approximation of actual material behaviour. The hyperelastic models used consider the materials to remain constant during: loading and unloading phases and repetitive loading cycles at different strain levels and different strain rates; they do not consider permanent strain deformation. To limit the inaccuracies of these shortcomings, it was essential to populate material models with data at the most appropriate strain level and strain rate. It was also important to consider the material response in a stable stress - strain state (post-Mullins softening).

The hyperelastic material coefficients established for each PDMS simulant were determined through evaluation of three pertinent and commonly used hyperelastic models and provided the closest description of their compressive material response. The viscoelastic properties of the materials were represented by a Prony series expansion based on data from stress relaxation tests conducted in a similar manner to characterisation studies for the target organic tissue datasets.

The Prony series provides a quasi-static representation of the viscoelasticity exhibited by the materials. A more dynamic analysis of the viscoelasticity of materials could also potentially be employed through measurement of the lag due to the materials internal damping when subject to oscillations. A recent study by Tirella *et al.* (2013) defined the viscoelastic material behaviour through application of short duration interactions with different compressive strain rates. The tests have no initial contact or pre-stress and analyse the initial viscoelastic region of compression to determine the time-dependent behaviour.

One of the key shortcomings of hyperelastic constitutive model types is in their inability to model materials through a range of strain rates and apply variable material properties based on the dynamic loading conditions within a simulation. Some studies in literature have attempted to overcome these issues through use of scaling parameters. Snedeker *et al.* (2005b) used the Cowper-Symonds material curve multiplication law (Cowper & Symonds, 1957) to model materials through a range of strain rates. The law multiplies the quasi-static material curve by a scalar function defined by p and D parameters (Equation (5.5)).

$$\sigma(\varepsilon, \dot{\varepsilon}) = \sigma_0(\varepsilon) \left[1 + \left(\frac{\dot{\varepsilon}}{D} \right)^{1/p} \right] \quad (5.5)$$

Where: ε = strain; $\dot{\varepsilon}$ = strain rate; ρ = density; σ_0 = quasi-static stress - strain material curve.

This is a simple model that can be applied to any set of stress - strain curves; however, the general curve response must be consistent between strain rates. Therefore, this could not be simply applied to the proposed PDMS silicones.

There is also a hysteresis model built into the Abaqus software which can be used alongside hyperelastic materials and is capable of representing the response of a material through a range of strain rates. However, this model is only currently available in Abaqus/Standard package not Explicit. Through a commercial VUMAT subroutine it is possible to use the Bergström-Boyce model in Abaqus/Explicit to model the rate dependent, dynamic and hysteresis material behaviour. This model decomposes the stress - strain material behaviour into two contributions: an equilibrium network defined by the stress - strain behaviour after a long time in stress relaxation tests; and a time dependent network which represents the rate dependent deviation from the equilibrium state (Bergström & Boyce, 2001). However, this model was not available to this research and represents an area for future improvement.

5.9. Conclusions

PDMS silicone simulants were formulated to match the quasi-static mechanical properties of selected target organic tissue datasets. An initial simplification of organic tissues and an intermediary stage of complexity involved the development of soft tissue simulants considering the mechanical behaviour of organic tissues in a single direction. The simulants were tested in uniaxial compression through quasi-static and intermediate strain rates and in compression stress relaxation tests to characterise their mechanical properties. The new PDMS simulants provided a superior representation of the target organic tissue datasets than previously-used single material soft tissue simulant, Silastic 3483. The mechanical responses were then used to describe the constitutive behaviour of the silicones in hyperelastic and viscoelastic material models.

Chapter 6 - Experimental Impact Testing of Soft Tissue Surrogates and FE Model Validation

6.1. Chapter Overview

Chapter 6 presents a comparison of the impact responses between developed PDMS silicones, previously-used single material simulant materials and organic tissue predictions. Experimental validation was first conducted on simple cylindrical puck surrogates under approximated cricket ball and knee impact conditions to ensure FE predictions were representative and believable. The validated material models were then used to predict surrogate behaviour in a geometrically more complex cylindrical surrogate. The responses of the simulant surrogates were compared to predicted organic tissue behaviour.

6.2. Introduction

6.2.1. Validation Approaches

FE models are a potentially powerful simulation tool for predicting the impact response of human surrogates. However without experimental validation under matched loading conditions it is not possible to have complete confidence in the accuracy of the simulation outputs. All simulation models are simplifications of their real structures (Zeigler, 1976). Therefore, a 100% accurate model will never be achieved because it is impossible to know everything about the real system (Robinson, 2008). One of the key challenges in modelling is to derive an appropriate simulation of reality, which is sufficiently accurate for the purpose at hand (Carson, 1986; Pidd, 2003).

There are two common approaches which have been adopted in FE model simulations (Fig. 6.1):

- *Investigative closed loop.* FE models are matched to, or partially validated by, an experiment and a series of experimental measures. This allows investigation of phenomena that have not or cannot easily be measured to add deeper insight into the response of the system. However, by definition, this is not knowledge fully validated otherwise the FE model offers no advantages over experimentation.
- *Predictive open loop.* Given validation of basic assumptions through experimentation (e.g. response of material models and contact conditions in simple geometries), exploratory predictions can be made under different conditions from those directly validated. The further that the simulations deviate from simpler validation experiments, the less assumed the predictions become; but, where best practice is followed, useful cost avoiding predictions can be made with adequate certainty.

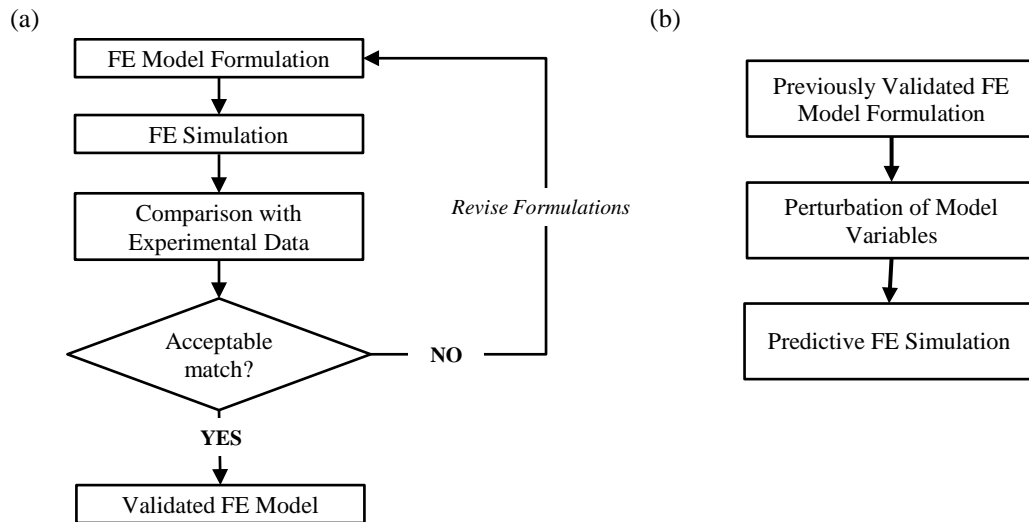


Figure 6.1 - Common FE model usage procedures: (a) Investigative closed loop; (b) Predictive open loop.

In the closed loop validation approach, an iterative optimisation is commonly adopted with the model being iteratively revised to adequately match the experimental data (Robinson, 2008). This approach can yield success and a representative model. However, many previous studies have only focussed on matching a particular kinematic parameter through manipulation of a few material variables within a complex system (Panzer *et al.*, 2011). This can provide an acceptable representation of global kinematic response for the situation in which it was calibrated but may not accurately predict local tissue strains or stresses. In most surrogate impact studies, the response corridor is defined by the mean \pm 1SD in experimental data (Cronin *et al.*, 2003; Panzer *et al.*, 2011).

To provide confidence in the accuracy of a FE model, it is beneficial to assess as many evaluation metrics as possible. However, it is experimentally very difficult to measure internal mechanical response phenomena without adversely affecting the biofidelity of the surrogate. Consequently, a common approach adopted is to validate external parameters that can be more easily measured and infer the internal response (Tiozzi *et al.*, 2013; Shin *et al.*, 2012). In rare sophisticated studies, authors have attempted to validate internal phenomena. For example, Shen *et al.* (2008) miniaturised pressurised catheters inserted within cadaver lungs to measure internal pressures; though this is very uncommon.

Chapter 3 (§3.5.5) outlined the mechanical response phenomena pertinent to both cricket ball and knee impact scenarios. Contusion injury outcomes in each scenario are predicted to be associated to the compressive stresses and strains at each of the tissue interfaces and intrinsically linked to the impact durations and tissue displacements. Given these relevant mechanical phenomena, the instrumentation that could potentially be used to experimentally measure impact response in surrogates has been evaluated. Practical considerations influencing the selection of the instrumentation include but are not limited to: the cost, the degree to which inclusion will influence surrogate biofidelity, adhesion between sensors and simulant materials and the ease of interpretation of instrumentation feedback.

6.2.2. Aims and Objectives

- 1) To establish the capabilities of current off-the-shelf instrumentation in human impact surrogate evaluations.
 - Experimental verification of instrumentation in surrogate impact configurations.
 - Identification of most appropriate available validation measures.
- 2) To determine whether experimental material characterisation, constitutive material modelling and dynamic FE load/deformation simulation techniques can be used to predict the response of single and multi-material surrogate constructions using common and bespoke formulated synthetic surrogate materials in closed-loop simulations.
 - Experimental determination of simulant material responses.
 - Comparison between FE model predictions and experimental test data.
 - Investigation and optimisation of differences in responses.
- 3) To determine whether a multi-material PDMS silicone surrogate more closely mimics multi-tissue organic human structures than current single surrogate material approaches through open loop simulations in a way that has value for injury and PPE assessment research.

6.3. Surrogate Instrumentation

6.3.1. Load Cells

Load cells are force transducers which transmit an electrical signal directly proportional to the load applied. The most common types of load cell are strain gauge based and piezoelectric, though piezoelectric load cells are more commonly used in dynamic impact scenarios. They are often used to determine mechanical response phenomena and as a validation measure in synthetic impact surrogates. A pertinent example of their usage is through safety standards where they have been widely used to measure the peak force transfer through PPE under set impact conditions (§2.2.3.b).

6.3.2. Pressure Measurement Systems

a) Tekscan F-Scan

The Tekscan F-scan mobile pressure measurement system (Tekscan Inc., Massachusetts, USA) uses thin film piezoresistive sensors. The sensors consist of electrically sensitive, pressure-sensitive resistive ink sandwiched between laminated polyester films. The system provides a lightweight, flexible sensor that can be used to measure dynamic impacts. Each sensor is 0.15 mm thick and consists of 954 sensels (measuring points) providing a fine spatial resolution.

Despite not being used for their original intended application (foot pressure measurements), the system is capable of recording at up to 750 Hz and as such can provide sufficient sampling frequency to measure the dynamic phenomena occurring in sports impacts. Prior to use, it is important to perform both an equilibration and calibration of the Tekscan pressure sensors. The equilibration procedure normalises the digital voltage output from the sensors at a known applied force, attributing an individual gain factor to each sensel, whilst calibration procedures are used to convert the digital outputs to engineering units (force or pressure).

A common method to equilibrate and calibrate the sensors is through a static pressure bladder system distributing an even pressure across the surface of the sensor. However, significant discrepancies in accuracy arise from the manner in which the sensors have been calibrated (Papaionnou *et al.*, 2008; Brimacombe *et al.*, 2009). Authors have observed differences in measured force dependent on the duration of force application, magnitude of load range, and presence and thickness of a material substrate (Morvan, 2012). A more accurate time-based calibration has recently been proposed by Cazzola *et al.* (2014) which applies a dynamic correction factor to all calibration data points. However, this approach still requires frame-based calibrations to be applied for each loading type to ensure accurate outputs. In addition, the Tekscan pressure sensors are subject to a positive logarithmic drift when a constant force is applied due to the non-linear response of the sensors (Cazzola *et al.* 2014).

Tekscan F-Scan sensors have been used previously in studies by Pain *et al.* (2008); Halkon *et al.* (2012) and Halkon *et al.* (2014) for rugby, American football and basketball impacts respectively. In these studies, the sensors have been used to measure the pressure, pressure distribution and net force from human gameplay sports impacts.

b) Tekscan FlexiForce

Tekscan FlexiForce pressure sensors (Tekscan Inc., Massachusetts, USA) are low cost, thin film piezoresistive force sensors whose electrical resistance changes with an applied force. The sensors have a similar construction to the Tekscan F-scan sensors and consist of a printed circuit made with layers of conductive silver and pressure-sensitive ink sandwiched by long strips of polyester film. The sensors have an active sensing area of 9.5 mm diameter and have a thickness of 0.2 mm. The sensors are supplied in three force ranges: 0 - 4.4 N, 0 - 110 N and 0 - 440 N.

FlexiForce pressure sensors have been widely used in impact injury biomechanics studies. They are typically arranged in an array to generate a pressure map or strategically positioned in areas of interest. For example, Johannsen & Schindler (2007) arranged a matrix of sensors on the abdominal region of a surrogate to measure the force - time history attained in automotive accident reconstructions.

6.3.3. Strain Gauges

The basic principle of a strain gauge dictates that when a conductive material is stretched the resistance of the material increases generating a measurable change, which is calibrated against known increases in displacement. Most conventional strain gauges are constructed from a foil conductive pattern sandwiched between a laminated substrate. This often introduces artificial stiffness when used in very compliant soft tissue surrogates. Conventional strain gauges are, therefore, most commonly applied in sports impact scenarios on rigid bodies such as skeletal components. For example, Found *et al.* (2006) used two conventional strains on a surrogate jaw assembly to assess the impact efficacy of different sports mouthguards.

In recent years, flexible strain gauges have been developed. Danfoss PolyPower sensors (Danfoss, Nordborg, Denmark) are compliant stretch sensors that use a variable parallel plate capacitor. They are Dielectric Electro Active Polymer (DEAP) materials which consist of a PDMS silicone polymer in conjunction with a corrugated metallic compliant electrode (Benslimane & Gravesen, 2002). When the DEAP material becomes strained the capacitance increases due to a reduction in thickness and increase in length. The sensors, however, are coupled with a data acquisition

system that permits a maximum sampling frequency of just 8Hz which is insufficient to accurately represent the strains induced in dynamic sports impact scenarios.

6.3.4. Accelerometers

Accelerometers are manufactured in many varieties and are frequently used to measure whole body motion and kinematics. Their primary usage in impact biomechanics applications has been through positioning a sensor on the impactor and, through knowledge of the impactor mass, calculating impact force using Newton's 2nd law (Kroell *et al.*, 1974; Cavanaugh *et al.*, 1986; Muggenthaler *et al.*, 2008). A disadvantage of this method is that it is limited to measuring forces in instances where rigid impactors were used since the effective mass in non-rigid impactors is constantly changing. In human surrogates, the accelerometer must be placed on rigid masses such as bone to be used in this way (Snyder, 1973).

6.3.5. Motion Tracking

a) 2D Single HSV Camera

A 2D single camera HSV is an instrument that enables a method of determining the relative positions of objects and can be used to calculate the magnitudes of deformations in surrogate impacts as well as the time course over which they are achieved. The Photron Fastcam DA1 675K-C1 HSV camera can capture at up to 50,000 fps at its full screen resolution of 1024 × 1024 pixels and has been used throughout this research.

Typically, when motion can be considered to be planar, a single HSV camera can be used to measure 2D position vs. time histories. In this scenario, positional markers are established on the objects of interest and tracked to determine displacements and subsequent velocities. The field of view needs to be calibrated using an object of known size in the same plane as the movement analysed. The numbers of pixels between the two ends of this length are then used to provide a scale factor to convert still images to 'real' distances when digitising the data. HSV is widely used in injury biomechanics research as physical deformation phenomena can be measured without invasively affecting the experiment (e.g. Pain *et al.*, 2008; Halkon *et al.*, 2012).

b) 3D Digital Image Correlation

Digital image correlation (DIC) techniques use multiple HSV cameras to measure the position of consistent marker points to track the surface deformation of an object. GOM ARAMIS (GOM, Braunschweig, Germany) is an example of a commercial system that is capable of performing semi-automated 3D tracking based on the positions of a large number of data points. The system requires a static reference state and then calculates changes from or with reference to this equilibrium position using algorithms within the software.

These techniques have been successfully applied in inverse optimisation methods to populate constitutive material models of standard mechanical tests. This is demonstrated by Takaza *et al.* (2013) who used DIC to track the intermediate strain rate deformation of *in vitro* muscle specimens and validate the deformation patterns of different materials in FE. Moerman *et al.* (2009) also applied DIC to validate an FE model on a silicone soft tissue phantom during indentation tests. The material models were optimised until the surface strain pattern generated by the FE models matched experimental data from the DIC software. However, in surrogate impact studies, the area of primary interest is directly beneath the impacting object, which is concealed

from the camera systems. Therefore, the response in this region must be inferred from measurements remote from the impact site.

c) **3D Positional Marker Tracking**

There are a number of commercially available motion tracking systems which are capable of determining the dynamic 3D position of a number of markers. These systems are most commonly used in human body biomechanical movement studies and are most applicable in scenarios measuring large scale displacements. However, they have been used in impact biomechanics applications. For example, Muggenthaler *et al.* (2008) used a passive optical marker tracking system to measure human volunteer kinematic responses to a series of controlled impacts.

Two types of system are typically adopted: passive and active marker tracking systems. Passive marker tracking systems (e.g. Vicon Motion Systems Ltd., Oxford, UK) track opto-reflective markers in real-time using infrared cameras, whilst active marker systems (e.g. CODAmotion, Charnwood Dynamics Ltd., UK) transmit infrared light from a LED to a series of sensors to determine marker position.

6.4. Instrumentation Evaluation

6.4.1. Selection of Instrumentation

Given the injury-related mechanical phenomena outlined in Chapter 3 for cricket ball and knee impacts (§3.5.5), the surrogate deformation, load transfer to deep tissues and stress between layers are believed to be most pertinent. Of the available instrumentation described previously, 2D planar single HSV capture enables determination of impactor penetration into the surrogate and so provides a simple measure of its overall deformation response. 3D imaging techniques, whilst possessing the capability of providing a more detailed description of surrogate deformation kinematics, would encounter visibility difficulties with small scale test samples where the impactor may obscure the view of the surrogate. Therefore, it is unlikely that these techniques could offer additional worth to the single HSV for the same resource expenditure. To determine the kinetic responses of the surrogate, load cell and Tekscan F-Scan techniques have been further investigated in simple surrogate experiments.

6.4.2. Mould Development

A 130 mm diameter puck surrogate was developed to both assess the effectiveness of different types of instrumentation and enable cost-effective validation of the simulant impact responses. A three-part cylindrical puck mould was developed with a 6 mm aluminium base plate that had mounting points to attach to the Instron Dynatup 9250HV drop tower. The mould was additive manufactured from PA 2200 Nylon using selective laser sintering (SLS) techniques. The material has sufficient tensile stiffness (1700 MPa) and tensile strength (48 MPa) for moulding applications and a melting temperature of 172 - 180°C which is appropriate for all simulant material moulding. A series of modular inserts were also developed to enable the insertion of different types of instrumentation between layers (Fig. 6.2).

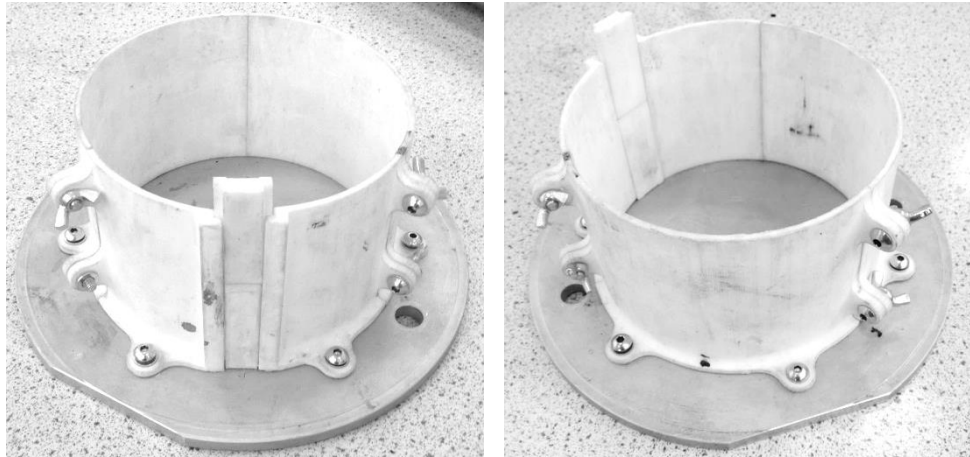


Figure 6.2 - Puck surrogate mould with instrumentation cable access point.

A 10% gelatin formulation was used initially as a low-cost surrogate material from which different sensors could be embedded and assessed.

6.4.3. Experimental Tests

a) Load Cells

The Instron 9250HV drop tower has a force measurement system with three dynamically calibrated piezoresistive load transducers integrated beneath the impact area. In sports impact evaluations the system is, however, limited by the minimum mass of the drop carriage (6.8 kg), which is significantly greater than either the cricket ball or knee impact mass approximations. Therefore, to perform these experiments, a stand-alone load cell was required.

The Dytran 1061V3 force sensor (Dytran Instruments, USA) was used and had a sensitivity of 1 mV/lbf with a 5000 lbs compressive force range. The sensor was mounted onto a rigid steel plate with a gelatin puck positioned on top. The load cell was calibrated using the known Instron 9250HV responses through a range of impact energies. A 6.8 kg drop mass with a 72 mm hemispherical striker was dropped from heights between 0.15 - 0.5 m. The outputs from the load cell and Instron were compared for each impact with the maximal load cell responses shown in Table 6.1.

Table 6.1 - Differences in peak force between Dytran and Instron 9250HV load cells.

Drop Height (m)	Instron Load Cell Force (N)	Dytran Load Cell Force (N)	Correction Factors
0.15	730	556	1.31
0.20	964	693	1.39
0.25	1180	833	1.42
0.30	1425	978	1.45
0.35	1743	1138	1.53
0.40	2138	1303	1.64
0.45	2500	1463	1.70
0.50	2877	1738	1.66

To ensure the accuracy of the response of the Instron load cell, the impulses were verified against momentum change calculated using HSV. The differences between the Dytran and Instron load cells is believed to be a sensitivity drift of the Dytran load cell charge amplifier system. A dynamic correction factor was subsequently applied to the Dytran load cell outputs based on a linear function (Fig. 6.3).

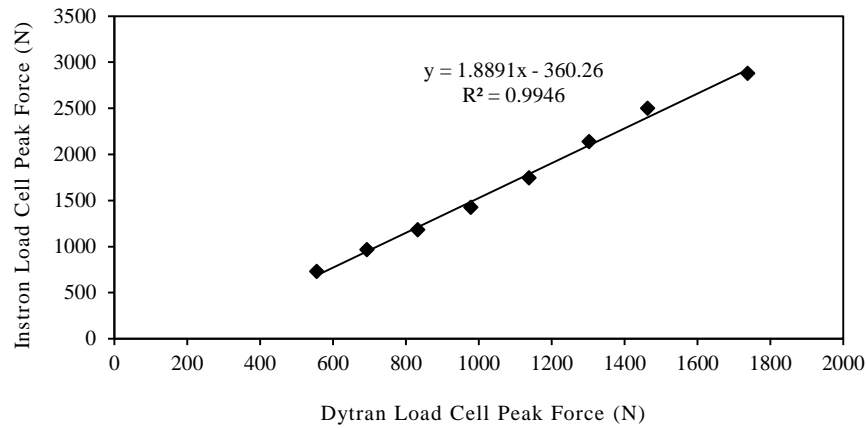


Figure 6.3 - Graph showing a comparison between Instron and Dytran load cell peak forces with a linear fit.

b) Tekscan F-Scan

Experimental tests were conducted with tethered F-scan sensors to determine their applicability in soft tissue surrogates. Sensors were positioned on the surface, base and embedded within the surrogate. To embed the sensors between layers, the mould was partially filled with gelatin and left to cure before the sensor was positioned and the remainder of the mould was filled. The Instron 9250HV drop tower was again used to conduct axial drop tests, central and perpendicular to the puck. A 6.8 kg, 72 mm hemi-spherical impactor was used from a drop height of 0.05 m.

(i) Pressure Visualisations

The pressure visualisations for each of the impacts are shown in Figure 6.4. The visualisations are each relative to the maximal pressure experienced in the individual trial (pink = highest pressure). The sensor gives a believable indication of pressure distribution when backed with by a relatively stiff and flat surface (Fig. 6.4.c) but (unless pre-shaped) crinkles when layer deformations are caused by a curved surface interacting with a deformable body (Fig. 6.4.a).

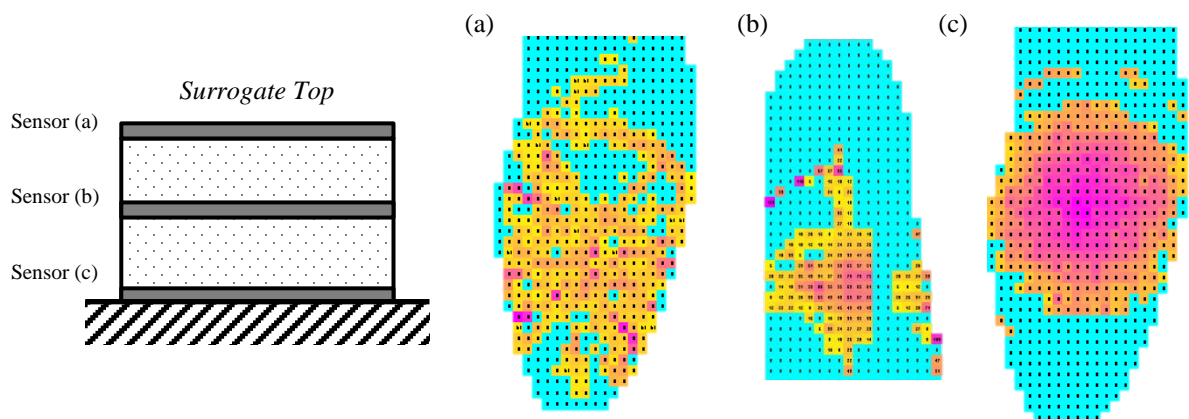


Figure 6.4 - Pressure map visualisation of: (a) surface sensor; (b) embedded sensor and (c) base sensor.

(ii) Accuracy of Force Measurement

The nett force data from the load cell on the Instron were compared with the Tekscan pressure sensor on the base of the surrogate (Fig. 6.5). The graph shows a significant divergence between the recorded load cell and Tekscan data (252% difference). This is likely to be due to issues extrapolating responses from static calibrations used for the Tekscan sensor to dynamic impact conditions. Therefore, to be useful as a load sensor for sports impact applications, it should be dynamically calibrated using the Instron load cell.

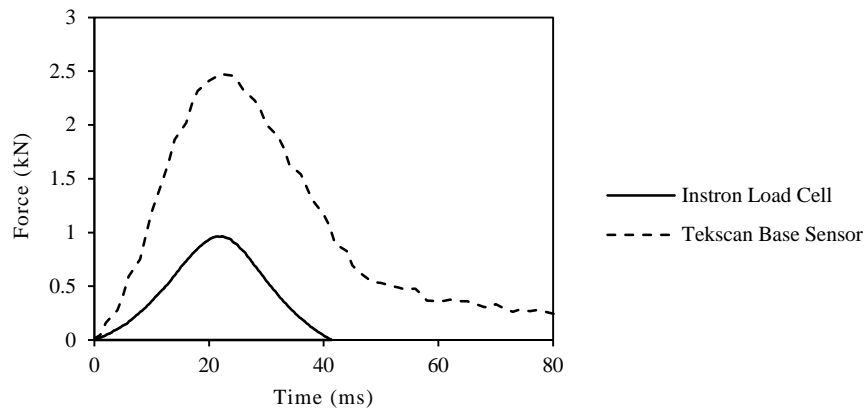


Figure 6.5 - Differences in nett force between the Instron 9250HV load cell and the Tekscan sensor (20cm, 6.8kg drop).

(iii) Sensor Response Interference

A further study was performed to determine the interference in surrogate biofidelity caused by the inclusion of a surface Tekscan F-scan sensor. Experiments were performed using a 6.8 kg, 72 mm hemi-spherical impactor from a drop height of 0.05 m with and without a surface sensor. The Instron load cell response from each trial is shown in Figure 6.6. The load cell data from the base of the surrogate showed the sensor caused a difference in peak force of 12.7% when the Tekscan sensor was positioned on the surface of the surrogate compared to a bare impact.

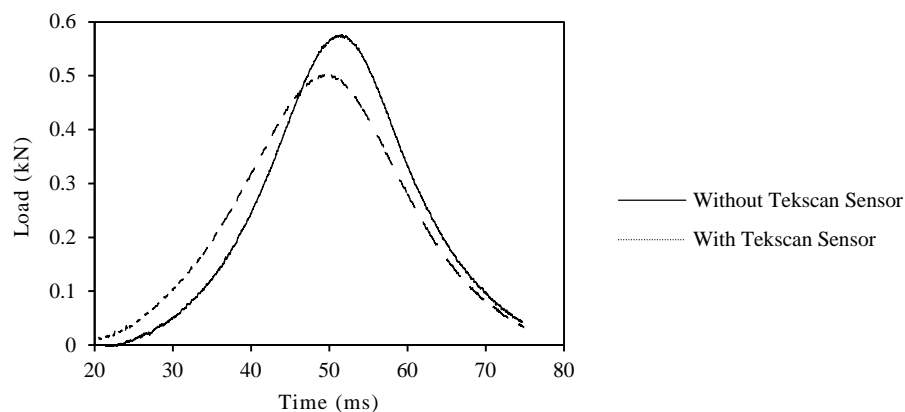


Figure 6.6 - Differences in Instron 9250 drop tower load cell output with and without a Tekscan F-Scan sensor on the surface of the gelatin puck.

Additional issues arose from the embedded sensor which created a delamination effect between layers and a point of artificial weakness (Fig. 6.7).

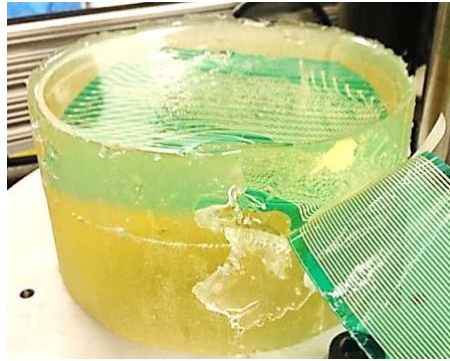


Figure 6.7 - Embedded Tekscan sensor creating delamination within the surrogate.

c) Summary

Tekscan F-scan sensors present an effective means of displaying relative pressures, particularly when located on a rigid surface (i.e. base of the surrogate). Their presence either embedded or on the surface of the surrogate has some merit but adversely affects the fidelity of the inherent material response and can cause artificial points of weakness. The significant variation between the net force recorded on the Tekscan sensor and Instron load cell (Fig. 6.5) necessitate the use of a full dynamic calibration. Further to this, previous research studies have reported a sensitivity drift of sensors (§6.3.2.a), which therefore have a limited useful life. This implies impact studies would require many sensors and hence time consuming dynamic calibrations. Therefore, the use of Tekscan F-scan within this study has been limited to relative comparisons rather than attempting to abstract absolute values from dynamic studies as was the case in the basketball human impact study (§3.4.2). Consequently, a load cell beneath the surrogate puck presents a preferable means of determining the force transmitted through the surrogate.

6.5. Closed Loop Surrogate Validation

6.5.1. Introduction

To provide confidence in the accuracy of FE model predictions, a closed loop experimental validation was performed on a simplified cylindrical puck surrogate. To provide a comprehensive evaluation of the potential benefits of the developed PDMS simulants developed (§5), comparisons have been made with single material soft tissue simulants previously-used in impact surrogates. Each of the synthetic material simulants has been validated against experimental data from cricket ball and knee impact conditions.

6.5.2. Materials

The PDMS tissue simulants (§5.5) and organic tissues (§4.3.3.a) characterised previously at representative strain rates have been used in the FE simulations. Elastomers from Silastic 3480 series silicones (Dow Corning Corporation, Michigan, USA) have been used in research studies to represent human soft tissues. Silastic 3481, 3483 and 3487 two-part cure silicone were fabricated in the same manner as the PDMS silicones (§5.3.2.c) and characterised in compression through a range of strain rates and in stress relaxation tests (§5.3.3). Ballistic gelatin was also formulated in 10% and 20% concentrations using the procedure outlined by Jussila (2004) and tested in the same manner as the PDMS simulants. The compressive stress - strain response of the single material simulants at representative strain rates have been shown in Figure 6.8. The hyperelastic and viscoelastic model coefficients for each material at representative strain rates are presented in Table 6.2.

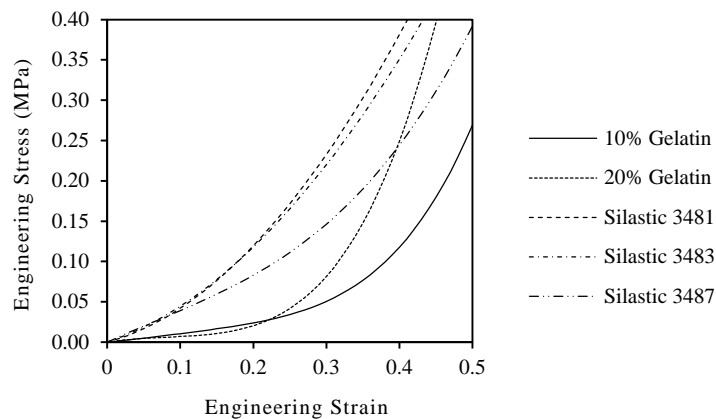


Figure 6.8 - Compressive engineering stress - strain graphs of Silastic simulants and ballistic gelatin at representative intermediate strain rates.

Table 6.2 - Hyperelastic and viscoelastic material coefficients for PDMS skin, adipose and relaxed muscle tissues.

	Mooney Rivlin Coefficients				Prony Series		
	D_{10}	C_{01}	C_{10}	i	$g(i)$	$k(i)$	$\tau(i)$
<i>PDMS Muscle</i>	-	4.25×10^2	1.57×10^4	1	1.28×10^{-1}	-	3.52×10^{-1}
				2	5.29×10^{-2}	-	8.07
				3	3.39×10^{-2}	-	7.61×10^1
<i>PDMS Adipose</i>	-	2.55×10^3	9.19×10^3	1	1.39×10^{-1}	-	7.51×10^{-5}
				2	1.70×10^{-1}	-	3.07
				3	7.41×10^{-2}	-	7.90×10^1
<i>Silastic 3481</i>	-	6.11×10^4	1.35×10^4	1	6.17×10^{-2}	-	1.80×10^{-1}
				2	3.85×10^{-2}	-	5.55
				3	3.30×10^{-2}	-	9.61×10^1
<i>Silastic 3483</i>	-	7.65×10^4	7.91×10^2	1	5.02×10^{-2}	-	2.18×10^{-1}
				2	2.87×10^{-2}	-	8.62
				3	2.60×10^{-2}	-	9.00×10^1
<i>Silastic 3487</i>	-	5.31×10^4	1.59×10^3	1	5.52×10^{-2}	-	2.32×10^{-1}
				2	3.51×10^{-2}	-	8.80
				3	3.92×10^{-2}	-	8.81×10^1
Ogden Model Coefficients							
	μ	α	D				
<i>PDMS Skin</i>	5.92×10^5	2.61	-	1	2.67×10^{-2}	-	8.51×10^{-1}
				2	8.07×10^{-3}	-	4.04×10^1
<i>Organic Skin</i>	2.20×10^6	12	-	1	5.01×10^1	3.80×10^{-1}	5.73×10^{-1}
				2	4.44×10^{-1}	5.59×10^{-1}	9.47
<i>Organic Adipose</i>	1.70×10^3	23	-	1	1.59×10^{-2}	-	7.83×10^{-5}
				2	7.97×10^{-2}	-	1.17×10^{-3}
				3	5.89×10^{-1}	-	1.61
				4	1.25×10^{-1}	-	7.29×10^1
<i>Organic Muscle</i>	3.63×10^4	4.5	-	1	3.39×10^1	-	2.37
				2	2.56×10^{-1}	-	7.02×10^1
<i>10% Gelatin</i>	2.52×10^4	2.93	2.26×10^5	1	2.27×10^{-1}	-	1.83
				2	3.88×10^{-1}	-	8.16×10^1
<i>20% Gelatin</i>	1.72×10^4	-6.08	3.29×10^{-5}	1	1.56×10^{-1}	-	1.80
				2	3.89×10^{-1}	-	9.39×10^1

6.5.3. Experimental Test Configuration

Material drop tests were performed on a series of puck shaped surrogates simulating both cricket ball and knee impacts using rigid impactor approximations. Puck surrogates with a 130 mm diameter (Fig. 6.9) were fabricated for each of the simulant materials using the mould previously developed for instrumentation tests (§6.4.2).

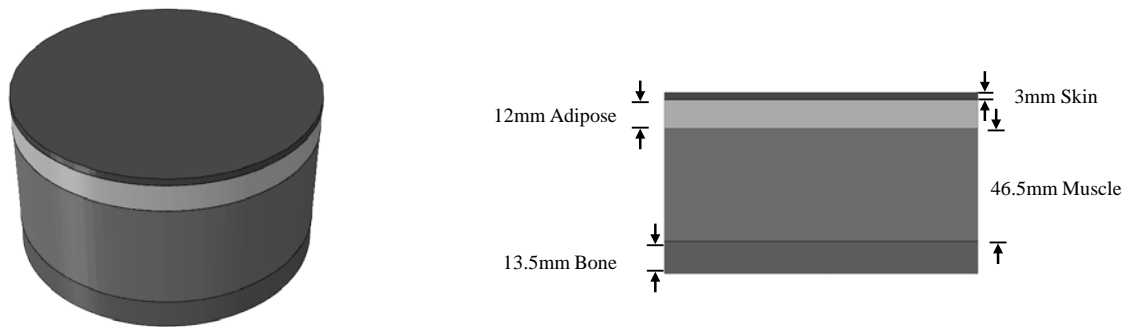


Figure 6.9 - Cylindrical puck geometry and sagittal plane section.

The impactors were dropped onto the puck surrogates through a vertical guidance system from heights of 0.5 m and 10 m for the knee and cricket ball impacts respectively (Fig. 6.10). The surrogate was positioned on a Dytran 1061V load cell (Dytran Instruments, USA). HSV was also captured with a Photron Fastcam DA1 675K-C1 camera positioned perpendicular to the surrogate, recording at 5000 fps with an image resolution of 1024×1024 pixels.

Four trials were conducted for each surrogate type with displacement - time and force - time outputs calculated from the video and load cell data. The experimental results were then compared with the predicted outputs from the FE models. The mean \pm 1SD has been defined as the response corridor for the surrogates.

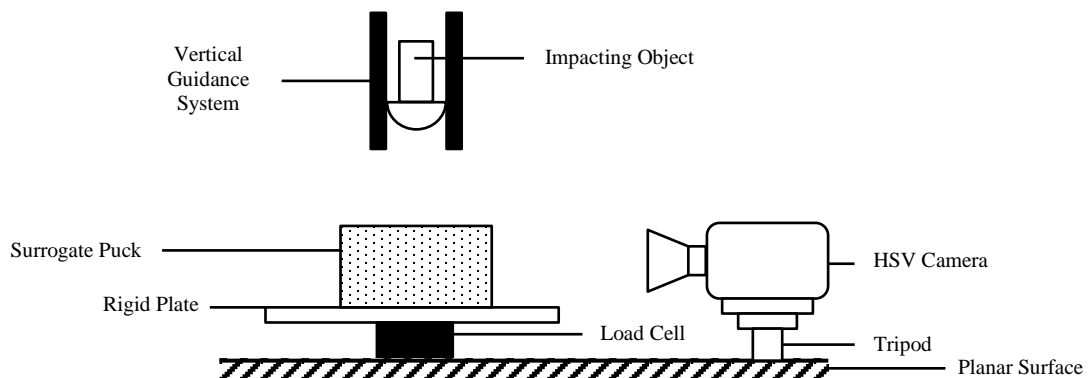


Figure 6.10 - Schematic showing experimental drop test configuration.

6.6. Results

6.6.1. Surrogate Validation Results: Knee Impact

A subset of HSV stills of the experimental knee impactor trials are shown in Figure 6.11 with combined simulant force - time and displacement - time graphs shown in Figure 6.12.

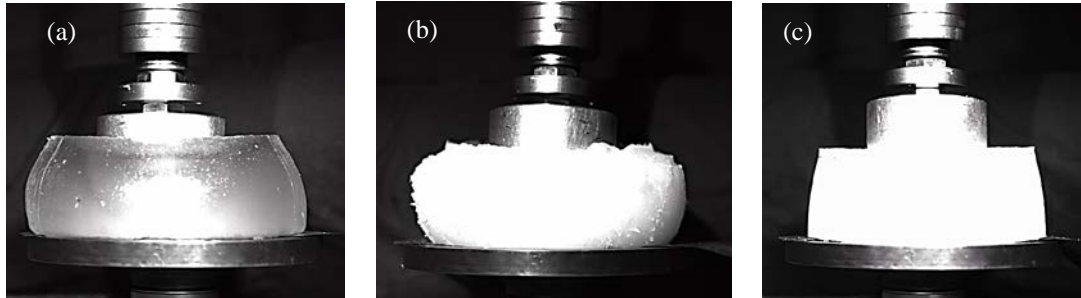


Figure 6.11 - HSV stills of puck surrogates at maximum displacement in: (a) 10% gelatin; (b) PDMS; (c) Silastic 3481.

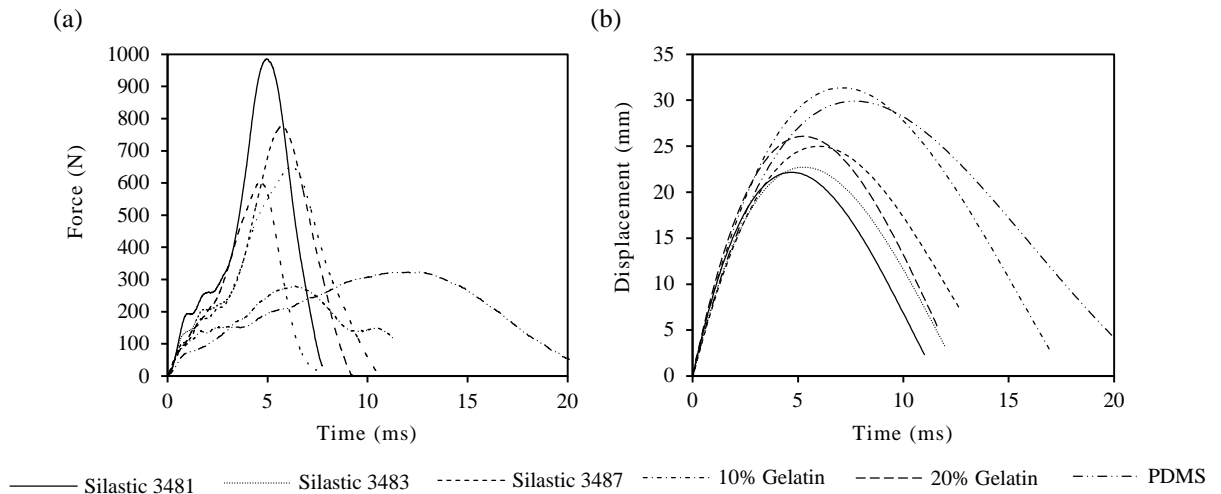


Figure 6.12 - Experimental differences in mean surrogate response in different simulants for knee impacts.

FE models of the puck impacts were initially formulated using the same model definitions as previously established in §4.3.4. The puck was modelled constrained to a rigid plate in all translational DOF.

Initial simulations were conducted using the material models documented in Table 6.2 and exhibited significant divergences in displacement and force from the experimental datasets. An investigation into the specific mechanical properties of the individual material batches used in the puck surrogates showed some process-induced variability of a similar magnitude to those reported in §5.5.5. The mechanical properties from the batch material were then used to populate the FE models.

The experimental data from each surrogate knee impact has been plotted on the same force - time and displacement - time graphs to show the relative differences in response between simulants (Fig. 6.12). The FE model outputs for the knee impact simulation have then been compared to experimental data in Figure 6.13. Experimental and FE force outputs were synchronised by matching the force traces at 10% of the peak FE force.

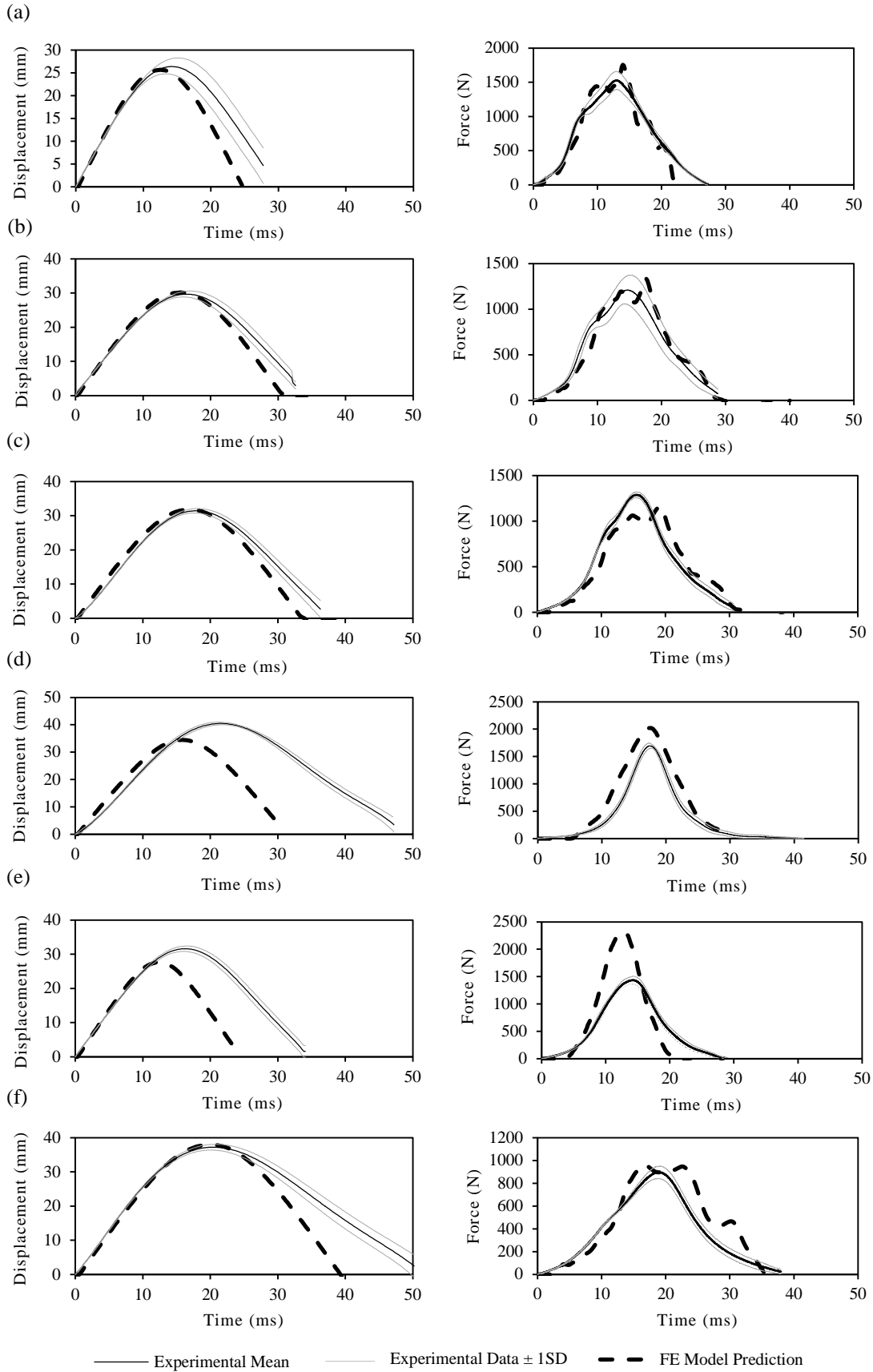


Figure 6.13 - Displacement vs. time and force vs. time graphs showing a comparison between experimental data and FE model predictions for knee impacts in: (a) Silastic 3481; (b) Silastic 3483; (c) Silastic 3487; (d) 10% Gelatin; (e) 20% Gelatin and (f) PDMS surrogates.

The 10% and 20% gelatin FE model predictions showed a significant divergence from the experimental test data, particularly with regards to the displacement exhibited with -14.8% and -12.5% differences from the experimental mean in 10% and 20% gelatins respectively. Both models exhibited an increased stiffness, therefore the material models were refined to provide a better representation of the experimental data. In both materials, the hyperelastic material was reduced to one third of its original stiffness. The resultant model outputs have been shown in Fig. 6.14 compared to experimental data.

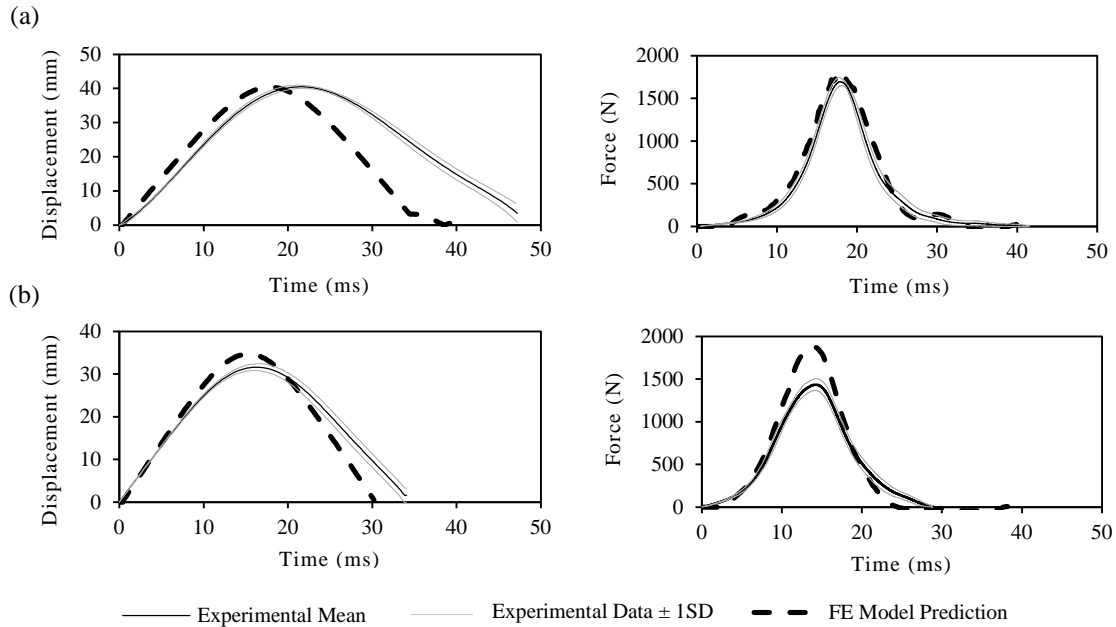


Figure 6.14 – Corrected displacement vs. time and force vs. time graphs showing a comparison between experimental data and optimised FE model predictions for: (a) 10% gelatin and (b) 20% gelatin.

The optimised gelatin material models provided a closer representation of the experimental data maximum displacement with divergences of just -0.20% and +8.90% in 10% and 20% gelatins respectively. The revised models also provided an improved prediction of the peak force in the 10% gelatin (+5.38% difference) but showed significant differences in the 20% gelatin model. Table 6.3 provides a comparison x_{max} , t_x , peak force (RF) and time to peak force (t_{rf}) between the experimental data and FE model predictions for the knee impact simulation.

Table 6.3 – Comparison of x_{max} , t_x , RF and t_{rf} between experimental data and FE model predictions in the knee impact.

	$x_{max}(mm)$			$t_x(ms)$			RF (N)			$t_{rf}(ms)$		
	Exp.	FE	% Error	Exp.	FE	% Error	Exp.	FE	% Error	Exp.	FE	% Error
PDMS Silicones	37.2	38.0	+2.04	20.4	20.0	-1.81	867	964	+7.72	19.0	16.6	-12.0
10% Gel	40.5	40.4	-0.20	21.5	17.8	-17.1	1690	1790	+5.38	17.6	17.8	+1.13
20% Gel	31.6	34.7	+8.90	16.5	15.4	-6.55	1440	1890	+31.3	14.3	15.8	+9.89
Silastic 3481	26.4	25.6	-2.77	14.2	12.6	-11.6	1530	1750	+14.9	13.0	12.9	-0.99
Silastic 3483	30.0	26.3	+1.54	16.5	17.2	+4.37	1210	1340	+10.3	14.7	17.6	+19.8
Silastic 3487	31.4	31.8	+1.27	18.0	17.0	-5.35	1290	1160	-9.89	15.5	19.2	+24.2

6.6.2. Surrogate Validation Results: Cricket Ball

A subset of HSV stills of the experimental cricket ball trials are shown in Figure 6.15 with combined simulant force - time and displacement - time graphs shown in Figure 6.16.

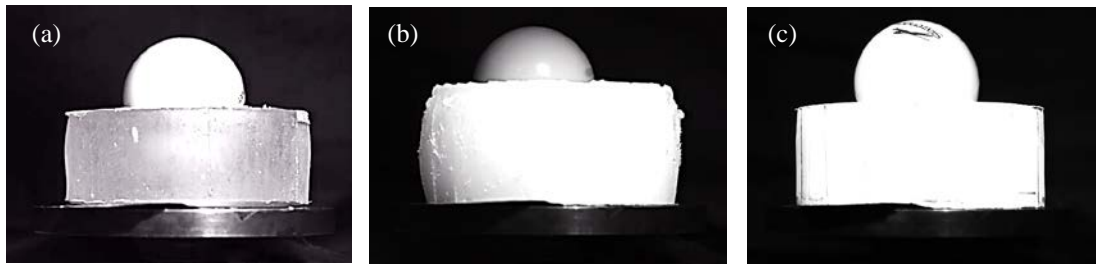


Figure 6.15 - HSV stills of cricket ball puck surrogates at maximum displacement: (a) 10% gelatin; (b) PDMS; (c) Silastic 3481.

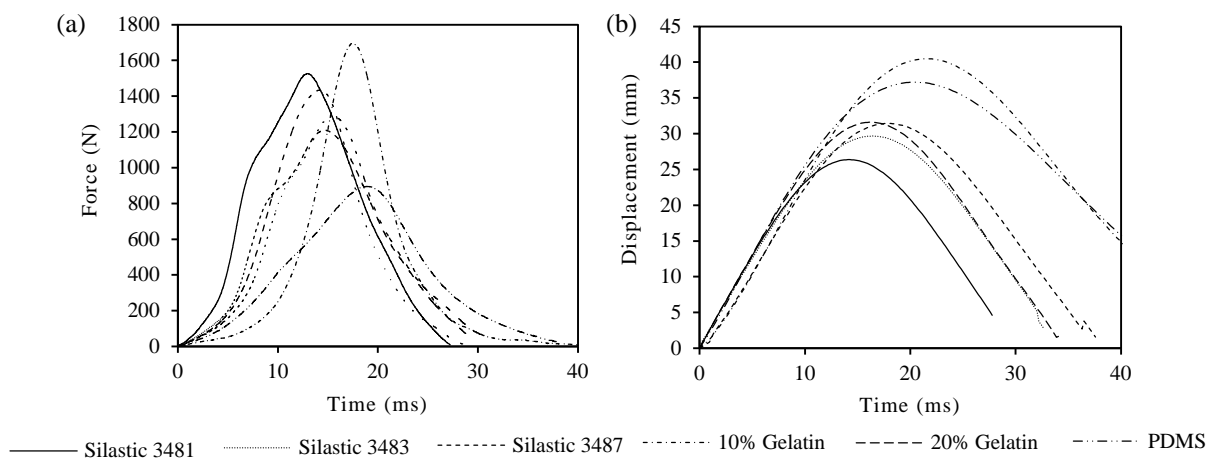


Figure 6.16 - Experimental differences in mean surrogate response in different simulants for cricket ball impacts.

The high strain rate cricket ball impact FEA simulations initially exhibited erroneous behaviour relating the manner in which the puck interacted with the rigid plate. A tied contact prevented the elements on the base of the surrogate from moving during impact, preventing lateral displacement and artificially stiffening the surrogate. A hard contact was also investigated but still generated similar artificial contact issues between the puck and the plate. This is likely to be due to mathematical instabilities introduced through this stringently enforced stiff contact type. Consequently, to overcome these issues, a softened exponential plate-puck contact (§4.3.4.c) was used with a pressure at zero clearance of 1.5×10^{-3} Pa and a clearance at zero pressure of 1.5×10^{-3} m.

Initial simulations were conducted using the original material models proposed and the revised one-third stiffness gelatin models. The simulations showed a near systematic divergence in displacements in silicone surrogates with all simulants predicting between 16.4% and 19.5% lower x_{\max} than the experimental data. The divergences between the experimental data and FE model predictions could have potentially been related to issues with the: material model; element type and attributes; mesh quality boundary conditions; contact; mass scaling; and damping. Each of the factors were explored to examine the effect on model predictions. It was determined that the mesh density was too coarse to accurately represent the estimated deformation behaviour of the materials and was resulting in both artificial stiffness and instabilities. The mesh of the FE puck was subsequently refined to a nominal element size of 1 mm throughout. The results from the revised impact simulations are shown in Figure 6.17.

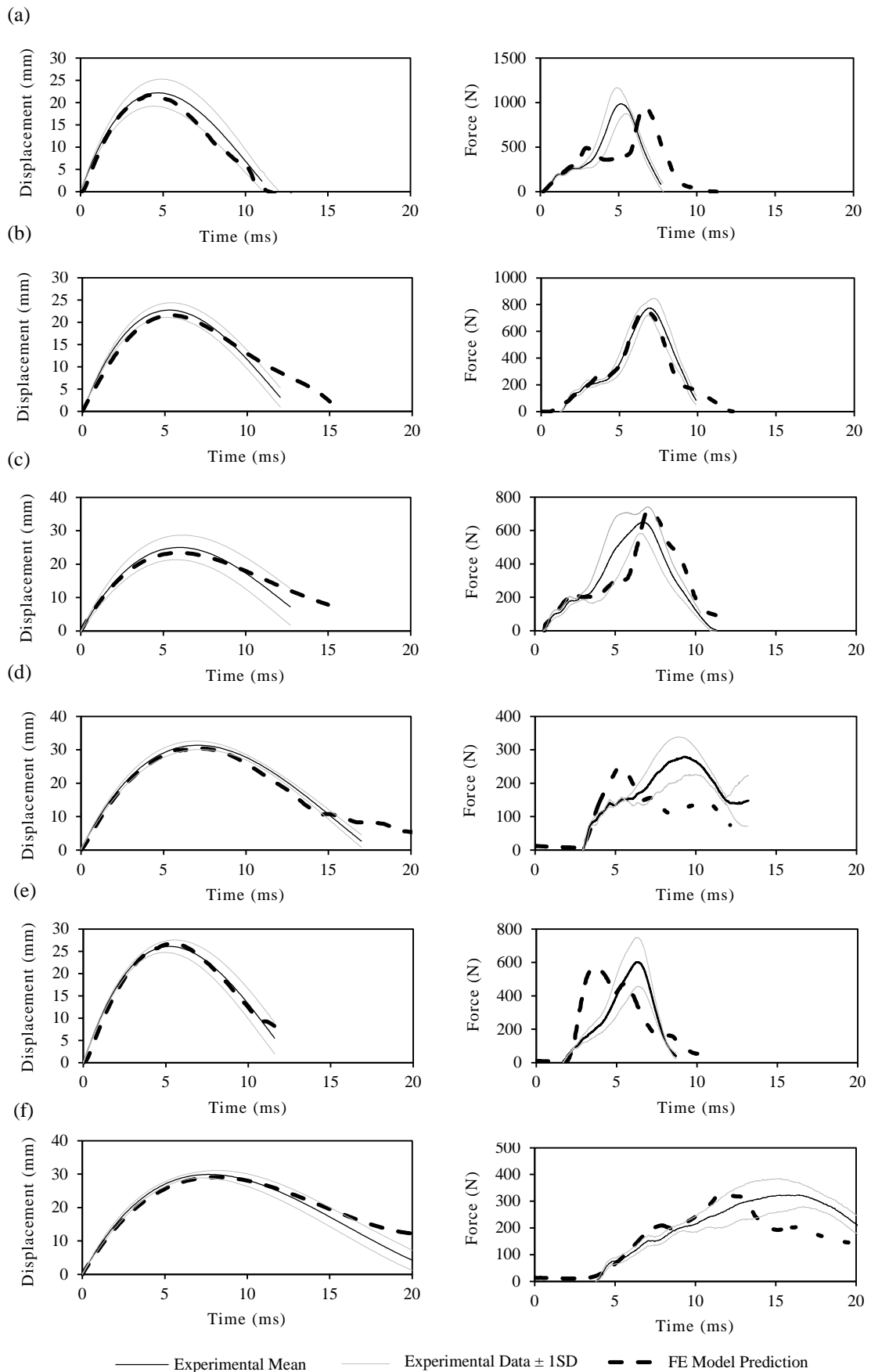


Figure 6.17 - Displacement vs. time and force vs. time graphs showing a comparison between experimental data and FE model predictions for cricket ball impacts in: (a) Silastic 3481; (b) Silastic 3483; (c) Silastic 3487; (d) 10% Gelatin; (e) 20% Gelatin and (f) PDMS surrogates.

Table 6.4 provides a comparison of x_{\max} , t_x , RF and t_{rf} between the experimental data and revised FE model predictions for the cricket ball impact simulation.

Table 6.4 - Comparison of x_{\max} , t_x , RF and t_{rf} between experimental data and FE model predictions in the cricket ball impact.

	x_{\max} (mm)			t_x (ms)			RF (N)			t_{rf} (ms)		
	Exp.	FE	% Error	Exp.	FE	% Error	Exp.	FE	% Error	Exp.	FE	% Error
PDMS Silicones	29.9	29.1	-2.77	7.70	8.55	+11.1	323	328	+1.54	16.1	11.7	-27.3
10% Gel	31.4	30.4	-2.93	7.10	7.20	+1.45	279	248	-11.1	9.23	5.24	-43.2
20% Gel	26.1	26.7	-2.43	5.20	5.23	+1.12	602	564	-6.25	6.27	3.70	-40.9
Silastic 3481	22.1	21.7	-2.12	4.70	4.40	-7.04	954	966	+1.19	5.14	6.67	+29.7
Silastic 3483	22.7	21.6	-5.14	5.30	5.40	+2.06	775	771	-0.49	6.87	6.55	-4.66
Silastic 3487	25.0	23.5	-6.49	6.00	5.94	-1.08	651	727	+11.6	6.74	7.08	+5.04

In the cricket ball impact simulations, each FE model provided a good prediction of the experimental surrogate displacements with maximum divergences of -6.49% and -7.04% in x_{\max} and t_x respectively. There was, however, a greater divergence from the force - time histories. The Silastic 3483, Silastic 3487, and PDMS surrogates all exhibited acceptable responses showing comparable force - time profiles and similar magnitudes of RF (max. +1.54% difference). The 10% gelatin, 20% gelatin and Silastic 3481 simulations showed significant differences in the force - time graphs, despite exhibiting a reasonable prediction of RF (<11.1% difference from experimental mean x_{\max} and RF). Overall, the results of this study indicate that a lower confidence should be placed upon the time course over which deep tissue pressures are experienced in the cricket ball impact simulations.

6.6.3. Discussion

Experimental data of the surrogate impacts were plotted in Figure 6.12 and Figure 6.16 and showed a significant difference in displacement and force responses between surrogates based on their constitutive materials. The FE models were validated against experimental tests of simplified puck surrogates under representative cricket ball and knee impactor conditions. The initial divergences observed were partially attributed to batch variability affecting the mechanical properties of materials. This has been previously shown to account for as much as 12.3% difference in maximal stress response (§5.5.5). The responses under the knee impact simulation subsequently showed an improved and an acceptable match with experimental data in all materials excepting gelatins within the experimental response corridor.

In the cricket ball impact simulation, a revised contact definition was required between the puck and the plate. The tied contact initially enforced artificially stiffened the surrogate and resulted in numerical instabilities as the surrogate deformed on impact. To overcome this, an exponential softened contact was introduced which significantly reduced the sudden impact loading being enforced and subsequent surrogate instabilities. The first batch of surrogate puck simulations exhibited an increased stiffness and reduced x_{\max} in the silicone simulants. This was due to the mesh definitions adopted failing to model predicted deformation modes in the high rate cricket

ball impacts resulting in artificial, stiffness and instabilities. To overcome this, a mesh refinement was conducted from which the nominal element size was reduced to 1 mm. The resultant silicone simulations exhibited magnitudes of x_{\max} and RF within a -6.49% difference of the experimental mean.

The gelatins showed significant divergences in both loading conditions and required an optimisation of the hyperelastic material parameter to ensure the predictions better mimicked the experimental data. Despite gelatin commonly being modelled as a hyperelastic material (Cronin, 2001; Minisi, 2006; Wen *et al.*, 2015), fundamental assumptions may be violated as the model is intended for materials which are incompressible, though gelatins exhibit a Poisson's ratio between 0.34 - 0.37 (Wen *et al.*, 2013). A further potential explanation for some of the divergences could be the increased stiffness introduced by the manner in which the viscoelasticity is applied. The Prony series expansion is a non-linear quasi-static representation of the viscoelasticity used widely in both organic tissue and elastomer based research (Lim *et al.*, 2009; Then *et al.*, 2012; Karimi & Navidbakhsh, 2014). This model was formulated by Fung (1993) and embodies the assumption that the shear modulus is independent of applied strain magnitude. Recent literature, however, suggests that some biological tissues have exhibited fully non-linear viscoelasticity whereby there is non-linearity in both the elastic and viscous aspects of the tissues mechanical behaviour (Duenwald *et al.*, 2009; Troyer & Puttlitz, 2011). This could also account for the increased divergence in the gelatins, which embody more significant viscoelastic behaviour.

6.7. Open Loop Predictive FE Simulation of Surrogate Behaviour

6.7.1. Introduction

To evaluate the differences between the surrogates in a more biofidelic geometry, and to compare responses against organic tissue predictions, an open loop predictive simulation was conducted using the FE model formulations established in the closed loop experimental puck validations.

In the investigatory closed loop validation, the meshing, material models and contact conditions used in the generic FE model formulation have been validated. Using these formulations, open loop predictive simulations were conducted in a geometrically more biofidelic cylinder shape to determine closeness of fit of each simulant material to an idealised organic tissue prediction. Further validations at this point, given only minor geometric variations from the puck simulations, do not represent a worthwhile activity considering the additional cost associated with synthetic surrogate fabrication.

6.7.2. Methodology

The 150 mm diameter target cylindrical surrogate developed previously (Fig. 4.4) has been used in cricket ball and knee impact simulations to determine the differences in mechanical response between surrogates.

The mechanical response metrics documented in §4.4.2.b have been assessed again with the maximum displacements (x_{\max}), time to maximum displacement (t_x), peak deep tissue pressure ($P_{\text{base,max}}$) and time to peak pressure (t_p). The displacements and maximum von Mises stress ($\sigma_{v,\max}$) on each layer surface have also been assessed to evaluate the worth of a layered approach.

6.7.3. Results

a) Surface Displacement

x_{skin} - time plots for each of the simulant surrogates are shown in Figure 6.18 with x_{\max} and t_x magnitudes shown in Table 6.5.

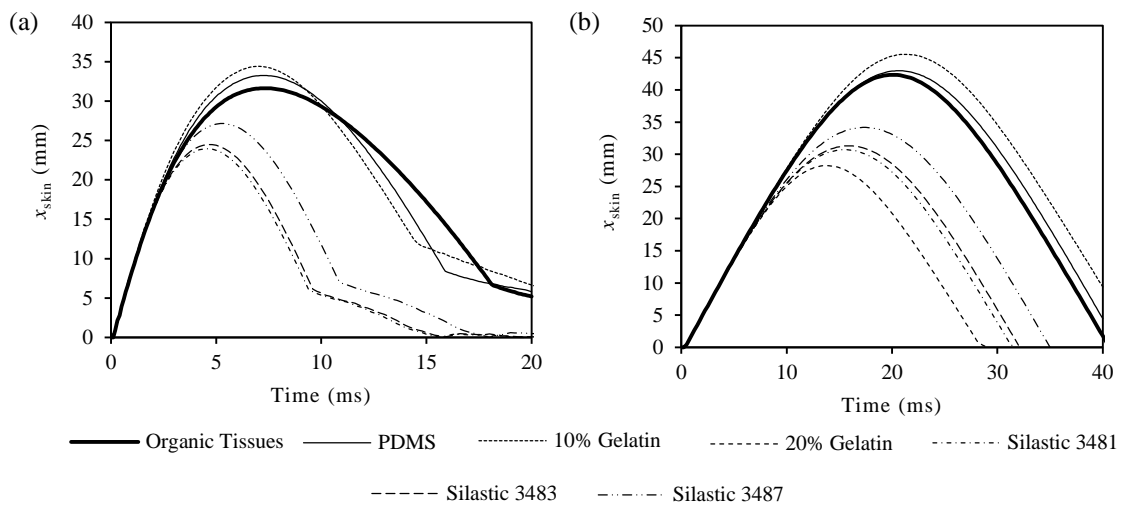


Figure 6.18 – x_{skin} - time plots of simulant surrogates in: (a) cricket ball and (b) knee impactor simulations.

Under both loading conditions the PDMS silicone surrogate exhibited the closest x_{max} and t_x values to the organic tissue surrogate predictions with maximal differences of -4.82% and +3.00% in x_{max} and t_x respectively. The 10% gelatin surrogate exhibited the closest single material simulant response, however showed increased x_{max} under both impact conditions (min. +7.57% difference). Silastic 3487 provided the closest single material responses with maximal differences in x_{max} of 14.2%.

Table 6.5 - x_{max} and t_x values for cricket ball and knee impacts (% difference from organic tissue predictions in brackets).

	Cricket Ball		Knee	
	x_{max} (mm)	t_x (ms)	x_{max} (mm)	t_x (ms)
<i>Organic Tissues</i>	31.6	7.30	42.3	20.0
<i>PDMS Silicones</i>	33.2 (-4.82%)	7.20 (-1.36%)	42.9 (-1.42%)	20.6 (+3.00%)
<i>10% Gel</i>	34.4 (+8.86%)	7.00 (-4.11%)	45.5 (+7.57%)	21.2 (+6.00%)
<i>20% Gel</i>	27.6 (-12.7%)	5.50 (-24.7%)	28.2 (-33.3%)	13.8 (-31.0%)
<i>Silastic 3481</i>	24.0 (-24.1%)	4.60 (-37.0%)	30.7 (-27.4%)	15.5 (-22.5%)
<i>Silastic 3483</i>	24.5 (-22.5%)	4.60 (-37.0%)	31.3 (-26.0%)	16.0 (-20.0%)
<i>Silastic 3487</i>	27.1 (-14.2%)	5.20 (-28.8%)	34.1 (-13.5%)	17.3 (-13.5%)

Figure 6.19 shows sagittal plane sections of the surrogates illustrating the differences in compression between the organic tissue, PDMS silicone and the most representative simulant (10% gelatin) models.

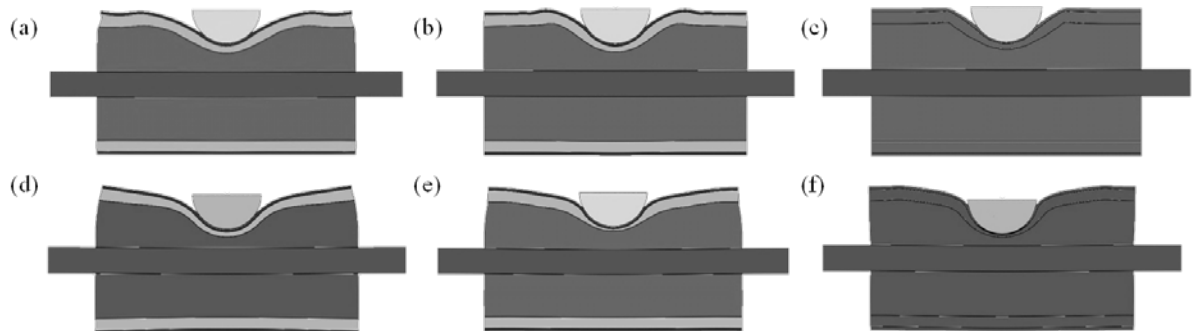


Figure 6.19 - Sagittal plane sections showing impactor penetrations of surrogate under cricket ball: (a) organic tissues, (b) PDMS, (c) 10% gelatin; and knee impactor loading conditions: (d) organic tissues, (e) PDMS, (f) 10% gelatin.

b) Deep Tissue Pressure

The $P_{\text{base,max}}$ and t_p were recorded (Table 6.6) alongside the percentage differences from the predicted organic tissue response.

Table 6.6 - $P_{\text{base,max}}$ and t_p values from cricket ball and knee impact simulations (% difference from organic tissue predictions in brackets).

	Cricket Ball		Knee	
	$P_{\text{base,max}}$ (MPa)	t_p (ms)	$P_{\text{base,max}}$ (MPa)	t_p (ms)
Organic Tissues	0.123	8.40	0.669	20.0
PDMS Silicones	0.152 (+23.5%)	9.50 (+13.1%)	0.567 (-15.2%)	20.8 (+4.00%)
10% Gel	0.196 (+59.3%)	9.50 (+13.1%)	0.733 (9.57%)	17.0 (-15.0%)
20% Gel	0.312 (+154%)	6.00 (-28.6%)	0.852 (+27.4%)	18.6 (-7.00%)
Silastic 3481	0.211 (+71.5%)	5.60 (-33.3%)	0.465 (-30.5%)	15.5 (-22.5%)
Silastic 3483	0.197 (+60.2%)	5.80 (-30.9%)	0.426 (-36.3%)	16.0 (-20.0%)
Silastic 3487	0.181 (+47.2%)	6.60 (-21.4%)	0.419 (-37.4%)	17.5 (-12.5%)

The PDMS simulant surrogate exhibited the closest $P_{\text{base,max}}$ magnitudes to the organic tissue surrogate predictions in the cricket ball impact simulation. The 10% gelatin provided the closest x_{max} approximation to the organic tissue predictions in the knee impact simulation, however exhibited significantly reduced t_p values (-15.0%). Figure 6.20 shows the differences in P_{base} between the predicted organic tissue model, PDMS simulants and select most representative simulants throughout the simulation.

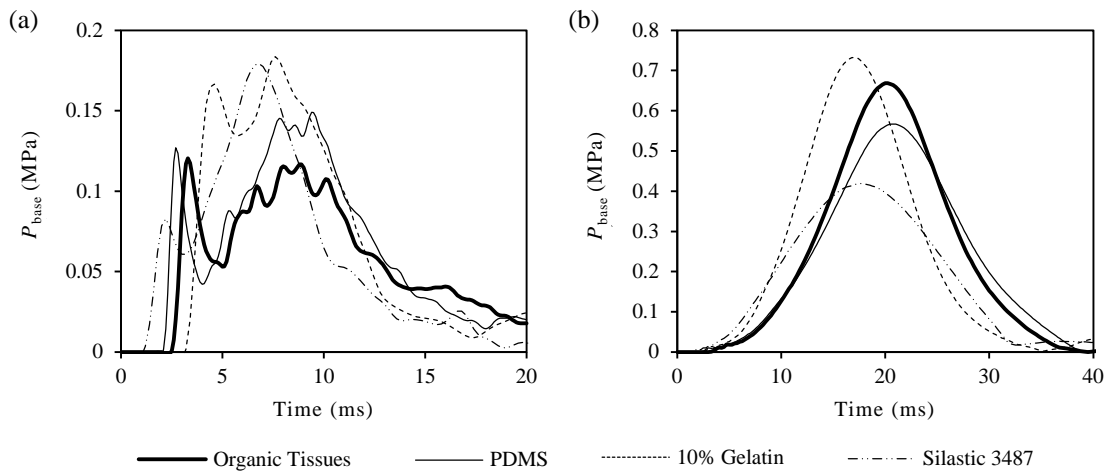


Figure 6.20 - P_{base} - time graphs for: (a) cricket ball and (b) knee impactor simulations.

c) Layer Effects

(i) Surface Stresses

The von Mises stresses experienced on the skin and muscle outer surfaces of the cylinder surrogates for the organic tissue predictions, PDMS simulants and most representative single material simulants (10% gelatin and Silastic 3487) have been shown in Figure 6.21.

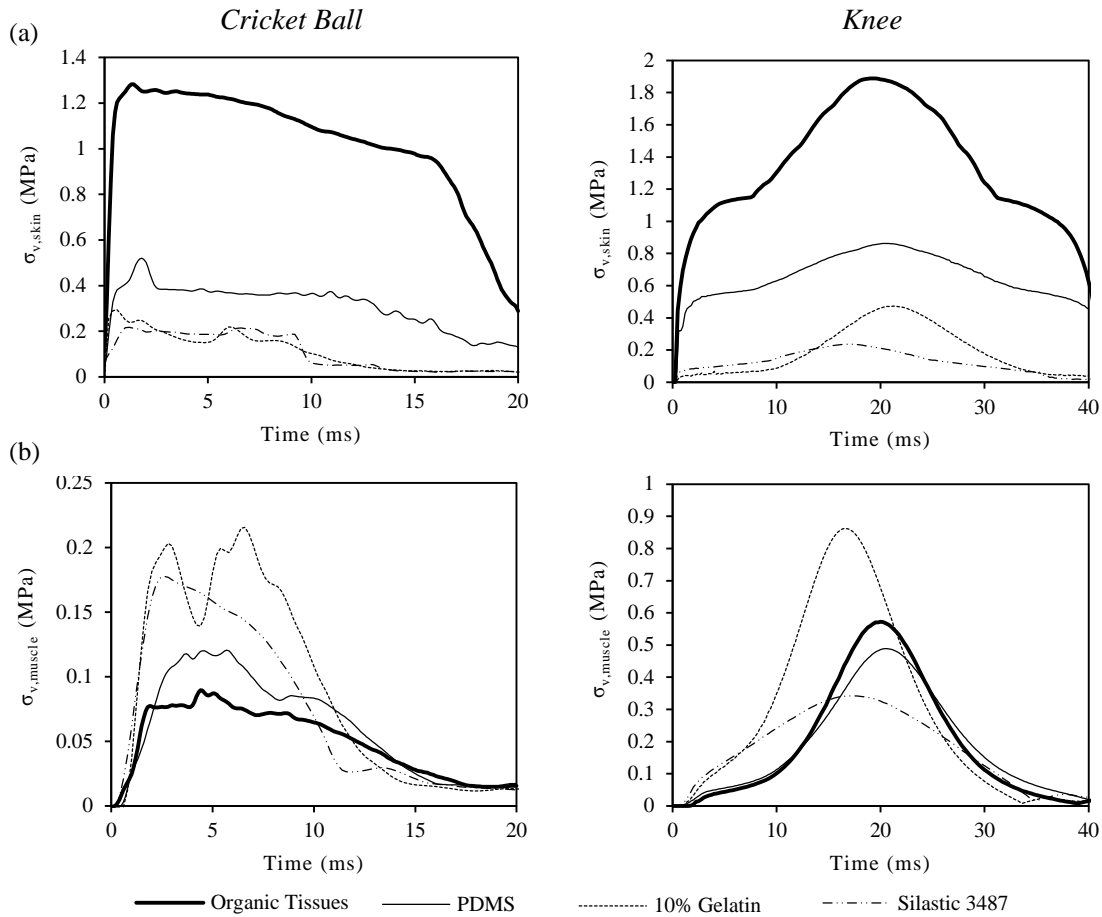


Figure 6.21 – (a) $\sigma_{v,skin}$ - time graphs and (b) $\sigma_{v,muscle}$ - time graphs (left: cricket ball; right: knee impacts).

The organic tissue surrogate exhibited the greatest magnitudes of $\sigma_{v,max}$ on the skin layer under both loading conditions. The PDMS simulant surrogate provided the closest $\sigma_{v,max}$ but still exhibited a -59.5% and -54.0% difference from the organic tissue predictions in cricket ball and knee impact simulations respectively. At the muscle layer, the PDMS simulant surrogate exhibited the closest $\sigma_{v,max}$ and t_{σ} under both loading conditions.

(ii) Layer Thicknesses

The thicknesses of the tissue layers throughout each impact simulation were compared in the organic tissue, PDMS, Silastic 3487 and 10% gelatin simulant surrogates in Figure 6.22.

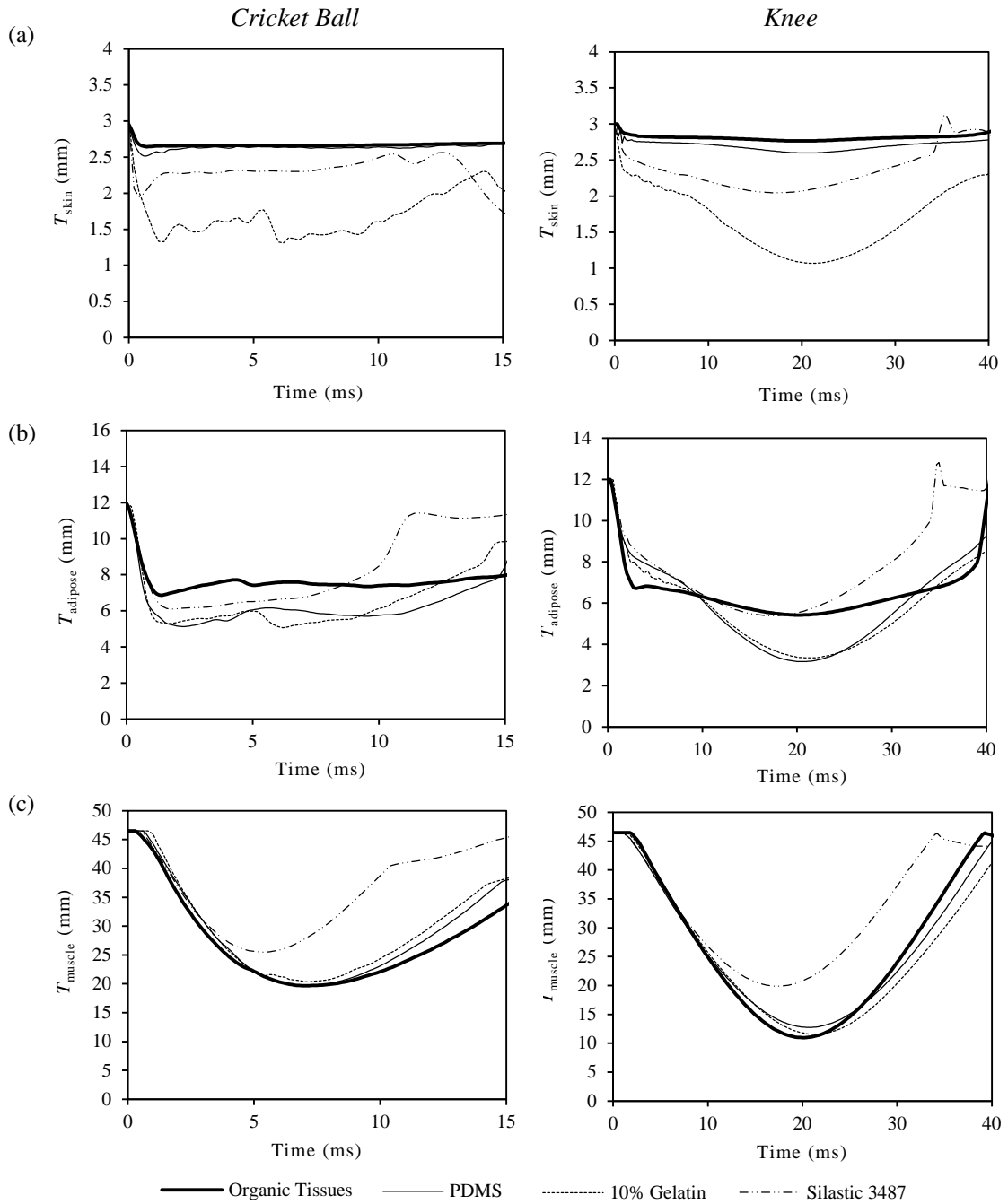


Figure 6.22 - Tissue layer thicknesses in the cylinder surrogate showing responses under the cricket ball (left graph) and knee impactor (right graph) loading conditions for: (a) skin; (b) adipose; (c) muscle tissues.

The results show the PDMS simulant and organic tissue surrogates exhibit significantly reduced tissue deformations compared to single material simulants. At the adipose layer, the organic tissue model exhibited reduced layer displacements compared to all surrogates in the cricket ball impact and the Silastic 3487 surrogate provided the best analogue for the knee impact with the PDMS simulants and 10% gelatin exhibiting increased displacements. At the muscle layer, the PDMS

simulant showed similar responses to the organic model predictions in the cricket ball impact but reduced displacements in the knee impact simulation in which the 10% gelatin provided a closer representation of organic tissue behaviour.

6.7.4. Discussion

The closed loop puck surrogate validations were conducted to establish confidence in the cylindrical model response predictions. The combined multi-material surrogate responses from the developed PDMS silicones show a significantly improved representation of the predicted organic tissue responses than single material constructions using existing simulants (Fig. 6.18; 6.20).

The top surface displacements (Table 6.5) provide a good indication of the composite dynamic impact response behaviour of all of the tissue layers in combination. The PDMS silicones provided better matched levels of overall compression than single material constructions under both loading conditions. Differences in x_{\max} of -4.82% and -1.42% and were recorded between the PDMS simulants and the target organic tissue model for cricket ball and knee impactor simulations respectively. The 10% gelatin simulant typically provided the closest representation of the x_{\max} of the organic tissue model, however exhibited softer overall behaviour with +7.57% and +8.86% differences from the organic tissue predictions. The Silastic 3487 was the most comparable durable simulant, however exhibited a significantly increased stiffness and a difference in x_{\max} of -14.2% and -13.5% from the organic tissue model predictions. The PDMS simulants also provided a better representation of t_x with -1.36% and 3.00% differences compared to -4.11% and +6.00% differences for 10% gelatin in cricket ball and knee impacts respectively.

The deep tissue pressures (Table 6.6) experienced are pertinent as they are a direct measure of the load transfer through the surrogate from the normal, axial impact. The PDMS silicones exhibited similar P_{base} - time profiles to organic tissue though showed +23.5% and -15.2% differences from the predicted organic tissue model. The 10% gelatin model provided a closer representation of the $P_{\text{base,max}}$ (+9.57%) in the knee impact, though differed in t_p by -15.0% compared to just +4.00% exhibited by the PDMS simulant model. The PDMS simulant model also better represents the onset and delay in pressures in the knee impact predicted by the organic tissue model with a significantly elongated P_{base} - time trace to all other simulants.

The importance of a biofidelic skin layer was demonstrated in the surrogate model through $\sigma_{v,\max}$ experienced on the top surface (Fig. 6.21.a). In the knee impact, the responses in the organic tissue and PDMS simulant models show comparable stress profiles with an initial sharp increase in stress followed by a gradual rise to the peak whilst all other simulants exhibited a more simple parabolic response. In the cricket ball simulations, the PDMS simulants similarly show the closest $\sigma_{v,\max}$ and stress profiles to the organic tissue data. Although the PDMS skin exhibited a significantly reduced $\sigma_{v,\max}$ compared to organic tissues in both conditions it still provides a closer match than other single material simulants. The importance of this layer is also emphasised by the lack of compression exhibited in the organic tissue and PDMS skin layers compared to other simulants (Fig. 6.22.a).

The importance of a biofidelic adipose layer is highlighted by the initial rapid decreases in layer thickness shown in Figure 6.22.b. Organic adipose exhibits initially very soft behaviour with a rapidly increasing stiffness at approximately 0.3 strain (§2.3.2.b). The organic adipose tissue layer experiences greater initial levels of compression than the PDMS simulant. The PDMS simulant

layer, however, experiences an overall greater level of compression than organic tissue most apparent in the knee impact simulation, which could be attributed to the lower strain hardening present under high strain deformations. The softer 10% gelatin simulant exhibits a slower initial displacement than the layered models but a similar level of overall compression to the PDMS simulant model.

At the muscle layer, the PDMS simulant model provided a close representation of the predicted organic tissue layer response exhibiting similar deformation responses and just a 16% difference at maximal compression. The $\sigma_{v,max}$ experienced on the muscle surface (Fig. 6.21.b) also showed that the PDMS silicone exhibited the closest response to the predicted organic tissue model with -5.54% and -14.5% differences compared to -17.4% and +50.7% differences in the 10% gelatin surrogate for cricket ball and knee impact simulations.

Overall, the simulations showed that the PDMS silicone surrogate was the most biofidelic simulant for all geometries and loading conditions. The 10% gelatin simulant model was the best alternate single material simulant; however, this material is innately inappropriate for sports impact surrogates due to its fragility. Frangible surrogates attain permanent damage from impacts, which are not suited to repeat testing required for PPE evaluations. Consequently, frangible surrogates are far more expensive per test than their durable alternatives and also often require specialised storage conditions and have limited shelf life. Given that the 20% gelatin surrogate was stiffer than the organic tissue predictions it could be assumed that an intermediate gelatin formulation could provide a closer approximation of the overall deformations. However, the significance of the layers shown indicates that key mechanical response phenomena will be ignored with a single material simulant. Silastic 3487 simulant provided the best existing durable synthetic representation of the multi-material response though still showed significant divergences from the target organic tissue predictions.

6.8. Conclusions

Multi-material PDMS human soft tissue surrogates were compared experimentally and computationally to previously-used single material surrogates and exhibit a more representative response when compared to organic tissue predictions. Puck surrogates were fabricated for PDMS and single material simulants and tested in closed loop validation trials under cricket ball and knee impact conditions. FE models were validated against the experimental results and in some cases, particularly gelatins, optimised to provide a good representation of their actual behaviour. In a more biofidelic cylindrical geometry, open loop predictive simulations were performed and the PDMS simulant model showed closer fits to organic tissue predictions in both loading conditions and through all evaluation metrics excepting maximal deep tissue pressure in the knee impact condition.

Chapter 7 – Investigation of the Importance of Anatomical Geometric Complexities and their Effect on PPE Interactions

7.1. Chapter Overview

Chapter 7 presents an investigation into the effects of surrogate geometry on impact response. The geometries used in previous sports impact surrogates have been reviewed and the need for such an investigation has been clearly identified. Established FE modelling practices (§4) have been used to predict the behaviour of different surrogate shapes (puck, shaped anvil, cylinder) at different anatomically selected positions on the thigh (50, 75, 100 mm radii of curvature). Cricket ball and knee impact simulations were conducted in each geometry and their behaviour through a series of key mechanical response metrics have been reported and compared. The surrogate responses were then compared in an anatomically contoured thigh surrogate exposed to multi-directional impacts. The extended worth of geometric complexities were then shown in the interactions of the different surrogates with PPE.

7.2. Introduction

7.2.1. Previous Surrogate Geometries

Previous impact surrogates in the sports equipment industry have utilised a range of geometries from simple pucks to more biofidelic cylindrical surrogates. The most simple surrogate designs are typically employed within safety standards (§2.2.3.a). The standards prescribed by the BSI commonly use hemispherical or half-cylinder shaped surrogates of varying curvature to represent the outer surface geometries of human limb segments (Fig. 7.1). The surrogate geometries are primarily adopted to enable compatibility with test equipment (e.g. Instron Dynatup 9250HV drop tower) as well as providing a consistent, repeatable structure.

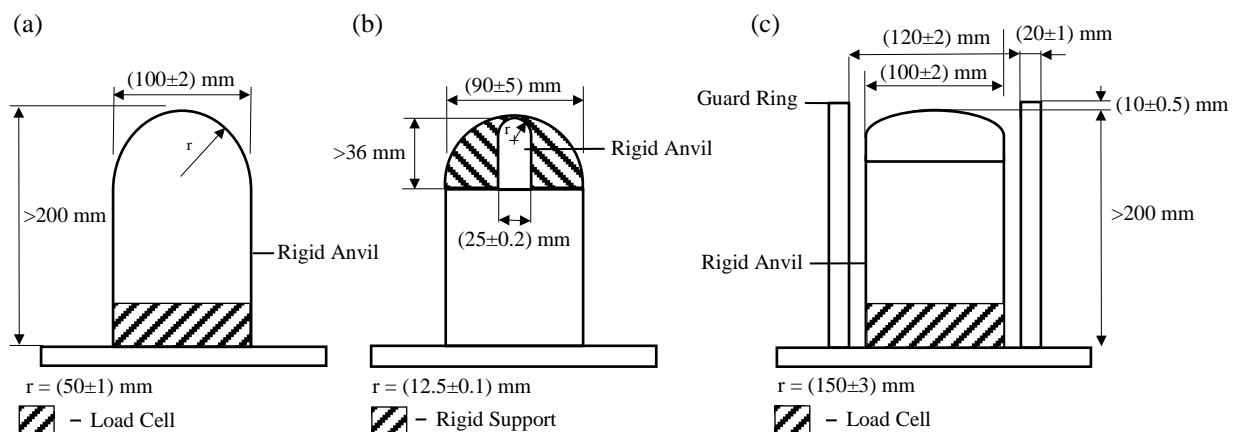


Figure 7.1 - (a) BS 6183:3:2000 Cricket Leg Guards - Shin Region; (b) BS:EN 13277 Martial Arts Limb Segment Protection – Shin, Instep and Forearm Protectors; (c) BS 13546:2002 – Field Hockey Goalkeeper Clothing – Abdominal, Chest, Breast Thigh, Hip Protection.

Non-standardised research surrogates have often adopted a more biofidelic simplified cylindrical geometry to represent the target limb segments (e.g. Hrysonmallis, 2009). These structures, similar to the previously adopted cylindrical FE surrogate (§4.3.2), commonly approximate both human anthropometric outer curvature, mass and inertial properties. Further to this, the most complex research surrogates have used either imaging or moulding techniques to provide a detailed representation of surface geometries, though these geometries have been almost exclusively used in automotive, military or medical research (e.g. Krstic *et al.*, 2002; Manning, 2007). These complex surrogate types potentially enable a better representation of human response to impact and more biofidelic interactions with PPE, though the level of detail required to elicit appreciable increases in biofidelity is currently unknown.

The differences in surrogate response have been extensively investigated when compared to PMHS in validation type studies (e.g. Krstic *et al.*, 2002; Hrysonmallis, 2009; Cronin *et al.*, 2011) where geometric differences are obvious. However, these studies do not specifically isolate the effects of different anatomical geometries as the constituent materials present (organic tissues) are likely to contribute significantly to any divergences in response. There is a paucity of information pertaining to the specific effects of surrogate geometries on impact response and the potential inaccuracies introduced from inadequate consideration of these factors. It is believed that improper consideration of surrogate geometries could affect the following impact related phenomena:

- Pressure distribution.
- Impactor penetration depths.
- Surrogate tissue stress/strain magnitudes.
- Stress/strain propagation rates and distributions.
- End distortions and edge effects.
- Surrogate-PPE interactions.

A previous study by Shen *et al.* (2010) investigated the effects of different surrogate geometries on body armour interactions in bullet impact simulations. It was noted that the geometry of surrogates, particularly outer curvatures, significantly affected the energy absorption of the PPE. Although flat and curved blocks exhibited similar impactor penetrations, the curved surrogate allowed PPE fibres to move in the direction of impact and absorb less energy ultimately suggesting the flat blocks would represent a non-conservative option. The presence and locality of a stiff interface was also reported to affect impact response. Shen *et al.* (2010) reported that the peak armour deformation was much greater in clay and gelatin surrogates compared to a human FE model due to the engagement of a stiff rib cage in the FE model slowing the bullet. Similarly, Lin *et al.* (2011) observed increases in contact pressures on compression garments around bony regions of the body such as the posterior ankle, patella and anterior calf.

Virtual surrogates are commonly used in shape optimisation studies in other industries (e.g. aerospace engineering – Krog *et al.*, 2002). A similar approach has been adopted in this chapter using FE models to investigate changes in mechanical response of different shaped surrogates when subject to impacts.

7.2.2. Aims and Objectives

- 1) To determine the differences in surrogate impact response in simple surrogate geometries. Evaluation of the following geometric factors:
 - Shape.
 - Radii of soft tissue curvature.
- 2) To assess the levels of surrogate complexity at which no appreciable change in response is observed.
- 3) To determine the extent to which different surrogate geometries affect the interaction of PPE with the surrogate. Evaluation of the following factors:
 - Proximity of the PPE to the surrogate and degree of surrogate-PPE interaction.
 - Pressure distribution on the surrogate.
 - Load transfer through the PPE to the surrogate.

7.3. Study 1 – Evaluation of Surrogate Shape

7.3.1. Introduction

An initial comparison between simple geometric shapes was performed to identify the differences in response based on the: shape, radius of soft tissue curvature and proximity of edges. Three geometries were studied in this evaluation: a puck, a shaped anvil and a cylinder. Each successive surrogate introduced increases in geometric complexity in the form of: layer configurations, curvature and levels of constraint. This study aimed to identify the levels of surrogate complexity necessary to elicit real surrogate response phenomena and determine what penalty in fidelity, if any, is associated with simpler geometries.

FE models have been used in an open loop predictive manner (Fig. 6.1) using the validated model formulations established in §6.6. The differences in geometries represent the only minor perturbation to these surrogate constructs and as such do not merit further incremental validations at this point considering the additional cost of synthetic surrogate fabrication. The FE simulations have been conducted to identify the relative cost vs. benefit of each surrogate shape. The cylindrical surrogate is inherently more biofidelic than the other shapes, therefore this study aims to determine whether similar responses are observed in puck or shaped anvil surrogates that would be more cost-effective

7.3.2. Methodology

a) Anthropometric Parameters

The anthropometric parameters for this study were obtained from the VHP in the same manner as presented in §4.3.3.a. Table 4.1 shows the measured distances from the femur bone centroid to each tissue layer. These measured parameters were used to inform the outer tissue radius of curvature at different positions along the thigh segment geometry. Using the data, a simplified approximation of the thigh at three positions along its length was determined: a 50 mm radius of curvature to represent inferior areas proximal to the bone; a 75 mm radius of curvature to represent a central section; and a 100mm radius of curvature to represent superior areas distal to the bone. Previously used tissue thicknesses of 12 mm and 3 mm have been approximated for adipose and skin thicknesses respectively.

b) Geometries

(i) Puck

The puck surrogate represents the most simple surrogate geometry in terms of shape complexity. It is commonly used in material specimen tests and is representative of the types of geometries used in some safety standards. A 130 mm diameter was selected as this is comparable with limb segment anvil approximations in safety standards (e.g. BS:EN 13546:2002). This size is also compatible with standardised test equipment (e.g. Instron Dynatup 9250HV drop tower). Figure 7.2 shows the puck surrogate configuration in the 75 mm model. The muscle layer thickness increases to 71.5 mm in the 100 mm surrogate and decreases to 21.5 mm in the 50 mm surrogate. The puck surrogate is intended to be fixed at the base of the bone layer.

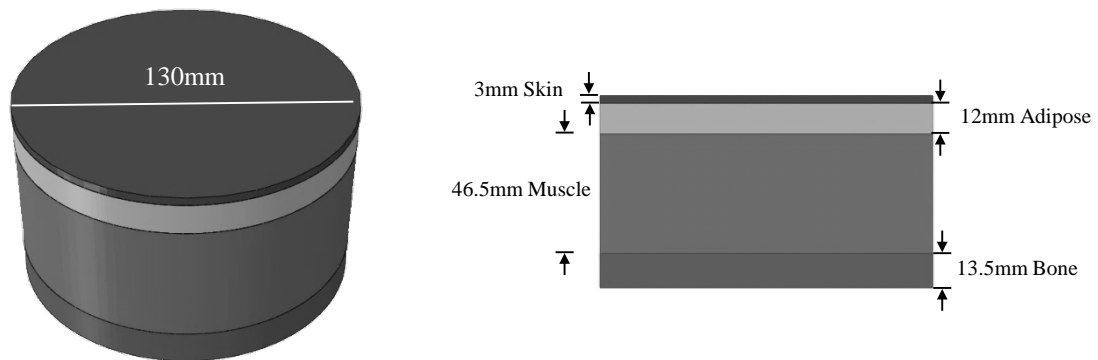


Figure 7.2 – 75 mm puck surrogate configuration dimensioned in sagittal plane section.

(ii) Shaped Anvil

The shaped anvil was designed to evaluate the potential of a cost-effective surrogate that could be used in safety standards evaluations. The surrogate embodies curved surfaces more representative of a human thigh than the puck, including the bone component which is located centrally on the base of the surrogate. Each surrogate has a total height of 100 mm and 130 mm × 130 mm base dimension to enable compatibility with a standard drop tower base plate. The radius of curvature is varied relative to the bone centre of curvature in 50, 75 and 100 mm surrogates with equivalent layer thicknesses to the puck surrogate (Fig. 7.3). The varied bone height relative to surrogate height provides different levels of soft tissue constraints. Due to its proposed use in a drop tower test configuration, all tissue structures located on the base of the surrogate were intended to be fixed.

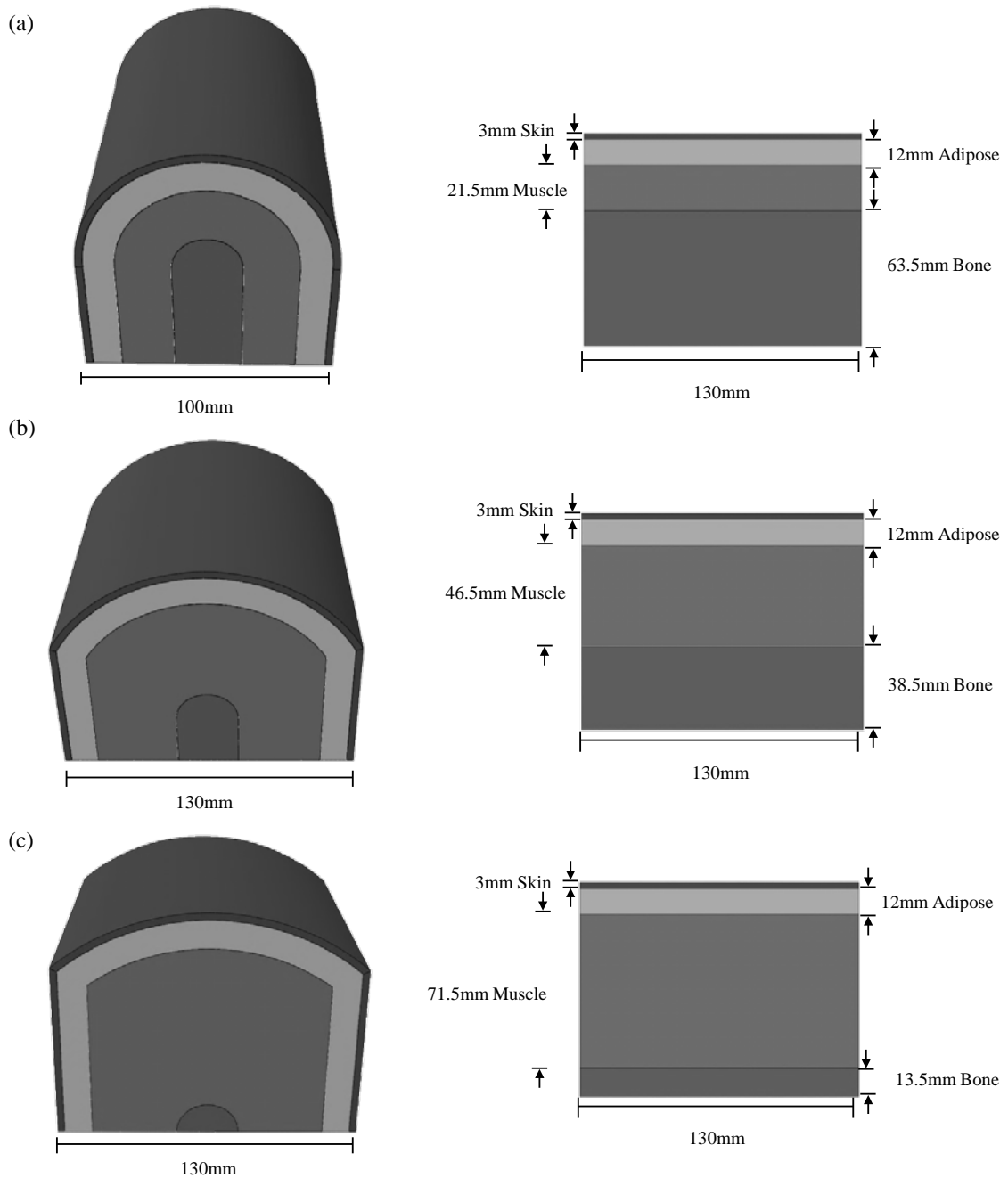


Figure 7.3 – Shaped anvil surrogate configurations and dimensions shown in sagittal plane section for: (a) 50 mm; (b) 75 mm and (c) 100 mm surrogates.

(iii) Cylinder

The cylinder surrogate, previously used in §4, provides complete continuous curved surfaces as a simplified representation of the human thigh. The soft tissue ends of the surrogate are left open; however, the length of the surrogate (276 mm) is sufficiently large to avoid edge effects given the relatively small impactor (72 mm diameter) and transient impact events. The geometry is intended to be remotely constrained in all translational axes at the ends of the bones creating an effective three-point bend scenario. The 75 mm cylinder surrogate configuration is shown in Figure 7.4. The skin, adipose and bone tissue dimensions remain constant in each surrogate configuration with the muscle thickness varying between 71.5 mm and 21.5 mm in 100 mm and 50 mm surrogates respectively.

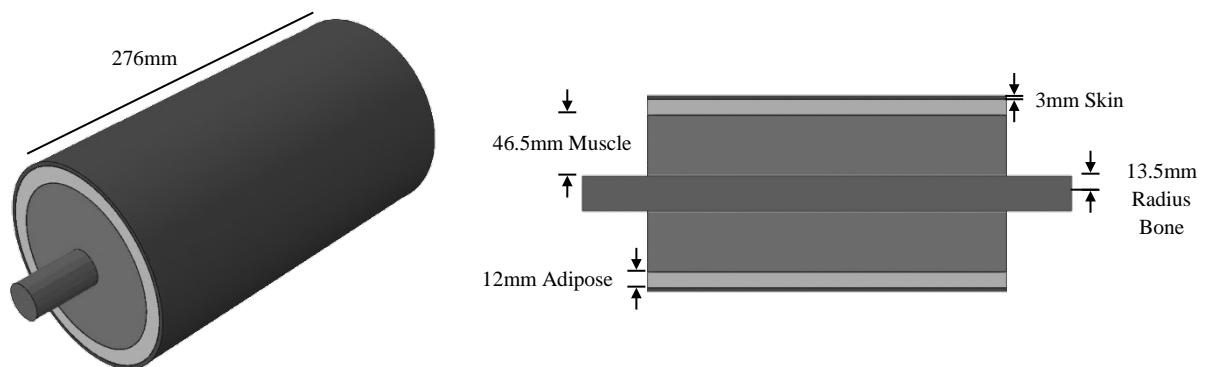


Figure 7.4 – 75 mm cylinder surrogate geometry and dimensions shown in sagittal plane section.

7.3.3. FE Modelling

a) Model Formulations

As in Chapter 4, organic tissue material properties (§4.3.2) have been used to assess the idealised state of each surrogate. Similarly, the FE modelling techniques and mesh densities of the puck, shaped anvil and cylinder surrogates are identical to those presented in §4.3.4.

b) Impact Parameters and Assessment Criteria

Each surrogate was impacted by both cricket ball and knee impactors using the impact parameters established (§3.5.4) and impactor approximation developed (§4.3.4.a). Both impactors are hemi-spherical with a 72mm diameter and have masses of 0.16 kg and 3 kg for cricket ball and knee impactor respectively. The knee impactor has an initial velocity of 3 m.s^{-1} , whilst the cricket ball is simulated at 10 m.s^{-1} .

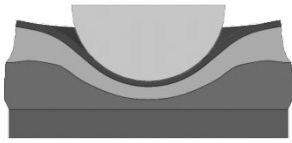
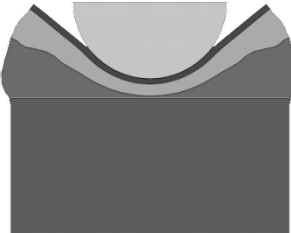
















In this study, the edge distortions introduced in each surrogate were first assessed through a visual comparison of sagittal plane sections at maximum displacement. The differences in surrogate response between surrogate shapes were then examined through comparisons of top surface displacements, deep tissue pressures and soft tissue layer stresses. The cylindrical surrogate represents the most biofidelic geometry considered; therefore, the simpler drop tower surrogates have been compared against this to evaluate responses. The responses at different outer surface radii of curvature were then also evaluated using these parameters. Finally, the merit of these surrogates has been expressed relative to their computational expenditure.

7.3.4. Results

a) Surrogate Sections at Maximum Displacement

Sagittal plane sections of each of the simple surrogates at maximum displacement are shown in Table 7.1.

Table 7.1 – Sagittal plane sections of simple surrogate at maximum deformation.

	Puck	Shaped Anvil	Cylinder
Cricket Ball			
50 mm			
75 mm			
100 mm			
Knee			
50 mm			
75 mm			
100 mm			

The images show that the puck and curved anvil surrogates both experienced significant edge effects where the size of the surrogate appears to influence the surrogate deformation response. This is most pronounced in 75 mm and 100 mm surrogates. The cylindrical surrogate exhibited no significant edge effects with the tissues distal from the impact site rarely recruited.

b) Top Surface Displacements

(i) Differences by Surrogate Shape

Figure 7.5 shows the differences in x_{skin} elicited in different surrogate shapes.

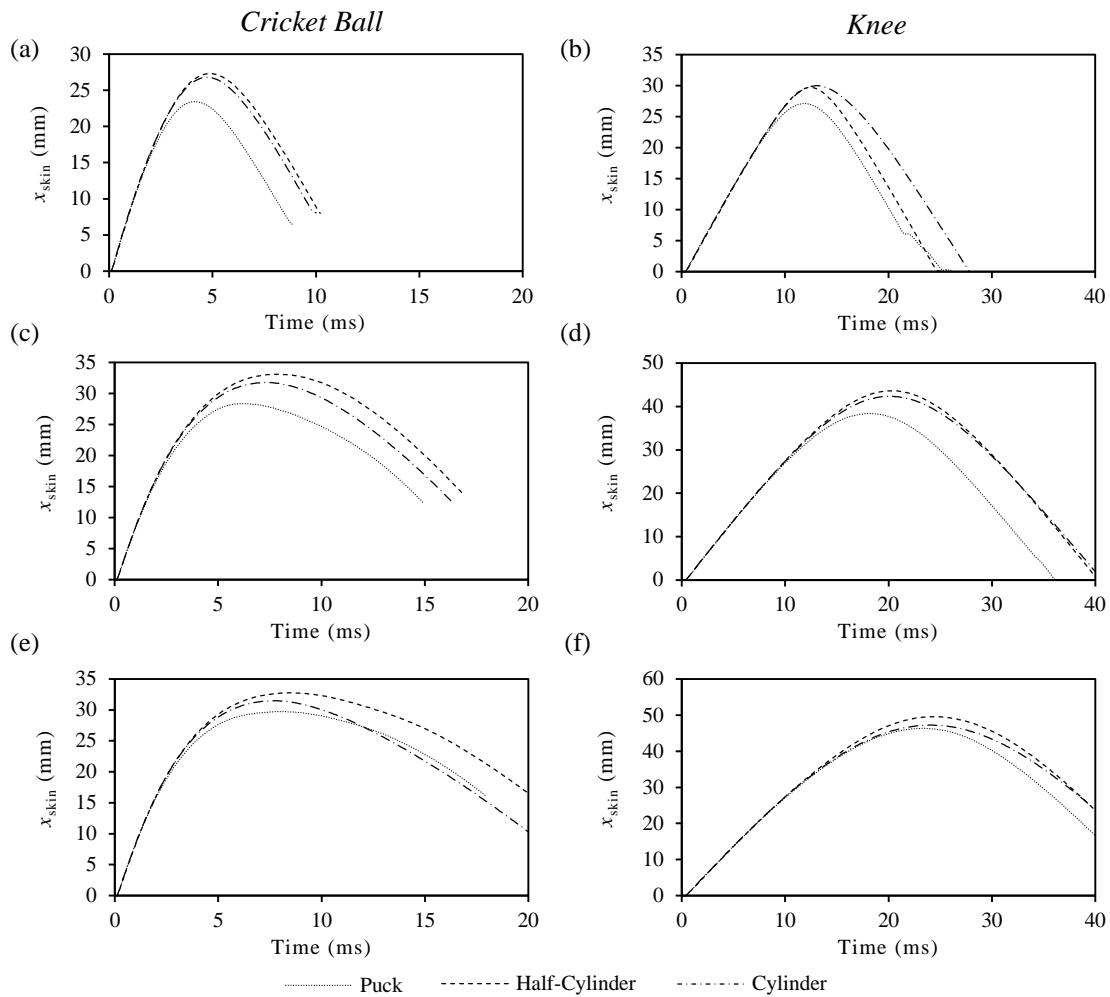


Figure 7.5 - x_{skin} - time comparisons between different surrogate geometries for: (a) 50 mm surrogate-cricket ball; (b) 50 mm surrogate-knee impact; (c) 75 mm surrogate-cricket ball; (d) 75 mm surrogate-knee impact; (e) 100 mm surrogate-cricket ball; (f) 100 mm surrogate-knee impact.

In all impact conditions, the puck surrogates exhibited the lowest x_{max} and t_x with minimum differences of -8.75% and -2.5% differences in cricket ball and knee impacts respectively. The differences were most pronounced in the 50 mm and 75 mm surrogates. The curved anvil and cylinder surrogates generally exhibited more comparable responses, though the curved anvil typically showed greater x_{max} and t_x values with divergences of up to +4.0% and +10.4% in cricket ball and knee impacts respectively.

(ii) Differences by Radii of Curvature

The differences in x_{skin} elicited at different outer tissue curvatures and soft tissue thicknesses are shown in Figure 7.6.

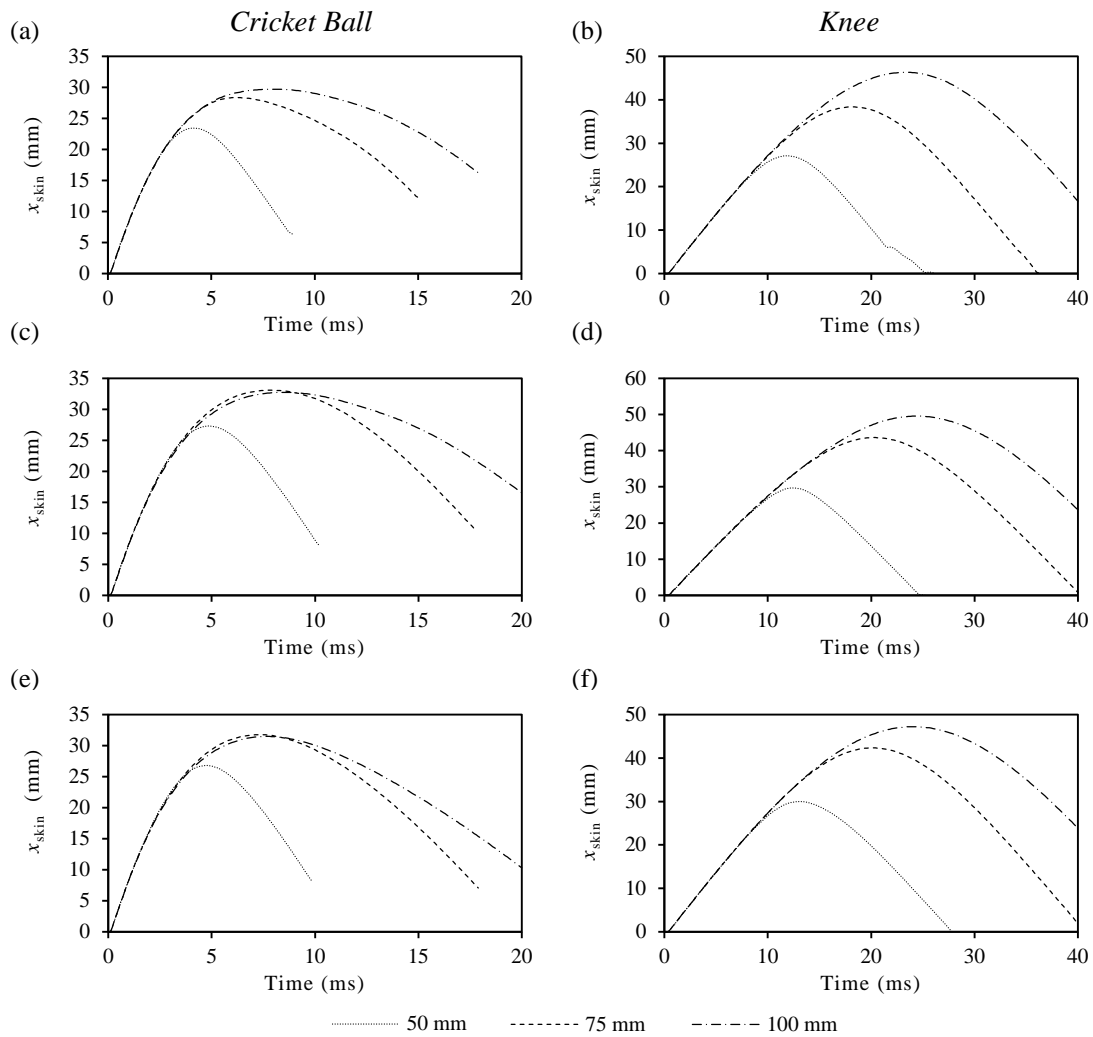


Figure 7.6 – x_{skin} - time graphs showing differences in response in the following impacts: (a) puck-cricket ball; (b) puck-knee; (c) shaped anvil-cricket ball; (d) shaped anvil-knee; (e) cylinder-cricket ball; (f) cylinder-knee.

The responses from both impact simulation show increased x_{max} and t_x at greater radii of curvature with the most significant differences being between the 50 mm and 75 mm surrogates (min. +20.1% difference).

The x_{max} and t_x for each surrogate impact simulation have been presented in Table 7.2.

Table 7.2 - x_{max} (mm) and t_x (ms) for surrogates in cricket ball and knee impacts.

	Cricket Ball						Knee					
	Puck		Shaped Anvil		Cylinder		Puck		Shaped Anvil		Cylinder	
	x_{max}	t_x	x_{max}	t_x	x_{max}	t_x	x_{max}	t_x	x_{max}	t_x	x_{max}	t_x
50 mm	23.4	4.10	27.3	4.80	26.8	4.70	27.1	11.8	29.7	12.4	30.0	13.0
75 mm	28.3	6.20	33.1	7.80	31.8	7.30	38.4	18.2	43.6	20.2	42.3	20.2
100 mm	29.7	7.80	32.8	8.50	31.5	7.70	46.3	23.4	49.6	24.4	47.2	24.0

c) Deep Tissue Pressure

(i) Differences by Surrogate Shape

The differences in P_{base} in surrogates of different shapes have been shown in Figure 7.7.

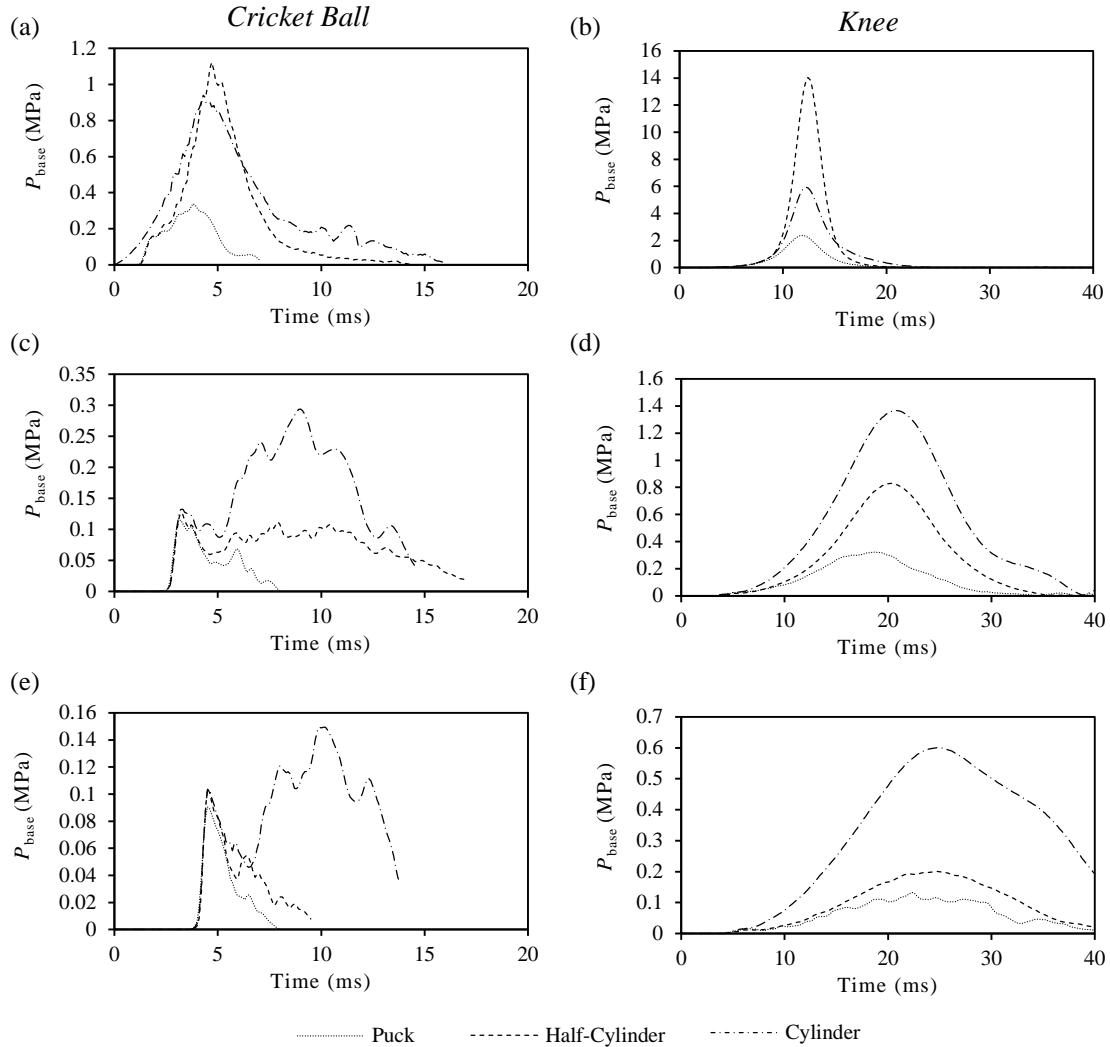


Figure 7.7 – P_{base} - time comparisons between different surrogate geometries for: (a) 50 mm surrogate-cricket ball; (b) 50 mm surrogate-knee impact; (c) 75 mm surrogate-cricket ball; (d) 75 mm surrogate-knee impact; (e) 100 mm surrogate-cricket ball; (f) 100 mm surrogate-knee impact.

Across all surrogate shapes and radii of curvature, the puck surrogate exhibited the lowest $P_{\text{base,max}}$ (min. -9.45% difference). The cylinder surrogate exhibited the highest pressures in all conditions expecting the 50 mm surrogates.

(ii) Differences by Radii of Curvature

The P_{base} in surrogates of different outer tissue curvature and soft tissue thicknesses have been shown in Figure 7.8.

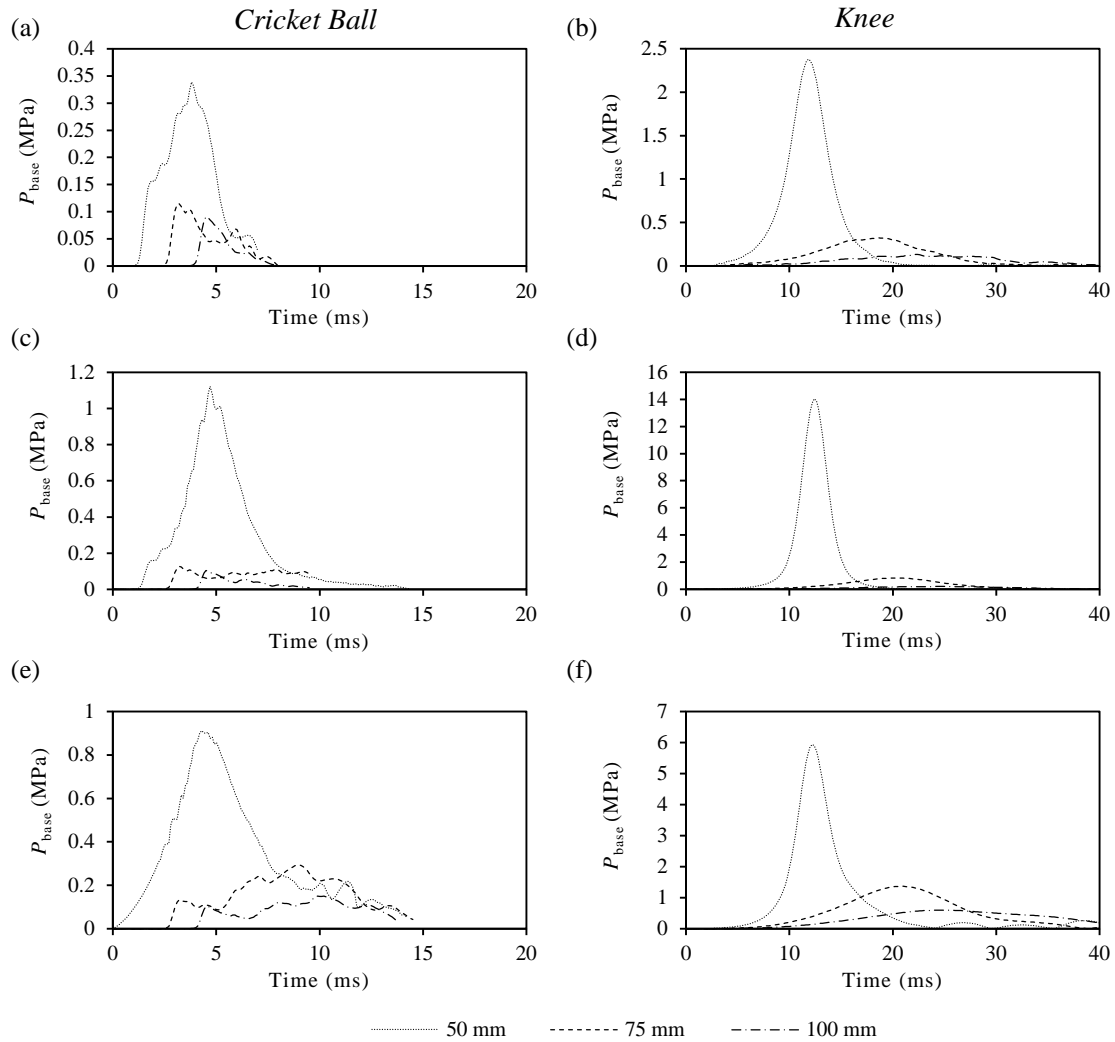


Figure 7.8 - P_{base} - time graphs for: (a) puck-cricket ball; (b) puck-knee; (c) shaped anvil-cricket ball; (d) shaped anvil-knee; (e) cylinder-cricket ball; (f) cylinder-knee.

In all shapes and impact conditions the 50 mm surrogate exhibited the highest P_{base} responses (mean +648% difference from 75 mm surrogates across all shapes and loading conditions) with decreasing magnitudes of pressure at greater radii of curvature.

The P_{base} and t_p on the bone surface for each surrogate impact simulation have been presented in Table 7.3.

Table 7.3 – $P_{\text{base,max}}$ (MPa) and t_p (ms) for surrogates in cricket ball and knee impacts.

	Cricket Ball						Knee					
	Puck		Shaped Anvil		Cylinder		Puck		Shaped Anvil		Cylinder	
	P_{base}	t_p	P_{base}	t_p	P_{base}	t_p	P_{base}	t_p	P_{base}	t_p	P_{base}	t_p
50 mm	0.338	3.80	1.12	4.70	0.911	0.20	2.38	11.8	14.0	12.4	5.94	12.2
75 mm	0.115	3.20	0.127	3.40	0.294	9.00	0.322	18.6	0.830	20.4	1.36	20.4
100 mm	0.0910	4.50	0.104	4.50	0.149	10.2	0.132	22.4	0.200	24.8	0.600	25.0

d) Layer Effects

(i) Skin Outer Surface Stress

The $\sigma_{v,max}$ and t_σ on the skin outer surface have been shown in Table 7.4

Table 7.4 – $\sigma_{v,max}$ (MPa) and t_σ (ms) for surrogates in cricket ball and knee impacts.

	Cricket Ball						Knee					
	Puck		Shaped Anvil		Cylinder		Puck		Shaped Anvil		Cylinder	
	$\sigma_{v,max}$	t_σ	$\sigma_{v,max}$	t_σ	$\sigma_{v,max}$	t_σ	$\sigma_{v,max}$	t_σ	$\sigma_{v,max}$	t_σ	$\sigma_{v,max}$	t_σ
50 mm	1.24	1.00	1.17	0.80	1.48	4.40	1.55	11.6	2.80	12.4	2.61	12.2
75 mm	1.24	0.90	1.22	1.00	1.29	0.30	1.60	22.2	1.07	20.8	1.72	19.2
100 mm	1.17	0.90	1.25	0.90	1.18	1.30	1.77	27.2	1.21	23.8	1.67	23.8

$\sigma_{v,skin}$ - time for the skin outer surface are shown in Figure 7.9 for different surrogate shapes. The magnitudes of differences in $\sigma_{v,max}$ between impacts were typically small, though differences in $\sigma_{v,max}$ and t_σ are most pronounced in the 50 mm surrogate knee impact simulations (min. 3.13% reduction).

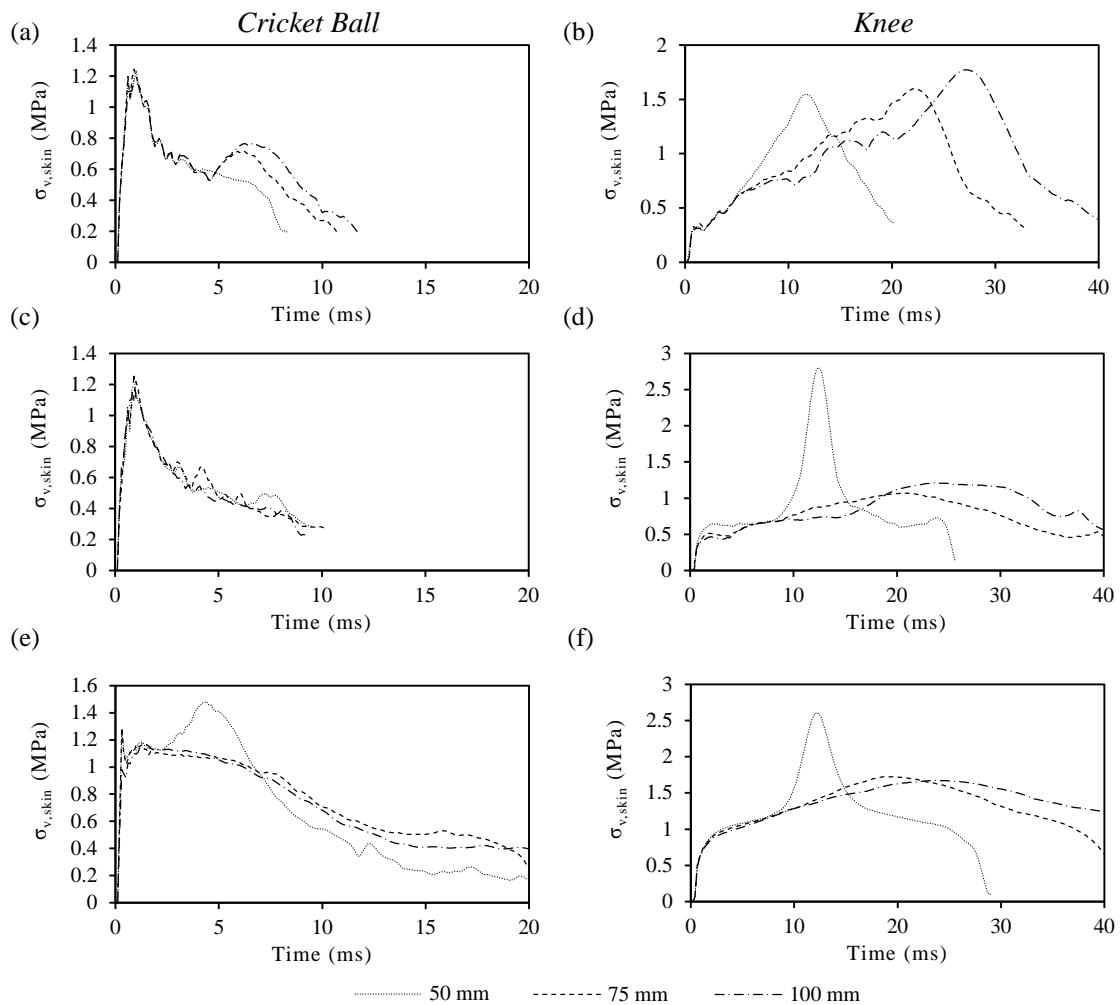


Figure 7.9 - $\sigma_{v,skin}$ - time plots in the following impacts: (a) puck-cricket ball; (b) puck-knee; (c) shaped anvil-cricket ball; (d) shaped anvil-knee; (e) cylinder-cricket ball; (f) cylinder-knee.

(ii) Muscle Outer Surface Stress

The $\sigma_{v,max}$ and t_σ on the muscle surface have been presented in Table 7.5.

Table 7.5 – $\sigma_{v,max}$ (MPa) and t_σ (ms) for surrogates in cricket ball and knee impacts

	Cricket Ball						Knee					
	Puck		Shaped Anvil		Cylinder		Puck		Shaped Anvil		Cylinder	
	$\sigma_{v,max}$	t_σ	$\sigma_{v,max}$	t_σ	$\sigma_{v,max}$	t_σ	$\sigma_{v,max}$	t_σ	$\sigma_{v,max}$	t_σ	$\sigma_{v,max}$	t_σ
50 mm	0.288	4.20	0.630	4.60	1.10	4.20	3.06	11.8	15.7	12.4	10.5	12.2
75 mm	0.0777	4.60	0.0827	1.90	0.0969	4.40	0.306	18.4	0.642	20.4	0.593	20.0
100mm	0.0719	2.20	0.0797	2.00	0.0807	3.30	0.167	25.2	0.169	23.2	0.178	23.6

$\sigma_{v,muscle}$ - time graphs for the muscle outer surface are shown in Figure 7.10 for different shapes. The $\sigma_{v,max}$ was greatest in the 50 mm surrogates across all shapes and loading condition with a typically decreasing magnitude of stresses at increasing radii of curvature. This is most pronounced in the knee impact simulations (min. 900% increase).

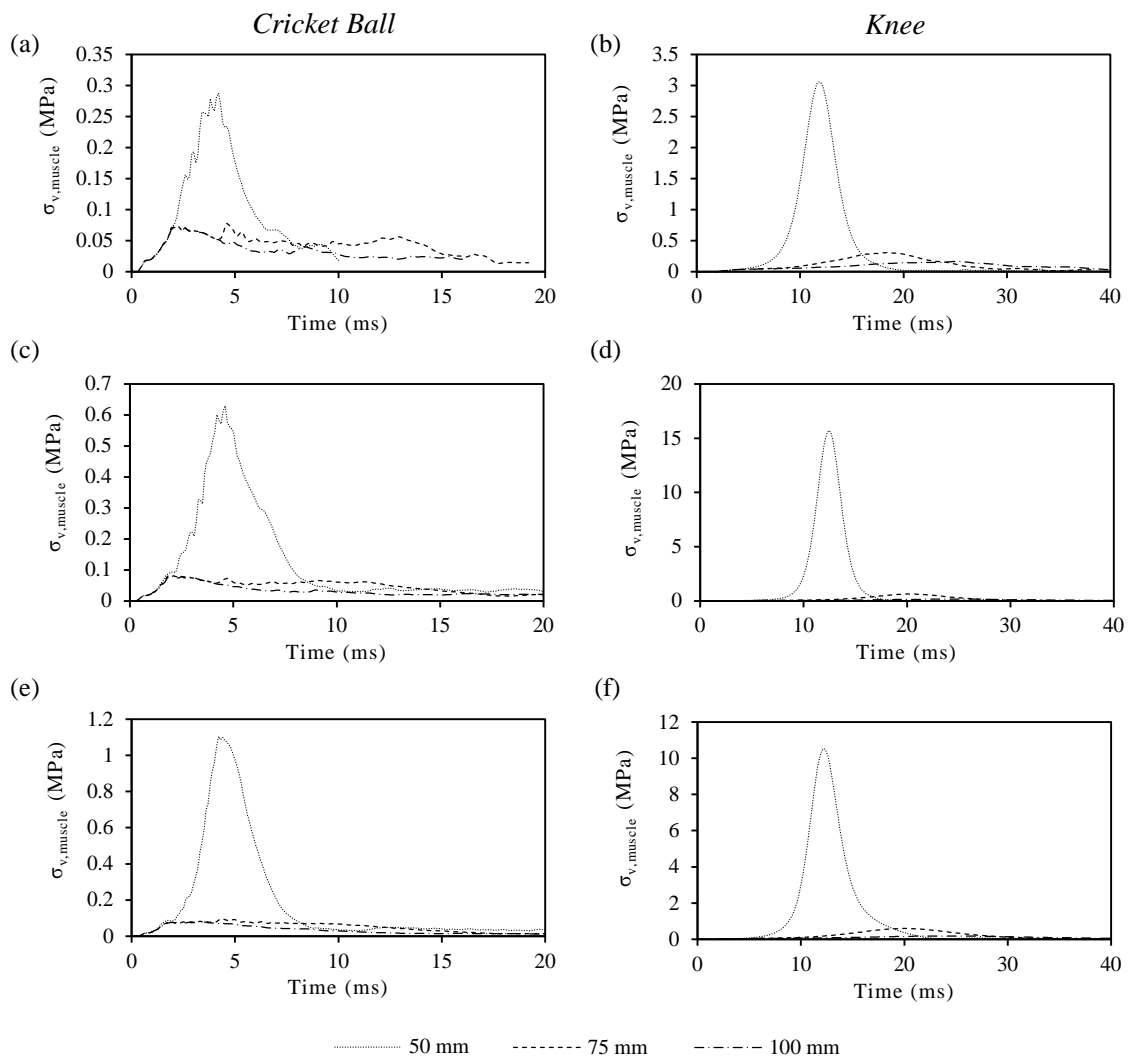


Figure 7.10 - $\sigma_{v,muscle}$ - time plots in the following impacts: (a) puck-cricket ball; (b) puck-knee; (c) shaped anvil-cricket ball; (d) shaped anvil-knee; (e) cylinder-cricket ball; (f) cylinder-knee.

e) Computational Expenditure

The computational expenditure has been compared for a knee impact simulation ($t = 40$ ms) between each surrogate type in Table 7.6. The computational time is classified as the time for a single CPU to complete the simulation.

Table 7.6 - Computational expenditure for each surrogate type.

Shape	Size	No. of Elements				Computational Time (hours)
		<i>Skin</i>	<i>Adipose</i>	<i>Muscle</i>	<i>Bone</i>	
Puck	50 mm	7,344	23,796	5,385	12,465	03:41
	75 mm	7,344	23,796	12,564	12,465	04:11
	100 mm	7,344	23,796	19,908	12,465	01:51
Shaped Anvil	50 mm	14,276	46,475	7,986	14,508	06:37
	75 mm	12,564	23,322	15,972	8,580	07:22
	100 mm	16,340	50,180	17,358	2,964	06:54
Cylinder	50 mm	38,640	110,814	41,676	20,536	14:50
	75 mm	57,776	169,740	61,065	20,536	16:40
	100 mm	76,912	231,840	112,608	20,536	18:12

7.3.5. Discussion

a) Surrogate Shape

Surrogate responses were first assessed based on the differences in surrogate shape. Considering the top surface displacements, the puck represented the most conservative geometry with lowest x_{\max} and t_x values in all simulations through both loading conditions with minimum differences in x_{\max} and t_x of -8.75% and -2.5% respectively from other shapes.

The deep tissue pressures on each of the surrogates show that the puck again represents the most conservative geometry with significantly lower $P_{\text{base,max}}$ in both loading conditions than other surrogates; this was particularly noticeable in knee impacts (min. -9.45% difference). This means that puck surrogate is likely to underestimate deep tissue stresses and potential related injury phenomena. This could potentially be due to the flat bone surface more capable of distributing stresses. The $P_{\text{base,max}}$ was greatest in the cylinder surrogate under both loading conditions in the mid-thigh 75 mm surrogates indicating that it is the least conservative surrogate geometry for assessing deep tissue injuries. However, in the 50 mm surrogate geometry, the shaped anvil surrogate had a significantly greater $P_{\text{base,max}}$ in the knee impact (136% greater than the cylinder $P_{\text{base,max}}$). This could be caused by a combination of the proximity of the bone to the surface and a narrow bone layer causing a local pinching effect (Table 7.1); this is also evident on the skin layer stresses (Fig. 7.9.d).

The $\sigma_{v,\max}$ on the skin outer layer surface generally shows less significant differences between surrogate shapes. The most notable differences were recorded on the 50 mm knee impact with the puck surrogate exhibiting the lowest $\sigma_{v,\max}$ (min. -40.6% difference). When considering the muscle layer stresses, in all radii of curvature and loading conditions the $\sigma_{v,\max}$ were lowest in the puck geometry (min. -6.05% difference in 75 mm surrogates) further indicating that it is the most conservative surrogate shape.

The 130 mm length of the puck and shaped anvil surrogates both clearly introduce edge effects, which have been illustrated in the sagittal plane sections in Table 7.1. This potentially influences the impact response in these surrogates and could introduce artificial deformation mechanisms unrepresentative of human impacts.

b) Radii of Curvature

In each of the surrogate shapes, the 50 mm surrogate exhibited significantly lower x_{\max} and t_x values than the 75 mm and 100 mm surrogates. This can be attributed to the smaller proportion of soft tissue in these surrogates. Smaller differences have been shown in x_{\max} between 75 mm and 100 mm surrogates and are most evident in the knee impact simulations with a mean difference of +17.7% between 75 mm and 100 mm surrogates. Through all shapes and impact conditions the models exhibited progressively greater t_x at increasing radii of curvature. This potentially indicates a bulk damping effect and a slowing of the impactor a greater proportion of soft tissue is present.

A clear trend is also present in increasing $P_{\text{base,max}}$ at smaller radii of curvature. This was most evident in the 50 mm surrogate where there were significantly increased pressures across all loading conditions with a mean +648% difference from 75 mm surrogate across all shapes and loading conditions. Differences in t_p were varied and not significant in the cricket ball impact condition but were evident in the knee impacts where t_p , similar to t_x , increased with radii of curvature.

There were no significant differences in $\sigma_{v,\max}$ on the skin outer layer surface, though differences in t_σ were present in the knee impact with increasing times associated with greater radii of curvature. More significant differences in $\sigma_{v,\max}$ were recorded on the muscle outer surface. Through all shapes and loading conditions, the 50 mm surrogates experienced the highest stresses. Similar to the $P_{\text{base,max}}$, less significant differences were observed between 75 mm and 100 mm surrogates and were most notable in knee impact conditions. There was also a trend to increasing t_σ at greater radii of curvature.

These results suggest the proximity of bone and thickness of soft tissues is significant to overall surrogate displacements, deep tissue pressures and layer stresses. This means that impacts to different regions of the thigh are likely to elicit different responses and models should be appropriately sized for their specific purpose. Surrogates with greater radii of soft tissue curvature are likely to represent conservative impact surrogate solutions.

c) Summary

There are significant difference in surrogate impact response exhibited based on both the shape and soft tissue curvature. The puck surrogate represents an inadequate solution with significant differences in response from the cylinder surrogate across both loading conditions. The shaped anvil provided a closer match to the cylinder surrogate responses but still showed large divergences in deep tissue pressures, particularly in the 50 mm surrogate. These factors indicate the merit of the cylinder geometry over these simpler surrogates that cannot accurately, in all impact conditions, predict the response of the most biofidelic geometry considered. This increased biofidelity is adopted with a penalty of a greater computational solution time (approximately 200% greater). However, given the processing capabilities of modern computers, this still represents a reasonably insignificant cost.

There were also large differences between the surrogates based on their outer tissue curvature, which was particularly apparent in the displacements exhibited between the 50 mm and 75 mm surrogates. In the human thigh, these tissue thicknesses vary greatly dependent on location. Therefore, it is important to examine a further level of surrogate complexity (i.e. non-uniform cross section) to determine whether these differences in tissue thickness elicit a significant difference in impact response.

7.4. Study 2 – Evaluation of Surrogate Response in an Anatomically More Representative Surrogate

7.4.1. Introduction

Given the established benefit of a remotely constrained cylindrical surrogate in §7.3 and the significant differences reported at different outer tissue curvature, a further level of anatomical complexity has been examined. A surrogate with anatomically derived features and representative local differences in tissue thickness has been considered.

This study again represents an open loop predictive simulation in which the FE formulations previously validated (§6.6) have been adopted to predict the relative behaviour of a series of surrogates. Although there is clearly a significant increase in complexity introduced in this anatomical model, it is contended that these FE simulations are necessary to discover the increase in biofidelity and how subsequently worthwhile the geometries are. The FE simulations have been conducted to identify the cost vs. benefit of this surrogate compared to those previously discussed. The varied cross-section introduced is inherently more biofidelic than simpler surrogate shapes, but, if similar phenomena are exhibited by the cylindrical surrogates, this is more cost-effective to achieve both experimentally and computationally making the additional complexity unnecessary.

7.4.2. Methodology

a) Geometries

The anatomically contoured surrogate used the point data extrapolated from the VHP images to provide a less simplified representation of both external and internal human tissue geometries. The data points were then converted into a series of splines at each cross-section and reconstructed in computer-aided design (CAD) software to provide a three-dimensional (3D) representation of the soft tissue structure relative to the femur. The surrogate contains detailed femur component and more biofidelic outer and internal surface geometries and hence inertial properties than the other surrogates. The surrogate is rigidly constrained at two positions: distally on the epicondyles of the femur and superiorly at the femoral head. The contoured cylinder surrogate configuration and constituent layers are shown in Figure 7.11.

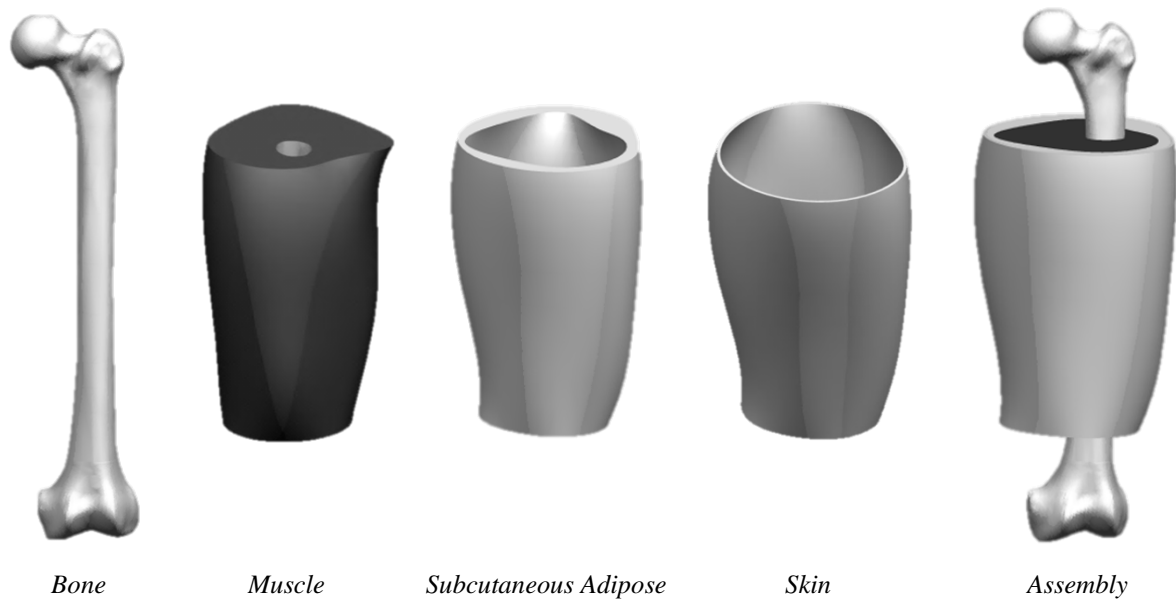


Figure 7.11 – Anatomically contoured cylinder surrogate and constituent tissue components.

The anatomically contoured cylinder surrogate was the most biofidelic level of geometric complexity addressed with this investigation and is more detailed than anything that has previously been researched in sports impact surrogates. Practical restrictions in both cost and time prevent further geometric complexity from being addressed but, even if this was possible, it is necessary to establish the worth of these geometries before attempting anything more complex.

b) FE Modelling

(i) Element Selection

Due to the increased geometric complexity of the anatomically contoured geometry, hexahedral elements were no longer a viable or computationally cost effective solution; tetrahedral elements were required. A 2nd order modified tetrahedral element C3D10M was selected due to its good convergence, minimal shear or volumetric locking and ability to model incompressible or near incompressible materials. Regular 2nd order tetrahedral elements (C3D10) have been reported to be poor in contact conditions and experience differences in stress under constant pressure between the corner and central nodes. The modified (C3D10M) formulation provides a robust element through finite deformation with accurate contact pressures (ABAQUS, 2014).

C3D10M elements are capable of providing accurate results with only a single element through the thickness, modelling bending accurately which cannot be accurately achieved using the C3D8R elements (Diehl & Carroll, 2000). Second order elements are also able to capture geometric features such as curved edges with fewer elements than first order elements and have been shown to outperform first order elements in problems where there are areas of significantly high stress concentrations, which are apparent in the more complex geometries (e.g. bony protrusions of the femur) (ABAQUS, 2014).

(ii) Mesh Refinement

A mesh refinement study was conducted for the new tetrahedral elements to determine the element density at which key evaluation metrics converge. Given the volume of the thigh segment a mesh biasing factor was introduced with elements concentrated towards the central impact regions. The convergence study showed that nominal element sizes of 4 mm, 3 mm, 5 mm and 4 mm exhibited the most accurate response relative to computational costs for skin, adipose, muscle and bone tissues respectively. Mesh descriptions for each tissue layer are shown in Table 7.7. An average computational time for an anatomically contoured surrogate knee impact simulation ($t = 40$ ms) is 70 hours on a single CPU.

Table 7.7 – Mesh descriptions for anatomically contoured surrogate.

	Nominal Element Size	No. of Elements
<i>Skin</i>	4 mm	56,406
<i>Adipose</i>	3 mm	240,744
<i>Muscle</i>	5 mm	90,149
<i>Bone</i>	4 mm	50,414

Images of the refined contoured VHP mesh are shown in Figure 7.12.

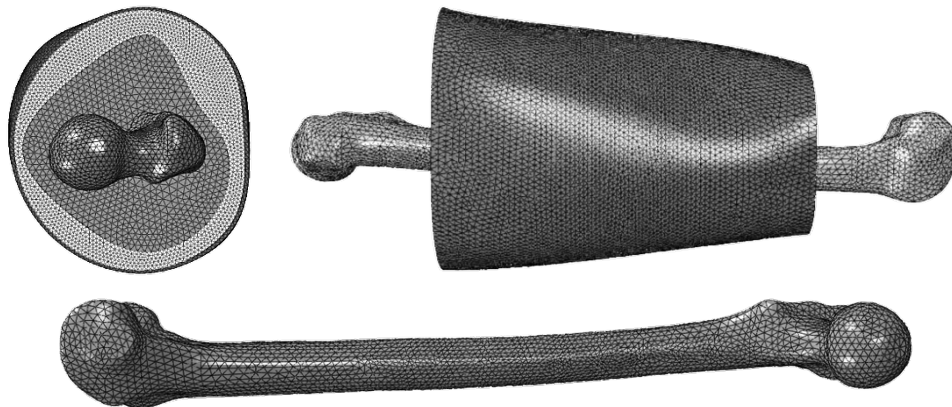


Figure 7.12 - Anatomical contoured cylinder mesh images showing density of tissue layers and mesh biasing.

c) Impact Simulations

Due to the non-symmetrical shape of the anatomically contoured surrogate, its responses will change dependant on the impact location. Three different impact types have been evaluated under both cricket ball and knee impact conditions: anterior, lateral and posterior. The impacts were all conducted in a central location on the surrogate and normal to the surface with the femur constrained rigidly distally on the epicondyles and superiorly on the greater trochanter and femoral head (Fig 7.13). The von Mises stress on the bone surface was used as the criterion for assessing stresses as opposed to the Cauchy stress tensor normal to the direction of impact due to the omnidirectional impacts simulated.

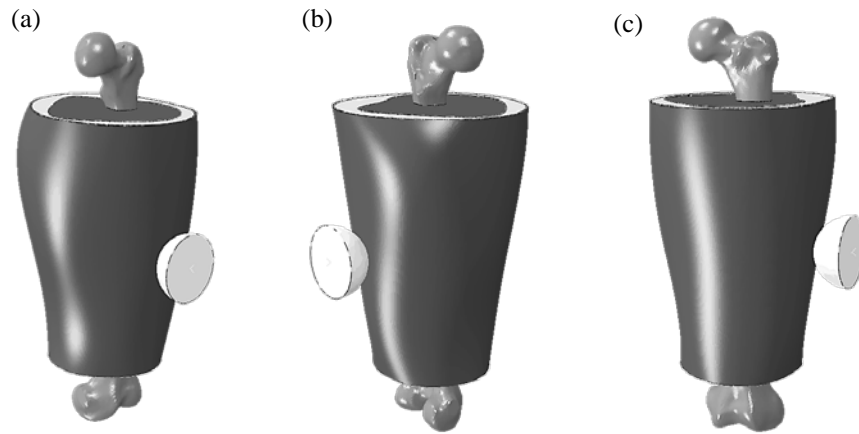


Figure 7.13 - Impact types to the anatomical contoured surrogate in: (a) anterior; (b) posterior and (c) lateral directions.

7.4.3. Results

a) Surrogate Sections at Maximum Displacement

Sagittal plane sections of the anatomical contoured cylinder surrogate at maximum displacement have been shown in Figure 7.14. Cricket ball and knee impacts in anterior, posterior and lateral directions have been presented. The simulations show significant differences in internal tissue composition dependent on the impact location with lower proportions of adipose tissue in the lateral impacts, particularly when compared to the posterior sections.

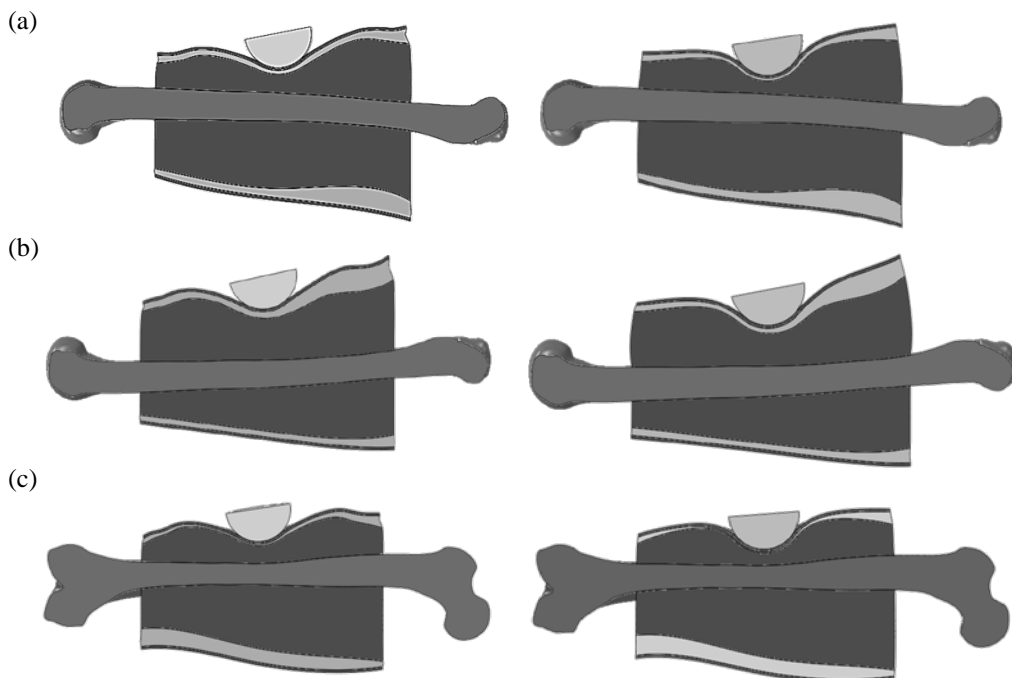


Figure 7.14 - Images of anatomical contoured cylinder at maximum displacement for: (a) anterior; (b) posterior; (c) lateral impacts (left: cricket ball; right: knee).

b) Top Surface Displacement

x_{skin} - time graphs of cricket ball and knee impacts in the anatomically contoured surrogate have been shown in Figure 7.15 for each impact direction.

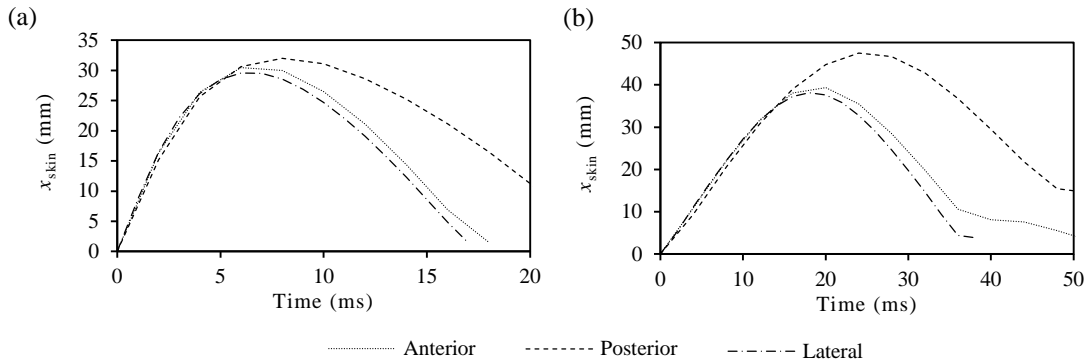


Figure 7.15 – x_{skin} - time graphs for the anatomically contoured surrogate in (a) cricket ball and (b) knee impact simulations.

The x_{max} and t_x values for each anatomically contoured surrogate impact are shown in Table 7.8.

Table 7.8 - x_{max} (mm) and t_x (ms) for the anatomical contoured surrogate in cricket ball and knee impact simulations.

	Cricket Ball		Knee	
	x_{max} (mm)	t_x (ms)	x_{max} (mm)	t_x (ms)
Anterior	30.5	6.90	39.4	19.1
Posterior	32.0	8.50	48.5	25.2
Lateral	29.5	6.70	38.1	18.3

Under both impact conditions, the posterior impact elicited the greatest x_{max} and t_x (minimum +4.91% and +25.2% difference respectively) whilst the lateral impact exhibited the lowest magnitudes.

c) Bone Stress

$\sigma_{v,bone}$ - time histories of each surrogate impact type have been presented in Figure 7.16.

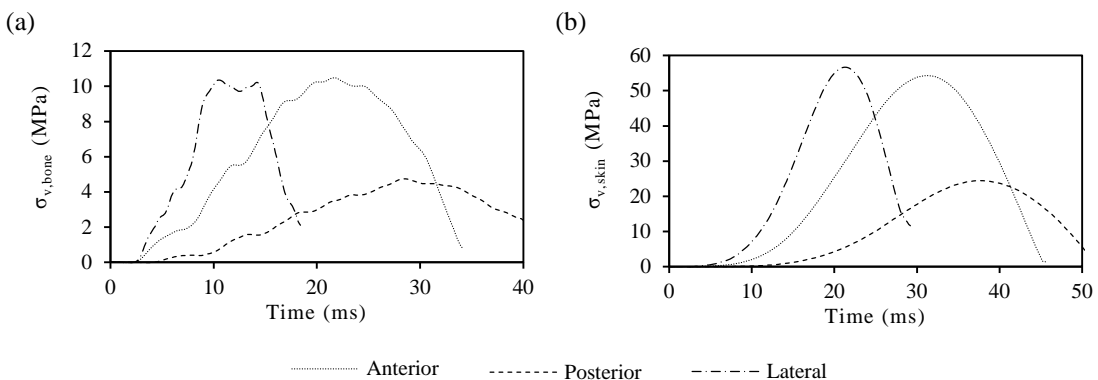


Figure 7.16 – $\sigma_{v,bone}$ - time graphs on the bone surface of the anatomical contoured surrogates in (a) cricket ball and (b) knee impact simulations.

The $\sigma_{v,max}$ and t_σ values for each anatomically contoured surrogate impact are shown in Table 7.9.

Table 7.9 – $\sigma_{v,max}$ and t_σ on bone surface of the anatomical contoured surrogate in cricket ball and knee impacts.

	Cricket Ball		Knee	
	$\sigma_{v,max}$ (MPa)	t_σ (ms)	$\sigma_{v,max}$ (MPa)	t_σ (ms)
<i>Anterior</i>	10.5	21.4	54.3	31.2
<i>Posterior</i>	4.75	28.4	26.3	37.6
<i>Lateral</i>	10.36	10.4	56.7	21.2

The anterior and lateral impacts, under both conditions, elicited similar magnitudes of $\sigma_{v,max}$ on the bone surface, significantly greater than those experienced in the posterior impacts (min. +106% difference). The lateral impacts, however experienced shorter t_σ (min. -47.4% difference) which is expected due to the lower proportions of soft tissue in the region and consistent with the surrogate curvature findings in the simple surrogates (§7.3.5.b).

d) Layer Stresses

$\sigma_{v,max}$ and t_σ values recorded on the skin, adipose and muscle surfaces for each surrogate impact have shown in Table 7.10.

Table 7.10 – $\sigma_{v,max}$ (MPa) and t_σ (ms) on skin, adipose and muscle surfaces of the anatomical contoured surrogate in cricket ball and knee impact simulations.

	Cricket Ball						Knee					
	Skin		Adipose		Muscle		Skin		Adipose		Muscle	
	$\sigma_{v,max}$	t_σ	$\sigma_{v,max}$	t_σ	$\sigma_{v,max}$	t_σ	$\sigma_{v,max}$	t_σ	$\sigma_{v,max}$	t_σ	$\sigma_{v,max}$	t_σ
<i>Anterior</i>	1.49	0.80	0.983	2.20	0.118	1.80	2.10	20.4	1.34	19.2	0.657	19.2
<i>Posterior</i>	1.88	0.60	1.12	2.10	0.133	1.60	2.13	25.2	0.597	24.4	0.185	23.6
<i>Lateral</i>	1.22	0.50	0.482	0.60	0.130	2.00	2.21	20.0	1.34	18.0	0.661	18.2

In the cricket ball impact simulations, the posterior impact elicited significantly increased magnitudes of $\sigma_{v,max}$ at the skin and adipose layers compared to anterior and lateral impacts though exhibited similar magnitudes of stress at the muscle layer to other impact types. In the knee impact simulation, the biggest differences were again shown in the posterior surrogate with significantly decreased $\sigma_{v,max}$ at the adipose (-55.4% difference) and muscle layers (-71.8% difference).

7.4.4. Discussion

a) Surrogate Responses

The anatomical contoured surrogate was impacted centrally and perpendicularly in three loading directions. Figure 7.14 shows images of sagittal plane sections of the surrogates at maximum displacement, illustrating tissue compositions and proximities of skeletal structures in each loading direction.

The posterior impacts exhibited the greatest x_{\max} and t_x and the lowest magnitudes of $\sigma_{v,\max}$ on the bone surface in both loading conditions. This is likely to be attributed to the additional thicknesses of muscle and adipose tissues in this region and is consistent with the results attained in the simple geometry curvature analysis (§7.3.5.b). The increased x_{\max} is most pronounced in the knee impact with a minimum increased x_{\max} of +23.1% compared to just +4.92% under cricket ball impact conditions. This could be due to the strain rate dependent response of the organic adipose tissue material, exhibiting an increased stiffness at higher strains pertinent to those elicited in the cricket ball impact. This is consistent with findings from §4.5.4.

The lateral and anterior impacts exhibited similar x_{\max} and t_x values across both loading conditions (min. +3.41% difference), which can be attributed to the similar thicknesses of the soft tissue around the bone (62.6 mm and 68.7 mm at mid-thigh respectively). The surrogates also showed similar $\sigma_{v,\max}$ magnitudes in both impacts (max. 4.23 % difference). However, the anterior surrogate exhibited a significantly greater t_σ in both impact conditions, which could be due to a slight increase in soft tissue in the region and the greater proportion of soft adipose tissue delaying the stress response.

At the muscle layer, the $\sigma_{v,\max}$ values from the cricket ball impacts were all of a similar magnitude (max. 11.2% difference). However, the knee impacts exhibited significant differences, the $\sigma_{v,\max}$ for the posterior knee impact were far lower than lateral and posterior impacts (min. -71.8% difference). This could be due to the greater proportion of soft tissues in this region and an increased adipose layer thickness slowing the impactor before load was transferred to the muscle layer surface.

b) Comparison with Cylinder Surrogate

The x_{skin} - time graphs of the anatomically contoured surrogate impacts compared to the 75 mm cylinder surrogate responses have been shown in Figure 7.17. A single cylindrical surrogate has been used, representative of the mid-thigh region in which the impacts were performed, in this comparison.

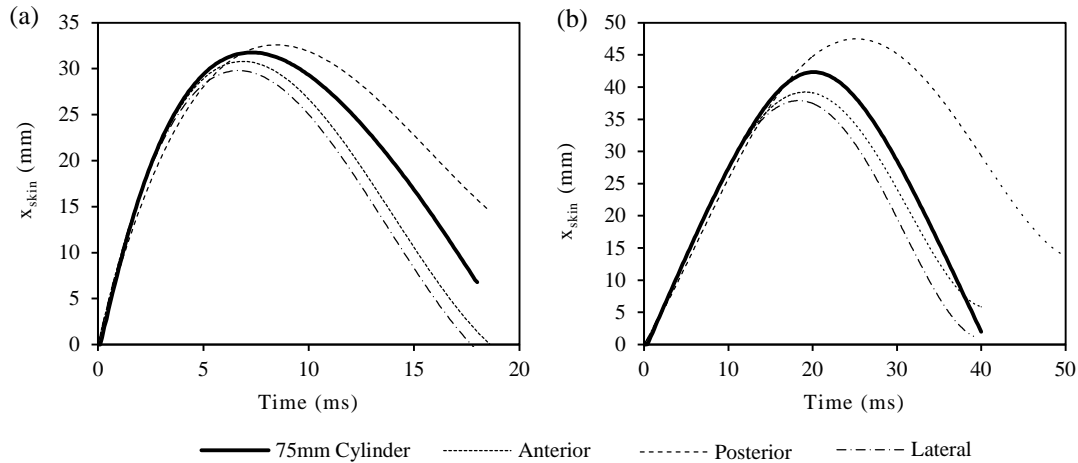


Figure 7.17 - x_{skin} - time graphs showing the differences in response between a 75 mm surrogate and the anatomically contoured surrogate in: (a) cricket ball and (b) knee impact simulations.

The graphs show that the 75 mm surrogate exhibited an x_{max} response between the ranges presented by different orientation anatomically contoured surrogate impacts. A closer response to the anatomically contoured surrogate was exhibited in the cricket ball impacts with a minimum difference of 3.14%, whilst a greater divergence was shown in the knee impact simulations with a minimum difference of -7.9% from anatomically contoured responses. This indicates that, whilst a single cylinder surrogate provides a reasonable approximation of all the anatomically contoured surrogate responses it does not accurately replicate any of them. Through manipulation of soft tissue curvatures and thicknesses, it could reasonably be anticipated that a cylindrical surrogate could be fabricated to match one of these responses, though would continue to show differences between others. Given that both surrogates have comparable volumes of tissues, it would not be cost-effective to approximate the more biofidelic surrogate response with a number of simplified alternatives.

Similarly, despite reduced computational costs in the cylinder model (approximately $4.5 \times$ lower than the anatomically contoured surrogate), it cannot replicate the local changes in tissue thickness. Therefore, a number of models would need to be formulated for different impact configurations, which would increase both the model set-up time and CPU running time to the point where there would be no benefit. The magnitudes of differences shown in Figure 7.17 could also be expected to be amplified when considering off-centre oblique impact type scenarios and scenarios in which the surrogate is free to recoil, as the tissue distributions differ significantly.

7.5. Study 3 - PDMS Divergence Study

7.5.1. Introduction

Having established that a more biofidelic anatomically contoured geometry is desirable, a further impact simulation study was conducted to investigate the differences in surrogate responses between PDMS and organic tissues across all impact types and loading conditions. The PDMS material models validated in §6.6 have been used to populate the anatomically contoured geometry. The degree of divergences in responses between the PDMS simulant models and the organic tissue model predictions has been reported.

7.5.2. Results

The differences in impact response of the PDMS simulant surrogate compared to organic tissue predictions have been shown in Table 7.11 and Table 7.12 with percentage differences in brackets.

Table 7.11 - x_{max} and t_x responses recorded for PDMS simulant surrogate impacts (percentage differences from organic tissue predictions in brackets).

	Cricket Ball		Knee	
	x_{max} (mm)	t_x (ms)	x_{max} (mm)	t_x (ms)
Anterior	30.0 (-1.51%)	6.70 (-2.90%)	40.4 (+1.00%)	19.7 (+3.14%)
Posterior	31.2 (-2.50%)	8.00 (-5.88%)	47.3 (-2.50%)	25.3 (+0.397%)
Lateral	29.4 (-0.03%)	6.50 (-2.99%)	39.2 (+2.88%)	19.5 (+6.56%)

Table 7.12 – $\sigma_{v,max}$ and t_σ responses on the bone surface recorded for PDMS simulant surrogate impacts (percentage differences from organic tissue predictions in brackets).

	Cricket Ball		Knee	
	$\sigma_{v,max}$ (MPa)	t_σ (ms)	$\sigma_{v,max}$ (MPa)	t_σ (ms)
Anterior	11.1 (+5.71%)	21.0 (+1.90%)	52.5 (-3.31%)	32.0 (+2.56%)
Posterior	5.47 (+15.1%)	25.4 (-10.6%)	29.3 (+11.5%)	38.4 (+2.13%)
Lateral	12.9 (+24.7%)	13.2 (+26.9%)	50.5 (-10.3%)	22.0 (+3.77%)

Table 7.11 shows the maximum divergences in x_{max} and t_x for each surrogate were +2.88% and +6.56% respectively across all loading conditions. Table 7.12 shows the most significant differences in $\sigma_{v,max}$ on the bone surface are shown in the cricket ball impact where a divergence of +24.7% was recorded in the lateral impact. In the knee impacts maximum divergences of +11.5% and +3.77% were shown in $\sigma_{v,max}$ and t_σ on the bone surface respectively.

The individual layer stresses recorded for each PDMS impact type have been presented in Table 7.13.

Table 7.13 – $\sigma_{v,max}$ (MPa) and t_σ (ms) layer stress responses recorded for PDMS simulant surrogate impacts.

	Cricket Ball						Knee					
	Skin		Adipose		Muscle		Skin		Adipose		Muscle	
	$\sigma_{v,max}$	t_σ	$\sigma_{v,max}$	t_σ	$\sigma_{v,max}$	t_σ	$\sigma_{v,max}$	t_σ	$\sigma_{v,max}$	t_σ	$\sigma_{v,max}$	t_σ
Anterior	0.742	2.00	0.164	1.80	0.150	6.00	0.734	18.0	0.326	18.8	0.502	18.8
Posterior	0.823	1.60	0.163	1.40	0.121	2.60	0.645	27.6	0.154	25.2	0.189	24.0
Lateral	0.853	1.40	0.164	1.80	0.160	5.80	0.771	20.0	0.276	19.2	0.567	19.2

7.5.3. Discussion

The PDMS simulant material models were employed with the anatomically contoured surrogate simulations to determine the differences in impact response in more biofidelic geometries. Initially considering the skin layer displacements, the PDMS simulations exhibited maximum divergence of 2.88% and -5.88% in x_{\max} and t_x respectively. This demonstrates that the developed simulant materials provide a close approximation of overall surrogate deformation.

Greater divergences were recorded in bone stresses. Under the cricket ball loading conditions, the PDMS simulants exhibited a maximum divergence of +24.7% and +26.9% in $\sigma_{v,\max}$ and t_σ respectively. Under the knee impact conditions, the PDMS simulants provided a better representation of organic tissue response with maximum differences of +11.5% and +3.70% in $\sigma_{v,\max}$ and t_σ respectively. The biggest differences in both impacts arose from lateral impacts. The greater divergence in the cricket ball impact conditions are consistent with results from §6.7.3 where the PDMS simulations again overestimated stresses under these conditions. The strain rate dependent response of organic tissues, in particular adipose, represent one of the key causal factors for these differences and should be addressed in future iterations of the silicones.

The $\sigma_{v,\max}$ recorded on the skin layer was lower than organic model predictions which is consistent with the results from §6.7.3 and can be attributed to the increased stiffness of the organic skin layer (§5.5.1). The PDMS muscle layer stresses exhibited more comparable responses. Maximum differences in $\sigma_{v,\max}$ at the muscle layer of +23.0% and -23.6% were recorded for cricket ball and knee impacts respectively.

7.6. Study 4 - Sensitivity Analysis: Tensile Soft Tissue Loads

7.6.1. Introduction

The anatomically contoured FE surrogate modelled only considers a discrete, non-continuous section of soft tissue. An impact study was conducted on the surrogate to investigate the differences in mechanical response when a continuous skin volume was approximated. This was simulated through application of a tensile load to the superior and inferior surfaces of the thigh (Fig. 7.18). Incrementally increasing loads were applied to the ends of the surrogate soft tissue components at the following magnitudes: 0 N, 10 N, 50 N and 100 N.

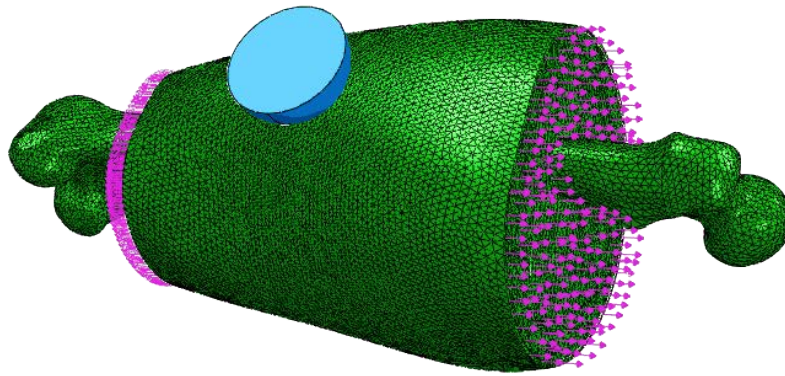


Figure 7.18 - Tensile soft tissue loads applied to ends of surrogate.

7.6.2. Results

The effects of tensile loads on the soft tissue ends of the surrogates have been shown in x_{skin} -time and $\sigma_{v,bone}$ -time plots (Fig. 7.19). The simulations show no significant changes in response when tensile loads were applied with maximal differences of +1.07% and -0.15% in $\sigma_{v,max}$ and x_{max} respectively.

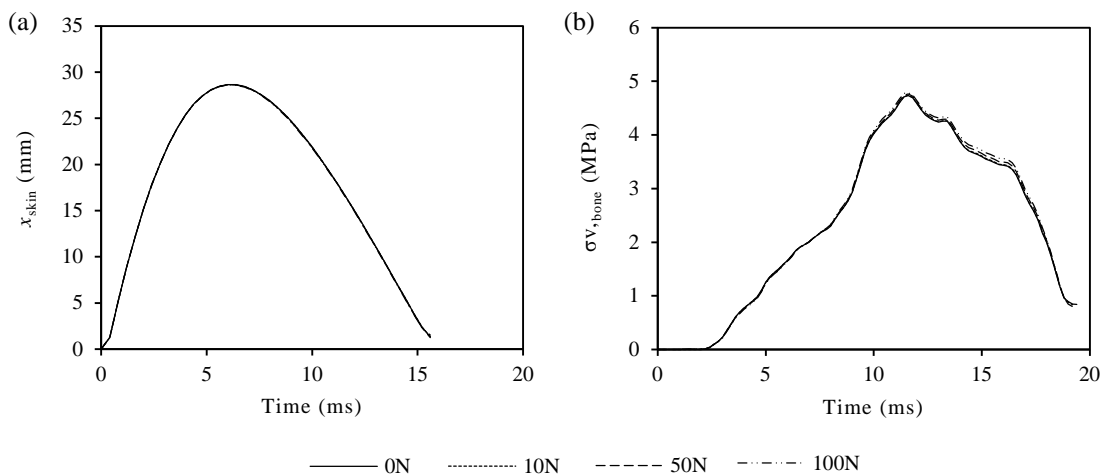


Figure 7.19 – x_{skin} - time and $\sigma_{v,bone}$ - time plots showing differences in response when different tensile loads were applied.

7.7. Study 5 - PPE Interactions

7.7.1. Introduction

Two different garments of sports PPE were used to assess PPE-surrogate interactions across surrogate designs: hard plate and soft foam protection (Fig. 7.20). Using FEA, PPE was modelled on the surrogates and impacted to examine its protective capabilities in each design type. Puck, cylinder, shaped anvil and anatomically contoured surrogates were all assessed. The PPE designs were kept intentionally simple and contrasting to show the relative differences introduced through each PPE type.

Exploratory open loop FEA simulations were conducted in this investigation using the model formulations validated in §6.6. Given the simplicity of the PPE modelled it is believed that substantial worth can be extracted from this study without warranting further validation at this stage.



Figure 7.20 - Commercial thigh PPE: (a) Nike Pro Combat Hyperstrong American Football Compression Hard Plate; (b) Kookaburra Blade Cricket Thigh Guard.

7.7.2. Methodology

a) Geometries

The geometry for the cricket thigh guard was predefined within BS 6183-3:2000 (2000) safety standard for cricket leg protectors. The shell hard plate PPE was modelled to match human geometries and used a 3 mm extrusion of the lateral region of the anatomical contoured cylinder surrogate (Fig.7.21).

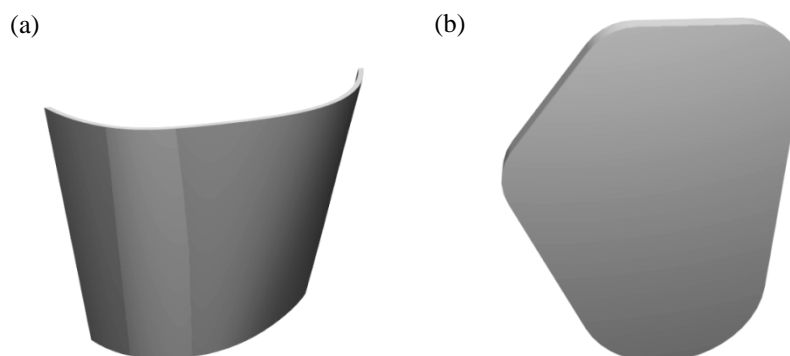


Figure 7.21 - CAD images of: (a) hard shell and (b) foam leg guard geometries.

b) FE Modelling

The material properties for the hard shell and foam leg guards have been approximated using a carbon-fibre-reinforced polymer (CFRP) and EVA foam materials respectively. The EVA foam material (Table 3.2; Table 3.3) was modelled using a single-term Ogden model proposed by Mills *et al.* (2003) (Table 7.14). The CFRP was approximated, for simplicity, using a simple linearly elastic material model with a derived representative stiffness (Table 7.14). It is believed that this is an appropriate approximation as the material is significantly stiffer than both the EVA foam and organic soft tissues and therefore significant differences should be elicited without having to model its known anisotropic material properties.

Table 7.14 – Single-term Ogden model coefficients for EVA foam (adapted from (Mills *et al.*, 2003)) and elastic material properties for CFRP (adapted from Davies *et al.* (2008)).

EVA Foam		CFRP	
ρ ($kg.m^{-3}$)	175	ρ ($kg.m^{-3}$)	1600
ν	0	ν	0
μ (kPa)	100	E (GPa)	70
α	0.5		

6,068 and 13,184 node C3D10M tetrahedral element meshes were used to discretise the hard shell and foam geometries respectively. To fit the PPE to the surrogates in the same manner as strapping, a pre-form was applied. The PPE was aligned to the top surfaces of the surrogates using manual translational and rotational commands within Abaqus. Once aligned, the surrogate surface was constrained as a rigid body and the PPE was fit to the surrogate surface with a uniform pressure of 1×10^6 Pa applied on the bottom surface of the PPE. This pressure was found to be the threshold to fit the PPE to the surrogate without inducing excessive deformation or instabilities in the contact. The fitted PPE was then exported from the model output database at the appropriate time point and imported to the impact assemblies (Fig. 7.22).

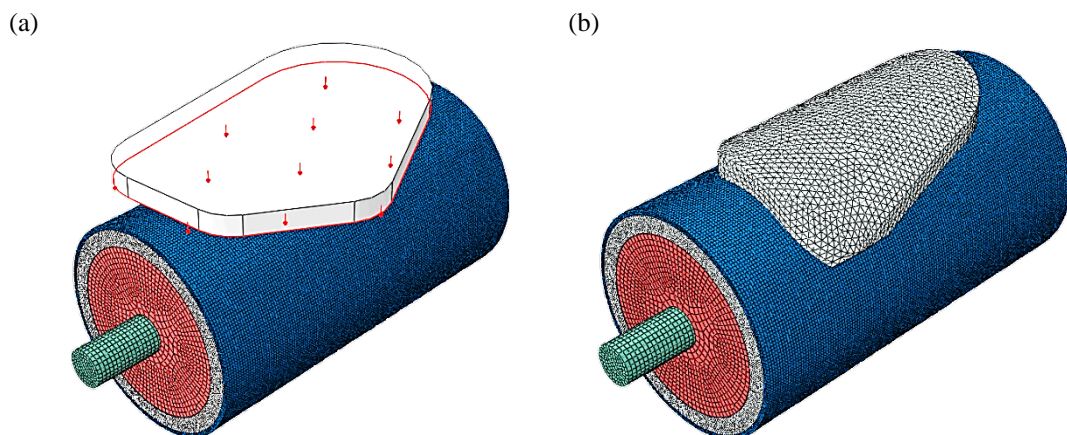


Figure 7.22 – (a) Undeformed PPE with pressure on underside; (b) deformed PPE configuration.

A hard normal contact has been applied between the PPE and skin with a tangential frictional coefficient of 0.5. This is within the range used for skin-to-textile frictional coefficients which have varied greatly in literature from 0.3 - 0.86 (Gerhardt *et al.*, 2009; Ankrah & Mills, 2003; Cottenden & Cottenden, 2012).

c) Impact Simulations

Given the established worth of the anatomically contoured surrogate (§7.4), an investigation into the effectiveness of each type of PPE has been conducted on the simple surrogates when compared with anatomically contoured surrogate. Mid-thigh 75 mm simple surrogates were selected in this evaluation as there is a requirement in PPE comparison studies for a single surrogate and this size was representative of the region from which the PPE was modelled.

An initial comparison of the PPE-surrogate interaction was performed through a visual assessment of the PPE fitted to each surrogate type. Following this, an impact study was conducted to show the effectiveness of both types of PPE when fitted to each of the surrogates considering the top surface displacements for each surrogate when subject to cricket ball and knee impacts. The pressure distributions elicited from each of these impacts has also been presented.

Finally, the load transfer has been evaluated between PPE types through consideration of the bone stresses experienced in the anatomically contoured surrogate in cricket ball and knee impact simulations. The load transfer has also been compared between the anatomically contoured surrogate and a rigid shaped anvil surrogate representative of those used in safety standards to indicate the potential degree of inaccuracy introduced.

7.7.3. Results

a) Surrogate-PPE Interactions

Figure 7.23 shows the interactions of each of the surrogates with foam and shell PPE types in both cricket ball and knee impact conditions. The images show the foam PPE conforms with each of the surrogate types, whilst the shell PPE shows a decreasingly poor fit from the anatomically contoured surrogate to the puck.

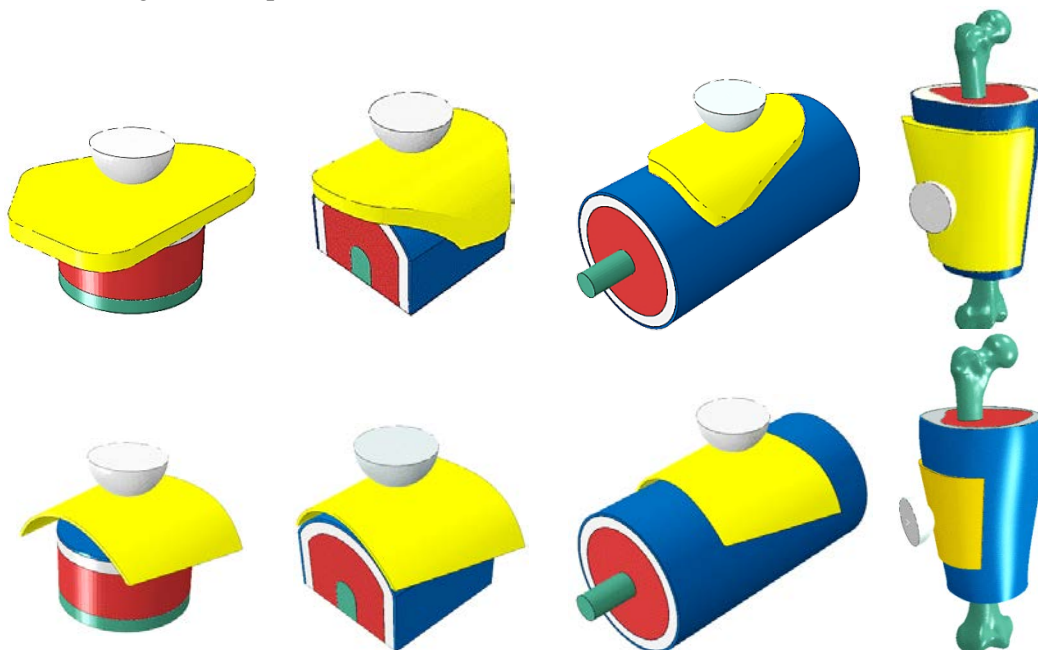


Figure 7.23 – PPE-surrogate configurations for foam and shell PPE across each surrogate.

b) Effectiveness of PPE Types

The x_{skin} exhibited by the surrogates when accompanied with each piece of PPE has been shown in Figure 7.24. This provides an indication of the capabilities of each surrogate type to assess both PPE types when compared to a representative anatomically contoured surrogate.

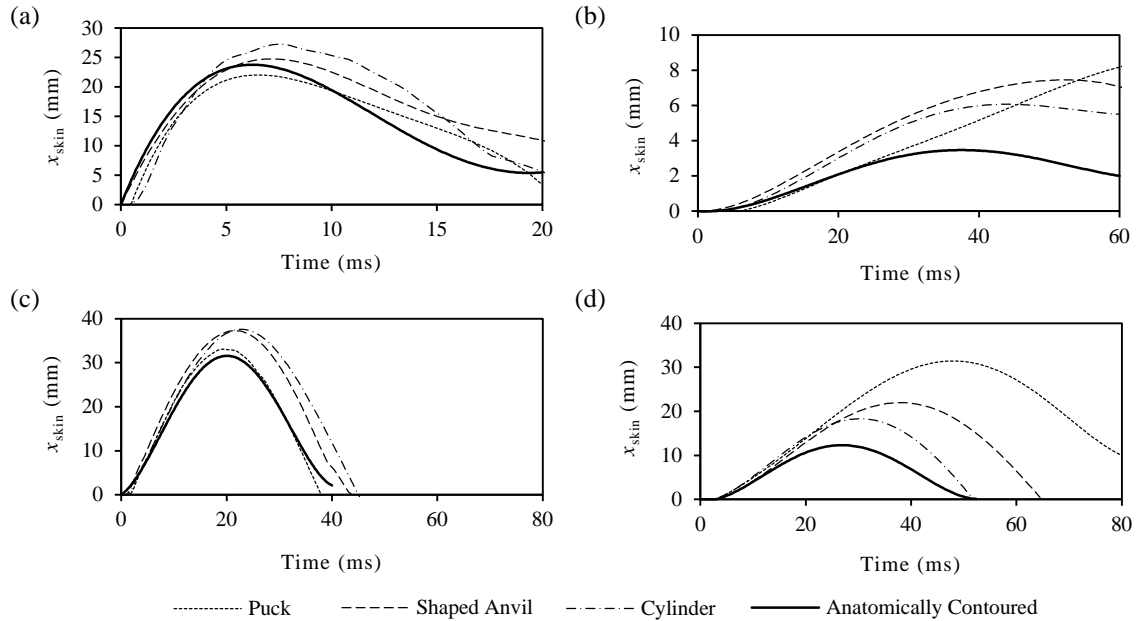


Figure 7.24 – x_{skin} - time plots for each surrogate geometry with PPE affixed: (a) cricket ball-foam; (b) cricket ball-shell; (c) knee-foam; (d) knee-shell.

The x_{max} and t_x values for each impact are shown in Table 7.15 with percentage differences from the anatomically contoured surrogate predictions in brackets.

Table 7.15 - x_{max} (mm) and t_x (ms) values for PPE impact simulations (percentage differences from anatomically contoured surrogate predictions in brackets).

	Foam				Shell			
	Cricket Ball		Knee		Cricket Ball		Knee	
	x_{max}	t_x	x_{max}	t_x	x_{max}	t_x	x_{max}	t_x
Anatomically Contoured	23.7	6.20	31.6	20.0	3.46	36.8	12.3	26.8
Puck	22.0 (-7.17%)	6.50	33.0 (+4.43%)	19.2	8.76 (+153%)	71.5	31.4 (+155%)	48.4
Shaped Anvil	24.7 (+4.22%)	7.40	37.3 (+18.0%)	21.6	7.45 (+115%)	52.4	22.0 (+78.9%)	38.0
Cylinder	27.2 (+14.8%)	7.60	37.6 (+19.0%)	22.8	6.07 (+75.4%)	44.0	18.3 (+48.7%)	30.4

Table 7.15 shows that simple surrogates typically provide a better representation of the anatomically contoured surrogate responses when modelled with the foam PPE with a maximum difference in x_{max} of +19.0%. In the foam PPE simulations the puck surrogate provides the best representation of the anatomically contoured surrogate with just -7.17% and +4.43% differences in cricket ball and knee impacts respectively. In the shell PPE simulations, all surrogates exhibited a significant difference in x_{max} from the anatomically contoured surrogate (minimum

+48.7% difference). This indicates that the simple surrogates would not be appropriate for assessing the effectiveness of this type of PPE.

c) Pressure Distribution

The stress distributions exhibited on the surrogate skin surfaces with the shell PPE modelled have been shown in Figure 7.25. The images were taken at the point of maximum displacement.

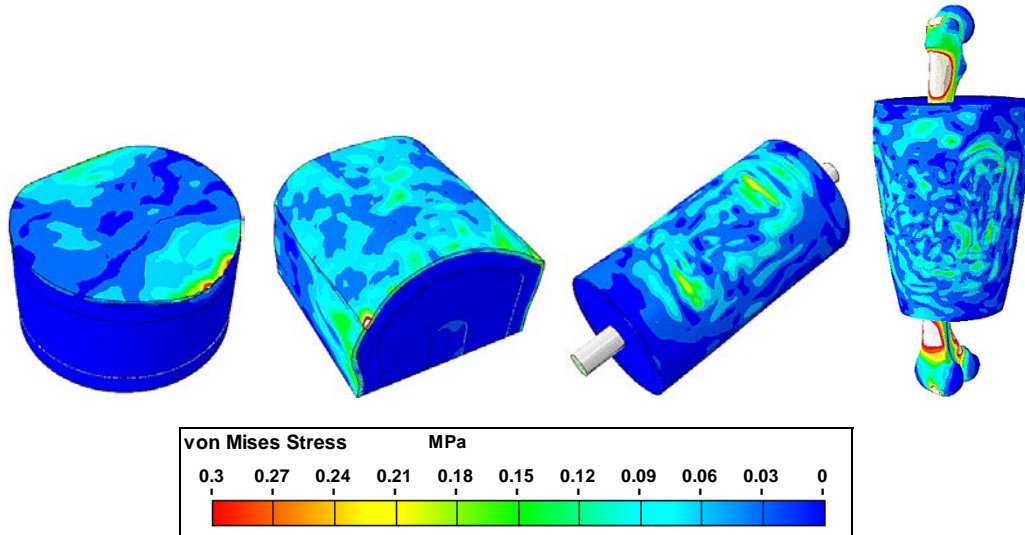


Figure 7.25 - von Mises stress distributions on surfaces of surrogates showing areas of high stress concentration immediately after impact when shell PPE was simulated.

The images shows regions of isolated high stress concentration in each of the simple surrogates where the rigid shell has failed to adequately fit to the surrogate geometries, whilst the anatomical surrogate exhibited a more continuous stress distribution. A comparison of the outer surface stresses between the shell and foam PPE has also been conducted on the anatomically contoured surrogate in Figure 7.26. Grey areas indicate stress has exceeded the stated scale.

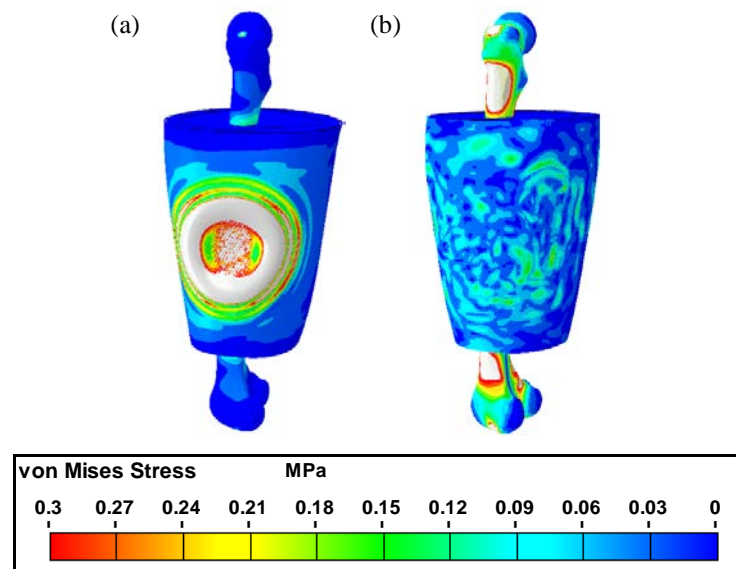


Figure 7.26 - von Mises stress distributions on the surface of anatomically contoured surrogates when: (a) foam and (b) shell were simulated.

The shell PPE demonstrated the ability to distribute pressure over a wider contact region, whilst the foam exhibited localised regions of high stress (shown by grey areas).

d) Load Transfer

The potential benefits of the shell PPE, which are potentially ignored by simple surrogates, have also been shown through the $\sigma_{v,bone}$ stresses experienced in the anatomically contoured surrogate. Figure 7.27 shows $\sigma_{v,bone}$ - time plots of the bone surface for foam and shell PPE simulations in both impact conditions.

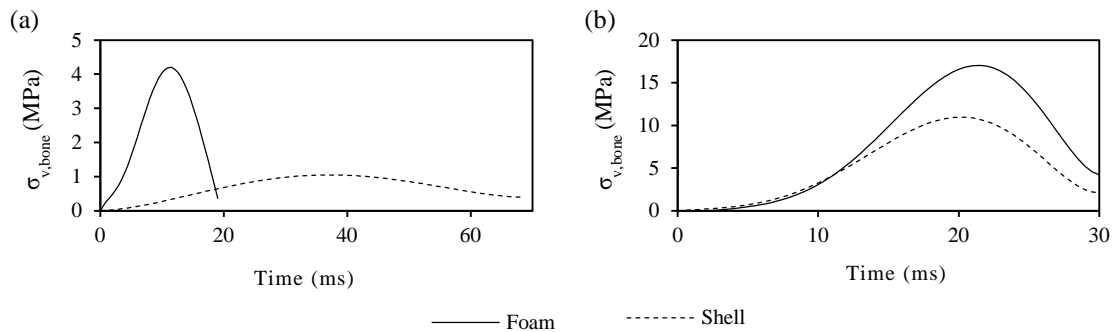


Figure 7.27 – $\sigma_{v,bone}$ - time plots for anatomical contoured surrogates with foam and shell PPE in: (a) cricket ball and (b) knee impact simulations.

The graphs show a significant increase in $\sigma_{v,max}$ when foam PPE was modelled in impact simulations with a 412% and 143% greater magnitudes compared to the shell PPE simulations. The shell PPE also dissipated the stress over a significantly longer time period in the cricket ball simulation and exhibited a 312% greater t_{σ} .

These simulated differences are not observed when considering a rigid shaped anvil surrogate, approximating those used in a test standard. The rigid surrogate predicted 1496% and 8044% greater $\sigma_{v,max}$ values in the shell PPE compared to the foam for cricket ball and knee impact simulations respectively.

7.7.4. Discussion

a) Proximity of PPE to Surrogate

The proximity of the PPE to the surrogate surface can significantly affect both the comfort and fit of the garment and subsequent load transfer phenomena on impact. With the preform applied assimilating the straps of a garment of PPE, the foam exhibited closer proximities to each of the surrogates than the shell PPE. The shell PPE, however, did fit closely to the anatomical contoured cylinder surrogate.

The gaps introduced through poor fit resulted in areas of significant isolated high pressure around the edges of the PPE (Fig. 7.25). This indicates that it is important when assessing PPE to select surrogate types that are representative of their target human geometries so that all PPE can be assessed with equal merit and result in better human conformity.

b) Pressure Distribution

A study by Ankrah & Mills (2004) investigating ankle protectors in association football concluded that a stiff shell will allow a larger volume of foam to be compressed and absorb energy. This same principle can be applied to human soft tissues, with a stiff shell distributing stresses over a wider contact area and hence reducing the potential for localised pressures and bruising to occur.

Although the foam PPE resulted in better conformity and fit across all surrogate types, it also introduced areas of significant high pressure beneath the contact area of the impactor. In the anatomical contoured surrogate where the shell PPE was well-fitted to the surrogate surface, the pressure was distributed over a much wider area beneath the PPE. Figure 7.26 shows a visualisation of skin surface pressure beneath the foam and shell PPE types in the anatomically contoured surrogate impacts. In the shell and foam PPE trials, peak magnitudes of von Mises stress on the skin surface of 0.17 MPa and 1.14 MPa were experienced respectively. An 85.1% reduction in the shell PPE. This demonstrates the importance of a rigid PPE interface in distributing blunt trauma impacts.

c) Load Transfer

The loads transferred through the surrogates to deep tissues are a key factor influencing the risk of sustaining deep tissue injuries (e.g. contusions) and their severity. The peak von Mises stresses experienced on the bone surface has been used as the evaluation metric to assess this. In the anatomically contoured surrogate, the shell PPE simulations induced reduced $\sigma_{v,max}$ on the bone surface of 72.7% and 33.3% compared to foam PPE simulations for the cricket ball and knee impacts respectively. This was not however represented in the rigid shaped anvil surrogate simulated where the foam PPE attenuated more impact force. Therefore, it is likely that effective, potentially safer PPE designs may fail the standardised tests.

7.8. Conclusions

A series of open loop predictive FEA simulations have been performed to investigate the effect of different geometric features on surrogate impact response. The importance of considerations to shape and size of impact surrogates were established initially through a simple surrogate shape investigation study using cricket ball and knee impacts. The study showed significant differences in response between shapes (puck, shaped anvil and cylinder) and outer tissue radii of curvature (50 mm, 75 mm, 100 mm). This highlighted the importance of developing surrogates to match the geometries of the impacted regions their target demographics. Consequently, an anatomically contoured surrogate was formulated which showed a directional dependent response, with posterior impacts typically exhibiting greater displacements though lower muscle and bone stresses. The lateral impact elicited lowest displacements due to the decreased volume of soft tissues in the region. These factors all indicate the importance of considerations to surrogate size and shape when approximating human geometries and the differences in response based on loading type and direction in more biofidelic anatomical geometries. The PPE simulations conducted indicated that current safety standards would be inadequate to assess certain types of PPE. Rigid shell PPE was shown to be inferior to foams when assessed in simple surrogates but showed superior fit, pressure distribution and load transfer in the anatomical surrogate. This further highlights the importance of such complex geometries in surrogate design.

Chapter 8 – Fabrication of an Anatomical Synthetic Thigh Surrogate

8.1. Chapter Overview

Chapter 8 presents the design and fabrication of a synthetic thigh surrogate informed by the simulant materials, geometries and methods of evaluation previously ascertained. Selection of an appropriate skeletal component has been detailed as well scanning techniques to create a virtual model. Design and manufacturing techniques used in the construction of moulds for the multi-material surrogate have been documented and the multi-material moulding process has been described. The success of the synthetic thigh has been appraised with reference to the production costs.

8.2. Introduction

The development of improved sport impact surrogates has considered: the importance of a multi-material surrogate (§4), appropriate soft tissue materials (§5) and the effects of different levels of anatomical geometric complexity (§7). Each of these studies has informed the development of a superior synthetic and computational impact surrogates. Given the range of requirements for sports industry applications based on differences in body shape and material properties, these surrogates have been produced as proof of the worth of the methodology rather than a final definitive solution.

8.2.1. Aims and Objectives

- 1) To develop a multi-material synthetic surrogate using the established soft tissue simulant materials and anatomical geometries.
 - Development of anatomical surrogate moulds and moulding procedure.
 - Feasibility study into the efficacy of surrogate moulding techniques.
 - Fabrication of the synthetic soft tissue thigh surrogate.
- 2) To establish the cost of a full synthetic thigh surrogate relative to other surrogate design solutions.

8.3. Methodology

8.3.1. Surrogate Skeletal Component

The development and analysis of appropriate soft tissue simulants have been extensively studied (§5). The skeletal femur component is also a key structure influencing the mechanical response of the thigh segment.

A large left fourth generation composite Sawbones[®] femur (Pacific Research Laboratories Ltd., Washington, USA) used previously in sports impact surrogates (§2.4.2.a) was selected as an appropriate surrogate skeletal component. The composite bone provides representations of both cortical and trabecular structures and embodies anatomical geometric properties (§2.3.2.d). The significantly increased strength and stiffness of the bone compared to surrounding soft tissues in this region means that compromises are often made with regards to the biofidelity of this structure. Despite reported issues regarding the strain rate dependency of the composite bone, the examined

impact types should elicit low strains and strain rates on the structure should therefore act as a representative skeletal component. The static mechanical properties for this structure are given in Table 2.5. The dimensions of the large composite femur are shown in Figure 8.1.

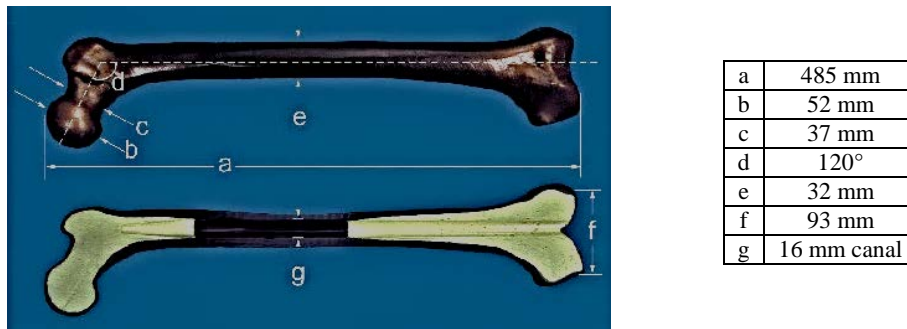


Figure 8.1 – Sawbones® 4th generation large left composite femur (www.sawbones.com).

The composite femur was scanned using a HandyScan™ hand-held range scanner (up to 0.04 mm accuracy) to create a digital copy of the geometry. Retroreflective markers were distributed around the surface of the bone to provide reference co-ordinates from which the scanner can align and determine the relative surface features (Fig. 8.2).



Figure 8.2 - Composite femur coated in developer spray and retroreflective markers.

8.3.2. Mould Tooling Development

a) Anatomical Simplifications

The Sawbones® composite femur selected for the surrogate had a longitudinal length of 485mm and was modelled on the femur of a 183 cm tall, 90.8 kg male. The soft tissue components, however, were adapted from data from the VHP which is based on a 180cm tall, 90.2 kg male (Spitzer *et al.*, 1996). These mismatched parameters, particularly the height will introduce small inaccuracies in soft tissue positioning on the bone.

Further simplifications have been made in the manner in which the VHP dataset was sampled. Data points were converted into a series of splines at each cross-section and reconstructed in computer-aided design (CAD) software to provide a three-dimensional (3D) representation of the soft tissue structure relative to the femur. This approach was adopted to provide a good representation of tissue thicknesses at different locations on the thigh, whilst avoiding specific elements of detail such as undercuts and sharp corners which may have introduced undesirable manufacturing challenges. The undercuts could result in air entrapment within the mould whilst sharp corners and re-entry angles could cause difficulties removing the parts from the mould. The skin layer was also simplified to a uniform 3 mm thickness to enable the silicone to pour into, and flow through, the mould cavity before the material begins to cure.

b) Manufacturing Approach

(i) Design Requirements

The proposed synthetic thigh surrogate soft tissue components needed to be moulded around the composite femur bone. The key requirements established for superior synthetic surrogate biofidelity were:

- Accurate geometric representation of outer and inner surface morphologies,
- Individual representative cross-sectional thicknesses for each tissue type,
- Continuity within tissue volume, without voids or other moulding flaws (e.g. contamination),
- Adhesion at tissue boundaries, and
- Consistent material properties within tissue boundaries.

(ii) Manufacturing Challenges

Achieving this, with the tissue structures, geometries and materials established presented a series of challenges:

- *Location and alignment of complex surface geometries.* At each process stage, the tissue simulant moulds must be aligned in a consistent orientation relative to the skeletal component.
- *Mixing consistency.* It is important that the mechanical properties of each tissue are continuous throughout despite the significant volumes of each simulant to be moulded.
- *Work times of silicones.* Each simulant contained different concentrations of cross-linker. Silicones with a greater concentration of cross-linker have shorter work times; the skin simulant, in particular, had a particularly short work time of approximately 120 min. The different volumes of uncured tissue simulant must flow through the available apertures well within material work time.
- *Viscosity of silicones vs. flow aperture variation.* The constituent formulations of the simulants affect their viscosity. The adipose simulant, in its uncured state, was the most viscous, while the skin simulant had the lowest viscosity. The challenge presented was related to the size of the cavity for each tissue type relative to the viscosity of the silicones.
- *Ease of void inclusion.* Owing to the mixing volumes, geometries of the mould cavities and viscosities of silicones, voids and other moulding flaws are easily introduced.

One of the most significant challenges when conceiving the manufacturing process was achieving accurate inner and outer skin geometry. If the adipose simulant were stiffer, a simple nested three stage moulding process (muscle-adipose-skin) with increasing girth would suffice, but since the adipose layer is the softest and does not retain its shape well such an approach was found to be unviable. Forming the skin layer, before introducing the adipose, using a mould tumbling process was considered but discounted because of the difficulty controlling the skin thickness and cure. The solution adopted was to introduce a sacrificial lost-wax like moulding stage using gelatin to define the inner skin boundary.

c) Moulding Process

To retain the structural integrity and mechanical properties of the PDMS silicone simulants, they each needed to be moulded in a single attempt. A series of process stages were employed to achieve this; an overview of the resulting multi-stage moulding process is shown in Figure 8.3, with each phase described as follows:

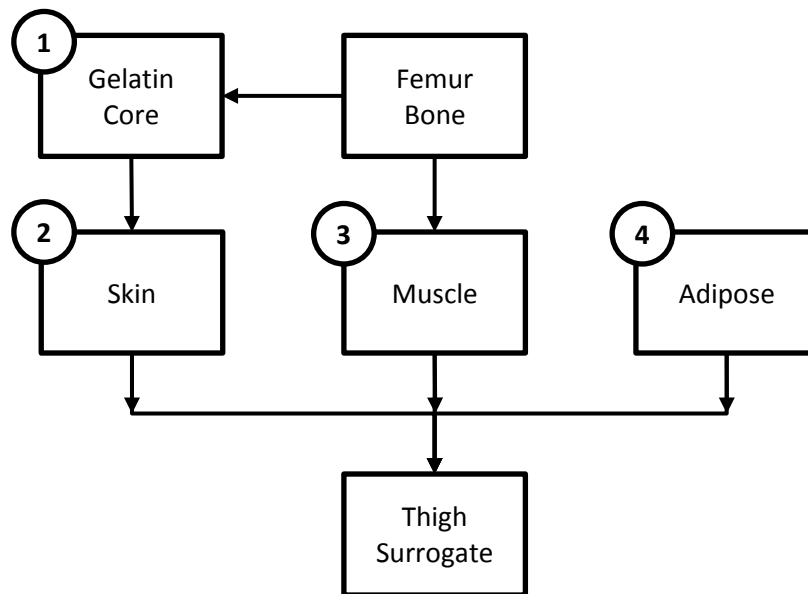


Figure 8.3 - Process stage diagram for thigh surrogate development.

1. Preparation

The initial stage of surrogate moulding involved the preparation of a support mould components and support structure, including:

- Making moulds for: muscle outer surface; skin inner surface; skin outer surface.
- Preparing an adaptive structural support system for the moulds to achieve consistent alignment with the skeletal component.

2. Stage 1

The first manufacturing stage involved the fabrication of a gelatin core required for the moulding of a thin continuous skin layer, including:

- Assembling the skin inner mould for the gelatin core in the mould support assembly.
- Moulding the gelatin core around the femur component.
- Setting the gelatin and removing it from disassembled mould.

3. Stage 2

The skin layer was the first surrogate tissue to be moulded and succeeded the fabrication of gelatin core, including:

- Assembling the skin outer mould in the mould support assembly and align the gelatin core using the femur component.
- Pouring the skin simulant into the cavity between the gelatin core and the skin outer mould and heat in an environmental chamber to melt gelatin and leave a continuous skin layer.
- Removing the skin layer from the mould support structure whilst attached to the outer skin mould.
- Cleaning the skin and femur components from gelatin contaminate.

4. Stage 3

Moulding of the muscle layer represented the third process stage; it consisted of the following constituent phases:

- Assembling the muscle outer mould in the mould support assembly around the femur.
- Pouring the muscle simulant in the mould and curing in an environmental chamber.
- Disassembling the mould and removing the muscle-femur component.

5. Stage 4

The final moulding phase involved the fabrication of the adipose layer and completion of the soft tissue surrogate. The constituent process stages have been listed:

- Positioning the skin outer mould with the skin layer attached in the mould assembly around the muscle femur component.
- Pouring the adipose simulant into the cavity between the skin and muscle tissues and curing in an environmental chamber.
- Disassembling the mould and removing the surrogate.

d) Pilot Testing – Small Scale Simple Moulds

To better understand the practicalities of this moulding process and the efficacy of such an approach, a small-scale pilot study was undertaken. Three cylindrical surrogate moulds were fabricated from acrylonitrile butadiene styrene (ABS) using a fuse deposition modelling (FDM) machine. The ABS material provided a stiff and strong material with sufficient melt temperature. The material was also less porous than the sintered Nylon powder used previously (§6.4.2) which improved the release agent coatings.

The moulds represented the skin outer, skin inner and muscle layers and were of diameter 65, 62 and 50 mm respectively. Each mould consisted of four quadrants with a height of 80 mm which joined to make the main cavity (Fig. 8.4). A base plate was also fabricated from ABS to complete the volume with a simple positioning stud located on the base to ensure a consistent alignment was maintained between moulding stages.

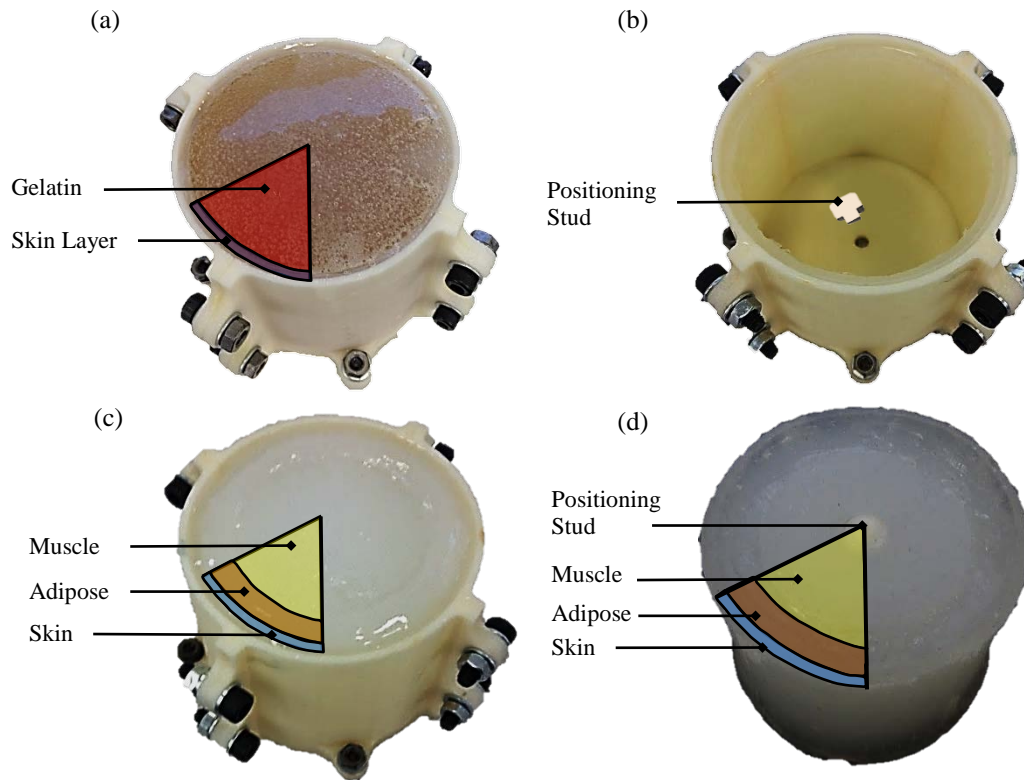


Figure 8.4 - Images of small scale surrogate development stages showing: (a) Stage 1 cured solid PDMS skin simulant and liquid sacrificial gelatin core; (b) Stage 1 cured PDMS skin on outside of mould with positioning stud; (c) Stage 4 final moulding of adipose; (d) Complete surrogate (inverted) showing positioning stud.

At stage 1, the gelatin core was moulded with a stud positioned on the base for subsequent alignment (Fig. 8.4b). The PDMS skin material was then poured into the cavity between the ABS mould and the gelatin core; the total pour time was 90 min for a mould of this scale. Figure 8.4a shows the cured skin simulant in the sacrificial gelatin core immediately after it was removed from the environmental chamber. The liquid gelatin was poured out of the mould and gelatin residue was cleaned from the surfaces with boiling water (Fig. 8.4b).

The PDMS muscle simulant was modelled independently, again with a stud located in the base plate. The cured muscle simulant was then positioned back into the skin mould using the locating stud and the adipose was poured in the resultant cavity (Fig. 8.4c, Fig. 8.4d). The time for the skin simulant to pour into the cavity was a particular issue and took a total of 90 min for a complete pour.

Given the pouring times observed, scaling up to a full-sized thigh required consideration of more than one pouring point. Exploration of this approach, during the pilot phase revealed difficulties maintaining alignment of the separate soft tissue regions if these were not: (i) adequately established by supporting structures; (ii) aided by even delivery from multiple pour points. Features to enable a rapid, even and consistent flow rate at multiple pour points were subsequently incorporated in the full scale mould tooling designs.

e) Full Scale Thigh Mould Development

Three full-scale anatomical moulds were fabricated out of FDM ABS for the skin outer, skin inner and muscle tissue structures using the detailed moulding approach. The mould assembly for the skin outer mould has been shown in Figure 8.5 and highlights many of the design features used in each of the cavity moulds.

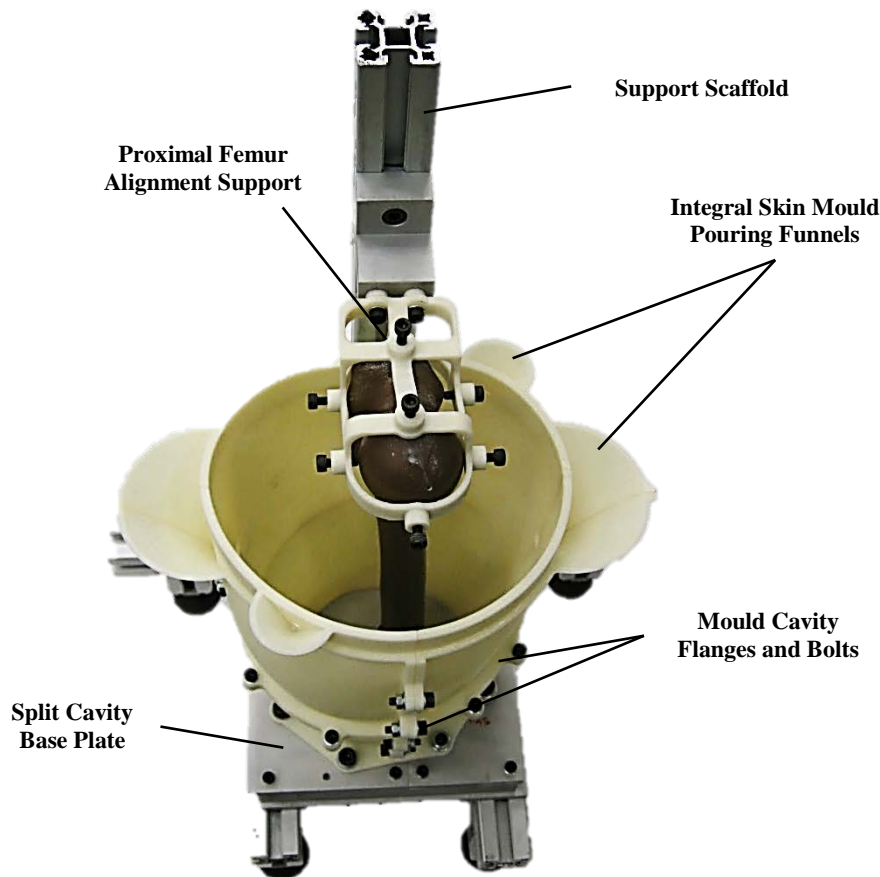


Figure 8.5 - Skin mould assembly with highlighted design features.

Each mould was segmented into eight pieces joined together on flanged surfaces with two 5 mm bolts to allow economic use of the FDM process (especially use of support material) and easy extraction of the moulded part without damage. The main ABS mould cavities were each mounted on a cavity base plate machined from 10 mm cast aluminium plate with a clearance cavity around the intersecting femur and a split line through the centroid of the femur on the plate (Fig. 8.6c). A scaffold support was constructed using 40 mm square sections of extruded aluminium profile. The scaffold provided a mounting point to which the mould cavities were attached and a consistent means of alignment for the composite femur. Alignment supports were used at the proximal and distal ends of the femur to rigidly constrain the bone in a specific, nominally vertical orientation. On each support, eight threaded nuts were embedded into the ABS in order that screws could be used clamp and manipulate the composite bone structure for optimal and consistent alignment (Fig. 8.6a).

The distal femur attachment support was connected to the cavity base plate through an intermediate plate structure, machined from aluminium (Fig. 8.6b). The intermediate plate was attached to the scaffold structure at the sides through 5 mm bolt holes and aligned against the upright scaffold using two 5 mm dowel pins. The intermediate plate and cavity base plate were then connected directly through two 15 mm × 200 mm aluminium upright supports.

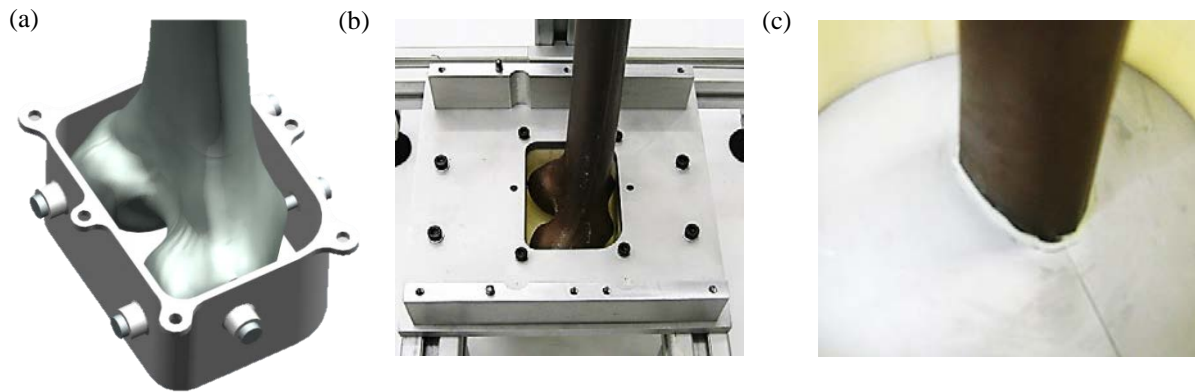


Figure 8.6 - Mould assembly components: (a) CAD image of distal femur attachment; (b) attachments between femur and intermediate base plates (c) cavity base plate femur seal.

As shown in Figure 8.5, pouring funnels were incorporated into the top of the skin cavity moulds to overcome issues associated with the pour and fill time of the PDMS skin layer. Two primary funnels were positioned on the anterior and posterior sides of the mould, 50 mm from the top, with 10 mm diameter feed holes. Two further secondary funnels were positioned above the top of the mould to enable the top 50 mm of the mould to fill evenly.

8.3.3. Surrogate Fabrication

The PDMS simulants were each formulated and mixed following the procedures outlined in §5.3.1 with 50% additional material to allow for wastage on the side of the mixing bowl and funnels. The quantities of materials used are detailed in Table 8.1.

Table 8.1 - PDMS simulant constituent quantities (kg) for full surrogate thigh.

	Part A				Part B	
	V46 (w/filler)	V31 (w/filler)	V21 (w/filler)	Heat Cure Catalyst	V31	H301
Skin	0.24	0.028	0.014	0.031	0.282	0.0314
Muscle	2.23	1.03	1.03	0.48	0.857	0.0953
Adipose	0.94	0.43	0.43	0.20	0.180	0.0200

Before each phase of moulding the components were assembled in the following order:

- 1) Bone ends fixed in supports.
- 2) Proximal femur support attached to intermediate base plate.
- 3) Dowel pins used to align intermediate base plate to R&K scaffold.
- 4) Intermediate base plate fixed to R&K scaffold.
- 5) Upright supports attached intermediate base plate to cavity base plate.
- 6) Cavity segments joined together and attached to cavity base plate.
- 7) Dowel pins used to align top of cavity to R&K scaffold.
- 8) Distal femur support fixed to R&K scaffold.

a) Skin Layer Fabrication

At stage 1, a sacrificial gelatin core was first fabricated. An iterative development study indicated that a 25% (by mass) gelatin concentration (250 Bloom) was optimal to develop a stiff but workable material which would retain its shape when stood vertical in a mould. The gelatin powder was mixed with water, heated at 50°C and poured into the mould cavity around the femur component (Fig. 8.7a) and left to cool for 10 hours at 4°C before removal from the mould (Fig. 8.7b).

At stage 2, the gelatin core was then placed inside the mould structure with the ABS skin outer cavity assembled around it (Fig. 8.7c). The PDMS skin material was then poured into the resultant cavity through the large moulded funnels which were continually refilled until the skin layer reached the level of the pour holes. At this point silicone was poured into the secondary funnels until the entire cavity was filled (Fig. 8.7d); the process took a total of 90 min.

The PDMS skin was left at room temperature to partially cure for 120 min before placing the entire mould assembly into the environmental chamber at 90°C. The mould was removed from the environmental chamber after 180 min and the molten gelatin was poured out of the mould. Water, just below boiling point, was then brushed onto the inside of the skin layer to remove the gelatin residue before being allowed to cool. The skin layer, attached to the mould cavity, was then carefully removed from the mould support assembly (Fig. 8.7e).

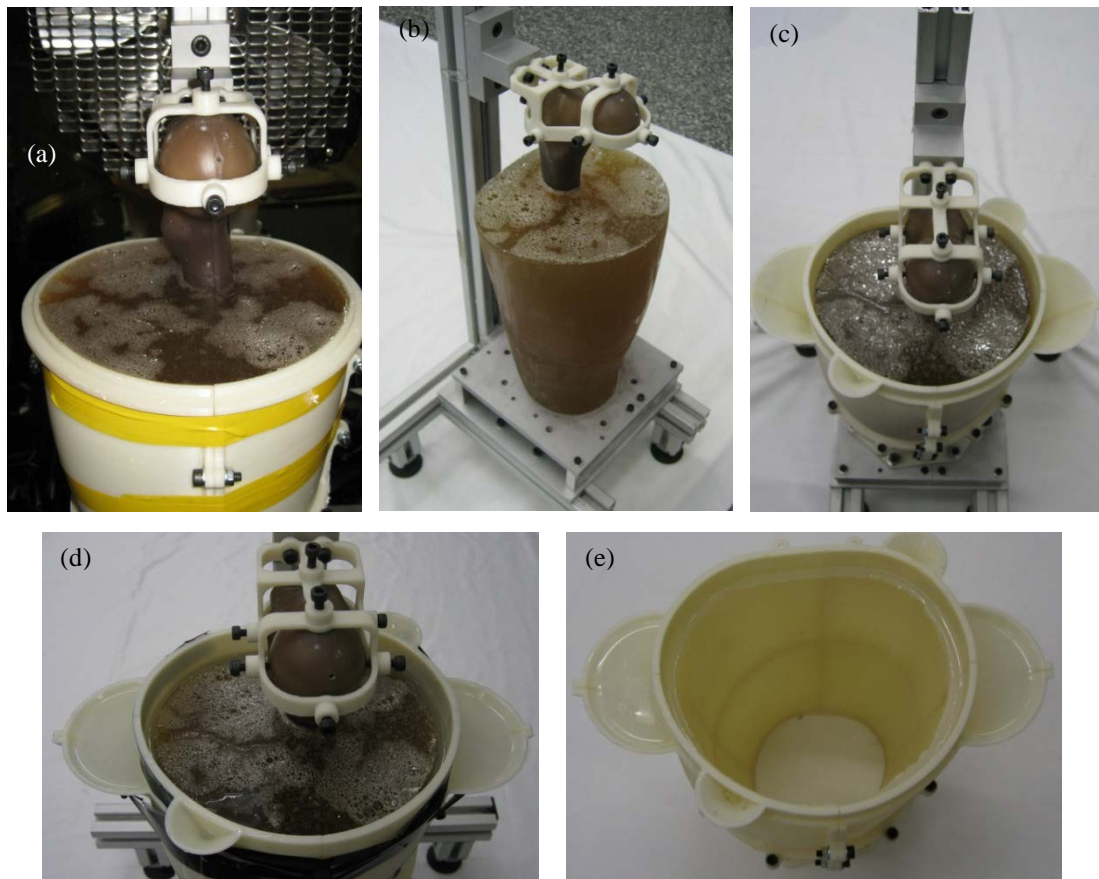


Figure 8.7 - Images showing the stage 1 and 2 development stages for the surrogate skin layer: (a) gelatin being cooled in skin inner mould; (b) cured gelatin removed from mould; (c) gelatin positioned in skin outer mould assembly; (d) PDMS skin simulant poured into gap between the gelatin and mould cavity through funnels; (e) gelatin removed from the mould and PDMS skin layer cleaned from contaminants.

b) Muscle Layer Fabrication

At stage 3, the muscle layer was moulded independently to the skin layer with the cleaned composite femur component positioned into the ABS muscle mould cavity. The PDMS muscle material was then poured into the cavity before the mould assembly was placed into the environmental chamber at 60°C for 6 hours until fully cured (Fig. 8.8a). The muscle layer, attached to the femur, was then carefully removed from the mould assembly (Fig 8.8b).

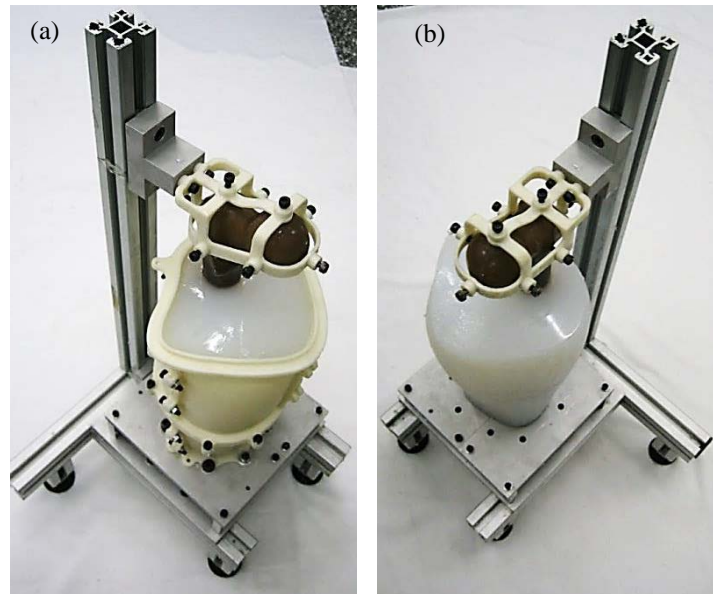


Figure 8.8 – Stage 3 moulding process: (a) PDMS muscle simulant moulded around femur; (b) cured PDMS simulant removed from the mould.

c) Adipose Layer Fabrication

At stage 4, the muscle-femur component was positioned inside the skin mould (with the skin layer attached) and fixed to the mould assembly (Fig. 8.9a). The PDMS adipose material was then poured into the resultant cavity between the PDMS skin and muscle material using a positioned funnel (Fig. 8.9b). Once filled, the complete mould assembly was placed in the environmental chamber at 60°C for 10 hours (Fig. 8.9c).

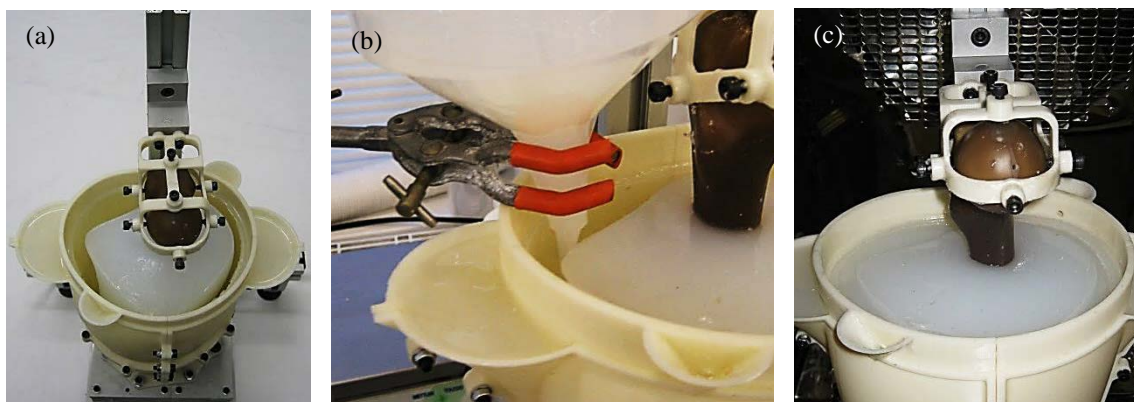


Figure 8.9 – Stage 4 Adipose layer moulding process: (a) muscle positioned in skin mould; (b) funnel used to pour adipose into cavity; (c) full leg assembly in environmental chamber.

The complete thigh surrogate was allowed to cool and removed from the mould (Fig. 8.10).

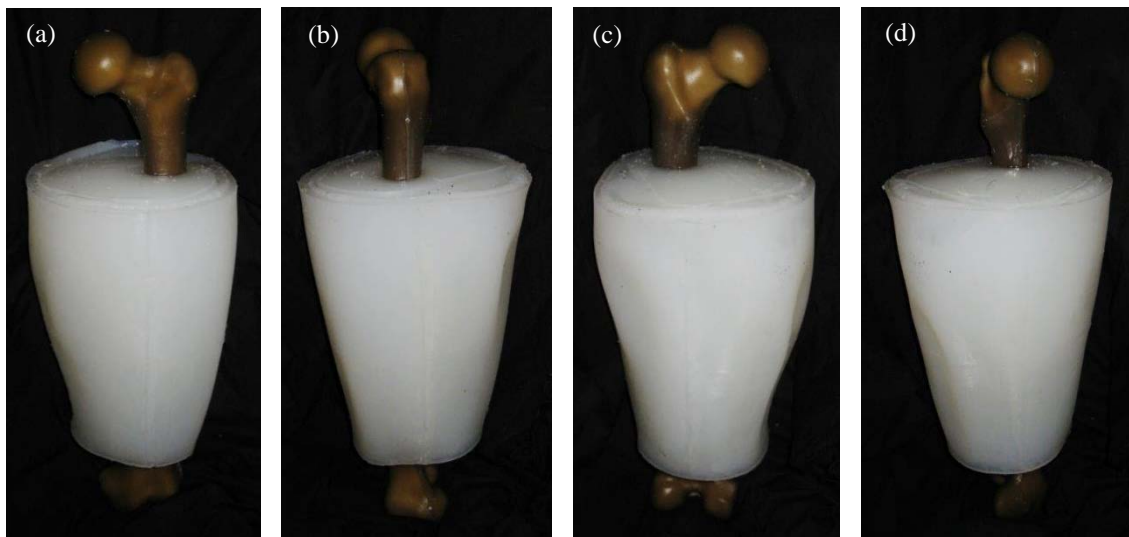


Figure 8.10 - Full synthetic thigh model in: (a) anterior; (b) lateral; (c) posterior; (d) medial views.

The synthetic thigh fabricated provided a full-scale multi-material human surrogate and good surface detail on anterior and lateral surfaces. The posterior and medial regions with large amounts of adipose simulant, however, failed to fully represent the desired geometry and wrinkled (Fig. 8.10c, 8.10d).

8.3.4. Costing

A key requirement established for improved human impact surrogates is that they can be manufactured affordably. A full cost breakdown for a single thigh surrogate has been detailed in Table 8.2.

Table 8.2 - Cost breakdown for single thigh surrogate manufacture.

Item		Cost Per Unit	Quantity	Line Cost
<i>ABS FDM Mould Parts</i>	Skin Outer Mould		574.9 cm ³	£488.67
	Skin Inner Mould	£0.85/cm ³	842.5 cm ³	£716.13
	Muscle Mould		542.9 cm ³	£460.70
<i>10 mm CERTAL Aluminium Base Plates</i>	Skin Base Plate		0.040 m ³	£8.80
	Muscle Base Plate	£220/m ³	0.040 m ³	£8.80
	Intermediate Plate		0.049 m ³	£10.79
<i>Silicone Constituents</i>	V46 Polymer (w/filler)	£55/kg	2.27 kg	£124.85
	V31 Polymer (w/filler)	£50/kg	0.99 kg	£49.50
	V21 Polymer (w/filler)	£50/kg	0.98 kg	£49.00
	Heat Cure Catalyst	£200/kg	0.47 kg	£94.00
	V31 Polymer	£30/kg	0.88 kg	£26.40
	H301 Cross Linker	£100/kg	0.097 kg	£9.70
<i>Gelatin</i>		£5/kg	1.36 kg	£6.80
<i>Sawbones® Composite Femur</i>				£115.00
<i>Laboratory Consumables</i>				£10.00
<i>Labour</i>		£25/hour	10 hours	£250.00
<i>Service Costs (Machining*, Blender, Vacuum Chamber)</i>				£50.00
Total Cost				£2,451.17

* (Custompartnet, 2014)

The surrogate costing's show that the total cost for surrogate manufacture was £2,451.17. This is the cost that would be incurred to develop an entirely new thigh segment which is an approach that may be desirable when considering individualised surrogate geometries for specific impact applications (e.g. frangible ballistic head developed for JFK assassination research (Adelaide T&E Systems, Australia)).

The costing for the surrogate detailed includes capital costs incurred in the development of mould tooling which would not be present in large volume production scenarios, likely to be pertinent in standardised PPE test environments. In most cases, it is desirable to develop a generalised surrogate broadly representative of the target demographic. This approach enables a single, cost-effective surrogate for repeat impact testing of PPE. Therefore, given geometric data representative of the target demographic group, one-off moulds could be developed and used in mass production reducing tooling costs. Economies of scale also suggest that the cost of silicone constituents could be reduced when the surrogates are manufactured in greater quantities.

Considering this, the costs for increased production runs for synthetic thigh surrogate manufacture have been estimated for PDMS, Silastic 3483 and gelatin simulants. In a larger volume manufacture scenario, each thigh surrogate will require a Sawbones® composite femur and soft tissue simulant materials. One-off costs for the PDMS surrogate include three moulds and a mould assembly structure, whilst the single material simulant surrogates only require a single skin outer mould and the assembly

structure. The estimated costings for increased production manufacture at different quantities have been shown in Table 8.3.

Table 8.3 - Estimation of cost per surrogate based on larger production volumes for: PDMS, Silastic 3483 and 10% ballistics gelatin.

	Quantity			
	1	5	5	50
<i>PDMS</i>	£2198	£728	£544	£397
<i>Silastic 3483</i>	£800	£270	£204	£151
<i>Gelatin</i>	£669	£139	£73.0	£20.0

The costings show that when manufacturing in quantities of 50, the PDMS surrogate can be fabricated at an additional expense of £246 compared to the Silastic 3483 surrogate. Although the gelatin surrogate can be fabricated at a significantly reduced cost, its frangibility means that it can only be used for a single impact application.

The elastomeric materials used to manufacture the synthetic surrogate are durable and are expected to withstand repeated impacts without failure. However, there will be an inevitable service life associated with the surrogate based on the damage incurred and repeat loading fatigue. The durability assessment of cylindrical specimens conducted in §5.5.4 showed that the materials were sufficiently robust not to fail through 1000 cycles at low strain rates. However, the softer materials did show some softening and degradation in material properties. It could be reasonably assumed that this would be exaggerated at increased loading rates. Therefore as a conservative estimate, a 100 impact product lifecycle has been selected. BS EN 13546:2002 (2002) stipulates that tests require two pairs of thigh PPE and five impacts per location. Therefore for assessment of a single garment of PPE, a minimum of 10 impacts are required. Given this, a standardised testing house could test approximately 10 pieces of PPE before replacing the surrogate.

8.4. Discussion

8.4.1. Quality of Synthetic Surrogate Thigh

The overall research aims for this study were principally concerned with determining the feasibility of designing and manufacturing a multi-material soft tissue surrogate for sports impact applications. The resulting surrogate is intended to exhibit dynamic response characteristics that, more closely than match those of the human equivalent than has previously been published for sports impacts. Anatomical simplifications were initially established through their function in impact applications, resulting in the selection of a four tissue surrogate with: skin, adipose, muscle and bone structures. Geometrical representations of each of these structures were determined through the sampling of anatomical imaging data in such a manner as to enable a greater ease of manufacture. The simulant materials used were then selected based on previously determined suitability in sports impact surrogate applications.

The mould assembly was constructed with such features to ensure that the skeletal components and moulds were oriented in a consistent alignment. A combination of precision engineered support structures, dowel pins and femur supports contributed to this. The multi-stage moulding process used enabled each of the tissues to be moulded individually and sequentially in a ‘single shot’ mould. This approach ensured that the tissues could be made without adversely affecting the mechanical properties

of the silicones. The novel use of a sacrificial gelatin core, in particular, was a key design feature of the moulding process, facilitating the thin, continuous, accurately formed skin simulant shape. Such a process could theoretically be effectively applied in other areas of future, more complex synthetic human surrogate models for example to generate vascular components.

Although these techniques were used to manufacture a simplified VHP anatomical dataset with PDMS simulants, the sequential, systematic nature of the process could be effectively applied to any given geometry in a fleshy region of the body surrounding bone with any combination of soft tissue elastomers. The resultant synthetic surrogate illustrates the potential for the construction techniques and materials to be effectively combined.

8.4.2. Further Surrogate Improvements

The otherwise successfully moulded full-sized thigh segment did exhibit an unanticipated flaw when released from the mould and left to stand. In medial and posterior regions (Fig. 8.10c, 8.10d) a crinkling effect developed on the surrogate surface. The location of this problem can be attributed to the increased proportions of the adipose simulant in these regions, which is particularly soft. Several potential reasons for why this may have occurred have been considered:

- Uneven cure rate through volume (e.g. heat source proximity),
- Loss of adipose simulant,
- Adipose simulant shrink back,
- Lack of interstitial fluid pressure, and/or
- Gravitational sagging.

Potential issues relating to the uneven curing rates and loss of adipose simulant in moulding can be easily eliminated through knowledge of the reliability of the environmental chamber used (Alpha 190H, Design Environmental Ltd.) and absence of any overspill from the mould. Similarly, this effect could also have been achieved through an under-fill or a void in the adipose simulant resulting in free space for the material to flow. However, the tissue structure dimensions were physically measured on both superior and distal surfaces and matched the desired dimensions from the CAD model. There could have also been a shrink back effect occurring whereby the skin was compressing the adipose simulant. However, there are no apparent environmental, chemical or physical reasons (e.g. heat shrinking) as to why this may occur.

The more likely reasons for these effects could be explained through examination of real human mechanical behaviour. All humans consist of approximately 16% interstitial fluid (by mass) which causes a hydrostatic pressure whereby tissues embody an equilibrium tonicity. This pressurisation is clearly absent in the currently proposed surrogate. Another contributory factor is adipose sagging under the influence of gravity caused by a lack of axial tension in the surrogate. The relatively low stiffness of the cured simulant, particularly at quasi-static strain rates, means that it exhibits some flow-type behaviour, which could result in deformation under static loads. The presence of such an effect has been investigated using FE models to simulate the effects of gravity when in a static vertical orientation. Figure 8.11 shows a significantly greater deformation of the adipose simulant in medial and posterior regions in these conditions. Although, the model is not sophisticated enough to predict the viscous flow type behaviour predicted and subsequent wrinkling, this does suggest that the movement of adipose in these regions due to gravity as another contributory cause.

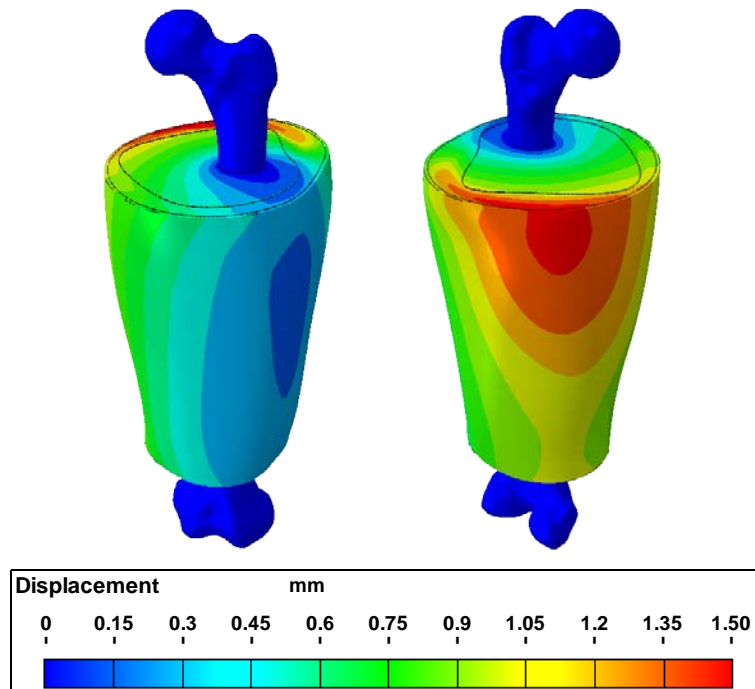


Figure 8.11 – FEA images of surrogate after 0.05s when subject to gravitational accelerations.

The discrete, shortened nature of the surrogate thigh could also contribute to this wrinkling effect. The human body consists of a series of continuous interconnected tissue structures with the skin in a state of biaxial tension stretching the local target region. In a discontinuous surrogate body segment, the soft tissues are free to move through the open ends. The presence of this effect has been simply demonstrated through manual stretching of the top of the skin layer. Figure 8.12 shows significantly reduced wrinkling of the surrogate when the superior surface of skin was manually stretched.

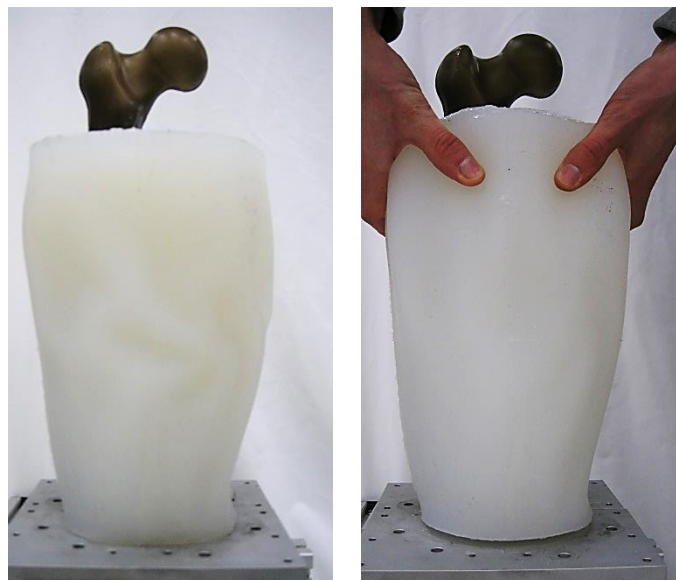


Figure 8.12 - Reduction of wrinkling effect when skin subject to manual axial tension.

Through a detailed examination of the potential causes, it has been determined that the reasons for wrinkling in the thigh surrogate are multifactorial. The gravitational sagging effect of the adipose tissue simulant, lack of skin tension in the discrete shortened thigh segment and lack of internal

pressure all contributed towards the resultant effect. Future work to overcome these issues should address the interstitial pressure within tissues and axial tension at the open ends of the surrogate.

8.4.3. Geometric Dataset and Anatomical Simplifications

Given the large variation in body shapes and material properties within and between demographic groups, this synthetic surrogate has been manufactured as a proof of the worth of the methodology. The VHP dataset used in this study was acquired from a 38-year-old male, which is not representative of an athletic population. The adipose tissue thicknesses of the elite-level basketball players tested in §3.4.2 were measured using a pulse-echo ultrasound scanner at predefined positions on the athletes thigh. The mean data collected has been shown in Table 8.4 and compared to equivalent measurements from the VHP.

Table 8.4 - Comparison of mid-thigh adipose thickness measurements between basketball players (mean \pm 1SD) and VHP.

	Adipose Thicknesses (mm)	
	VHP	Basketball players ($N = 15$)
<i>Anterior</i>	6.08	4.81 (\pm 1.84)
<i>Posterior</i>	9.88	4.16 (\pm 1.60)
<i>Lateral</i>	2.85	3.84 (\pm 1.00)
<i>Medial</i>	16.9	6.79 (\pm 2.36)

There are significant discrepancies between the VHP and athletic demographic measurement datasets particularly in the medial and posterior regions. Therefore, the adipose effects are likely to be exaggerated by the sedentary VHP male dataset from which the surrogate was moulded.

The VHP geometries were also interpolated from sampled data. Therefore, despite providing a more biofidelic representation of human geometries, the model still embodies inaccuracies and approximations which could be improved upon. As a first attempt of full-scale synthetic moulding, some simplifications were also made to ensure that the structures could be moulded (e.g. increased skin thickness). However, the success shown moulding a uniform 3 mm thick skin demonstrated the possibility of the techniques to model more complex geometries. A small scale trial was conducted to investigate whether the same moulding technique could be effectively applied to mould reduced skin thicknesses. A uniform 1.5 mm skin layer was designed and successfully moulded in a small scale surrogate (Fig. 8.13). The skin simulant material did, however, take 90 minutes to fill the mould which would be unsuitable for a full scale thigh. Further refinement of the moulding technique would be required to manufacture a skin layer of this thickness in a large scale mould.



Figure 8.13 - Small scale cylindrical surrogate with 1.5mm skin layer.

In most cases, it is desirable to develop a generalised surrogate broadly representative of the target demographic. This approach enables a single, cost-effective surrogate for repeat impact testing of PPE. Therefore future surrogates should focus on better matching the 3D tissue morphologies representative of the intended sports population. However, in spite of the shortcomings of the VHP dataset, it has provided an accessible and practically geometries from which to begin to model complex human structures. The presence of complex morphologies and extreme tissue dimensions has demonstrated the potential of the moulding techniques used, possibly beyond what could have been shown in athletic geometries. The adipose wrinkling effects experienced are also likely to be exaggerated by the sedentary VHP male dataset from which the surrogate was moulded.

8.4.4. Cost of Manufacture

The cost of surrogate manufacture, largely underpinned by additive manufacturing process used in the fabrication of the mould cavities proved expensive and cost £2,451.17. This cost could, however, be reduced significantly when considering the cost per unit if the tooling costs are shared in increased volume production. In this scenario, the mould tooling would only need to be fabricated once. Offsetting the capital costs of mould manufacture, assuming a batch of 50 surrogates, the cost of a single surrogate would be £397. This is more than twice the cost of a Silastic surrogate, but with greater biofidelity, and almost twenty times the cost of a gelatin surrogate, but with greater durability and testing efficiency.

The cost of rigid surrogate manufacture has been estimated as £240 using a manufacturing quote generator based on the geometries of the BS 13546:2002 safety standard (Custompartnet, 2014). Whilst this again provides an inexpensive solution, it embodies similar but exaggerated shortcomings to the Silastic surrogate in its lack of biofidelity.

The 3 mm wall thickness used in mould manufacture was potentially over engineered for the purposes of moulding silicones. Given the stiffness of the mould parts, a proposed reduced wall thickness of 1 mm could effectively reduce costs significantly. Given the size of the moulds, the additive manufacturing approach may also be more expensive than a conventional milling approach.

The repeated usage expected from the durable silicone materials lessens the financial burden. However, there will be a finite lifetime for the surrogate. Given the potential for material softening over time, the impact response under specific impact stimulus could be calibrated to ensure consistency of response is maintained. Once the recorded response is outside of the acceptable experimental limits, the surrogate should be recommended for replacement.

Chapter 9 –Experimental Impact Testing of the Synthetic Surrogate Thigh and Validation of a Parallel FEA Model

9.1. Chapter Overview

Chapter 9 presents experimental testing procedures used to determine the impact response of the synthetic surrogate thigh under representative impact conditions. Impact tests were conducted recording the accelerations of the impacting object, displacements of the skin outer surface and bone, and the surface strain from each impact. The experimental responses were compared to FE model predictions through each of these evaluation metrics to determine the correlation of fit and subsequent predictive validity of the FE models.

9.2. Introduction

9.2.1. FEA Approaches

The shape evaluation studies conducted in Chapter 7 showed the importance of a full anatomically contoured surrogate when considering impact response and PPE evaluations. FEA model formulations were generated for the surrogate based on the closed loop validated experimental puck impacts conducted in §6. Assumptions of the models accuracy were considered to be necessary to predict the worth of the surrogates and justify its expense. For the model to be used in a true predictive capacity (e.g. to optimise PPE design performance before committing to manufacture) it must be validated through closed loop experimental trials to prove the accuracy of the simulations.

9.2.2. Impact Testing Configurations

The configurations in which surrogates are tested are an important element of sports PPE evaluations. Two key components associated directly with impact testing configurations are the impact parameters and methods of constraint. Many previous sports impact tests have used a vertical-guided drop tower consisting of a gravity-driven carriage section with an end effector (e.g. Hysomallis, 2009; Francisco *et al.*, 2000; Ankrah & Mills, 2003).

In this configuration the impact surrogate is rigidly constrained to a massive base. This restricts the ability of the surrogate to recoil on impact, which is a phenomenon present, to some degree, in all real sports impacts. This could affect both the magnitude of force transfer to the surrogate and the duration of impact. The impact parameters used in drop tower tests are another issue. In specifying test conditions to model sports impacts, the selection of an appropriate mass and impact velocity for the striker is a common problem. In drop tower configurations, the mass of this carriage is often constrained by the guidance mechanisms and robustness requirements of the drop tower and it is therefore not uncommon for the minimum carriage mass of 5 kg or more.

9.2.3. Aims and Objectives

- 1) To determine the impact response behaviour of the developed surrogate under representative impact conditions.
 - Establish an appropriate experimental test configuration.
 - Determine appropriate instrumentation and evaluation metrics.
- 2) To compare the experimental impact data of the synthetic thigh to FEA model simulations and determine their predictive capabilities.

9.3. Test Methodology

9.3.1. Experimental Test Configuration

To assess the impact response of the synthetic impact surrogate, a representative impact configuration was required. The requirements for representative cricket ball and knee impact tests were established in §3.5. An unbraced leg strike was modelled to aid in the simulation of the boundary conditions enforced.

Given the issues associated with vertical-guided drop tests on sports impact surrogates (§9.2.2), a pendulum impact configuration was adopted (Fig. 9.1). The surrogate was suspended from an A-frame using light inextensible strings. The strings attached to the composite femur bone proximally through use of jubilee clips attached to the neck of the femur. The surrogate was also supported distally through strings attached to the upright supports of the A-frame which permitted a greater ease of alignment of the surrogate. A rigid, 3 kg striking object was used for surrogate testing.



Figure 9.1 – Pendulum test rig configuration with mounted striker and surrogate bodies.

9.3.2. Instrumentation and Methods of Evaluation

To determine the magnitudes of acceleration experienced during the impact event an accelerometer was mounted on the striking object. A Brüel & Kjær 4375 piezoelectric charge accelerometer (Brüel & Kjær, Nærum, Denmark) was calibrated mounted on a handheld electromagnetic exciter (Brüel & Kjær Type 4294) and connected to a conditioning amplifier (Brüel & Kjær Nexus 2692). The calibrated accelerometer was then screw mounted onto the rear of the striking object (Fig. 9.2). Data were recorded from the accelerometer using a LeCroy Wavejet 324 200 MHz oscilloscope at a sampling frequency of 10,000Hz (Teledyne LeCroy, New York, USA).

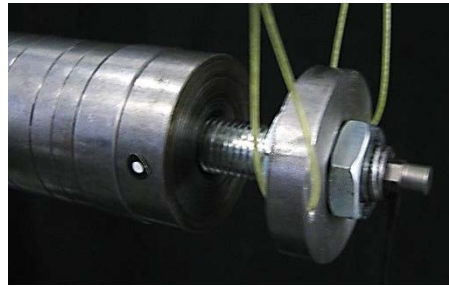


Figure 9.2 – Accelerometer screw mounted into rear of the striking object.

A combination of HSV and DIC were used to determine the kinematic response phenomena. A Photron Fastcam Colour HSV camera (§6.3.5.a) was aligned perpendicular to the impact site with an approximate 300×300 mm field of view (Fig. 9.3). The camera was set with a temporal resolution of 5000 fps and shutter speed of 1/5000 s. The field of view was calibrated against objects of known distance. Positional markers on the impactor and surrogate bone were tracked used to calculate the displacements of both bodies throughout the impact event.

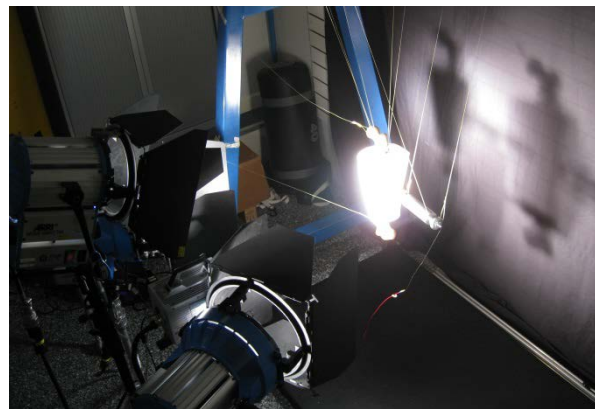


Figure 9.3 – High speed video camera and lighting arrangement for impact testing.

A GOM ARAMIS DIC system was also used (§6.3.5.b). The system used two Basler A505K HSV cameras (Basler AG, Schleswig-Holstein, Germany), which were calibrated using a regular pattern board aligned in a series of defined orientations. The cameras were consequently separated by a known distance (39 cm) relative to the impact site. The cameras were operated at their maximum operating frequency of 500 Hz with a shutter speed of 0.01 s. Tracking points were manually drawn onto the surrogate skin using a permanent marker pen in an irregular speckle pattern (Fig 9.4). Three 12,000 W lights (ARRI Group, Munich, Germany) were positioned behind the cameras with their intensity varied to achieve the maximum marker visibility without saturation (Fig. 9.4).



Figure 9.4 – Images showing the speckle pattern on surrogate surface for GOM ARAMIS DIC tracking and the camera and lighting orientation.

For the ARAMIS tracking algorithms to operate the positional markers must be in view through the entire capture duration. This caused difficulty when the impactor entered the field of view as this significantly obscured visibility of the speckle pattern. Consequently, two captures were performed, one with the cameras positioned beneath the striking object in the normal direction and the other with the cameras aligned at approximately 45° to the impact location (Fig. 9.5).

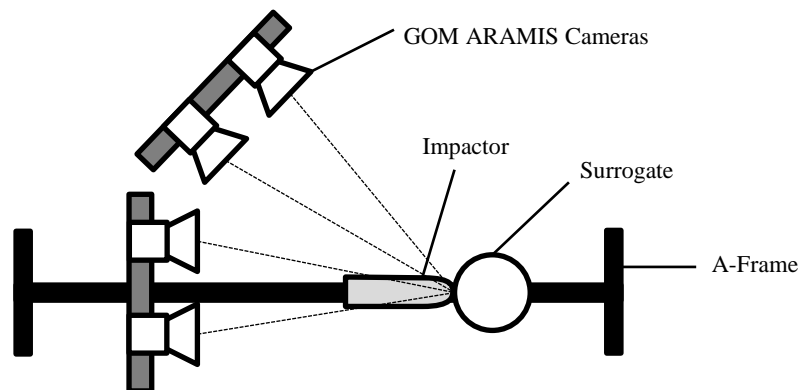


Figure 9.5 - GOM ARAMIS camera orientations for impact trials

9.3.3. Impact Parameters

Given spatial constraints, the A-frame pendulum test rig configuration can achieve velocities up to 5 m.s⁻¹. The impact parameters selected were, therefore, based on the knee impact scenario. A 3 kg mass was used, consistent with that from FE impact simulations. The impact velocity was increased in 1 m.s⁻¹ intervals from 1 - 4 ms⁻¹. Five trials were conducted at each velocity level.

The surrogate was impacted in the lateral and anterior directions as these regions are pertinent to sports impacts and were not affected by the adipose wrinkling effect (Fig 8.10).

9.3.4. FE Modelling

a) Model Formulation

FE modelling of the surrogate thigh was conducted using the modelling parameters established in §7.4. The PDMS soft tissue simulant batch variability has been investigated and accounted for in the FE models. Material specimens from the thigh surrogate material batches were compared to reported reference data for each PDMS simulant (§5.5.1). The specimen responses under quasi-static loading conditions are shown in Figure 9.6.

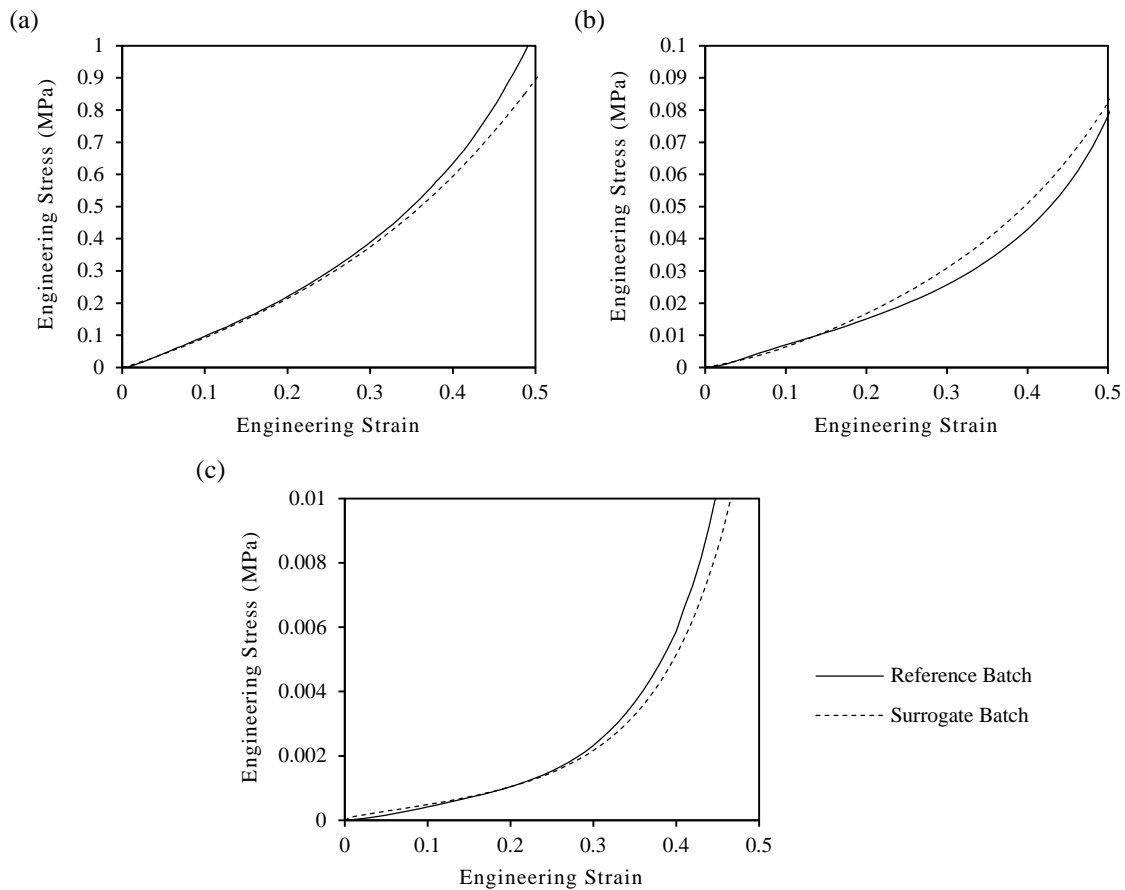


Figure 9.6 - Comparison in quasi-static mechanical response between specimens from the reference and surrogate material batches for: (a) skin; (b) relaxed muscle; and (c) adipose simulants.

The material batches used in the surrogate exhibited some differences from the previously reported reference datasets. At 0.4 strain, the surrogate batch exhibited -1.75%, +3.77% and -8.26% differences from the reference batch in skin, relaxed muscle and adipose simulants respectively. The skeletal representation was also changed from the models in §7 with the Sawbones[®] femur used in the synthetic surrogate modelled using the parameters in Table 9.1.

Table 9.1 - Material properties for 4th generation composite femur (adapted from Heiner *et al.* (2008) and Thielen *et al.* (2014)).

ρ ($kg.m^{-3}$)	1,640
ν	0.3
E (GPa)	16.6

b) Methods of Evaluation

Three primary evaluation criteria were assessed in the FE model validation study: impactor acceleration, bone displacement and impactor displacement. The impactor acceleration was measured considering the normal accelerations using a reference point on the rear of the rigid impactor. The impactor and bone displacements were measured through determination of the associated virtual nodes representative of the markers being tracked in the experimental tests.

A further comparison was conducted investigating the surface strains elicited on the skin layer. The maximum principle strain on the FE model was visualised for a qualitative comparison between experimental data and FE models. The differences in response were also quantitatively assessed through extraction of point strain data from a series of predefined locations around the impact. The surrogate was divided into a series of sampling points based on the proximity to the impactor at maximum displacement (Fig. 9.7).

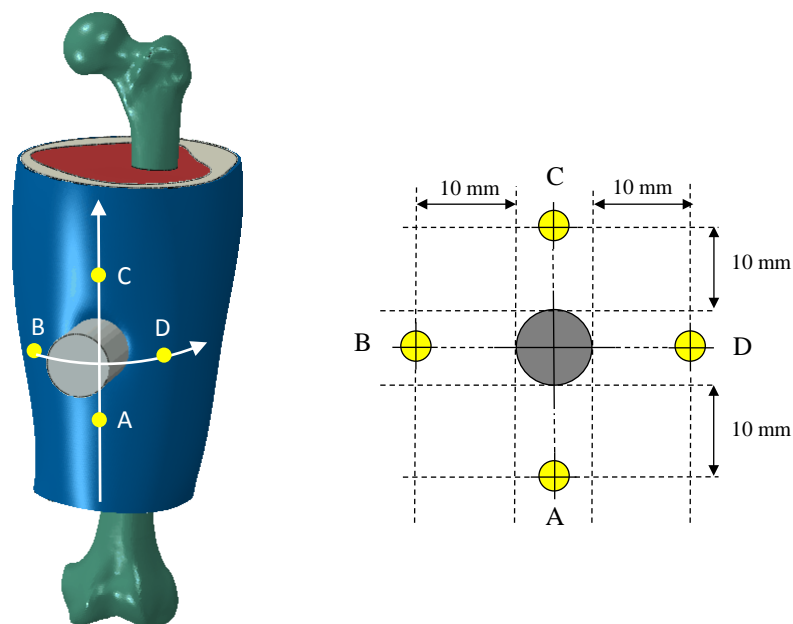


Figure 9.7 - Image showing the distribution of sampling points relative to the impact location at x_{\max} .

9.4. Results

9.4.1. Synthetic Surrogate Responses

The surrogate was impacted centrally and perpendicularly in anterior and lateral regions at nominal velocities between 1 - 4 m.s⁻¹. Actual impact velocities were attained by post-processing of the HSV data and showed a SD of no greater than 0.11 m.s⁻¹ across all velocity increments. High speed video stills demonstrating the types of impacts conducted have been shown in Figure 9.8.

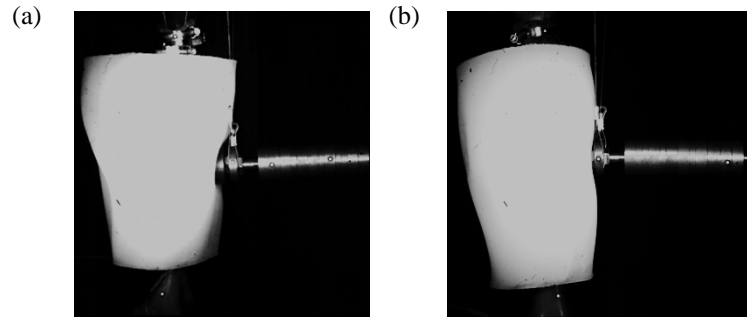


Figure 9.8 – Perpendicular high speed video stills of 2 m.s⁻¹ impacts at maximum displacement to: (a) anterior and (b) lateral thigh regions.

The synthetic surrogate responses for anterior and lateral impacts have been reported in Table 9.2. Mean (± 1 SD) values for maximum acceleration (a_{\max}), time to maximum acceleration (t_{acc}), maximum impactor displacement (x_{\max}) and time to maximum displacement (t_x) have been recorded.

Table 9.2 - Mean synthetic surrogate outputs in anterior and lateral impacts (± 1 SD).

	Velocity (m.s ⁻¹)	a_{\max} (m.s ⁻²)	t_{acc} (ms)	x_{\max} (mm)	t_x (ms)
<i>Anterior</i>	1 (± 0.03)	12.3 (± 0.59)	23.3 (± 1.23)	23.1 (± 0.975)	48.5 (± 1.64)
	2 (± 0.03)	68.8 (± 2.81)	17.9 (± 0.893)	32.4 (± 0.563)	41.7 (± 1.16)
	3 (± 0.05)	94.3 (± 5.55)	16.6 (± 0.327)	42.3 (± 1.23)	37.7 (± 1.90)
	4 (± 0.11)	129 (± 10.7)	14.2 (± 0.736)	56.1 (± 1.04)	32.1 (± 0.50)
<i>Lateral</i>	1 (± 0.02)	23.7 (± 1.53)	20.7 (± 1.66)	20.9 (± 0.82)	43.2 (± 1.34)
	2 (± 0.05)	65.1 (± 3.27)	15.9 (± 0.234)	30.8 (± 1.46)	38.5 (± 0.891)
	3 (± 0.06)	126 (± 7.12)	16.1 (± 0.355)	46.8 (± 3.02)	37.1 (± 3.21)
	4 (± 0.09)	199 (± 13.8)	14.7 (± 1.07)	46.8 (± 2.77)	31.9 (± 2.40)

The data shows a directional-dependent response with a trend to greater magnitudes of a_{\max} and inhibited x_{\max} in lateral impacts compared to anterior impacts, particularly at higher velocities. There was also an expected increase experimental variance in responses at higher impact velocities.

Acceleration - time and force - time graphs showing the magnitudes of differences in experimental response under different impact conditions have been shown in Figure 9.9 and Figure 9.10.

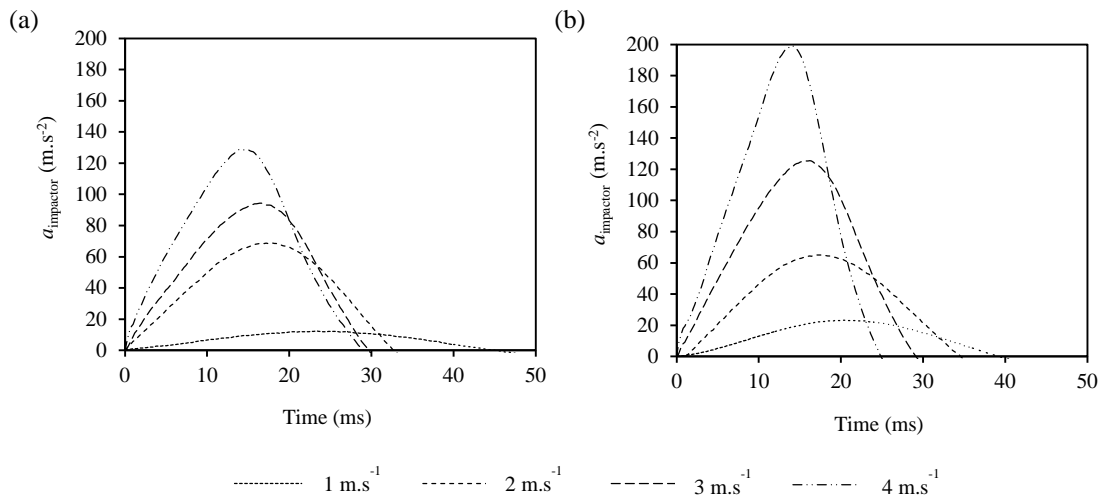


Figure 9.9 – Mean acceleration - time graphs for the impactor in: (a) anterior and (b) lateral impacts.

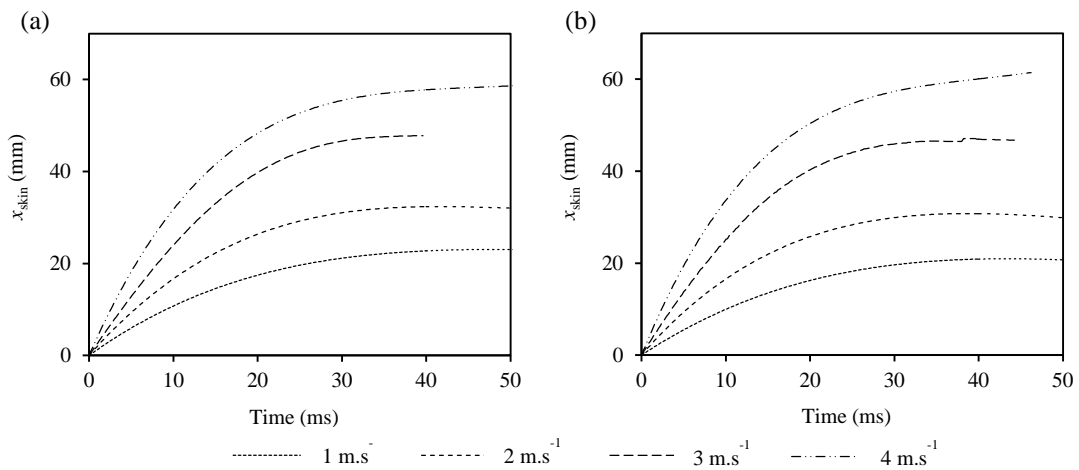


Figure 9.10 – Mean displacement - time graphs for the impactor in: (a) anterior and (b) lateral impacts.

Example surface strain data generated from synthetic surrogate trials have been presented in Figure 9.11.

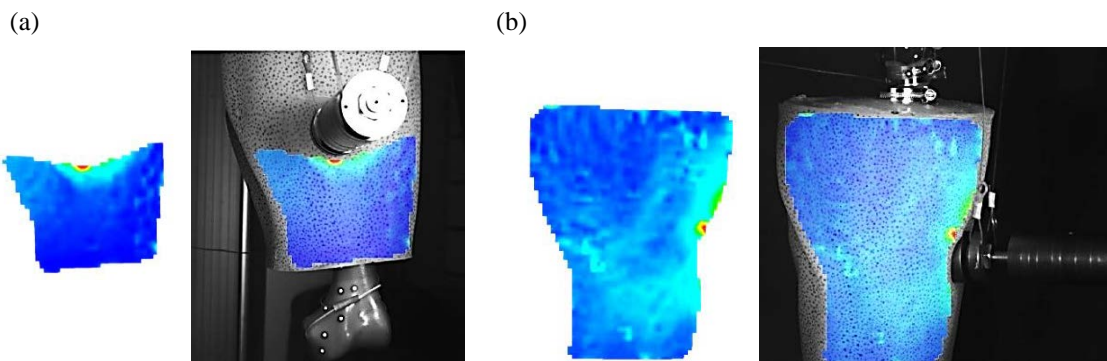


Figure 9.11 - Examples of surface strain maps generated in GOM ARAMIS, attained from anterior impacts using: (a) frontal and (b) side camera arrangements.

During experimental testing, damage was inflicted upon the surrogate. A tear formed in the skin from an off-centre 4 m.s^{-1} impact due to edge effects on the impactor (50 mm frontal diameter) (Fig. 9.12.a). There was also a delamination effect which occurred on the lateral surface where there was a separation of skin and adipose layers (Fig. 9.12.b).

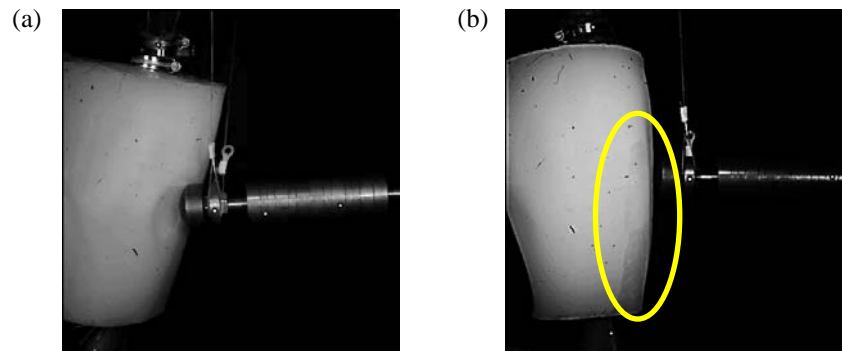


Figure 9.12 – (a) Torn skin on anterior surrogate surface due to off-centre impact; (b) Delamination of skin and adipose tissues in lateral regions.

9.4.2. FE Model Comparison

When running FE simulations on an unconstrained thigh segment (without translational restrictions on femur ends), the level of mass scaling previously employed (to a minimum time increment of 1×10^{-6} s) influenced the surrogate response kinematics. This resulted in an inhibited translation of the surrogate on impact. To correct this, a reduced mass scaling was employed with semi-automatic mass scaling when below a minimum time increment of 1×10^{-7} s.

a) Kinematics of Striker and Surrogate

A comparison of the kinematic responses of the impactor and bone between experimental data and FE model predictions has been shown in x_{skin} - time and x_{bone} - time graphs in Figure 9.13 and Figure 9.14 (left: impactor penetration; right: bone displacement). Positive displacements have been reported in the direction of the impact.

(i) Lateral Impacts

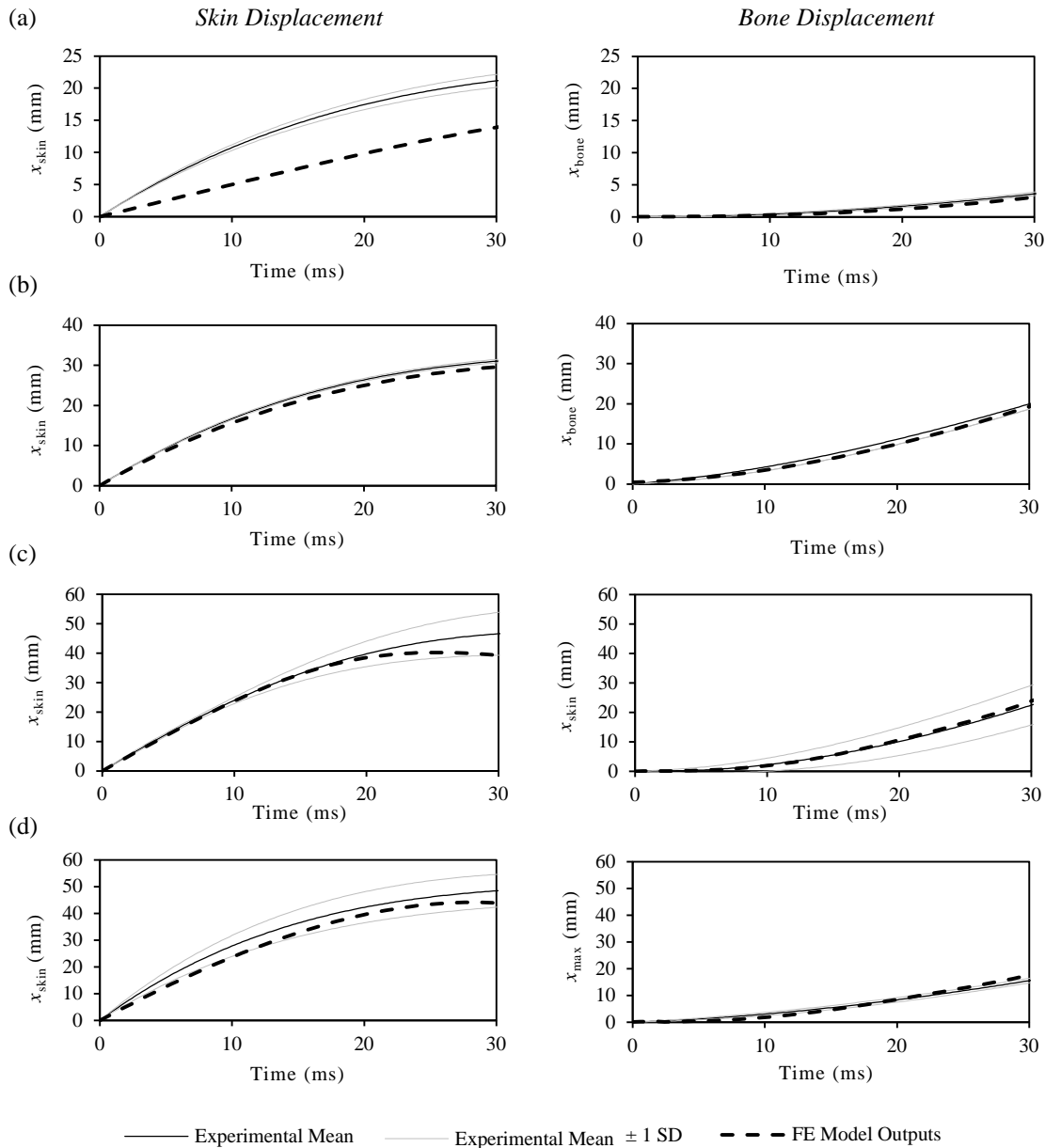


Figure 9.13 - x_{skin} - time and x_{bone} - time graphs showing the differences in impact kinematics between experimental data and FE model predictions in lateral impacts: (a) 1 m.s⁻¹; (b) 2 m.s⁻¹; (c) 3 m.s⁻¹; (d) 4 m.s⁻¹.

(ii) Anterior Impacts

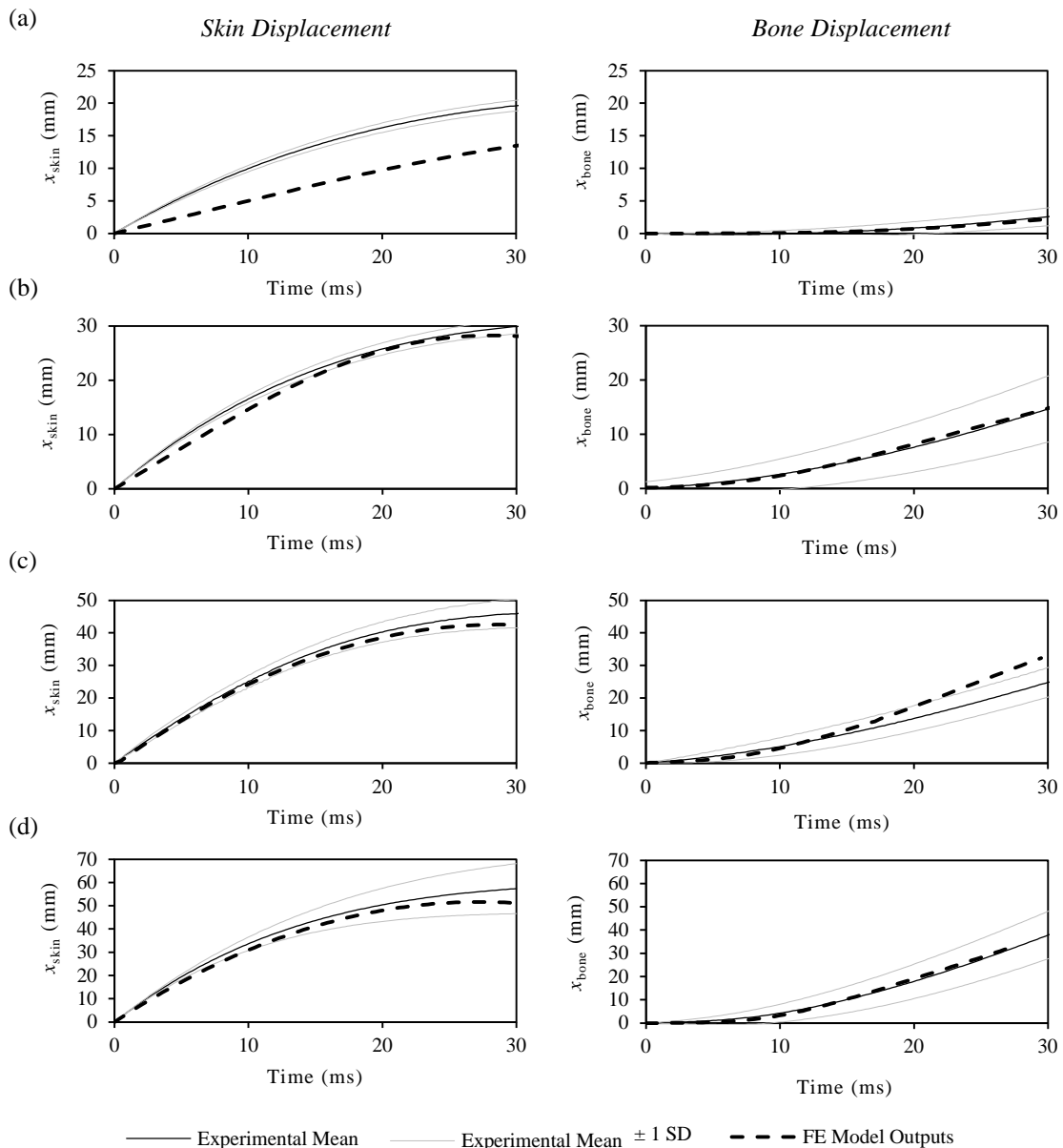


Figure 9.14 – x_{skin} - time and x_{bone} - time graphs showing the differences in impact kinematics between experimental data and FE model predictions in anterior impacts: (a) 1 m.s^{-1} ; (b) 2 m.s^{-1} ; (c) 3 m.s^{-1} ; (d) 4 m.s^{-1} .

The experimental data follows an expected trend whereby, at increasing velocities, greater magnitudes of skin and bone displacements are exhibited. The FE models generally provided a good prediction of the impact kinematics with all FE responses within the experimental response corridor with the exception of 1 m.s^{-1} in both lateral and anterior directions.

In these impacts an inhibited skin displacement was exhibited. This could be due to the strain rates of these FE impact simulations being below the experimental characterisation strain rate resulting in an artificially stiff FE model prediction.

b) Impactor Accelerations

The accelerations of the impactor have also been compared between with FE model predictions in a series of a_{impactor} - time graphs. In these graphs, the acceleration traces were synchronised at 10% of the peak FE acceleration magnitude.

(i) Lateral Impacts

a_{impactor} - time graphs for lateral impacts at 1 - 4 m.s^{-1} have been shown in Figure 9.15.

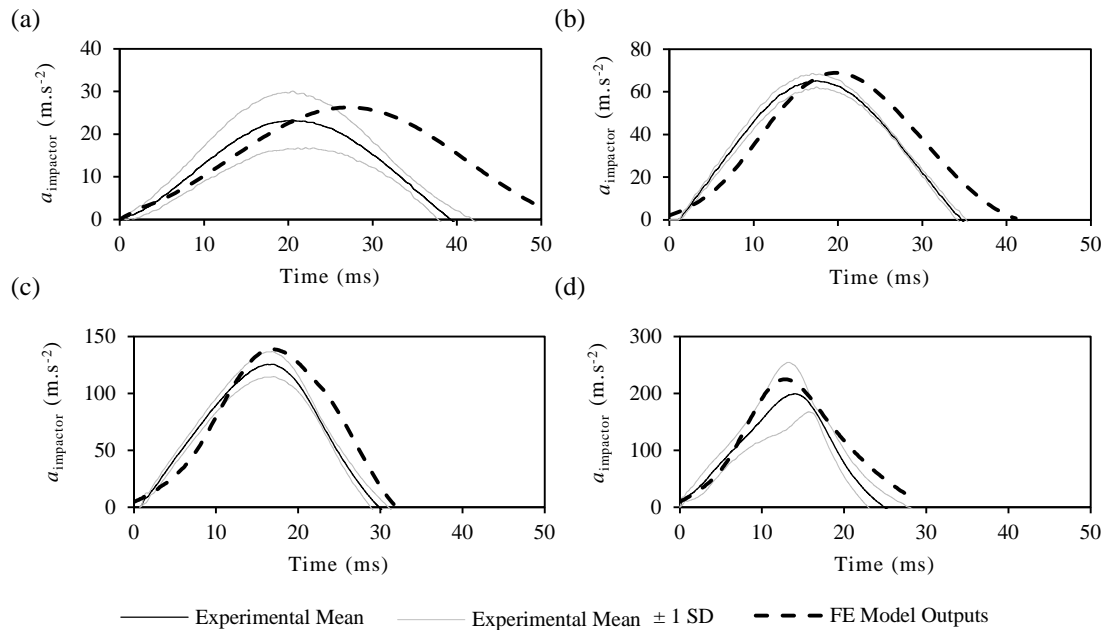


Figure 9.15 – a_{max} - time graphs showing the differences in impactor decelerations between experimental data and FE model predictions in lateral impacts: (a) 1 m.s^{-1} ; (b) 2 m.s^{-1} ; (c) 3 m.s^{-1} ; (d) 4 m.s^{-1} .

The peak acceleration (a_{max}), time to peak acceleration (t_{acc}) and total impact time (t_{impact}) for experimental and FE lateral impacts have been shown in Table 9.3.

Table 9.3 - Comparison of accelerometer outputs between experimental data and FE model predictions for lateral impacts.

	$a_{\text{max}} (\text{m.s}^{-2})$			$t_{\text{peak}} (\text{ms})$			$t_{\text{impact}} (\text{ms})$		
	Exp.	FE	% Error	Exp.	FE	% Error	Exp.	FE	% Error
1 m.s^{-1}	23.3	26.3	+12.8	20.5	27.3	+33.2	39.3	52.8	+34.4
2 m.s^{-1}	65.1	68.9	+5.84	17.5	19.8	+13.1	34.6	41.1	+18.8
3 m.s^{-1}	126	139	+10.3	16.9	16.7	-1.18	29.9	31.9	+6.69
4 m.s^{-1}	199	224	+12.5	14.0	12.9	-7.86	24.9	29.1	+16.9

The FE model predictions typically provided a good prediction of experimental acceleration responses with maximum divergences in a_{max} of +12.8% across all trials. These divergences were most significant in the 1 m.s^{-1} impact where there was also a large difference in t_{peak} (+33.2%) and t_{impact} (+34.4%) values. Across all trials there was also an elongated a_{impactor} - time trace with a minimum difference in t_{impact} of +6.69% from experimental data.

(ii) Anterior Impacts

a_{impactor} - time graphs for anterior impacts at 1 - 4 m.s^{-1} have been shown in Figure 9.16.

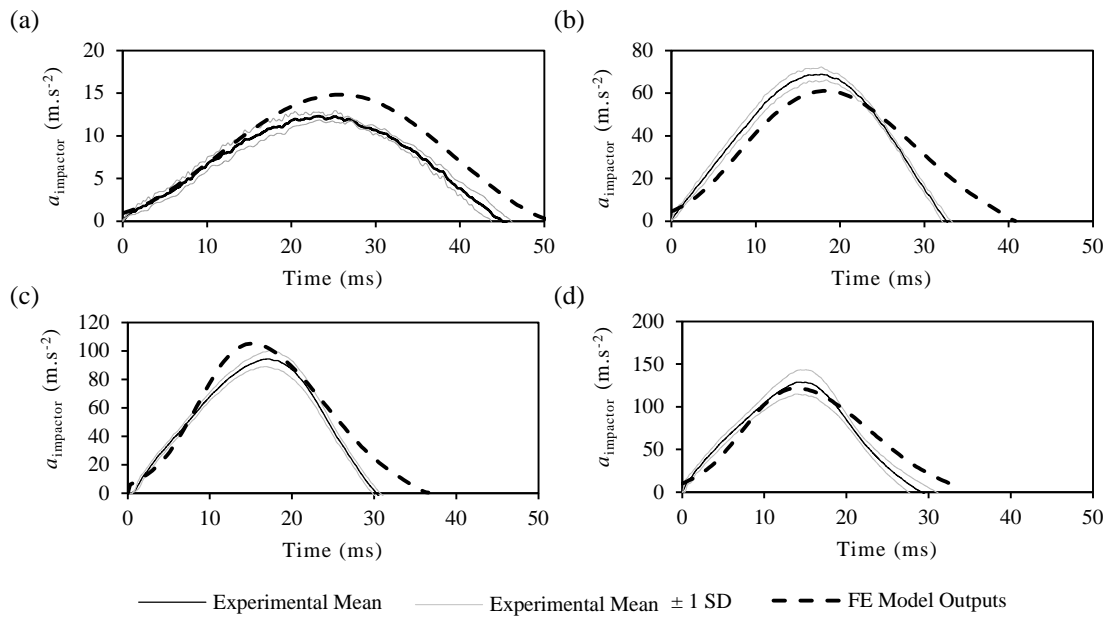


Figure 9.16 - a_{impactor} - time graphs showing the differences in impactor accelerations between experimental data and FE model predictions in anterior impacts: (a) 1 m.s^{-1} ; (b) 2 m.s^{-1} ; (c) 3 m.s^{-1} ; (d) 4 m.s^{-1} .

The a_{max} , t_{acc} and t_{impact} values for experimental and FE anterior impacts have been shown in Table 9.4.

Table 9.4 - Comparison of accelerometer outputs between experimental data and FE model predictions for anterior impacts.

	$a_{\text{max}} (\text{m.s}^{-2})$			$t_{\text{peak}} (\text{ms})$			$t_{\text{impact}} (\text{N})$		
	Exp.	FE	% Error	Exp.	FE	% Error	Exp.	FE	% Error
1 m.s^{-1}	12.3	14.8	+20.3	23.3	26.0	+11.6	45.0	51.2	+13.8
2 m.s^{-1}	68.8	61.1	-6.14	17.9	18.6	+3.91	32.7	40.8	+24.8
3 m.s^{-1}	94.3	105	+11.3	16.6	15.3	-7.83	29.7	36.6	+23.2
4 m.s^{-1}	129	121	-6.20	14.2	14.1	-0.71	29.0	33.2	+14.4

The FE predictions of anterior impact response showed good correlation with the peak acceleration magnitudes in all velocities excepting the 1 m.s^{-1} impact where there was a +20.3% difference from experimental data. At the other impact velocities, this divergence decreased significantly with a_{max} values all within +11.3% of the experimental mean. The FE predictions of t_{impact} showed significantly increased impact durations (min. +13.8% difference), which was consistent with the responses of the lateral impacts.

c) Surface Strain

The surface strain patterns generated by GOM ARAMIS for the synthetic thigh surrogate have also been compared to FE model predictions. A representative subset of comparison images have been shown in Figure 9.17.

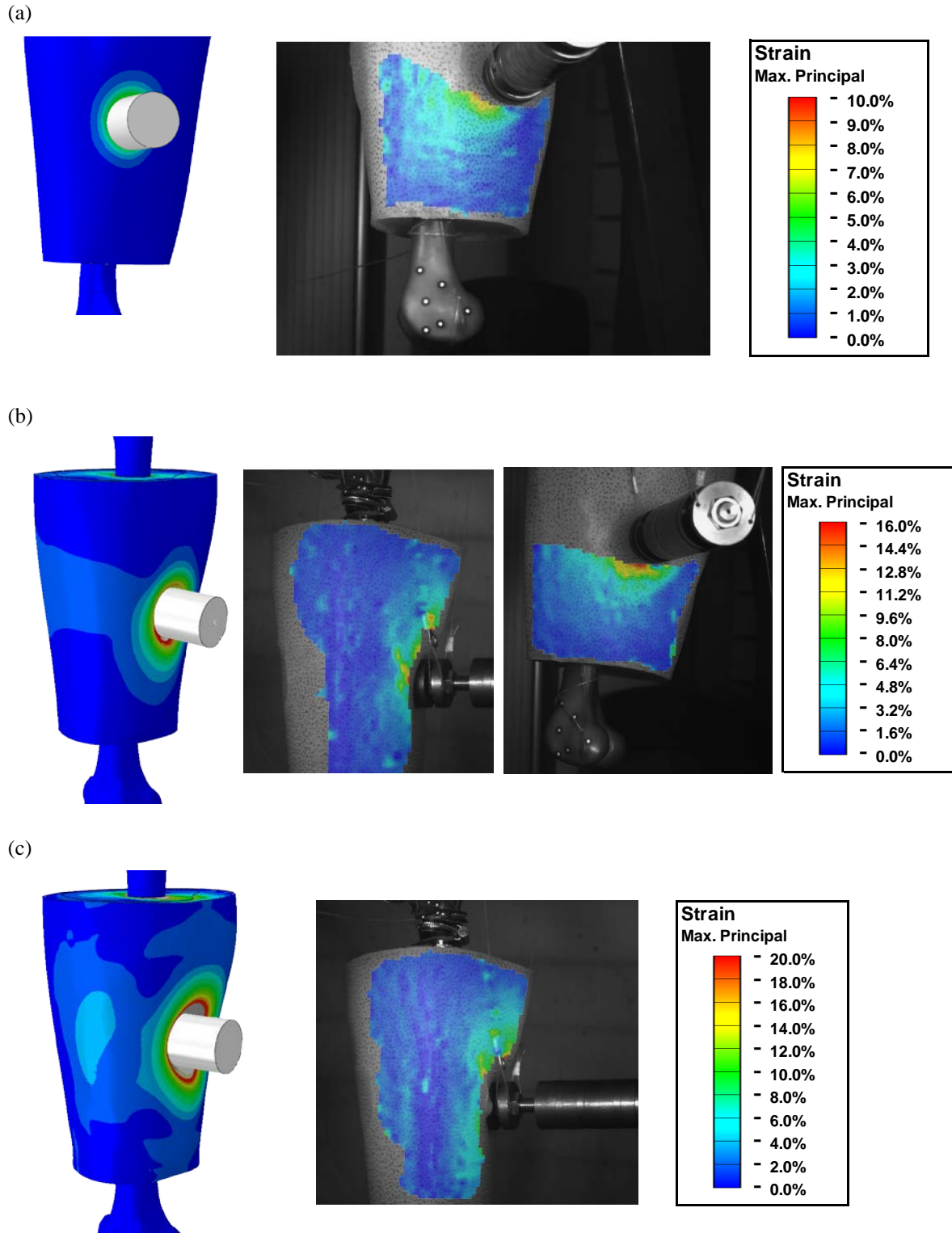


Figure 9.17 – Surface strain images of lateral impacts at x_{max} showing differences in response between GOM ARAMIS data and FE model predictions in (a) 1 m.s^{-1} ; (b) 2 m.s^{-1} ; (c) 3 m.s^{-1} .

At each of the surrogate sampling points (Fig. 9.7), the strain experienced was recorded and has been shown in Table 9.5. Sampling point D was not visible to the GOM ARAMIS cameras in either capture orientation and hence was not available for comparison in any of the trials. Sampling point C was not visible in the 1 m.s⁻¹ anterior impact.

Table 9.5 - Maximum principal strain magnitudes experienced at each sampling point in FE and experimental trials.

Vel. (m.s ⁻¹)	Maximum Principal Strain (%)															
	Experimental Data								FE							
	Anterior				Lateral				Anterior				Lateral			
	A	B	C	D	A	B	C	D	A	B	C	D	A	B	C	D
1	7.23	6.10	-	-	4.53	5.23	3.50	-	2.11	0.69	2.00	0.95	0.97	0.51	1.32	2.51
2	10.8	6.57	9.50	-	9.21	11.5	7.54	-	12.5	7.40	10.3	7.39	11.2	8.43	9.20	6.49
3	14.9	8.56	15.4	-	19.4	16.2	17.4	-	19.8	12.6	19.5	16.6	21.2	17.8	20.9	17.4

A series of graphs were also plotted to show the degree of divergence between FE simulations and experimental data (Fig. 9.18)

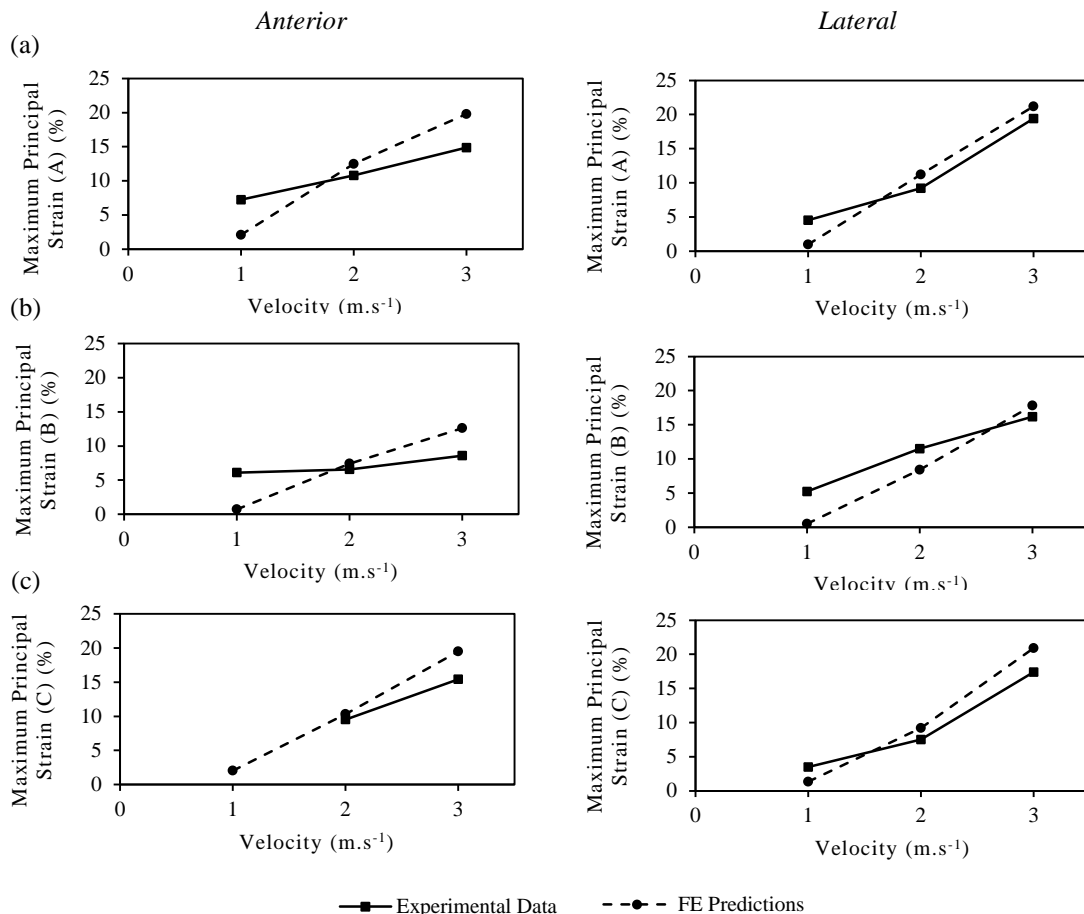


Figure 9.18 - Graphs showing the divergence in response between experimental data and FE model predictions at sampling point: (a) A; (b) B; and (c) C (left: anterior; right: lateral).

Overall, across all sampling points and velocities, there was a mean difference of -14.0% between experimental data and FE model predictions. The graphs show the greatest degree of divergence in 1 m.s⁻¹ impacts in both anterior and lateral directions (-79.8% and -77.0% differences respectively). This was consistent with the findings from both the impact kinematics and acceleration traces which

suggested that the FE model was behaving artificially stiff at these velocities. The extent of this divergence can be clearly seen in Figure 9.17a.

At higher velocities the FE model typically provided a better prediction of the experimental data, though typically exhibited greater magnitudes of strain. Differences were lowest in the 2 m.s^{-1} impacts where there were mean differences of +5.64% and -6.28% between the FE model predictions and experimental data in anterior and lateral impacts respectively. There was a greater divergence at 3 m.s^{-1} with mean differences of +35.6% and +24.3% from the experimental data. This could potentially be attributed to difficulties identifying exact sampling points when the surrogate was more deformed.

9.5. Discussion

9.5.1. Correlation between Experimental Data and FE Model Responses

The FE models generally provided a good prediction of the experimental kinematic responses of the impactor and bone with a maximal deviation from the mean of just 6.86% in all trials excepting 1 m.s^{-1} impacts. At these low impact velocities, there was a greater divergence in skin displacement with -26.7% and -23.1% differences in x_{\max} in lateral and anterior impacts respectively. These lower displacements could potentially be due to the lower strain rates experienced in experimental impacts than what was used to populate the FE material models. These divergences in the 1 m.s^{-1} impacts were also reflected in the surface strain measurements where there was a significantly lower strain magnitude in the 1 m.s^{-1} FE model prediction (min. -77.0% difference).

GOM ARAMIS generally presented a useful measure of experimental strain experienced by the surrogate surface and, ignoring the 1 m.s^{-1} impacts, showed a mean variance of +12.0% with FE models through the sampling points measured (Fig. 9.18). However, the region of interest was obscured by both the suspension supports and impactor and only a partial strain distribution could be attained. These limitations restrict the application of this technique as a primary validation tool but show promise as perhaps a secondary measure verifying similarities in relative strain patterns

In all trials except the 1 m.s^{-1} velocity impacts, the FE models provided a good prediction of impactor decelerations, particularly a_{\max} magnitudes with a maximum deviation of +12.5% from the experimental response corridor (Table 9.3; Table 9.4). In general, the FE models typically predicted greater impact durations than experimental trials (mean +19.1% difference) and a delayed time of peak deceleration (mean +5.53% difference).

The differences reported in a_{\max} were not systematic with simulations both under and over predicting the experimental responses. Therefore, these differences cannot be attributed to errors in the model formulation or constitutive material descriptions. This also excludes the possibility that the divergences could be due calibration errors in the experimental instrumentation which would result in a systematic difference.

Some of these differences could be due to the angular alignment of the impactor. In experimental trials, a uni-axial accelerometer was used, which only measured accelerations perfectly normal to the orientation of the impactor. This means that, in any off centre impacts, a rotational component of acceleration would not have been registered and the magnitude of normal acceleration would have been reduced.

With a greater experimental control afforded by the FE trials, impacts could be aligned normal and perpendicular to the surface and underlying skeletal components. The potential divergences from the surface normal can be estimated through knowledge of the magnitudes of both accelerations. Using mean experimental and FE predicted a_{max} values, trigonometry can be applied to estimate the angle deviation from the surface normal on impact (Fig. 9.19).

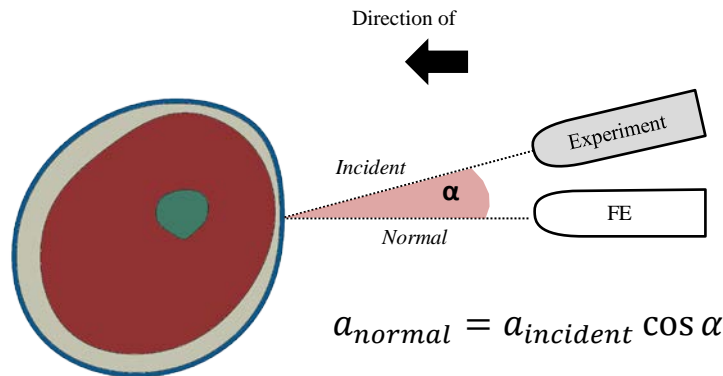


Figure 9.19 – Axial cross-section of the thigh showing the potential error introduced through impactor misalignment.

The differences in acceleration magnitude that could be introduced through these misalignments are shown in Table 9.6.

Table 9.6 - Differences in a_{max} magnitude introduced through angular impactor deviation.

Angular Deviation	Difference in a_{max}
1°	0.015%
5°	0.38%
10°	1.50%
20°	6.00%
30°	18.5%

It is therefore unlikely that the deviation in impactor alignment could account for the 12.5% divergence recorded. Given the experimental control and impactor stability introduced through the wide support impactor suspension method and the quality control enforced throughout the experimental trials, it would be reasonable believe that this could not be greater than 5° (0.38%).

These differences could also be attributed to differences in impact velocity. A comparison between the peak impact accelerations at different velocities is shown in Figure 9.20 and indicates that the a_{max} behaves in a near linear manner with respect to velocity in both impact directions.

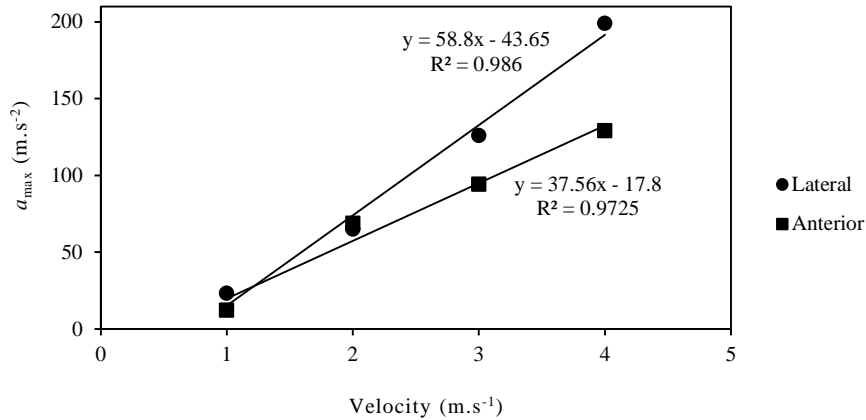


Figure 9.20 - a_{\max} vs. velocity plot for anterior and lateral impacts

Given the standard deviations in experimental impact data (Table 9.7), the differences in a_{\max} can be estimated. Table 9.7 shows estimations of changes in a_{\max} at different impact velocities if the standard deviations in velocities are applied.

Table 9.7 - Estimations of divergences in a_{\max} at different velocities.

Anterior Velocity (m.s ⁻¹)	Potential Error	Lateral Velocity (m.s ⁻¹)	Potential Error
1 (± 0.03)	+69.8%	1 (± 0.02)	-29.9%
2 (± 0.03)	-15.0%	2 (± 0.05)	+18.1%
3 (± 0.05)	+2.61%	3 (± 0.06)	+8.16%
4 (± 0.11)	+5.87%	4 (± 0.09)	-1.08%

Table 9.7 shows that significant divergences in a_{\max} could be introduced through variability in impact velocity. Ignoring the responses at 1 m.s⁻¹ where the linear fit is a poor representation of the experimental data, errors of up to +18.1% could be accounted for through variability in velocities.

These differences in response could also potentially be attributed to variability in impactor alignment in the sagittal planes (Fig. 9.21). Given, the contoured surface of the surrogate thigh, minor deviations in alignment from the surface normal are all possible and could account for some of the differences.

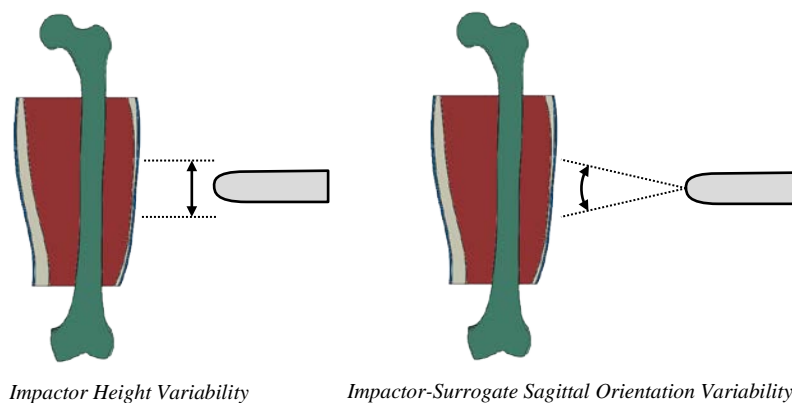


Figure 9.21 - Cross-sectional sagittal plane images showing potential alignment issues introduced in experimental trials,

9.5.2. Test Rig Configuration

The test rig configuration used in this study provided a time-efficient, cost-effective experimental set-up for surrogate impact testing that satisfied each of the requirements stipulated in §3.5. The suspension supports allowed both bodies to be freely suspended and permitted an ease of alignment of both surrogate and impactor bodies. The experimental configuration adopted was also simple, in that it could, and was shown to be, easily replicated in FE model simulations.

The experimental configuration used in this study, however, did embody some simplifications of the actual impact scenarios experienced in sports which could be improved upon. A revised test rig may give greater consideration to the stiffness of the striker element, the levels of constraint for both the target and striker bodies and the abilities of test rig to perform any sports impact ranging from low mass, high velocity projectile impacts to high mass, low velocity human impacts.

In the thigh region, there are constraints present at the hip and knee joint (§2.3.1.f) and influencing masses from the upper body mass and the lower leg. In both defined injury scenarios (Table 3.2; Table 3.3), the thigh segment is freely positioned without any interfering constraints (e.g. turf-stud interactions). It is believed that a more cost-effective and accurate representation of the thigh segment could be achieved through developing a high fidelity thigh region with effective remote inertias (ERIs) and constraints (Fig. 9.22).

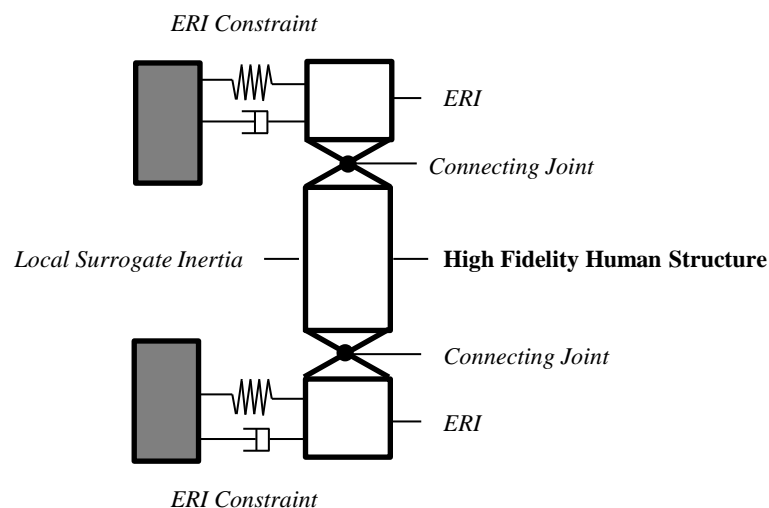


Figure 9.22 – Schematic showing the constraints in the thigh region.

Through estimation of the effective impact energies (defined by Ankrah & Mills (2003)) involved in impacts, an improved simplified representation of the impacts could potentially be achieved using a drop tower test configuration. This approach could be further improved through incorporation of a compliant spring element backing the target or striker surrogates to represent the underlying stiffness of the tissues. This has been adopted in hip protection standards, in which a spring with a stiffness of 47 kN/m and length of 0.37 m backed the striker to represent the response of the pelvis (Robinovitch *et al.*, 2009; Davison *et al.*, 2013).

9.6. Conclusions

The experimental responses of the synthetic surrogate thigh were determined through impact testing. The surrogate was tested in a pendulum impact configuration with the surrogate aligned in both anterior and lateral directions. The experimental responses were compared to parallel FE model predictions and showed comparable responses in acceleration, impactor and bone displacements through all velocities above $1 \text{ m}\cdot\text{s}^{-1}$ where the FE model typically experienced increased magnitudes of acceleration and inhibited impactor displacements. There were also similarities in surface strain patterns between the FE model and experimental data above $1 \text{ m}\cdot\text{s}^{-1}$. The closeness of correlations with synthetic surrogate responses demonstrate the predictive capabilities of the model and indicate that confidence could be placed upon future predictions within these experimental ranges.

Chapter 10 – Discussion, Conclusions and Recommendations for Future Work

10.1. Chapter Overview

The overall research aim and specific research questions established in §1 have been reviewed. Each question has been individually addressed with specific reference to major findings from experimental chapters. The limitations of the presented studies have also been outlined. Finally, the wider implications of the research have been concluded and future work in the research field has been identified with a measure of their importance and recommendations for which parties should be potentially be engaged in such activities.

10.2. Discussion

Prior to this research study, Hrysomallis (2009) presented the only previous investigation of sports injury and PPE effectiveness in the thigh region using human surrogates. A key requirement of this study, established in §3.5, was to produce synthetic and computational surrogates that exceed the biofidelity demonstrated in that study and to establish a method to enable the continued development of improved surrogates. This has been objectively assessed through a comprehensive review of the research questions (§1.4).

Q1. Can Finite Element models be formulated to better inform the development of improved human surrogates?

FE models have demonstrated practical uses as a design tool throughout this research study. The ease of model formulation has permitted investigation of many permutations of different variables relating to surrogate design. This has perhaps been best demonstrated in §4 where FE models were used to evaluate the relative importance of different organic tissue layers in a simplified geometry. Although there were many simplifications to the actual target human thigh segment (e.g. materials, geometries, contact), the models provided merit as a design tool to investigate the relative benefits of tissue structures in this configuration.

In §6, the predictive merit of the FE models were initially established through a closed loop validation study. The FE models were able to provide a good correlation with the synthetic surrogate in both cricket ball and knee impact conditions demonstrating their predictive capabilities. This was also shown in §9, where the full anatomically contoured FE model exhibited comparable responses to the synthetic surrogate thigh under representative knee impact conditions. In addition, open loop predictive studies have been used to show the relative differences between different design features. In §6, this was applied to show the relative differences in impact response of identical surrogates with different material properties, whilst in §7, this was applied to show the differences in surrogate response through different geometries when identical material models were used.

Furthermore, the superior measurement capabilities introduced by FE models (e.g. continuous stress profiles) means that individual elements of surrogate or PPE design can be assessed without affecting the biofidelity of the bodies. This has been successfully shown, to a greater level than what could be achieved in synthetic surrogates, in the PPE evaluations conducted (§7.7).

Q2. Can durable, biofidelic human soft tissue simulants be fabricated using materials that exhibit a consistent impact response?

Silicones have been previously used in impact surrogates due to their consistent, repeatable, durable responses. PDMS soft tissue simulants were developed for skin, contracted muscle, relaxed muscle and adipose tissues. The simulants each exhibited an improved response individually in standardised materials tests and when combined in FE simulations compared to previously used single material simulants.

Compressive mechanical tests were performed to attempt to match the isotropic response of the PDMS silicones to a specific *in vitro* organic tissue dataset. The simulants were matched to experimental data under quasi-static loading conditions and all, excepting skin, exhibited responses within 250% of the respective datasets across each strain increments. All simulants, however, exhibited a different stress response to organic tissues whereby they experienced greater stresses at low strains and a less significant strain hardening effect at higher strains. The PDMS simulants did, however, provide a significantly improved response when compared to single material simulant, Silastic 3483, which exhibited a 410%, 5860% and 323% greater divergence than PDMS simulants when compared to organic tissue datasets at 0.3 strain in relaxed muscle, adipose and skin tissues respectively. The responses at increased strain rates, more representative of sports impacts, showed a greater divergence from the target datasets. In all simulants excepting skin the PDMS simulants typically exhibited an increased stiffness when compared to organic tissues at these rates. This was particularly notable in the PDMS adipose tissue simulant.

In cylindrical geometries (§6), the impact responses of the surrogates showed that the PDMS soft tissue simulant constructions exhibited a better representation of organic tissue surrogate predictions than previously-used single material simulants, particularly other silicones. Under both cricket ball and knee impact conditions the PDMS simulants showed an improved composite response through more representative top surface displacements (max. difference -4.82%) and deep tissue pressures as well as more representative layer responses through more comparable tissue layer surface displacements and stresses.

The most significant differences between the developed PDMS silicones and organic tissue predictions were under higher strain rate cricket ball impact conditions. This was expected due to the differences in mechanical response under the standardised compressive specimen tests and could be expected to increase if the surrogates were simulated under higher rate impact conditions (e.g. cricket ball impact at 40ms^{-1}) with PDMS simulants and organic tissues characterised under comparable associated high rate impact conditions.

Q3. Is a significant difference in surrogate response elicited in more anatomically complex geometries?

The geometries used in impact surrogates range from very primitive cylindrical pucks to much more complex human-shaped structures. In §7, FE models were formulated to investigate the importance of different aspects of surrogate shape on the impact response. The responses under both cricket ball and knee impact simulations, initially, showed the need for curved outer tissue geometries as the flat puck surrogates experienced lower x_{\max} (min. difference -8.75%) and $P_{\text{base,max}}$ (min -9.45% difference) than curved surrogates. The study also showed significant differences in response dependent on the soft tissue radii of curvature indicating the importance of bone proximity relative to the outer surrogate surface (min. +20.1% difference between 50 and 75 mm surrogates). These findings highlight the necessity to develop surrogates to match the geometries of the specific region of interest in order to elicit a more representative impact response.

There was typically a smaller difference in response exhibited between the shaped anvil and cylinder surrogates across both loading conditions. Therefore, if there is an overwhelming requirement for mounted drop tower surrogates, it is recommended that this surrogate embodies, as closely as possible, soft tissue thicknesses and radii of curvature of the target body region. This could be effectively achieved using a shaped anvil type surrogate configuration to generate a more representative segment response than puck type surrogates.

However, the responses of the anatomical contoured surrogate showed a clear location dependent response between anterior, posterior and lateral impact directions. A superior thigh shaped surrogate would permit testing of PPE in each of these impact directions as opposed to approximating the response of all through a single radius of curvature.

Q4. To what extent do different human soft tissue structures influence impact response?

In §4, FE models were formulated using organic hyperelastic and viscoelastic material models to describe the behaviour of skin, adipose, relaxed muscle and bone tissues. A study was performed to predict the effects of skin and adipose tissues in a cylinder surrogate when subject to representative cricket ball and knee impact conditions. The presence of both skin and adipose tissues clearly demonstrated a significant effect on the mechanical impact response of human surrogates in both the overall composite responses and layer effects. Notably, the skin layer introduced increased surface stresses with 787% and 476% differences from the muscle-only surrogate for cricket ball and knee impacts respectively, whilst the adipose layer introduced increased top surface displacements in both impact conditions (mean. +6.38% difference). These layer effects were also observed in the surrogate material comparison in §6.7. There was a notable difference in stresses and tissue displacements between the layered organic and PDMS surrogates and the single material simulant surrogates.

These structures can influence both measures of PPE effectiveness and injury causation. For example, deep tissue injuries such as contusions may be poorly predicted when using single material surrogates where load transfer phenomena differ due to the presence of skin and adipose layers. In addition, most studies evaluating stresses or strains in surrogates have typically used surface pressure sensors; these sensors could potentially underestimate the surface stresses when using single material surrogates without a specific skin layer.

Q5. Given thorough consideration of kinetic and kinematic impact parameters of specific injury scenarios, can bespoke reconstructions provide the basis for more realistic PPE evaluations?

The PPE impact evaluations conducted in safety standards are not typically representative of the impacts experienced in play. The potential degrees of divergence in kinetic energy and momentum between safety standards and actual ‘in play’ impacts were explored in §2.2.3.b. The DCS model presented in §3 provided a comprehensive systematic method of describing the kinetics and kinematics pertaining to a particular impact scenario. This model and its subsequent applications were used to determine more representative impact parameters for cricket ball (0.16 kg, 10 m.s⁻¹) and knee (3 kg, 3 m.s⁻¹) impacts.

Most safety standards evaluations of sports PPE typically use impact parameters similar to those established for the knee impact even when they are concerned with projectile impacts. Given the differences in response measured between cricket ball and knee impacts in representative surrogates (e.g. 33.8% difference in x_{\max} in organic cylinder surrogate), the sports safety standards will unquestionably provide a poor representation of projectile impacts that could be improved through better consideration of gameplay impact kinematics.

Q6. Can human impact surrogates be developed at an affordable cost when compared to previous surrogates?

The judgement of whether the surrogate is cost-effective is largely subjective and dependent on the application context. When the cost of not adequately showing the benefits of the surrogate (e.g. more representative tissue deformations) are higher than the surrogate cost it becomes cost-effective. For example, sporting goods manufacturers may inadequately evaluate the protective capabilities of a piece of PPE to be produced in large volumes if a simple surrogate is chosen instead.

The value of virtual FE surrogates in sports impact research has been addressed in Q1. Validated FE models provide a tool from which PPE can be assessed more cost effectively than having to develop physical prototypes reducing the number of necessary design iterations. However, the sporting goods industry requires physical testing of PPE prior to product launch and subsequent human use due to the inevitable inaccuracies introduced in the virtual modelling of PPE. Therefore, it is believed that synthetic impact surrogates will always be required.

The complete costing for a single human thigh impact surrogate indicated that the improved surrogate incurred a significantly increased financial burden when compared to existing standardised test surrogates. The total surrogate cost was £2,451.17 compared to approximately £240 estimated for a rigid surrogate (§8.4.4). These one-off manufacturing costs are not insignificant but also not unaffordably expensive, especially when compared to existing commercial surrogate products such as the Hybrid III crash test dummy (§2.4.2.a) which cost an estimated £4000 for a thigh segment (based on a total cost of \$35,000). When manufacturing in larger volumes, the surrogate production costs significantly reduced as tooling costs become shared (§8.3.4). Considering a 50 surrogate production run, the cost of PDMS surrogate manufacture was £397. When compared to the Hybrid III surrogate estimates, this is approximately 10× less expensive and exhibits a greater biofidelity for sports impacts.

Despite the increased cost of the improved surrogate compared to rigid anvils, standardised test facilities could offer a superior service using more biofidelic surrogates and hence command a higher fee per PPE test. Existing testing houses charge approximately £3,000 - £5,000 for each piece of PPE.

It is estimated that for just an additional £200 a significantly improved service could be offered, therefore if just a single thigh can be used per test this is < 10% of the costs. A series of high profile injuries and mounting public pressure for improved PPE could also lead to a legislative call for improved standardised tests and consequently improved surrogates.

There are many stakeholders in the development of PPE who could potentially influence the adoption of improved human surrogates. The participants of the sport, particularly at an elite level, may demand superior PPE to either enhance safety or performance of the protection in use. Both of these goals could be achieved using improved human surrogates. Similarly, the coaches and clubs who own players may demand improved PPE to reduce the likelihood of their missing important competition. An elite level sports person can be paid up to £400,000 per week; there is a significant financial burden to clubs and sponsors if players are unable to play. There is also a financial burden to society from recreational players becoming injured resulting in days off work and cost to employers. The surrogates may also be purchased by sporting goods manufacturers to improve their understanding of their own PPE through in-house tests.

Q7. Can the developed surrogates provide a better understanding of injury causation and PPE effectiveness?

In §7, FE models were used to investigate the differences in PPE-surrogate interactions through a range of impact surrogate types under cricket ball and knee impact conditions. The anatomically contoured surrogate was the only surrogate which conformed well and provided a good fit for the shell PPE. All other surrogate shapes experienced isolated regions of high stress at the edges of the PPE. The shell PPE resulted in lower impactor penetration (mean +370% difference), wider pressure distribution and lower peak bone stresses (mean -175% difference) than the foam PPE in the anatomically contoured surrogate. This illustrates the importance of an anatomically shaped soft tissue surrogate in assessing the effectiveness of PPE. This could potentially lead to the development of person-specific PPE, particularly in elite level sports competition where there are fewer financial constraints.

There is currently no consensus opinion on mechanical phenomena required to elicit soft tissue injuries (§2.2.2). Whilst the developed anatomical surrogates do not directly improve our understanding of the causal factors pertaining to injuries, they offer a more representative interface from which to further explore these effects. The developed surrogate has incrementally adopted important additional elements of human complexity from previous surrogates and as such should provide a more biofidelic impact response. For example, a significant difference was observed in surrogates with multiple soft tissue layers in §6. These differences could affect measurements on the surrogate surface (e.g. pressure sensors on skin) and deep tissue (e.g. strain gauges, load cells on bone) and their subsequent predictions of injury causation. The anatomically contoured thigh surrogates developed in §7, §8 and §9 indicated differences in response based on impact location due to the presence of different tissue types and thicknesses. These structures are present in this form in actual humans and as such it could be inferred, to a reasonable degree of confidence, that this represents a better prediction of human response.

10.3. Limitations of Study and Recommendations for Future Work

10.3.1. Diversity and Range of Tissue Structures

The organic tissue structures considered within this research study (bone, muscle, adipose, skin) were shown to contribute significantly to impact response. There are, however, many other tissue structures which were not explicitly considered in this study. It is hypothesised that, of these other tissues, modelling the individual muscles, muscle compartments and tendons could elicit the most significant differences in response. In addition, the fascia surrounding the individual muscles consist of a thick sheath of connective tissue which could represent an area for future study.

Furthermore, a greater diversity of skin layers (e.g. hypodermis and stratum corneum) as well as vascular and nerve tissues could influence the mechanical behaviour of the surrogates and merit some further consideration. For example, Geerligs (2010) stated that the hypodermis has a function in the body to protect from mechanical shocks. Some previous research surrogates have considered these additional tissue structures. For example, Davison *et al.* (2013) modelled hypodermis and dermis layers in a hip surrogate for assessing impact protectors.

It is recommended that further activity in this area will be conducted by research and concerns medical, automotive, military and sports domains. It is suggested that for cost-effective analysis this research will be conducted using FE tools.

10.3.2. Organic Soft Tissue Characterisation

Organic soft tissue characterisation, particularly human tissue, represents a key area for future work in this area. Most previous studies have examined the mechanical properties of *in vitro* tissue specimens from porcine or bovine sources. The mechanical behaviour of tissues *in vitro* are likely to differ significantly from *in vivo* due to the shortened/discrete nature of specimens and lack of physiological and neurological activity making specimens atonal. Animal sources, despite providing good analogues do not exactly replicate human mechanical response. For example, Balaraman *et al.* (2012) noted that human muscle tissue exhibited stiffer responses than porcine tissues. Future research activity in this area should focus on increasing the understanding of *in vivo* human mechanical response.

Target datasets were all obtained from compressive test specimens tested in the cross-fibre direction. Whilst this is pertinent to blunt force trauma in the normal direction in fleshy regions of the body, characterisations could be improved through consideration of the mechanical behaviour in other loading directions. This is potentially particularly relevant to skin tissue which exhibits known tensile responses to impact. A recent study by Ottenio *et al.* (2015) has presented tensile test data on human skin at sports impact relevant strain rates. Although this data was unavailable at the inception of the study, it could be used in future surrogates to generate more representative simulants and material models.

The effects of muscle contraction are pertinent in some sports applications (e.g. when the player is anticipating the impact). Dynamic human FE models have attempted to represent muscle contraction effects (e.g. Teran *et al.*, 2005; Lemos *et al.*, 2005), however this has been reported to be challenging, particularly due to the increased computational expenditure. Nevertheless the differences in mechanical properties at varying levels of muscle contraction represent an important area of future work.

Many previous studies have also only focussed on quasi-static or low strain rate mechanical behaviour of tissues. Organic tissues typically exhibit greatly anisotropic, non-linear and strain rate dependent mechanical responses. To fully understand their behaviour it is necessary to characterise the tissues through the full strain rate range of their expected application. There is currently a paucity of information on the mechanical response of organic tissues at intermediate strain rates ($50 - 500 \text{ s}^{-1}$) representative of many sports impacts. Future research should consider characterisation at these strain rates in order to adequately populate material models and associated computational surrogates. Similarly, the viscoelastic behaviour of organic tissues must be better understood under dynamic impact conditions.

Significant variability has been exhibited between current characterisation studies based on factors related to the species type, specimen location and mechanical testing conditions. Therefore, all studies will present an entirely individualised representation of the particular tissue. Consequently, it is important that surrogate studies that consider the behaviour of organic tissues select particular datasets from the most representative species, demographics, specimen locations and strain rates for their respective impact applications.

10.3.3. Synthetic Soft Tissue Materials

The PDMS synthetic soft tissues developed for skin, adipose and muscle tissues provided an improved representation of organic tissue behaviour compared to previously used single material simulants. The simulants, however, only attempted to match the isotropic behaviour of the organic tissues through compressive behaviour in a single loading mode (compressive). A consideration of the anisotropic mechanical properties of organic tissues would represent a key future research area for improved simulant materials, particularly skin and muscle tissues. This could be achieved through development of simulants to match organic tissue properties for the respective strain rate range of their applications or through reinforcement matrix techniques. Reinforcement matrices have been attempted previously through electrospinning and textile processing techniques where a reinforcement fibre matrix has been introduced to artificially stiffen simulant materials. This is an approach that could be used in combination with the existing PDMS simulant formulations to elicit more biofidelic impact response.

10.3.4. Constitutive Modelling

The material models used to describe the organic tissues offer a simplification of their actual mechanical behaviour and responses typically provide a partial description of the actual responses. The hyperelastic and viscoelastic material models used provide a description of the non-linear compressive responses from a single strain rate loading curve and time-dependent behaviour under quasi-static loading conditions. These models were capable of providing an acceptable approximation of experimental impact response under the low strain rate knee impact condition but showed a greater divergence under the higher rate cricket ball impact, exhibiting increased stiffness and requiring optimisation.

The only viscoelastic material model built in and compatible with the Abaqus/Explicit solver is the Prony series which is a QLV model. A key assumption of this model is that shear modulus is independent of strain level. This is not necessarily satisfied in elastomers or organic soft tissues. There is a need for improved modelling capabilities to predict the dynamic elastic and viscous response of these materials

Similarly, the hyperelastic models present in the software only enables modelling of an experimental dataset at a single strain rate. Improved material models such as the Bergström-Boyce model potentially offer a solution and present capabilities in modelling elastomers through a range of strain rates. However, the absence of such models in Abaqus/Explicit solver is problematic. Future improvements in this area could be in enhanced elastomer modelling capabilities to enable superior predictive capabilities.

10.3.5. Geometric Representation of External and Internal Tissue Structures

Improvements in the capabilities of imaging technologies such as CT and MRI scans and their accessibility have enabled higher quality and more cost-effective geometric descriptions of human tissues. The dataset sampled in this research study was from the VHP which is an anatomical dataset from a 180 cm, 90.2 kg sedentary male. This dataset is not representative of an athletic demographic likely to sustain the sports impacts. Future improved human impact surrogates would ideally select the data from a directly representative sample (e.g. rugby players for rugby tackle impacts).

The manner in which the data were sampled for the impact surrogate provided a simplified representation of both internal and external geometries. This enabled a greater ease of manufacture in the first instance, however given the success shown through the presented manufacturing techniques, future work may consider use of more representative sampling techniques. Through use of commercial software such as Mimics® (Materialise, Leuven, Belgium) imaging data can be sampled automatically using algorithms in the software. This can enable an enhanced description of internal and external tissue geometries. Similarly, companies such as Simpleware (Simpleware Ltd., Exeter, UK) provide a service in which scan geometries are sampled, constructed and meshed for clients. Use of such companies could also present an area of improvement for the research.

10.3.6. Measurement and Injury Evaluation

The two primary applications of impact surrogates in injury biomechanics research are in the evaluation of PPE and the prediction of impact injuries. There is currently a paucity in knowledge of the direct mechanical causal factors pertaining to common impact injuries, particularly contusions and lacerations from blunt force trauma. Further work is required to better understand these factors and relate them to measurable mechanical response phenomena (i.e. magnitudes of stresses and strains). This would greatly enhance the potential of impact surrogates and enable superior specific designs of PPE to protect against particular injury modes.

The measurement capabilities of impact surrogates are currently somewhat limited. They typically either provide an indirect measure of the mechanical response phenomena occurring (e.g. video) or introduce foreign bodies and artificial stresses within the surrogate (e.g. pressure sensors). Elastomeric sensors present a potential method of measuring the mechanical response phenomena within impact surrogates without significantly affecting the biofidelity of the tissue simulants. Future advancements in this area could enable calibrated measurement tools for strain and pressure at various positions within the surrogate. Elastomeric sensors have been developed by Danfoss (Danfoss, Nordborg, Denmark), however lack sufficient temporal resolution to be used in dynamic impact events; though still offer potential in this field. Research studies have also developed elastomeric sensors (e.g. Mattman *et al.*, 2008) and are likely to contribute significantly to future enhancements in this area.

Further advancements could also be made through non-invasive imaging based techniques. For example, Moerman *et al.* (2011) used sequenced MRI data based on spatial modulation of magnetism

(SPAMM) of *in vivo* non-invasively measured quasi-static 3D soft tissue deformations. The study was conducted on a silicone soft tissue phantom of a human upper arm and demonstrated that, through six acquisitions, validated quasi-static measurements could be achieved with a mean subvoxel displacement difference of 72 μm between experimental data.

The application for these techniques in human surrogate research is potentially substantial and could enable more accurate determination of *in vivo* tissue properties and measurement of synthetic surrogate responses. However, as yet, the techniques have only been validated under quasi-static strain rates. In addition, the processes are very resource intensive and, in most cases, require a medical facility to perform.

10.3.7. Human Impact Testing

Although the FEA simulations conducted predicted that the developed synthetic human surrogate behaved in a similar manner to organic tissues, in order to truly evaluate the biofidelity of the surrogate, it is necessary to compare the impact responses with real humans. Ideally, tests would be conducted on a group of humans with representative anthropometrics to the VHP, particularly in the thigh region. The tests could potentially be ethically conducted at low impact intensities using the techniques established in §9.3.1 in a similar manner to Muggenthaler *et al.* (2008).

10.3.8. Safety Standards

The current safety standards for sports PPE embody many flaws which detract from their usefulness in understanding the protective capabilities of PPE. The rigid surrogates used and unrepresentative surface geometries have been shown to introduce inaccuracies in PPE pressure distribution and load transfer when compared to a more representative impact surrogate (§7.7). Similarly, the fixed impact test rig constraints used are not representative of the scenarios in which the participants commonly sustain impact injuries. The kinematic data used in safety standard impact trials were also shown to be unrepresentative of common impacts within the sport (§2.2.3.b).

Future work by standards institutions such as the BSI should consider improved surrogates, which represent the key soft tissue structures outlined. Improved test methods may also consider test rig designs similar to the universal impact rig previously proposed (§9.5.2) and provide a more accurate consideration of the kinematics of specific sports impacts to enable superior assessment of sports PPE.

10.4. Conclusions

The research aim formulated in §1 was “to establish a method to enable the development of superior, complementary, increasingly complex synthetic and computational surrogates for improved assessment of sports personal protective equipment”. This research study presented a method, using parallel synthetic and computational models, to systematically investigate each constitutive human surrogate component. The study successfully demonstrates the potential of using these techniques to produce surrogates that can provide an improved assessment of the effectiveness of sports PPE.

This was achieved, firstly, through a detailed review of the components of a sports impact assessment and the formulation and practical usage of a conceptual impact injury model to describe specific impact injuries to the thigh region. This model enabled a structured and detailed consideration of the improved impact assessment specifications and surrogate design approach.

Three key elements were identified as being integral to improved sports impact surrogates: consideration to the tissue structures, simulant materials and geometries. FE models were used as a design tool to evaluate the relative differences in surrogate response. This was first applied to determine the importance of surrogate tissue layers. Differences in surrogate response were observed with a skin tissue layer present due to the increased skin outer surface stresses and reduced surface displacements induced. The importance of an adipose layer was shown through increased surface displacements and a more rapid rate of layer displacement when this tissue structure was present.

FE models were further applied as a design tool to determine the relative differences in surrogate impact response across surrogate shapes. The study showed that puck surrogates with a flat outer surface significantly underestimated surrogate displacements and layer stresses. Large differences were also shown between surrogates with different radii of soft tissue curvature with the greatest variation in response between 50 mm and 75 mm surrogates. An anatomically contoured thigh surrogate was fabricated and predicted differences in response dependent on the orientation of the surrogate on impact based on the underlying tissue thicknesses and compositions. This indicated the importance of a representative contoured surrogate with local changes in tissue thickness representative of the target impact region.

Further benefits of this geometry were shown through a PPE evaluation study in which a rigid shell and foam PPE were assessed on simple surrogates. The soft foam padding exhibited a good fit with all surrogate types; however, the rigid shell PPE failed to form to the surrogate outer surface of the simple surrogates and caused areas of isolated high stress concentrations on the surrogate surface. The rigid shell PPE type was shown to be most protective against the cricket ball and knee impacts when modelled in an anatomically contoured geometry. However, each simple surrogate significantly overestimated the magnitudes of surrogate deformation when modelling the shell PPE type demonstrating their inadequacies for these evaluations.

Novel synthetic soft tissue simulants were formulated using bespoke blends of PDMS soft tissue simulants to match the dynamic responses of specific organic tissue datasets for skin, adipose, contracted and relaxed muscle tissues. The study showed that the PDMS simulants exhibited comparable responses at quasi-static strain rates in all tissues but the skin. The responses of the simulants were significantly closer to the organic tissue dataset than could be attained through using a single soft tissue simulant. This was shown in comparisons with Silastic 3483 which exhibited +324%, +11,140% and -15.8% greater differences greater divergence than PDMS simulants when compared to organic tissue datasets at 0.3 strain in relaxed muscle, adipose and skin tissues respectively.

These simulants were fabricated into two synthetic surrogates used at different stages of the research. Firstly, as a validation tool in simple experimental drop test validations to establish the impact response of the surrogates and validate FE models and, finally, in the full-scale anatomically contoured synthetic thigh surrogate.

The simple puck surrogate experimental drop tests were used to validate the responses of a series of previously used synthetic soft tissue simulants to enable open loop predictive simulations to be conducted with greater confidence. The validated FE models were used to show the benefits of the PDMS formulations when compared to previously used single material simulants. The surrogates showed a closer response to organic tissue predictions through all impact types and evaluation metrics than silicone elastomers and ballistic gelatin.

The synthetic thigh represented the ultimate level of complexity considered in this research study and was based on the important tissue structures, materials and geometries established previously. The surrogate was fabricated using a novel multi-material moulding process to ensure PDMS simulants of varying stiffness, work time, viscosity and tissue thickness could be formed in a single shot, contoured surrogate mould. A key design feature of these moulds that enabled surrogate manufacture was the use of a sacrificial gelatin core, which was used to provide a dummy surface that formed a temporary cavity for the thin (3 mm) skin layer. The resultant PDMS thigh surrogate provided a geometrically accurate test structure with representative tissue thicknesses.

The synthetic surrogate thigh was tested experimentally through a series of impact tests in anterior and lateral surrogate orientations. The surrogate exhibited an expected increase in magnitudes of impactor acceleration, skin and bone displacement at increasing impact velocities. The responses of the parallel FE thigh model were compared to experimental impact data and showed good correlations in all impacts excepting 1 m.s^{-1} trials with a maximum divergences of +6.86% and +12.5% in impactor displacement and peak acceleration respectively across all trials. The FE models also showed a good correlation with surface strain data generated using GOM ARAMIS DIC techniques with a mean variance, ignoring 1 m.s^{-1} impacts, of only 13.3%.

The total cost of the PDMS soft tissue surrogate was £2,451. Considering the reduced tooling costs distributed through increased production runs, the cost per surrogate is estimated to reduce to £397 in a production run of 50 units. The PDMS surrogate is still £246 more expensive than the cost of an identically sized Silastic 3483 surrogate and £156 more expensive than estimates of a rigid anvil, though offers significantly greater biofidelity.

Reference List

- AA. 2013. *Crash Test Dummies: Meet the Family*. [online]. Available at: http://www.theaa.com/motoring_advice/euroncap/dummies.html> Accessed on: 22nd April 2014.
- ABAQUS. 2014. *Abaqus Documentation*. Dassault Systèmes Simulia Corp: Providence, RI, USA.
- Ackerman, M.J. 1998. The visible human project. *Proceedings of the IEEE*; 86 (3), pp. 504-511. DOI: 10.1109/5.662875.
- Adharapurapu, R.R., Jiang, F. and Vecchio, K.S. 2006. Dynamic fracture of bovine bone. *Materials Science and Engineering: C*; 26 (8), pp. 1325-1332. DOI: 10.1016/j.msec.2005.08.008.
- Agel, J., Evans, T.A., Dick, R., Putukian, M. and Marshall, S.W. 2007. Descriptive epidemiology of collegiate men's soccer injuries: National Collegiate Athletic Association Injury Surveillance System, 1988–1989 through 2002–2003. *Journal of Athletic Training*; 42 (2), pp. 270-277.
- Ahmed, E.M. 2013. Hydrogel: Preparation, characterization, and applications. *Journal of Advanced Research*; 6 (2), pp. 105-121. DOI: 10.1016/j.jare.2013.07.006.
- Akkus, O., Oguz, A., Uzunlulu, M. and Kizilgul, M. 2012. Evaluation of skin and subcutaneous adipose tissue thickness for optimal insulin injection. *Journal of Diabetes & Metabolism*; 3 (8), pp. 216. DOI: 10.4172/2155-6156.1000216.
- Al Nazer, R. 2008. *Flexible Multibody Simulation Approach in the Dynamic Analysis of Bone Strains During Physical Activity*, PhD Thesis. Lappeenranta University of Technology, Finland.
- Alaoui, A.H., Woignier, T., Scherer, G.W. and Phalippou, J. 2008. Comparison between flexural and uniaxial compression tests to measure the elastic modulus of silica aerogel. *Journal of Non-Crystalline Solids*; 354 (40), pp. 4556-4561. DOI: 10.1016/j.jnoncrysol.2008.06.014.
- Albright, A.L. and Stern, J.S. 1998. Adipose tissue. *Encyclopedia of Sports Medicine and Science*, Internet Society for Sport Science.
- Alexander, R. 2004. Bipedal animals, and their differences from humans. *Journal of Anatomy*; 204 (5), pp. 321-330. DOI: 10.1111/j.0021-8782.2004.00289.x.
- Ali, A., Fouladi, M.H. and Sahari, B. 2010. A review of constitutive models for rubber-like materials. *American Journal of Engineering and Applied Sciences*; 3 (1), pp. 232-239. DOI: 10.3844/ajeassp.2010.232.239.
- Alkhouli, N., Mansfield, J., Green, E., Bell, J., Knight, B., Liversedge, N., Tham, J.C., Welbourn, R., Shore, A.C., Kos, K. and Winlove, C.P. 2013. The mechanical properties of human adipose tissues and their relationships to the structure and composition of the extracellular matrix. *Am J Physiol Endocrinol Metab.*; 305 (12), pp. E1427-35. DOI: 10.1152/ajpendo.00111.2013.
- Ambrósio, J.A.C., Pereira, M.F.O.S. and da Silva, F.P. 1997. *Crashworthiness of transportation systems: structural impact and occupant protection*. Kluwer Academic Pub: Tróia, Portugal.
- Animal Welfare Act. 2006. *Animal Welfare Act 2006 (c.45) (Act of Parliament)*. London: HMSO: Great Britain Parliament;
- Ankersen, J., Birkbeck, A., Thomson, R. and Vanezis, P. 1999. Puncture resistance and tensile strength of skin simulants. *Proceedings of the Institution of Mechanical Engineers, Part H: Journal of Engineering in Medicine*; 213 (6), pp. 493-501. DOI: 10.1243/0954411991535103.
- Ankrah, S. and Mills, N. 2003. Performance of football shin guards for direct stud impacts. *Sports Engineering*; 6 (4), pp. 207-219. DOI: 10.1007/BF02844024.
- Ankrah, S. and Mills, N. 2004. Analysis of ankle protection in Association football. *Sports Engineering*; 7 (1), pp. 41-52. DOI: 10.1007/BF02843972.
- Arbogast, K.B., Thibault, K.L., Pinheiro, B.S., Winey, K.I. and Margulies, S.S. 1997. A high-frequency shear device for testing soft biological tissues. *Journal of Biomechanics*; 30 (7), pp. 757-759. DOI: 10.1016/S0021-9290(97)00023-7.

- Arensdorf, S.C. and Tobergte, E.H. 2012. Athletic Protective Padding. Stromgren Athletics Inc., *United States Patent*. US 8272073 B2.
- Ashman, R.B. and Rho, J.Y. 1988. Elastic modulus of trabecular bone material. *Journal of Biomechanics*; 21 (3), pp. 177-181. DOI: 10.1016/0021-9290(88)90167-4.
- Assassi, L., Charbonnier, C., Schmid, J., Volino, P. and Magnenat-Thalmann, N. 2009. From MRI to anatomical simulation of the hip joint. *Computer Animation and Virtual Worlds*; 20 (1), pp. 53-66. DOI: 10.1002/cav.266.
- ASTM D1349. 2009. *Standard Practice for Rubber-Standard Temperatures for Testing*. ASTM International: West Conshohocken, PA.
- ASTM D395. 2008. *Standard Test Methods for Rubber Property—Compression Set*. ASTM International,: West Conshohocken, PA.
- ASTM D6417. 2014. *Standard Test Method for Vulcanised Rubber and Thermoplastic Elastomer - Determination of Force Decay (Stress Relaxation) in Compression*. West Conshohocken, PA: ASTM International.
- Avon, S. and Wood, R. 2005. Porcine skin as an *in vivo* model for ageing of human bite marks. *J Forensic Odontostomatol*; 23 (2), pp. 30-39.
- Azar, F.S., Metaxas, D.N. and Schnall, M.D. 2002. Methods for modeling and predicting mechanical deformations of the breast under external perturbations. *Medical Image Analysis*; 6 (1), pp. 1-27. DOI: 10.1016/S1361-8415(01)00053-6.
- Backaitis, S.H. and Mertz, H.J. 1993. *Hybrid III: The first human-like crash test dummy*. 1st ed. Society of Automotive Engineers: Warrendale, PA.
- Bahr, R. and Krosshaug, T. 2005. Understanding injury mechanisms: a key component of preventing injuries in sport. *British Journal of Sports Medicine*; 39 (6), pp. 324-329. DOI: 10.1136/bjsm.2005.018341.
- Bahr, R. and Mæhlum, S. 2004. *General injury prevention measures*. Human Kinetics: Hong Kong.
- Bailly, L., Toungara, M., Orgéas, L., Bertrand, E., Deplano, V. and Geindreau, C. 2014. In-plane mechanics of soft architected fibre-reinforced silicone rubber membranes. *Journal of the Mechanical Behavior of Biomedical Materials*; 40, pp. 339-353. DOI: 10.1016/j.jmbbm.2014.09.012.
- Balaraman, K., Mukherjee, S., Chawla, A. and Malhotra, R. 2012. Dynamic Compressive Response of Human Passive Muscle using Split Hopkinson Pressure Bar. *Indian Journal of Biomechanics*; 3 (1-2).
- Banks, S. and Hodge, W. 2004. Design and activity dependence of kinematics in fixed and mobile-bearing knee arthroplasties. *J Arthroplasty*; 19 (7), pp. 809-816. DOI: 10.1016/j.arth.2004.04.011.
- Barclays. 2005. *Survey Reveals Sporting Injury rate in the UK*. [online]. Available at: <<http://www.personal.barclays.co.uk/BRC1/jsp/brcontrol?task=popup1group&value=11147&target=blank&site=pfs>> Accessed on: August 22nd 2012.
- Basdogan, C. 2012. Dynamic material properties of human and animal livers. *Soft Tissue Biomechanical Modeling for Computer Assisted Surgery*, Berlin Heidelberg: Springer, pp. 229-241.
- Bathgate, A., Best, J., Craig, G. and Jamieson, M. 2002. A prospective study of injuries to elite Australian rugby union players. *British Journal of Sports Medicine*; 36 (4), pp. 265-269. DOI: 10.1136/bjsm.36.4.265.
- BCC Research. 2013. *Protective Sports Equipment: The North American Market*. BCC Research: Market Forecasting: MA, USA.
- Beach, D., White R. Jr., T. Shams and N. Rangarajan. 1998. THOR Advanced Test Dummy - Biofidelity and Injury Assessment. *FAA International Aircraft Fire and Cabin Safety Conf*. 16-20 November 1998. Atlantic City, New Jersey.
- Bedewi, P.G. 2001. A review of biomechanics in automotive safety. *International Journal of Vehicle Design*; 26 (4), pp. 407-429. DOI: 10.1504/IJVD.2001.005215.
- Been, B., F. Bermond, K. Bortenschlager, D. Hynd, L. Martinez, G. Ferichola and R. Meijer. 2007. WorldSID small female Side Impact Dummy specifications and prototype evaluation. *20th Conference on the Enhanced Safety of Vehicles*, 18-21 June, 2007. Washington DC, USA.

- Beiner, J.M. and Jokl, P. 2002. Muscle contusion injury and myositis ossificans traumatica. *Clinical Orthopaedics and Related Research*; 403 (Suppl.), pp. S110-S119. DOI: 10.1097/00003086-200210001-00013.
- Bensamoun, S.F., Ringleb, S.I., Littrell, L., Chen, Q., Brennan, M., Ehman, R.L. and An, K. 2006. Determination of thigh muscle stiffness using magnetic resonance elastography. *Journal of Magnetic Resonance Imaging*; 23 (2), pp. 242-247. DOI: 10.1002/jmri.20487.
- Benslimane, M., P. Gravesen and P. Sommer-Larsen. 2002. Mechanical properties of dielectric elastomer actuators with smart metallic compliant electrodes. *SPIE's 9th Annual International Symposium on Smart Structures and Materials*, 2-6 Mar. . 150-157.
- Bergeron, D.M. 2004. *Test Methodologies for Personal Protective Equipment Against Anti-Personnel Mine Blast*. NATO: Springfield, Virginia, USA.
- Bergeron, D.M., Anderson, I.B., Coley, C.G. and Fall, R.W. 2006. *Assessment of Lower Leg Injury from Land Mine Blast – Phase 1: Test Results using a Frangible Surrogate Leg with Assorted Protective Footwear and Comparison with Cadaver Test Data*. Defence Research and Development Canada.: Valcartier, Canada.
- Bergeron, D.M. and Chichester, C. 2003. Protecting Deminers from APLs: A Review of US/Canada Cooperation in R&D. *Journal of Mine Action*; 7 (1).
- Bergeron, D.M., G.G. Coley, M.S. Rountree, I.B. Anderson and R.M. Harris. 2001. Assessment of Foot Protection Against Anti-Personnel Landmine Blast Using a Frangible Surrogate Leg. *UXO Forum*, 9-12 April. New Orleans, USA.
- Bergström, J. and Boyce, M. 1998. Constitutive modeling of the large strain time-dependent behavior of elastomers. *Journal of the Mechanics and Physics of Solids*; 46 (5), pp. 931-954. DOI: 10.1016/S0022-5096(97)00075-6.
- Biokinetics and Associates Ltd. 2003. *The Complex Lower Leg*. Biokinetics: Ontario, Canada.
- Bir, C., Barbir, A., Dosquet, F., Wilhelm, M., van der Horst, M. and Wolfe, G. 2008. Validation of lower limb surrogates as injury assessment tools in floor impacts due to anti-vehicular land mines. *Military Medicine*; 173 (12), pp. 1180-1184.
- Blackburn, J.T., Bell, D.R., Norcross, M.F., Hudson, J.D. and Kimsey, M.H. 2009. Sex comparison of hamstring structural and material properties. *Clinical Biomechanics*; 24 (1), pp. 65-70. DOI: 10.1016/j.clinbiomech.2008.10.001.
- Blemker, S.S., Asakawa, D.S., Gold, G.E. and Delp, S.L. 2007. Image-based musculoskeletal modeling: Applications, advances, and future opportunities. *Journal of Magnetic Resonance Imaging*; 25 (2), pp. 441-451. DOI: 10.1002/jmri.20805.
- Böl, M., Kruse, R., Ehret, A.E., Leichsenring, K. and Siebert, T. 2012. Compressive properties of passive skeletal muscle - The impact of precise sample geometry on parameter identification in inverse finite element analysis. *Journal of Biomechanics*; 45 (15), pp. 2673-2679. DOI: 10.1016/j.jbiomech.2012.08.023.
- Bourget, D., Bergeron, D.M., Williams, K., Salisbury, C. and Cronin, D. 2008. Simplified Biofidelic Lower Leg Surrogate. Canada. CA 2438950 A1.
- Brekelmans, W., Poort, H. and Slooff, T. 1972. A new method to analyse the mechanical behaviour of skeletal parts. *Acta Orthopaedica*; 43 (5), pp. 301-317. DOI: 10.3109/17453677208998949.
- Brooks, J., Fuller, C., Kemp, S. and Reddin, D. 2005. Epidemiology of injuries in English professional rugby union: part 1 match injuries. *British Journal of Sports Medicine*; 39 (10), pp. 757-766. DOI: 10.1136/bjism.2005.018135.
- Brown, I.A. 1973. A scanning electron microscope study of the effects of uniaxial tension on human skin. *British Journal of Dermatology*; 89 (4), pp. 383-393. DOI: 10.1111/j.1365-2133.1973.tb02993.x.
- BS 6183-3:2000. 2000. *Protective equipment for cricketers - Part 3: Leg protectors for batsmen, wicketkeepers and fielders, and thigh, arm and chest protectors for batsmen*. United Kingdom: British Standards Institute.
- BS:EN 13061:2009. 2009. *Protective clothing - Shin guards for association football players - Requirements and test methods*. United Kingdom: British Standards Institute.

BS:EN 13546:2002. 2002. *Protective clothing – Hand, arm, chest, Abdomen, leg, foot and genital protectors for field hockey goal keepers and shin protectors for field players – Requirements and test methods*. United Kingdom: British Standards Institute.

Bu, N., Huang, Y., Wang, X. and Yin, Z. 2012. Continuously tunable and oriented nanofiber direct-written by mechano-electrospinning. *Materials and Manufacturing Processes*; 27 (12), pp. 1318-1323. DOI: 10.1080/10426914.2012.700145.

Caldwell, E., Gernhardt, M., Somers, T., Younker, D. and Newby, N. 2012. *Evidence report: risk of injury due to dynamic loads*. Human Research Program Human Health and Countermeasures Element: NASA, Lyndon B. Johnson Space Center, Houston, Texas.

Carson, J.S. 1986. Convincing users of model's validity is a challenging aspect of the modeler's job. *Industrial Engineering*; 18 (6), pp. 74-85.

Carter, D.R. and Hayes, W.C. 1976. Bone compressive strength: the influence of density and strain rate. *Science*; 194 (4270), pp. 1174-1176. DOI: 10.1126/science.996549.

Carter, D.R. and Hayes, W.C. 1977. The compressive behavior of bone as a two-phase porous structure. *The Journal of Bone and Joint Surgery. American Volume*; 59 (7), pp. 954-962.

Cassagnau, P. and Mélis, F. 2003. Non-linear viscoelastic behaviour and modulus recovery in silica filled polymers. *Polymer*; 44 (21), pp. 6607-6615. DOI: 10.1016/S0032-3861(03)00689-X.

Cavaleri, P. and Singer, P. 1993. *The great ape project: Equality beyond humanity*. St Martins Pr: .

Cavanaugh, J.M., Nyquist, G.W., Goldberg, S.J. and King, A.I. 1986. Lower abdominal tolerance and response. *SAE Technical Paper 861878*; pp. 41-63. DOI: 10.4271/861878.

Cazzola, D., Trewartha, G. and Preatoni, E. 2013. Time-based calibrations of pressure sensors improve the estimation of force signals containing impulsive events. *Proceedings of the Institution of Mechanical Engineers, Part P: Journal of Sports Engineering and Technology*; 228 (2), pp. 147-151. DOI: 10.1177/1754337113504397.

Chaloner, E., McMaster, J. and Hinsley, D. 2002. Principles and problems underlying testing the effectiveness of blast protective footwear. *Royal Army Medical Corps*; 148 (1), pp. 38-43.

Champion, H.R. 2012. Abbreviated Injury Scale. In: J. Vincent and J.B. Hall eds., *Encyclopedia of Intensive Care Medicine*, Berlin Heidelberg: Springer, pp. 1-5.

Chawla, A., Mukherjee, S. and Karthikeyan, B. 2009. Characterization of human passive muscles for impact loads using genetic algorithm and inverse finite element methods. *Biomechanics and Modeling in Mechanobiology*; 8 (1), pp. 67-76. DOI: 10.1007/s10237-008-0121-6.

Choi, H., Hwang, S., Kang, Y., Kim, J. and Kang, B. 2002. Comparison of implicit and explicit finite-element methods for the hydroforming process of an automobile lower arm. *The International Journal of Advanced Manufacturing Technology*; 20 (6), pp. 407-413. DOI: 10.1007/s001700200170.

Chomiak, J., Junge, A., Peterson, L. and Dvorak, J. 2000. Severe injuries in football players influencing factors. *The American Journal of Sports Medicine*; 28 (suppl 5), pp. S-58-68. DOI: 10.1177/28.suppl_5.S-58.

Chong, A., Miller, F., Buxton, M. and Friis, E.A. 2007. Fracture toughness and fatigue crack propagation rate of short fiber reinforced epoxy composites for analogue cortical bone. *Journal of Biomechanical Engineering*; 129 (4), pp. 487-493. DOI: 10.1115/1.2746369.

Cifuentes, A. and Kalbag, A. 1992. A performance study of tetrahedral and hexahedral elements in 3-D finite element structural analysis. *Finite Elements in Analysis and Design*; 12 (3), pp. 313-318. DOI: 10.1016/0168-874X(92)90040-J.

Clavert, P., Kempf, J., Bonnet, F., Boutemy, P., Marcelin, L. and Kahn, J.L. 2001. Effects of freezing/thawing on the biomechanical properties of human tendons. *Surgical and Radiologic Anatomy*; 23 (4), pp. 259-262. DOI: 10.1007/s00276-001-0259-8.

Cohen, R., Hooley, C. and McCrum, N. 1976. Viscoelastic creep of collagenous tissue. *Journal of Biomechanics*; 9 (4), pp. 175-184. DOI: 10.1016/0021-9290(76)90002-6.

- Comley, K. and Fleck, N. 2012. The compressive response of porcine adipose tissue from low to high strain rate. *International Journal of Impact Engineering*; 46, pp. 1-10. DOI: 10.1016/j.ijimpeng.2011.12.009.
- Comley, K. and Fleck, N.A. 2010. A micromechanical model for the Young's modulus of adipose tissue. *International Journal of Solids and Structures*; 47 (21), pp. 2982-2990. DOI: 10.1016/j.ijsolstr.2010.07.001.
- Conforti, M. 2013. The Treatment of Muscle Hematomas. In: G.N. Bisciotti and C. Eirale eds., *Muscle Injuries in Sports Medicine*, InTech, pp. 203-220.
- Cosgrove, T., Turner, M.J. and Thomas, D.R. 1997. The adsorption of polydimethylsiloxane onto silica from the melt. *Polymer*; 38 (15), pp. 3885-3892. DOI: 10.1016/S0032-3861(96)00955-X.
- Cottenden, D.J. and Cottenden, A.M. 2013. A study of friction mechanisms between a surrogate skin (Lorica soft) and nonwoven fabrics. *Journal of the Mechanical Behavior of Biomedical Materials*; 28, pp. 410-426. DOI: 10.1016/j.jmbbm.2013.04.024.
- Crandall, J.R. and Kent, R. 2011. *A Systems Approach to Sports Injuries: Turf Toe and Lisfranc Injuries in American Football*. [Presentation]. Available at: <<http://www.ircobi.org/downloads/2011-lecture-crandall.pdf>> Accessed on: 9th June 2012.
- Crandall, J. and W. Pilkey. 1994. Preservation of Human Surrogates for Impact Studies. *Proceedings of 13th Southern Biomedical Engineering Conference*, April 1994. 582-585.
- Crandall, J.R., Bose, D., Forman, J., Untaroiu, C.D., Arregui-Dalmases, C., Shaw, C.G. and Kerrigan, J.R. 2011. Human surrogates for injury biomechanics research. *Clinical Anatomy*; 24 (3), pp. 362-371. DOI: 10.1002/ca.21152.
- Crisco, J., Hentel, K., Jackson, W., Goehner, K. and Jokl, P. 1996. Maximal contraction lessens impact response in a muscle contusion model. *Journal of Biomechanics*; 29 (10), pp. 1291-1296. DOI: 10.1016/0021-9290(96)00047-4.
- Crisco, J.J., Jokl, P., Heinen, G.T., Connell, M.D. and Panjabi, M.M. 1994. A muscle contusion injury model. Biomechanics, physiology, and histology. *The American Journal of Sports Medicine*; 22 (5), pp. 702-710. DOI: 10.1177/036354659402200521.
- Cristofolini, L., Juszczak, M., Martelli, S., Taddei, F. and Viceconti, M. 2007. In vitro replication of spontaneous fractures of the proximal human femur. *Journal of Biomechanics*; 40 (13), pp. 2837-2845. DOI: 10.1016/j.jbiomech.2007.03.015.
- Cronin, D., Williams, K., Bass, C.R.D., Magnan, P., Dosquet, F., Bergeron, D.M. and van Bree, J.L.M.J. 2003. *Test Methods for Protective Footwear Against AP Mine Blast*. NATO: Springfield, Virginia, USA.
- Cronin, D., M. Worswick, A. Ennis, D. Bourget, K. Williams and G. Pageau. 2001. Behind Armour Blunt Trauma for ballistic impacts on rigid body armour. *Proc. of the 19th International Symposium on Ballistics*, 7-11th May. Interlaken, Switzerland.
- Cronin, D.S., Williams, K. and Salisbury, C. 2011. Physical surrogate leg to evaluate blast mine injury. *Military Medicine*; 176 (12), pp. 1408-1416.
- Crowninshield, R. and Pope, M. 1974. The response of compact bone in tension at various strain rates. *Annals of Biomedical Engineering*; 2 (2), pp. 217-225. DOI: 10.1007/BF02368492.
- Currey, J.D. 1988. The effect of porosity and mineral content on the Young's modulus of elasticity of compact bone. *Journal of Biomechanics*; 21 (2), pp. 131-139. DOI: 10.1016/0021-9290(88)90006-1.
- Currey, J. 1989. Strain rate dependence of the mechanical properties of reindeer antler and the cumulative damage model of bone fracture. *Journal of Biomechanics*; 22 (5), pp. 469-475. DOI: 10.1016/0021-9290(89)90207-8.
- Currey, J.D. 1985. The mechanical adaptations of bones. *American Journal of Physical Anthropology*; 68 (1), pp. 141-142. DOI: 10.1002/ajpa.1330680117.
- Currey, J.D. and Butler, G. 1975. The mechanical properties of bone tissue in children. *The Journal of Bone and Joint Surgery. American Volume*; 57 (6), pp. 810-814.
- Custompartnet. *Manufacturing Cost Estimation*. [online]. Available at: <<http://www.custompartnet.com/>> Accessed on: 2014.

- Davies, S.I.J. 2008. The effect of processing parameters on the flexural properties of unidirectional carbon fibre-reinforced polymer (CFRP) composites. *Mater Sci Eng A*; 498 (1-2), pp. 65-68. DOI: 10.1016/j.msea.2007.11.148.
- Davison, M., Jones, J. and Allan, T. 2013. *Hip Region Soft Tissue Whitepaper*. Locus Research & Delloch Ltd.: Tauranga, New Zealand.
- DD 7971-9:2005. 2005. *Protective clothing and equipment for use in violent situations and in training - Part 9: Training suits and equipment - Requirements and test methods*. United Kingdom: British Standards Institute.
- DD CEN/TS 15256:2005. 2005. *Protective clothing - Hand, arm, leg, genital and neck protectors for use in ice hockey - Protectors for players other than goalkeepers - Requirements and test methods*. United Kingdom: British Standards Institute.
- Derraik, J.G., Rademaker, M., Cutfield, W.S., Pinto, T.E., Tregurtha, S., Faherty, A., Peart, J.M., Drury, P.L. and Hofman, P.L. 2014. Effects of Age, Gender, BMI, and Anatomical Site on Skin Thickness in Children and Adults with Diabetes. *PLoS One*; 9 (1), pp. e86637. DOI: 10.1371/journal.pone.0086637.
- Desmoulin, G.T. and Anderson, G.S. 2011. Method to Investigate Contusion Mechanics in Living Humans. *Journal of Forensic Biomechanics*; 2 (1), pp. 1-10.
- Diani, J., Fayolle, B. and Gilormini, P. 2009. A review on the Mullins effect. *European Polymer Journal*; 45 (3), pp. 601-612. DOI: 10.1016/j.eurpolymj.2008.11.017.
- Diaz, J.A., Fischer, D.A., Rettig, A.C., Davis, T.J. and Shelbourne, K.D. 2003. Severe Quadriceps Muscle Contusions in Athletes: A Report of Three Cases. *The American Journal of Sports Medicine*; 31 (2), pp. 289-293. DOI: 10.1177/03635465030310022201.
- Dick, R., Hootman, J.M., Agel, J., Vela, L., Marshall, S.W. and Messina, R. 2007a. Descriptive epidemiology of collegiate women's field hockey injuries: National Collegiate Athletic Association Injury Surveillance System, 1988–1989 through 2002–2003. *Journal of Athletic Training*; 42 (2), pp. 211-220.
- Dick, R., Romani, W.A., Agel, J., Case, J.G. and Marshall, S.W. 2007b. Descriptive epidemiology of collegiate men's lacrosse injuries: National Collegiate Athletic Association Injury Surveillance System, 1988–1989 through 2003–2004. *Journal of Athletic Training*; 42 (2), pp. 255-261.
- Dick, R., Hertel, J., Agel, J., Grossman, J. and Marshall, S.W. 2007d. Descriptive epidemiology of collegiate men's basketball injuries: National Collegiate Athletic Association Injury Surveillance System, 1988–1989 through 2003–2004. *Journal of Athletic Training*; 42 (2), pp. 194-201.
- Dick, R., Ferrara, M.S., Agel, J., Courson, R., Marshall, S.W., Hanley, M.J. and Reifsteck, F. 2007c. Descriptive epidemiology of collegiate men's football injuries: National Collegiate Athletic Association Injury Surveillance System, 1988-1989 through 2003-2004. *Journal of Athletic Training*; 42 (2), pp. 221-233.
- Diehl, T. and D. Carroll. 2000. Utilizing ABAQUS' 10-Node Modified Tet for Analyzing Impact Problems Involving Thin-Walled Structures. *Proceedings of the ABAQUS Users' Conference*, 31 May - 2 June. Newport, RI.
- Donnelly, B.R. and Roberts, D. 1987. *Comparison of cadaver and hybrid III dummy response to axial impacts of the femur*. Society of Automotive Engineers: Warrendale, PA.
- Dorfmann, A. and Ogden, R. 2004. A constitutive model for the Mullins effect with permanent set in particle-reinforced rubber. *International Journal of Solids and Structures*; 41 (7), pp. 1855-1878. DOI: 10.1016/j.ijsolstr.2003.11.014.
- Douglas, W.R. 1972. Of pigs and men and research: a review of applications and analogies of the pig, *sus scrofa*, in human medical research. *Space Life Sciences*; 3 (3), pp. 226-234. DOI: 10.1007/BF00928167.
- Duenwald, S.E.; Vanderby, R. Jr.; Lakes, R.S. 2009. Viscoelastic relaxation and recovery of tendon. *Annals of Biomedical Engineering*, 37 (6), pp. 1131-1140. DOI: 10.1007/s10439-009-9687-0
- Dunn, M.G., Silver, F.H. and Swann, D.A. 1985. Mechanical analysis of hypertrophic scar tissue: structural basis for apparent increased rigidity. *Journal of Investigative Dermatology*; 84 (1), pp. 9-13. DOI: 10.1111/1523-1747.ep12274528.
- Edwards, C. and Marks, R. 1995. Evaluation of biomechanical properties of human skin. *Clinics in Dermatology*; 13 (4), pp. 375-380. DOI: 10.1016/0738-081X(95)00078-T.

- Egelbretsson, K. 2011. *Evaluation of material models in LS-DYNA for impact simulation of white adipose tissue*, Masters Thesis. Chalmers University of Technology.
- Erdemir, A., Viveiros, M.L., Ulbrecht, J.S. and Cavanagh, P.R. 2006. An inverse finite-element model of heel-pad indentation. *Journal of Biomechanics*; 39 (7), pp. 1279-1286. DOI: 10.1016/j.jbiomech.2005.03.007.
- Erickson, G.M., Catanese, J. and Keaveny, T.M. 2002. Evolution of the biomechanical material properties of the femur. *The Anatomical Record*; 268 (2), pp. 115-124. DOI: 10.1002/ar.10145.
- Esat, I.I. and Ozada, N. 2010. Articular human joint modelling. *Robotica*; 28 (02), pp. 321-339. DOI: 10.1017/S0263574709990592.
- Evans, L. 2001. Female compared with male fatality risk from similar physical impacts. *Journal of Trauma-Injury, Infection, and Critical Care*; 50 (2), pp. 281-288. DOI: 10.1097/00005373-200102000-00014.
- Evans, L. and Gerrish, P.H. 2001. *Gender and age influence on fatality risk from the same physical impact determined using two-car crashes*. Society of Automotive Engineers: Warrendale, PA.
- Fackler, M.L. 1988. Ordnance gelatin for ballistic studies: Detrimental effect of excess heat used in gelatin preparation. *American Journal of Forensic Medicine & Pathology*; 9 (3), pp. 218-219. DOI: 10.1097/00000433-198809000-00008.
- Farvid, M., Ng, T., Chan, D., Barrett, P. and Watts, G. 2005. Association of adiponectin and resistin with adipose tissue compartments, insulin resistance and dyslipidaemia. *Diabetes, Obesity and Metabolism*; 7 (4), pp. 406-413. DOI: 10.1111/j.1463-1326.2004.00410.x.
- Ferreira, F., Vaz, M. and Simoes, J. 2006. Mechanical properties of bovine cortical bone at high strain rate. *Materials Characterization*; 57 (2), pp. 71-79. DOI: 10.1016/j.matchar.2005.11.023.
- Fidanza, F., Keys, A. and Anderson, J.T. 1953. Density of body fat in man and other mammals. *Journal of Applied Physiology*; 6 (4), pp. 252-256.
- Finlay, J.B. 1978. Thixotropy in human skin. *Journal of Biomechanics*; 11 (6), pp. 333-342. DOI: 10.1016/0021-9290(78)90066-0.
- Flynn, C. and McCormack, B.A. 2008. Finite element modelling of forearm skin wrinkling. *Skin Research and Technology*; 14 (3), pp. 261-269. DOI: 10.1111/j.1600-0846.2008.00289.x.
- Fontanella, C., Matteoli, S., Carniel, E., Wilhjelm, J.E., Virga, A., Corvi, A. and Natali, A. 2012. Investigation on the load-displacement curves of a human healthy heel pad: In vivo compression data compared to numerical results. *Medical Engineering & Physics*; 34 (9), pp. 1253-1259. DOI: 10.1016/j.medengphy.2011.12.013.
- Found, M., Patrick, D. and Pearson, J. 2006. The influence of strain measurement on the impact performance of sports mouthguards. *Composites Part A: Applied Science and Manufacturing*; 37 (11), pp. 2164-2170. DOI: 10.1016/j.compositesa.2005.11.011.
- Francisco, A.C., Nightingale, R.W., Guilak, F., Glisson, R.R. and Garrett Jr, W.E. 2000. Comparison of soccer shin guards in preventing tibia fracture. *The American Journal of Sports Medicine*; 28 (2), pp. 227-233.
- Fung, Y. 1993. *Biomechanics: mechanical properties of living tissues*. 2nd ed. Springer: The University of Michigan, USA.
- Gallagher, A., A. Ní Annaidh and K. Bruyère. 2012. Dynamic tensile properties of human skin. 2012 *International Research Council on the Biomechanics of Injury*, 12 - 14 September 2012. Dublin, Ireland. 494-502.
- Gardner, M.P., Chong, A.C.M., Pollock, A.G. and Wooley, P.H. 2010. Mechanical evaluation of large-size fourth-generation composite femur and tibia models. *Annals of Biomedical Engineering*; 38 (3), pp. 613-620. DOI: 10.1007/s10439-009-9887-7.
- Garraway, W. and Macleod, D. 1995. Epidemiology of rugby football injuries. *The Lancet*; 345 (8963), pp. 1485-1487. DOI: doi:10.1136/bjism.2005.018135.
- Geerligs, M., Peters, G.W., Ackermans, P.A., Oomens, C.W. and Baaijens, F. 2010. Does subcutaneous adipose tissue behave as an (anti-) thixotropic material? *Journal of Biomechanics*; 43 (6), pp. 1153-1159. DOI: 10.1016/j.jbiomech.2009.11.037.
- Geerligs, M., Peters, G.W., Ackermans, P.A., Oomens, C.W. and Baaijens, F.P. 2008. Linear viscoelastic behavior of subcutaneous adipose tissue. *Biorheology*; 45 (6), pp. 677-688. DOI: 10.3233/BIR-2008-0517.

- Gefen, A. and Haberman, E. 2007. Viscoelastic properties of ovine adipose tissue covering the gluteus muscles. *Journal of Biomechanical Engineering*; 129 (6), pp. 924-930. DOI: 10.1115/1.2800830.
- Gerhardt, L., Lenz, A., Spencer, N., Münzer, T. and Derler, S. 2009. Skin–textile friction and skin elasticity in young and aged persons. *Skin Research and Technology*; 15 (3), pp. 288-298. DOI: 10.1111/j.1600-0846.2009.00363.x.
- Geurts, J., M. van der Horst, P.J. Leerdam, C. Bir, H. Van Dommelen and J. Wismans. 2006. Occupant Safety: Mine Detonation under Vehicles - A Numerical Lower Leg Injury Assessment. *2006 International Conference on the Biomechanics of Impact*, 22-26 September 2006. Madrid, Spain. 373-377.
- Gholami, T., J. Lescheticky and R. PaBmann. 2003. Crashworthiness simulation of automobiles with ABAQUS/Explicit. *Proceeding of Abaqus Users' Conference*, 4-6 June. Munich, Germany.
- Ghoreishy, M.H.R. 2012. Determination of the parameters of the Prony series in hyper-viscoelastic material models using the finite element method. *Materials & Design*; 35, pp. 791-797. DOI: 10.1016/j.matdes.2011.05.057.
- Gissane, C., White, J., Kerr, K. and Jennings, D. 2001. An operational model to investigate contact sports injuries. *Medicine and Science in Sports and Exercise*; 33 (12), pp. 1999-2003. DOI: 10.1097/00005768-200112000-00004.
- Goldsmith, L.A. 1990. My organ is bigger than your organ. *Archives of Dermatology*; 126 (3), pp. 301-302. DOI: 10.1001/archderm.1990.01670270033005.
- Gray, H. 1918. *Anatomy of the human body*. 20th ed. Lea & Febiger: Philadelphia.
- Grood, E.S., Stowers, S.F. and Noyes, F.R. 1988. Limits of movement in the human knee. *J Bone Joint Surg A*; 70 (1), pp. 88-97.
- Guedes, R., Simões, J. and Morais, J. 2006. Viscoelastic behaviour and failure of bovine cancellous bone under constant strain rate. *Journal of Biomechanics*; 39 (1), pp. 49-60. DOI: 10.1016/j.jbiomech.2004.11.005.
- Guillotin, B., Bourget, C., Remy-Zolgadri, M., Bareille, R., Fernandez, P., Conrad, V. and Amédée-Vilamitjana, J. 2004. Human primary endothelial cells stimulate human osteoprogenitor cell differentiation. *Cellular Physiology and Biochemistry*; 14 (4-6), pp. 325-332. DOI: DOI:10.1159/000080342.
- Haddon, W.J. 1980. Options for the prevention of motor vehicle crash injury. *Israel Journal of Medical Sciences*; 16 (1), pp. 45-65.
- Hagel, B. and Meeuwisse, W. 2004. Risk compensation: a “side effect” of sport injury prevention? *Clinical Journal of Sport Medicine*; 14 (4), pp. 193-196. DOI: 10.1097/00042752-200407000-00001.
- Häggglund, M., Waldén, M. and Ekstrand, J. 2009. Injuries among male and female elite football players. *Scandinavian Journal of Medicine & Science in Sports*; 19 (6), pp. 819-827. DOI: 10.1111/j.1600-0838.2008.00861.x.
- Halkon, B., J. Webster, S. Mitchell and M. Mientjes. 2012. Development of a test methodology for the assessment of human impacts in sport. *9th Conference of the International Sports Engineering Association (ISEA)*, 9-13 July 2012. Boston, MA. 813-818.
- Halkon, B.J., Mitchell, S.R., Payne, T. and Carbo, J. 2014. Biomechanical measurements of human impacts in basketball. *Procedia Engineering*; 72, pp. 214-219. DOI: 10.1016/j.proeng.2014.06.038.
- Hansen, U., Zioupos, P., Simpson, R., Currey, J.D. and Hynd, D. 2008. The effect of strain rate on the mechanical properties of human cortical bone. *Journal of Biomechanical Engineering*; 130 (1), pp. 011011-1-011011-5. DOI: 10.1115/1.2838032.
- Harewood, F. and McHugh, P. 2007. Comparison of the implicit and explicit finite element methods using crystal plasticity. *Computational Materials Science*; 39 (2), pp. 481-494. DOI: 10.1016/j.commatsci.2006.08.002.
- Harris, R., M. Rountree, R. Hayda, L. Griffin, S. Mannion and T. Bice. 2001. The Efficacy of Current Landmine Protective Footwear: Changes in Medical Outcomes. *Proceedings of the 2001 UXO conference*, 9-12 April. New Orleans, USA.

- Haut, R. 1989. The effects of orientation and location on the strength of dorsal rat skin in high and low speed tensile failure experiments. *Journal of Biomechanical Engineering*; 111 (2), pp. 136-140. DOI: 10.1115/1.3168354.
- Heald, J. and Pass, D. 1994. Ball standards relevant to risk of head injury. *ASTM Special Technical Publication*; 1229, pp. 223-238.
- Heiner, A.D. 2008. Structural properties of fourth-generation composite femurs and tibias. *Journal of Biomechanics*; 41 (15), pp. 3282-3284. DOI: 10.1016/j.jbiomech.2008.08.013.
- Heiner, A.D. and Brown, T.D. 2001. Structural properties of a new design of composite replicate femurs and tibias. *Journal of Biomechanics*; 34 (6), pp. 773-781. DOI: 10.1016/S0021-9290(01)00015-X.
- Helelä, T. 1969. Age-dependent Variations of the Cortical Thickness of the Clavicle. *Annals of Clinical Research*; 1 (2), pp. 140-143.
- Henry, R.P. 2014. Multi-Material Impact Protection for Contact Sports. Nike Inc., *United States Patent*. US20140259322 A1.
- Hoare, T.R. and Kohane, D.S. 2008. Hydrogels in drug delivery: progress and challenges. *Polymer*; 49 (8), pp. 1993-2007. DOI: 10.1016/j.polymer.2008.01.027.
- Hoffer, J. and Andreassen, S. 1981. Regulation of soleus muscle stiffness in pre-mammillary cats: intrinsic and reflex components. *Journal of Neurophysiology*; 45 (2), pp. 267-285.
- Hogan, H.A., Ruhmann, S.P. and Sampson, H.W. 2000. The mechanical properties of cancellous bone in the proximal tibia of ovariectomized rats. *Journal of Bone and Mineral Research*; 15 (2), pp. 284-292. DOI: 10.1359/jbmr.2000.15.2.284.
- Holzapfel, G.A. 2004. Computational biomechanics of soft biological tissue. *Encyclopedia of Computational Mechanics*, Graz, Austria: Wiley Online Library.
- Horsman, M.D.K., Koopman, H., Veeger, H. and van der Helm, F. 2007. *The Twente Lower Extremity Model: a comparison of maximal isometric moment with the literature*. Gildeprint Drukkerijen: Enschede, The Netherlands.
- Hrysomallis, C. 2009. Surrogate thigh model for assessing impact force attenuation of protective pads. *Journal of Science and Medicine in Sport*; 12 (1), pp. 35-41. DOI: 10.1016/j.jsams.2007.07.013.
- Huard, J., Li, Y. and Fu, F.H. 2002. Muscle injuries and repair: current trends in research. *The Journal of Bone & Joint Surgery*; 84 (5), pp. 822-832.
- Human Tissue Act. 2004. *Human Tissue Act 2004 (c.30) (Act of Parliament)*. London: HMSO: Great Britain Parliament; 15 November 2004.
- Ihde, S., Goldmann, T., Himmlova, L. and Aleksic, Z. 2008. The use of finite element analysis to model bone-implant contact with basal implants. *Oral Surgery, Oral Medicine, Oral Pathology, Oral Radiology, and Endodontology*; 106 (1), pp. 39-48. DOI: 10.1016/j.tripleo.2007.12.005.
- Ionescu, V. and P. Wernicke. 2006. Assessment of Side Impact Simulation Using ABAQUS/Explicit. *SAE 2006 World Congress & Exhibition*, 3-6 April. Detroit, MI, USA.
- ISO 3384-1. 2011. *Rubber, vulcanized or thermoplastic — Determination of stress relaxation in compression — Part 1: Testing at constant temperature*. International Organization for Standardization: Geneva, Switzerland.
- Jain, S.M., Pandey, K., Lahoti, A. and Rao, P.K. 2013. Evaluation of skin and subcutaneous tissue thickness at insulin injection sites in Indian, insulin naive, type-2 diabetic adult population. *Indian Journal of Endocrinology and Metabolism*; 17 (5), pp. 864-870. DOI: 10.4103/2230-8210.117249.
- James, M.R. 1991. Spinal fractures associated with ejection from jet aircraft: two case reports and a review. *Archives of Emergency Medicine*; 8 (4), pp. 240-244. DOI: 10.1136/emj.8.4.240.
- Jamison, C., Marangoni, R. and Glaser, A. 1968. Viscoelastic properties of soft tissue by discrete model characterization. *Journal of Biomechanics*; 1 (1), pp. 33-46. DOI: 10.1016/0021-9290(68)90036-5.
- Jansen, L. and Rottier, P. 1958. Comparison of the mechanical properties of strips of human abdominal skin excised from below and from above the umbilic. *Dermatologica*; 117 (4), pp. 252-258. DOI: 10.1159/000255597.

- Jarvinen, T.A., Jarvinen, T.L., Kaariainen, M., Kalimo, H. and Jarvinen, M. 2005. Muscle injuries: biology and treatment. *The American Journal of Sports Medicine*; 33 (5), pp. 745-764. DOI: 10.1177/0363546505274714.
- Jee, T. and Komvopoulos, K. 2014. Skin viscoelasticity studied in vitro by microprobe-based techniques. *Journal of Biomechanics*; 47 (2), pp. 553-559. DOI: 10.1016/j.jbiomech.2013.10.006.
- Johannsen, H. and V. Schindler. 2007. Development and Assessment of a Surface Force Abdominal Sensor. *Proc. of the 20th International Conference on Enhanced Safety of Vehicles*, 18-21 June. Lyon, France.
- Johner, R., Stäubli, H., Gunst, M. and Cordey, J. 2000. The point of view of the clinician: a prospective study of the mechanism of accidents and the morphology of tibial and fibular shaft fractures. *Injury*; 31 (Suppl 3), pp. 45-93. DOI: 10.1016/S0020-1383(00)80031-5.
- Johnson, T., Socrate, S. and Boyce, M. 2010. A viscoelastic, viscoplastic model of cortical bone valid at low and high strain rates. *Acta Biomaterialia*; 6 (10), pp. 4073-4080. DOI: 10.1016/j.actbio.2010.04.017.
- Joldes, G.R., Wittek, A. and Miller, K. 2009. Suite of finite element algorithms for accurate computation of soft tissue deformation for surgical simulation. *Medical Image Analysis*; 13 (6), pp. 912-919. DOI: 10.1016/j.media.2008.12.001.
- Junge, A., Dvorak, J. and Graf-Baumann, T. 2004. Football injuries during the World Cup 2002. *The American Journal of Sports Medicine*; 32 (1 Suppl), pp. 23S-27S. DOI: 10.1177/0363546503261246.
- Jussila, J. 2004. Preparing ballistic gelatine—review and proposal for a standard method. *Forensic Science International*; 141 (2), pp. 91-98. DOI: 10.1016/j.forsciint.2003.11.036.
- Kajzer, J., Matsui, Y., Ishikawa, H., Schroeder, G. and Bosch, U. 1999. *Shearing and bending effects at the knee joint at low-speed lateral loading*. Society of Automotive Engineers: Detroit, Michigan, USA.
- Kajzer, J., Schroeder, G., Ishikawa, H., Matsui, Y. and Bosch, U. 1997. *Shearing and Bending Effects at the Knee Joint at High Speed Lateral Loading*. Society of Automotive Engineers: Warrendale, PA.
- Kaliske, M., Nasdala, L. and Rothert, H. 2001. On damage modelling for elastic and viscoelastic materials at large strain. *Computers & Structures*; 79 (22), pp. 2133-2141. DOI: 10.1016/S0045-7949(01)00061-X.
- Karimi, A. and Navidbakhsh, M. 2014. Mechanical properties of PVA material for tissue engineering applications. *Materials Technology*; 29 (2), pp. 90-100. DOI: 10.1179/1753555713Y.0000000115.
- Keaveny, T.M. and L Bouxsein, M. 2008. Theoretical implications of the biomechanical fracture threshold. *Journal of Bone and Mineral Research*; 23 (10), pp. 1541-1547. DOI: 10.1359/JBMR.080406.
- Keaveny, T.M., Morgan, E.F., Niebur, G.L. and Yeh, O.C. 2001. Biomechanics of trabecular bone. *Annual Review of Biomedical Engineering*; 3 (1), pp. 307-333. DOI: 10.1146/annurev.bioeng.3.1.307.
- Kent, R. and Bass, C. 2007. Experimentacion con animales (Experimentation With Animals). In: C. Arregui-Dalmases, J. Luzon and M. Segui-Gomez eds., *Fundamentos de Biomecanica en las Lesiones por Accidente de Trafico. (Fundamentals of Biomechanics and Road Traffic Injuries)*, 2nd ed. Madrid: .
- Kent, R., Lessley, D. and Sherwood, C. 2004. Thoracic response to dynamic, non-impact loading from a hub, distributed belt, diagonal belt, and double diagonal belts. *Stapp Car Crash Journal*; 48, pp. 495-519.
- Kerrigan, J.R., Bhalla, K.S., Funk, J.R., Madeley, N.J., Bose, D. and Crandall, J.R. 2003. *Experiments for establishing pedestrian-impact lower limb injury criteria*. SAE 2003 World Congress & Exhibition: Detroit, MI.
- Khattak, M.J., Ahmad, T., Rehman, R., Umer, M., Hasan, S.H. and Ahmed, M. 2010. Muscle healing and nerve regeneration in a muscle contusion model in the rat. *The Journal of Bone and Joint Surgery. British Volume*; 92 (6), pp. 894-899. DOI: 10.1302/0301-620X.92B6.22819.
- Kimpara, H., Lee, J., Yang, K. and King, A. 2010. Effects of Body Weight, Height, and Rib Cage Area Moment of Inertia on Blunt Chest Impact Response. *Traffic Injury Prevention*; 11 (2), pp. 207-214. DOI: 10.1080/15389580903554863.
- King, A.I., Viano, D.C. and Mizeres, N. 1995. Humanitarian benefits of cadaver research on injury prevention. *The Journal of Trauma*; 38 (4), pp. 564-569. DOI: 0.1097/00005373-199504000-00016.
- Kragh Jr, J.F., Svoboda, S.J., Wenke, J.C., Brooks, D.E., Bice, T.G. and Walters, T.J. 2005. The role of epimysium in suturing skeletal muscle lacerations. *Journal of the American College of Surgeons*; 200 (1), pp. 38-44. DOI: 10.1016/j.jamcollsurg.2004.09.009.

- Kraus, C., Bock, H.G. and Mutschler, H. 2005. Parameter estimation for biomechanical models based on a special form of natural coordinates. *Multibody System Dynamics*; 13 (1), pp. 101-111. DOI: 10.1007/s11044-005-4081-7.
- Kroell, C.K., Schneider, D.C. and Nahum, A.M. 1974. *Impact tolerance and response of the human thorax II*. Society of Automotive Engineers: Warrendale, PA, USA.
- Krog, L., Tucker, A. and Rollema, G. 2002. *Application of topology, sizing and shape optimization methods to optimal design of aircraft components*. Altair Engineering: MI, USA.
- Krosshaug, T., Andersen, T., Olsen, O.E.O., Myklebust, G. and Bahr, R. 2005. Research approaches to describe the mechanisms of injuries in sport: limitations and possibilities. *British Journal of Sports Medicine*; 39 (6), pp. 330-339. DOI: 10.1136/bjism.2005.018358.
- Krouskop, T.A., Wheeler, T.M., Kallel, F., Garra, B.S. and Hall, T. 1998. Elastic moduli of breast and prostate tissues under compression. *Ultrasonic Imaging*; 20 (4), pp. 260-274. DOI: 10.1177/016173469802000403.
- Krstic, A. 2005. Surrogate. Adelaide, *Australia Patent*. WO/2002/009068.
- Krstic, A.R., Bergeron, D.M., Bourget, D., Softley, I. and Neades, D. 2002. *Development of a Lower Leg Physical Model for Enhanced Soldier Survivability against Landmines*. The Technical Cooperation Program: South Australia, Australia.
- Kulin, R.M., Jiang, F. and Vecchio, K.S. 2011. Effects of age and loading rate on equine cortical bone failure. *Journal of the Mechanical Behavior of Biomedical Materials*; 4 (1), pp. 57-75. DOI: 10.1016/j.jmbbm.2010.09.006.
- Laboratory Animal Welfare Act. 1966. *Laboratory Animal Welfare Act 1966 (P.L. 89-544) (US Government Publication)*; Washington, United States: USDA, 24 August 1966.
- Lakes, R.S. and Katz, J.L. 1979. Viscoelastic properties of wet cortical bone—II. Relaxation mechanisms. *Journal of Biomechanics*; 12 (9), pp. 679-687. DOI: 10.1016/0021-9290(79)90017-4.
- Lanir, Y. and Fung, Y. 1974. Two-dimensional mechanical properties of rabbit skin—I. Experimental system. *Journal of Biomechanics*; 7 (1), pp. 29-34. DOI: 10.1016/0021-9290(74)90067-0.
- Lawrence, G.J.L. and B.J. Hardy. 1998. Pedestrian safety testing using the EEVC pedestrian impactors. *16th International Technical Conference on the Enhanced Safety of Vehicles*, May 31- June 4. Ontario, Canada.
- Leary, T. and White, J.A. 2000. Acute injury incidence in professional county club cricket players (1985–1995). *British Journal of Sports Medicine*; 34 (2), pp. 145-147. DOI: 10.1136/bjism.34.2.145.
- Lee, D., Glueck, M., Khan, A., Fiume, E. and Jackson, K. 2009. A survey of modeling and simulation of skeletal muscle. *ACM Transactions on Graphics*; 28 (4), pp. Article 106. DOI: 10.1145/1559755.1559763.
- Lee, K.E. and Pelker, R.R. 1985. Effect of freezing on histologic and biomechanical failure patterns in the rabbit capital femoral growth plate. *J Orthop Res*; 3 (3), pp. 514-515. DOI: 10.1002/jor.1100030415.
- Li, W., Zhang, C., Li, C. and Liao, H. 2009. Modeling aspects of high velocity impact of particles in cold spraying by explicit finite element analysis. *Journal of Thermal Spray Technology*; 18 (5-6), pp. 921-933. DOI: 10.1007/s11666-009-9325-2.
- Li, Z., Zou, D., Liu, N., Zhong, L., Shao, Y., Wan, L., Huang, P. and Chen, Y. 2013. Finite element analysis of pedestrian lower limb fractures by direct force: The result of being run over or impact? *Forensic Science International*; 229 (1), pp. 43-51. DOI: 10.1016/j.forsciint.2013.03.027.
- Lim, J., Hong, J., Chen, W.W. and Weerasooriya, T. 2011. Mechanical response of pig skin under dynamic tensile loading. *International Journal of Impact Engineering*; 38 (2), pp. 130-135. DOI: 10.1016/j.ijimpeng.2010.09.003.
- Lim, Y., Deo, D., Singh, T.P., Jones, D.B. and De, S. 2009. In situ measurement and modeling of biomechanical response of human cadaveric soft tissues for physics-based surgical simulation. *Surgical Endoscopy*; 23 (6), pp. 1298-1307. DOI: 10.1007/s00464-008-0154-z.
- Liu, Z. and Yeung, K. 2008. The preconditioning and stress relaxation of skin tissue. *Journal of Biomedical & Pharmaceutical Engineering*; 2 (1), pp. 22-28.

- Lotz, J.C., Gerhart, T.N. and Hayes, W.C. 1990. Mechanical properties of trabecular bone from the proximal femur: a quantitative CT study. *Journal of Computer Assisted Tomography*; 14 (1), pp. 107-114. DOI: 10.1097/00004728-199001000-00020.
- Lowenhielm, P., Voigt, G.E., Ljung, C.B. and Wihlberg, B.G. 1977. Influence of post mortem changes on experimental safety belt injuries. *Zeitschrift Fur Rechtsmedizin*; 80 (3), pp. 171-182. DOI: 10.1007/BF02114612.
- Lucksanasomboon, P., Higgs, W., Higgs, R. and Swain, M. 2003. Interfacial fracture toughness between bovine cortical bone and cements. *Biomaterials*; 24 (7), pp. 1159-1166. DOI: 10.1016/S0142-9612(02)00464-7.
- Manning, J. 2007. Development Of A Pedestrian Legform To Assess Sensors Used In Active Pedestrian Protection Systems. *Proceedings of the 20th International Technical Conference on the Enhanced Safety of Vehicles (ESV)*, 18-21 June. Lyon, France.
- Marckmann, G. and Verron, E. 2006. Comparison of hyperelastic models for rubber-like materials. *Rubber Chemistry and Technology*; 79 (5), pp. 835-858. DOI: 10.5254/1.3547969.
- Martin, B. 1993. Aging and strength of bone as a structural material. *Calcified Tissue International*; 53 (1), pp. S34-S40. DOI: 10.1007/BF01673400.
- Martin, R.B. 1972. The effects of geometric feedback in the development of osteoporosis. *Journal of Biomechanics*; 5 (5), pp. 447-455. DOI: 10.1016/0021-9290(72)90003-6.
- Martinez, J.S., Le Cam, J., Balandraud, X., Toussaint, E. and Caillard, J. 2013. Filler effects on the thermomechanical response of stretched rubbers. *Polymer Testing*; 32 (5), pp. 835-841. DOI: 10.1016/j.polymertesting.2013.04.003.
- Mather, B.S. 1968. Variation with age and sex in strength of the femur. *Medical and Biological Engineering and Computing*; 6 (2), pp. 129-132. DOI: 10.1007/BF02474265.
- Mattmann, C., Clemens, F. and Tröster, G. 2008. Sensor for measuring strain in textile. *Sensors*; 8 (6), pp. 3719-3732. DOI: 10.3390/s8063719.
- McBrier, N.M., Neuberger, T., Okita, N., Webb, A. and Sharkey, N. 2009. Reliability and validity of a novel muscle contusion device. *Journal of Athletic Training*; 44 (3), pp. 275-278. DOI: 10.4085/1062-6050-44.3.275.
- McElhaney, J.H. 1966. Dynamic response of bone and muscle tissue. *Journal of Applied Physiology*; 21 (4), pp. 1231-1236.
- McElhaney, J.H., Fogle, J.L., Melvin, J.W., Haynes, R.R., Roberts, V.L. and Alem, N.M. 1970. Mechanical properties of cranial bone. *Journal of Biomechanics*; 3 (5), pp. 495-511. DOI: 10.1016/0021-9290(70)90059-X.
- McHenry, R.R. 1963. Analysis of the dynamics of automobile passenger restraint systems. *7th Stapp Car Crash Conference*, 11-13 Nov. Berkeley Institute of Transportation and Traffic Engineering. 207-249.
- McIntosh, A.S. 2011. Biomechanical considerations in the design of equipment to prevent sports injury. *Proceedings of the Institution of Mechanical Engineers, Part P: Journal of Sports Engineering and Technology*; 226 (3-4), pp. 193-199. DOI: 10.1177/1754337111431024.
- McIntosh, A. 2005. Risk compensation, motivation, injuries, and biomechanics in competitive sport. *British Journal of Sports Medicine*; 39 (1), pp. 2-3. DOI: 10.1136/bjism.2004.016188.
- McPherson, M. and Pickett, W. 2010. Characteristics of martial art injuries in a defined Canadian population: a descriptive epidemiological study. *BMC Public Health*; 10 (1), pp. 795-802. DOI: 10.1186/1471-2458-10-795.
- Meeuwisse, W.H. 1994. Assessing Causation in Sport Injury: A Multifactorial Model. *Clinical Journal of Sport Medicine*; 4 (3), pp. 166-170. DOI: 10.1097/00042752-199407000-00004.
- Meeuwisse, W.H., Tyreman, H., Hagel, B. and Emery, C. 2007. A dynamic model of etiology in sport injury: the recursive nature of risk and causation. *Clinical Journal of Sport Medicine*; 17 (3), pp. 215-219. DOI: 10.1097/JSM.0b013e3180592a48.
- Meeuwisse, W. 1991. Predictability of sports injuries. *Sports Medicine*; 12 (1), pp. 8-15. DOI: 10.2165/00007256-199112010-00002.
- Mendez, J. and Keys, A. 1960. Density and composition of mammalian muscle. *Metabolism*; 9 (2), pp. 184-188.

- Menetrey, J., Kasemkijwattana, C., Fu, F.H., Moreland, M.S. and Huard, J. 1999. Suturing versus immobilization of a muscle laceration. A morphological and functional study in a mouse model. *The American Journal of Sports Medicine*; 27 (2), pp. 222-229. DOI: 10.1016/S0196-0644(99)80077-8.
- Menz, L.J. 1971. Structural changes and impairment of function associated with freezing and thawing in muscle, nerve, and leucocytes. *Cryobiology*; 8 (1), pp. 1-131. DOI: 10.1016/S0011-2240(69)80416-5.
- Merkle, A.C., Carneal, C.M., Wing, I.D., Wickwire, A.C., Paulson, J.M., Ott, K.A., Ward, E.E., Harrigan, T.P., Roberts, J.C. and Carkhuff, B.G. 2013. Biomechanics and Injury Mitigation Systems Program: An Overview of Human Models for Assessing Injury Risk in Blast, Ballistic, and Transportation Impact Scenarios. *Johns Hopkins APL Technical Digest*; 31 (4), pp. 286-295.
- Mertz, H. and Patrick, L. 1967. *Investigation of the kinematics and kinetics of whiplash*. SAE International: Warrendale, PA, USA.
- Messerer, O. 1880. *Über Elasticität und Festigkeit der menschlichen Knochen*. *Cotta'schen Bunchhandlung*; Cited in: Nahum AM and Melvin J, *Accidental Injury, Biomechanics and Prevention*, New York, Springer-Verlag, 1993 .
- Meunier, L., Chagnon, G., Favier, D., Orgéas, L. and Vacher, P. 2008. Mechanical experimental characterisation and numerical modelling of an unfilled silicone rubber. *Polymer Testing*; 27 (6), pp. 765-777. DOI: 10.1016/j.polymertesting.2008.05.011.
- Miller, K. 2000. *Testing Elastomers for Hyperelastic Material Models in Finite Element Analysis*. Axel Products Inc: Ann Arbor, MI, USA.
- Miller-Young, J.E., Duncan, N.A. and Baroud, G. 2002. Material properties of the human calcaneal fat pad in compression: experiment and theory. *Journal of Biomechanics*; 35 (12), pp. 1523-1531. DOI: 10.1016/S0021-9290(02)00090-8.
- Mills, N., Fitzgerald, C., Gilchrist, A. and Verdejo, R. 2003. Polymer foams for personal protection: cushions, shoes and helmets. *Composites Science and Technology*; 63 (16), pp. 2389-2400. DOI: 10.1016/S0266-3538(03)00272-0.
- Minisi, M. 2005. *Gelatin Impact Modelling*. Natural Defense National Association;: New Jersey, USA.
- Mitchell, B. 2000. Efficacy of thigh protectors in preventing thigh haematomas. *Journal of Science and Medicine in Sport*; 3 (1), pp. 30-34. DOI: 10.1016/S1440-2440(00)80045-6.
- Moerman, K.M., Holt, C.A., Evans, S.L. and Simms, C.K. 2009. Digital image correlation and finite element modelling as a method to determine mechanical properties of human soft tissue in vivo. *Journal of Biomechanics*; 42 (8), pp. 1150-1153. DOI: 10.1016/j.jbiomech.2009.02.016.
- Moerman, K.M., Sprengers, A.M., Simms, C.K., Lamerichs, R.M., Stoker, J. and Nederveen, A.J. 2011. Validation of SPAMM tagged MRI based measurement of 3D soft tissue deformation. *Medical Physics*; 38 (3), pp. 1248-1260. DOI: 10.1118/1.3533942.
- Morvan, T. 2012. *Sports Personal Protective Equipment Testing*, [Unpublished]. MSc. Thesis. Loughborough University.
- Mottahedi, M., Dadalau, A., Hafla, A. and Verl, A. 2011. Numerical Analysis of Relaxation Test Based on Prony Series Material Model. In: M. Fathi, A. Holland, F. Ansari and C. Weber eds., *Integrated Systems, Design and Technology 2010*, Berlin Heidelberg: Springer, pp. 79-91.
- Muggenthaler, H., von Merten, K., Peldschus, S., Holley, S., Adamec, J., Praxl, N. and Graw, M. 2008. Experimental tests for the validation of active numerical human models. *Forensic Science International*; 177 (2), pp. 184-191. DOI: 10.1016/j.forsciint.2007.12.005.
- Mullins, L. 1969. Softening of rubber by deformation. *Rubber Chemistry and Technology*; 42 (1), pp. 339-362. DOI: 10.5254/1.3539210.
- Murtaugh, K. 2001. Injury patterns among female field hockey players. *Medicine & Science in Sports & Exercise*; 33 (2), pp. 201-207. DOI: 10.1097/00005768-200102000-00005.
- Natali, A., Fontanella, C. and Carniel, E. 2012. A numerical model for investigating the mechanics of calcaneal fat pad region. *Journal of the Mechanical Behavior of Biomedical Materials*; 5 (1), pp. 216-223. DOI: 10.1016/j.jmbbm.2011.08.025.

NATO. 2007. *Test Methodology for Protection of Vehicle Occupants against Anti-Vehicular Landmine Effects*. NATO: Springfield, United States.

NFL. 2013. *2013 Official Playing Rules of the National Football League*. [online]. Available at: <<http://static.nfl.com/static/content/public/image/rulebook/pdfs/2013%20-%20Rule%20Book.pdf>> Accessed on: April 12th 2014.

Ní Annaidh, A., Bruyère, K., Destrade, M., Gilchrist, M.D. and Otténio, M. 2012. Characterization of the anisotropic mechanical properties of excised human skin. *Journal of the Mechanical Behavior of Biomedical Materials*; 5 (1), pp. 139-148. DOI: 10.1016/j.jmbbm.2011.08.016.

Nicholl, J.P., Coleman, P. and Williams, B.T. 1995. The epidemiology of sports and exercise related injury in the United Kingdom. *British Journal of Sports Medicine*; 29 (4), pp. 232-238. DOI: 10.1136/bjism.29.4.232.

Ogden, R. 1972. Large deformation isotropic elasticity-on the correlation of theory and experiment for incompressible rubberlike solids. *Proceedings of the Royal Society of London.A.Mathematical and Physical Sciences*; 326 (1567), pp. 565-584. DOI: 10.1098/rspa.1972.0026.

Oomens, C., Maenhout, M., Van Oijen, C., Drost, M. and Baaijens, F. 2003. Finite element modelling of contracting skeletal muscle. *Philosophical Transactions of the Royal Society of London.Series B: Biological Sciences*; 358 (1437), pp. 1453-1460. DOI: 10.1098/rstb.2003.1345.

Orchard, J., James, T., Alcott, E., Carter, S. and Farhart, P. 2002. Injuries in Australian cricket at first class level 1995/1996 to 2000/2001. *British Journal of Sports Medicine*; 36 (4), pp. 270-274. DOI: 10.1136/bjism.36.4.270.

Ore, L.S. 1992. *Design Requirements and Specifications: Dummy Lower Extremity Development Task*. U.S. Department of Transportation: Washington, DC.

Osterhoff, G., Löffler, S., Steinke, H., Feja, C., Josten, C. and Hepp, P. 2011. Comparative anatomical measurements of osseous structures in the ovine and human knee. *The Knee*; 18 (2), pp. 98-103. DOI: 10.1016/j.knee.2010.02.001.

Otténio, M., Tran, D., Annaidh, A.N., Gilchrist, M.D. and Bruyère, K. 2015. Strain rate and anisotropy effects on the tensile failure characteristics of human skin. *Journal of the Mechanical Behavior of Biomedical Materials*; 41 , pp. 241-250. DOI: 10.1016/j.jmbbm.2014.10.006.

Owen, C., Lowne, R. and McMaster, J. 2001. *Requirements for the Evaluation of the Risk of Injury to the Ankle in Car Impact Tests*. 17th International Technical Conference on the Enhanced Safety of Vehicles: Amsterdam, The Netherlands.

Owens, B.D., Kragh Jr, J.F., Macaitis, J., Svoboda, S.J. and Wenke, J.C. 2007. Characterization of extremity wounds in operation Iraqi freedom and operation enduring freedom. *Journal of Orthopaedic Trauma*; 21 (4), pp. 254-257. DOI: 10.1097/BOT.0b013e31802f78fb.

Pailler-Mattei, C., Bec, S. and Zahouani, H. 2008. In vivo measurements of the elastic mechanical properties of human skin by indentation tests. *Medical Engineering & Physics*; 30 (5), pp. 599-606. DOI: 10.1016/j.medengphy.2007.06.011.

Pain, M.T.G., Tsui, F. and Cove, S. 2008. In vivo determination of the effect of shoulder pads on tackling forces in rugby. *Journal of Sports Sciences*; 26 (8), pp. 855-862. DOI: 10.1080/02640410801910319.

Panzer, M.B., Fice, J.B. and Cronin, D.S. 2011. Cervical spine response in frontal crash. *Medical Engineering & Physics*; 33 (9), pp. 1147-1159. DOI: 10.1016/j.medengphy.2011.05.004.

Parthasarathy, V., Graichen, C. and Hathaway, A. 1994. A comparison of tetrahedron quality measures. *Finite Elements in Analysis and Design*; 15 (3), pp. 255-261. DOI: 10.1016/0168-874X(94)90033-7.

Patel, P.N., Smith, C.K. and Patrick, C.W. 2005. Rheological and recovery properties of poly (ethylene glycol) diacrylate hydrogels and human adipose tissue. *Journal of Biomedical Materials Research. Part A*; 73 (3), pp. 313-319. DOI: 10.1002/jbm.a.30291.

Patton, D.A., McIntosh, A.S. and Kleiven, S. 2013. The biomechanical determinants of concussion: finite element simulations to investigate brain tissue deformations during sporting impacts to the unprotected head. *Journal of Applied Biomechanics*; 29 (6), pp. 721-730. DOI: 2012-0191 [pii].

- Paus, R., Klein, J., Permana, P., Owecki, M., Chaldakov, G., Böhm, M., Hausman, G., Lapière, C., Atanassova, P. and Sowiński, J. 2007. What are subcutaneous adipocytes really good for...? *Experimental Dermatology*; 16 (1), pp. 45-47. DOI: 10.1111/j.1600-0625.2006.00519_1.x.
- Payne, T., Mitchell, S. and Bibb, R. 2013. Design of human surrogates for the study of biomechanical injury: a review. *Critical Reviews™ in Biomedical Engineering*; 41 (1), pp. 51-89. DOI: 10.1615/CritRevBiomedEng.2013006847.
- Penrose, T., Foster, D. and Blanksby, B. 1976. Release velocities of fast bowlers during a cricket test match. *Australian Journal for Health, Physical Education and Recreation*; 71 (Supplement to Australian Journal for Health, Physical Recreation & Education), pp. 2-5.
- Perillo-Marcone, A., Alonso-Vazquez, A. and Taylor, M. 2003. Assessment of the effect of mesh density on the material property discretisation within QCT based FE models: a practical example using the implanted proximal tibia. *Computer Methods in Biomechanics & Biomedical Engineering*; 6 (1), pp. 17-26. DOI: 10.1080/1025584031000064470.
- Petersen, C.J., Pyne, D., Dawson, B., Portus, M. and Kellett, A. 2010. Movement patterns in cricket vary by both position and game format. *Journal of Sports Sciences*; 28 (1), pp. 45-52. DOI: 10.1080/02640410903348665.
- Petit, P., L. Portier, J. Foret-Bruno, X. Trosseille, C. Parenteau, J. Coltat, C. TARRIERE and J. Lassau. 1997. Quasistatic characterization of the human foot-ankle joints in a simulated tensed state and updated accidentological data. *1996 International Conference of the Biomechanics of Impact*, September 11-13. Dublin, Ireland.
- Pidd, M. 2003. *Tools for Thinking: Modelling in Management Science*. 2nd ed. John Wiley & Sons: Chichester, UK.
- Podnos, E., Becker, E., Klawitter, J. and Strzepa, P. 2006. FEA analysis of silicone MCP implant. *Journal of Biomechanics*; 39 (7), pp. 1217-1226. DOI: 10.1016/j.jbiomech.2005.03.019.
- Potts, R.O., Buras Jr, E.M. and Chrisman Jr, D.A. 1984. Changes with age in the moisture content of human skin. *Journal of Investigative Dermatology*; 82 (1), pp. 97-100. DOI: 10.1111/1523-1747.ep12259203.
- Prior, A. 1994. Applications of implicit and explicit finite element techniques to metal forming. *Journal of Materials Processing Technology*; 45 (1), pp. 649-656. DOI: 10.1016/0924-0136(94)90413-8.
- Ramasamy, A., Hill, A. and Clasper, J. 2009. Improvised explosive devices: pathophysiology, injury profiles and current medical management. *JR Army Med Corps*; 155 (4), pp. 265-272. DOI: 10.1136/jramc-155-04-05.
- Ramasamy, A., Masouros, S.D., Newell, N., Hill, A.M., Proud, W.G., Brown, K.A., Bull, A.M.J. and Clasper, J.C. 2011. In-vehicle extremity injuries from improvised explosive devices: current and future foci. *Philosophical Transactions of the Royal Society B: Biological Sciences*; 366 (1562), pp. 160-170. DOI: 10.1098/rstb.2010.0219.
- Rashid, B., Destrade, M. and Gilchrist, M.D. 2012. Mechanical characterization of brain tissue in compression at dynamic strain rates. *Journal of the Mechanical Behavior of Biomedical Materials*; 10 , pp. 23-38. DOI: 10.1016/j.jmbbm.2012.01.022.
- Rebelo, N., Nagtegaal, J., Taylor, L. and Passmann, R. 1992. Comparison of implicit and explicit finite element methods in the simulation of metal forming processes. In: J.L. Chenot, R.D. Wood and O.C. Zienkiewicz eds., *Numerical Methods in Industrial Forming Processes*, The University of Michigan: CRC Press, pp. 99-108.
- Reilly, D.T., Burstein, A.H. and Frankel, V.H. 1974. The elastic modulus for bone. *Journal of Biomechanics*; 7 (3), pp. 271-275. DOI: 10.1016/0021-9290(74)90018-9.
- Rey, T., Chagnon, G., Le Cam, J. and Favier, D. 2013. Influence of the temperature on the mechanical behaviour of filled and unfilled silicone rubbers. *Polymer Testing*; 32 (3), pp. 492-501. DOI: 10.1016/j.polymertesting.2013.01.008.
- Rho, J.Y., Ashman, R.B. and Turner, C.H. 1993. Young's modulus of trabecular and cortical bone material: ultrasonic and microtensile measurements. *Journal of Biomechanics*; 26 (2), pp. 111-119. DOI: 10.1016/0021-9290(93)90042-D.

- Rivlin, R. 1948. Large elastic deformations of isotropic materials. II. Some uniqueness theorems for pure, homogeneous deformation. *Philosophical Transactions of the Royal Society of London. Series A, Mathematical and Physical Sciences*; 240 (822), pp. 491-508. DOI: 10.1098/rsta.1948.0003.
- Roach, M. 2003. *Stiff: The curious lives of human cadavers*. WW Norton & Company: United States.
- Robbins, S.E., Gouw, G.J. and Hanna, A.M. 1989. Running-related injury prevention through innate impact-moderating behavior. *Medicine and Science in Sports and Exercise*; 21 (2), pp. 130-139.
- Roberts, J., Merkle, A., Biermann, P., Ward, E., Carkhuff, B., Cain, R. and O'Connor, J. 2007. Computational and experimental models of the human torso for non-penetrating ballistic impact. *Journal of Biomechanics*; 40 (1), pp. 125-136. DOI: 10.1016/j.jbiomech.2005.11.003.
- Robertson, D.D., Debski, R.E., Almusa, E., Armfield, D.R., Stone, D.A. and Walker, P.S. 2003. Knee joint biomechanics: relevance to imaging. *Seminars in Musculoskeletal Radiology*; 7 (01), pp. 043-058.
- Robinovitch, S., Evans, S., Minns, J., Laing, A.C., Kannus, P., Crompton, P.A., Derler, S., Birge, S., Plant, D. and Cameron, I.D. 2009. Hip protectors: recommendations for biomechanical testing—an international consensus statement (part I). *Osteoporosis International*; 20 (12), pp. 1977-1988. DOI: 10.1007/s00198-009-1045-4.
- Robinson, S. 2008. Conceptual modelling for simulation Part I: definition and requirements. *Journal of the Operational Research Society*; 59 (3), pp. 278-290. DOI: 10.1057/palgrave.jors.2602368.
- Rohan, C., Badel, P., Lun, B., Rastel, D. and Avril, S. 2013. Biomechanical response of varicose veins to elastic compression: A numerical study. *Journal of Biomechanics*; 46 (3), pp. 599-603. DOI: 10.1016/j.jbiomech.2012.10.043.
- Rosiak, J.M. and Yoshii, F. 1999. Hydrogels and their medical applications. *Nuclear Instruments and Methods in Physics Research Section B: Beam Interactions with Materials and Atoms*; 151 (1), pp. 56-64. DOI: 10.1016/S0168-583X(99)00118-4.
- Rubin, C.T. and Lanyon, L.E. 1982. Limb mechanics as a function of speed and gait: a study of functional strains in the radius and tibia of horse and dog. *The Journal of Experimental Biology*; 101, pp. 187-211.
- Sakezles, C. 2009. Synthetic Human Tissue Models Can Reduce the Cost of Device Development. *Medical Device Technology*; 20 (1), pp. 32-34.
- Salem, R.O., Laposata, M., Rajendram, R., Cluette-Brown, J.E. and Preedy, V.R. 2006. The total body mass of fatty acid ethyl esters in skeletal muscles following ethanol exposure greatly exceeds that found in the liver and the heart. *Alcohol and Alcoholism (Oxford, Oxfordshire)*; 41 (6), pp. 598-603. DOI: 10.1093/alcalc/agl069.
- Samani, A. and Plewes, D. 2004. A method to measure the hyperelastic parameters of ex vivo breast tissue samples. *Physics in Medicine and Biology*; 49 (18), pp. 4395-4405. DOI: 10.1088/0031-9155/49/18/014.
- Samani, A., Zubovits, J. and Plewes, D. 2007. Elastic moduli of normal and pathological human breast tissues: an inversion-technique-based investigation of 169 samples. *Physics in Medicine and Biology*; 52 (6), pp. 1565-1576. DOI: 10.1088/0031-9155/52/6/002.
- Samani, A., Bishop, J., Luginbuhl, C. and Plewes, D.B. 2003. Measuring the elastic modulus of ex vivo small tissue samples. *Physics in Medicine and Biology*; 48 (14), pp. 2183-2198. DOI: 10.1088/0031-9155/48/14/310.
- Sapozhnikov, S. and Ignatova, A. 2013. Experimental and theoretical investigation of deformation and fracture of subcutaneous fat under compression. *Mechanics of Composite Materials*; 48 (6), pp. 649-654. DOI: 10.1007/s11029-013-9309-7.
- Saraf, H., Ramesh, K., Lennon, A., Merkle, A. and Roberts, J. 2007. Mechanical properties of soft human tissues under dynamic loading. *Journal of Biomechanics*; 40 (9), pp. 1960-1967. DOI: 10.1016/j.jbiomech.2006.09.021.
- Sarvazyan, A.P., D. Goukassian, E. Maevsky and G. Oranskara. 1994. Elasticity imaging as a new modality of medical imaging for cancer detection. *Proc of International Workshop "Interaction of Ultrasound with Biological Media"*, 69-81.
- Sarvazyan, A.P., Rudenko, O.V., Swanson, S.D., Fowlkes, J.B. and Emelianov, S.Y. 1998. Shear wave elasticity imaging: a new ultrasonic technology of medical diagnostics. *Ultrasound in Medicine & Biology*; 24 (9), pp. 1419-1435. DOI: 0.1016/S0301-5629(98)00110-0.

- Sato, Y., T. Sasama, N. Sugano, K. Nakahodo, T. Nishii, K. Ozono, K. Yonenobu, T. Ochi and S. Tamura. 2000. Intraoperative simulation and planning using a combined acetabular and femoral (CAF) navigation system for total hip replacement. *Medical Image Computing and Computer-Assisted Intervention–MICCAI 2000*, October 11-14. Pennsylvania, USA.
- Scheepers, F., R.E. Parent, W.E. Carlson and S.F. May. 1997. Anatomy-based modeling of the human musculature. *Proceedings of the 24th Annual Conference on Computer Graphics and Interactive Techniques*, 3 - 8 August. Los Angeles, CA.
- Schmikli, S.L., Backx, F.J., Kemler, H.J. and van Mechelen, W. 2009. National survey on sports injuries in the Netherlands: target populations for sports injury prevention programs. *Clinical Journal of Sport Medicine: Official Journal of the Canadian Academy of Sport Medicine*; 19 (2), pp. 101-106. DOI: 10.1097/JSM.0b013e31819b9ca3 [doi].
- Schmitt, J., Meiforth, J. and Lengsfeld, M. 2001. Development of a hybrid finite element model for individual simulation of intertrochanteric osteotomies. *Medical Engineering & Physics*; 23 (8), pp. 529-539. DOI: 10.1016/S1350-4533(01)00085-6.
- Schmook, F.P., Meingassner, J.G. and Billich, A. 2001. Comparison of human skin or epidermis models with human and animal skin in in-vitro percutaneous absorption. *International Journal of Pharmaceutics*; 215 (1), pp. 51-56. DOI: 10.1016/S0378-5173(00)00665-7.
- Schneider, L. 1983. *Development of anthropometrically based design specifications for an advanced adult anthropomorphic dummy family*. Transportation Research Institute: Ann Arbor, Michigan.
- Schoenfeld, C., Lautenschlager, E. and Meyer Jr, P. 1974. Mechanical properties of human cancellous bone in the femoral head. *Medical and Biological Engineering*; 12 (3), pp. 313-317. DOI: 10.1007/BF02477797.
- Schreiber, P., Crandall, J., Hurwitz, S. and Nusholtz, G. 1998. Static and dynamic bending strength of the leg. *International Journal of Crashworthiness*; 3 (3), pp. 295-308. DOI: 10.1533/cras.1998.0077.
- Sellier, K.G. and Kneubuehl, B.P. 1994. *Wound ballistics and the scientific background*. Elsevier Science Health Science Division: New York.
- Sharkey, E., Cassidy, M., Brady, J., Gilchrist, M. and NicDaeid, N. 2012. Investigation of the force associated with the formation of lacerations and skull fractures. *International Journal of Legal Medicine*; 126 (6), pp. 835-844. DOI: 10.1007/s00414-011-0608-z.
- Shaw, G., Crandall, J. and Butcher, J. 2002. Comparative evaluation of the THOR advanced frontal crash test dummy. *International Journal of Crashworthiness*; 7 (3), pp. 239-254. DOI: 10.1533/cras.2002.0217.
- Shen, W., Niu, Y., Bykanova, L., Laurence, P. and Link, N. 2010. Characterizing the interaction among bullet, body armor, and human and surrogate targets. *Journal of Biomechanical Engineering*; 132 (12), pp. 121001-121012. DOI: 10.1115/1.4002699.
- Shen, W., Niu, Y., Mattrey, R.F., Fournier, A., Corbeil, J., Kono, Y. and Stuhmiller, J.H. 2008. Development and validation of subject-specific finite element models for blunt trauma study. *Journal of Biomechanical Engineering*; 130 (2), pp. 021022-1-021022-13. DOI: 10.1115/1.2898723.
- Shergold, O.A., Fleck, N.A. and Radford, D. 2006. The uniaxial stress versus strain response of pig skin and silicone rubber at low and high strain rates. *International Journal of Impact Engineering*; 32 (9), pp. 1384-1402. DOI: 10.1016/j.ijimpeng.2004.11.010.
- Sherman, D., C. Bir, D. Viano and E.M. Haacke. 2005. Evaluation and Quantification of Bruising. *International Society of Biomechanics XXth Congress - ASB 29th Annual Meeting*, July 31 - August 5. Cleveland, USA.
- Shin, J., Yue, N. and Untaroiu, C.D. 2012. A finite element model of the foot and ankle for automotive impact applications. *Annals of Biomedical Engineering*; 40 (12), pp. 2519-2531. DOI: 10.1007/s10439-012-0607-3.
- Silvestri, C. and Ray, M. 2009. Development of a finite element model of the knee-thigh-hip of a 50th percentile male including ligaments and muscles. *International Journal of Crashworthiness*; 14 (2), pp. 215-229. DOI: 10.1080/13588260802671399.
- Sims, A., Stait-Gardner, T., Fong, L., Morley, J., Price, W., Hoffman, M., Simmons, A. and Schindhelm, K. 2010. Elastic and viscoelastic properties of porcine subdermal fat using MRI and inverse FEA. *Biomechanics and Modeling in Mechanobiology*; 9 (6), pp. 703-711. DOI: 10.1007/s10237-010-0207-9.

- Skelton, C., Cannon, L., and Trimble, K. 2000. Development of a Lower Limb Physical Model to assess the severity of Land Mine injury. *J Bone and Joint Surg Br*; 85-B (SUPP II), pp. 177.
- Smith, C., Kruger, M.J., Smith, R.M. and Myburgh, K.H. 2008. The inflammatory response to skeletal muscle injury. *Sports Medicine*; 38 (11), pp. 947-969. DOI: 10.2165/00007256-200838110-00005.
- Smith, J.W. and Walmsley, R. 1959. Factors affecting the elasticity of bone. *Journal of Anatomy*; 93 (4), pp. 503-523.
- Snedeker, J., Barbezat, M., Niederer, P., Schmidlin, F. and Farshad, M. 2005b. Strain energy density as a rupture criterion for the kidney: impact tests on porcine organs, finite element simulation, and a baseline comparison between human and porcine tissues. *Journal of Biomechanics*; 38 (5), pp. 993-1001. DOI: 10.1016/j.jbiomech.2004.05.030.
- Snedeker, J., Niederer, P., Schmidlin, F., Farshad, M., Demetropoulos, C., Lee, J. and Yang, K. 2005a. Strain-rate dependent material properties of the porcine and human kidney capsule. *Journal of Biomechanics*; 38 (5), pp. 1011-1021. DOI: 10.1016/j.jbiomech.2004.05.036.
- Snyder, R., Hodgson, V., Nahum, A., King, A., Burstein, A., McHenry, R., Patrick, L., Walt, A., Wilson, R., Lange, W. and Mertz, H. 1973. *Biomechanics and Its Application to Automotive Design P-49 - A Continuing Engineering Education Course developed by SAE Automobile Body Activity, Passenger Protection Committee*. Society of Automotive Engineers: Warrendale, USA.
- Sommer, G., Eder, M., Kovacs, L., Pathak, H., Bonitz, L., Mueller, C., Regitnig, P. and Holzapfel, G.A. 2013. Multi-axial mechanical properties and constitutive modeling of human adipose tissue: A basis for preoperative simulations in plastic and reconstructive surgery. *Acta Biomaterialia*; 9 (11), pp. 9036-9048. DOI: 10.1016/j.actbio.2013.06.011.
- Song, B., Chen, W., Ge, Y. and Weerasooriya, T. 2007. Dynamic and quasi-static compressive response of porcine muscle. *Journal of Biomechanics*; 40 (13), pp. 2999-3005. DOI: 10.1016/j.jbiomech.2007.02.001.
- Souza, J.d. and Gottfried, C. 2013. Muscle injury: Review of experimental models. *Journal of Electromyography and Kinesiology*; 23 (6), pp. 1253-1260. DOI: 10.1016/j.jelekin.2013.07.009.
- Spitzer, V., Ackerman, M.J., Scherzinger, A.L. and Whitlock, D. 1996. The visible human male: a technical report. *Journal of the American Medical Informatics Association : JAMIA*; 3 (2), pp. 118-130. DOI: 10.1136/jamia.1996.96236280.
- Stolk, J., Verdonschot, N. and Huiskes, R. 2001. Management of stress fields around singular points in a finite element analysis. *Computer methods in biomechanics and biomedical engineering*. 3rd ed. London: Gordon and Breach Science Publishers, pp. 57-62.
- Stromsoe, K., Hoiseth, A., Alho, A. and Kok, W. 1995. Bending strength of the femur in relation to non-invasive bone mineral assessment. *Journal of Biomechanics*; 28 (7), pp. 857-861. DOI: 10.1016/0021-9290(95)95274-9.
- Stronge, W.J. 2000. *Impact mechanics*. 1st ed. Cambridge University Press: Cambridge, UK.
- Sugihara, T., Ohura, T., Homma, K. and Igawa, H. 1991. The extensibility in human skin: variation according to age and site. *British Journal of Plastic Surgery*; 44 (6), pp. 418-422. DOI: 10.1016/0007-1226(91)90199-T.
- Sun, E.Q. 2006. *Shear locking and hourglassing in MSC Nastran, ABAQUS, and ANSYS*. MSC Software Corporation's 2006 Americas Virtual Product Development Conference: Evolution to Enterprise Simulation.
- Sun, J., Lee, K. and Lee, H. 2000. Comparison of implicit and explicit finite element methods for dynamic problems. *Journal of Materials Processing Technology*; 105 (1), pp. 110-118. DOI: 10.1016/S0924-0136(00)00580-X.
- Takaza, M., Moerman, K.M. and Simms, C.K. 2013. Passive skeletal muscle response to impact loading: experimental testing and inverse modelling. *Journal of the Mechanical Behavior of Biomedical Materials*; 27, pp. 214-225. DOI: 10.1016/j.jmbbm.2013.04.016.
- Tang, Y.M. and Hui, K.C. 2009. Simulating tendon motion with axial mass-spring system. *Computers & Graphics*; 33 (2), pp. 162-172. DOI: 10.1016/j.cag.2009.01.002.
- Tatar, Y., Ramazanoglu, N., Camliguney, A.F., Saygi, E.K. and Cotuk, H.B. 2014. The Effectiveness of Shin Guards Used by Football Players. *Journal of Sports Science and Medicine*; 13 (1), pp. 120-127.

- Taylor, Z.A., Comas, O., Cheng, M., Passenger, J., Hawkes, D.J., Atkinson, D. and Ourselin, S. 2009. On modelling of anisotropic viscoelasticity for soft tissue simulation: Numerical solution and GPU execution. *Medical Image Analysis*; 13 (2), pp. 234-244. DOI: 10.1016/j.media.2008.10.001.
- Tencer, A.F. and Johnson, K.D., 1994. *Biomechanics in Orthopaedic Trauma: Bone Fracture and Fixation*. Martin Dunitz: London.
- Tencer, A.F., Kaufman, R., Ryan, K., Grossman, D.C., Henley, M.B., Mann, F., Mock, C., Rivara, F., Wang, S. and Augenstein, J. 2002. Femur fractures in relatively low speed frontal crashes: the possible role of muscle forces. *Accident Analysis & Prevention*; 34 (1), pp. 1-11. DOI: 10.1016/S0001-4575(00)00097-X.
- Teran, J., Sifakis, E., Blemker, S.S., Ng-Thow-Hing, V., Lau, C. and Fedkiw, R. 2005. Creating and simulating skeletal muscle from the visible human data set. *IEEE Transactions on Visualization and Computer Graphics*; 11 (3), pp. 317-328. DOI: 10.1109/TVCG.2005.42.
- Then, C., Vogl, T. and Silber, G. 2012. Method for characterizing viscoelasticity of human gluteal tissue. *Journal of Biomechanics*; 45 (7), pp. 1252-1258. DOI: 10.1016/j.jbiomech.2012.01.037.
- Thielen, T., Maas, S., Zuerbes, A., Waldmann, D., Anagnostakos, K. and Kelm, J. 2009. Mechanical behaviour of standardized, endoskeleton-including hip spacers implanted into composite femurs. *International Journal of Medical Sciences*; 6 (5), pp. 280-286. DOI: 10.7150/ijms.6.280.
- Tiossi, R., Vasco, M.A., Lin, L., Conrad, H.J., Bezzon, O.L., Ribeiro, R.F. and Fok, A.S. 2013. Validation of finite element models for strain analysis of implant-supported prostheses using digital image correlation. *Dental Materials*; 29 (7), pp. 788-796. DOI: 10.1016/j.dental.2013.04.010.
- Tirella, A., Mattei, G. and Ahluwalia, A. 2013. Strain rate viscoelastic analysis of soft and highly hydrated biomaterials. *Journal of Biomedical Materials Research Part A*; 102 (10), pp. 3352-3360. DOI: 10.1002/jbm.a.34914.
- Torell, V.B. 2011. As fast as possible rather than well protected: experiences of football clothes. *Culture Unbound: Journal of Current Cultural Research*; 3 , pp. 83-99.
- Treloar, L. 1943. The elasticity of a network of long-chain molecules—II. *Transactions of the Faraday Society*; 39, pp. 241-246. DOI: 10.1039/tf9433900241.
- Troyer, K.L. and Puttlitz, C.M. 2011. Human cervical spine ligaments exhibit fully nonlinear viscoelastic behavior. *Acta Biomaterialia*; 7 (2), pp. 700-709. DOI: 10.1016/j.actbio.2010.09.003.
- Tschoegl, N.W. 1989. *The Phenomenological Theory of Linear Viscoelastic Behavior: An Introduction*. Springer: New York.
- Tsui, F. and M. Pain. 2008. The effects of muscle tension on human biomechanical response and perceived impact intensity. *Proceedings of the 4th North American Congress on Biomechanics*, August 2008. Ann Arbor, USA.
- Turner, N.J., Badylak, J.S., Weber, D.J. and Badylak, S.F. 2012. Biologic scaffold remodeling in a dog model of complex musculoskeletal injury. *Journal of Surgical Research*; 176 (2), pp. 490-502. DOI: 10.1016/j.jss.2011.11.1029.
- Untaroiu, C.D., Yue, N. and Shin, J. 2013. A finite element model of the lower limb for simulating automotive impacts. *Annals of Biomedical Engineering*; 41 (3), pp. 513-526. DOI: 10.1007/s10439-012-0687-0.
- Van der Horst, M., C. Simms, R. Van Maasdam and P. Leerdam. 2005. Occupant lower leg injury assessment in landmine detonations under a vehicle. *IUTAM Symposium on Impact Biomechanics: From Fundamental Insights to Applications*, Dublin, Ireland. 41-49.
- Van Ee, C., Chasse, A. and Myers, B. 2000. Quantifying skeletal muscle properties in cadaveric test specimens: effects of mechanical loading, postmortem time, and freezer storage. *Journal of Biomechanical Engineering*; 122 (1), pp. 9-14. DOI: 10.1115/1.429621.
- Van Houten, E.E.W., Doyley, M.M., Kennedy, F.E., Weaver, J.B. and Paulsen, K.D. 2003. Initial in vivo experience with steady-state subzone-based MR elastography of the human breast. *Journal of Magnetic Resonance Imaging*; 17 (1), pp. 72-85. DOI: 10.1002/jmri.10232.
- Van Loocke, M., Lyons, C. and Simms, C. 2006. A validated model of passive muscle in compression. *Journal of Biomechanics*; 39 (16), pp. 2999-3009. DOI: 10.1016/j.jbiomech.2005.10.016.

- Van Loocke, M., Lyons, C. and Simms, C. 2008. Viscoelastic properties of passive skeletal muscle in compression: stress-relaxation behaviour and constitutive modelling. *Journal of Biomechanics*; 41 (7), pp. 1555-1566. DOI: 10.1016/j.jbiomech.2008.02.007.
- Van Loocke, M., Simms, C. and Lyons, C. 2009. Viscoelastic properties of passive skeletal muscle in compression-Cyclic behaviour. *Journal of Biomechanics*; 42 (8), pp. 1038-1048. DOI: 10.1016/j.jbiomech.2009.02.022.
- Van Slightenhorst, C., Cronin, D.S. and Wayne Brodland, G. 2006. High strain rate compressive properties of bovine muscle tissue determined using a split Hopkinson bar apparatus. *Journal of Biomechanics*; 39 (10), pp. 1852-1858.
- Velani, N., Wilson, O., Halkon, B.J. and Harland, A.R. 2012. Measuring the risk of sustaining injury in sport a novel approach to aid the re-design of personal protective equipment. *Applied Ergonomics*; 43 (5), pp. 883-890. DOI: 10.1016/j.apergo.2011.12.010.
- Verhagen, E. and van Mechelen, W. 2010. The pragmatic approach. *Sports injury research*, New York: Oxford University Press, pp. 143-144.
- Verriest, J. 1984. Thorax and upper abdomen kinematics and tolerance levels and injury criteria. *The Biomechanics of Impact Trauma: Proceedings from course given at International Centre for Transportation Studies*, May 30 - June 4. Amalfi, Italy.
- Viano, D.C., King, A.I., Melvin, J.W. and Weber, K. 1989. Injury biomechanics research: an essential element in the prevention of trauma. *Journal of Biomechanics*; 22 (5), pp. 403-417. DOI: 10.1016/0021-9290(89)90201-7.
- Walker, H., Carr, D., Chalmers, D. and Wilson, C. 2010. Injury to recreational and professional cricket players: Circumstances, type and potential for intervention. *Accident Analysis & Prevention*; 42 (6), pp. 2094-2098. DOI: 10.1016/j.aap.2010.06.022.
- Walton, M. and Rothwell, A.G. 1983. Reactions of thigh tissues of sheep to blunt trauma. *Clinical Orthopaedics and Related Research*; 176, pp. 273-281. DOI: 10.1097/00003086-198306000-00040.
- Wang, C., Y. Zheng, Y. Xiao, W. Qiu and H. Zheng. 2012. Using vibro-ultrasound method to assess the vastus intermedius stiffness over the entire range of step isometric contraction of knee extensors. *Ultrasonics Symposium (IUS), 2012 IEEE International, 7th-10th October 2012*. Dresden, Germany.
- Wang, Z., Deurenberg, P., Wang, W. and Heymsfield, S. 1997. Proportion of adipose tissue-free body mass as skeletal muscle: Magnitude and constancy in men. *American Journal of Human Biology*; 9 (4), pp. 487-492. DOI: 0.1002/(SICI)1520-6300(1997)9:4<487::AID-AJHB8>3.0.CO;2-T.
- Ward, S.R. and Lieber, R.L. 2005. Density and hydration of fresh and fixed human skeletal muscle. *Journal of Biomechanics*; 38 (11), pp. 2317-2320. DOI: 10.1016/j.jbiomech.2004.10.001.
- Weber, C. Chirurgische Erfahrungen und Untersuchungen nebst zahlreichen Beobachtungen aus der chirurgischen Klinik und dem evangelischen Krankenhause zu Bonn: Mit neun Tafeln. 1859. Reimer, Berlin, pp. 171-174. .
- Webster, J. and Roberts, J. 2011. Determining the effect of cricket leg guards on running performance. *Journal of Sports Sciences*; 29 (7), pp. 749-760. DOI: 10.1080/02640414.2011.553962.
- Wen, Y., Xu, C., Wang, H., Chen, A. and Batra, R. 2013. Impact of steel spheres on ballistic gelatin at moderate velocities. *International Journal of Impact Engineering*; 62, pp. 142-151. DOI: 10.1016/j.ijimpeng.2013.07.002.
- Wen, Y., Xu, C., Wang, S. and Batra, R. 2015. Analysis of Behind the Armor Ballistic Trauma. *Journal of the Mechanical Behavior of Biomedical Materials*; 45, pp. 11-21. DOI: 10.1016/j.jmbbm.2015.01.010.
- Wichterle, O. and Lim, D. 1960. Hydrophilic gels for biological use. *Nature*; 185, pp. 117-118. DOI: 10.1038/185117a0.
- Winter, D.A. 1990. Anthropometry. *Biomechanics and Motor Control of Human Movement*, 2nd ed. John Wiley & Sons Inc, pp. 51-57.
- Wismans, J., Janssen, E.G., Beusenbergh, M., Koppens, W.P., Happee, R. and Bovendeerd, P.H.M. 2000. *Injury Biomechanics (4J610)*. Eindhoven University of Technology: Eindhoven, The Netherlands.

- Woo, S.L.Y., Hollis, J.M., Adams, D.J., Lyon, R.M. and Takai, S. 1991. Tensile properties of the human femur-anterior cruciate ligament-tibia complex. The effects of specimen age and orientation. *The American Journal of Sports Medicine*; 19 (3), pp. 217-225. DOI: 10.1177/036354659101900303.
- World Medical Association. 2008. *Declaration of Helsinki - Ethical Principles for Medical Research Involving Human Subjects*. [online]. Available at: <<http://www.wma.net/en/30publications/10policies/b3/>> Accessed on: 14th November 2012.
- Wu, J.Z., Cutlip, R.G., Andrew, M.E. and Dong, R.G. 2007. Simultaneous determination of the nonlinear-elastic properties of skin and subcutaneous tissue in unconfined compression tests. *Skin Research and Technology*; 13 (1), pp. 34-42. DOI: 10.1111/j.1600-0846.2007.00182.x.
- Wu, J.Z., Dong, R.G., Smutz, W.P. and Schopper, A.W. 2003. Nonlinear and viscoelastic characteristics of skin under compression: experiment and analysis. *Bio-Medical Materials and Engineering*; 13 (4), pp. 373-385.
- Yamada, H. 1970. *Strength of biological materials*. Williams & Wilkins: Baltimore, Maryland, USA.
- Yan, L., Dillard, D.A., West, R.L., Rubis, K.J. and Gordon, G.V. 2012. Strain rate and temperature dependence of a nanoparticle-filled poly (dimethylsiloxane) undergoing shear deformation. *Journal of Polymer Science Part B: Polymer Physics*; 50 (13), pp. 929-937. DOI: 10.1002/polb.23088.
- Yang, K.H., Hu, J., White, N.A., King, A.I., Chou, C.C. and Prasad, P. 2006. Development of numerical models for injury biomechanics research: a review of 50 years of publications in the Stapp Car Crash Conference. *Stapp Car Crash Journal*; 50, pp. 429-490.
- Yeni, Y., Brown, C. and Norman, T. 1998. Influence of bone composition and apparent density on fracture toughness of the human femur and tibia. *Bone*; 22 (1), pp. 79-84. DOI: 10.1016/S8756-3282(97)00227-5.
- Young, D.A. and Christman, K.L. 2012. Injectable biomaterials for adipose tissue engineering. *Biomedical Materials*; 7 (2), pp. 024104. DOI: 10.1088/1748-6041.
- Yucesoy, C.A., Koopman, B.H., Huijing, P.A. and Grootenboer, H.J. 2002. Three-dimensional finite element modeling of skeletal muscle using a two-domain approach: linked fiber-matrix mesh model. *Journal of Biomechanics*; 35 (9), pp. 1253-1262. DOI: 10.1016/S0021-9290(02)00069-6.
- Zdero, R., Shah, S., Mosli, M. and Schemitsch, E.H. 2010. The effect of load application rate on the biomechanics of synthetic femurs. *Proceedings of the Institution of Mechanical Engineers. Part H, Journal of Engineering in Medicine*; 224 (4), pp. 599-605. DOI: 10.1243/09544119JEIM742.
- Zeigler, B.P. 1976. *Theory of modelling and simulation*. Wiley: New York.
- Zheng, Y., Mak, A.F. and Lue, B. 1999. Objective assessment of limb tissue elasticity: development of a manual indentation procedure. *Journal of Rehabilitation Research and Development*; 36 (2), pp. 71-85